LEABHARLANN CHOLÁISTE NA TRÍONÓIDE, BAILE ÁTHA CLIATH
Ollscoil Átha Cliath
TRINITY COLLEGE LIBRARY DUBLIN
The University of Dublin

Terms and Conditions of Use of Digitised Theses from Trinity College Library Dublin

Copyright statement

All material supplied by Trinity College Library is protected by copyright (under the Copyright and Related Rights Act, 2000 as amended) and other relevant Intellectual Property Rights. By accessing and using a Digitised Thesis from Trinity College Library you acknowledge that all Intellectual Property Rights in any Works supplied are the sole and exclusive property of the copyright and/or other IPR holder. Specific copyright holders may not be explicitly identified. Use of materials from other sources within a thesis should not be construed as a claim over them.

A non-exclusive, non-transferable licence is hereby granted to those using or reproducing, in whole or in part, the material for valid purposes, providing the copyright owners are acknowledged using the normal conventions. Where specific permission to use material is required, this is identified and such permission must be sought from the copyright holder or agency cited.

Liability statement

By using a Digitised Thesis, I accept that Trinity College Dublin bears no legal responsibility for the accuracy, legality or comprehensiveness of materials contained within the thesis, and that Trinity College Dublin accepts no liability for indirect, consequential, or incidental, damages or losses arising from use of the thesis for whatever reason. Information located in a thesis may be subject to specific use constraints, details of which may not be explicitly described. It is the responsibility of potential and actual users to be aware of such constraints and to abide by them. By making use of material from a digitised thesis, you accept these copyright and disclaimer provisions. Where it is brought to the attention of Trinity College Library that there may be a breach of copyright or other restraint, it is the policy to withdraw or take down access to a thesis while the issue is being resolved.

Access Agreement

By using a Digitised Thesis from Trinity College Library you are bound by the following Terms & Conditions. Please read them carefully.

I have read and I understand the following statement: All material supplied via a Digitised Thesis from Trinity College Library is protected by copyright and other intellectual property rights, and duplication or sale of all or part of any of a thesis is not permitted, except that material may be duplicated by you for your research use or for educational purposes in electronic or print form providing the copyright owners are acknowledged using the normal conventions. You must obtain permission for any other use. Electronic or print copies may not be offered, whether for sale or otherwise to anyone. This copy has been supplied on the understanding that it is copyright material and that no quotation from the thesis may be published without proper acknowledgement.

Modelling a Network of Turloughs

Trinity College Library
Dublin



University of Dublin
THIS THESIS MAY BE READ ONLY IN THE LIBRARY

Bound By:
THE
THESIS CENTRE
65 Camden St. Lwr.,
Dublin 2. Ph: 475 3616
www.thesiscentre.com

Modelling a Network of Turloughs

Laurence Gill

A thesis submitted for the Degree of Doctor of Philosophy
to the University of Dublin, Trinity College

May 2010

Department of Civil, Structural and Environmental Engineering
University of Dublin
Trinity College
Dublin

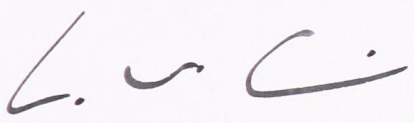
TRINITY COLLEGE
2 7 AUG 2010
LIBRARY DUBLIN
8913

Declaration

I declare that this thesis has not been submitted as an exercise for a degree at this or any other University and is entirely my own work.

I agree that the Library may lend or copy the thesis upon request. This permission covers only single copies made for study purposes, subject to normal conditions of acknowledgement.

SIGNED



LAURENCE GILL

for Charlie Whimbrel, the kipper

Summary

Turloughs are depressions in karst, which are intermittently flooded on an annual cycle via groundwater sources and have substrate and/or ecological communities characteristic of wetlands. The flooding in turlough basins could occur as a result of several different hydraulic settings and configurations but for many it is due to insufficient capacity of the underground karst system to take increased flows following excessive precipitation events, causing the conduit-type network to surcharge. Turloughs in Ireland have been the continuing focus of research interest mainly due to the unique flora and fauna in this type of aquatic environment, but also from the point of view of risks of localised flooding. This research has taken continuous water level measurements in five turloughs (Blackrock, Coy, Coole, Garryland and Caherglassaun) in the Gort lowlands area of south Galway over a three year period. The monitoring of water level fluctuations, in conjunction with river inputs and precipitation, has then been used to elucidate the hydrogeological controls and physical mechanisms forming the hydraulic system beneath the ground.

A model of the karst network has been developed using a pipe network model with the turloughs represented as ponds. The contribution to the karst network from diffuse flow through the epikarst via the matrix and fracture flow has also been modelled using a combination of a groundwater infiltration module and network of permeable pipes in series. The linkages comprising the network system have been determined through several different avenues of research: the relationship between turlough water level and net flows into / out of the underground conduits; time series analytical techniques (Fast Fourier Transform, Discrete and Continuous Wavelet Transforms) applied to the non-stationery turlough water level profiles; and hydro-chemical analysis of water samples at different points on the network which has included the use of stable isotope ^{18}O.

The final model was calibrated against two separate hydrological years taking gauged river flows as inflows at discrete points into the network. In general the model provided a good simulation for all of the turloughs, particularly for the lower three turloughs (Coole, Garryland and Caherglassaun) which are situated closest to the sea. Indeed the model

accurately pickled up the tidal response observed in these turloughs at shallow depths. The model however, did not accurately simulate the Blackrock and Coy system in response to heavy rain events following significant periods of dry weather. This could be due to the storage of flow in the drained epikarst which is not being explicitly modelled or possibly due to a more complex pipe network in the area than has been considered, possibly as a result of a karst collapse structure.

Finally, a rainfall-runoff model has also been developed to simulate the river flows draining off the Old Red Sandstone mountains down into the karst underground network. The combination of the rainfall-runoff model to provide inputs into the karst system and the pipe network model did promote the right patterns of water level fluctuation in the simulated turloughs but did not provide enough flow to fill the turloughs adequately.

Acknowledgements

My sincere appreciation goes to Paul Johnston for suggesting this topic of research to me originally and his depth of knowledge and wisdom of all things "turlough" during his long supervision of my work. His dedication to the monitoring of the south Galway lowland karst hydrogeology over the past 20 years is noble. Special acknowledgments go to the Box for the turlough water level data and other fieldwork, esoteric discussions on modelling and the legendary yurt, as well as to Pat Veale for fine days out west wandering the turloughs and long evenings camping on the coast. Other help from within the College for which I am indebted includes: Biswajit Basu and Bidisha Ghosh for help on the use of Fourier analysis and wavelets; Ted McCormack for river gauging fieldwork; Paul Hynds and Clare O'Farrell for analysis on the ICP; Robbie Goodhue (TCD Geology) for stable isotope analysis; Mark Kavanagh (TCD Centre for the Environment) for Total N and TOC analysis.

I would also like to acknowledge Mike Reeves and Susan Anderson from Wallingford software for advice regarding *Infoworks*, Met Eireann for meteorological data, the Marine Institute for tidal data and the OPW for the river gauging data. My thanks go to the Coole park estate and the local farmers in south Galway on whose land the turloughs emerge every year, for access. I also acknowledge the National Parks and Wildlife Service for funding the *Conservation status of turloughs* project in Trinity College which has been running in parallel to this work and has informed the work in this thesis.

My deepest appreciation goes to my wife Olivia for her constant love and support during this process, as well as for help with fieldwork and proof reading. Her selfless composure throughout my turloughian rhapsody has been sublime, particularly following the arrival of the young Archduke Skudinand. And eternal gratitude to my parents who taught me to follow my own passions through life, to delight in the pursuit of knowledge and the liberating adventure of discovery. Hopefully this thesis acts as some tribute to them.

Finally, my thoughts go to Prof. Simon Perry for having faith in me at the start of my academic career and suggesting that I nip upstairs to talk to Paul about a possible research topic 10 years ago.

Table of Contents

Disclaimer i

Executive Summary iii

Acknowledgements v

Abbreviations xi

1 INTRODUCTION **1**

1.1 Background **1**

1.2 Project Aims and objectives **3**

1.3 The Generated Soul **5**

2 LITERATURE REVIEW **6**

2.1 Overview of Karst Hydrology **6**

2.2 The Conceptual Framework for Karst Aquifers **7**

2.2.1 Recharge 7

2.2.2 Underground flow systems 9

2.2.3 Discharge 13

2.2.4 Chemistry 14

2.3 Evolution of Conduit Permeability and Karst Network Development **15**

2.3.1 Fracture enlargement 16

2.3.2 Conduit network development 17

2.4 Investigative Techniques for the Characterisation of Karst Aquifers **20**

2.4.1 Cave mapping 21

2.4.2 Geomorphology 21

2.4.3 Tracer tests 23

2.4.4 Spring water chemistry (geochemistry) 26

2.4.5 Spring hydrographs 33

2.4.6 Use of test wells in karst 36

2.4.7 Remote sensing and surface geophysics 37

2.4.8 Other methods 38

2.5 Mathematical Modelling of Karst Aquifers 40
2.5.1 Lumped parameter, linear systems models 42
2.5.1.1 Parametric transfer function methods 43
2.5.1.2 Non-parametric transfer function methods 49
2.5.2 Equivalent porous media models 56
2.5.3 Tank-and-pipe models 58
2.5.4 Dual porosity distributed parameter models 67
2.5.5 Other modelling approaches 70
2.5.5.1 Geochemical models 70
2.5.5.2 Contaminant transport modelling 72
2.5.5.3 Sediment transport modelling 73
2.5.5.4 Neural networks 74

3 BACKGROUND AND AREA DESCRIPTION 76
3.1 Introduction 76
3.2 Geology and Hydrogeology 76
3.3 Turloughs 82
3.3.1 Turlough hydrology and hydrogeology 82
3.3.2 Turlough ecology 84
3.3.3 Pressures and impacts upon turloughs as Groundwater Dependent Terrestrial Ecosystems 90
3.4 Previous Studies in the Gort Lowlands 91
3.4.1 Field work 92
3.4.2 Hydraulic model 95

4 INSTRUMENTATION AND DATA COLLECTION 98
4.1 Introduction 98
4.2 Turlough Water Depth Monitoring 98
4.3 Rainfall Monitoring 99
4.4 River Gauging 100
4.4.1 Determination of rating curves 103

4.5 Sea level monitoring **107**

4.6 Turlough surveying **109**

4.7 Visual surveying **113**

4.8 Hydrochemical data **118**

4.8.1 Chemical analysis 119

4.8.2 Isotope analysis 119

5 DATA ANALYSIS **121**

5.1 Introduction **121**

5.2 Water Level Profiles **121**

5.3 Hydraulic Gradients **123**

5.4 Depth-Volume-Area relationships **127**

5.5 Flow and residence time analysis **129**

5.5.1 Recession curves 129

5.5.2 Filling periods 136

5.5.3 Flows into the system 138

5.5.4 Mean residence time 143

5.6 Rainfall and Evapotranspiration Analyses **145**

5.6.1 Rainfall 145

5.6.2 Evapotranspiration 147

5.7 River Flows **148**

5.7.1 Rating curves 148

5.7.2 River flows 153

5.7.3 Calculating diffuse recharge from epikarst 154

5.8 Turlough Water Quality Analyses **157**

5.8.1 Stable isotope monitoring 158

5.8.2 Turlough water quality 164

6 TIME SERIES ANALYSIS **171**

6.1 Introduction **171**

6.2 Correlation analysis of turlough water levels **171**

6.3 Fourier analysis 176
6.3.1 Fast Fourier Transform analysis 177
6.3.2 Short Term Fourier Transform analysis 187
6.4 Wavelet analysis 190
6.4.1 Discrete wavelet transform (DWT) analysis 192
6.4.2 Continuous wavelet transform (CWT) analysis 196

7 PIPE NETWORK MODELLING 199
7.1 Introduction 199
7.2 Hydraulic Principles of the Pipe-Network Model 199
7.3 Generic model of single turlough – preliminary investigations 202
7.3.1 Change in pond volume 203
7.3.2 Downstream pipe diameter 204
7.3.3 Short throttle section 207
7.3.4 Comparison of throttle versus smaller downstream pipe 208
7.3.5 Comparison of length of pipe versus tidal effect 209
7.3.6 Comparison of different entry pipe diameters into pond 210
7.3.7 Balance between throttle pipe and pond entry pipe diameters 210
7.3.8 Difference between two methods of modelling pressurised flow 212
7.3.9 Comparing elliptical pipes to circular pipes 212
7.4 Representing surveyed turlough by ponds in *Infoworks* 214
7.5 Modelling Diffuse Infiltration into the Network 215
7.5.1 Rainfall runoff and routing models 215
7.5.1.1 Runoff surfaces 217
7.5.1.2 Groundwater infiltration module 221
7.5.1.3 Contributing catchment area and pipe network 224
7.6 Calibration of diffuse flow component of network model 229

8 RAINFALL RUNOFF MODELLING 233
8.1 Introduction 233
8.2 Background to model 233
8.3 Data 236
8.4 Model calibration 237
8.5 Reservoir Routing across Lough Cutra 240

9 OVERALL MODEL OF LINKED TURLOUGH SYSTEM 243
9.1 Overall Turlough Conceptual Model 243
9.2 Linked pipe network model 244
9.2.1 Initial network development 245
9.2.2 Model calibration 246
9.2.3 Model validation 254
9.2.4 Gort lowland system statistics 260
9.3 Linked Model validation 262

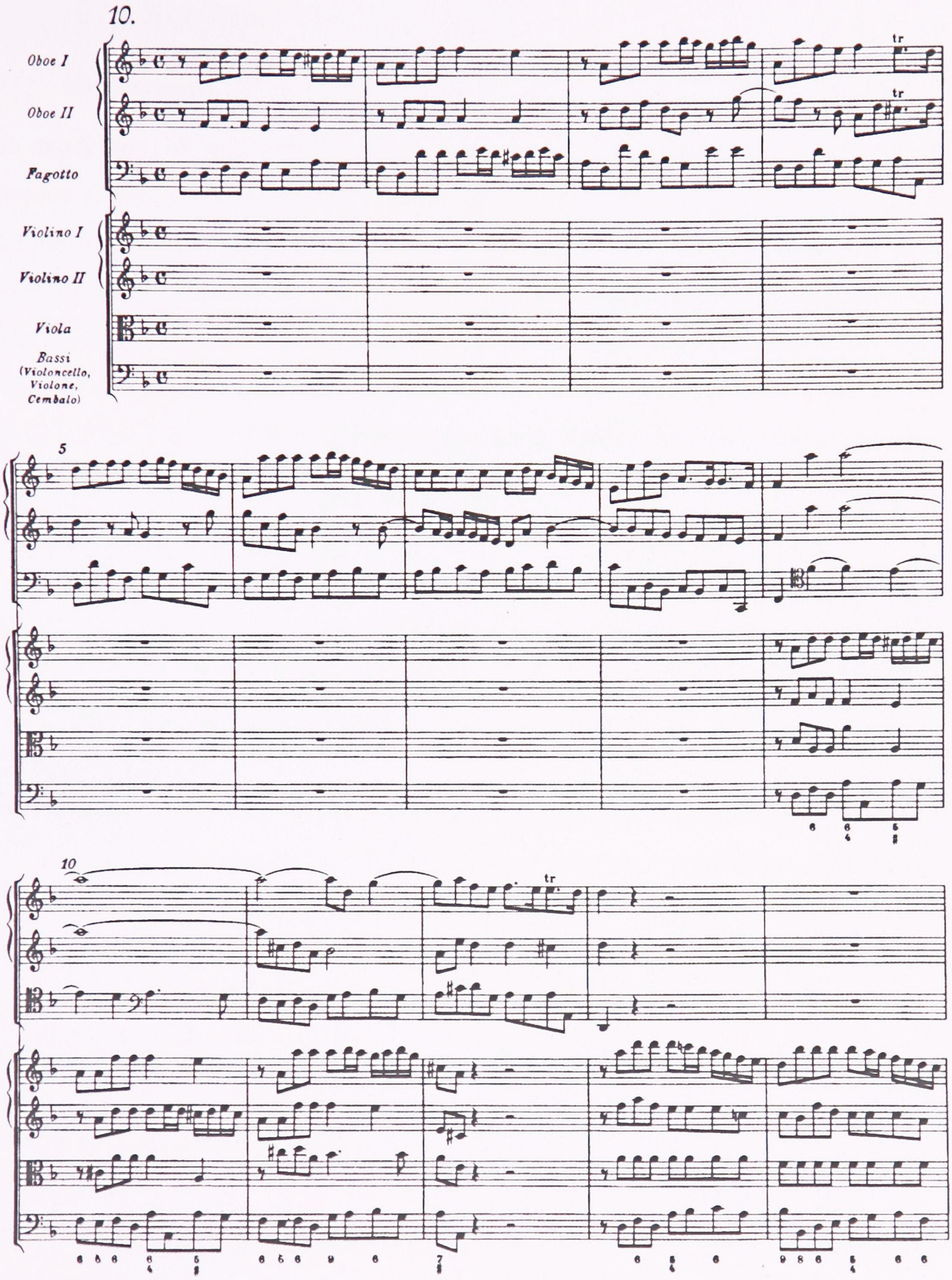
10 CONCLUSIONS 265
10.1 Conclusions 265
10.2 Further Research 266

REFERENCES 270

APPENDIX A Maps
APPENDIX B Topographic Surveys
APPENDIX C Flow Analysis
APPENDIX D Rating Curves
APPENDIX E Water Quality Results
APPENDIX F Time Series Analysis
APPENDIX G Pipe Network Modelling

Abbreviations

CFD	computational fluid dynamics
CWT	continuous wavelet transform
CSTR	continuously stirred tank reactor
DIC	dissolved inorganic carbon
DNAPL	dense non-aqueous phase liquid
DWT	discrete wavelet transform
δ^2H	deuterium (δD)
$\delta^{18}O$	oxygen 18 isotope
EC	electrical conductivity
FFT	fast Fourier transform
STFT	short tem Fourier transform
GIM	groundwater infiltration module
GMWL	global meteoric water line
GPS	global positioning system
GWDTE	groundwater dependent terrestrial ecosystems
^2H	(deuterium) isotope
K	hydraulic conductivity
λ (or *f*)	friction factor
μ	viscosity
MRS	magnetic resonance sounding
NPWS	National Parks and Wildlife Service
^{18}O	oxygen isotope
OPW	Office of Public Works
Ø	diameter
PE	potential evapotranspiration
RTD	residence time distribution
SUDS	sustainable urban drainage systems
TOC	total organic carbon
UTC	Temps Universel Coordonné (*Coordinated Universal Time equivalent to Greenwich Mean Time*)
VSMOW	Vienna standard mean ocean water
WFD	Water Framework Directive



Handel's Water Music – Suite I in F-major (HWV 348) 10. *Molto allegro*

1 INTRODUCTION

1.1 Background

The modelling of underground flows through karst aquifers has received plenty of attention across many regions throughout the world. In general, the studies aim to link a precipitation input to a discrete and measurable outflow from the karst system at a spring. Various different conceptual, analytical and numerical approaches have been used to form such a relationship from black box models to detailed physically-based models. The lowland karst area of south Galway in the west of Ireland provides a different setting for karst hydrogeological studies to many other karst regions however, due to its low-lying nature whereby most of the catchment is less than 30 m above sea level. Indeed, the main spring from this area discharges the groundwater slightly below mean sea level at the coast which, critically, means that it is not possible to measure the net flows from the karst network. However, this low-lying landscape does provide unique karstic hydrogeological signatures in the form of fluctuating water levels of intermittently flooded topographic depressions - temporary lakes which are known as *turloughs*.

Turloughs are depressions in karst, which are intermittently flooded on an annual cycle via groundwater sources and have substrate and/or ecological communities characteristic of wetlands. The flooding in turlough basins could occur as a result of several different hydraulic settings and configurations but for many it is due to insufficient capacity of the underground karst system to take increased flows following excessive precipitation events, causing the conduit-type network to surcharge. Hence, the monitoring of water level fluctuations can be used to elucidate the hydrogeological controls and physical mechanisms forming the hydraulic system beneath the ground.

Turloughs in Ireland have been the continuing focus of research interest mainly due to the unique flora and fauna in this type of aquatic environment, but also from a more anthropocentric point of view, due to the risks of localised flooding. The Gort-Ardrahan area of south Galway experienced severe flooding during the winters of 1989-90, 1991,

1994 and 1995, the latter being the most severe. High levels were also experienced in 1998 and 1999 which led to a detailed hydrological study of this karst limestone area.

Measurements of relevant hydrological parameters are used to describe quantitatively the behaviour of turloughs and the development of characteristic hydrological indicators for use in the conservation of these protected groundwater dependent ecosystems. Turloughs provide a habitat for many protected flora and fauna species and are designated a Priority Habitat in Annex 1 of the EU Habitats Directive (92/43/EEC) (EEC, 1992). Hydrology is the primary driver of these unique ecosystems, and a better understanding of the flooding regime is therefore required for their future sustainability and conservation. Equally, under the Water Framework Directive (WFD) (EC, 2000) turloughs are designated as Groundwater Dependent Terrestrial Ecosystems (GWDTE). Indeed, an ongoing multi-disciplinary project entitled the *Conservation Status of Turloughs* is currently being sponsored funded by the National Parks and Wildlife Service (NPWS) in order to provide a more comprehensive understanding of the pressures on these ecosystems, integrating the hydrology with land-use and catchment management.

The monitoring of the water levels in the turloughs in the low-lying karst near Gort in Galway has been taking place over several years. The turloughs are thought to be connected together in a linked conduit drainage network which receives the rainfall-runoff draining off the Old Red Sandstone Slieve Aughty mountains, flows which disappear underground when reaching the karst bedrock. This research has taken the continuous water level measurement in five turloughs (Blackrock, Coy, Coole, Garryland and Caherglassaun) over the last three years in order to develop a mathematical model which will be verified using different analytical techniques to establish the nature of the underground links. The model of the karst is represented by a pond and pipe flow model to represent the turlough and conduit network. This takes the river flows as inflows at points into the network. A second rainfall-runoff model has also been developed to generate the flows draining off the Old Red Sandstone mountains down into the karst underground network for use in periods when river flow records are not available.

The development of a calibrated mathematical model of the karst network is needed for two reasons: as a tool to predict future flooding levels; and as a calibrated model to tie in with the ecology to establish seasonal flooding levels which can be correlated against specific ecology.

1.2 Project Aims and Objectives

The overall aim of the research is to develop a mathematical model which accurately simulates the behaviour of five turloughs in the lowland karst (and by corollary the behaviour of the underground karstic network) in response to meteorological input (precipitation and potential evapotranspiration).

This has been achieved via several targeted objectives as follows:

- To monitor the turlough water level, precipitation and river flows in the Gort lowland area for several different hydrological years.

- To carry out a topographic survey of each turlough from which depth-volume and depth surface area relationships can be determined.

- To provide rating curves for the three main rivers draining off the Slieve Aughty mountains down into the low-lying karst.

- To quantify the relationship between turlough water level and net flows into / out of the underground network.

- To develop the conceptual model of the linkages comprising the network system through a combination of time series analytical techniques and hydro-chemical analysis of samples taken at different points on the network.

- To gain an understanding of the dynamics of different pipe and tank network configurations using a hypothetical network.

- To quantify the contribution to the karst network from diffuse flow through the epikarst and then to model this dynamic in the karst mathematical model.

- To develop a calibrated rainfall-runoff model for the main rivers draining the Old Red sandstone Slieve Aughty mountains to provide an input at specific points into the karst model.

- To investigate the nutrient water quality and stable oxygen isotopic signatures in the turloughs and rivers.

- To quantify the net flows through the system and discharging into Galway Bay.

- To calibrate and validate a pipe network model of the Gort lowland karst network with respect to measured levels in five turloughs (Blackrock, Coy, Coole, Garryland and Caherglassaun).

1.3 The Generated Soul

Coole Demesne was the home of Lady Gregory in the early 20th century and acted as a focus for many artists of the day; poets, novelists, dramatists and philosophers used to gather there forming what is now termed the Irish Literary Revival. W.B. Yeats was a frequent visitor to Coole during this time which he vividly describes in the following poem which also contains relevant knowledge of karst hydrology in the area.

"Coole and Ballylee, 1931"
by W.B. Yeats

Under my window-ledge the waters race,
Otters below and moor-hens on the top,
Run for a mile undimmed in Heaven's face
Then darkening through 'dark' Raftery's 'cellar' drop,
Run underground, rise in a rocky place
In Coole demesne, and there to finish up
Spread to a lake and drop into a hole.
What's water but the generated soul?

Upon the border of that lake's a wood
Now all dry sticks under a wintry sun,
And in a copse of beeches there I stood,
For Nature's pulled her tragic buskin on
And all the rant's a mirror of my mood:
At sudden thunder of the mounting swan
I turned about and looked where branches break
The glittering reaches of the flooded lake.

Another emblem there! That stormy white
But seems a concentration of the sky;
And, like the soul, it sails into the sight
And in the morning's gone, no man knows why;
And is so lovely that it sets to right
What knowledge or its lack had set awry,
So arrogantly pure, a child might think
It can be murdered with a spot of ink.

Sound of a stick upon the floor, a sound
From somebody that toils from chair to chair;
Beloved books that famous hands have bound,
Old marble heads, old pictures everywhere;
Great rooms where travelled men and children found
Content or joy; a last inheritor
Where none has reigned that lacked a name and fame
Or out of folly into folly came.

A spot whereon the founders lived and died
Seemed once more dear than life; ancestral trees,
Or gardens rich in memory glorified
Marriages, alliances and families,
And every bride's ambition satisfied.
Where fashion or mere fantasy decrees
Man shifts about—all that great glory spent—
Like some poor Arab tribesman and his tent.

We were the last romantics—chose for theme
Traditional sanctity and loveliness;
Whatever's written in what poets name
The book of the people; whatever most can bless
The mind of man or elevate a rhyme;
But all is changed, that high horse riderless,
Though mounted in that saddle Homer rode
Where the swan drifts upon a darkening flood.

2 LITERATURE REVIEW

2.1 Overview of Karst Hydrology

Karst terrains are estimated to cover 10-15% of the earth's land surface and the aquifers in karst rocks act as a water resource for approximately a quarter of the world's population (Ford and Williams, 2007). Karst aquifers contain dissolution conduits which permit rapid transport of groundwater, usually in turbulent flow which may often short-circuit the granular or fracture permeability of the acquifer. For example, the change in sediment carried by a karst discharge after rain storms can vary drastically due to the movement of sediment laden surface water disappearing into the underground conduits to re-emerge with more or less the same energy and sediment load (Mahler and Lynch, 1999). Conversely, during times of low flow the water comes from the matrix and fractures within the aquifer and is therefore very clean.

Up until the 1960s although the existence of conduits within karst was obviously acknowledged (caves etc.), hydrogeologists (pumping at the ground surface) assumed that the aquifer behaved equivalently to a porous medium and did not generally consider the conduits to be significant in terms of the groundwater hydrology, being viewed merely as water-filled cavities which did not interrupt the flow field. Speleologists have held different views historically, presuming that karst aquifers are dominated by conduit flow. Extensive developments in the 1970s and 1980s in the disciplines of hydrogeology and speleology with regards to carbonate aquifers however, have provided a more convergent approach between the disparate views (Sasowsky, 2000), particularly as a result of physical and chemical studies of karst springs (including tracer studies). Equally, the study of cave growth (speleogenesis) with time scales of thousands of years has contributed to the understanding of carbonate aquifers as much as the study of existing karst porosity distribution. Hence, in the past decade, researchers generally considered the combined effects and interactions between conduit flow, fracture flow and matrix flow. Conduit flow has more in common with surface water hydrology and engineered hydraulic networks than it does with the classical study of groundwater and so the study of karst hydrology involves the confluence of both surface and ground water hydrology concepts.

2.2 The Conceptual Framework for Karst Aquifers

2.2.1 Recharge

Karst is fed by surface water either via a network of surface drainage channels (carrying streams fed by groundwater and/or surface runoff) or diffuse infiltration from direct rainfall. Unlike other aquifers, recharge to karstic groundwater systems may first be concentrated into runoff at or near to the surface before discharging into the aquifer as a sinking stream. Such flow concentration may occur internally, on the limestone outcrop via vertical shafts or via *dolines*; or it may occur where streams flow onto the limestone from adjacent non-carbonate rocks and sink underground through *swallets* (or swallow holes) at or close to the geological boundary - known as *allogenic* concentrated recharge (Drew, 2002).

Diffuse infiltration can be considered to be the same as in any other hydrogeological setting. The initial precipitation is taken up as soil moisture and when the soil is saturated the water begins to percolate downwards through the matrix porosity or along fractures in the bedrock until it reaches the water table and is stored in the phreatic zone of the aquifer (Shaw, 1994). However, the existence of an epikarst (or subcutaneous zone) in which the soil / carbonate rock interface is usually very sharp means there is very little existence of any weathered rock (C-horizon) in karst terrains. The karst soil tends to be well leached and little carbonate material remains and the bedrock is often very irregular with deep crevices which have formed due to dissolution between the fractures, as shown on Figure 2.1. Water moving downward from overlying soil into the epikarst must often move laterally for substantial distances before finding an open fracture or shaft that will permit vertical movement into the unsaturated zone of the bedrock and hence the epikarst can hold the water in temporary storage for days or weeks before the water may enter the groundwater system, depending on the depth of the epikarst (Williams, 1983). However, in areas of very thin soils and highly fractured bedrock the spring hydrographs lag only slightly behind the precipitation as demonstrated in Slovenia for example (Kogovsek, 1981).

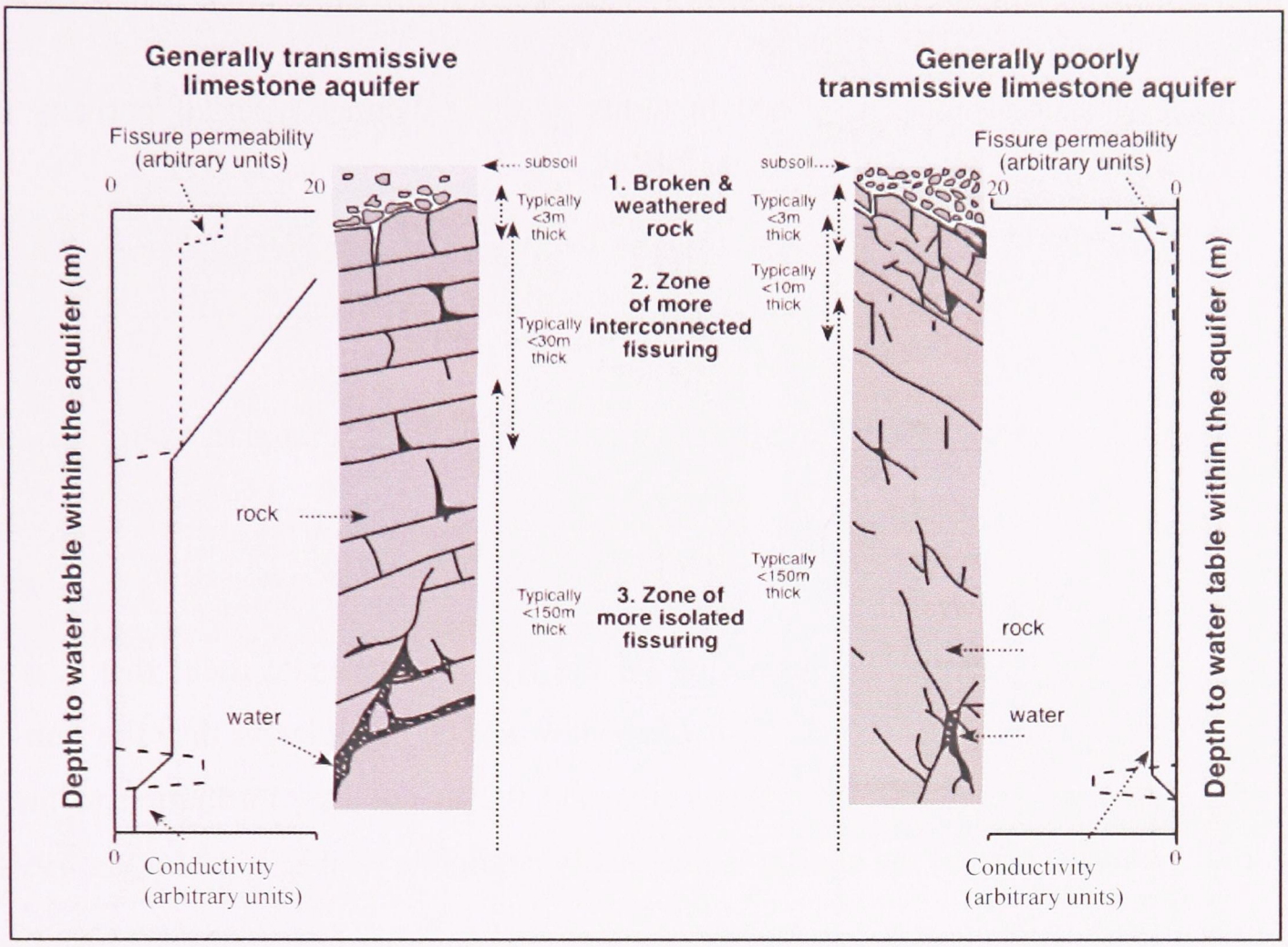


Figure 2.1 A schematic model of the vertical distribution of permeability in Irish limestone (after Fitzsimons *et al.*, 2005).

As the recharge enters the karst aquifer several different scenarios can occur according to the carrying capacity of the conduit system. The underground system could be capable of carrying all of the allogenic runoff even from the most intense storms. Alternatively, the storm flow may be too much for both the carrying capacity of the conduits and any discharge to the baseflow leading to storm runoff spilling over, backing up and remaining as surface water. Finally, if the carrying capacity is not sufficient to carry even the minimum surface flow this will result in a permanent surface stream, although such surface runoff may also occur if the rainfall exceeds the infiltration capacity of the soil overlying the karst system. There can also be significant temporary effects due to intermediate storage within the system. For example, intermediate storage can occur within the epikarst or soil without necessarily creating surface runoff. Equally, fluctuations of the water table can store large amounts of water following a storm event.

2.2.2 Underground flow systems

Karst aquifers are usually described in terms of three distinct types of porosity (triple permeability) models (White and White, 2005).

(i) Matrix permeability - the intergranular permeability of unfractured rock

(ii) Fracture permeability - mechanical joints, joint swarms and bedding plane partings all of which may be enlarged by solution.

(iii) Conduit permeability - pipe-like openings with apertures ranging from 1 cm to tens of metres.

MATRIX

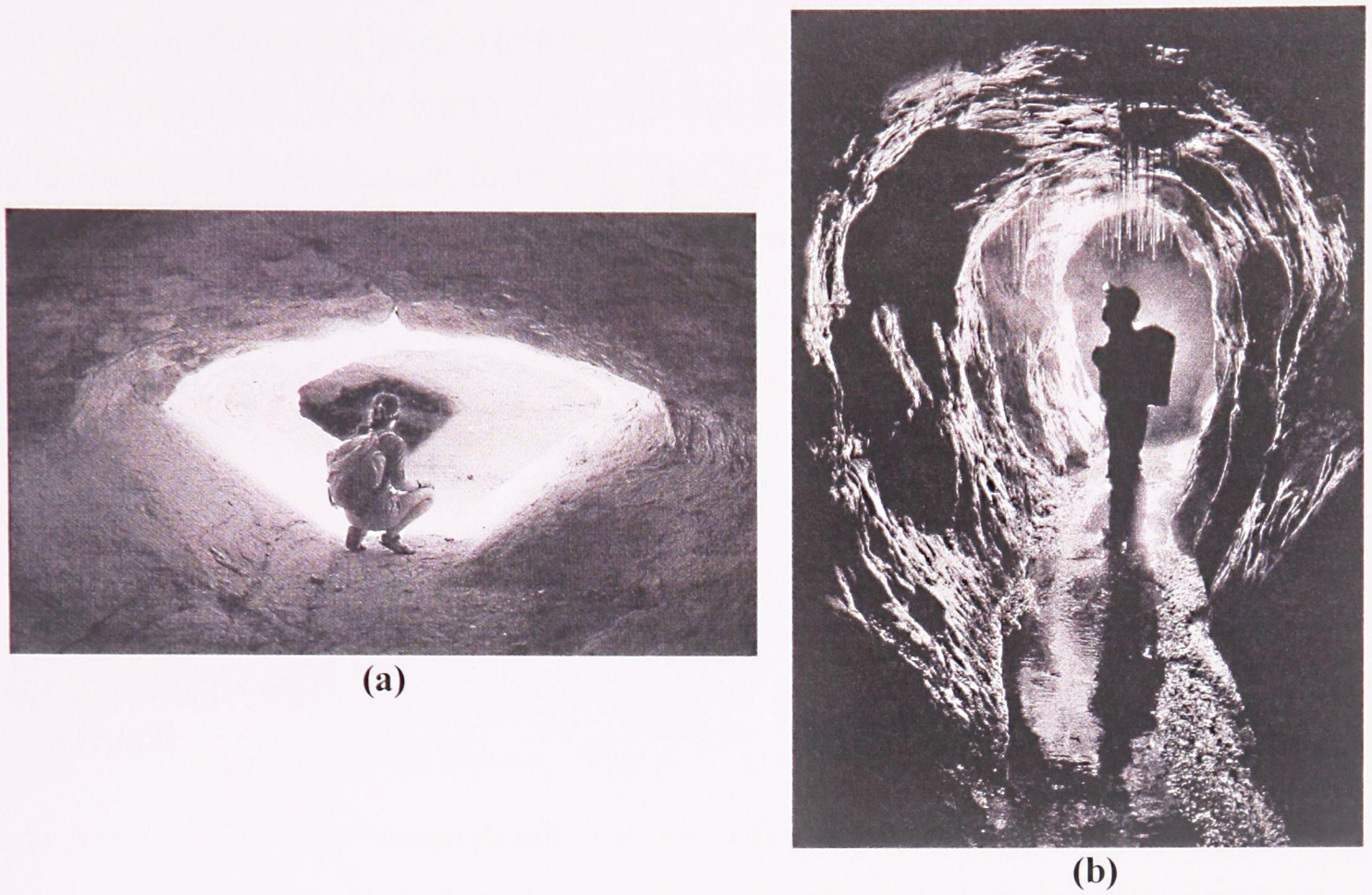
Matrix flow can be so small (depending on the type of carbonate rock) that it is often ignored. The matrix porosity (2-11%) is often shown to be much larger than the sum of the conduit and fracture / fissure porosities (0.5 and 0.2%) but its contribution to the total hydraulic conductivity of the aquifer is practically negligible (Zuber and Motyka, 1998).

FRACTURES

Fractures (or fissures) normally have apertures in the range 50-500 μm. At the point where they reach a width of 1 cm, they are deemed to turn into conduits (White and White, 2005).

CONDUITS

Conduits are solutionally enlarged pathways through the carbonate aquifer. The onset of non-Darcian behaviour (i.e. turbulent flow) has been demonstrated to occur at apertures greater than 1 cm (Massey, 1989; White, 1999) and so groundwater flow in conduits is normally in a turbulent hydraulic regime. Studies have shown that as much as 80% of subterranean flow in karst terrains occurs in conduits (Atkinson, 1977; Palmer 1991). Conduits down to 0.5 m wide are accessible through exploration by cavers but various studies on spring hydrochemistry and tracer tests as discussed later in Section 2.4 (Martin and Gordon, 2000; Maloszewski *et al.*, 2002 etc.) have demonstrated that there must be a very large component of conduit porosity within the width range 0.01 to 0.5 m range. The typical shape of flood prone passages are elliptical (Figure 2.2) since corrosion is equal in all directions when flooded but concentrates along the guiding bedding planes (Ford and Williams, 2007).



(a) **(b)**

Figure 2.2 Elliptical conduits in cave systems **(a)** Ghar Hassan, Malta **(b)** Ogof Draenen, Wales (Howes, 1997).

Within these stark definitions there are often irregularities. For example, fracture swarms can form zones of high permeability and individual fractures are observed to have apertures in excess of 0.01 m although they may not be continuous at such an aperture.

An interesting study on matrix, fracture and conduit components of storage and flow was undertaken on almost 3000 sinking streams and springs on the central Kentucky karst (Worthington *et al.*, 2000) which found that almost all of the storage (95.6 to 97.3%) was within the rock matrix whereas almost all of the permeability (99 to 99.8%) was accounted for by the conduits. Hydraulic conductivity results were as follows: matrix (2×10^{-11} m/s); fracture (6×10^{-6} to 3×10^{-5} m/s); channels (3×10^{-3} m/s). Other studies on karst aquifers in Canada, England and Mexico as summarised in Ford and Williams (2007) and Germany (Einsiedl, 2005) have found similar statistics with 94 to 99.7% of the storage within the matrix.

Another study on the Edwards aquifer in central Texas attempted to segregate the proportional influence of matrix, fracture and conduit flow from a number of test wells by comparing the field results with various hypothetical models (Halihan *et al.*, 2000). A Reynolds number of 10 was used to represent the onset of non-linear laminar flow in the fractures (with apertures of 3.1 to 4.8 mm) and full turbulence was estimated in fractures 18 to 28 mm apertures at Reynolds numbers of 2000 or over. Matrix permeability was modelled as a lognormal distribution with geometric mean of 1.3×10^{-15} m^2. Fracture permeability can be modelled using the cubic law (Ford and Williams, 2007):

$$Q = \frac{\rho g b^3}{12\mu} \frac{dh}{dL} \qquad \text{Eqn. 2.1}$$

whereby,

$$K = \frac{\rho g b^3}{12\mu} \qquad \text{Eqn. 2.2}$$

where b is the full aperture of the fracture, μ is the dynamic viscosity of water, w is the fracture width, and dh/dL is the hydraulic gradient; K is the hydraulic conductivity.

This is derived from the Hagen-Poiseuille equation (Chadwick *et al.*, 2004) which describes laminar flow through a smooth pipe whereby discharge (Q) is proportional to the fourth power of the diameter:

$$Q = \frac{\pi d^4 \rho g}{128\mu} \frac{dh}{dL} \qquad \text{Eqn. 2.3}$$

Fracture apertures are also generally assumed to follow a lognormal distribution.

Conduit permeability can be calculated from the Darcy-Weisbach equation assuming both laminar and smoothly turbulent flows (Adams and Parkin, 2001) using typical values of roughness coefficient, ks/D = 0.25.

Laminar hydraulic conductivity modelled as:

$$K_l = \frac{g}{\upsilon} \frac{d^2}{32} \qquad \text{Eqn. 2.4}$$

Turbulent hydraulic conductivity modelled as:

$$K_t = 4.706 \frac{g^{4/7}}{\upsilon^{1/7}} \left(\frac{d}{2}\right)^{5/7} \qquad \text{Eqn. 2.5}$$

A study on an active phreatic conduit in Norway (Lauritzen *et al.*, 1985) showed a dramatic decrease in the Darcy-Weisbach friction factor, *f* (or more commonly, λ) with discharge until it attained a constant value at discharges over about 10 m^3/s (see Figure 2.3). Moreover, friction factors calculated over a range of karst investigations have been spread across a wide range from f = 0.039 to 340 (Ford and Williams, 2007). The range might be explained by the experimental methods for example, mean values of f = 23 to 340 were calculated in the Mendip Hills, Somerset by Atkinson (1977) across whole conduit systems compared to much lower values (f = 0.028 to 0.13) found by Gale (1984) across much shorter conduit sections in good condition in 13 caves in the UK and North America. Equally, this may be related to the "hydraulic conductivity scale effect" whereby measured hydraulic conductivities have been shown to increase with the scale of rock tested (Sánchez-Villa *et al.*, 1996; Rovey, 1998; Ford and Williams, 2007).

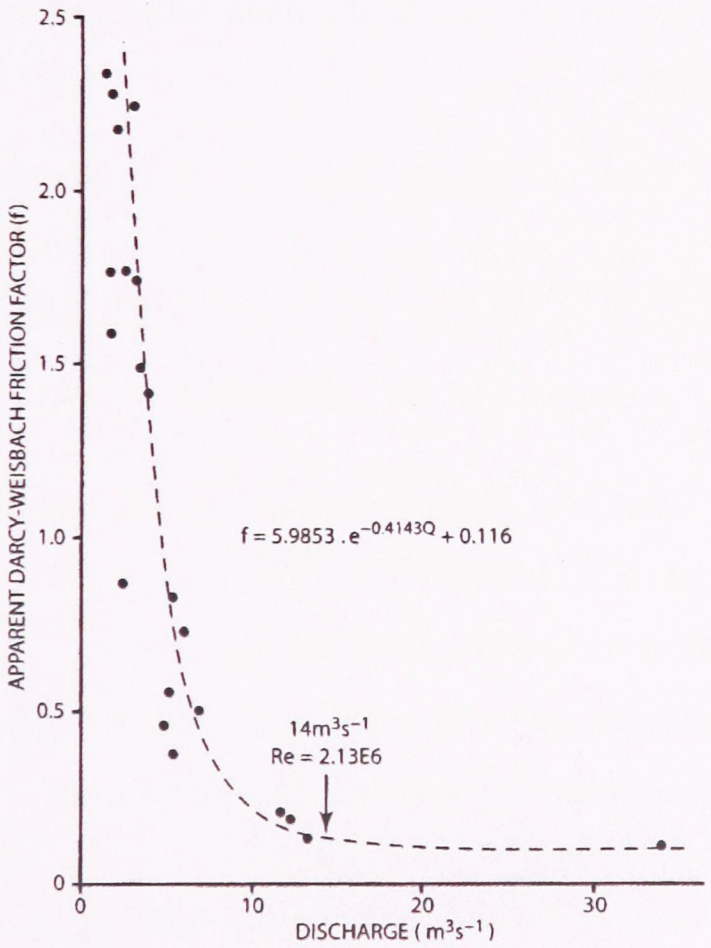


Figure 2.3 Relationship between Darcy-Weisbach friction factor and discharge in a phreatic conduit in Norway (Lauritzen *et al.*, 1985).

It should be noted that permeability can be measured in laboratory conditions on rock samples or by pumping tests on wells drilled into the aquifer. However, pumping tests are

highly sensitive to the exact location and in order to establish the fracture permeability the initial placements really need to be decided by means of fracture mapping. It is thus almost impossible to establish the permeability of conduits using wells since the density of such developed conduits is invariably very low.

The recognition of *overflow* tributaries or streams is also very important to consider when analysing karst systems. These are conduits that come into use seasonally or intermittently due to excessive flow in the normal flow carrying conduits (increase in head in the groundwater system) or partial blockage / collapse of existing conduits (Ray, 1997). Such routes can be crucial for the successful modelling / diagnosis of the systems Turloughs, temporary lakes which are expressions of the hydraulic gradient coming to the surface at times of high groundwater flow, fall into the above category as they store large quantities of water linked directly to the groundwater regime. As the main subject of the thesis, these are discussed in more detail in Chapter 3.

2.2.3 Discharge

Groundwater from karst usually discharges back to the surface through large springs which can be categorised into:-

(i) open conduit gravity springs

(ii) alleviated conduit springs where the water emerges from a rise pool formed by a blockage of material (glacial or alluvial).

(iii) rise pools discharging water from shallow flooded conduits

(iv) artesian springs where water rises under pressure from considerable depths.

(v) springs that discharge from solutionally widened fracture swarms.

(White, 2002)

Springs exhibit a wide variety of rates of discharge and have been extensively used as gauging points, sampling points and monitoring points for karst aquifers. The type (v) spring (above) is often referred to as a diffuse flow spring from which water issues at a constant temperature and a chemical composition seemingly independent to any surface storms; in comparison the so-called conduit flow springs discharge water which typically varies in temperature and chemical composition. Another distinction has been made

(White, 2002) between "underflow" springs, carrying the baseflow from ground water basins and "overflow" springs which carry only part of the discharge or become active during storm flow. It should be noted that for hydrogeological studies, springs may be located beneath the surface of streams or even beneath the sea, as is the case for part of the day for the karst network studied in this thesis.

2.2.4 Chemistry

The chemistry of the dissolution of calcite and dolomite was formulated in the 1980s with the publication of reliable values for the equilibrium constants (Plummer and Busenburg, 1982) identification of pertinent complexes and the establishment of useful interpretative parameters, hardness, saturation index and calculated carbon dioxide partial pressure. Such chemical calculations can now be performed on several computer applications WATEQ4F, PHREEQC (available from the US Geological Survey) etc. (White, 1999; Lipson *et al.*, 2007).

The development of the karst aquifers is more to do with the kinetics of the dissolution reactions rather than the final equilibrium state of these reactions. Karst porosity generally develops when meteoric waters become enriched with CO_2 forming carbonic acid (H_2CO_3) which is aggressive to calcite. The individual chemical reactions are set out below:

$$CaCO_3 + H^+ \Rightarrow Ca^{2+} + HCO_3^- \qquad \text{Eqn. 2.6}$$

$$CaCO_3 + H_2CO_3 \Rightarrow Ca^{2+} + 2HCO_3^- \qquad \text{Eqn. 2.7}$$

$$CaCO_3 + H_2O \Rightarrow Ca^{2+} + HCO_3^- + OH^- \qquad \text{Eqn. 2.8}$$

(Plummer *et al.*,1978)

Each reaction is described for a forward reaction rate which together provides the overall dissolution rate for calcite:

$$Rate = k_1 a_{H^+} + k_2 a_{H_2CO_3} + k_3 a_{H_2O} - k_4 a_{Ca^{2+}} a_{HCO_3^-} \qquad \text{Eqn. 2.9}$$

where k is the respective reaction rate constant and a is concentration of the activated species.

The first term is mass transfer controlled but the second and third terms are reaction rate controlled so that in the pH range expected in karst water, the dissolution rate is only slightly dependent on flow regime.

Additional progress has been made towards understanding carbonate dissolution kinetics using the following generic rate equation (Palmer, 1991).

$$Rate = \frac{A}{V}\frac{dC}{dt} = k\left(1 - \frac{C}{C_s}\right)^n \qquad \text{Eqn. 2.10}$$

where, A = area, V = volume of solution, C = conc. of dissolved carbonate, C_s = equilibrium saturation concentration of dissolved carbonate, n = reaction order.

The reaction order can be determined empirically and shows that there is a break in the reaction rate order at about 85% saturation. When the water is under-saturated, the reaction kinetics are roughly first order but this reaction rate increases to near fourth order as the water approaches saturation.

Further investigations of dissolution kinetics under turbulent flow conditions and also conditions of near equilibrium have shown that the hydration reaction of aqueous CO_2 to H_2CO_3 is shown to be rate controlling when A/V ratios are high and under some conditions of turbulent flow. The absorption of ions on the reactive surface becomes rate controlling under near-saturation conditions and a diffusion boundary layer becomes important under conditions of laminar flow (White, 1999).

2.3 Evolution of Conduit Permeability and Karst Network Development

On a geologic timescale, dissolution is a very rapid process with significant modifications of flow paths and development of new flow paths requiring only thousands of years. The fractures are solutionally enlarged by flow under laminar flow conditions into conduits at which point turbulent flow conditions tend to prevail. Although this study is primarily involved in modelling the storm response of an existing karst system in the Gort lowlands in the west of Ireland, a knowledge of the development of karstic networks is pertinent as it

yields information into the likely size, distribution and form of the main conduits which are almost impossible to access directly due to their size and inherent remoteness.

2.3.1 Fracture enlargement

Fracture flow is not unique to carbonate rocks, for example it occurs in consolidated sediments such as shale and in crystalline rocks such as granite and basalt. However, what is different about carbonate fractures is that they enlarge with time under continued water circulation. Fracture flow is laminar and hence the flow field (on average) can be considered to follow Darcy's Law (Darcy, 1856). When unsaturated water enters a fracture there is a rapid reaction and uptake of dissolved carbonate. It was recognised that most CO_2 (and hence acidity) was imparted to the groundwater in the soil zone which raises the question of how caves can form at substantial depth if their dissolving power has been expended near the surface with the initial contact with the limestone. If the kinetics were linear, the water would quickly become saturated and there would be no dissolutional enlargement of fractures deeper within the aquifer. However, the rate slows down (by some orders of magnitude) shifting from 1^{st} order to 4^{th} order when the water is 85% saturated (Svensson and Dreybrodt, 1992), permitting the slow laminar flow to penetrate deeper into the aquifer carrying unsaturated water; hence the dissolution continues along the whole flow path at a slow rate. Field and laboratory data has shown that slightly aggressive meteoric water may persist to great depths in limestone due to the sluggish reaction kinetics at conditions near equilibrium. The non-linear relationship between calcite solubility and CO_2 concentration (known as mixing corrosion) allows for two waters saturated with respect to calcite to mix and become aggressive. A further mechanism which has also been postulated may contribute to erosion at depths in karst is the deep generation of CO_2 by microbial oxidation of carbon (Sasowsky, 2000).

There will be one particular pathway through the aquifer which will gradually enlarge until its aperture is such that water with less than 85% saturation can penetrate. At this point the kinetics shift from 4^{th} order to 1^{st} order and the rate of dissolution dramatically increases. This work combined with modelling has shown that so called "kinetic triggering" can account for most cave formation (Palmer, 1991). The evolution from a fracture to a conduit

is inherently discontinuous but the thresholds appear to be when the aperture reaches roughly 0.01 m (White, 1999). At this point there is an onset of turbulent flow (and hence loss of Darcian behaviour); the shift in the dissolution rate from 4^{th} order kinetics to linear kinetics; and the apertures and flow velocities start to become large enough to transport *clastic* material. Hence, there are likely to be very few fully developed conduits passing through an area of karst bedrock.

The laminar flow of water in small fractures can be modelled as smooth parallel planes by the cubic law – see Eqn. 2.1 (Ford and Williams, 2007). When the Reynolds number is around 2000 (Massey, 1989) the flow will start to become turbulent, which for the typical hydraulic gradients observed in karst aquifer occurs when the aperture reaches 0.01 m.

2.3.2 Conduit network development

Initiation

As discussed, the apertures will gradually widen under 4^{th} order kinetics until they become wide enough to allow the total penetration of under-saturated water from entry to exit. At some point (in a relatively short time of 5000 -10000 years) "breakthrough" occurs which is defined as the time at which turbulent flow is first encountered (i.e. Reynolds number of 2000) (Dreybrodt, 1990). The breakthrough time is thought to be very sensitive to initial aperture size and also length of the fissure and the hydraulic gradient. After this breakthrough, flow becomes turbulent and the widening of karst channels dramatically increases to an even rate of 10^{-2} to 10^{-1} cm / year from thereon in (Dreybrodt, 1996).

The governing equations for fissure dissolution are the coupled equations for flow, transport of Ca^{2+}, and dissolutional enlargement. One important result from the modelling of this initiation phase (Dreybrodt, 1992, 1996) is the case of a wide initial fracture, short path length and high hydraulic gradient in which the breakthrough is thought to happen in less than 100 years if:

$$\frac{i}{\lambda} > (5.3x10^{-8}) a_0^{-2.63} P_{CO_2}^{-0.77} \qquad \text{Eqn. 2.11}$$

where, i = hydraulic gradient, λ = path length (m), a_0 = initial fracture aperture (cm),

P_{CO2} = carbon dioxide partial pressure of water entering the fracture (atm).

From this understanding and study of single fractures, models have been developed to attempt to represent the network of fractures which make up a realistic flow path. Groves and Howard (1994) developed a model which started on a hypothetical grid of fractures at very large spacings. A model with smaller spacings was then built to analyse each grid (Siemers and Dreybrodt, 1998) which introduced the concept of a probability that any given fracture segment on the grid would be connected to other fractures. Many of these attempts assume a simple geometry of plane parallel fractures of fixed apertures and uniform cross-section. As such, the flow through the fracture is proportional to the cube of the aperture. However, if the reality of rough walls, variable apertures and tortuosity is appreciated then a correction to the cube law is required (Oron and Berkowitz, 1998). These models confirm what is seen in nature that the hydraulic evolution of karst networks is for very few large conduit channels with diffuse flow through numerous small fractures.

An attempt to model dissolutional widening of rough and irregular features (Hanna and Rajaram, 1998) predicts breakthrough times to be approximately half of that which is predicted by the hypothetical smooth fractures previously considered. Two-dimensional geochemical models were developed with a single fracture, but unlike previous studies the fissure aperture varied according to a random field. The results of several sets of statistical parameters showed that aperture variability will accelerate conduit growth by a factor of two (compared to fixed width apertures) for mild variations and up to ten-times for highly heterogeneous aperture fields.

Conduit enlargement and integration

Once the aperture size has reached the value of approximately 0.01 m and an optimum flow path has been determined, the under-saturated water will now traverse the entire width of the aquifer. The dissolution kinetics move into a more or less linear range and the rate of retreat of the conduit has been shown (Palmer, 1991) to depend only on the degree of under-saturation described by:

$$S = \frac{31.56k_1\left(1-\frac{C}{C_s}\right)^n}{\rho_R} \qquad \text{Eqn. 2.12}$$

where, S = rate of wall retreat (cm/yr), k_1 = 1st order reaction rate constant, C = conc of dissolved carbonate, C_s = saturation conc. of dissolved carbonate, n = reaction order, ρ_R = density of bedrock

Values of k_1 and n have been determined experimentally and findings are that wall retreat is from 0.01 to 0.1 cm/yr, hence indicating that a threshold conduit (0.01 m) can enlarge to the diameter of a metre in a few thousand years.

The actual pattern of the conduit system has not been researched with much success. The enlargement phase is marked by fairly uniform conduit growth under the conditions of turbulent flow (Howard and Groves, 1995) (when compared with the highly selective development phase). The direction of individual passages is mainly controlled by the geologic structure (bedding planes, joints etc) and distribution of phreatic and vadose flow. However, whether these form single conduit, branchwork caves, or network (or maze) caves etc. is dependent on the geological constraints and the arrangement of recharge and discharge areas. The nature of groundwater recharge is the most important factor in deterring whether a cave system will be branchwork or network (Palmer, 1991). Sinkhole recharge forms branching caves with tributaries that join downstream as higher order passages (as shown in Figure 2.4). Maze caves form where either: (i) surface runoff enters the soluble rock either as sinking streams or bank storage along entrenched rivers during floods, producing hydraulic gradients steep enough to produce uniform passage enlargement along several alternate routes; (ii) diffuse recharge through overlying permeable rock contributes uniform flows to every fracture in the limestone; or (iii) discharge or renewal of under-saturated water is uniform long many alternative routes. Diffuse recharge can also form spongework caves (interconnected solution cavities) as well as network caves.

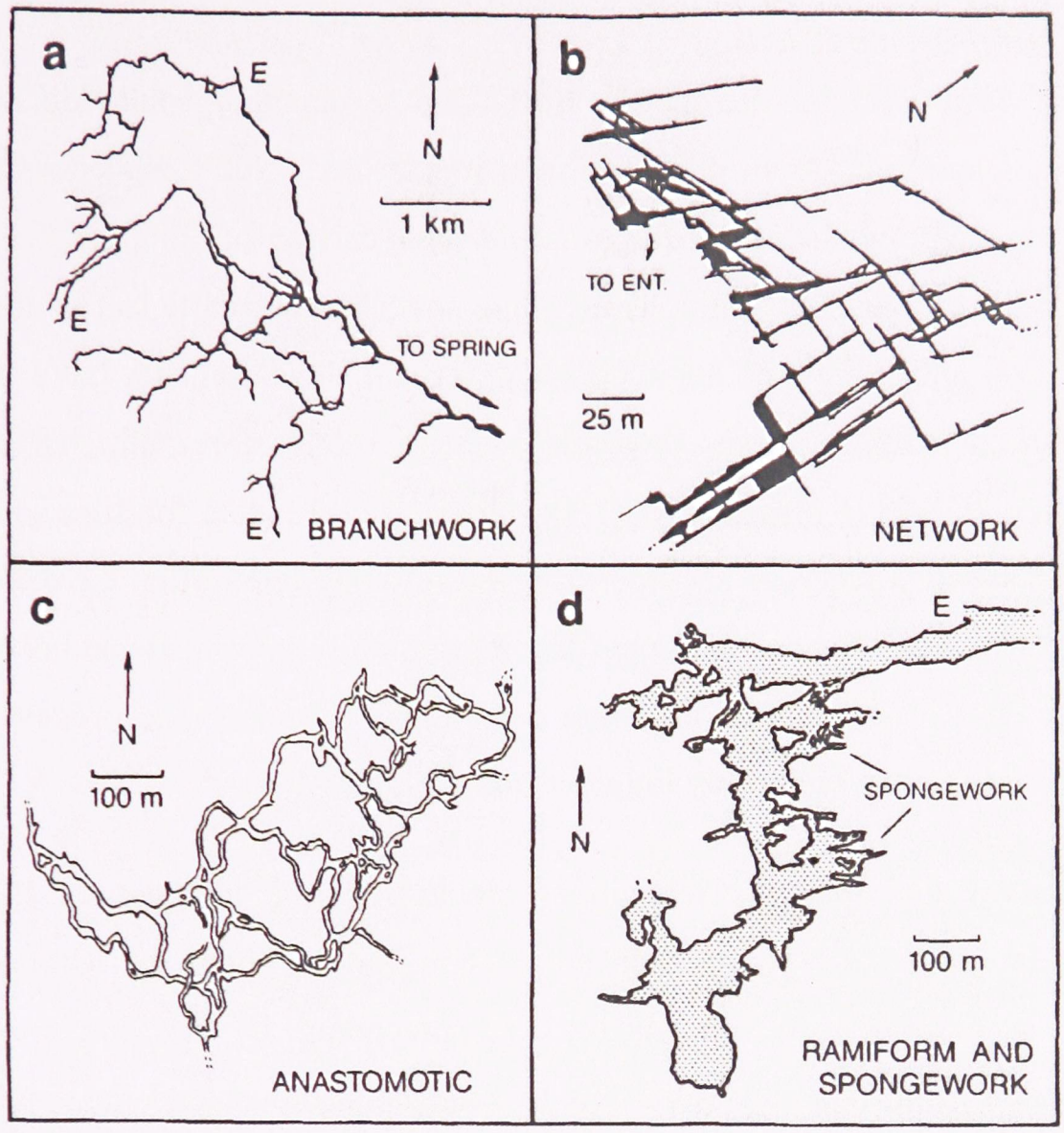


Figure 2.4 Common patterns of solutional caves: (a) branchwork, (b) network, (c) anastomotic and (d) ramiform and spongework (Palmer, 1991).

2.4 Investigative Techniques for the Characterisation of Karst Aquifers

Numerous characterisation techniques have been applied to karst areas in an attempt to reveal the hydrogeology. One of the simplifying factors is that (due to the conduit nature of the flow paths) the groundwater resurfaces at a single or limited group of springs which enables either a water budget approach or mass balance on natural or anthropogenic tracers to be undertaken to reveal the hydrological characteristics. The results of such studies are often used nowadays to help to formulate a mathematical model of the aquifer which is covered in Section 2.5.

2.4.1 Cave mapping

Maps of caves systems are mainly developed by amateur speleologists using tapes and compasses and many may only be found in the local club newsletters (the University of Bristol Spelæological Society for example have carried out mapping in the Galway karst over a period of several years). These have contributed greatly to the understanding of the distribution and modes of karst porosity. Recent developments have used cave surveys from saturated cave systems to produce an interactive three-dimensional geometric and parameter models (Kincaid, 2000). The greatest accuracies for surveying are possible in dry cave systems whereas accuracies in saturated systems often have to be compromised due to the obvious time constraints (decompression requirements and diver's breathing gas supply). However, recent work using cave sonar has made the process much quicker as profiles can now be constantly logged throughout the dive.

Cave survey and mapping techniques are thoroughly documented (Ellis, 1988). Cave survey data, normally recorded in polar coordinates (where the location of each survey station is described relative to the one preceding it) are converted into Cartesian coordinates using mapping programs to produce contours and the final 3D cave model. These models can then be viewed from any direction and cave volume calculations can be made. The three-dimensional gridded data can also be used to resolve the fractal dimension of the cave system which describes the volume filling character of the cave and can also be used as scaling factors to predict permeability throughout groundwater catchments of karst aquifers (on the assumption that the process of dissolution porosity development is similar for the largest caves and smallest tubes).

2.4.2 Geomorphology

Morphology has been used on 3 scales: specific features within the cave, the overall form of the cave and the cave in relation to the rest of its environment. Within the cave, the shape of the conduit can help to determine whether the cave formed in the phreatic or vadose zone. Equally, by measuring the cross-sections of dissolutional scallops (asymmetrical concavities eroded into the passage walls) on the walls, paleohydraulic techniques can be used to estimate discharge and velocities in the conduits (Curl, 1974; Atkinson, 1977; Gale, 1984; Jeannin, 2001) and also used to estimate mean values of

friction factors and shear stresses on the wall. For example, scallops are reckoned to form around the laminar-turbulent transition phase at stable scallop Reynolds numbers in the range 1000 to 3000 and their size is inversely proportional to flow velocity with the relationship proposed (Curl, 1974) as follows:

$$u = \upsilon \frac{\mathrm{Re}_L}{L_{32}} \qquad \text{Eqn. 2.13}$$

where, u = mean flow velocity (m/s), Re_L = Reynolds no. for scallops based on the fluid velocity at a distance from the wall equal to L_{32} = mean length of scallop (= L_i^3 / L_i^2, where L_i is the greatest length in direction of flow of the *i*th scallop), υ = kinematic viscosity cm^2/s.

Caves can be considered as fractal objects with a distribution consisting of a very large number of short caves and a very small number of long caves. Hence, fracture porosity can be estimated using the technique of fractal scaling as was done on surface exposures (outcrops) (Mace and Hovorka, 2000). Feeler gauges and image analysis have been used to characterise and interpret hundreds of fracture apertures and the cross-sectional area of thousands of dissolutional features in a variety of exposures and then tested for scale invariance (i.e. fractal behaviour) using frequency-size distribution plots.

Finally, the evaluation of the cave in the context of its geologic setting can aid an understanding of the groundwater flow patterns (Sasowsky, 2000). For example, the discharge from the Gort lowland karst hydraulic network - the focus of this research - currently outlets just below sea level into Galway Bay. The development of much of the conduit network in the area however, is thought to have formed during previous periods of glaciation when sea levels were much lower (as described later in Chapter 3). On a macro-scale, a 3D geological model has been used to develop a hydrological model of a karst area in northern Switzerland using the geometry of aquifers, aquitards and fault lines (Butscher and Huggenburger, 2007). The gradient of the aquifer base has then been used to delineate spring catchment areas and determine dominant flow processes without the need to carry out costly physical monitoring studies over an extensive time period.

2.4.3 Tracer tests

Tracing the path of ground water using conservative substances injected at known upstream points which can be detected when they reappear at the outlet points is a common procedure for groundwater flows. A qualitative tracer test may be carried out by injecting a tracer and simply looking for it downstream in order to establish a hydrologic connection between a specific input point and a discharge point. However, if accurate water budgets are required, the concentration of the tracer and discharge at a recovery point need to be measured in order to calculate travel times and flow velocities. Tracing studies have also been able to delineate karst groundwater basins which often do not coincide with the respective surface topographic water basins (Sasowsky, 2000).

The most common tracing method is to use a fluorescent dye, examples include Rhodamine WT, fluorescein (or uranine), Eosine, Sulphorhodamine B and optical brightener. The analysis of the concentration of dye in a water sample can be done by fluorescence spectroscopy whereby each type of dye has a specific wavelength which can be picked up and extremely low detection limits are now possible down to the parts-per-trillion levels. For example, fluorescent dyes (as well as Iodine-131 and indium-EDTA) have been used in the Cordru Moma, karst mountains in Romania to establish conduit flows and links (Oraseanu and Mather, 2000). Techniques using multiple dyes have also been used whereby deconvolution of the dye spectra flows allows the separation of overlapping bands (Tucker and Crawford, 1999).

Dye breakthrough curves (i.e. Residence Time Distributions, RTDs) can be used to determine the time of travel from the injection point to the spring. The shape of the RTD curve also yields information in relation to the flow path through the aquifer and in terms its plug flow / complete mix nature due to dispersion (Einsiedl, 2005). Such fluorescent dye tracing methods though must take account of variable background readings which may occur during the tracer study (Lane and Smart, 1999). RTD curves have also been used to yield information on the geometry of the conduits. An interesting study was carried out in the Jura Mountains in Switzerland (Hauns *et al.*, 2001) which compared the tracer breakthrough curves to a variety of conduit geometries including different sizes of channel,

pools, rapids and waterfalls from which CFD simulations were run. The breakthrough curves were interpreted according to the shape parameters for both the rising limb (time to peak and time to half peak) and the retardation (ratio of mass passed through to mass retarded etc.) which showed that dispersion was linearly related to water velocity in a straight conduit; and that the effect of retardation by side walls for realistic conduit dimensions was less than 10% (although it did lead to greater dispersion). However, the effect of different conduit geometries with longitudinal distance downstream such as pools, caverns etc. created the most retardation and dispersion due to the secondary currents set up in such structures.

Tracer tests have been used to establish the flow rates through conduit networks. For example, a quantitative tracer test conducted on the Beech Creek karst aquifer in Indiana (Baedke and Krothe, 2000) used two tracers simultaneously: Rhodamine WT as a qualitative tracer (as shown in Figure 2.5) and ionic bromide tracer (which does not absorb to soil or rock materials) for the quantitative test results to ascertain the true velocity of the flow in the conduit. Approximate travel times were calculated from the ionic tracer breakthrough data revealing the major conduit velocity to be 286 m/hr. Another tracer study in Missouri (Dreiss, 1982) revealed average flow rates over 65 km/d of up to 342 km/d. A tracer study in upper cretaceous chalk in Berkshire, UK (Banks *et al.*, 1995) using fluorescin demonstrated that the chalk was behaving as a karstic aquifer with numerous swallow holes over the outcrop, swallow holes which incidentally were often used for the disposal of effluent from motorway runoff and agricultural runoff. The tracers established high transport velocities (up to 7 km/d) and low dispersion indicating karst-like (i.e. discrete) flow pathways. Similarly dye tracing was also used to establish connections and flow velocities in the cretaceous chalk aquifer in Northern Ireland (Barnes, 1999) again demonstrating that flow occurs along discrete conduits rather than through fissure/ fracture networks. Interestingly, in this case the dispersion coefficient (which was low) appeared to be independent of flow velocity.

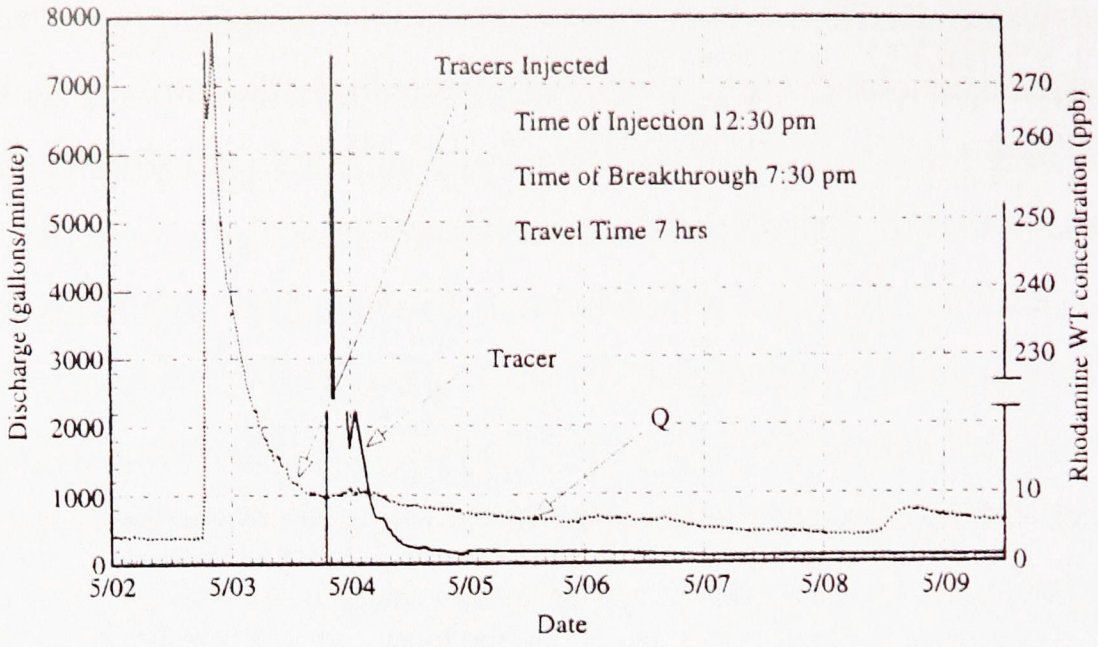


Figure 2.5 Example of tracer output using Rhodamine WT at Beech Creek aquifer, Indianna (Baedke and Krothe, 2000).

Tracer breakthrough curves in karst are typically associated with strong tails. A more representative fit to such tails has been achieved by using a two-region non-equilibrium model which takes account of partitioning solute into mobile and immobile fluid regions. This model was trialled on conduits in karstic aquifers (Field and Pinsky, 2000) which resulted in increases in flow velocities and decreases in longitudinal dispersion coefficients compared to equilibrium model estimates.

Tracer studies using fluorescent dyes have also been used to identify the source of faecal pollution at springs. For example, the source of faecal pollution at the spring bathing pool at Sulphur Springs, Florida was eventually revealed to be from a leaking storm water retention pond (Wallace, 1993).

Finally, the natural fluorescence of cave waters has also been shown as a potential means to source karst waters in England (Baker and Genty, 1999), the water having the signature of the overlying soil conditions in this case from a humic-like (probably fulvic acid) source. Alternatively, UV spectrophotometry has been used to evaluate flow conditions in karstic aquifers whereby the molecular absorption of the UV spectra is a function of the chemical compounds in the water sample (Winiarski *et al.*, 1995).

POLLUTION AS A TRACER

Indirect tracer tests have also been carried out by looking at concentrations of persistent chemical or bacterial pollutants from the recharge. For example, PCB concentrations in rain runoff have been correlated against spring discharge in Illinois (Talarovich and Krothe, 1998). Indeed several studies have specifically looked at the pollution potential from karst networks which display a lack of filtration / degradation for example with respect to faecal contamination. One study in the Peak District, UK confirmed this (Tranter *et al.*, 1997), studying faecal coliforms in the sinks and the springs although the relationship between input and output was found to be very complex. Other studies (Mahler *et al.*, 2000; Pronk *et al.*, 2006; 2007; 2009) have looked at the association of bacteria with suspended sediment after rain events, as described later in Section 2.4.8.

Finally, micro-organisms, particularly bacteriophages have been used as tracers. For example, phages T7, Psf2, H6/1, H40/1 and H4/4 were used by Drew *et al.* (1997) in the Gort lowlands study area to trace river sinks to the coastal springs, as discussed later in Chapter 3.

2.4.4 Spring water chemistry (geochemistry)

The process of carbonate dissolution exerts the most apparent geochemical effect on the behaviour of carbonate aquifers by controlling groundwater flow. Analyses of spring waters show that the hardness (the amount of divalent cations Ca^{2+} and Mg^{2+}), temperature and calcite saturation index of the water will fluctuate with the seasons and often also respond to storm water inputs into the groundwater basin. The use of spring records by combining the hydrographs and chemographs and catchment precipitation can yield insights about the karst aquifer.

Many studies have quantified the relative proportions of diffuse and conduit flow on the basis of chemographs of chemical composition and temperature of spring discharge and their coefficients of variation (Shuster and White, 1971; Toran *et al.*, 2007). Springs with a high coefficient of variation, i.e. systematic seasonal variations in temperature and hardness (calculated as $CaCO_3$), are believed to be dominated by conduit flow due to rapid

infiltration of surface water and short residence times in the subsurface (thus limiting equilibration with the wall rocks). Springs characterised by low coefficients of variation are commonly close to saturation with respect to calcite or dolomite and hence are believed to come from intergranular porosity reflecting the long residence time in the rock. Low variation, however, does not necessarily imply an absence of conduits only that the recharge is mainly from diffuse infiltration (as opposed to allogenic or internal runoff water). One study (Wicks, 1997) for example, separated out the conduit flow source which was found to have a residence time of only 3 to 4 days which was considered to be an insufficient time for thermal or chemical equilibrium to be achieved compared to the residence time for the internally drained sources of 8 days. Other studies have claimed that the key variable was the fraction of allogenic recharge rather than the flow pathway within the rock mass (Sasowsky, 2000).

One premise that has been used is that after the pressure heads drop following a rainfall event, water starts to drain back into the conduits from the fine fractures and pores. This water will have spent long residence time in contact with the limestone and hence will have high concentrations of the ions. Hence, the water at the spring will be a combination of the water draining from this secondary porosity and the relatively dilute storm-derived water associated with the recent rainfall event. Specific conductance is often used as a surrogate scale for hardness in carbonate water. The continuous record of concentrations of dissolved ions Ca^{2+}, Mg^{2+} and HCO_3^- monitored at a spring can be used to separate out the proportion of flow arriving at the spring from the new rainfall and old secondary porosity water in response to rainfall events, on the premise that there is a significant difference between the ionic concentration of old water and new water. Such a technique was used to compare three springs in south-eastern Missouri (Dreiss, 1989a) which showed that a plug of old water was pushed through in the rising limb of the spring hydrograph which was then taken over by the new rainfall; it took several days for the ion concentrations to return to pre-storm levels. This effect was also seen in an interesting study carried out on the Big Spring basin in the south-central Kentucky karst (Ryan and Meiman, 1996) where dye tracing was also used to back up results from the chemical investigations. The results

indicated that the pollutants came through in a pulse but a pulse that greatly lagged the rising limb of the hydrograph.

A study in the Haute-Normandie region of France (Valdes *et al.*, 2006) used both the response of both conductivity and turbidity measurements at wells and springs following rain storms to separate out slow and fast flow. The responses were analysed using an autocorrelation function and conductivity-turbidity hysteresis curves which showed clear differences in the systems: some exhibiting a long memory effect whereby water was being stored in the conduits resulting in deposition of suspended solids; others with a short memory effect where the flow through capacity was sufficient for direct transport to occur with little deposition or resuspension. From this work, three conceptual models of the hydrodynamic functioning were proposed as shown in Figure 2.6.

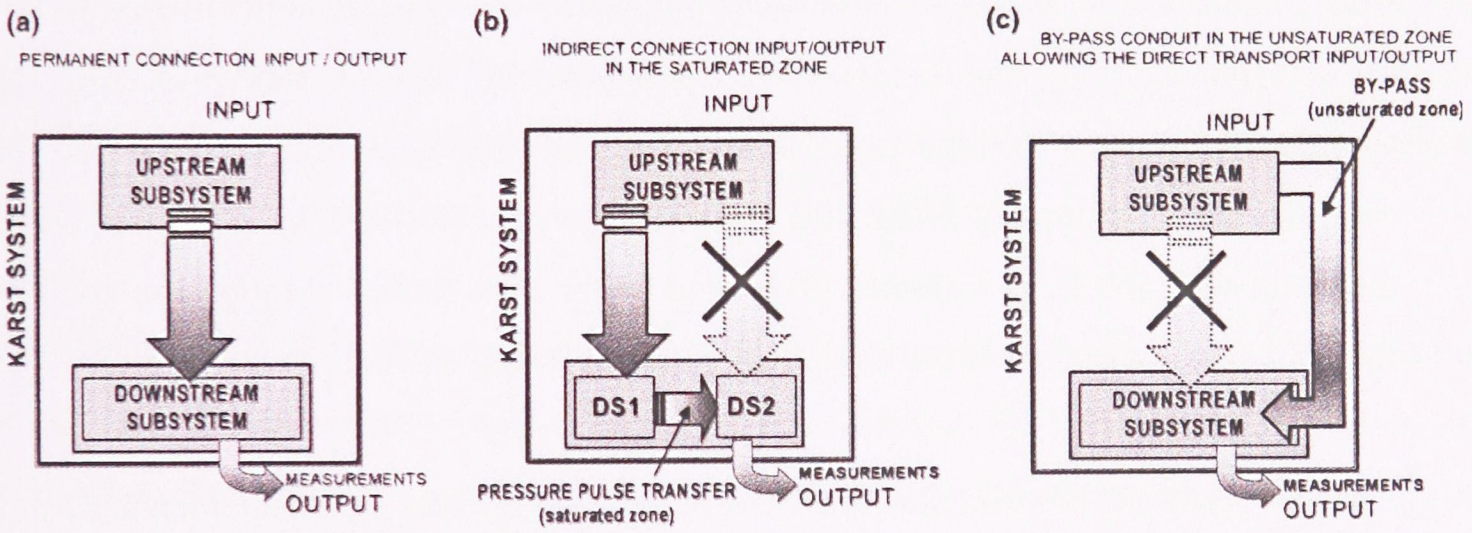


Figure 2.6 Three conceptual models of karst functioning following the Valdes *et al.* (2006) study in Haute-Normandie.

Similar work comparing dissolved species to turbidity was investigated in the karst system in the Seine valley in France (Massei *et al.*, 2006) but this time a variety of numerical techniques were applied (correlation, spectral analyses and wavelets) to determine the relationships between the signals and response of the system to rainfall events. Again, a short memory effect was detected for turbidity with respect to rainfall events compared to a much longer memory effect to specific conductance (i.e. dissolved species). Another study analysed calcium, bicarbonate, nitrate and saturation indices at both a spring and a well in order to understand the flow paths (Toran *et al.*, 2007). Higher concentrations of calcium

and bicarbonate in the springs (and the much longer response following storm events) indicated the longer travel times through dispersed flowpaths compared to the spring water which was more conduit based – although evidence of dispersed fracture flow was evident as well at the spring.

Other studies have investigated concentrations of numerous dissolved components, for example the major study on the Ichetucknee spring discharges in Florida (Martin and Gordon, 2000; Martin and Dean, 2001). Variations in O_2, Cl, SO_4, NO_3, DIC, alkalinity, pH, Mg and Ca with respect to time were used to establish the relative mixing of surface and ground water and heterogeneity of flow paths within a small region. Although various tracer studies carried out on the catchment had shown flow velocities of 1.6 to 2.0 km/d indicating predominantly conduit flow, the results of the chemical compositions from the study indicated low coefficients of variation across the seasons indicative of water with a long residence time and hence flow dominated by diffuse pathways. This apparent anomaly was due to the high water table in the unconfined aquifer which meant that most conduits were continually filled with water. Recharge water following rainfall events could then mix with the large volumes of ground water as it flowed through the conduits, thus buffering rapid changes in the composition of the spring discharge water.

Another study on 6 springs in the Betic Cordilleras, Spain (López-Chicano *et al.*, 2001) used hydrochemical analyses (Ca, Mg, Cl, SO_4, HCO_3, EC, temp and pH) on spring discharges. The Piper diagram plots of the proportions of all major anions and cations showed that the water type changed along the direction of flow from predominantly Ca-HCO_3 to Ca-Mg-HCO_3. The study was also able to determine that the piston effect (i.e. displacement of older mineralised groundwater by new recharge, as discussed elsewhere) between dry periods and intense rainfall recharge was picked up at the springs.

Spring water chemistry has also been used by looking at the relationship between stage (flow) from springs and nitrate concentrations in the spring water which was washed down from fertilizer (poultry waste) from the surface (Peterson *et al.*, 2000). A number of regression analysis techniques were used which revealed that there was a correlation

between stage increase and nitrate concentration. The relationships, which were specific to each spring, appeared to vary according to the degree of conduit to diffuse flow proportions which fed each spring. A study in central France (Vaute *et al.*, 1997) looked at a series of different chemical compounds both naturally present in the water and as a result of sewage effluents. This study showed that in areas where the sewage effluent was discharged directly into a permeable zone as a point source (for example, from a centralised WwTW) the movement was rapid through the conduits. However, if the pollutive discharge was into a low-permeability zone (for example, diffuse pollution from septic tanks) the flow did not allow rapid movement of the polluted water.

The hydrochemistry of coastal limestone regions is of special interest, particularly to this thesis. A relationship between coastal landform evolution and fresh groundwater discharge, where increased dissolution via mixing corrosion is taking place has been developed (Back *et al.*, 1979). Caves are often found on carbonate islands, which form in discharge zones where the salt and fresh water mix, being found at various elevations due to changes in sea level.

Monitoring of rainfall volumes and drip rates and hydrochemistry in caves have also been used to understand the temporal and spatial variations in karst water hydrology and chemistry. For example, study of speleothem-forming drip water in southwest Ireland (Tooth and Fairchild, 2003) demonstrated that both soil matrix and preferential flow influence the karst water chemistry, soil matrix flow being dominant during dry periods whereas preferential flow through soil macropores was the most important during recharge.

Another study looking at the Vaucluse karst system in France found that the water originating in the infiltration zone was very important to the flow characteristics of the system and acted as a hanging reservoir (Lastennet and Mudry, 1997).

STABLE ISOTOPES

Stable isotopes, particularly ^{2}H (deuterium) and ^{18}O, have been used to investigate the age of recharge water moving through an aquifer following rain events. Isotopes of an element

have the same atomic number but different atomic weights due to a different number of neutrons in the nucleus which tends to be significant in the lighter elements (e.g. oxygen and hydrogen). The resulting difference in mass (isotropic fractionation) can result from any processes that cause the ratio of isotopes in a particular phase to differ from one another, including evaporation, radioactive decay, and chemical and biological reactions. Stable isotopes are those that are not involved in any type of radioactive decay process. Hence, they are used in hydrogeological studies to differentiate water sources, flow paths or residence times. For example, a reservoir undergoing evaporation would become enriched with the heavier isotopes of oxygen and hydrogen, since the lighter isotopes preferentially evaporate. The principles behind the use of such stable isotopes in hydrogeology are discussed in detail in Section 5.8.

Examples of major studies include the Knox aquifer in Alabama USA where stable isotopes $\delta^{18}O$ and δD (i.e. ^{2}H) in addition to major cation and anions were analysed (Redwine and Howell, 2001). Another study in Switzerland (Perrin *et al.*, 2003) demonstrated the degree of buffering associated with the soil and epikarst regions, finding that the seepage water into the conduits (see Section 2.5.3) showed very little variation in isotopic values compared to the new rainwater which demonstrated seasonal trends (maximum values in summer, minimum in winter). Equally, the Madison aquifer in North Dakota was studied using naturally occurring $\delta^{18}O$ to examine the dynamics of transient fluid interchange between conduit and diffusive networks (Long and Putnam, 2004).

Long term measurements (over 20 years) of environmental tritium (^{3}H) and stable isotopes (^{18}O and/or ^{2}H) were also used to study Austrian karst systems (Maloszewski *et al.*, 2002) and to develop a lumped parameter model formulated as two interconnected parallel flow systems of fissured-porous aquifer and karstic channels. Separation of the two different water paths at the output spring concentrations was achieved by analysing the isotope tracer concentrations at very high and very low discharges respectively. This approach enabled the mean transit times in both flow systems to be calculated and showed (as discussed earlier) that the volume of water stored in the karstic channels was insignificantly small (<1%) in comparison to the volume of water stored in the fissured-

porous aquifer. However, the karstic channels were shown to discharge the whole water flux. The volumetric flow rate of water entering via sinkholes (which thus moves quickly through the system and poses a potential pollution threat) was found to be 17.5%. The study also showed that the total porosity of the karst system was about 1.5%.

A study in the karstified Tauras mountains (discharging into the Mediterranean Sea) used stable and radioactive isotopes, CFCs and He to identify hydraulic connections (Nativ *et al.*, 1999). The groundwater components were separated by altitude source using $\delta^{18}O$ and δD isotopes whilst separation of groundwater components by residence time was achieved using tritium, CFCs, carbon isotopes and helium. Other similar techniques of isotopic composition include a study to differentiate between slow and fast drip recharge mechanisms within caves in response to rainfall events and thickness and fracture system of the rock cover (Ayalon *et al.*, 1998). Also, a study in Syria (Kattan, 1997) demonstrated high level interconnections during storm periods between different parts of the Figeh aquifer which established that the two neighbouring aquifers were independent from each other. The study was also able to show that the mean turnover time of water in the aquifer had decreased due to over-pumping of the aquifer.

Another study in South Australia used the isotopes $\delta^{2}H$, $\delta^{18}O$, ^{36}Cl to distinguish between point source and diffuse recharge into the karstic aquifer, finding that water recharging the groundwater via point source features were detectable only on a local scale and became indistinguishable from regional scale groundwater compositions (Herczeg *et al.*, 1997). Studies carried out in Malaga, Spain (Caballero *et al.*, 1996) in Georgia, USA (Plummer *et al.*, 1998) and in the Mount Xishun area of China (Zhang, 1993) have also used stable isotopes research to differentiate the spring waters between the unconfined and deeper confined aquifers with much older groundwater.

Finally, a study in Southern France used major and trace elements in conjunction with Sr and Pb isotopes on karstic springs to identify the hydrology of the karstic area (Petelet-Giraud *et al.*, 2003). The study was able to evaluate water originating from different layers in the aquifer (internal circulation) and also (in the case of Pb isotopes) water from natural

or anthropogenic sources. The Sr isotopes were particularly adapted for a binary karst system where part of the recharge area is not composed of carbonates (such as granite for example).

2.4.5 Spring hydrographs

Springs are the natural outlet for groundwater in karst aquifers and temporal variations in discharge can provide insight into the storage and transport characteristics of the aquifer. The analysis of the hydrographs has often been used in conjunction with quantitative dye tracing or variation in some chemical parameter (Sections 2.4.3 and 2.4.4) and as discussed earlier, such studies show that the flood pulses can be considered to consist of two components: displaced storage water and fresh recharge.

One of the main ways of analysing the hydrographs is based on the original hypothesis developed by Maillet (1905) where the recessional limb of the hydrograph is assumed to have a consistent exponential response related to the hydraulic parameters of the aquifer. This approach uses the empirical assumption that the storm response is due to flow through different permeability regions with the fastest response in the conduits and the slowest in the matrix. During a storm event, the internal conduit network of the karst can be considered as a transfer function in order to modify the input to the system deriving from swallets and internal runoff, into the outlet flow as observed in the form of hydrographs at springs (see Figure 2.7). A karst aquifer with a fast response time means that the storm pulses should be evident at the storm hydrographs. The hydrologic complexity of a karst aquifer is caused by highly variable recharge conditions and by heterogeneous subsurface flow conditions. The response time of a karst aquifer depends on: the contribution of allogenic recharge and internal runoff; the carrying capacity and internal structure of the conduit system; and the area of the ground water basin. However, a lack of individual storm pulses in a spring hydrograph does not necessarily imply that an aquifer does not contain conduits. A smoother hydrograph may merely indicate that the aquifer is recharged by diffuse infiltration rather than sinking streams of internal runoff. Equally, a sinking stream located close to the spring may produce a fast response hydrograph in a basin which is predominantly slow response.

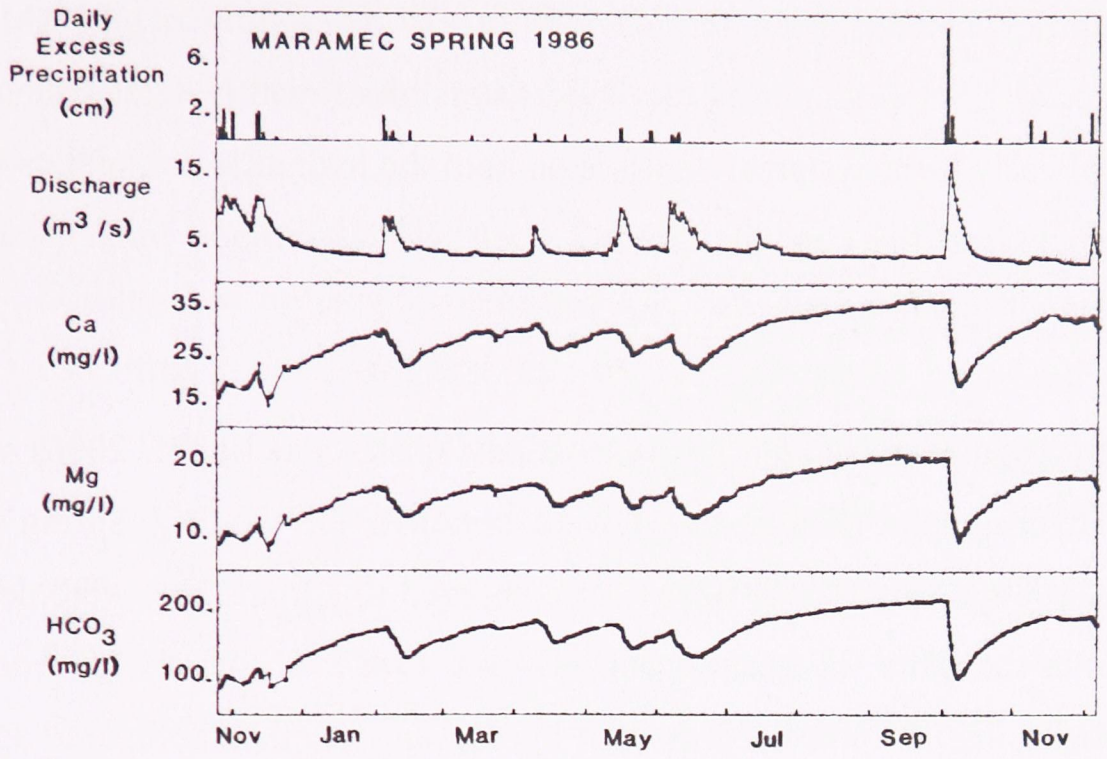


Figure 2.7 Example of spring hydrograph (Maramec spring, Missouri) with corresponding chemical signatures (Dreiss, 1989).

Much of the original work of analysing the hydrographs was by Atkinson (1977) and Milanovic (1976) following which a linear systems approach has been used for large springs (Dreiss, 1982; Estrela and Sahuquillo 1997). The approach allows one to obtain a transfer function (unit hydrograph, linear transform, kernel) which can be used to predict the response of a spring basin to varying hydrologic conditions, as discussed in Section 2.5.

In general, the recession limbs of individual storm hydrographs should be exponential.

$$Q = Q_0 e^{-t/\tau} \qquad \text{Eqn. 2.14}$$

where τ is the aquifer response time.

Often a semi-log plot of recession limbs in karstic aquifers may show two straight lines, whereby one portion of the aquifer drains quickly and another portion drains slowly. Possibly the "quickflow" represents the conduits draining whilst the "slowflow" represents the draining of the fractures into the conduits. During the baseflow recession of mature karst systems it is assumed that the hydraulic parameters of the conduits do not influence the drainage of the low permeability matrix. Hence, this flow condition is a function of the

low permeability blocks and has been termed *matrix-restrained flow regime* (MRFR) (Kovács *et al.*, 2005). Alternatively, during the flood recession of mature karst systems (or baseflow recession of early karst systems) depends on both the hydraulic parameters of the low permeability blocks and the conduits and has been termed, *conduit-influenced flow regime* (CIFR).

The use of a unit hydrograph technique has been tried (Wicks and Bohm, 2000) where dimensionless unit hydrographs (Shaw, 1994) were obtained for the Big Spring basin (Missouri) from six storm events. These were then compared to kernels that were derived by deconvolution from the same six storm events (Dreiss, 1982). The discharge from the springs was calculated using the dimensionless unit hydrograph and then compared against the actual discharge from the springs. This was done by multiplying the daily value of the transfer function by the amount of excess precipitation to the basin, the area of the basin and a scaling factor (used to close the water budget). Baseflow was then subsequently added to the calculated event flow to give the calculated discharge. The match between the kernels and dimensionless unit hydrograph was very good showing little difference between the transfer functions. The transfer function was then used on other single peak events and with recharge events with multiple peaks with generally good overall agreement although several peaks were off timing within each data set.

Spring hydrographs have been used to estimate the specific yields associated with each part of the aquifer storage, conduit, fracture and matrix (Shevenell, 1996) by looking at the speed of response to rainfall events (fast response = conduits) and also the shape and gradient of the recession curves for the proportion of fracture and matrix flow.

Finally, the continuous flow monitoring of spring flows can also be used to calculate the water budget of the aquifer, based on the principle of a mass balance of the water moving through the aquifer. A concept of *normalised* baseflow (i.e. the mean spring flow divided by the catchment area) has been used due to the fact that dry weather flow from springs is very low. This concept has been used on a large number of drainage basins in order to

provide estimates of basin area and also to help to confirm basin boundaries which may have been determined via other techniques (Quinlan and Ray, 1995; White, 2002).

2.4.6 Use of test wells in karst

Drilling test wells is the standard approach for most aquifer types but for karst aquifers it can often prove a fruitless activity unless extreme care (and good luck) is taken in the placement of the wells. For, example, in a study on the central Kentucky karst the chances of a borehole intersecting a channel was estimated to be between 0.4 to 3% (Worthington *et al.*, 2000). Wells that penetrate conduits can be used to install instrumentation to measure parameters such as temperature, conductance etc. A transducer can allow the well to be used to gain the pressure head in the conduit under flood flow conditions. However, often voids encountered during drilling can be laterally discontinuous dissolution features which are only hydraulically connected by fractures (Halihan *et al.*, 2000). Research on the Edwards aquifer in central Texas which looked at the permeability of a number of test wells revealed (by mathematical modelling) that for the majority of test wells the observed permeability could only be explained by the flow through fractures (as opposed to the matrix or conduits) (Halihan *et al.*, 2000). This was due to the low probability of intersecting a well-connected conduit in a karst aquifer. However, they found that increasing permeability with scale is to be expected for a fractured karst aquifer.

Wells can also be drilled into the fractures and fracture intersections to carry out pump tests to gain the hydraulic conductivity but such data can be unreliable. A project which used several different techniques to define the porosity and permeability of the Edwards karstic aquifer in Texas again demonstrated the strengths and weaknesses of the different techniques (Mace and Hovorka, 2000). Core plugs were found to be useful for defining the relationship between matrix porosity and permeability to stratigraphy and geophysical log response, although the estimates of porosity and permeability were acknowledged to be only approximate. Outcrop measurements were found to be useful for estimating secondary porosity due to fractures and dissolution features although they tend to be biased towards higher values because of unloading effects and weathering, but were still felt to be better than estimates based on core plugs or poor resolution geophysical logs. Another

recent study modelled the hydraulic behaviour of a fissured-karstic aquifer by a linear function using the dynamic level in a borehole against cumulative yield. This found that such a linear function suited 80% of the curve although floods followed by heavy storms could not be taken into account (Debieche *et al.*, 2002). Transmissivity and hydraulic conductivity of karstic aquifers in Slovenia have also been estimated using specific capacity (i.e. discharge divided by corresponding drawdown in the well) and specific capacity index (i.e. discharge divided by saturated aquifer thickness) (Verbovšek, 2008), techniques normally reserved for more alluvial (rather than fractured) aquifers.

Finally, fluctuations in the groundwater levels in both natural holes and boreholes have been used to determine characteristics about the karst. For example, levels monitored on an hourly basis over a period of two years clearly picked up evidence of saltwater intrusion due to tidal cycles in the Dinaric karst in Croatia (Bonacci and Roje-Bonacci, 2000).

2.4.7 Remote sensing and surface geophysics

Techniques such as airborne surveys and infrared photography, spectral scanning and thermal scanning have proved successful when surveying broad areas to identify karst features such as springs and sinking streams. Surface geophysics has been used to locate buried sinkholes or voids (Sasowsky, 2000). In areas underlain by carbonate rock the most common techniques are electromagnetic, gravity and ground penetrating radar surveys but little attempt has been made to integrate such information into the overall function of the aquifer.

Borehole geophysical methods allow observation of the aquifer in regions where humans are physically not able to travel. Porosity and permeability trends can be evaluated using classical tools (used in the petroleum industry) such as calliper, gamma ray, density and porosity, but with the advent of the borehole video camera, views into fractures and conduits are now possible, as used for example in the Kentucky karst study (Worthington *et al.*, 2000).

Magnetic Resonance Sounding (MRS) has proved a useful tool to detect the actual groundwater in the conduits/ caves but only works when there is a high enough quantity of water to be detected (Vouillamoz *et al.*, 2003). The technique was shown to accurately plot the known conduit location and depth and the cross-sections of the conduits were accurately calculated from tranmissivity and permeability estimators. Conduits have been identified by cavers using magnetic induction (cave radio) location devices.

Dipole-dipole D.C. resistivity techniques have also been used (Lambert *et al.*, 1997) which involves measuring the apparent resistivity of the subsurface by introducing a current. Karst features (conduits etc) typically show up as high resistivity anomalies which enable generalised interpretations for further modelling purposes.

The use of the natural electrical potential - the naturally occurring voltage at the ground surface resulting from ambient electrical currents in the earth - has been used successfully to locate groundwater flow in karst terrains (Wanfrang *et al.*, 1999). Electrical potential gradients are generated by the horizontal flow of the water along the fractures or conduits which can thus be picked up. A study in Cuba successfully determined transmissivity in a karst aquifer (when compared against pumping tests carried out in the same area) finding that longitudinal conductance was the geoelectrical parameter which was the best predictor of aquifer transmissivity (Ortega and Espinosa, 1999).

Another method is using seismic surface waves (Luke and Chase, 1997). Here a spectral analysis of surface waves is analysed based on the dispersive nature of Rayleigh waves. The technique enabled the depth to the roof of cavities to be detected but not the depth of the cavity itself.

2.4.8 Other methods

SEDIMENT ANALYSIS

Generally sediment transport is assumed to be negligible when modelling karst aquifers and is ignored. However, the physical and hydraulic properties of sediment from karst aquifers can be used to determine the similarity of sediment between karst aquifer systems

and also the importance of modelling flow through karst aquifers (Peterson and Wicks, 2003). Sediment cores have been taken from sediment in the main conduits and physical properties such as bulk density, porosity, mass wetness and percentage saturation were determined. The grain size distribution was determined and then the hydraulic conductivity (K) of the sediment. Equally the organic content was measured as was the mineral composition with respect to quartz, plagioclase, calcite and total clay. The results from the sediments from different caves showed nearly identical compositions (not surprising perhaps since they are located in the same area). The minerals were a mixture of both minerals from the karst rock (autochthonous) and those transported into the karst aquifer (allochthonous). Note, there was a distinct lack of carbonate material in the sediments probably as it had been dissolved or the carbonate strata was not actively being eroded. Finally, the K values of the sediments came out to be about 10^{-7} ms^{-1} which is within the range for carbonate rocks in general and therefore suggests that the sediment can be ignored or included in the unit corresponding to the carbonate matrix in flow models.

Research in Switzerland comparing sediments and suspended particles / colloids to faecal and pathogenic micro-organisms (Pronk *et al.*, 2006; 2007; 2009; Goldscheider, 2009) through karstic systems following rain storms showed that the first turbidity signal received at the spring was from autochthonous material (i.e. sediment from within the aquifer that is resuspended) which is then followed by a second turbidity signal from the allochthonous particles (i.e. from the soil and sinking streams) which was associated with the possible presence of faecal bacteria (see Figure 2.8). Hence, turbidity alone as an early warning signal for spring pollution signal is not good enough. Particle Size Analysis showed that the autochthonous material consisted of a mixture of particle sizes compared to the allochthonous particles which were composed of mainly very fine particles / colloids.

Temperature profiles

Stream-air temperature relationships have been used to distinguish between ground water and surface water components of different rivers in karst areas (O'Driscoll and DeWalle, 2006). The study also compared energy exchanges / budgets for the different rivers.

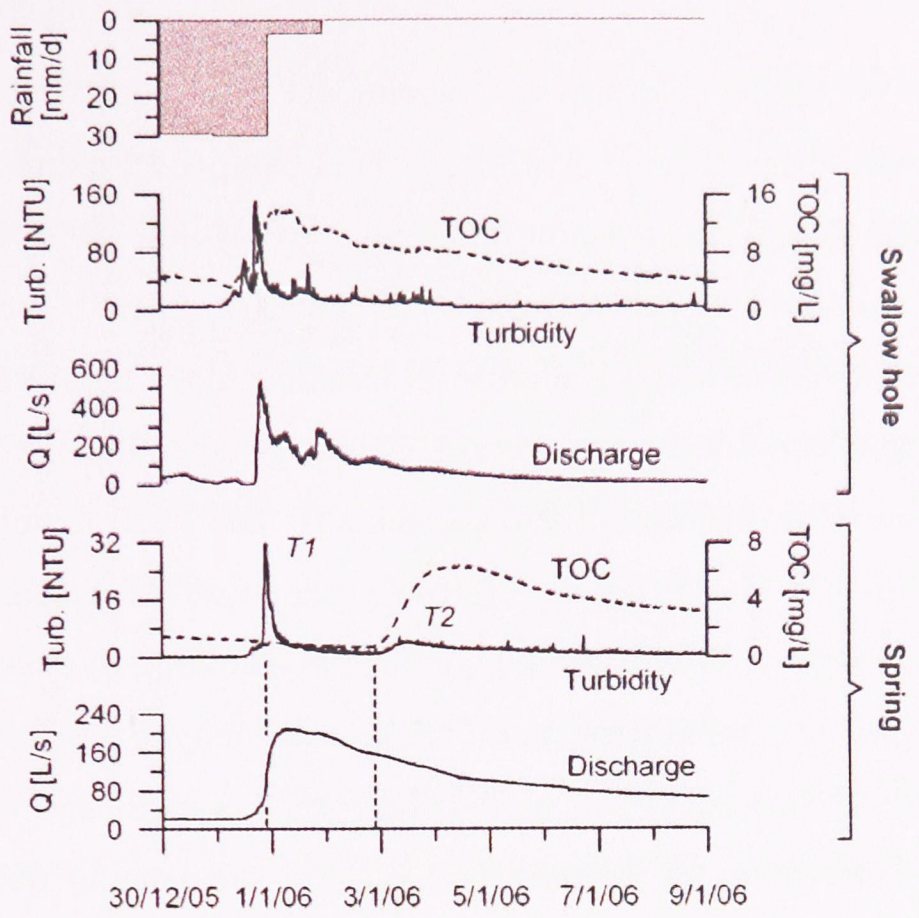


Figure 2.8 Autochthonous (T1) and allochthonous (T2) turbidity signals at the Moulinet karst spring , Switzerland following a heavy rainfall event after a prolonged dry period (Pronk *et al.*, 2007).

LABORATORY EXPERIMENTS

Very little work has been done at a laboratory scale apart from geochemical studies examining dissolution rates of minerals under varying conditions (Rauch and White, 1977).

2.5 Mathematical Modelling of Karst Aquifers

Numerical modelling of karst aquifers can be divided into three generic types: models of present day groundwater flows (the focus of this thesis); geochemical models of aqueous reactions taking place within the aquifer; and growth models which combine aspects of flow and geochemical models to study the development of cave growth. This section concentrates on the different approaches applied to the modelling of present day flows through karst aquifers.

Karstic systems are highly heterogeneous geological formations which are characterised by multi-scale temporal and spatial hydrologic behaviour. Modelling groundwater flow in karst aquifers has to take into account laminar (Darcian) flow in fissures, turbulent flow in open channels and diphasic flows through the epikartsic zone. Moreover, karstic aquifers present different levels of karstification from less developed karst, "diffuse flow aquifers" to developed karst "conduit flow aquifers" (Atkinson, 1977). Equally, infiltration processes vary from diffuse, slow infiltration into small matrix and fracture volumes to concentrated flow or rapid infiltration into the channel network, as do the discharge conditions (from diffuse seepage from the low hydraulic conductivity volume to concentrated discharge at karst springs from the conduit network). This heterogeneity is why most karst models have been characterised according to global responses which try to account for their hydrodynamic behaviour; for example, relating an input to an output using a transfer function. However, a wide variety of different deterministic modelling approaches have been attempted on karst aquifers, some assuming linear relationships between input and output and others trying to model the inherent non-linearity.

Overall it seems that karstic models have been developed based upon one of two distinct approaches. One approach, based on the analysis of the recessional limb of spring hydrographs, suggests that the response is due to regional changes in hydraulic conductivity (due to the relative difference between matrix and conduit flows for example). Other models, based on a network of conduits and tanks, suggest a much more physical mechanism - these include more local controls on flows due to constriction or boulder choked sections of conduits.

The conceptually simplest types of model have been so-called *black box* models (e.g. Dreiss, 1982) which contain no spatial information on the karst aquifer but can predict the outflow spring discharge from the system. More deterministic models for groundwater flow (which can also often be linked to transport processes) may either have distributed or lumped parameters. The lumped models lack the spatial dimension in the equations describing flow and transport and hence only linear differential equations must be solved.

Distributed parameter models are normally chosen to increase the accuracy of predictions or achieve a high degree of spatial resolution which can extend right up to finite element models of aquifer systems. Dual porosity distributed parameter models have also been developed for karst aquifers, representing both conduit and diffuse flow.

It has been suggested that the most appropriate modelling approach for karstic aquifers depends on whether the inputs to the aquifer are point or diffuse and whether the observed output is point (such as a well) or diffuse (such as a spring) (Teutsch and Sauter, 1998). The objective of the model should also dictate its conceptual structure: whether it's being used to evaluate groundwater flow from a water management perspective, the assessment of contaminant transport, or the assessment of aquifer vulnerability (Scanlon *et al.*, 2003). Porous media models for example, can be used for the evaluation of regional groundwater issues but cannot simulate local flow directions or rates since the major conduits are not explicitly represented.

2.5.1 Lumped parameter, linear systems models

A typical rainfall-runoff model postulates that water discharge at the catchment outlet is given by a linear convolution between effective rainfall and a physically based transfer function (Beven, 2001). This approach was first derived for hydrologically closed surface water basins where the output series is river discharge and input series excess recharge. In karst basins, the output series is discharge from springs. The input series is recharge to the groundwater system through the unsaturated zone and seepage through sinkholes (autogenic recharge) and losing streams (allogenic recharge). An advantage of this approach is that it does not rely on the specification of the size, shape or location of the internal structure of the aquifer - i.e. it is a *black box* modelling approach. The drawback to the approach is that there is generally no simple method which will derive the transfer functions which can be used to model the response to individual storm events, multiple-day events and year-long series. Also, a linear systems model is being used to simulate what is recognized as a non-linear system; the kernel functions are effectively lumping all the effects of several complex processes together.

Several methods have been used to identify the transfer functions which can be separated into two generic groups. The first group determine parametric transfer functions, i.e. a form of Instantaneous Unit Hydrograph determined from a conceptual model (the Nash-reservoir model, for example); the parameters are then optimised to fit the data. The second group uses numerous different numerical methods for the determination of non-parametric transfer functions which include Fourier transforms, least squares approaches, statistical methods (such as the Wiener-Hopf method) and more recently techniques based on spectral analyses and wavelets.

2.5.1.1 Parametric transfer function methods

The linear systems approach treats the karst system as a black box operating on input functions to produce an output function response, represented by,

$$y(t) = \int_{t=0}^{\infty} h(t-\tau)x(\tau)d\tau \qquad \text{Eqn. 2.15}$$

where y(t) is the output series, x(τ) is the input series and h(t- τ) is a transfer function (t = time, τ = variable of integration). Hence, if both series x(τ) and y(t) are known then the transfer function h(t- τ) can be found by the method of deconvolution (i.e. solution methods) using a variety of different algorithms (Neuman and de Marsily, 1976). The hydraulic behaviour of karst systems is described as a relationship between input and output where the rainfall-runoff relation is characterised statistically by a unique, time-invariant transfer function which may be interpreted as the unit impulse response of the karstic basin. This approach describes the regional scale transport through the karst under natural conditions only using the readily available spring flow properties.

The shape of the transfer functions can be characterised by the known physical structure of the karstic system. The delay of the response is due to delay in the non-karstic soil and subsoil during surface infiltration and runoff. There may also be delay due to the exchange of water between micro and macro fissure systems. Another characteristic is the presence of several modes and plateaux or tails. These are due to rapid infiltration after a storm passes through the primary mode (large holes / main conduits) and then the tail coming from the annex of secondary fissures, drains and reservoirs in the flooded zone. Hence, the

more important the water storage capacity of the system, the longer the tails would be expected to be.

Several researchers (Dreiss, 1982; Labat *et al.*, 2000a; Denić-Jukić and Jukić, 2003 etc.) have shown that the derivation of the transfer function by the method of deconvolution results in unstable (oscillatory) functions due to the sensitivity of the method - small data errors can cause large oscillations in identified kernel functions. In such cases the volume of excess precipitation turns out to be much greater than the volume of the storm response of a spring since some of the effective precipitation goes into surface runoff, interflow and deep groundwater circulation as well as the spring recharge water. This can be dealt with in the model by a simple scaling factor applied to the input series. However, it has generally been found that kernel functions identified for large springs from different isolated storms are similar in shape and time to peak. The linear systems analysis for the storm-derived component of spring hydrographs (Dreiss, 1989b) have also been calculated by looking at variations in ionic concentrations in spring discharges (Dreiss 1989a). These were then adjusted to represent variations in the ionic composition of the secondary porosity (which is normally considered to be constant) and achieved closer fits. The single empirically derived linear transfer function (or *kernel*) which was required was then analysed using time moment analysis. This describes the shape of the function and statistical properties of the residence time distribution of the rapid groundwater recharge in the conduit network, as shown schematically in Figure 2.9. These were used to represent the mean travel times and degree of mixing that occurs during rapid transport in the aquifer. For conduit-type aquifers, the relatively low variance reflected the fact that little mixing occurred during transport indicating plug flow conditions, as expected.

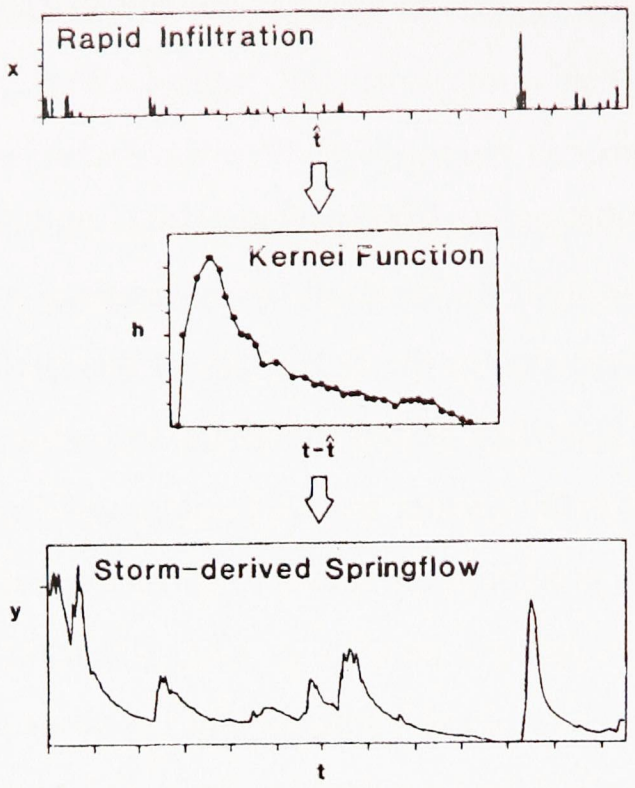


Figure 2.9 Schematic diagram of linear system analysis of karst conduit-type spring flow (Dreiss 1989b).

More recent work (Estrela and Sahuquillo, 1997) has used the relationship between the slopes for the line segment along the recessional limbs to derive the values of the transfer function. This method however, accounts for the response of the basins to year-long recessional, not isolated recharge events since it does not use deconvolution. Another linear systems approach was applied to the Madison aquifer in South Dakota where instead of spring discharge, the hydraulic head in a well was considered to be the output (Long and Derickson, 1999). Calculations were carried out on the transformed data to get the transformed function which was then inversed to return the actual transfer function. In this approach the baseflow from the aquifer was first determined and then subtracted from the actual head to give the output that was responding to the system input according to a calculated transfer function. Curves were fitted to the short-term recession of hydraulic head which were then used to predict the long term recession. This long term recession was then used to determine a transfer function that characterises the aquifer. Deconvolution of the linear system was carried out using the Fourier transform. In this particular study a logarithmic curve was found to be the most appropriate transfer function for this system which had a long-term, heavily damped response.

There seems to be a general conclusion with the use of a single transfer function models that they do not simulate the long recessional limbs of typical karst discharges (i.e. when the quick flow in the conduits has passed through and subsequent drainage occurs due to the gradual emptying of pores, smaller fractures and fissures). The tails are often irregular shapes and seem to have no physical representation in terms of karst system. This is due to the underlying assumptions for the linear systems approach that the transfer function is time invariant and also the linearity of the technique (i.e. founded on the principle of proportionality and superposition). To improve this, a composite transfer function has been proposed (Denić-Jukić and Jukić, 2003) in what could be described as a *grey system* approach using the superposition of two transfer functions: one to represent the quick flow component and the other to represent the slow flow component as follows:

$$y(t) = y^{D} + \int_{0}^{t} h^{s}(\tau)x(t-\tau) + \int_{0}^{t} h^{Q}(\tau)x(t-\tau)d\tau \qquad \text{Eqn. 2.16}$$

where, $h^{S}(\tau)$ is the slow transfer function, $h^{Q}(\tau)$ is the quick transfer function, and y^{D} represents the antecedent recession.

The slow flow component was modelled in four different conceptual ways and fitted to the data from the Jado spring in Croatia using a constrained least squares method. The four parametric methods, as illustrated in Figure 2.10, are: the Nash-reservoir model (based on the concept of a cascade of unequal linear reservoirs (Beven, 2001)); the Zoch model (based on a linear channel and linear reservoir in series); two parallel unequal linear reservoirs with recession coefficients; and finally a time variant linear reservoir with recession coefficient. All four methods produced a much closer fit than the standard non-parametric transfer function especially for the tails and also made more physical sense, with smooth recessions to the function compared to the typical erratic function of the non-parametric transfer function.

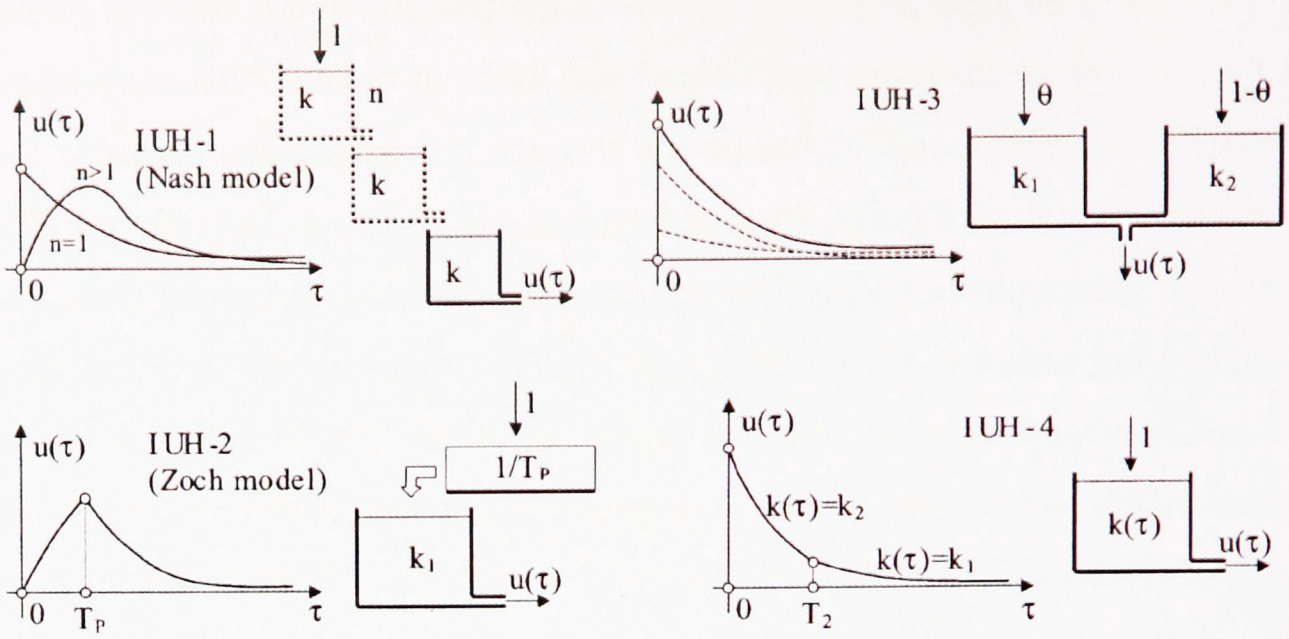


Figure 2.10 Conceptual models and their normalised unit hydrographs for the slow flow component (Denić-Jukić and Jukić, 2003).

Lumped parameter models based on reservoirs in series and /or parallel have also been developed, such as the model of the Fontaine de Vaucluse aquifer in the south of France as shown in Figure 2.11 (Fleury *et al.*, 2007b). In this conceptual model one reservoir simulates the infiltration through the soil using effective rainfall and a transfer function. This then feeds to two parallel reservoirs, one of which models slow discharge (i.e. fracture flow), the other models rapid discharge (i.e. conduit dominated flow). The slow discharge transfer function was determined by hydrodynamic analysis of the recession.

The diffuse recharge to a karst aquifer was specifically looked at in Switzerland in order to characterise the amount of storage in the soil and epikarst using field data (Perrin *et al.*, 2003). Input and output isotopes in the system were looked at to separate the fresh rain water from the older stored water which showed heavily buffered concentrations at the spring indicating the existence of an important storage component allowing mixing of the infiltrated water with the stored water which led to the conceptual model below (Figure 2.12). The system was modelled as two successive reservoirs: a soil reservoir with mixing function and an epikarst reservoir which provides the dynamic storage, producing a sharp hydraulic response but damped solute concentrations. It also created a bottleneck effect in the epikarst by decreasing the hydraulic conductivities with depth in this region, storage and mixing and piston flow for rapid hydraulic pulses but delayed transport response. The

mixing reservoir for the soil could be physically interpreted by the fact that in unsaturated soils the water is mainly stored in the matrix.

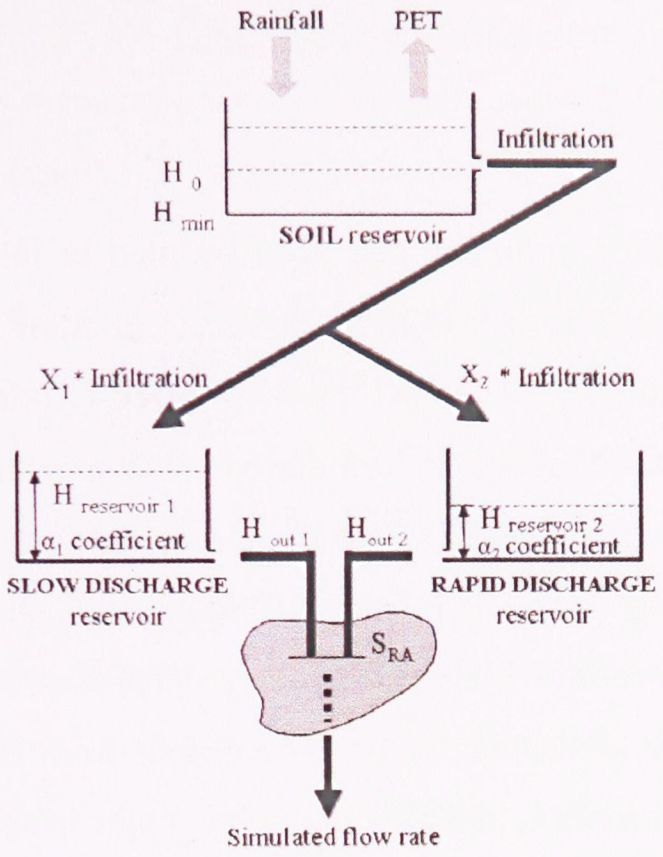


Figure 2.11 Conceptual model used for the Fontaine de Vaucluse karst aquifer (Fleury *et al.*, 2007b).

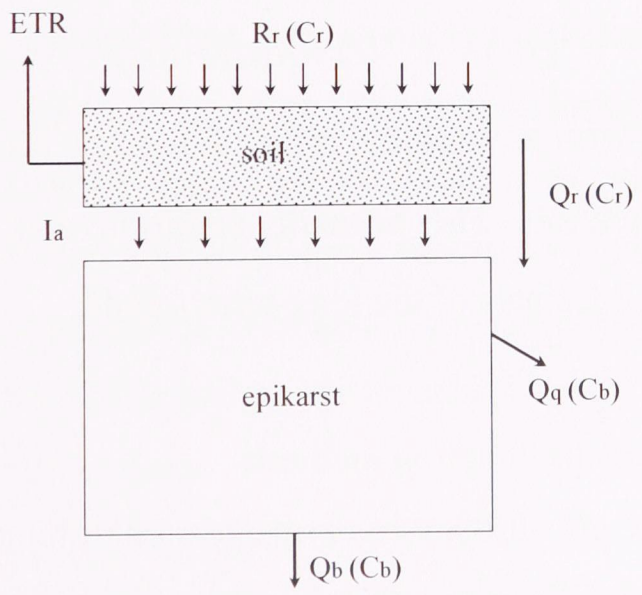


Figure 2.12 Conceptual model of flow and storage in the soil/epikarst layer where, ETR is evapotranspiration, R_r is rainfall (at concentration C_r), I_a is actual infiltration, Q_f is excess by-pass infiltration, Q_b is baseflow and Qq is quickflow (Perrin *et al.*, 2003).

When recharge occurs, the hydraulic conductivity increases drastically and some of the fresh water will bypass the matrix through macropores. Hence the matrix water becomes completely mobile and can mix with the fresh water – modelled as a reservoir in the model.

A similar *grey box* modelling approach has been adopted to investigate the three major source tributaries of the River Jordan in northern Israel draining the karstic catchment of Mount Hermon using a model with the acronym HYMKE (Rimmer and Salingar, 2006). The daily rainfall-streamflow model was formulated using four modules: the surface layer (rainfall minus evaporation), the vadose zone, the groundwater and surface flow. The percolation into the vadose zone (i.e. from the epikarst) included both a slow flow (depending on soil moisture and hydraulic conductivity) and high flow component to represent the karstic nature of the landscape. The output from the vadose zone then fed three groundwater reservoir models in parallel, one per major tributary.

Long term karst spring discharges in China have been analysed as a *grey system* using a composite function but this time comprised of their long-term trends, periodic variation and random fluctuations (Hao *et al.*, 2007).

$$Q(t) = \hat{x}^{(0)}(t) + S(t_i) + R(t) \qquad \text{Eqn. 2.17}$$

where, $\hat{x}^{(0)}(t)$ is the long term trend of the spring flow, $S(t_i)$ is the periodic variation and $R(t)$ is the random fluctuation. The periodic variation and random fluctuations were obtained by analyzing the residuals of the long-term trends.

2.5.1.2 Non-parametric transfer function methods

Certain studies (Labat *et al.*, 2000a) have discovered limitations to the time-invariant transfer function techniques discussed in the previous section when trying to reconstruct the temporal structure of relatively infrequent flow events such as floods or low water periods. The inadequacy of such a linear-output approach is not surprising due to the significant physical and geometric heterogeneity at all levels and scales of karstic aquifers (e.g. fine fissures up to large caverns and conduits) which produces dynamic and temporal

type heterogeneity as well - after intense precipitation the flow follows the most transmissive conduits (quickflow) whereas in depletion the relative importance of the flow through these large conduits is much less or even negligible with respect to baseflow. Hence, to get the most realistic models for such hydrologic basins the non-linear and non-stationary aspects should be included

Time series of rainfall and spring discharge over long periods can be studied by both univariate and cross analysis (Padilla and Pulido-Bosch, 1995). Univariate analysis characterizes the individual structure of the time series, the functions applied being autocorrelation (in the time domain) and spectral density (in the frequency domain). Cross analysis characterises the transformation of an input function into an output function (i.e. a transfer function). The cross-correlation function is analysed in the time domain and the cross-amplitude, phase, coherence and gain functions are analysed in the frequency domain. The coherence function expresses the intensity of the input-output link for example and its linearity, linearity being regarded as a characteristic of a highly karstified aquifer (Larcroque *et al.*, 1998). Interpretation of such correlation and cross-spectral analyses has been used to separate the quickflow from the baseflow. This was first tested using three theoretical time series obtained by deconvolution (Padilla and Pulido-Bosch, 1995) representing highly karstified, virtually non-karstified (i.e. porous media) and then combined quickflow / baseflow aquifers. The interpretation was then tested on four real karstic aquifers (two in the Pyrénées and two in the south-east of Spain). The results of the study of the correlogram and amplitude cross functions were used to obtain the duration of the impulse response of the aquifer. The gain function allowed the quickflow, intermediate flow and baseflow to be differentiated whilst delays in the responses were deduced from the phase and coherence functions.

Correlation and spectral analyses were also used to analyse different types of spatially distributed time series on the La Rochefoucauld karst aquifer in France (Larocque *et al.*, 1998). Correlations were performed on river flow rates into aquifer and spring outputs. Spectral analyses were also then performed on precipitation as an input and piezometric heads in different parts of the aquifer which yielded information about the dynamics of

water level changes and infiltration whereby a low coherence function indicated limited karstification. Cross-correlation analysis was also used on electrical conductivity readings of water in the input rivers and output spring water. This found that during high water periods, as electrical conductivity decreased in the input rivers due to dilution, there was a corresponding increase in the output conductivity due to the flushing effect (i.e. displacement of existing stored water). However, during low water periods the aquifer displayed different behaviour whereby decreasing input conductivity lead to decreasing output conductivity. This led to the conclusion that the aquifer must be comprised of variable levels of karstification with the more karstified sections nearer to the surface. Water temperature time series were also studied but with less success.

A linear convolution model was developed and tested on three karstic springs in the Ariège region of the Pyrénées mountains (Labat *et al.*, 2000a). Three different deconvolution techniques were compared: the substitution method, the statistical Wiener-Hopf method and the ordinary least squares method. The results showed that whilst the ordinary least squares method proved slightly better than the statistical methods, the linear convolution models were not very accurate at simulation at the daily sampling rate. The study also showed that the simulation results became poorer as the degree of karstification increased when comparing the three different aquifer basins. An alternative method was then tried on the same data sets based on the statistical properties of the runoff processes alone where the runoff synthesis was based on stationary runoff process statistics (spectral density function). The Fast Fourier transform, although efficient for stationery signals was found to be rather poor when used for reconstructing non-stationery and non-Gaussian processes.

Following on from the premise that karstic systems are non-linear and non-stationary systems, the identification of characteristic time-scales for such models is crucial for accurate modelling. Multifractal analyses have been applied to hydrological signals in several studies, for example rainfall time series (Olsson and Niemczynowicz, 1996; Svenson *et al.*, 1996; de Lima and Grasman, 1999) whereby the (multiple) scaling of the probability distributions of rainfall intensity were used to investigate the multifractal temporal structure of the process. This same approach was used to study the same three

karstic springs in the French Pyrénées (which have long data sets) at two different time scales (Labat *et al.*, 2002). Initially, generalised moment distributions were found for both the rainfall and spring flow runoff at the three springs. In general, large moments highlight strong singularities in the process (such as high rainfall intensities or floods) whereas small moments highlight small singularities (small rainfall or low flow). Spectral analysis then consists of the variance density distributions around certain scales - the determination of pulsation intervals on which the spectrum follows a power-law behaviour. As above, the spectra of all the time series (one rainfall and three spring runoffs) exhibited the normal power-law behaviour, as shown in Figure 2.13.

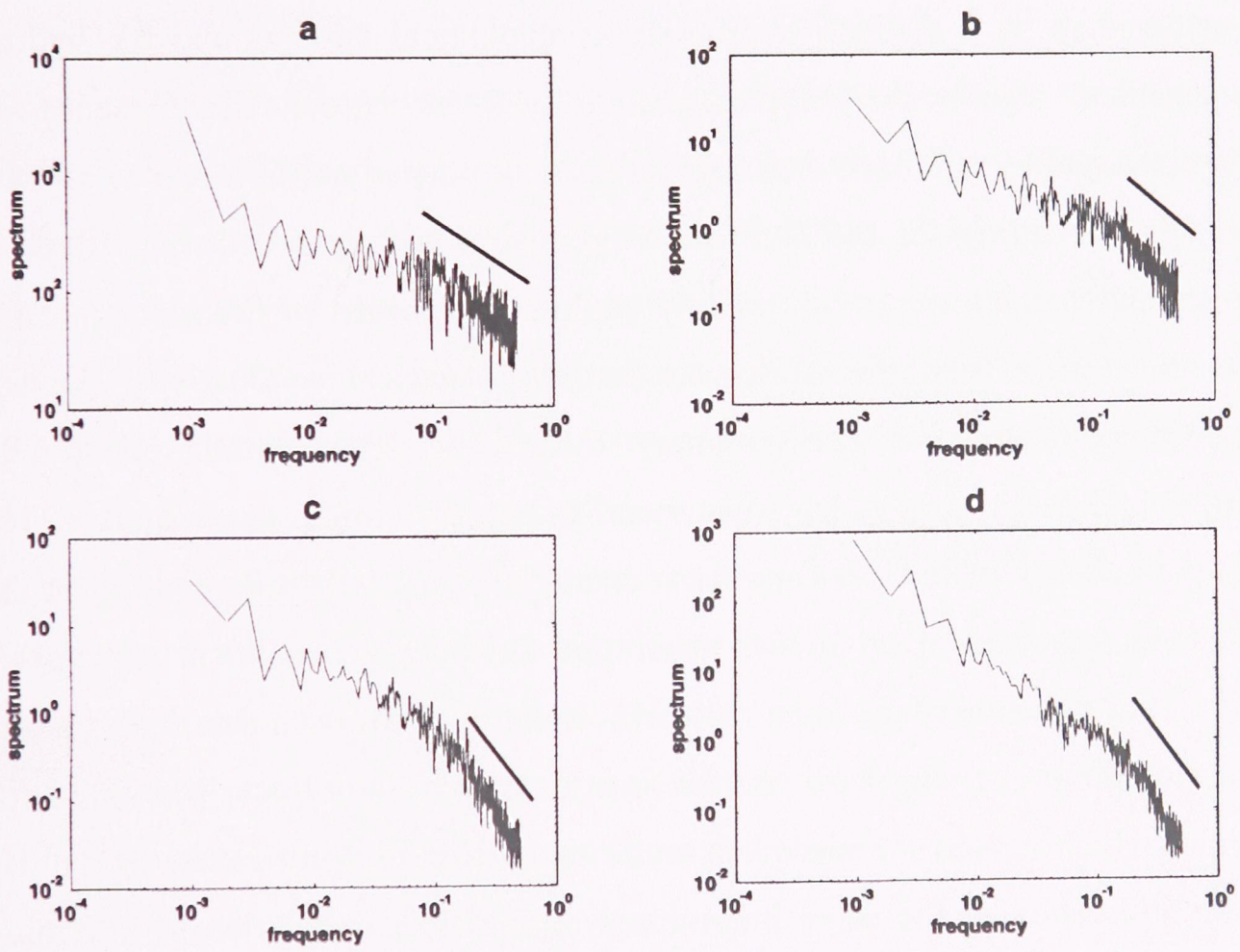


Figure 2.13 Spectral analysis: variance spectra of **(a)** daily rainfall and **(b, c, d)** spring flow runoff rates from 3 karstic basins in the Pyrénées, France (Labat *et al.*, 2002).

The multifractal analysis consists of a more systematic investigation of the different empirical moments of the signal function of the scale observation. Multifractal analysis was carried out on both the large time scale and short time scale processes for both data sets at different sampling rate. The daily sampling rate data showed no difference between

the three aquifer types, even though they were known to have different internal structures from previous studies. However, when the data was analysed at the half-hourly sampling rate, two distinctly different multifractal signals were obtained for the runoff time series indicating different behaviours at this timescale. This shows that the choice of appropriate time steps needs to be carefully considered when modelling karstic systems.

More recently multifractal analyses have been carried out on the spring behaviour in the Italian Dolomites (Majone *et al.*, 2004) looking at hydrological signals (precipitation and spring flow) and geochemical (electrical conductivity) signals to infer the residence time of the water emerging. A non-linear, multifractal model was chosen since scaling is considered to be a distinctive property of geological systems and the hydrological and geochemical signals were typically non-linear in nature. The presence of a highly organized and hierarchized drainage network introduced multiple scales of variability into the signals (calling for the multi-scale approach) and the non-linear effects due to soil moisture dynamics were conveniently explored by means of the multifractal framework. One conclusion from the work was that the electrical conductivity signals were less intermittent and more non-stationary than either the rainfall or spring discharge multifractal parameters which were found to be very similar to each other. This suggests that the network of fractures and karst channels exerted a strong control on the residence time and less control on runoff generation (i.e. the geochemical signals reflected the underlying structure of the karst network). It was hypothesised that during storm flows the effect of the underlying karst system was masked by non-linear processes controlled by rainfall which caused the pre-event water to contribute significantly to runoff generation while still retaining the same intermittent spring flow in relation to intermittent rainfall pattern. The similarity between the rainfall and spring flow signals suggested that the spring flow could be obtained by fractional convolution of the rainfall signal with a non-stationary power law transfer function.

Groundwater recharge rates in karst are generally orientated to groundwater balance and soil-moisture balance calculations. However, because of the complex internal structures of karst aquifers, groundwater balances are normally difficult to ascertain without extensive

knowledge of the internal structure. A groundwater recharge model for a karst aquifer in Croatia was developed using the frequency domain method (i.e. spectral analysis) to determine the parameters of the model (Jukić and Denić-Jukić, 2004). By transforming the problem into the frequency domain, the groundwater balance was avoided and the groundwater recharge rates could be calculated by using the soil-moisture balance approach where only the easily obtained hydro-meteorological and spring discharge time series were required. The conceptual model of the aquifer was a lumped system with phreatic and vadose zone: the rainfall rates were transformed into groundwater recharge beneath the vadose zone and the phreatic zone represented by a linear, time-invariant filter transforming the groundwater recharge rate into spring discharges.

The interactions between karst groundwater and ephemeral rivers in the Mediterranean was studied as a black box binary system, using rainfall and river flow as input variables and karst spring flows as the output (Bailly-Comte *et al.*, 2008). The karst / river interactions were cross-correlated and simple linear systems relationship used to understand how the flood energy was stored or released by the karst aquifer. Spectral analyses were used to show the frequency response of the karst / river system whereby the karst subsystem acts as a tank which stored and released surface water during flood transfer using shallow underground flow paths which bypass the surface flow (i.e. in the epikarst). At other times, however, the karst aquifer contributed a significant flow to the river flow. The study shows that the energy exchange between the karst and river can be interpreted in the time domain by the use of auto- and cross-correlation analyses and in the frequency domain by power spectral density, cross-amplitude, coherence gain and phase functions.

Wavelet Analyses on karstic basins

As seen above, spectral or correlation analyses are often applied to rainfall rates and karstic spring discharges. However, such analyses tend to lose temporal information since they operate globally on the signal in a statistical way. The different moments of the time series are supposed to be constant in time, a strong hypothesis which is never the truth when the measured data is examined, being based on time-invariance and stationery assumptions. Runoff from karstic systems is influenced by the time structure of the rainfall rates but also

the high non-linearity of the karstic system. Hence, correlation and spectral analyses cannot provide information, for example, on the occurrence of localized flood events or intermittent processes in rainfall or runoff time series. Therefore, attempts have been made to introduce a new type of analysis which takes account of the fact that hydrological signals are not stationary rather than these classical statistical methods. The relatively new technique uses the concept of *wavelets* to give a time-scale representation of the non-stationary processes and of their relationships. From this a more detailed physical interpretation of the hydrological structure of the rainfall / runoff relationship for karstic springs is possible. The wavelet analysis is principally used in two ways: extraction of local time-scale information and representation of processes in appropriate bases. The principles of wavelets are discussed in more detail in Section 6.2.2.

There are several different types of wavelet used including the Haar wavelet, the complex Morlet wavelet and successive derivatives of the Gaussian function (e.g. the Mexican Hat function) (Labat *et al.*, 2000b). The use of wavelets in hydrology has been expanding recently, for example the technique based on the Morlet wavelet has been used to compare large scale river basin discharges with respect to climate change (Labat *et al.*, 2005) or to analyse and transform rainfall statistics which then feed a neural network model used to predict droughts (Kim and Valdés, 2003). Such wavelets have also been applied to the Licq-Atherey karstic system in the Pyrénées of France and compared with classical spectral and correlation analyses (as described previously) based on the rainfall and runoff data over a period of 30 years (Labat *et al.*, 2001). The composite nature of the basin composed of a highly karstified subsystem (with a fast one day response) and less developed subsystem was also confirmed by the analysis. Continuous Morlet wavelet analysis was applied to both the rainfall and runoff data at different sampling rates from daily to half-hourly sampling rates (Labat *et al.*, 2000b). The wavelet spectrum of rainfall rates was characterised by the presence of high frequency patterns corresponding to scales of less than one month. The wavelet spectrum of the runoff data highlighted two components: a 6 month component and classical one year component (i.e. the annual recharge). High-frequency or short-scale patterns were much less visible than in the rainfall spectrum. These wavelets were then used to investigate the rainfall-runoff

relationship which clearly showed it was scale dependant (monthly, yearly and three to seven year components). In addition the discrete orthogonal Haar wavelet transform was used for multi-resolution analyses in order to visualise the energy distribution at different scales and compare this against the energy distribution across frequencies (i.e. the Fourier spectrum). This suggested that different models (temporal or physical) are necessary to simulate the rapid response, the annual recharge or the multi-annual components. Another strength of the wavelet analysis approach is that it allows the rapid and efficient decomposition of input and output signals in several components without loss of information. It also allows a finer analysis of these different components and of their variability using Morlet wavelet co-spectrum or multi-resolution cross-analyses. The results obtained can distinguish between the two components in a karstic spring runoff response to rainfall: a fast response due to conduit flow; and a slower response probably due to the slower flow of internal reserves of water located in the porous matrix and fissures (fractures).

2.5.2 Equivalent porous media models

The early attempts to model karst aquifers assumed Darcian flow conditions (ignoring conduit flow) on the basis that at sufficiently large scales, the spaces in a carbonate aquifer (pores, fissures and conduits) can be assumed to be homogeneous with arbitrary boundaries and characterised by mean values of the parameters.

Modelling approaches have used an equivalent porous media model which can be either lumped parameter (effectively black box models as detailed earlier) or physically based, semi-distributed models. The distributed parameter models can be separated into single continuum or dual continuum where one continuum represents moderately karstified system (diffuse flow, low conductivity) and the other represents highly karstified zones (high conductivity, low retention times) (Teutsch and Sauter, 1998). Exchange between the continua is achieved by equations with exchange coefficients (for example, superposition of two MODFLOW grids).

A finite element model approach was used for example to develop a two-dimensional regional flow model of a karstic aquifer in Greece to study the effects of groundwater lowering for a proposed mine adjacent to the aquifer (Kavvadas and Marinos, 1994).

A comparison between modelling the Barton Springs Edwards karstic aquifer in Texas using an equivalent porous media model and tanks in series model was undertaken (Scanlon *et al.*, 2003). One model was formulated as a simple lumped parameter model represented as 5 reservoirs as shown later in Figure 2.14, each representing a major river in the study area. The other model as a more involved distributed parameter model was comprised of 14 400 cells on the finite difference MODFLOW modelling software. The hydraulic conductivity of each cell represents all types of flow (i.e. conduit, fracture and matrix). Both models were calibrated against steady state and then compared against 10 year transient flow events. In general, the two types both returned similar results with the simpler lumped parameter model slightly out performing the more complicated model in terms of goodness of fit. However, it was considered that if the model was used for the assessment of non-point sources of contamination, then the distributed model would be more appropriate.

The finite difference modelling approach has also been used to simulate the complex groundwater flow through karstic environments by incorporating MODFLOW's "drain" feature (used to simulate agricultural tiles) assigned with high conductance as an analogue for preferential flowpaths or conduits (Quinn and Tomasko, 2000; Quinn *et al.*, 2006). The beginning of the preferred flowpath coincides with a known surface feature (e.g. sinkhole or fracture etc) and terminates at a known emergent surface discharge point. Two models were built to simulate separate karstic aquifers in Hohenfels, Germany and in Missouri, USA, both of which had a set of tracer studies used for calibration. In both sites good comparisons were obtained between the model and the field measurements. The same principal using MODFLOW to model dual porosity using the drain feature to represent the conduit flow was used in Israel to model perched karstic aquifers (Weiss and Gvirtzman, 2007).

Other examples of where MODFLOW has been used to model karstic aquifers include a karstic spring in Italy (Angelini and Dragoni, 1997) and a karst area in Florida where it was used to study the potential impacts of extra abstraction (Dufresne and Drake, 1997). A three-dimensional MODFLOW model was also developed of the flows through the Corallian aquifer in North Yorkshire which were lost from the bed of the River Derwent through solution hollows flowing over the top (Carey and Chadha, 1998).

2.5.3 Tank-and-pipe models

The investigation of the physical mechanisms which could generate the observed storm responses has been another generic approach to the mathematical analysis and representation of karst systems. Such models span from physically-based, distributed to simple presumptions about the internal geometry. In particular, conduits in karstic aquifers have been modelled as pipe networks based upon engineering hydraulics concepts; the role of constrictions in cave passages has been specifically studied for instance. Such models can work well both in the prediction of spring discharge hydrographs and the peaks and recession of hydrographs due to storm flow.

One of the first documented studies of karst using a pipe flow model was for an aquifer in Kentucky (Thrailkill, 1974) which proved reasonably successful. Since then several different karst systems have been modelled on this pipe flow (non-Darcian) basis with the latest generation of models being described as discrete models containing an explicit conduit system developed either based on actual exploration or by estimation as to where the conduits should lie (Mohrlok and Sauter, 1997; Jeannin, 2001; White, 2002). A simple branched pipe network system, for example, has been successfully used to model conduit dominated flow karst systems through Europe's longest cave – the 185 km Hölloch cave network in Switzerland (Jeannin, 2001). The system was shown to be strongly non-linear due to the epiphreatic conduits. Similarly, models using reservoirs and pipes in various combinations have been used, for example, the model of so-called rhythmic (i.e. intermittent) springs in Yugoslavia developed by Bonacci and Bonjanić (1991) based upon two reservoirs connected by a siphon as shown in Figure 2.14.

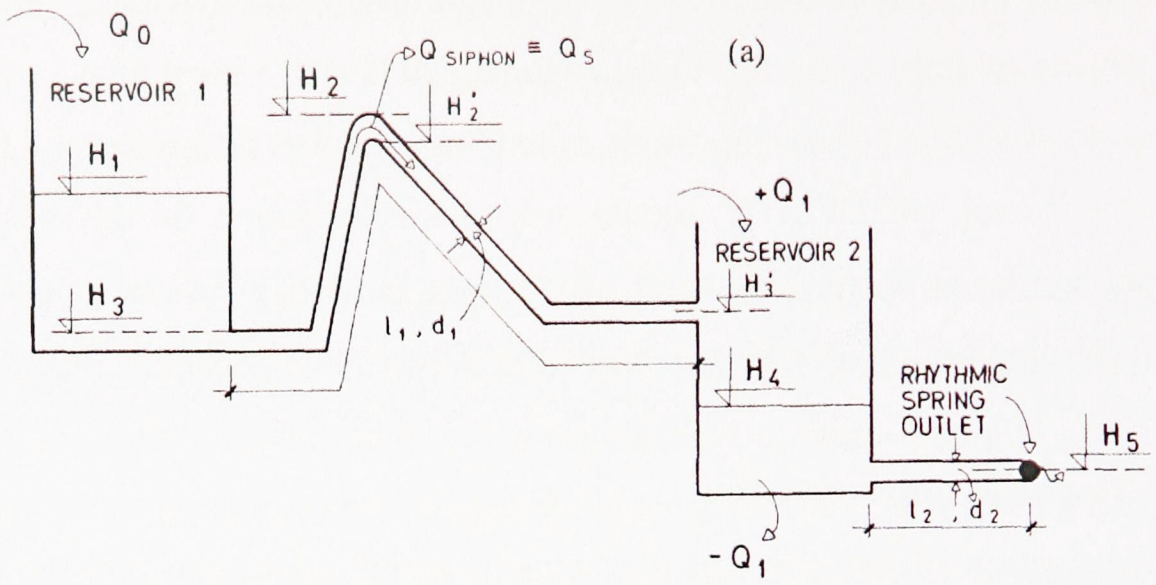


Figure 2.14 Schematic cross-section through a rhythmic karst spring (Bonacci and Bonjanić, 1991).

A one-dimensional closed conduit model has been developed (Springer, 2004) based upon idealised elliptical conduit geometries as shown in Figure 2.15. The assumption was that overall headloss along the conduit was a combination of the headloss due to friction on the side walls plus the headlosses due to expansions and contractions and bends, as would be conventional for pressurised pipe flow design in engineered networks (see Chadwick *et al.*, 2004).

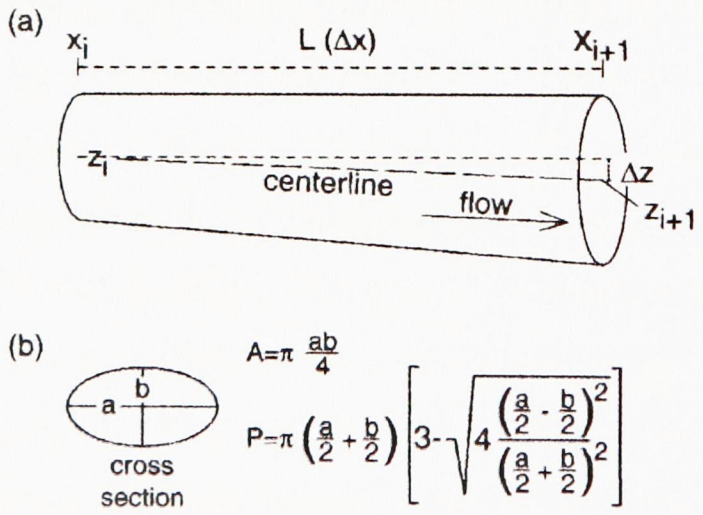


Figure 2.15 Schematic diagram of idealised conduit geometries **(a)** pipe of variable diameter and **(b)** elliptical conduit cross-section with geometric variables (Springer, 2004).

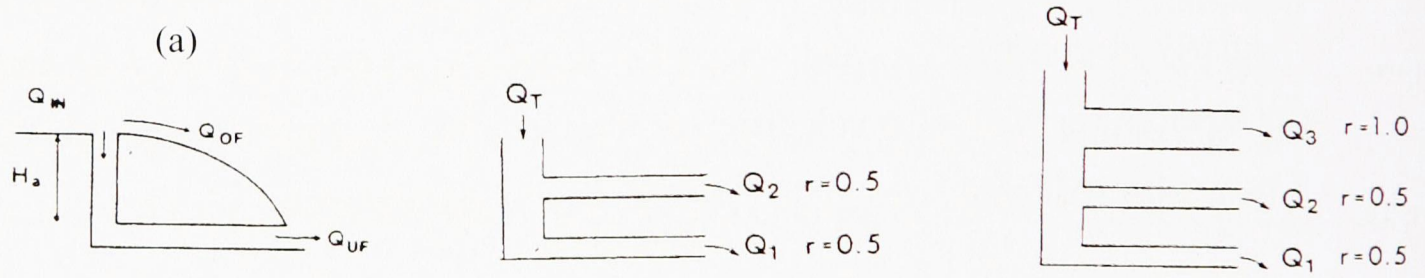
The model was then formulated based on a set of simultaneous equations based on the energy (Bernoulli's) equation across each change of section. The geometry of the whole

conduit (Buckeye Creek Cave, West Virginia) was measured and also paleohydraulic indicators were looked at to establish head levels and suitable range of friction factors. Expansions and bends were also measured and empirical loss coefficients associated with each one. The model was divided into 16 different sections over the 1.6 km conduit and then the discharge was varied through the system until the correct overall headloss was achieved. This gave the overall result that 25% head loss was from the expansions, 68% from the bends and only 7% from the sidewall friction. This would be surprising in manufactured pipe flow systems where normally the so-called *minor* losses (expansions and bends) are dwarfed in comparison to the wall friction losses. However, in natural cave passages, the shape can repeatedly change over short distances (Palmer, 1991; Springer 2004) whereby head losses from so-called diffusers lead to flow separation and turbulence which dissipates energy. This has been corroborated by looking at scallops which have indicated reverse flow along the pipe sides (Springer and Wohl, 2002). The model above did show high sensitivity to the expansion coefficient giving very high localised headlosses particularly at constrictions and was only carried out at steady flow rates. Interestingly, shear stresses (τ) were also calculated at the modelled flow rates to see whether it could compare with sediment sizes in the passage way (with mixed results).

As described in Section 2.2.2, several studies have examined conduits to determine their hydraulic properties (for example, friction factors etc) based upon pipe flow calculations. Such research indicates the appropriate scale of coefficients which should be used in pipe flow models. However, the range of derived friction factors found by different researchers for karst conduits is fairly broad. For example, Gale (1984) found localised friction factors (λ) to be in the range 0.028-0.13. This can be compared to friction factors calculated across the whole systems, lumping together all minor losses, where the values can increase to a range 0.12-104 (Jeannin, 2001) although this range can be tightened to the systems without significant obstruction from sediments to λ = 0.12-0.24. Equally, a model based on numerical solutions of the dispersion equation was developed to simulate solute transport for a single karstic conduit in the Basque Country, Spain under variable recharge and velocity conditions (Morales-Juberías *et al.*, 1997). The model had different hypothetical

structures which were fitted to experimental tracer breakthrough results to determine the optimum conduit structure.

The interpretation of flow data from karst aquifers was examined by the application of a simple model on theoretical conduit aquifers in terms of exceedance probability of discharge (Smart, 1988). The distribution of daily flows was expressed in terms of the exceedance probability or a flow duration curve. The karst aquifers modelled were: a single conduit (Figure 2.16(a)) high level conduits and internal overflow (Figure 2.16(b)) and several conduit systems (Figure 2.16(c)) with a range of radii from 0.1 to 1.0 m. The results showed that although the model was inaccurate in terms of storage considerations, the internal structure of the aquifer (different levels of conduits etc) has a profound effect on the flow through its constituent conduits.



Q_{of} = overflow, Q_{uf} = underflow, Q_T = inflow, Q_1 = underflow, Q_I = internal inflow, r = radius (m)

Figure 2.16 Different conceptual models for karst aquifers for **(a)** single conduit, **(b)** twin conduit and **(c)** three conduit system (Smart, 1988).

Another study (Halihan *et al.*, 1998) attempted to determine whether the storm response of a spring was a local or regional effect (or combination of both). The model consisted of water flowing through a tank (ephiphreatic conduit) and pipe (phreatic conduit) to simulate the Devil's Icebox cave system in Missouri, as illustrated schematically in Figure 2.17. The model showed that the storm response of the system could be simulated by a constricted flow scenario which was confirmed by the increase in kinetic head at the spring during storm events. The discharge from the constriction was calculated using the Darcy-Weisbach equation assuming that the flow was smoothly turbulent. This also provided an explanation for the observed water level variations in the cave passages upstream

compared with the variation at the spring. The model was found to be very sensitive to recharge (which needed hourly precipitation measurements at least) and also illustrated the transition from local control due to the constriction, to regional controls due to the aquifer matrix after the effects of the storm had passed, since the model no longer fitted the observed data at such times. The differentiation between conduit and matrix flow was also studied using a specific energy analysis of the springflow, on the basis that in a "conventional" Darcian flow aquifer, the kinetic head is much smaller than the pressure and potential (elevation) head, whereas in karstic aquifers this is not true. Specific energy was calculated at the discharge spring for the system using Bernoulli's Law whereby,

$$E = d_{avg} + \frac{v_{avg}^2}{2g} \qquad \text{Eqn. 2.18}$$

where, d = average depth and v = average velocity.

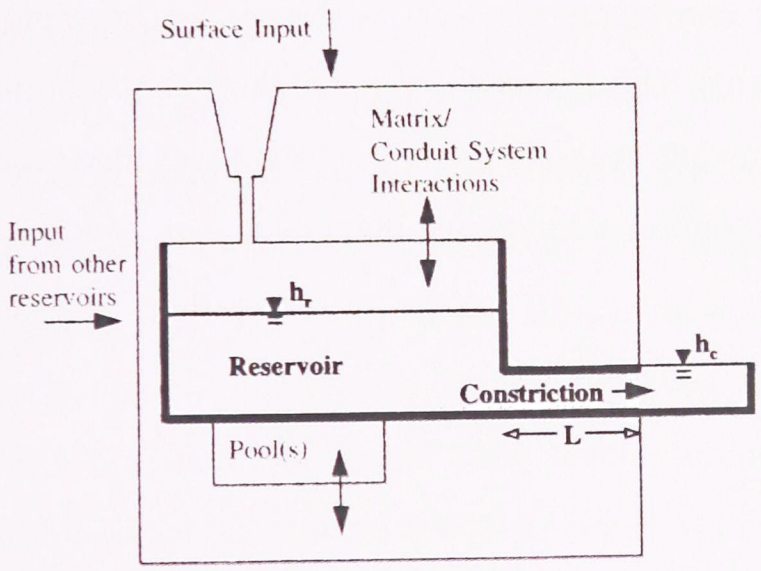


Figure 2.17 Schematic model of the Devil's Icebox cave system (Halihan *et al.*, 1998).

Further interesting work was carried out by Halihan and Wicks (1998) whereby conduit flow systems were modelled as different combinations of pipes connecting to reservoirs. A range of different hypothetical systems were looked at starting with a one tank-one pipe model, as shown in Figure 2.18. This was found to be very sensitive to the input values - i.e. if the input signal occurred very quickly the mechanism caused a sharp peak with highly asymmetric hydrograph limbs - but if the input signal duration was long the model did little to alter the signal. This simple system also proved to be very sensitive to the pipe parameter (length to diameter ratio).

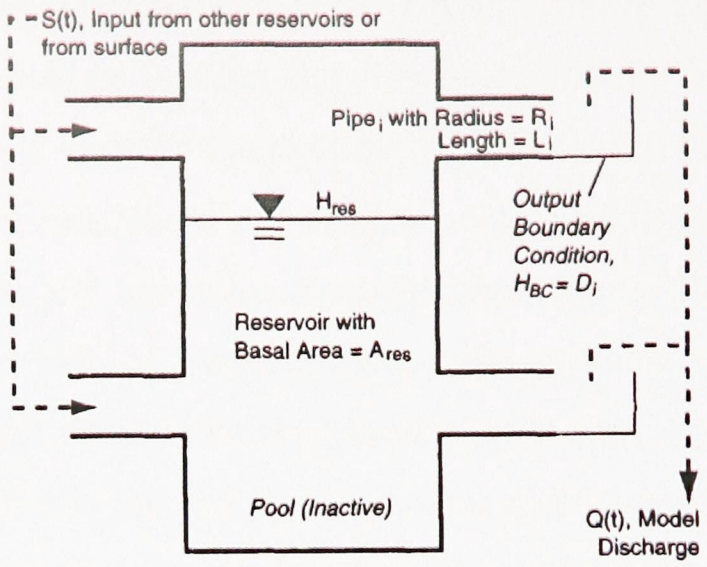


Figure 2.18 Schematic cross-section of the reservoir model used (Halihan and Wicks, 1998).

Other more complicated model configurations were assessed, for example with several overflow levels (see Figure 2.19(b)). This showed that the highest conduit mimics the input signal but will lag behind it somewhat. A tanks-in-series system was also modelled (Figure 2.19(c)) whereby the smallest conduit connecting the tanks was found to control the response.

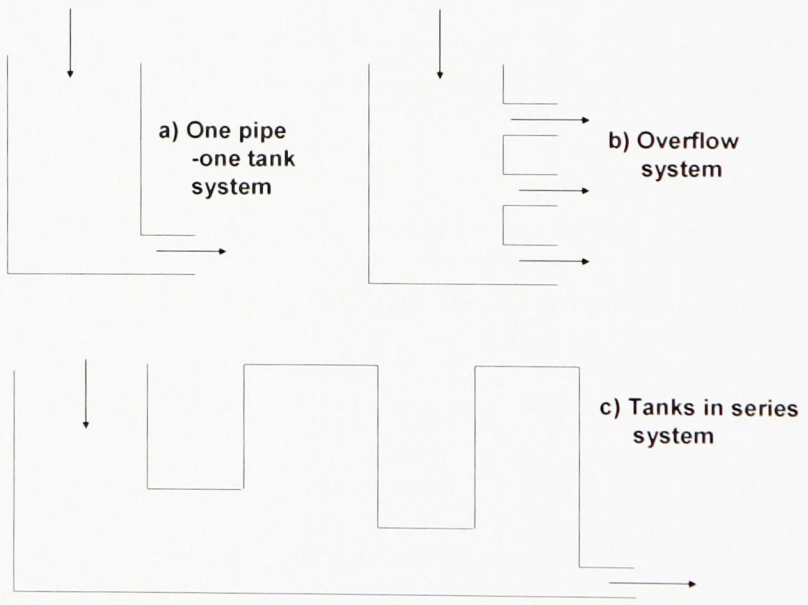


Figure 2.19 Schematic cross-sections of other reservoir models compared by Halihan and Wicks (1998).

The responses in the reservoirs varied from a single response to responses that contain recessional limbs with multiple components. One very interesting observation from the reservoir constriction model was that it indicated that the variations in hydrograph

responses were not based upon the regional draining of the aquifer. It also showed that the baseflow component in hydrographs (normally assumed to be the Darcian response from the fracture matrix) could also have come from constricted passages or have been generated from overflow or feedback mechanisms. Hence, baseflow conditions in karstic systems do not necessarily mean that the aquifer is flowing under Darcian conditions.

The sensitivity of a pipe network model using the U.S. Environmental Protection Agency's Storm Water Management Model (SWMM) software was used to model the same Devil's Icebox cave system (Peterson and Wicks, 2006). Ten percent changes in the length or width of the conduits produced statistically different outflows compared to the calibrated baseline model. The model was also found to be extremely sensitive to changes in the Manning's roughness coefficient but was relatively insensitive to changes to slope and infiltration rates.

A multicell groundwater model for karstic aquifers was developed which used a mixed equation to represent both free surface and pressure flow in the conduits (Rozos and Koutsoyiannis, 2006). They found that it was of no advantage to the prediction of springflow when compared to the system built using the MODFLOW software which treats flow as Darcian if internal water levels were not known (i.e. rainfall related to spring flow) but it was of advantage if aquifer levels were known and needed to calibrate against this. A plot of measured spring flow against estimated hydraulic conductivity (K) for the system resulted in a significant variation in K and a hysteresis loop as found by other researchers (e.g. Bonacci and Roje-Bonacci, 2000) resulting from the stage dependent internal routing of the water.

An essentially lumped parameter model (so-called *parsimonious* model) was developed for a section of the Edwards aquifer in Texas (Barrett and Charbeneau, 1997) in order to simplify the representation of the physical structure of the processes involved. This included vertical variations in aquifer properties (normally only allowed on a horizontal plane) but tried to simplify the data requirements and calibration parameters by reducing the number of cells. Each aquifer in this system was treated as a tank whereby a parameter

relates fluctuations in water surface elevations to volume of water in each cell (Figure 2.20). The cells were then assigned different yields according to the elevation of water level in them (generally divided into three distinct zones) which could be estimated during the calibration process. This equated to the change of flow and storage characteristics in the aquifer as water levels rose and fell and caves and conduits became submerged, hence strongly affecting flow in the aquifer. This model proved to be very responsive to the different types of flow regime (from basal flow up to storm flow response).

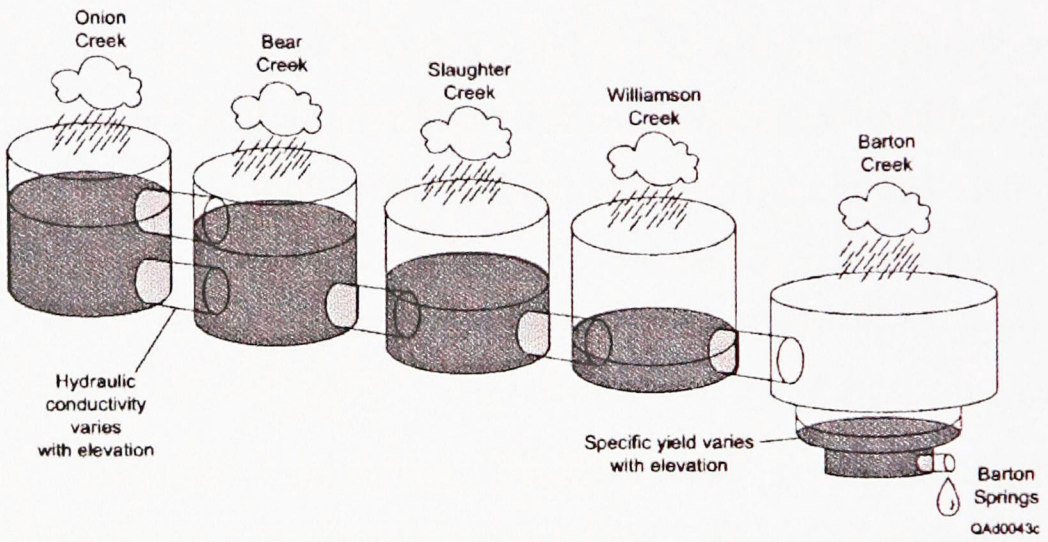


Figure 2.20 Schematic diagram of the lumped parameter model cells and connections used to model the Barton Springs Edwards aquifer (Scanlon *et al.*, 2003).

A model was built to simulate brackish karstic springs and tested on the Almiros Spring in Crete (Maramanthas *et al.*, 2003). A conceptual model of three reservoirs was developed whereby two reservoirs simulated the karstic aquifer and one (infinitely large) reservoir simulated the sea (see Figure 2.21). The two karst reservoirs represented two types of karstic subsystem that feed the spring: the section of karst that drains quickly (i.e. large conduits) and the other which drains rather slowly (smaller conduits / fractures). The model was based on the principle of continuity (mass balance) and energy balances were carried out across each reservoir. The model simulated both the discharge and also the chloride concentrations of the spring; it was found to be very good at simulating the levels during depletion periods but only satisfactory during recharge periods (the latter was felt to be due to limited rainfall measurements).

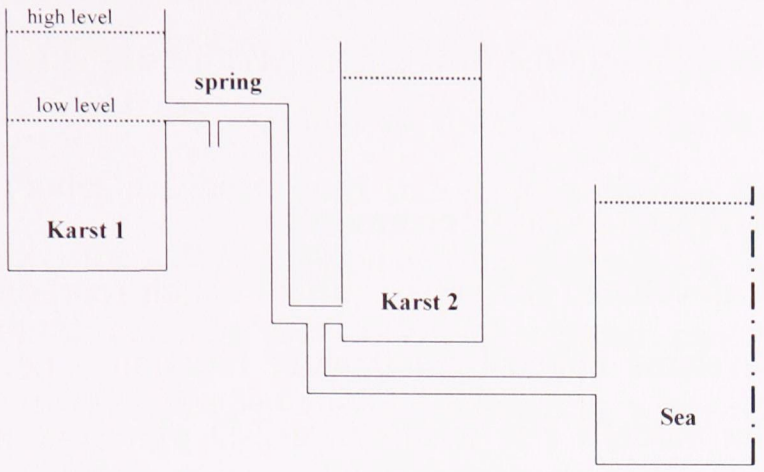


Figure 2.21 Conceptual model of karstic springs (after Maramanthas *et al.*, 2003).

Many karst networks around the world discharge via well developed conduits (caverns) below the current sea water level which developed during previous periods of lower sea levels (Fleury *et al.*, 2007a). This karstification at depth can allow a flux of seawater to enter which can also create a possible siphoning effect whereby salt water is drawn from below into the freshwater discharging at sea level outflow during flood times. The density difference between the saline sea water intrusion and fresh water is the major factor governing the relative movements (and boundary) between these two fluids (and can be determined by the Ghyben-Herzberg formula).

Interesting work was carried out by Zhou (2000) where three physical models were built to simulate the typical drainage pattern in karst aquifers where flow is channelized and concentrated along discrete conduits. Recharge was controlled by upstream water tanks and karst conduits by plastic pipes of different diameters. The relationship between water velocity and hydraulic gradient was found to be closely associated with the internal structure of the model and the situation where there was no correlation between the two parameters could easily be achieved with a relatively simple combination of structures. Hence, it is no surprise that in real karstic systems with complex internal networks and chambers it is rare to find such a correlation. Equally, attempts were made to apply mixing cell models (i.e. networks of continually-stirred tank reactors (CSTRs)) to simulate flow through the karstic system using a finite difference scheme for convection. These mixing

cell models were calibrated in conjunction with dye traces to get the best fit and hence the optimum number of cells to represent the flow characteristics of the aquifer.

2.5.4 Dual porosity distributed parameter models

Several models have been developed for karst aquifers which represent conduit flow and diffuse flow as separate systems linked by a transfer function – i.e. often a combining network and porous media models. For example, a 2-D pipework model coupled to a single layer MODFLOW model was developed as part of the EU GRACE project to simulate flow and transport in conduit systems which feed karst springs in Germany and the United Kingdom (Younger *et al.*, 1997).

Techniques have been employed to model karst which originated from models of Mine Water Rebound; the network of mine shafts and tunnels are not dissimilar to the conduits in karst, although they are also distinguished from their closest natural relations by the particular geometries of voids present and lateral scale of inter-connection. For example, natural karst-systems have hundreds of kilometres of passageways beneath a relatively small surface area whereas mined systems tend to be more laterally extensive (Aldous *et al.*, 1986). Discharges of polluted water from abandoned mines following ground water rebound are a major cause of water resource pollution due to the so-called acid mine drainage which arises from the bacterially catalysed oxidation of pyrite (FeS_2) which leads to a production of acidity (Younger, 1995). The flow in the large open mine voids is often turbulent during the rebound process and hence standard techniques for modelling groundwater flow which assume laminar flow conditions are inappropriate.

A strategy for groundwater modelling has been proposed (Adams and Younger, 2001) for which a 3-D pipe network model is used for relatively modest systems (<200km^2), a semi-distributed model (GRAM) which uses a conceptual framework of interconnected volumes working as ponds for regions up to 3000 km^2, and then for the largest scale simple water-balance calculations are proposed as the most suitable. The techniques relevant to karst modelling are the first two modelling approaches. The minewater rebound model uses the VSS (Variably Saturated Subsurface) component of SHETRAN which simulates the

combination of saturated and unsaturated conditions typically found in abandoned coalfields. However, in the regions where the flow regime is turbulent, a pipe network model was adopted and coupled to the VSS model to create the VSS-NET combined model. The model has been used successfully on the Bishop-Auckland and Ynysarwed-Blaenant mines. The GRAM (Groundwater Rebound in Abandoned Mineworkings) model uses the central concept that a mined system can be resolved into a number of hydraulically discrete ponds which can exchange water with each other via a small number of interpond overflow points as shown schematically in Figure 2.22 (Younger and Adams, 1999). Different ponds are assumed to fill independently until the time when the water level in one overflows creating interpond transfer. The overflow feature can be unrestricted (i.e. minimal head difference ponds) or throttled. Monte-Carlo simulations were also used to quantify uncertainties – i.e. probability distributions for pipe roughness etc. GRAM has been used successfully on several coalmines: Durham Coalfield, Dysat-Leven Coalfield, South Yorkshire Coalfield (Burke and Younger, 2000) and Whittle Colliery for example.

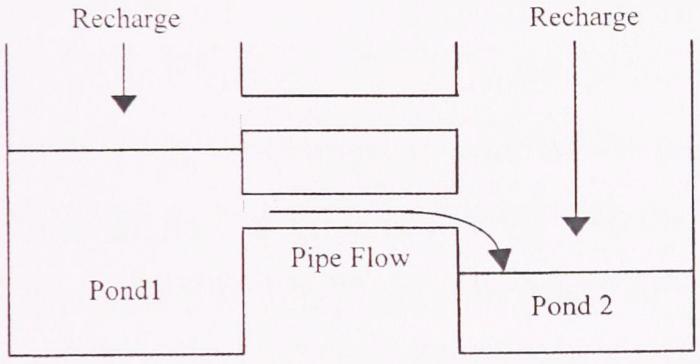


Figure 2.22 Schematic diagram of flow between two ponds in a roadway in a flooded mine (Younger and Adams, 1999).

The SHETRAN hydrological model has been used to model karstic groundwater movement as part of the European Commission's Sustainable Management of Groundwater in Karstic Environments (STALAGMITE) project (Adams and Parkin, 2001). SHETRAN is a physically-based distributed hydrological modelling system which is comprised of a modular system of interconnected components which represents the hydrological cycle. It couples surface and subsurface processes together into an integrated 3-D model of water flow and transport (Ewen *et al.*, 2000). The hydrological catchment is discretised into a series of elements and non-linear equations which govern the flow of

water and transport of catchments and sediments, which are solved by numerical methods. The model for the karst aquifer was set up as physically based which means that the model parameters have some physical meaning. Flow in the sub-horizontal cave network in the saturated zone was modelled using the VSS-NET component of the model originally developed to model to simulate groundwater rebound in abandoned mines, as described above. The exchange of flows between the conduits and matrix cells were modelled using Darcy's Law and flows in the conduit modelled using Darcy-Weisbach or Hazen Williams. A boundary condition with a fixed head was required for each network of conduits (i.e. spring discharge). Shafts were also modelled whereby they could receive either rainfall or flow from sinking streams or inflow from a connected network. The water levels in the shaft also fixed the boundary conditions for the saturated cave network. The epikarst region near the surface absorbs and then transmits infiltration into the subsurface region and requires two parameters to calculate an instantaneous transfer flux: the threshold water depth and a constant of proportionality. The model has been successfully used in Slovenia, Slovakia and Bulgaria as part of the project.

One study on karst basins in the Swiss Jura (Eisenlohr *et al.*, 1997) used an indirect method of verification of such models by introducing a well defined theoretical karst structure into a finite element model and then analysing the simulated global response according to a series of fixed interpretation schemes. The karst system studied included the soil cover, non-karst terrains, the unsaturated part of the aquifer and the saturated zone connected to the principal output (the karst spring). This model was used to test the sensitivity of some statistical methods used in ground flow interpretation such as auto-correlation between discharge-discharge and cross-correlation between rainfall–discharge. The numerical simulations were modelled both as simplified 2-D and 3-D networks which include both the low conductivity fractured flow network and the higher conductivity conduit flow. Overall the work found that the climatic regime (storm frequency and spatial / temporal distribution of rainfall) and infiltration mechanisms of karst (ratio between diffused and concentrated infiltration) had a major influence on the form of the hydrograph. The numerical simulation, however, did behave as an effective cross-correlation between precipitation and discharge.

A process-based flow and transport model has been developed by coupling a pipe-flow model (for fast conduit flow) to MODFLOW (to represent flow in fissured porous rock) and used on a relatively simple hypothetical karst aquifer (Birk *et al.*, 2006). Interesting results showed that the conduit volume estimated from the time lag between hydraulic and physico-chemical spring responses tended to be larger than the actual volume.

2.5.5 Other modelling approaches

2.5.5.1 Geochemical models

Geochemical models give insights into the geochemical processes acting on an aquifer through time or through space. Some models such as NETPATH define reaction models consistent with given data whereas other models, PHREEQE are useful for applying an assumed reaction to some specified initial conditions. Attempts have been made to join flow models with reactive geochemical models to simulate cave growth (Dreybrodt, 1992; Groves and Howard, 1994; Palmer, 1991). For example, a model Carbonate Aquifer Void Evolution (CAVE) couples the flow in the karst with a reaction module, simulating the dissolutional enlargement of conduits (Clemens *et al.*, 1998; Liedl *et al.*, 2003). CAVE has also been extended by the gypsum dissolution module Evaporite Void Evolution (EVE) accounting for different dissolution kinetics of gypsum and different boundary conditions (Birk *et al.*, 2005). Such models are very useful from a contemporary hydrogeological perspective by helping to understand the observed porosity distribution.

A global systems approach has been taken to model karst structures and thus infer the structure of the karst network (Grasso and Jeannin, 2002). Models based on the changing concentrations of calcite in the spring discharges have been considered based on the premise that there is a relationship between flow rate and water mineralistaion of a karst spring during a flood event. The variation in dissolution rates depends on the groundwater flow velocity through the conduit network and thus variations in dissolved carbonate concentrations at the spring are related to changes in flow velocity. This looks at the chemically based recession flow of the emptying karst system after the initial piston flow, which is the pressurised expulsion of all the pre-event existing water in the aquifer. An

empirical relationship has been noticed in this recession flow (Grasso and Jeannin, 2002) whereby the concentration variations at the discharge of a karstic system can be described by a negative power of the flow rate (Grasso *et al.*, 2003) as follows:

$$C = AQ^{-\alpha} = Ae^{-\alpha \ln(Q)} \qquad \text{Eqn. 2.19}$$

where, C is the solution concentration, A and α are empirical coefficients and Q is the flow rate.

A deterministic model was formulated based on calcite dissolution kinetics and hydraulics (Grasso *et al.*, 2003) and the physically based parameters compared to the empirical model parameters (A and α) to provide some physically based interpretation to them. Limestone dissolution in karstic conduits is a function of both chemical characteristics (the relationship between solution concentration and equilibrium) and hydraulic characteristics (water velocity). Hence, as discussed before, there is a drop in dissolution rate as the system approaches equilibrium. The deterministic model was developed on the basis of this dissolution rate occurring in the laminar layer of flow adjacent to the wall during turbulent flow conditions in the conduit. This model was trialled on a theoretical network of reservoirs and pipes to predict the concentration of Ca^{2+} at different discharges and velocities. These results were compared against the global empirical relationship model (Eqn. 2.19) and hence able to give some physical meaning to the empirical parameters (A and α) which proved a relationship between α and the conduit network dimensions. The model was then applied to 5 karst aquifers in the Jura Mountains to determine the degree of karstification and also correlated with the global empirical model parameters. An interesting result from the modelling process was that it suggested that the piston flow pushes some of the fissured matrix flow water into the conduit at the beginning of the flow peak (as well as the "old water" in the conduit expelled due to the pressure wave, as discussed previously).

The evolution and flow in a karstic aquifer was studied using a KARST model (Karstic Aquifer Simulation Tool) which starts as a 3-D network of conduits to represent fractures and porous rock matrix to represent fine fissures (Kaufmann, 2009). Fractures are enlarged with time by chemical dissolution which causes a dramatic increase in the hydraulic

conductivity of the aquifer with time and lowering of the water table down to almost the base level (steady state after 10 000 years was achieved but modelled over 50 000 years). The karst bedrock was also overlain by a landscape which evolves with time due to river erosion, denudation etc.

2.5.5.2 Contaminant transport modelling

Insight into karst modelling can also be gained from the modelling attempts at tracking pollutants through karstic aquifers. For example, dense non-aqueous phase liquid (DNAPLs) can easily be released into aquifers through sinkholes or sinking streams and the discharge of such liquids delayed depending on the transport mechanism, storm water recharge and storage sites within the karst aquifer. Interestingly a conceptual model is based on the transport of the DNAPL stored during storm flow pulses by the exceedance of thresholds in terms of the conduit stream power. (i.e. due to shear between liquid and water flowing over it) (Loop and White, 2001). Whilst the mechanism of transport and storage of DNAPL are not that relevant to this study, the model of the conduit flow (and hence evaluation of contaminant transport related to the flow regime) is of concern. In this context such transport includes: dissolution, transport on suspended sediment, bulk transport and transport within entrained bulk sediment (Vesper *et al.*, 2003). At low to moderate flows DNAPLs will be constantly flushed with fresh water and hence dissolution will take place across the liquid-liquid interface, predicted by mass transfer coefficients. Under flood flows the DNAPL may be dragged along the channel and then at even higher flows, entrained and transported in suspension as well as sediment, which could be calculated in terms of stream power under different conditions.

A linear systems approach has been used to model aqueous contaminant movement through karst aquifers (Hoke and Wicks, 1997). Using the lumped, time-invariant linear systems as described in Dreiss (1982), where the input is related to the output via a kernel function, instead of having flow as the input function, the mass of contaminant can be used. Such as study was made in Missouri after a nitrogen fertilizer pipeline broke above a karst aquifer. A linear kernel function for the flow path was derived by a fluorescent dye test. This function was then applied for the system to predict the breakthrough curve for

this point source of nitrogen contamination which compared closely to the actual sampled findings.

An overall methodology to assessing the vulnerability of carbonate aquifers has been developed at a European level (Daly *et al.*, 2002; Ravbar and Goldscheider, 2009). Such aquifers are especially vulnerable to various human impacts since the water can move rapidly through fissures, sinking streams provide direct entry points to the groundwater with little or no attenuation of contaminants and the soil cover is often thin or absent. The approach is based upon a series of factors: P factor (rainfall), C factor (concentration of flow) O factor (overlying layers, subsoil etc) and K factor (karst network development) as shown schematically in Figure 2.23.

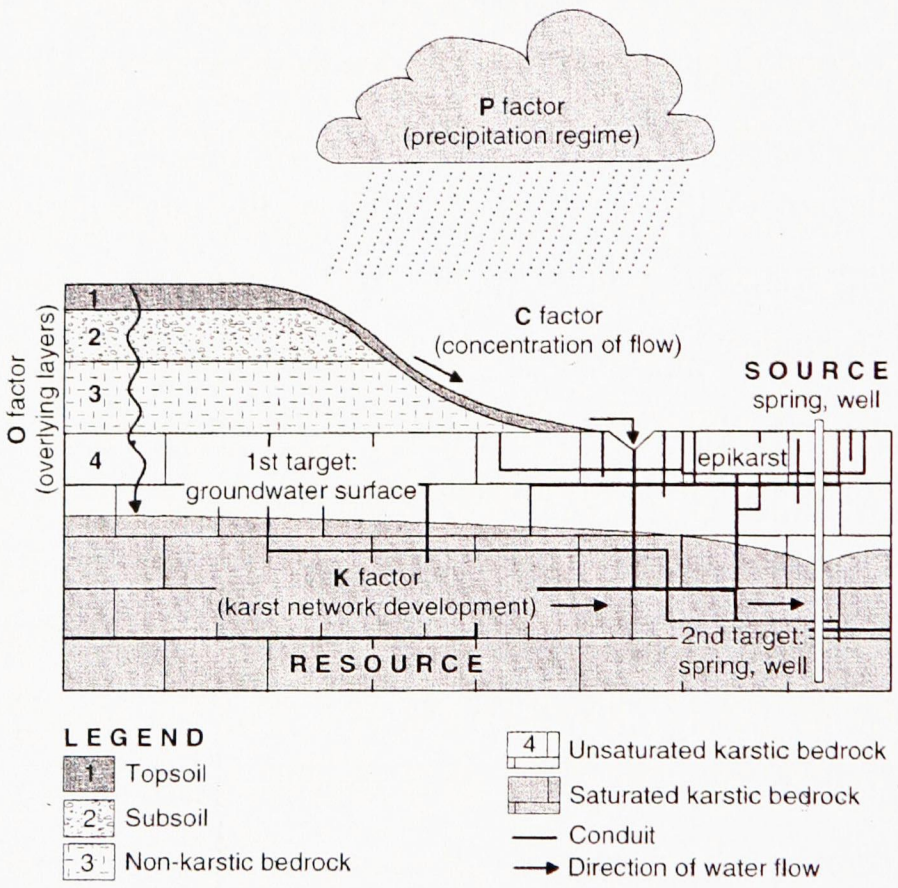


Figure 2.23 Diagrammatic cross-section showing factors which input into intrinsic vulnerability maps (Daly *et al.*, 2002).

2.5.5.3 Sediment transport modelling

So called "turbidigraph" separation (i.e. the turbidity observed at a karstic spring) has been used to determine more about the nature of flow and structure of karstic aquifers (Massei *et al.*, 2003). The turbidity measured at a karstic spring can be considered to be made up of

part direct transfer of suspended particulates and part resuspension of particulate material previously deposited in the conduits. The storm component of the spring hydrograph was compared to the particle flux breakthrough curves in terms of transfer time in order to distinguish between the intrakarstic resuspension and the allochthonous, direct transfer material. The relationship between resuspended element and flows through the aquifer were then compared to infer how the resuspension of deposited particles occurs in response to storm derived water flux. This seemed to be non-linear relationship and was caused by three distinct factors: the initial pressure transfer of the water; the rising head over the whole system pushing out the old water; and then finally resuspension caused by the actual fast flow rate coming through from the rain event. Further work by these researchers (Massei *et al.*, 2006) has examined turbidity dynamics of karst aquifers using correlation, spectral and wavelet analyses as discussed earlier in Section 2.4.4. Interestingly, the wavelet analysis highlighted a strong relationship between the rainfall and turbidity which could not be detected from the correlation or spectral analyses.

2.5.5.4 Neural networks

Neural networks have been applied to karstic aquifers (see Figure 2.24 for architecture) (Johannet *et al.*, 1994). The network will "learn" by a backpropagation algorithm to minimise the difference between the spring discharge and model output.

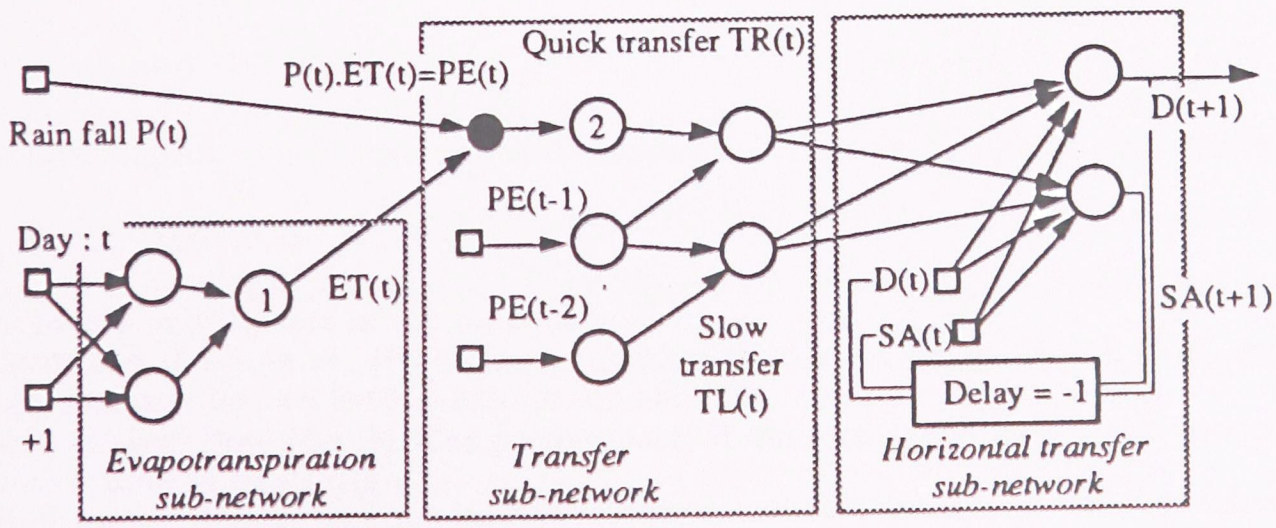


Figure 2.24 Architecture of the global network for modelling a karstic aquifer (Johannet *et al.*, 1994).

In another study in Normandy, France a model based upon an artificial neural network was developed to predict turbid spikes associated with floods from the aquifer based on water level in a well and precipitation (Beaudeau *et al.*, 2001). A multi-layered feed forward architecture was employed based on a hierarchy of two iterative processes: at the upper level, the Simplex algorithm was performed to optimise the runoff parameters which were the trained up at each step of the main loop of the neural network.

3 BACKGROUND AND AREA DESCRIPTION

3.1 Introduction

Carboniferous limestone is the outcrop or near outcrop rock across over 50% of Ireland (Drew, 2008). Most of the purest limestones lies to the west of the River Shannon and have developed full karstic landforms and drainage compared to the more impure limestones to the east and in the Midlands. Ireland is unusual in that more than 75% of its karst is lowland (i.e. less than 100 m above sea level) in comparison to the remainder of Europe where most karst terrain is mountain or plateau (Drew, 2002). Hence, a distinctive feature of such lowland karst is the considerable degree of interaction between surface and groundwater, whereby water is exchanged between the two systems via losing and gaining rivers, via swallow holes and springs and via turloughs often fed by *estavelles* which are bi-directional openings that may function as springs or swallow holes depending on hydrologic conditions. In addition to being the primary aquifer in the region, the lowland karst underlies some of the most productive agricultural land (as well as a few major centres of population). The Gort-Ardrahan area of south Galway, the subject area of this research, is bounded to the east by the Slieve Aughty mountains and by the edge of the Burren to the west. The 500 km^2 catchment drains north-west from the mountains across the Gort lowlands to the sea in Galway Bay as shown in Figure 3.1.

3.2 Geology and Hydrogeology

The Slieve Aughty mountains to the south-east are of relatively low permeability sandstones and mudstones of Devonian age (Old Red Sandstone). The lowlands of higher permeability Carboniferous limestone (see Figure 3.2) are intensively karstified in places, as shown by the number of karst features on the GSI karst database shown in Figure A.5 in Appendix A. The stratigraphy of the region has been described as a thick succession of fairly pure limestones of Early Carboniferous age, sandwiched between two thick clastic sequences of Devonian (mainly) and late Carboniferous age respectively (Simms, 2003). Three geological cross-sections through the area are shown in Figures 3.3, 3.4 and 3.5.

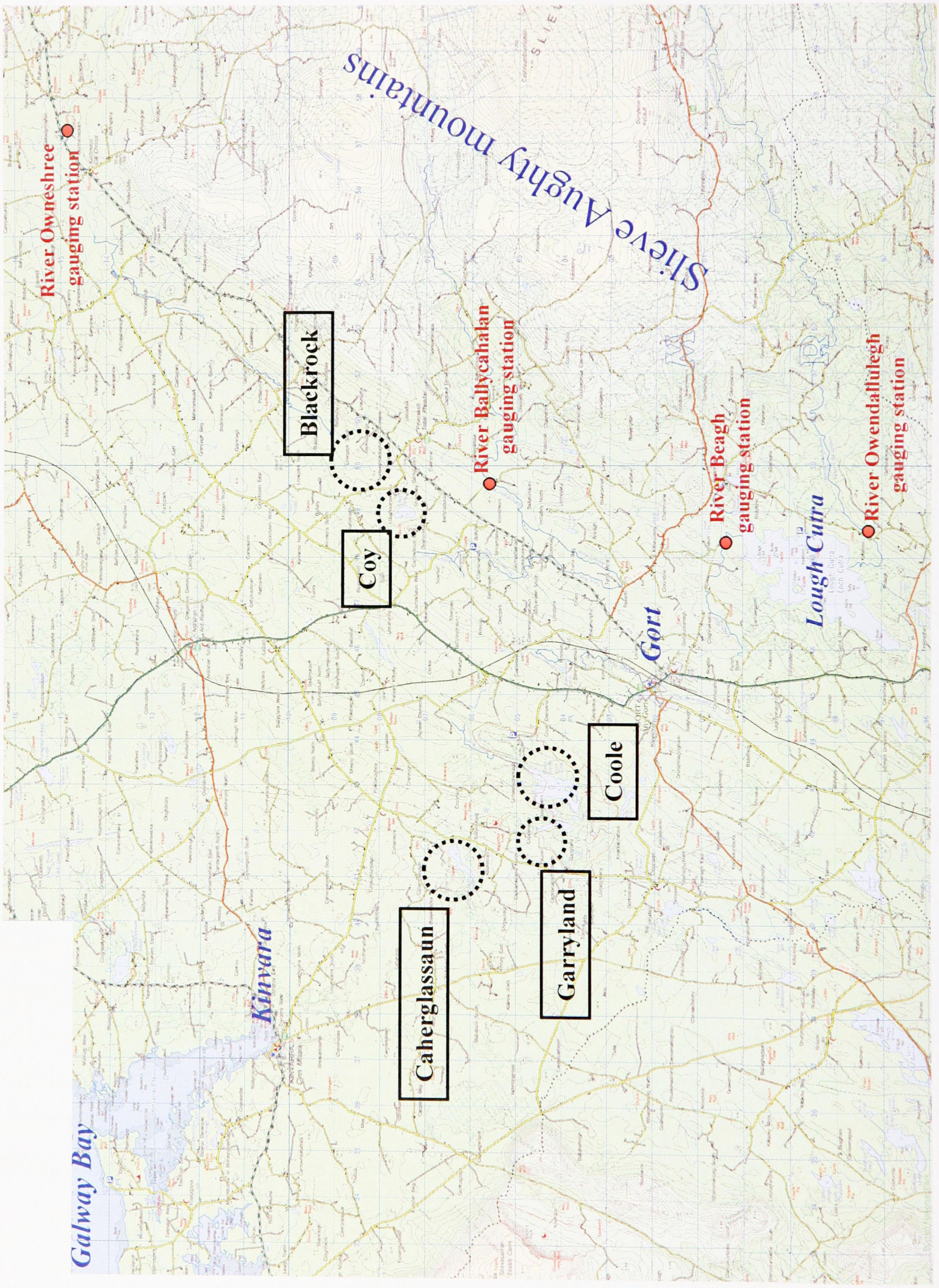


Figure 3.1 Map of Gort lowlands showing the location of the 5 turloughs investigated in this research.

In the east of the region, near the Slieve Aughty Mountains, the succession has been folded into a broad anticline across which limestone and overlaying clastics have been stripped to reveal older clastics beneath. To the west, the succession is less disturbed and has been tilted only gently to the south. To the north, the Upper Carboniferous clastics have been stripped away and in the south, the limestone dips beneath the surviving clastic cover.

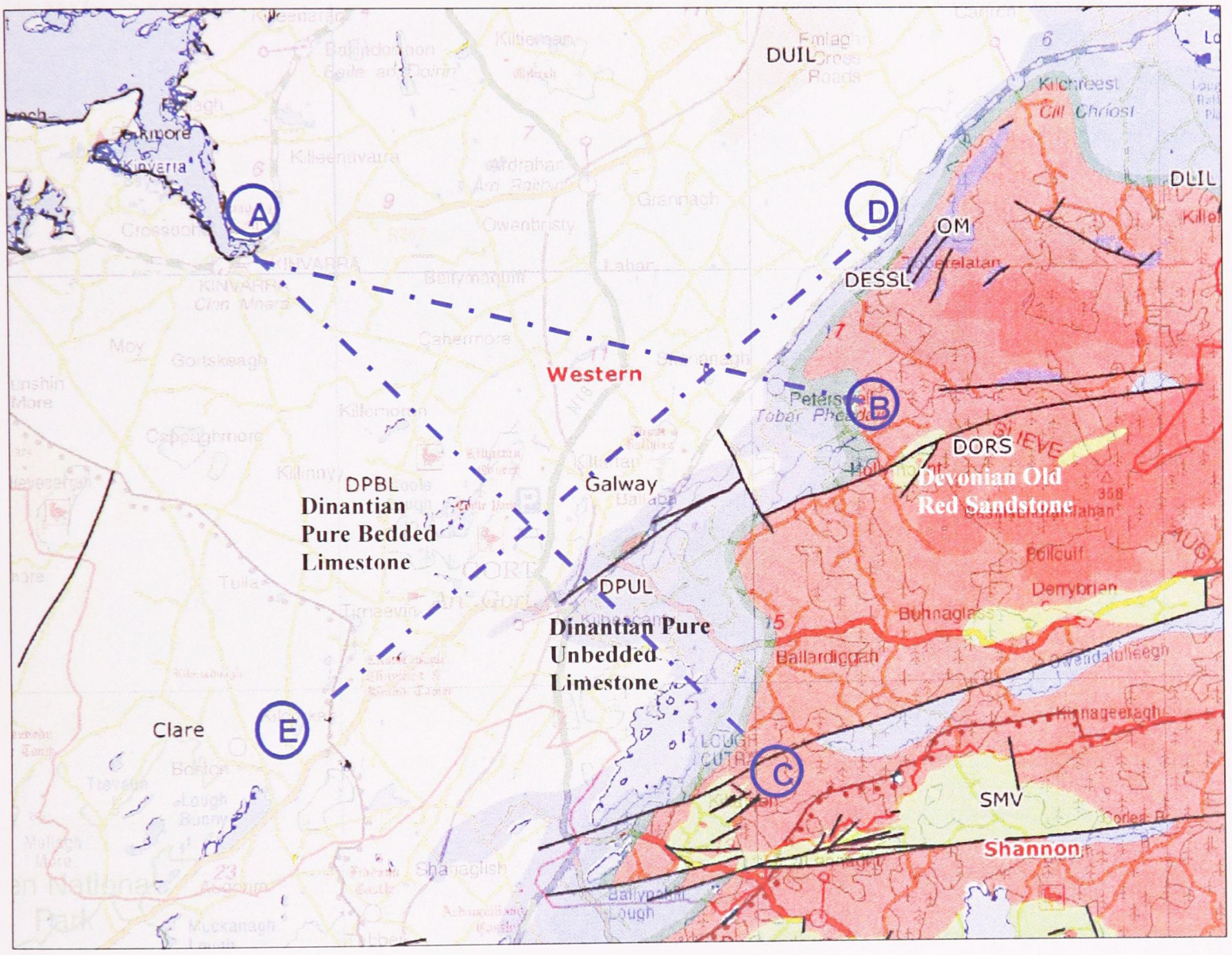
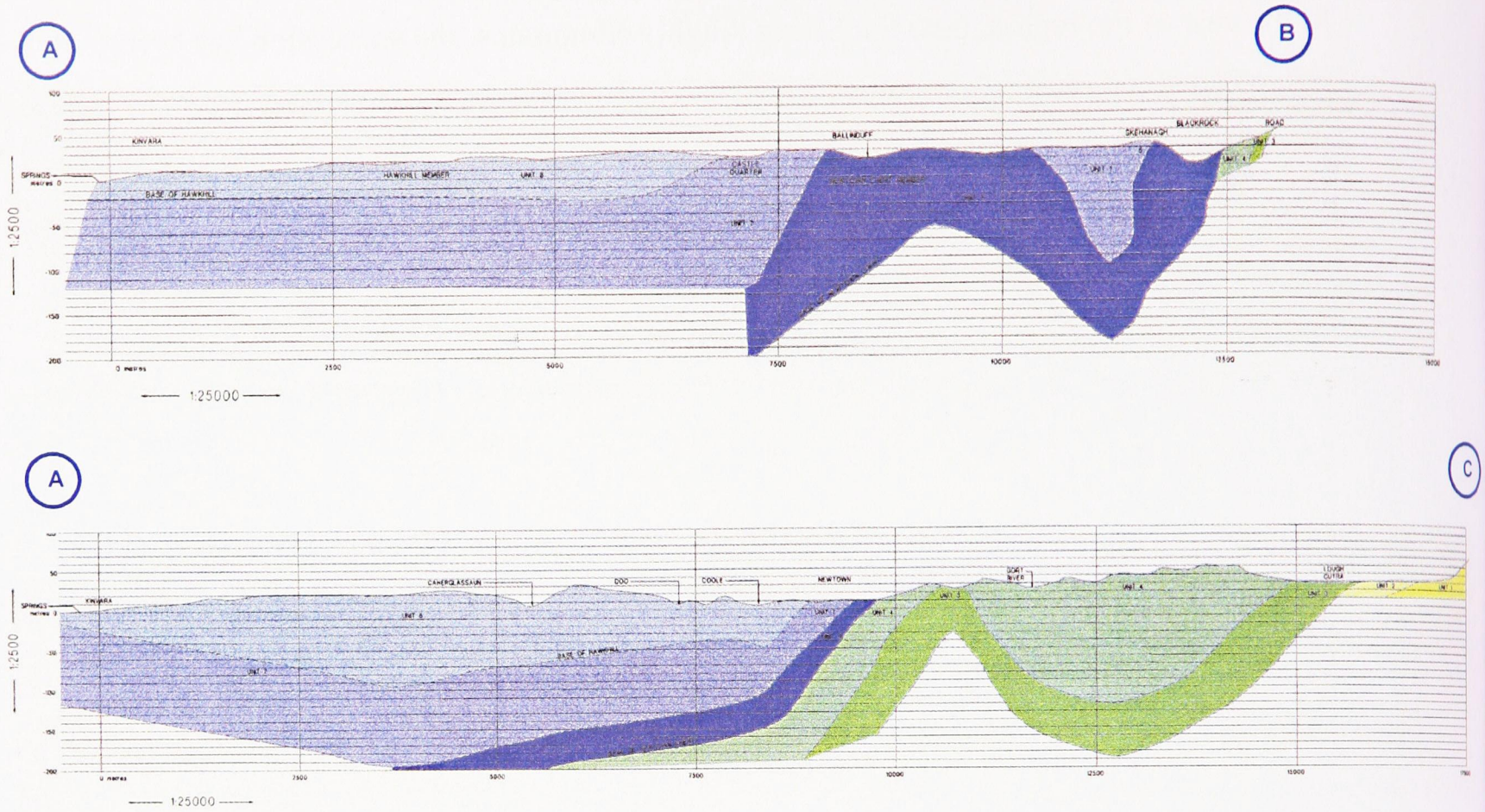


Figure 3.2 Bedrock geology and faults of the Gort lowlands (GSI, 2009).

DPBL (Dinantian Pure Bedded Limestone); DPUL (Dinantian Pure Unbedded Limestone); DORS (Devonian Old Red Sandstone); DUIL (Dinantian Upper Impure Limestone); OM (Ordovician Metasediments); SMV (Silurian Metasediments & Volcanics); DESSL (Dinantian Early Sandstones, Shales & Limestone).



LEGEND		
FORMATION	MAP UNIT	GRAPHIC LOG
BURREN LIMESTONE FORMATION	9	
	8	
TUBBER LIMESTONE FORMATION	7	
	5	
	4	
WAULSORTIAN LIMESTONE Fm	3	
BALLYMARTIN LIMESTONE Fm BALLYSTEEN LIMESTONE Fm	2	
OLD RED SANDSTONE	1	

Figure 3.3 Geological cross-sections through the Gort lowlands (as shown on plan in Figure 3.2).

The karst aquifer in the Gort lowlands is defined as Regionally Important with High to Extreme vulnerability as shown in Figures A.2 and A.3 in Appendix A. It is fed by several sinking streams draining from Devonian sandstones on the Slieve Aughty uplands, the three main streams being, the Owenshree, the Ballycahalan (or Boleyneedonish) and the Owendallulaegh (or Derrywee). The lowland area thus contains major karst conduits associated with these chemically aggressive water inputs (Skeffington *et al.*, 2006); streams frequently disappear into underground fissures and conduits and then reappear again in surface reaches or turloughs (glacially formed depressions). It has been concluded in the past that all of the drainage eventually converges to meet at Lough Coole to the north-west of Gort, as detailed later. From here the drainage takes the flows underground to the north–west to the sea at Kinvarra reappearing once en route at the tidally affected Caherglassaun. The rivers from the Slieve Aughty mountains have relatively low dissolved solids, low alkalinity and high iron concentrations. The Kilchreest river periodically fills Blackrock and Coy turloughs, whilst the Ballycahalan and Owendallulleagh rivers flow underground to the Coole basin. Figure 3.4 shows the previous tracer studies that have been done although caution must be taken when interpreting such lines for such a system as they only link the entry and sampled exit points, which did not necessarily include intermediate points between.

The major intertidal springs on the south Galway bay coast (Ballyvaughan, Bellharbour, Corranroo and Kinvarra) are all located close to the head of funnel-shaped sea inlets. These may have partly resulted from glacial erosion from the last ice advance but may also reveal evidence that the preferential solution of the limestone has taken place in the dominant north-south joints in the zone where fresh and saline waters mix to produce subsaturated waters (Drew, 1990). This would lead to accelerated enlargement of the fissures and subsequent collapse of overlying strata causing headwards migration of the spring – i.e. the narrow bays seen today.

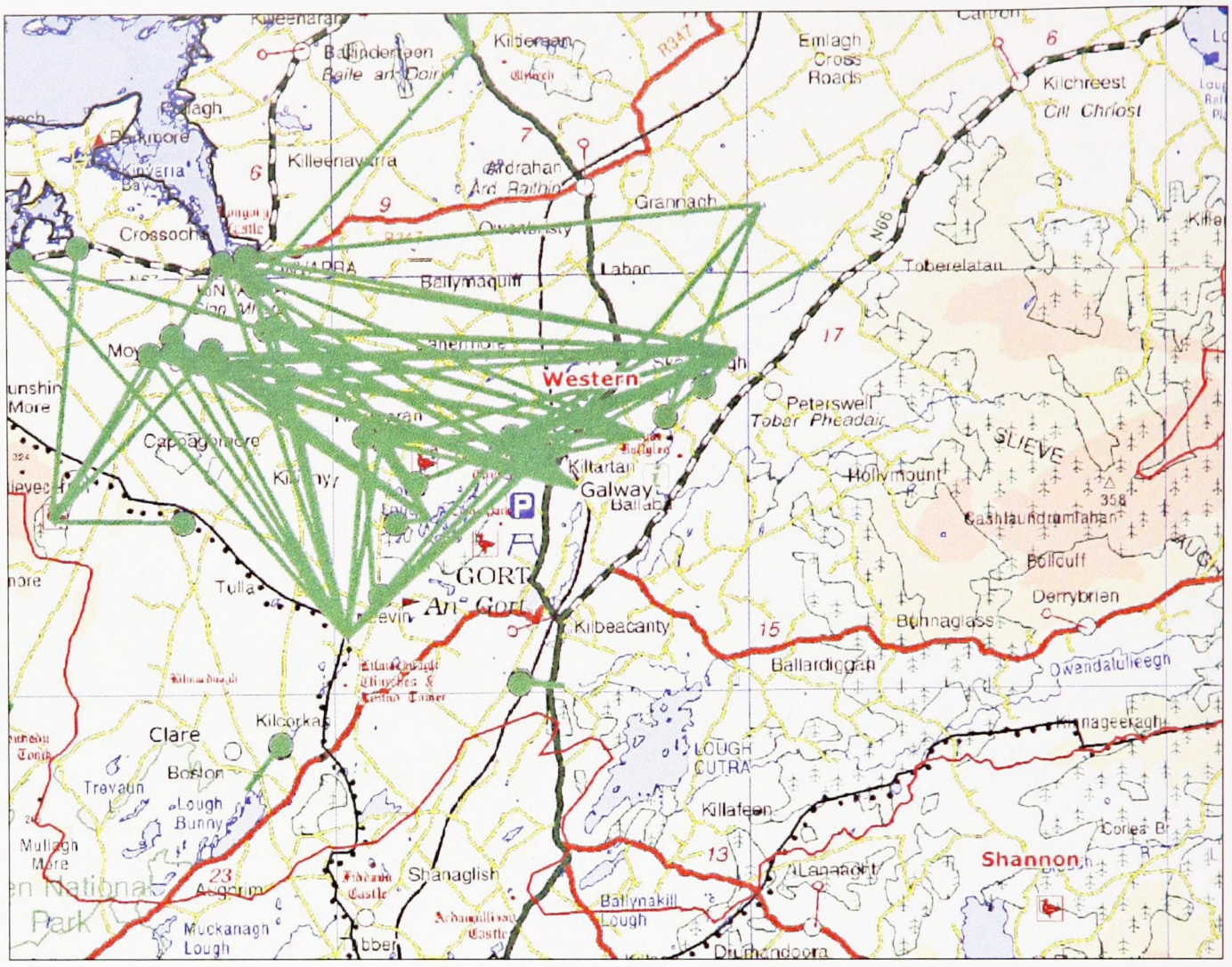


Figure 3.4 Karst tracer lines in the Gort lowland area (GSI, 2009).

The karstification in the area is not homogeneous from a spatial perspective but is complex, evolving under lithostratigraphic control whereby cherty beds within the limestone have exerted a strong influence (Johnston and Peach, 1999). Folding and faulting, associated with the north-northwest trending Fergus shear zone have also influenced the development of the karst. There seems to be at least two levels of ages of karstification: a shallow epikarst (associated with the last glaciation) which is often less than 15m in depth and at least one level of deeper palaeokarst occuring up to 50m below sea level. It has been conjectured that many karstic drainage systems on the lowlands (which are thought to have originally formed during the karstification of the Tertiary period) were blocked and rendered inoperative by sediment infilling due to glacial and fluvioglacial deposition and that present day groundwater flow systems have developed in immature fissure or conduit systems of the Holocene age, or in reactivated ancient conduits from which sediment has been eroded (or a mixture of both) (Drew and Daly, 1993). Most of the karst development is often less than 15m in depth with very variable fissures from a

few mm in width to several metres as found in conduits and caves. The depression on the surface acts as a focus for collection of rainfall as well as an emergent route for subsurface flows in the fissures. The larger depressions, the turloughs, often flood in winter and store temporarily huge volumes of water, forming a key component in the hydrogeological regime. In summer, however, these turloughs normally dry out. Hence, it seems that the turloughs behave as surge tanks in the system, attenuating flow in the subterranean conduit network (Johnston and Peach, 1999). Water levels have been seen to vary very quickly in response to a hydrological event: such large volumes of water moving over a short period of time are highly unlikely to have come from an epikarst fracture system. Hydraulic gradients in the lowland aquifer range have been estimated between 0.001 and 0.01 with flow rates determined from tracing studies ranging from 5 to 250 m/h (Drew, 2008). There are also a few permanent lakes (particularly Lough Cutra) and several bog areas across the Slieve Aughty mountains which act as buffers on the overall drainage system.

The superficial deposits in the area (see Figure A.4) are inferred to play a relatively minor role in the overall hydrological response of the catchment but could be locally important in providing groundwater storage and slowing the runoff rate. They could also act to confine the aquifer underneath (depending on nature of deposit) or, at the other extreme, function as an intergranular aquifer with high storage, feeding water into the highly transmissive limestone aquifer beneath (Drew, 2008). Most of the limestone outcrop (pavements etc) is exposed west of the northeast-southwest line passing through Coole. East of this line are a few drumlins and modest thickness of sandy till along the sandstone/limestone contact. In the west, along the edge of the Burren, drilling has shown evidence of a former glacial outwash channel with an excess of 40 m thickness of sands and gravels.

3.3 Turloughs

3.3.1 Turlough hydrology and hydrogeology

Turloughs (from the Irish *tuar loch*, dry lake) are described by the Working Group on Groundwater (EPA, 2004) as topographic depressions in karst, which are intermittently flooded on an annual cycle via groundwater sources and have substrate and/or ecological communities characteristic of wetlands. The flooding in the turlough basin is due to

insufficient capacity of the underground karst flow system following excessive precipitation events, causing the conduit-type network to surcharge. Turloughs can fill and empty relatively quickly (a few weeks) via swallow holes or estavelles. As such they can also act as a buffered source of point recharge to the aquifer (Drew, 2008). Turloughs exist in Ireland due to the combination of high precipitation (relative to evapotranspiration) and low-lying karst limestone which is not widely found elsewhere (Drew, 1990). They mainly occur on the west coast on the Dinantian pure bedded limestones as shown by their distribution in Figure 3.5. However, similar lakes have been reported in Wales, Catalonia, Eastern Canada and Slovenia (Goodwillie and Reynolds, 2003; Skeffington and Scott, 2008). Equally, such temporary lakes in karst can form in areas where there are enclosed depressions close to the hydrological base level which receive periods of high rainfall, known as *poljes*, as detailed, for example, in the Dinaric karst in Croatia (Bonacci, 2004) and southern Spain (López-Chicano *et al.*, 2002).

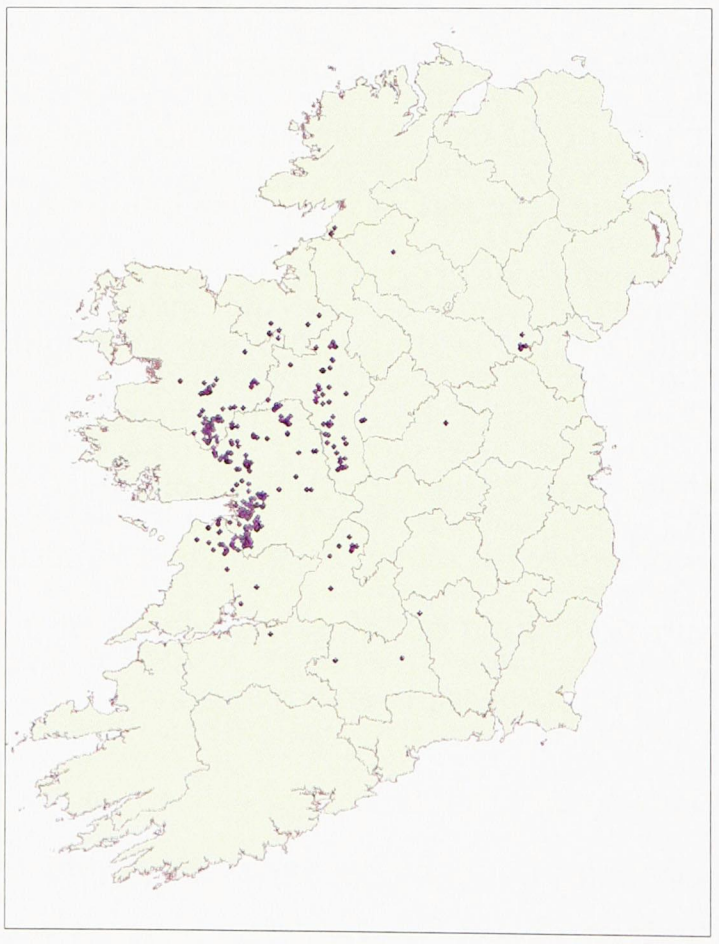


Figure 3.5 Distribution of 304 turloughs on GSI database.

Turloughs often have an impermeable floor of lake clay with one or several obvious connections to the groundwater system which may occur way above the lowest point in the

basin. The underground water carries dissolved limestone in the form of calcium bicarbonate and when it appears above ground in a turlough some of the lime may be precipitated. This is predominantly a physical process but may also be mediated by planktonic organisms (Coxon, 1994a). In long lasting pools marl accumulates providing an effective impermeable barrier to drainage. However, there is evidence (sediment cores) that the hydrology of turloughs can change naturally over time where white marl (indicating open water conditions) is overlain by peat (showing colonization of the water body by plants etc) which is then overlain again by marl, indicating reflooding. Such shifts have been attributed to changes in the drainage system and sediments as swallow holes and fissures have become blocked or opened. A survey of the deposits in the turloughs of interest in this research project revealed that Blackrock and Coole had no marl deposits whilst Coy, Garryland and Caherglassaun did contain significant marl deposits (Coxon, 1994b). The existence of marl in turloughs probably indicates that these were permanent lakes at sometime in the past (possibly Late-glacial to early Holocene times); the cessation of marl deposition being when the seasonal flooding regime occurred. This raises the tantalizing theory that Blackrock and Coole have always operated as turloughs since these depressions first started to become inundated. As Blackrock is at the top of the system it is perhaps not so surprising that it has always drained on an annual basis, however Coole is closer to sea level and (as will be seen later) is normally fairly slow to empty. Hence, this might indicate that in the past there was an easier route to the sea which, by implication, was not hydraulically connected to Caherglassaun at the time. One hypothesis that could be drawn is that some collapse structure may have subsequently fully or partially blocked this route forcing a new direction for the major conduit which brought Caherglassaun into the network. Indeed, collapse structures near Caherglassaun point to the fact that it was originally created as a cave that collapsed with local hearsay telling that the most recent collapse was due to Lisbon earthquake in 1750s because of a tidal wave (Goodwillie and Reynolds, 2003).

3.3.2 Turlough ecology

Turloughs provide a habitat for many protected flora and fauna species and are designated a Priority Habitat in Annex 1 of the EU Habitats Directive (92/43/EEC) (EEC, 1992).

Indeed, many turloughs have been designated as Special Areas of Conservation (SACs). Under the Water Framework Directive (WFD) (EC, 2000) turloughs are designated as Groundwater Dependent Terrestrial Ecosystems (GWDTE). Hydrology is the primary driver of these unique ecosystems, and a better understanding of the flooding regime is therefore required for their future sustainability and conservation.

There have been several attempts to classify turloughs in relation to their flooding regime, geomorphology and trophic status (Tynan *et al.*, 2007) but it is also apparent that each turlough has its own unique hydrological features which in turn have a bearing on substrate, vegetation type and invertebrate communities (Skeffington *et al.*, 2006). A large interdisciplinary research project is currently being undertaken by Trinity College Dublin funded by the National Parks and Wildlife Service (NPWS) entitled, *Assessing the Conservation Status of Turloughs*, due for completion in 2010. This has targeted 22 turloughs (four of which are featured in this research) and is looking for linkages between the hydrology, turlough soils, vegetation, invertebrates, water quality and land management within each turlough catchment area.

A short section on the ecology of turloughs is presented since it is anticipated that one of the main uses of the hydrological model developed in this research will be to tie in with studies on plant species and invertebrates in relation to degree of inundation. The other main use of such a model would be to predict flooding events, more of which is discussed in Section 3.4.

Flora

Since not many plants are adapted to such unpredictable flooding, turloughs tend to have a regular zonation of vegetation for the relatively low number of species. The factors that lead to the differential spread of these species have received extensive study and are: inundation, nutrients and soil, grazing and other threats. Inundation (obviously directly linked to the hydrogeology of the area) is related to the depth and the period of the flooding every year. The species can be divided into those that can withstand flooding in

situ (amphibious species) and those that are able to colonise the land quickly after the flood waters have retreated.

The period of flooding appears to be particularly relevant at the base of the turlough where the inundation lasts longest. Some correlations were found for example as part of the OPW study in the Gort lowland karst area (Jennings O'Donovan / Southern Water Global, 1997) for the two flood years 1995 and 1997. The inundation affects the plants since gaseous interchange is interrupted and those that survive must have some special adaptation to survive. For example, annual plants may change their oxygen demand by seed dormancy whilst perennials may have to change from aerobic to anaerobic respiration, withstand root death or develop aerenchyma to allow oxygen to get to the roots. Many turlough species have rhizomes on the surface to compensate for root die off (e.g. *Potentilla anserina*, *Agrostis stolonifera*, *Trifolium repens*). Fully aquatic plants such as reeds *Phragmites australis* and *Schoenoplectus lacustris* have a direct connection to the atmosphere.

A few species will occur from the edge of the turlough to the base such as bent grass (*Agrostis stolonifera*), silverweed (*Potentilla anserina*), sedge (*Carex panacea*) and the buttercup (*Ranunculus repens*). The less tolerant species are restricted to specific zones which are controlled by depth within the basin (e.g. trees), nutritional quality of the water and /or substrate (sedges and grasses) or by the presence of non-vegetated areas (annuals) (Goodwillie and Reynolds, 2003). However, these patterns may be concealed by anthropogenic interference, for example, intensive fertilisation within the turloughs.

The presence of holly (*Ilex aquifolium*) can often be used as a rough guide to the top water level of a turlough or, if there are rocks, a better indicator is the black moss (*Cinclidotus fontinaloides*) – hence the eponymous "Blackrock" turlough. For example, Coxon (1987) carried out a study on the depth of flooding in 60 turloughs by taking the upper limit to be indicated by the black moss which revealed that depths typically varied between 0.5 to 6 m with a median depth of 1.5 m. It also showed that most turloughs contain an upper and lower zone with the upper zone with rock surfaces dominated by *Cinclidotus* and the lower zone dominated by willow moss (*Fontinalis antipyretica*). In 35% of the 60 sites studied,

the *Cinclidotus* was found in the base of the turlough indicative of shorter flood duration conditions, where the turlough fills and drains more frequently.

The upper reaches of the turlough basins are often surrounded by woodland (e.g. Coy, Garryland and Coole) and the woody plants die out as one moves down into the upper part of the turlough, e.g. from buckthorn, *Rhamus catahrtica*, blackthorn, *Prunus spinosa* and shrubby cinquefoil, *Potentilla fructicosa* to alder buckthorn, *Frangula alnus* being the last to persist. Tree roots are particularly susceptible to oxygen depletion meaning that summer growth may be delayed in years where the flooding has been higher than normal.
Herbaceous vegetation can be particularly affected in spring if the flooding persists. The leaves will start to grow underwater, producing narrow leaves (*Phalaris arundinacea*) or more dissected leaves (*Ranunculus repens*) for plants growing in more flooded regions compared to the same species found in non-flooded locations. This is thought to result in a higher photosynthetic capacity required when submerged (Lynn, and Waldren, 2001).

Below the woody plants large grasses (e.g. *Festuca arundinacea, Deschampsia caespitosa and Phalaris arundinacea*) and tall herbs such as meadowsweet (*Filipendula ulmaria*) occupy the next zone. Below this the vegetation tends to split into two distinct types depending on the availability of nutrients. On the nutrient rich sites plantain (*Plantago lanceolata*), *Carex nigra* and *Potentilla anserina* will be found whilst on nutrient poor sites, sedge stands of *Carex hostiana*, *Carex panacea* and *Mollina caerulea* are more common. At this level species such as northern bedstraw (*Galium boreale*), adder's tongue (*Ophioglossum vulgatum*) and the violets (*Viola canina*) will also be found. Finally, in the base of the turlough where conditions are most frequently inundated, there is usually sedge (*Carex nigra*) with rushes (*Juncus articulatus*, *Eleocharis palustris*), marsh marigold (*Caltha palustris*) etc.

Dissolved nutrients are brought down into the turlough every year which must get trapped in the basin to some extent but its affect on plant communities is not well understood (Otte, 2003). For example, the western and southern turloughs in the region are most clearly fed purely from karstic groundwater and can be the most productive with an abundant, dense

growth of filamentous algae, which bleach white on drying (known as "algal paper") evident (for example, Hawkhill turlough).

It should be noted that most turloughs have been extensively grazed which totally alters the vegetation balance that might be expected in a pristine turlough. For example, the larger species are removed which tends to shade smaller species which can then proliferate. In addition it is not clear what the relative contribution of in-turlough nutrient enrichment due to manure from grazing animals is – potentially very high for certain hydraulic configurations.

Fauna

The same features which contribute to the development of different floral zonation, as discussed above, also promote different fauna according to their sensitivities to depth, temperature, frequency and pattern of flooding. Hence, characteristic fauna tends to be short-lived, adapted to drought and herbivorous or detritivorous since the breakdown of exposed aquatic plants provides further detritus to feed on. In general invertebrate communities are at their richest in the concentrated conditions: when turlough levels decrease to a shallow residual pool, the faunal diversity appears to be controlled mainly by seasonal dry periods (normally in summer). However, the less common combination of low winter levels and frost has also been shown to be a controlling factor in macrophyte and invertebrate communities. Recent research into macroinvertebrates in turloughs showed that biodiversity and community structure varied monthly and inter-annually with permanent residents dominating during the start of the hydrocycle with an increase in ephemeral taxa over time (Porst *et al.*, 2009). Disturbance was shown to be an important factor in community structure with more highly fluctuating hydrological regimes generally supporting lower faunal diversity. The influence of disturbance, however, generally decreased with time leading to a stabilisation of communities.

Most invertebrate species in turloughs, however, are found elsewhere but there are two rare crustaceans, *Tanymastix stagnalis* and *Eurycerus gacialis* (remnants of earlier ice ages) which are found in turloughs since the temporary water bodies preclude fish populations

which would otherwise prey on the crustaceans' unprotected nature and large sizes. The localised environment around the sink holes of turloughs may provide a refuge for aquatic organisms such as *Gasterosteus aculeatus*, *Gammarus duebeni celticus* or *Polcelis nigra* (Reynolds, 1996) since the water temperature does not vary much (around 7-10˚C all year). In the turlough basin bivalve molluscs such as *Pisidium* may burrow as will many other invertebrates in order to survive brief dry periods due to the changing water levels. Warm weather and persistent low water levels may result in a dense growth of filamentous algae, i.e. algal paper.

Many other faunal components from frogs and newts to beetles, mayflies and dipterans are amphibious or terrestrial during the dry period. The highest predator in such ephemeral systems tends to be the newt *Triturus vulgaris* which colonises field ponds and congregated over the breeding season in the water bodies. Fish are not normally present unless they have been washed into a turlough from surface waters (Reynolds and Marnell, 1999).

Birds

Few studies have been carried out on birds but an Internationally Important population of Whooper swans and Nationally Important population of Bewick's Swans were found to be wintering on the Lough Coole system (Heery and Madden, 1997). In addition to this a wide diversity of birds can be found such as dabbling duck, diving duck and waders (lapwing, snipe, common sandpiper, whimbrel, redshank, and ringed plover). The wintering birds clearly seemed to favour the river fed turlough with their large throughput of water (and large fluctuations). There appeared to be a strong link to the movement of birds between turloughs and water heights. The birds typically moved at a frequency in terms of hours (as opposed to days which is more common for wintering birds trying to conserve energy and finding safe places to roost). Hence, it seems that the birds favoured turloughs which were at low to moderate rather than moderate to higher levels since there are more plentiful marginal feeding areas. Ideal conditions for breeding waders would be for the turloughs to dry out gradually through spring and early summer which promotes

suitable nesting sites. The smaller the turlough, the more unpredictable the water levels and thus they are least likely to support such populations.

3.3.3 Pressures and impacts on turloughs as GWDTEs

A study was recently carried out which reviewed all previous research on turloughs in Ireland with the objective to produce a risk assessment framework for these GWDTEs and to develop a methodology for characterising these karstic groundwater bodies (Tynan *et al.*, 2007). 128 turlough sites were first collated in an inventory almost all of which were located on Dinantian pure bedded limestone. In summary, the work found that they were hydrological parameters (frequency-duration curve gradients and recession constants) that could be related to ecological indicators, although it was difficult to be too generic as every turlough had unique inputs due to different land-use practices on the catchment. For example, an attempt was made to relate vegetation to factors such as flood duration whereby exceedance curves for different turloughs were compared against vegetation mapping. This suggested (albeit on a limited number of turloughs) that four broad groups of species could be identified: communities that appeared to be constrained by a maximum flooding duration limit; communities that appeared to be constrained by a minimum flooding duration limit; communities which occur across a wide range of flooding conditions; and a specific community occurring on flooded limestone pavement. In another analysis flood recessions and vegetation wetness indices were also compared. Stage recession constants for the falling limb of the turlough hydrographs (in terms of water levels) were calculated and plotted against vegetation indices which only found a low degree of correlation but did show that as the rate of emptying decreased that the vegetation communities were more dominated by wet vegetation categories. The influence of a marl substrate in some of the turloughs was found to have a distinct effect on vegetation patterns and rate of drainage. A relationship between turlough trophic status and karstic flow system was also investigated. Karstic flow was broadly divided into shallow epikarst versus conduit or fracture/conduit dominated karstic flow systems whilst trophic status was derived from Ellenberg Scores. This showed that the more conduit flow dominated the turlough the higher the trophic status, however this simple pattern was

greatly complicated by other impacts such as riverine inputs and significant anthropogenic impacts.

More recent work on 22 turloughs in Galway, Mayo and Roscommon as part of the ongoing NPWS research project showed that the turloughs in the Gort lowlands seem to be different in terms of nutrient relationships between phosphorus and chlorophyll A; they showed high nutrient levels but relatively low chlorophyll compared to other turloughs monitored which showed the more usual linear relationship between the two parameters (Pereira *et al.*, 2009). This has provisionally been attributed to the fact that they are fed by allogenic (non-limestone) water from the Slieve Aughty hills and lie along a major conduit system whereas other turloughs are though to be fed by autogenic, diffuse recharge. A couple of reasons postulated as to why there is relatively low algal growth despite the high phosphorus concentrations is that the highly coloured peaty waters may suppress light (and hence photosynthesis) and/or that the turloughs experience rapid flushing rate – as will be investigated later in this thesis.

3.4 Previous Studies in the Gort Lowlands

An extensive investigation of the Gort lowland region was carried out under the Gort Flood Study which was set up after the major flooding events during the winters of 1989-90, 1991, 1994 and 1995, the last being the most severe. This project included drilling, surface geophysics, geological and topographic modelling and the main output of the work was the hydrological model which was then used to model various engineering options to alleviate the flooding. However, the concept of a minimum level (Ecological Control level) to which turloughs were allowed to rise in order to protect their unique ecology was also incorporated. Engineering strategies included: improving the facility for water to get from Caherglassaun to the coast; holding back water upstream of the major flooded areas; and diverting water upstream of the major flooded areas from the principal water courses (McCarthy, 2002) – none of which incidentally, have been undertaken to date.

3.4.1 Field work

Tracing studies

Tracing studies were undertaken mainly to establish point-to-point flow routes using a variety of tracers such as dyes (Leucophor, Rhodamine WT and Fluorescein) salt and bacteriophages, the results of which are included in Figure 3.3. Tracing experiments were carried out at 5 inputs simultaneously to indicate flow paths under the same stage conditions, with the premise that higher level conduits systems might come into operation at higher depths. The flow tracing also revealed that the velocities could be very high and increase with stage. Mean flow rates were calculated to be around 4-5 m^3/s but up to 15 m^3/s in winter with flow velocities ranging from 60-1000 m/h (most around 200 m/h) in the vicinity of Lough Coole. Tracer breakthrough curves conducted between Gort and the springs at Kinvarra using bacteriophages (types T7, Psf2, H6/1, H40/1 and H4/4) with intermediate samples taken at known deep conduits, shallow epikarst sites and deeper borehole locations revealed the existence of at least three groundwater flow regimes of which the conduit system was clearly dominant (Drew *et al.*, 1997). The conduit system exhibited rapid times to peak concentration at the Kinvarra spring and equally rapid falloff (decay) showing plug flow conditions. However, there also appeared to be a shallow flow system probably at depths 2 – 5 m in the epikarstic layer as revealed from a rapid initial rise in the tracer but prolonged tail. Equally, there was some evidence of a deeper flow system (independent of the major conduits) which exhibited much longer response characteristics which may be due to the deep cave systems behind Kinvarra formed during older periods of karstification.

Other findings from the tracer studies showed that there is a direct route from Ballylee / Owenshree into the main conduit system with some evidence of flow passing through Coole and Caherglassaun. The study also indicated that only water from the Gort River seems to flow wholly through Coole, other inputs are partial only. The groundwater catchment boundaries for the system were also estimated from the following results:

- Kinvarra east spring seems to derive its flow from separate sources to those feeding the central and west springs.

- Corranroo, particularly Corranroo West, is the western limit of the conduit system and also takes water from the Burren.
- The south-western area drains south to the Fergus River
- The north-eastern Burren plateau including Slieve Carran drains to Corranroo
- Tullanafrankagh, a turlough 9 km to the north of the Blackrock-Coy line, drains to the Dunkellin river (further north again) and so does not end up in the same system.

Hydrometric measurements

The water level dynamics in turloughs were measured, a process that has continued to date and forms the main data for this thesis. In general, the level data showed a rapid response to indirect recharge inputs from the Slieve Aughty mountains and also produced very similar shaped curves. Blackrock and Lough Coy were the first to respond to recharge events closely followed by Coole, Garryland and Caherglassaun. During periods of recession, Coole and Garryland dropped more quickly, suggesting that they are more directly in hydraulic connection to Caherglassaun and the main cave system.

Borehole water level monitoring

Water levels in 50 boreholes were monitored to establish regional flow gradients and directions and the measurement of water levels in caves was also used. This confirmed that the overall drainage focussed on the outlet at the sea beside Kinvarra. Water level monitoring in the caves just south of Kinvarra, as discussed above, showed the clear effects of the cyclical tidal influence on their water levels. Equally, the areas of tidal fluctuations and low groundwater levels in the Coole / Garryland / Caherglassaun area identify the major cave / conduit system and the hydraulically connected surface water bodies along this flow route. The tidal response again confirmed the high transmissivities and low storage in this area. Equally, rapid responses to recharge events (and subsequent recessions during dry periods) were observed, for example, rapid recharge events from the Slieve Aughty river sinks through the karst system to the coast and also from the Burren in the epikarst of the limestone pavement to the west of the Gort lowlands. This again implies low storage and high transmissivity within the karst bedrock.

Groundwater divides were established for the catchment from groundwater contour maps which appeared to remain stable at both low and high water levels (Jennings O'Donovan / Southern Water Global, 1997).

- A groundwater divide runs from near Kilchreest to Cloghballymore with waters to the north of it flowing to the Dunkelin River. High water levels also create a groundwater divide from Cahermore to Tullirin Castle.
- Groundwater from the Grannagh-Castle Boy area (from the Owenshree River) appear to flow north of Cahermore towards Kinvarra East spring.
- Groundwater from the Slieve Aughty river sinks flows south to the Coole area and towards Kinvarra.
- In the south of the study area a groundwater divide was more difficult to interpret but was assumed to be between Turloughmore and Roo with groundwater flowing east towards low levels in Bunny-Hawkhill (Clonteen catchment) and onto the central low area around Coole Lough. North-west of this divide groundwater flows north towards Kinvarra.

However, it has been stated (Drew, 2008) that such sharp divides on a map mask the high heterogeneity of the groundwater environment and specific flow paths cannot be reliably determined (for example, a connection between Castle Daly to Kinvarra East Spring is known from tracing studies).

Hydrochemistry

Some samples were also taken for hydrochemical analyses which confirmed the very rapid travel of peaty water from the uplands to the north-western extremities of the karstic conduit system. Results from across the study area divided the water into 3 main types based mainly on their carbonate alkalinity and iron levels.

Type I waters were defined as recharge waters split into,

Type Ia: surface water or very rapid conduit travel.

Type Ib: direct recharge having undergone rapid surface water/groundwater flow.

Type Ic: indirect river recharge

Type Id: direct (rainfall) recharge undergoing moderate to slow groundwater flow

Type II: waters are mixes of Type I waters (mixes of rapid groundwater throughflow) or (direct and indirect recharge)

Type III: waters affected by the marine environment (saline intrusion)

Spring discharge at Kinvarra

An attempt was made to quantify the flows from the Kinvarra springs using spot gauging techniques but this proved impractical because of the density effects of saline and fresh water and also the short time available between high tides. Conductivity surveys of Kinvarra and Corranoo Bay were also carried out to see whether large volumes of fresh water could be detected out in the bay, which was the case in the shallow levels at Kinvarra but not at Corranoo Bay.

Rainfall measurement

Spatial rainfall estimation was essential to the calibration and operation of the model. Correlation studies were carried out to link five new rain gauges with existing rain gauges. A spatially variable stochastic model of daily rainfall was then established through which synthetic sequences of rainfall could be input into the model. Evidence showed that there seemed to be long-term changes in the pattern of mean rainfall on wet days, i.e. intensities increasing potentially due to climate change.

3.4.2 Hydraulic model

The fissured nature of the karstic bedrock in much of the area and the thin cover of the glacially derived subsoils meant that the hydrological regime could not be neatly divided between surface water and groundwater components and hence the traditional boundaries had to be merged to some extent. The direct recharge was likely to be routed to discrete pathways both surface and underground. The surcharging of these discrete pathways was felt to have been causing the flooding (Johnston and Peach, 1999) and hence a conventional equivalent porous media model could not be used. Thus a network model was chosen to be the most suitable approach for simulating flow in the karstified limestone areas.

The important missing link for the flow model was the absence of any reliable discharge measurement at the catchment outlet, the springs of Kinvarra. As discussed, the distributed nature of the springs and the location of many of them below tide level made discharge measurement impractical. Hence, the downstream boundary condition for the model was represented by the known cyclical tidal head only.

Three types of flow regimes were identified in the area for groundwater flow: the epikarstic system comprised of groundwater flow in the upper 2-5 m of limestone in solution opened joints and fissures and major conduits supporting major flows; deep karst flow systems involving major cave / conduit systems often several metres in diameter and fracture conduit systems that can also be deep seated but are smaller and more distributed; and distributed groundwater flow systems characterised by some of the older Carboniferous limestone (which is of limited storage and is slow to respond) and the superficial deposits, widespread in the northern half of the study area, the most abundant being the sandy till.

Groundwater network model

The network representation of the karstic drainage was felt to represent an intermediate approach between a linear systems approach and a detailed pipe network model for which the geometry of every pipe would need to be known. Hence, the individual links were characterised according to a hydraulic resistance derived from the real hydrological response from the field work data – i.e. a single link could represent a single conduit or equally could represent an active fracture system operating under a pressure head (Johnston and Peach, 1999). *Hydroworks* (a sewer network model from Wallingford) was chosen to represent the network of conduits connecting nodal storages (turloughs). The outlet was controlled by the cyclical tidal head and inflow came from recharge from net rainfall and from surface water inflows from the three streams draining the Slieve Aughty mountains. It is not clear how accurately the turlough volumes were defined as they were not topographically surveyed although it is stated that a Digital Terrain Model was used – presumably from Ordnance Survey mapping data.

The direct recharge to the model was calculated on the basis of 250 m^2 grid squares using soil moisture deficits (from rainfall and evapotranspiration calculated on Penman-Grindley estimates). Six land use categories were defined with rooting constants and wilting points. Daily values of direct recharge were put into the network model at nodal points.

Surface water flows

The upland areas of the Slieve Aughty mountains with a cover of peat and glacially derived soils, partially planted with forestry were shown to promote a conventional rainfall-runoff response (even though the permeability of the underlying sandstone is relatively low) producing fairly rapid runoff and a baseflow. The IHACRES (Institute of Hydrology) rainfall-runoff model was chosen to yield a continuous simulation of runoff and thus a suitable discrete input into the karst groundwater network model at the three stream gauging points. The model had two components: a non-linear loss model to convert rainfall into effective rainfall, and the second routing component which routes the rainfall into two linear conceptual storages, one representing "quickflow" and the other a baseflow, as described later in Chapter 8. Rainfall data from the five installed rain gauges was reduced to areal rainfall using Thiessen polygons and combined with the discharge data from the gauging stations.

4 INSTRUMENTATION AND DATA COLLECTION

4.1 Introduction

A variety of different data was collected for the project. Continuously monitored parameters were the water levels in the turloughs, precipitation, the water levels of the three main rivers draining off the Slieve Aughty mountains and the tidal level in Galway Bay. In addition discrete samples of water were taken periodically from the turloughs, rivers and the main outlet spring at Kinvarra for hydrochemical analysis.

4.2 Turlough Water Depth Monitoring

The water depth was continuously measured using Mini-Diver® DI501 and DI502 monitors (Schlumberger Water Services) placed in the bottom of each turlough which measured the pressure of the water column from which the water level was calculated. The divers also recorded the water temperature for every time step which automatically provided a correction to the water level measurement. The internal dataloggers in the divers were programmed to record one measurement every hour with a memory capacity of 24(or 48)000 measurements per parameter. The Mini-Diver® DI501 had a range of 10 m of water with an accuracy of 0.5 cm and resolution of 0.2 cm; the depth range of the Mini-Diver® DI502 was 20 m of water with an accuracy of 1 cm and resolution of 0.4 m.

The Mini-Divers® were placed at the lowest point in each turlough at the end of the summer when the turloughs were empty. They were fastened to a concrete platform, shown in Figure 4.1(a), which had a buoy attached to it via a rope to mark its position; this allowed the divers to be retrieved during period of inundation if necessary (as was the case in the 2008/09 hydrological year during which many of the turloughs did not dry out). However, in most cases the divers were left in position until the turloughs had receded at the end of the hydrological year in the summer. The divers were downloaded using a Reading Unit (see Figure 4.1(b)) into which the end of the diver was inserted having removed the mounting cap. The Reading Unit was connected to a laptop and the data downloaded using specific Mini-Diver® software. The data was then imported into an Excel® spreadsheet format.



Figure 4.1 (a) Diver and concrete platform and **(b)** downloading diver to laptop.

In order to determine the true groundwater level accurately, compensation for the variation in prevailing air pressure was made by means of a BaroDiver® (DI500). This was installed at a height of 2 m in a tree at Coy turlough and set to record one measurement every hour - the range of the BaroDiver® was 1.5 m (water pressure head) with an accuracy of 0.5 cm and resolution of 0.1 m. The BaroDiver® air pressure readings were converted into equivalent water head and then taken away from the water levels recorded by the Mini-Divers®. The corrected depth readings were then referenced to Ordnance Datum which was achieved by GPS surveying the position of the Mini-Divers® in each turlough when empty. This fixed the 0 m depth in terms of mAOD and all other depth data were adjusted appropriately to this reference.

4.3 Rainfall Monitoring

Tipping bucket ARG100 rain gauges (Environmental Measurement Ltd.) were installed at Kilchreest (70 mAOD) and Francis gap (elevation 250 mAOD). The gauges were set level and it was ensured that they were away from any interference – i.e. a maximum of 15° sight line to any nearby trees or walls and equally not too over-exposed (Shaw, 1994). The rain gauges were enclosed by a small fence in order to keep livestock away from the gauge, as shown on Figures 4.2(a and b). The data logger recorded the time of every tip of the bucket which equated to 1 mm of rain. The gauges were downloaded about once every six months.

The data from other rain gauges in the area operated by Met Eireann were also gathered in order to provide comparison with the two project gauges. There are only two *synoptic* weather stations reasonably close to the Gort lowland area which record all meteorological data (rainfall, relative humidity, solar radiation, wind speed and direction and temperature) on an hourly basis: at Shannon Airport (42 km from Gort), and Birr (61 km from Gort). Other *climatological* stations operated by Met Eireann are at Galway (27 km from Gort) and Carron (17 km from Gort) record daily data which was also obtained. Daily rainfall data was also gained from stations in Gort, Loughrea (19 km from Gort), and Ballyvaughan (22 km from Gort). Note, for all daily precipitation values the sums are calculated from 09UTC to 09UTC.



Figure 4.2 Tipping bucket rain gauges sited at **(a)** Kilchreest and **(b)** Francis gap.

4.4 River Gauging

The flows in the three main rivers draining off the Slieve Aughty hills – the Owenshree river, the Ballycahalan / Boleyneendoorish river and the Owendalulleegh river - were constantly gauged at the positions indicated on Figure 3.1 located just on the edge of the sandstone before the rivers cross over onto the karst limestone. These were gauging stations operated by the Office of Public Works (OPW), each of which consisted of a pressure transducer embedded into the river, referenced against a staff gauge beside (see Figure 4.3). The data loggers were downloaded on average once every 6 months to provide a plot of stage against time with the levels recorded once every 15 minutes. The data from a fourth OPW gauging station on the Beagh river, just as it drains Lough Cutra, were also

collected in order to investigate the flood routing of the Owendalulleegh river across the lough before the river disappears underground at the Devil's punchbowl.



Figure 4.3 OPW gauging stations at **(a)** the Ballycahalan / Boleyneendoorish river **(b)** Owendalulleegh river and **(c)** Beagh river.

A fifth gauging station was set up on the Owenshree river at the bridge near Pollacurra (Figure 4.4) downstream from the gauging station at Kilchreest after the river had passed over approximately 12 km of karst limestone. This was achieved using a Mini-Diver® set in the base of the river and a Baro-Diver® on the river bank in a tree. A comparison of the

river flows at Kilchreest and Pollacurra could then be used to determine the addition of water from the karst (or possible losses to the underlying karst) over this section.



Figure 4.4 Gauging station installed at the Owenshree river just upstream of Blackrock turlough (12 km downstream of Kilchreest).

A recently felled tree was found to be blocking one of the bridge piers just downstream of the Kilchreest gauging station on 1st May 2009, just before the intensive flow monitoring survey started in order to produce the flow rating curve. This was creating a significant backwater effect and so had to be removed, as shown in Figure 4.5. The river data from before this period for at least two weeks showed a distinct rising trend and so was used with caution.



Figure 4.5 Removing the tree blocking one of the bridge piers just downstream of the Kilchreest gauging station.

There were no rating curves available for any of the rivers being monitored and so such curves were determined for the river sections over the course of the project by sequential visits, as discussed in the following section.

4.4.1 Determination of rating curves

A *rating curve* (i.e. flow against stage relationship) was needed for each of the five gauging stations on the rivers. This was achieved by measuring the flow at different times (stages) by a combination of the mid-section velocity depth surveying method (at moderate to high flows) or dilution gauging method at low flows in order to build a comprehensive data-base of flows against stage as contained in Appendix A. This relationship was then used to convert the historic stage measurements (as measured continuously by the pressure transducers in the base of the rivers) into flow. The main problem with getting the data was for the high flow events whereby it was difficult to remain in the river when the depths were over about 1.2 m deep due to the velocity – although attempts were made to get a few higher values as shown in Figure 4.6.



Figure 4.6 Measuring the flow in the Owendalulleegh river during high flows.

Mid-section method

The mid-section method involves measuring the river velocity and depth at several points across the gauging section of the river to calculate the discharge. An acoustic digital ultrasonic current meter (OTT ADC) was used to measure the point velocity in the river (see Figure 4.7). This meter was able to measure both the velocity distribution across the river section but also the respective depth of the sensor. The velocity measuring range was -0.2 to 2.5 m/s (with a resolution 0.001 m/s and accuracy 1%). The depth measurement range was 0 to 5 m with an accuracy of 1%. The river cross-section selected for discharge measurement had to be hydraulically suitable – i.e. a straight length of channel with regular cross-section and a consistent bed gradient. The sections did not have any still areas or any counter or eddy currents. The number and position of the vertical measuring points was chosen according to the European / International Standard EN – ISO 748 (2007) as set out on Table 4.1.



Figure 4.7 ADC meter used to measure river flows (Owenshree river).

River width (m)	No. of verticals
>1 to <3	5 - 8
>3 to <5	8 - 10
>5 to <10	10 - 20
>10	> 20

Table 4.1 Number of vertical measurement points required in relation to river width.

The mid-section method was chosen to calculate the discharge as it is quicker to calculate and generally considered to be more accurate than the mean-section method. The 3-point velocity measurement was made at each vertical at 0.2, 0.6 and 0.8 the depth of the river at each point. The mean velocity (v_m) for that vertical section was then calculated according to Equation 4.1.

$$v_m = 0.25(v_{0.2} + 2v_{0.6} + v_{0.8}) \qquad \text{Eq. 4.1}$$

The flow in the river (for each different stage visit) was then calculated by the cumulative addition of the flows through each section according to Equation 4.2 and shown in Figure 4.8.

$$Q = \sum_{i=1}^{n} v_{m(i)} h_i b \qquad \text{Eq 4.2}$$

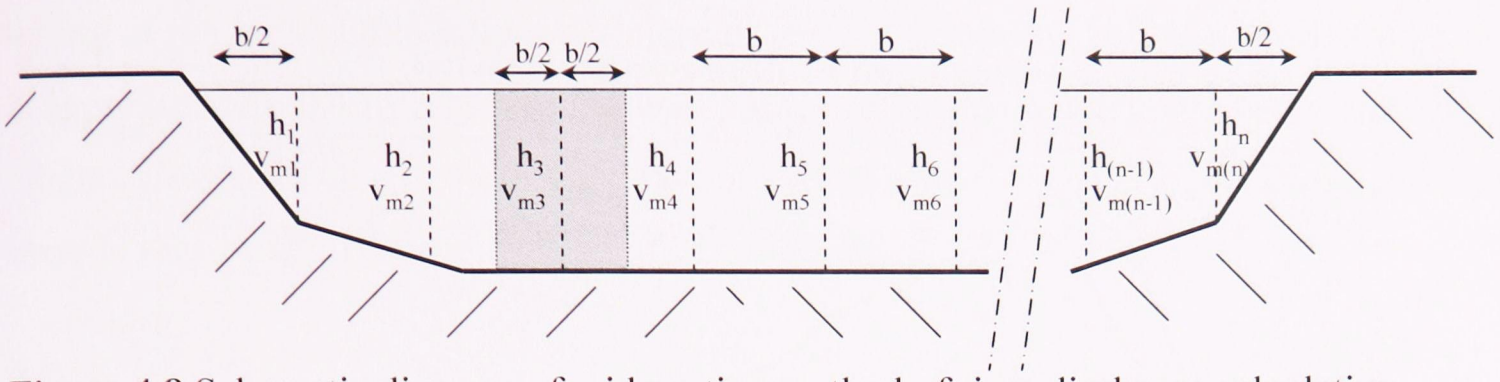


Figure 4.8 Schematic diagram of mid-section method of river discharge calculation.

Dilution gauging method

For certain flows the depth of water in the river was not sufficient to place the meter and so a more accurate method of flow measurement was to use the dilution gauging technique whereby a known mass of conservative tracer (normally a dye or salt) is added to the river at one point, just upstream of a turbulent zone. For this project table salt (sodium chloride) was used – usually 2 kg – which was mixed into a bucket of the river water until was totally dissolved. At time t = 0, the full contents were thrown instantaneously into the middle of the turbulent water at the upstream point in the river. The concentration of the salt in river was measured over time at a location downstream (usually about 20 to 30 m on these rivers) using an electrical conductivity (EC) meter (WTW® Cond.197i) which measures the ease of transmitting a current through the water in units, µS/cm. A relationship between the salt concentration (mg/l) and EC (µS/cm) was carried out above the background conductivity. The tracer was measured at the downstream point (where the salt was considered to have been totally mixed into flow) until the effect of the salt had passed and the EC had fallen away to background levels again. A typical profile downstream and calculated salt concentration is shown in Figure 4.9 which shows the background conductivity was around 595 µS/cm on this particular day.

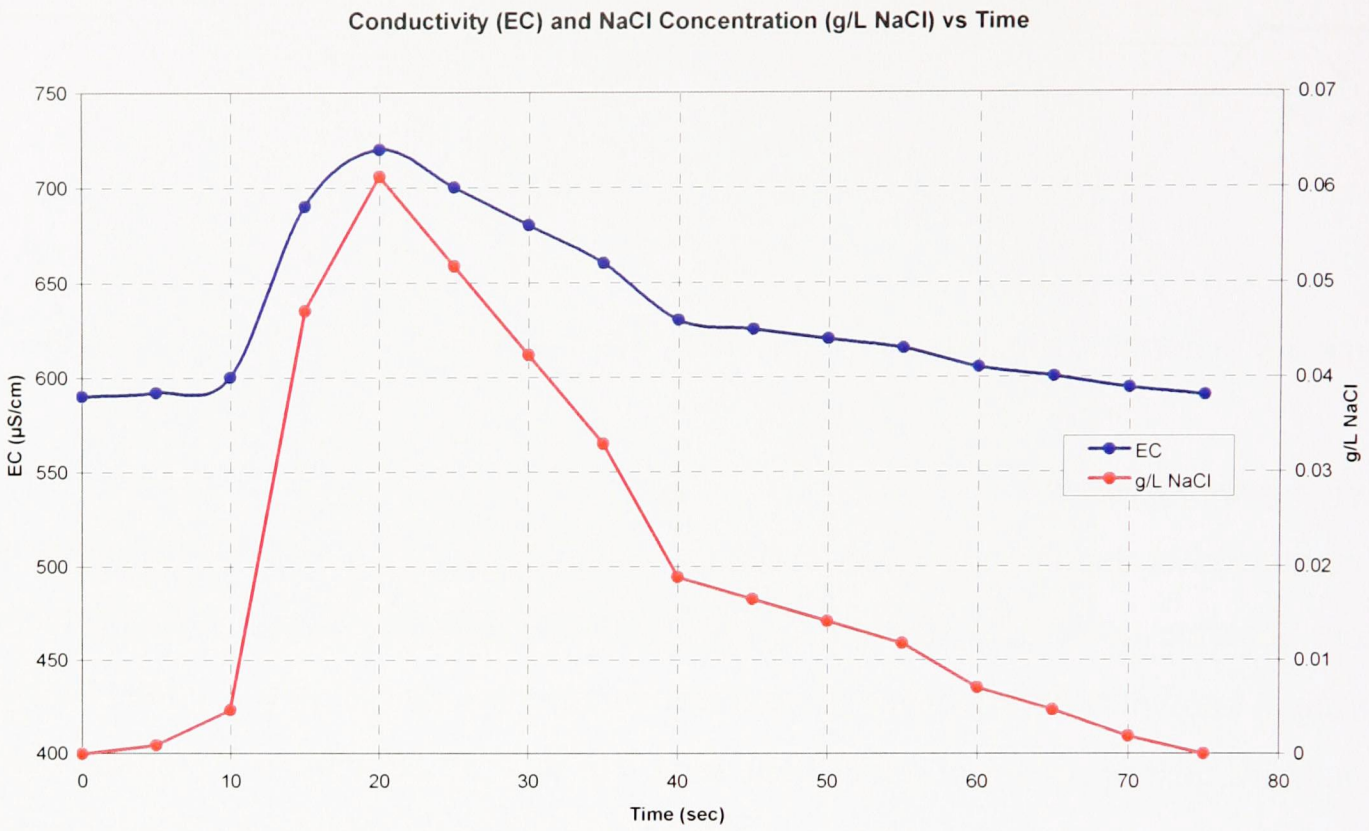


Figure 4.9 Dilution gauging results for Owenshree river on 9th January 2009.

The area under the curve but above the background level was determined by a macro written in Excel© and equates to the mass of salt added to the river. The flow was then calculated according to Equation 4.3.

$$Q = \frac{VC_s}{\int (C - C_0)dt} \qquad \text{Eq. 4.3}$$

where, V = volume of tracer solution added at concentration C_s (hence, $V.C_s$ = mass of salt added), C is the concentration of salt measured downstream at tine t and C_o is the background concentration in the river.

4.5 Sea Level Monitoring

Tide level data was obtained from the Marine Institute for the Galway Port tide gauge and also the Inishmore tide gauge (Arann Islands). All tide levels are recorded with respect to Ordnance Datum Malin and the time is reported as Coordinated Universal Time (UTC) Hence, all data sets in this thesis are standardised to Greenwich Meantime. A comparison between the tide levels in Galway Port (15 km away from Kinvarra across the bay) and the Inishmore tide gauge is shown on Figure 4.10 for several tidal cycles. This shows that the

timing of the high and low tides are more or less synchronous. The tidal level at high tide is approximately 0.4 m higher at Galway port (~ 30% higher compared to Insishmore) as would be expected due to the slight tidal bore effect of the tide entering a bay. At low tides there is very little difference between the tidal levels.

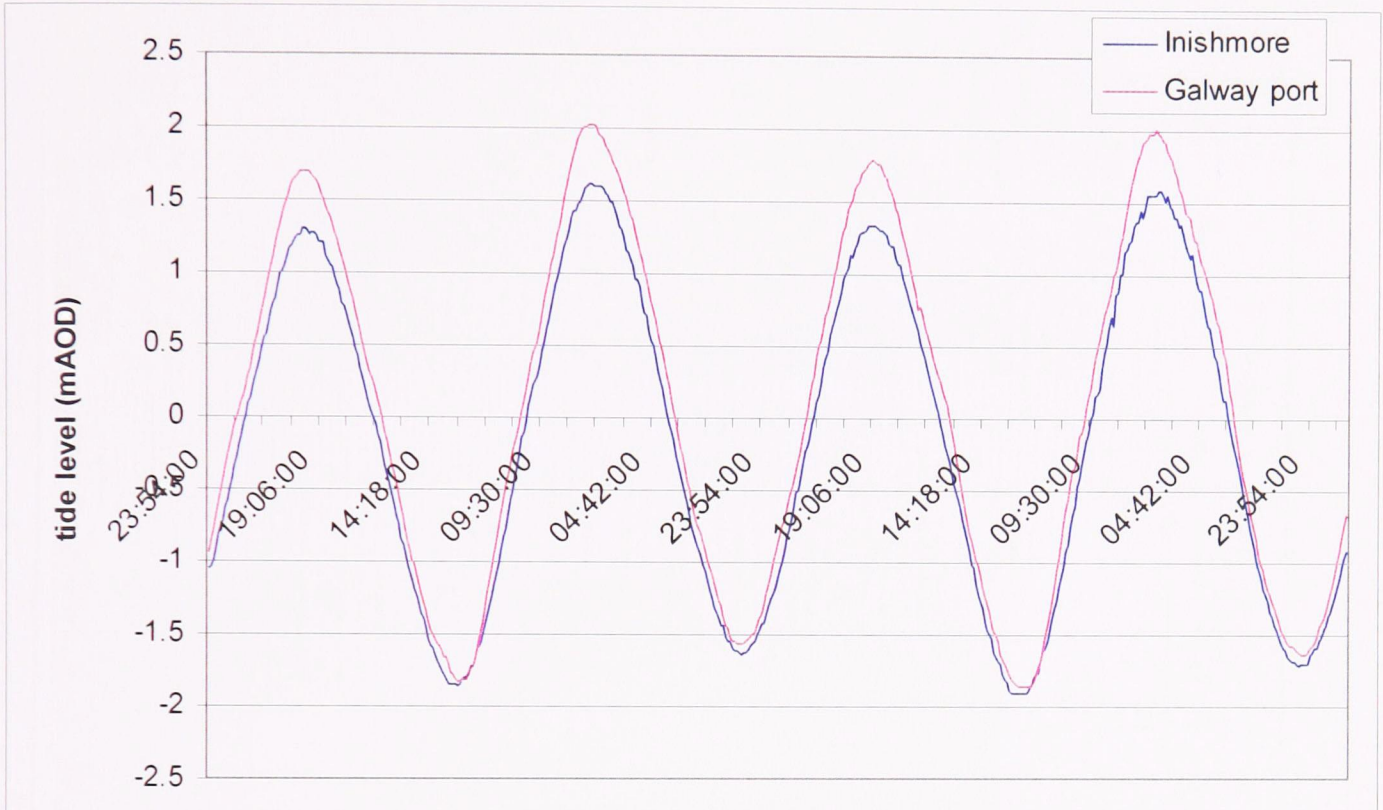


Figure 4.10 Comparison of tide levels in December 2008 at Inishmore and Galway tide gauges.

The raw tidal data from the Marine Institute had a number of errors and omissions in it. For example, at several time steps the same time and level was given twice; alternatively there were many points at which two to three hours of data were missing. At times where the data was missing the equivalent data from the Inishmore tide gauge was used to fill in the gaps as there was little difference between the data (both tide gauges being so close). If data was required either side of the high tide level (down to 0.5 mAOD) then the Inishmore data was augmented by 30% to account for the extra levels in the bay as discussed above.

A plot of the tidal levels at Galway is shown (Figure 4.11) for the month of January in 2008 which clearly shows the spring tides (i.e. high tides when the sun and moon are in alignment with either the new or full moon) and neap tides (when moon is in first or third

quarter and the sun partly counteracts the moon's gravity). There is a slight lag of approximately a day between full or new moon and spring tides due to the momentum and viscosity of the huge water movements involved. The mean sea level measured at Galway was 0.081 mAOD – a figure used later when considering at hydraulic gradients across the hydrological system.

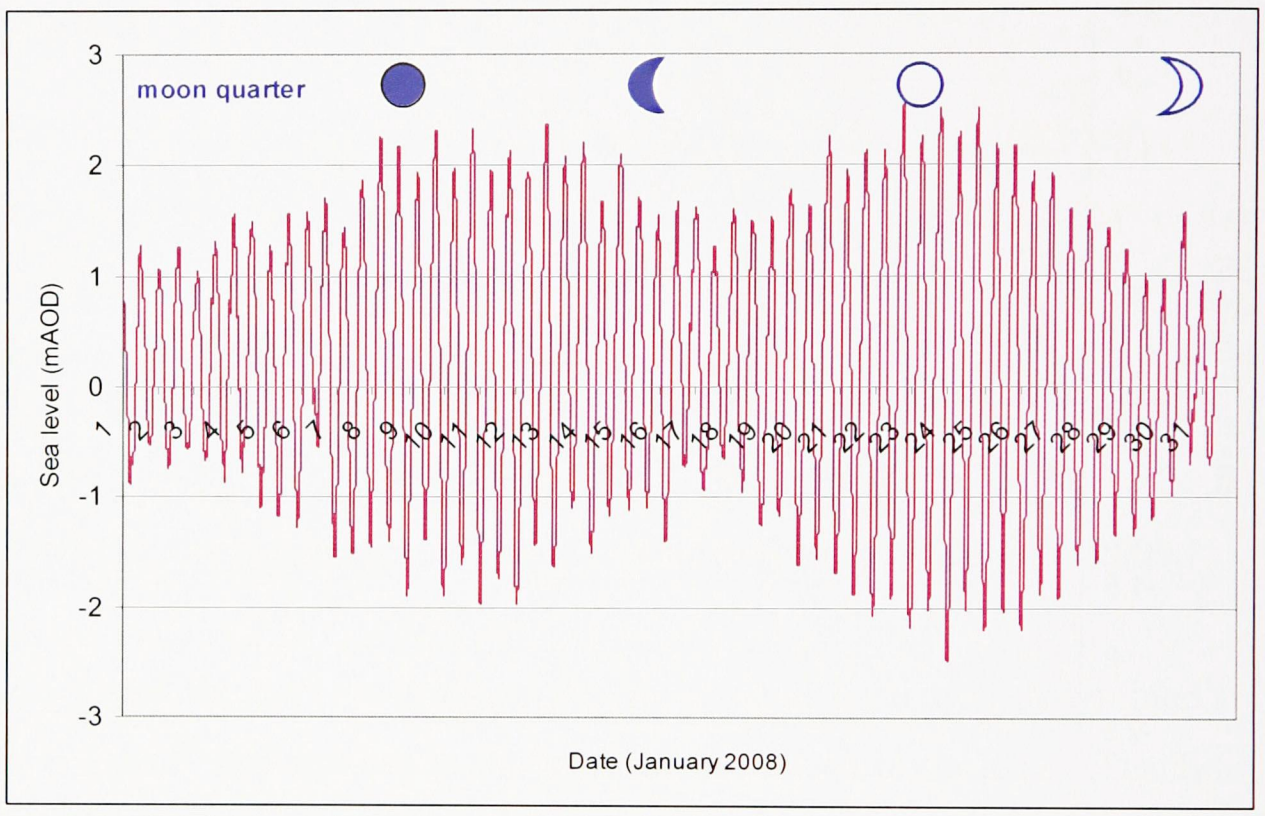


Figure 4.11 Tidal measurement at Galway harbour for January 2008.

4.6 Turlough Surveying

The turloughs were surveyed during the summer periods when the waters had receded. However, it should be noted that the summers of 2008 and 2009 were exceptionally wet and the turloughs did not completely dry out. The survey was carried out using a Trimble 4700 GPS system with R6 Rover and Base Station and TSC2 Survey Controller as shown on Figure 4.12. The surveying could be carried out by one person by establishing the base station coordinates and then using the rover to get all the topographic points.





Figure 4.12 GPS equipment at Garryland turlough **(a)** base station and **(b)** rover.

The procedure to set up the GPS was as follows. Initially the base station was set up, ideally in the middle of the area to be surveyed. The base station was levelled in on top of the tripod and distance from the ground to the height of the base station measured. The base station was then set running to establish links with satellites to fix its position. A mobile phone with Bluetooth enabled was also switched on and linked to the base station. The phone then established the base station position in terms of the Irish Ordnance Datum. Once the base station has been set via connection to the phone it was then set to communicate with the rover. The rover was positioned at a 2 m height on top of the staff and the survey points were then made with this. At each point required on the survey the

rover was held vertically by means of a bubble level and the point entered on the hand set. The minimum accuracy required was 0.02 m in both the horizontal and vertical direction – this was generally obtained when the rover was in contact with 9 or more satellites – however, often better accuracies down to 1 cm were achieved. The position is fixed by the direct satellite communication with the rover but this is then refined and converted into AOD by communication between the base station and the rover. Points were taken on average every 20 to 30 m but this would depend on the topography (more frequently if it was variable – less frequently if there was little change in slope). It should be noted that it was not possible to survey underneath trees which often occur near the high water mark around the turloughs (particularly Garryland and Coole). In these cases as many spot measurements within the forest in clearings or on tracks were taken. The surveying of each turlough often took more than one day - the data from the previous foray was stored on a file which was opened and surveying continued.

Towards the end of the 2009 hydrologic year the turloughs had not dried out sufficiently for the base of Coole and Garryland to surveys to be completed. Therefore, the flooded turloughs were surveyed by setting up the GPS base station and then gaining a series of spot depth measurements across each turlough from a kayak with depth gauge as shown on Figure 4.13.



Figure 4.13 GPS base station set up at Coole with kayak used to gain spot depths.

The GPS data (Easting, Northing and elevation) was stored on the handset and then downloaded to an Excel .CSV file. This was then exported to Surfer® version 8.6 software in which a survey point grid was built using the Kriging method set to 2 m spacing. The 2 m grid spacing was chosen by comparison of the *residuals* (i.e. the difference between the measured spot levels from the survey against the levels computed at those same points from the Surfer® derived surface) at several different spacings from 0.5 m up to 20 m. A significant improvement was found from 20 m down to 2 m spacing after which the improvement was minimal –2 m was thus chosen as the optimum spacing.

Once the surface has been computed the software was used to produce contour maps as shown for Coy turlough in Figure 4.14. These were also combined with a wireframe plot to give a 3-D representation of each turlough as shown in Figure 4.15. The contour plots and 3-D surfaces of all of the turloughs are given in Appendix B.

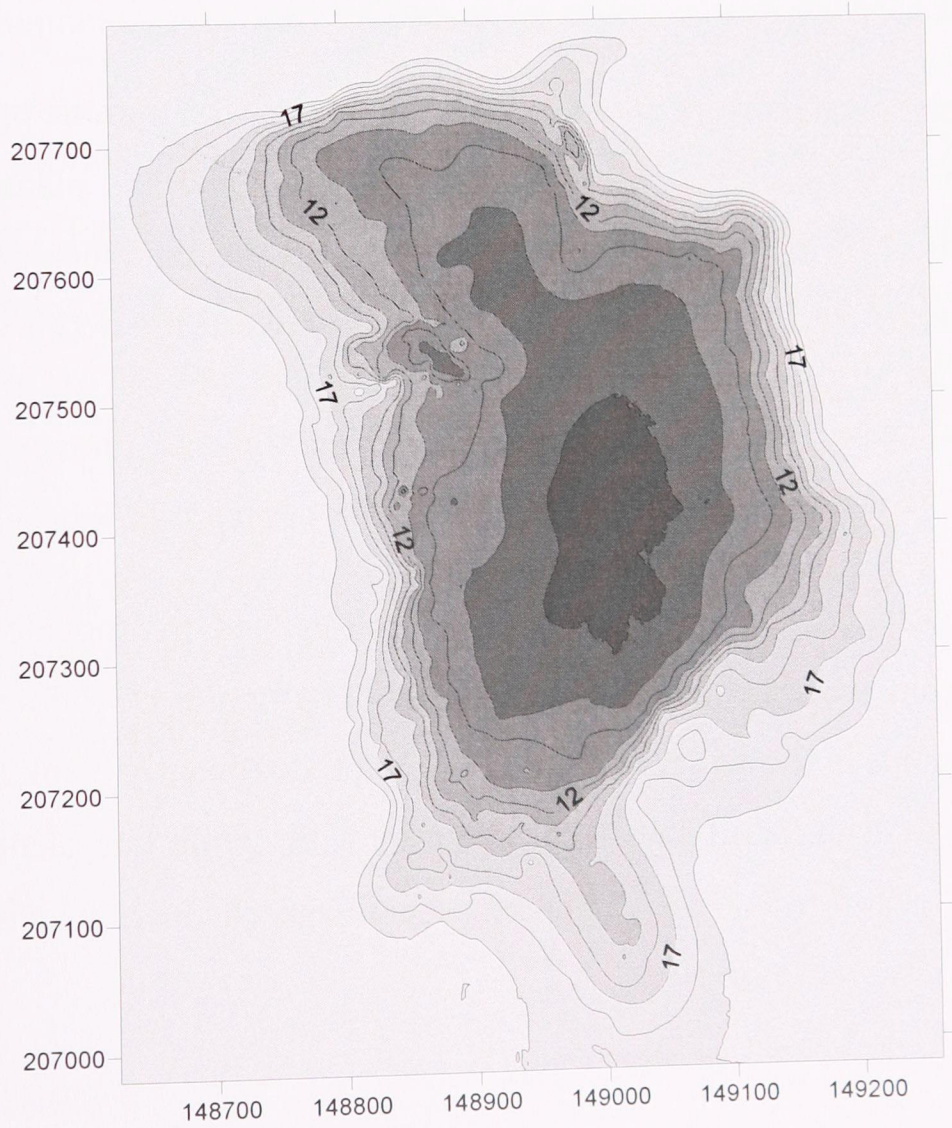


Figure 4.14 Contour map produced by Surfer® from survey data of Coy turlough.

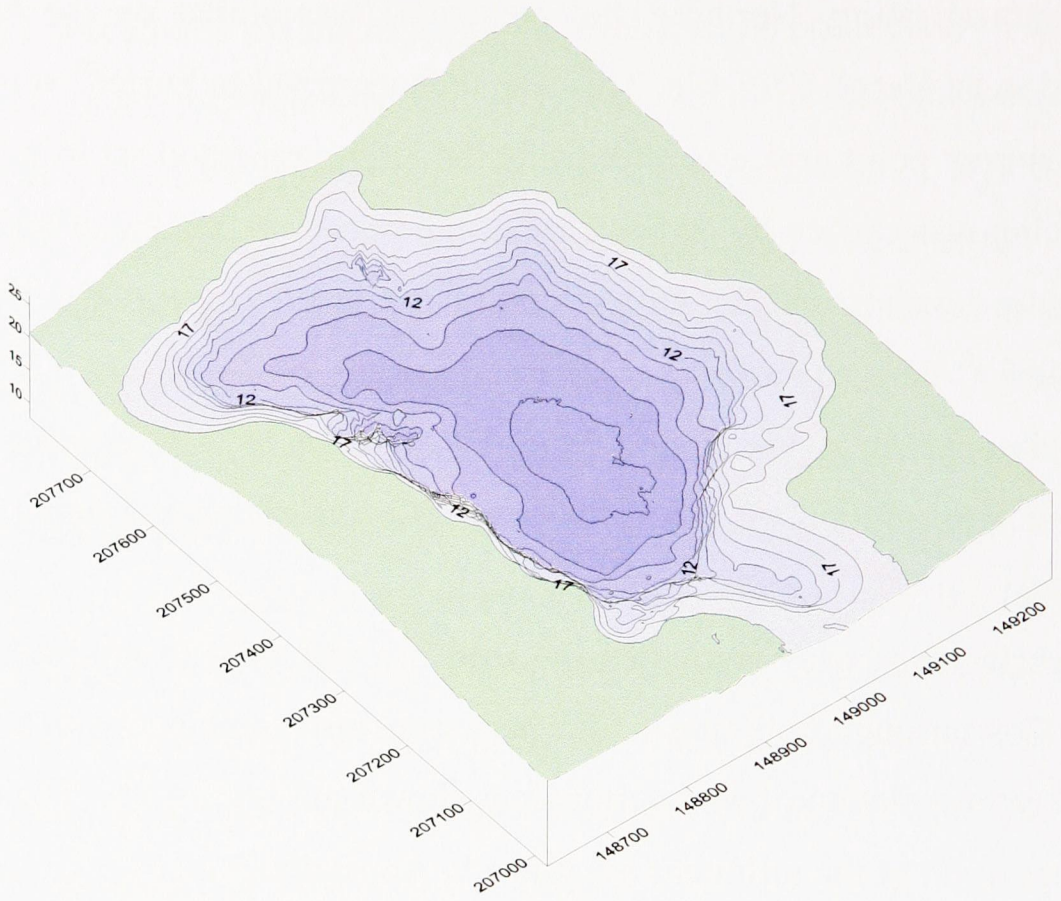


Figure 4.15 Three-dimensional surface and contour plot of Coy from Surfer®.

Depth-area relationships were computed via the Surfer® programme by means of a Surfer® script written in Visual Basic which computes the volume and planar area at a range of depth intervals (0.02 m). The specific turlough depths (i.e. data measured by Divers) could then be converted into volumes via interpolation between the depth-volume relationships in Excel®, as discussed later in Section 5.4.

4.7 Visual Surveying

Many aspects and deductions about the hydrology and hydrogeology of the area was ascertained from walking the catchment areas. The nature of runoff high on the Slieve Aughty mountains is shown on Figure 4.16 with predominantly blanket peat coverage of at least 3 m depth with significant areas forested with coniferous plantations. A lot of the surface water runoff was seen in the forest drainage channels which fed the three main rivers.



Figure 4.16 Runoff on the Slieve Aughty hills following rain event **(a)** peaty runoff in forest drainage channel and **(b)** Ballycahalan river at an early stage in the mountains.

During the GPS surveying of each turlough many springs and swallow holes were noted and their position referenced. For example, in Garryland during recession of the turlough in summer a spring was noticed as shown on Figure 4.17 at the water's edge. The temperature of the water was very cold in comparison to the Garryland turlough water indicating that the spring was probably issuing water from the epikarst (fractures etc.), not water from an adjacent turlough which would have been a lot warmer at that time of year. The main estavelle in Blackrock turlough is shown during a period of recession in winter (Figure 4.18) which also shows the brown vegetation due to the fact that it the land had been submerged for several months.



Figure 4.17 Spring in Garryland during recession of the turlough in August 2009.



Figure 4.18 Estavelle in the base of Blackrock turlough (January 2009).

Visits to the north-east end of Coole demesne at several times of the year clearly showed the river feeding the turlough confirming the suspicion that it operated as a river fed turlough taking the main flows from the Blackrock / Coy conduit and the river Beagh through Gort. Significant high flows were seen during periods of peak turlough inundation as shown in Figure 4.19 which was taken following exceptionally heavy rainfall period in the summer and clearly shows the peaty runoff from the Slieve Aughty mountains. Equally, the main river feeding Coole could be seen to be carrying significant flows at all times of year,

Some previous reports had suggested that the main discharge from the Gort lowland system was at Corranroo Bay to the west of Kinvarra. However, in major periods of recession it was obvious (particularly at low tide) that the high flows were discharging at Kinvarra as shown on Figure 4.20.



Figure 4.19 River discharging into Coole from the north-east (August 2009).



Figure 4.20 Main spring discharging into Galway Bay at low tide at Kinvarra.

Other places of hydrogeologic interest were the sink at Ballylee where the Ballycahalan river joins the main Blackrock-Coy conduit and the Devil's punchbowl and resurgence (Figure 4.21) which takes the flows from the river Beagh draining Lough Cutra.



Figure 4.21 Resurgence from Devil's Punchbowl outside Gort (June 2009).

4.8 Hydrochemical Data

A number of discrete water samples were collected from several key points on the karst network between December 2008 and June 2009. At each visit samples were collected from the middle of each of the five turloughs by kayak and then at the following places by grab sample:

- 2 springs at Kinvarra (east and west) at low tide
- 2 samples from the River Owenshree at Kilchreest and 12 km downstream at the bridge at Ballynackagh grid ref. [516 102]
- River Ballycahalan at Ballylee just before it disappears underground
- River Beagh as it flows through Gort

In addition samples were taken of rainfall of the Slieve Aughty mountains, of peat runoff and forestry runoff, as well as at different distances down the Ballycahalan river as it drains off the mountains. These were analysed in the laboratory for stable oxygen isotopes, nutrient (N and P) and multi-elements whilst conductivity and temperature was measured directly in the turlough and river water using an electrical conductivity (EC) meter (WTW® Cond.197i).

The robustness of taking single samples of water from a turlough as representative of its water quality was assessed by an intensive survey of an individual turlough, whereby several samples were taken (spatially) across Coy turlough and also at three different depths. The samples were taken using a Discrete Interval Sampler (Solinst) which allowed samples to be taken at specific depths (surface, 2 m and 4 m depth) as shown on Figure 4.22.



Figure 4.22 Multi-depth sampling on Coy turlough, showing Discrete Interval Sampler and glass sample bottles.

4.8.1 Chemical analysis

Samples were collected in 200 mL glass jars at a depth of 0.5 m from the middle of the turlough. Nitrogen and total organic carbon (TOC) analysis was carried out using a *vario TOC cube* (Elementar, Germany) based on thermo-catalytic oxidation and subsequent infrared analysis of the oxidation products.

The samples for ICP analysis were acidified as soon as possible whereby 10 mL of each sample was added to 1 mL of 60% nitric acid. The sample was then stored in the fridge until analysed on the Varian Liberty AX – sequential ICP-AES (Inductively Coupled Plasma) machine. The phosphorus standards were 0, 0.25, 0.5, 1.0, 2.0 and 5.0 mg/l and multi-element standards 0, 0.25, 0.5, 1.0 and 2.0 mg/l for Al, Fe, Mg and Mn and 0 2.5, 5, 10 and 20 mg/l for K.

4.8.2 Stable isotope analysis

Separate samples were collected at each visit in 20 mL glass jars at a depth of 0.5 m which were flooded before sealing under water to ensure that there was no air trapped in the bottle, as shown in Figure 4.23. These were then transferred to a cool box before being stored in a fridge until ready for the stable isotope analysis by mass spectrometry.



Figure 4.23 Sample collected for ^{18}O isotope analysis.

The analysis of the samples to yield the $^{18}O/^{16}O$ ratio was carried out in two batches using continuous flow-isotope ratio mass spectrometry (Thermo Delta^{plus} CF-IRMS). The sample preparation to find the $\delta^{18}O$ of water by equilibration was as follows.

- 0.5 mL of water was pipetted into a 12 mL exetainer which is capped with a rubber septum.
- The exetainer was flushed with a 0.3% CO_2 in helium for 800 seconds.
- The exetainer was allowed to equilibrate in the sample block for >20 hours.

Two equilibrations occur:

(1) $CO_2(g) <=> CO_2\ (aq)$
where CO_2 is exchanged between the gaseous and aqueous phase.

(2) $CO_2\ (aq) + H_2O <=> H_2CO_3$
where dissolved CO_2 reacts with water to form carbonic acid.

- Samples were run with the standard method (5 reference CO_2 peaks, 10 sample peaks and 2 reference CO_2 peaks). The middle 8 sample peaks were then averaged to give the $\delta^{18}O$ value.

Corrections to the standard were made and the Standard Deviation was reported as 1SD for all standards run with unknowns.

5 DATA ANALYSIS

5.1 Introduction

The continuously monitored field data collected throughout the 3 years were the water levels in the five turloughs, precipitation and river stages. GPS surveys were also carried out for all turloughs when empty in order to define the depth-volume-surface area relationship. Using this information, the net flows into or out of each turlough could then be calculated. Finally, some discrete samples of water quality were taken throughout 2009 in order to augment the other data and provide further insight into the hydraulic network of the turloughs. All this data has been analyzed in order to determine the linkages and hydraulic pathways between the turloughs and then down to the sea.

5.2 Water Level Profiles

The water depths for all five turloughs Blackrock, Coy, Coole, Garryland and Caherglassaun from autumn 2006 to summer 2009 are shown on Figure 5.1. The 2006/07 and 2007/08 hydrological years showed what might be considered to be a classic turlough response with the turloughs filling in November, reaching a peak in the middle of winter (January to February) and then starting to recede through the spring until more or less empty throughout the summer. The 2008/09 hydrological year however, showed a different pattern with several filling and emptying events throughout the year. Blackrock turlough at the top of the chain shows a sharp response to rainfall with Coy providing a more muted version, lagging behind Blackrock during recession but starting to fill earlier which is investigated later in Chapter 6. The statistics of turlough water levels (Table 5.1) and the time series (Figure 5.1) reveal that Coy seems to get capped at a maximum depth of around 17 mAOD despite the much higher fluctuations of Blackrock turlough just one kilometre upstream. This might be significant i.e. indicative of another drain at this level which sends flows into a higher level system that might bypass the lower system or head direct to Coole. Alternatively it indicates a certain remoteness (due to a constriction) from the main conduit system.

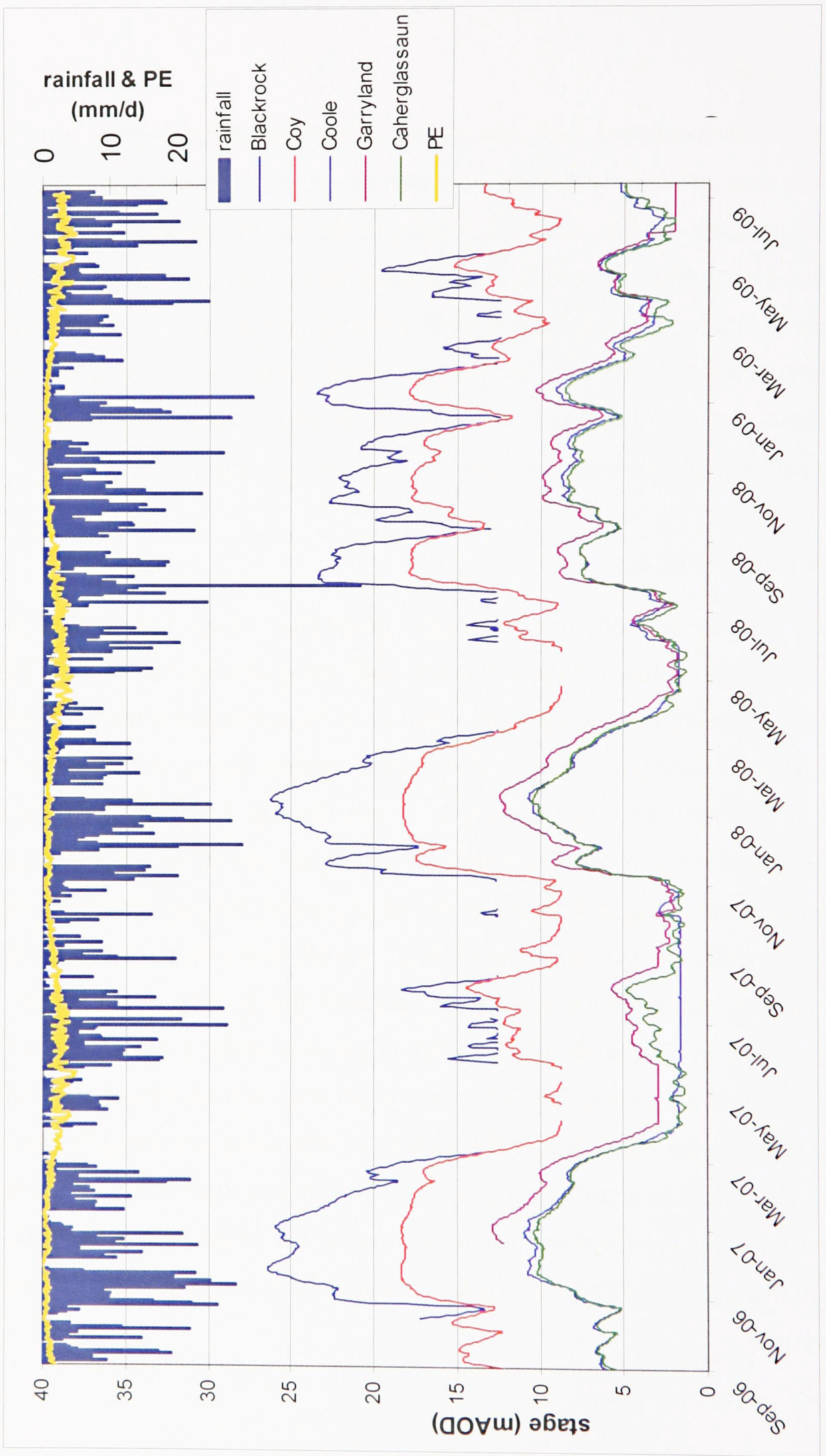


Figure 5.1 Water depths (stage) for all turloughs and rainfall at Gort from autumn 2006 to summer 2009.

The three turloughs lower down the system, Coole, Garryland and Caherglassaun, show very similar profiles with little lag, indicating their close proximity but also possibly relatively unconstrained hydraulic connections between them. The filling of the turloughs appears to be correlated to intense, prolonged rainfall periods particularly in winter time. Such rainfall conditions in summer (for example June, July 2007) can also be seen to promote filling but at a much smaller scale due to the higher initial losses for the rainfall (higher evapotranspiration etc) and also the fact that the antecedent condition of the network is likely to have more capacity to take higher flows before surcharging. The data (Table 5.1) also shows that the turloughs further down the system (and therefore closer to the sea) were more inundated for longer periods i.e. more constant flooding regimes – although Coole seems to drain fairly freely compared to Garryland and Caherglassaun. The mean water levels in the turloughs are also fairly common throughout the years from 4 to 6 m, with the exception of Blackrock which is more flashy.

Table 5.1 Statistics on turlough inundation 2006 to 2009.

	Oct.06 to Sept.07		Oct.07 to Sept.08		Oct.08 to Jul.09	
	Days empty (no.(%))	Max (*mean*) water depth (m)	Days empty (no.(%))	Max (*mean*) water depth (m)	Days empty (no.(%))	Max (*mean*) water depth (m)
Blackrock	137 (*38%*)	14.1 (*6.8*)	159 (*44%*)	13.9 (*9.0*)	58 (*21%*)	11.1 (*4.9*)
Coy	70 (*19%*)	9.7 (*6.0*)	58 (*16%*)	9.6 (*5.5*)	0 (*0%*)	9.3 (*5.2*)
Coole	73 (*20%*)	9.6 (*3.8*)	91 (*25%*)	9.4 (*3.8*)	0 (*0%*)	7.7 (*4.7*)
Garryland	10 (*3%*)	11.3 *(4.8)*	18 (*5%*)	10.9 *(4.0)*	0 (*0%*)	8.7 *(5.5)*
Caherglassaun	0 (*0%*)	9.3 (*4.3*)	0 (*0%*)	9.4 (*3.9*)	0 (*0%*)	7.4 (*4.4*)

5.3 Hydraulic Gradients

The temporal hydraulic gradients between each turlough and down to the sea (the mean sea level = 0.081 mAOD) are shown on Figure 5.2 over the 3 year period for the study. This shows the pressure head acting on the underground conduit system and is reflective of the nature of the hydraulic capacity of the underground conduits. The hydraulic gradients in general range between 5×10^{-4} to 2×10^{-3} m/m. Blackrock seems more peaky indicating

perhaps it is more constrained downstream than the others. Interestingly Caherglassaun shows a relatively high hydraulic gradient, particularly on the first two years (2006 to 2008) even though it is closest to the sea again indicating some form of constriction between it and the free flow to the sea.

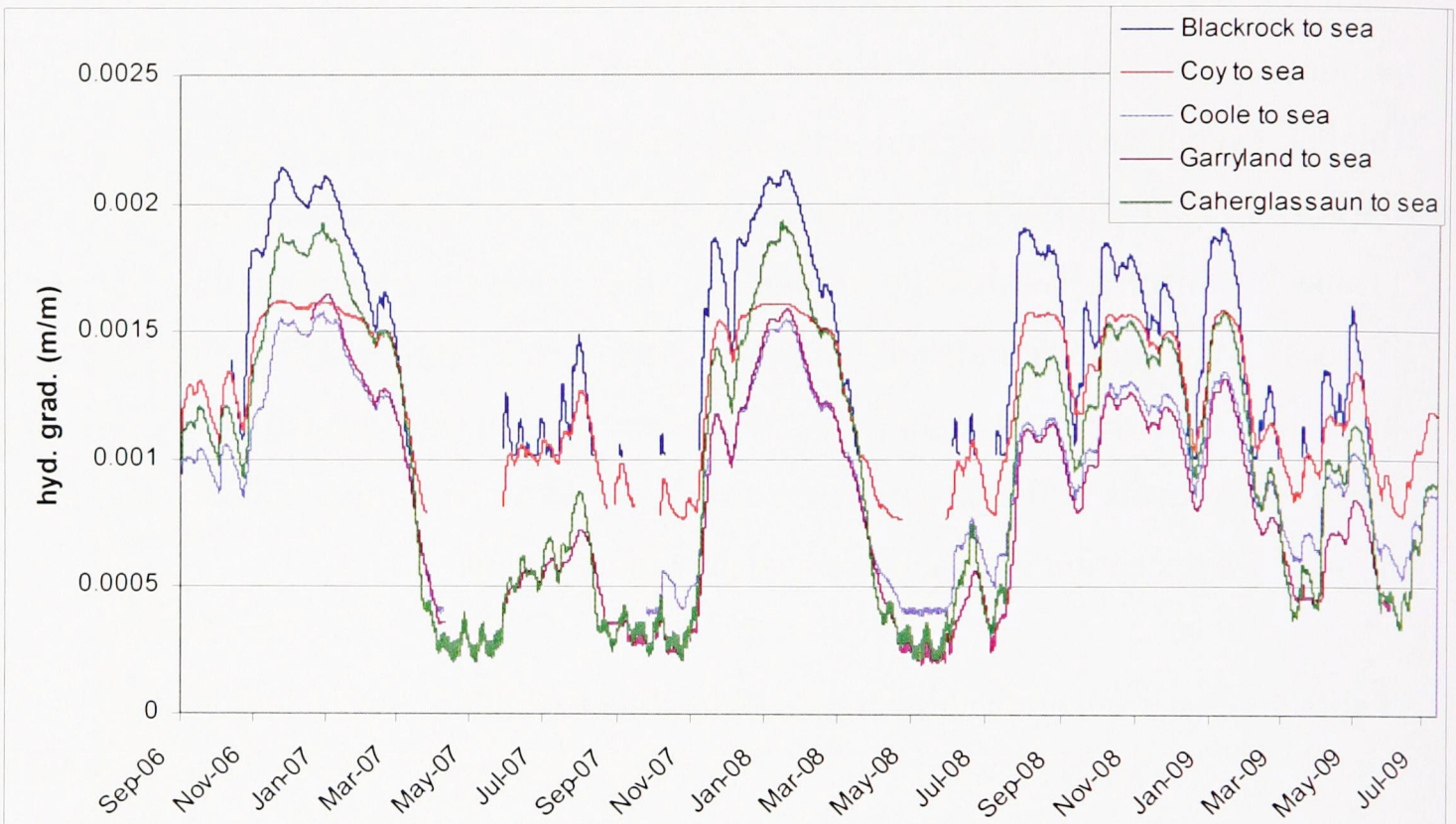


Figure 5.2 Hydraulic gradients of turloughs with respect to sea level.

A more realistic comparison of hydraulic gradients can be made if the outlet from the higher network (i.e. the Blackrock to Coy section) is at Coole - i.e. the flow outlets at the open channel (at atmospheric pressure) which enters Coole. This does not make a significant difference although the spread is more compressed. There is a period between June to October 2007 where the hydraulic gradient of Blackrock and Coy is heightened with respect to Figure 5.2. This is due to the fact that Coole totally emptied during this summer (whereas Garryland and Caherglassaun just flooded slightly (being slightly lower downstream).The hydraulic gradients in general were between 5×10^{-4} to 2×10^{-3} m/m although they are a bit lower during summer periods when the downstream turloughs were almost empty.

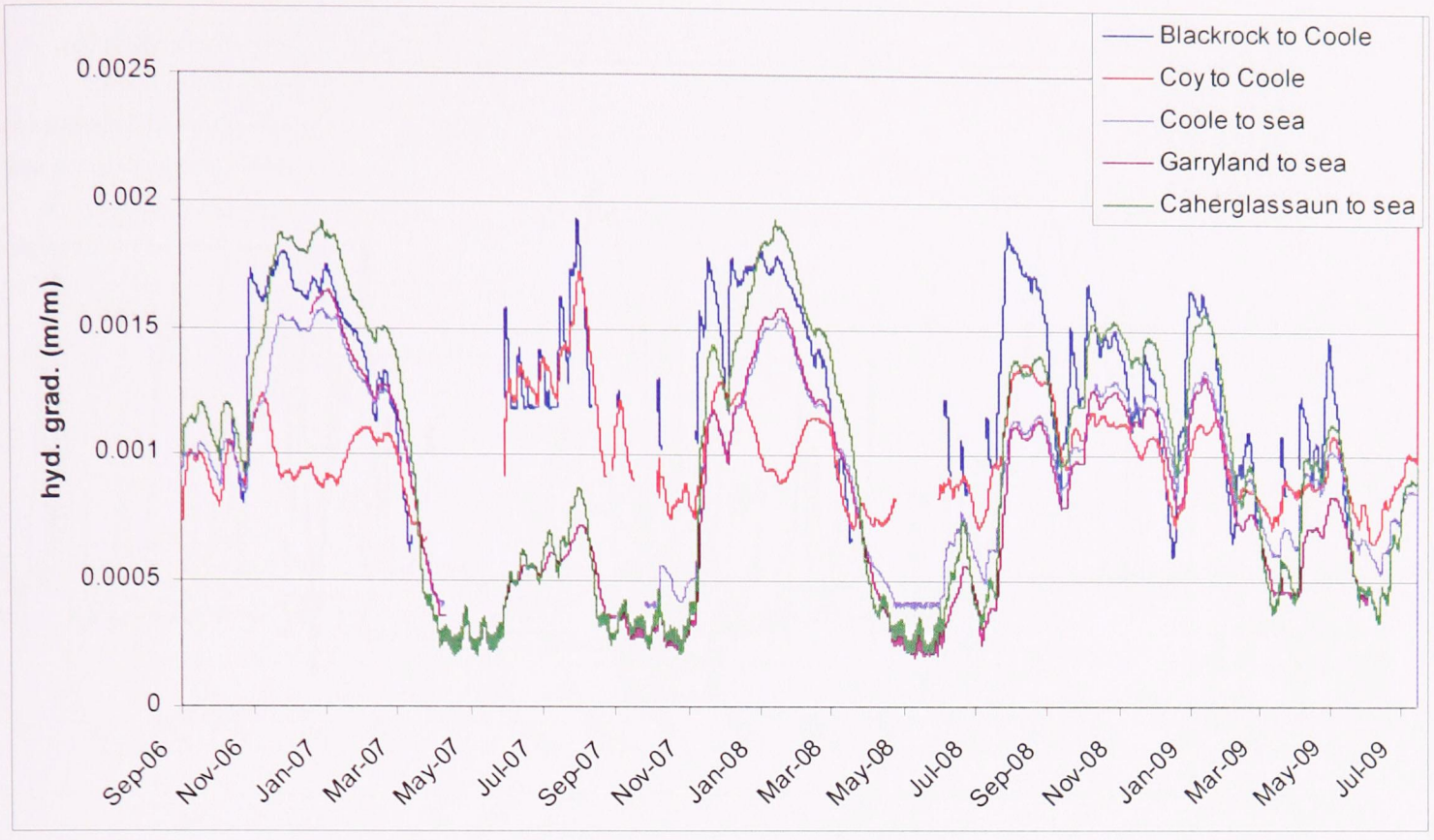


Figure 5.3 Hydraulic gradients of Blackrock and Coy to Coole outlet and other turloughs to the sea.

Finally, the hydraulic gradients calculated between the different turloughs in series (Figure 5.4) also yield pertinent information concerning the nature of any connection and dynamics between the temporary lakes. The hydraulic gradients between most of the turloughs are fairly constant and less than 2×10^{-3} with the exception of the gradient between Blackrock and Coy where the signal is erratic and often peaks up to over 6×10^{-3} m/m. These sharply fluctuating hydraulic gradients over the season indicate that there must either be a significant hydraulic constriction between Blackrock and Coy or a very fast rapidly varying input upstream of Blackrock which the turlough modifies / mutes to some extent. The more constant hydraulic gradients revealed across all years between Coy to Coole and between the lower three turloughs of Coole, Garryland and Caherglassaun, however, indicates little restriction between them. Caherglassaun does shows a more peaky response (muted compared to Blackrock though) which implies some backing up between the turlough and the sea i.e. some hydraulic restriction backing-up the whole system.

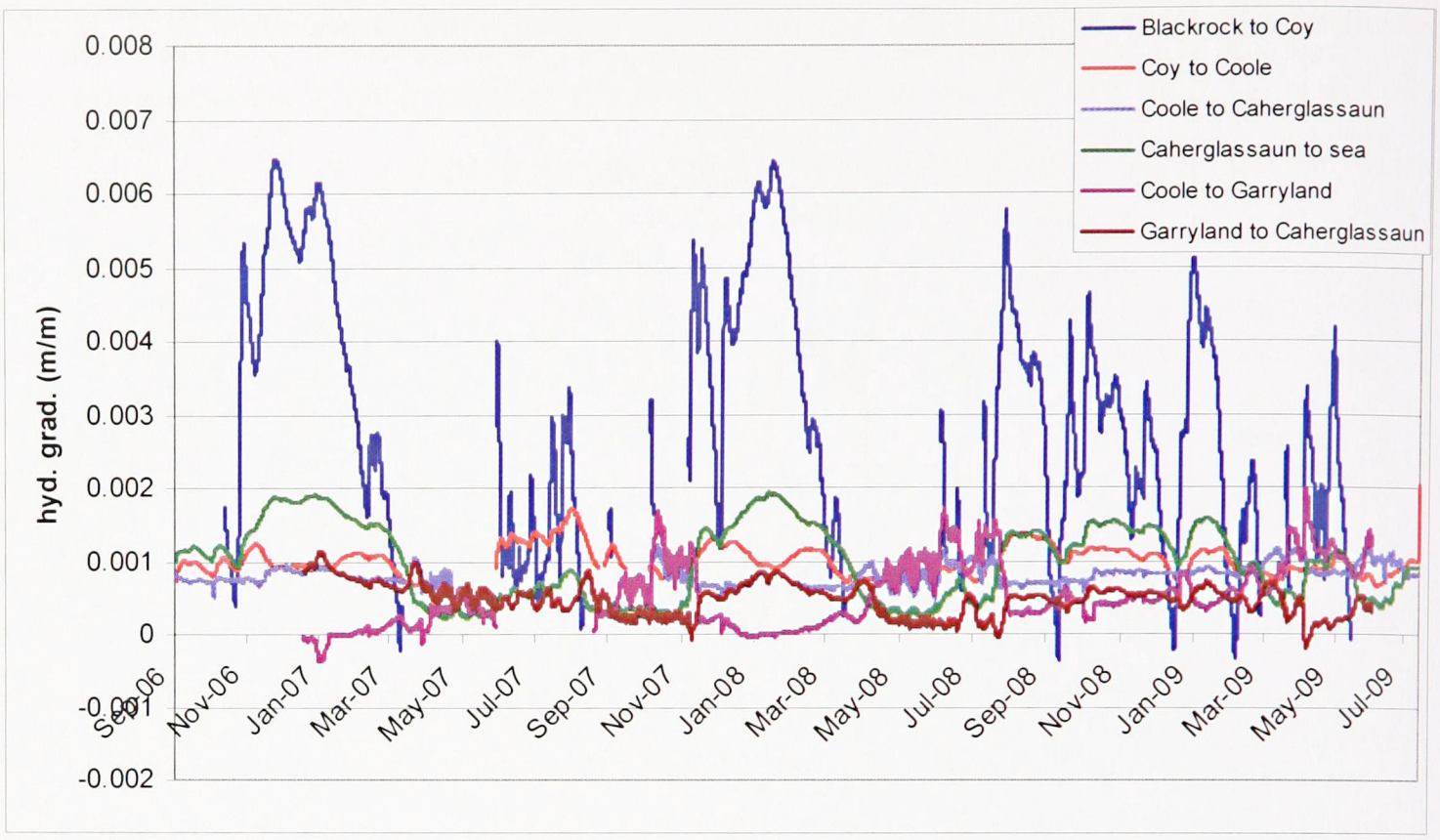


Figure 5.4 Hydraulic gradients between Blackrock, Coy, Coole, Caherglassaun turloughs and the sea at Kinvarra (2006 to 2009).

There is an interesting period in the summer of 2007 where the levels of Coole drop below Garryland. This is thought to be due to the positioning of the diver in Garryland during this period which was not down at the lowest point in the turlough but in a higher position which was probably isolated from the water table at low stages as it was in a sealed hollow. It should be noted that the diver's position was changed that summer after the annual data download, being relocated to the bottom of the main sink hole – it's depth was resurveyed to tie it in with Ordnance Datum. It is also interesting to compare this recent data to data that was collected in four of the turloughs (Garryland not being monitored during this time) between 1999 and 2003 (Figure 5.5) which reveals the same patterns and values i.e. high fluctuations in Blackrock and more muted peaks in Caherglassaun with the rest more or less flat.



Figure 5.5 Hydraulic gradients between Blackrock, Coy, Coole, Caherglassaun turloughs and the sea at Kinvarra (1999 to 2003).

5.4 Depth-Volume-Area Relationships

As described in Section 4.6, the GPS survey data was imported into Surfer® 8.6 in order to produce depth-volume-surface area relationships. Hence, knowing the change in volume across each time step enabled the net flow into or out of each turlough to be calculated. The depth-volume relationship for Blackrock turlough with fitted trend line is shown in Figure 5.6 below whilst all other relationships are in Appendix B.

The maximum volumes of the 5 turloughs and mean / median volumes (when full) are shown on Table 5.2. Coole is at least twice the size of the next biggest turlough (Blackrock) with a maximum amount of water at 9 million cubic metres. The maximum to mean volume ratios are plotted on Figure 5.6 which clearly show a common pattern for Coole, Garryland and Caherglassaun over the three years (again indicating intimate hydraulic linkage). Coy shows a remarkably consistent ratio across the three years which were very different in terms of rainfall and turlough response. Again, this may indicate some control on the maximum level in the turlough such as a high level overflow. Finally,

Blackrock shows a different, almost opposite, pattern from the three downstream turloughs with the smallest variation in the 2007/08 year.

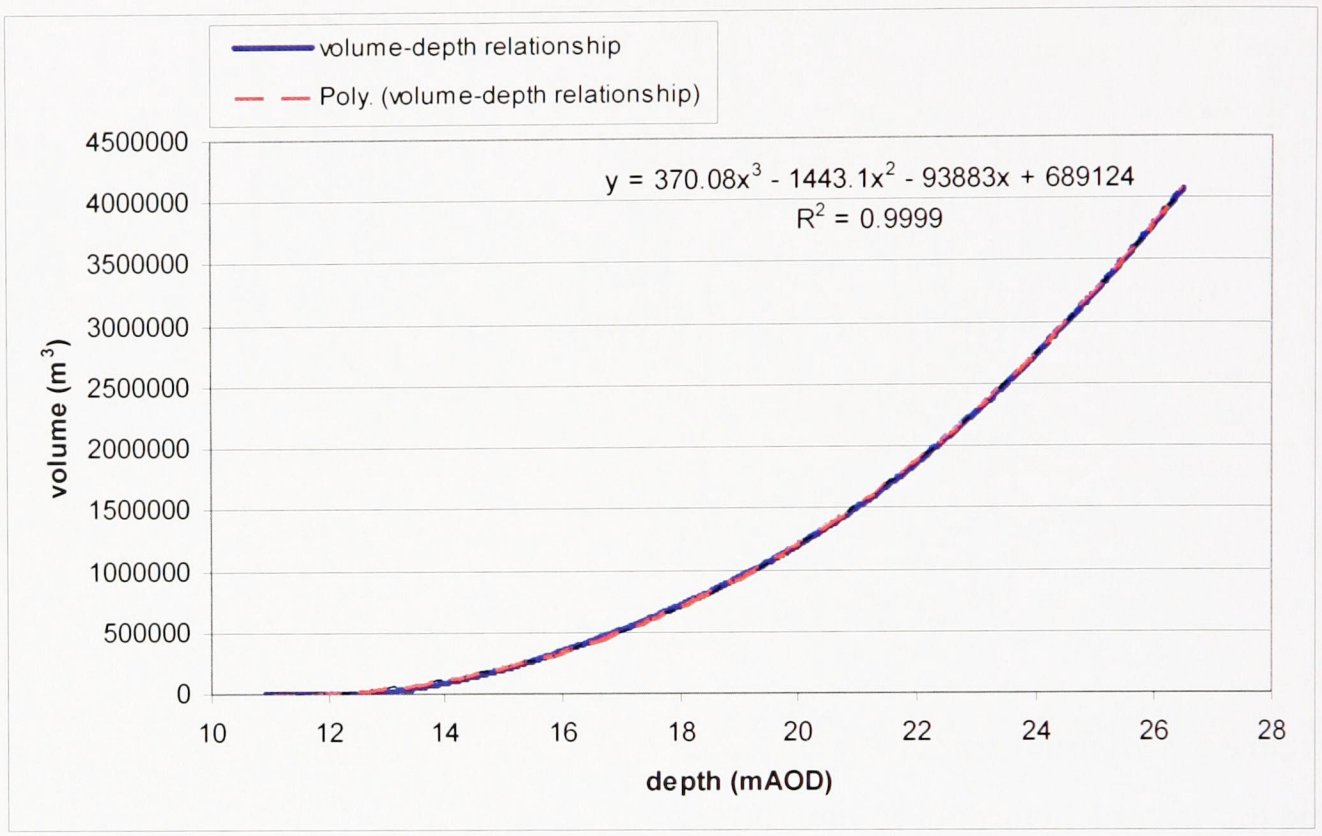


Figure 5.X Depth-volume relationship for Blackrock turlough.

Table 5.2 Statistics on turlough volumes for 2006 to 2009.

	Oct.06 to Sept.07		Oct.07 to Sept.08		Oct.08 to Jul.09	
	Max vol. (10^6 m^3)	Mean vol. (10^6 m^3)	Max vol. (10^6 m^3)	Mean vol. (10^6 m^3)	Max vol. (10^6 m^3)	Mean vol. (10^6 m^3)
Blackrock	4.16	1.45	4.05	1.89	2.47	0.76
Coy	1.48	0.80	1.45	0.75	1.38	0.66
Coole	9.09	2.90	8.70	2.62	6.36	3.00
Garryland	2.33	0.63	2.14	0.53	1.39	0.63
Caherglassaun	3.03	1.02	3.06	0.91	1.93	0.90

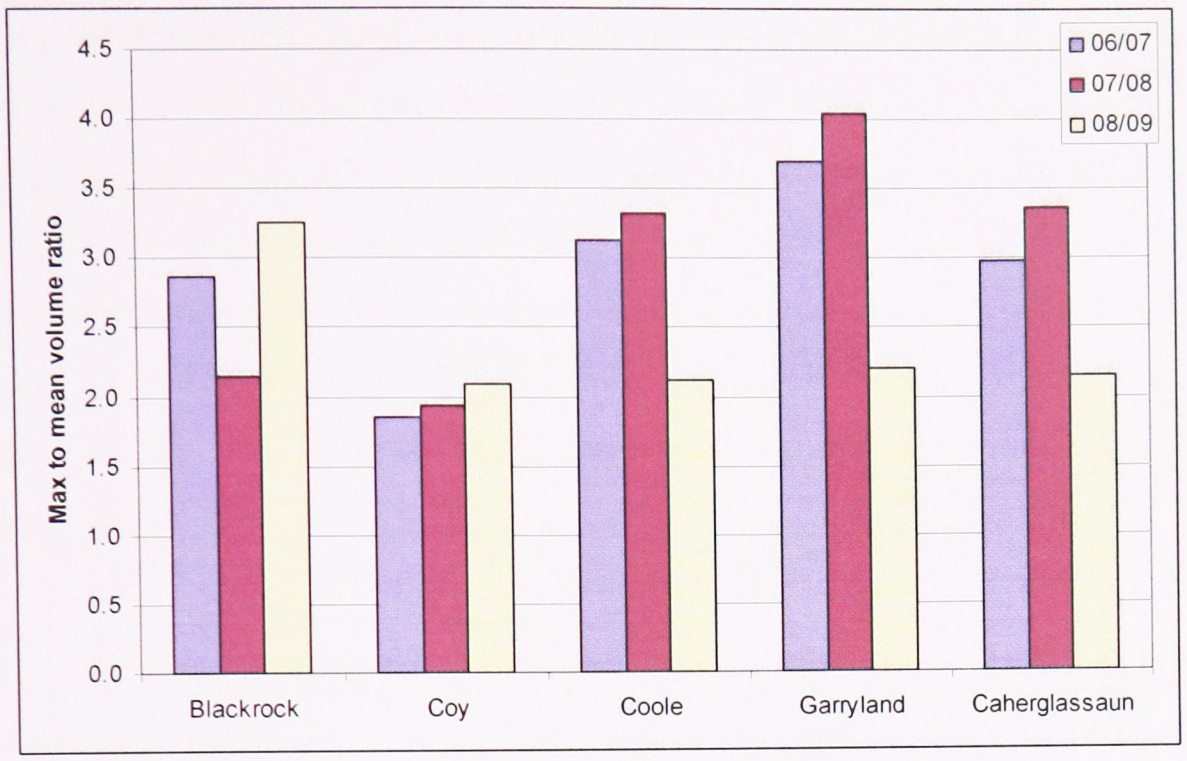


Figure 5.6 Max to mean volume ratios for three consecutive hydrological years.

5.5 Flow and residence time analysis

From these depth-area analyses for each turlough basin, the changes in water level (as recorded by the divers) can be turned into net flow rates into or out of each turlough. A series of recessions and filling periods have been analysed which can be seen on the main chart, Figure 5.1, or more clearly on the water level plots for individual hydrological years in Appendix C.

5.5.1 Recession curves

The analysis of the periods when the turloughs were draining (in recession) can yield key information about the nature of the network. Two examples of major recession periods in 2009 are shown on Figure 5.7 - the rest are contained in Appendix C. These show an interesting relationship between Blackrock and Coy whereby flows start to drain out of Blackrock at an increasing rate up to a peak of about 2 m^3/s and then drop away more as would be expected for a raised tank draining back down through an orifice into the underlying network (like a bath emptying). So, the initial period whereby flows increase is somewhat unexpected but can be explained by the capacity of the underlying network changing with time. Coy meanwhile shows increasing rates of draining up to a maximum of about 0.9 m^3/s but these maxima occur much later than the peak flows out of Blackrock

and only when Blackrock has generally dropped to flows of under 1 m^3/s during periods when the recession water level in the turlough is in the range 15.5 to 16.5 mAOD. So the higher head at Blackrock effectively pushes its water preferentially down the network until this time.

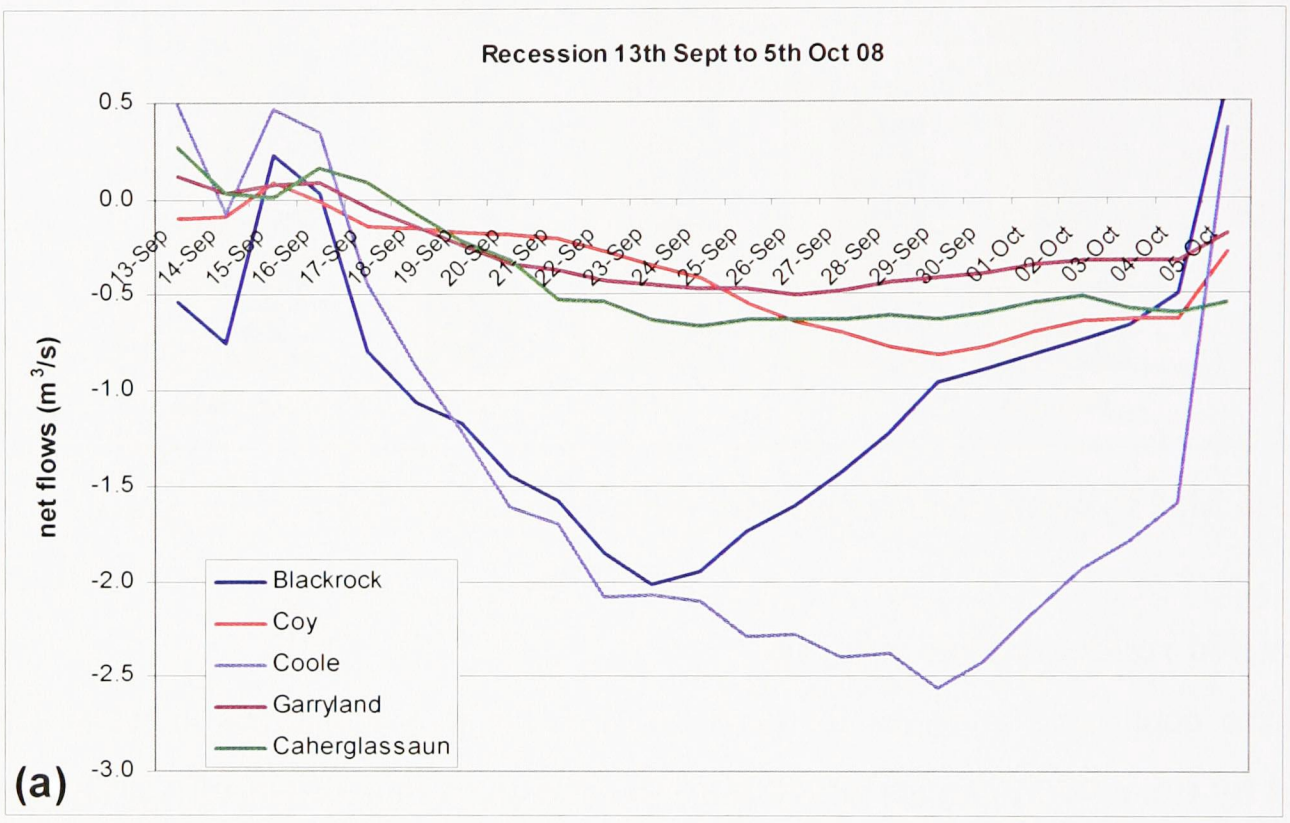


Figure 5.7 Two periods of turlough recession in (a) 2008/09 season and (b) 2007/08 season.

The flow response from the lower turloughs shows a delayed recession as would be expected being lower down the system although, interestingly, the start of the recessions all occur at approximately the same time. Also, interesting is that the maximum flows out of Coole are more or less the same as Blackrock (~2 m^3/s). This pattern (Figure 5.7(a)) is the more normal response during recessions. However, there is another type of recession as shown in Figure 5.7(b) whereby Blackrock and Coole show a more similar profile in terms of timing, possibly due to different rainfall patterns across the Slieve Aughty range which has slightly delayed the Blackrock recession with respect to Coole.

The net water leaving both Blackrock and Coy is shown below (Figure 5.8) for several periods of recession, plotted so they all start at the same time. This shows that the peak flow entering the downstream network is about 2.4 m^3/s (depending on upstream head and flow still passing through from the Owenshree river); other recessions which start from lower turlough depth levels show smaller net flow rates. However, it can be seen that the rate of increase in flow rates at the start is similar for most of the recessions. Also of interest is that once the peak draining flows start to fall, it seems to be a very similar gradient for several of the recessions, reducing at a rate of approximately 0.11 m^3/s per day. The traces all show the same pattern whereby the net flows increase as the drainage network underneath starts to have spare capacity to a peak value from which the flows start to decrease as the head drops, as discussed above and as illustrated theoretically on Figure 5.9. Following the rainfall, the contribution from the river decays away exponentially. The contribution from the turlough then starts to increase to make up for the spare capacity up to the maximum limit of the network. After some time (arbitrarily = 15 on Figure 5.9) the turlough is draining more or less freely, regulated by its own discharge orifice whereby the flow rate drops exponentially with reducing head.

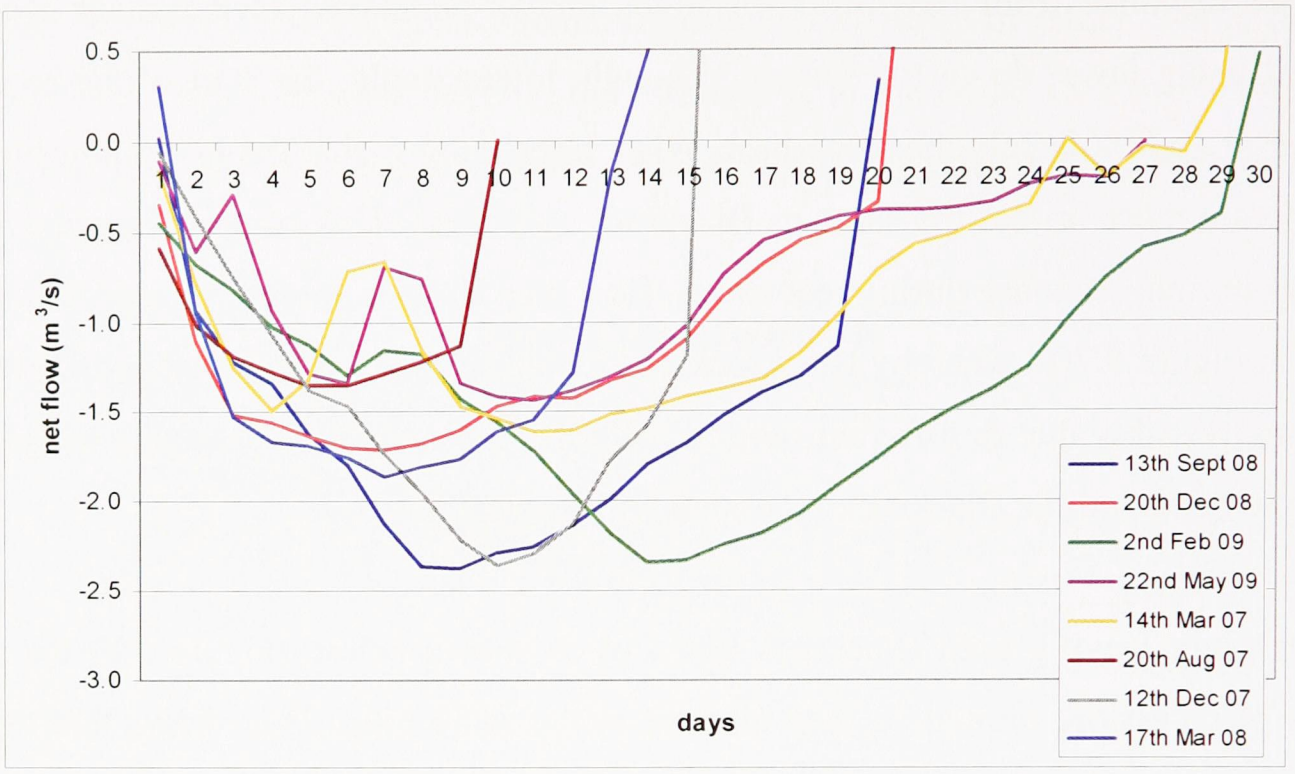


Figure 5.8 Net flow leaving Blackrock and Coy during different periods of recession.

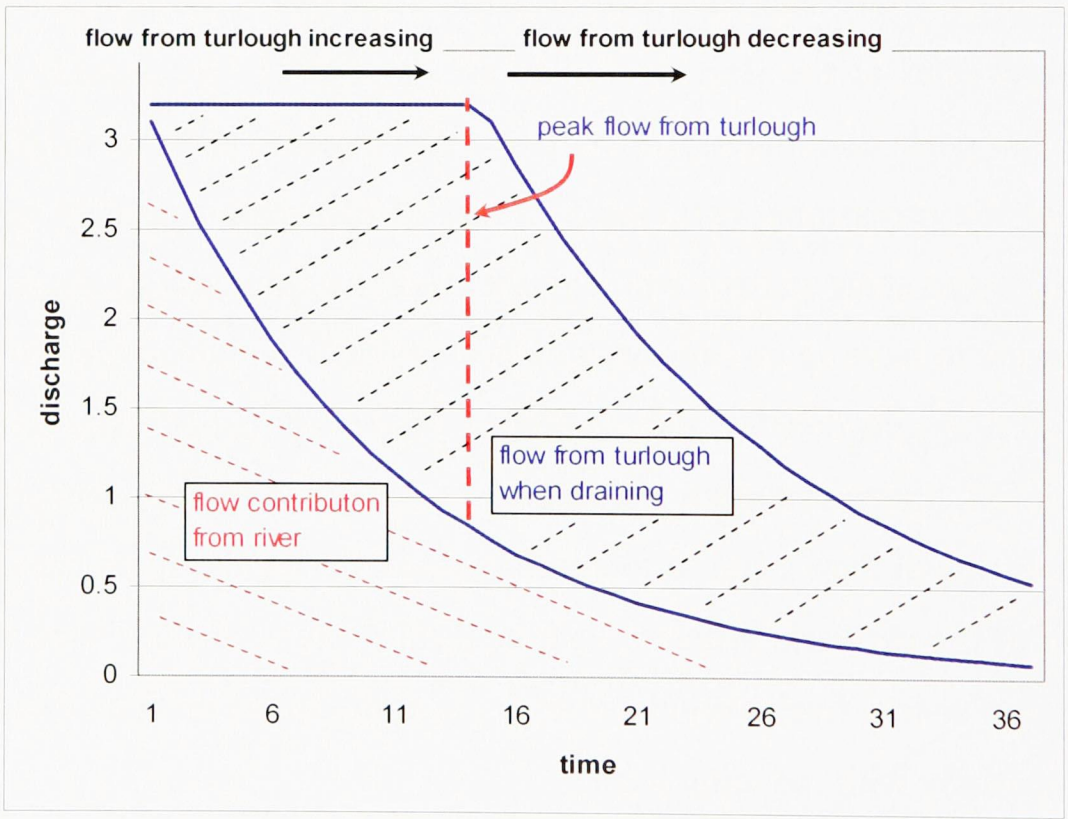


Figure 5.9 Illustration of proportion of flows in underground network during turlough recession periods.

An analysis of the net flows from Blackrock with respect to head difference with the water level in Coy is shown in Figure 5.10 which again illustrates how the flows out of Blackrock increase as the relative head drops (which might initially appear counter-intuitive for a draining tank) until reaching a peak at just over 2 m head difference between

the levels from which point the system seems to drain more as expected. Similar plots for the other recessions periods are included in Appendix C. Figure 5.11 shows the same plot but the head difference is taken with respect to Coole (where the network discharges out into an open channel) which is perhaps more pertinent. This shows a similar pattern, with peak flows of 2 m^3/s reached at a head difference of about 12 m.

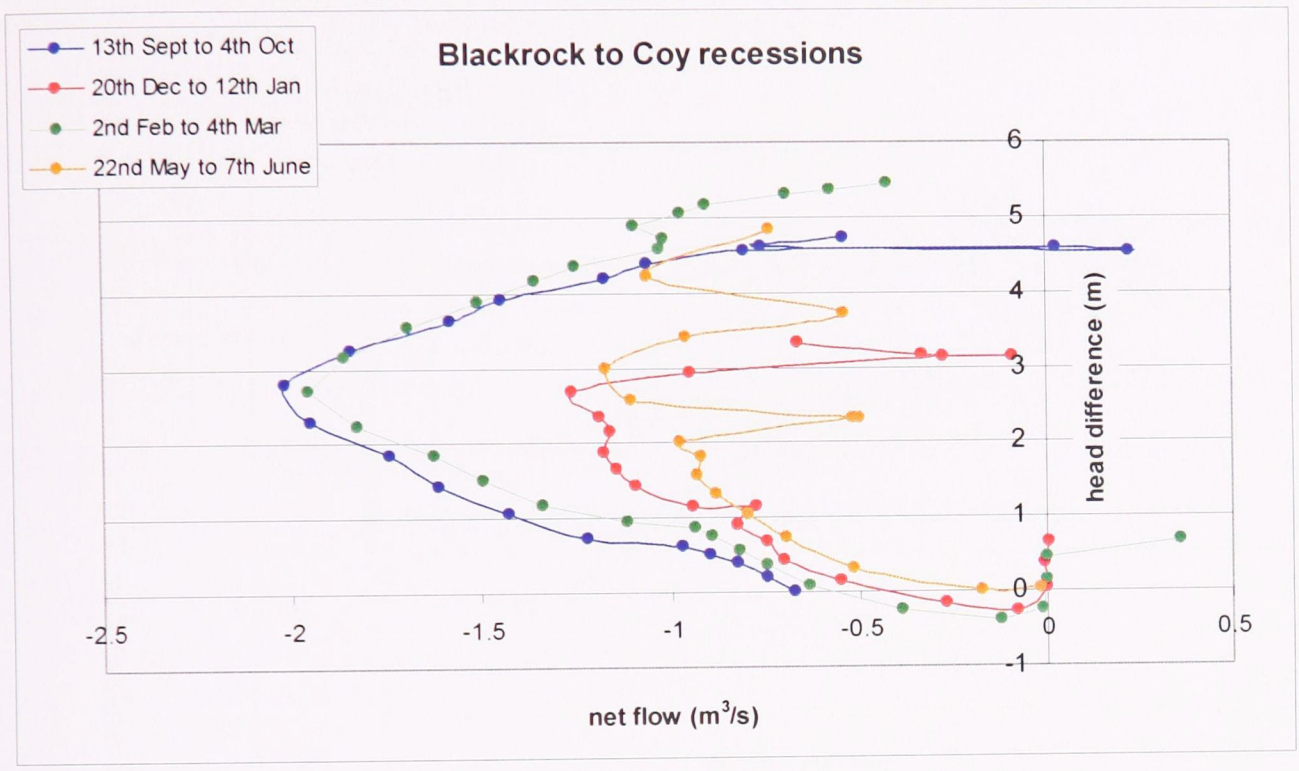


Figure 5.10 Net flows from Blackrock against head difference to Coy for four periods of turlough recession in 2008/09 season.

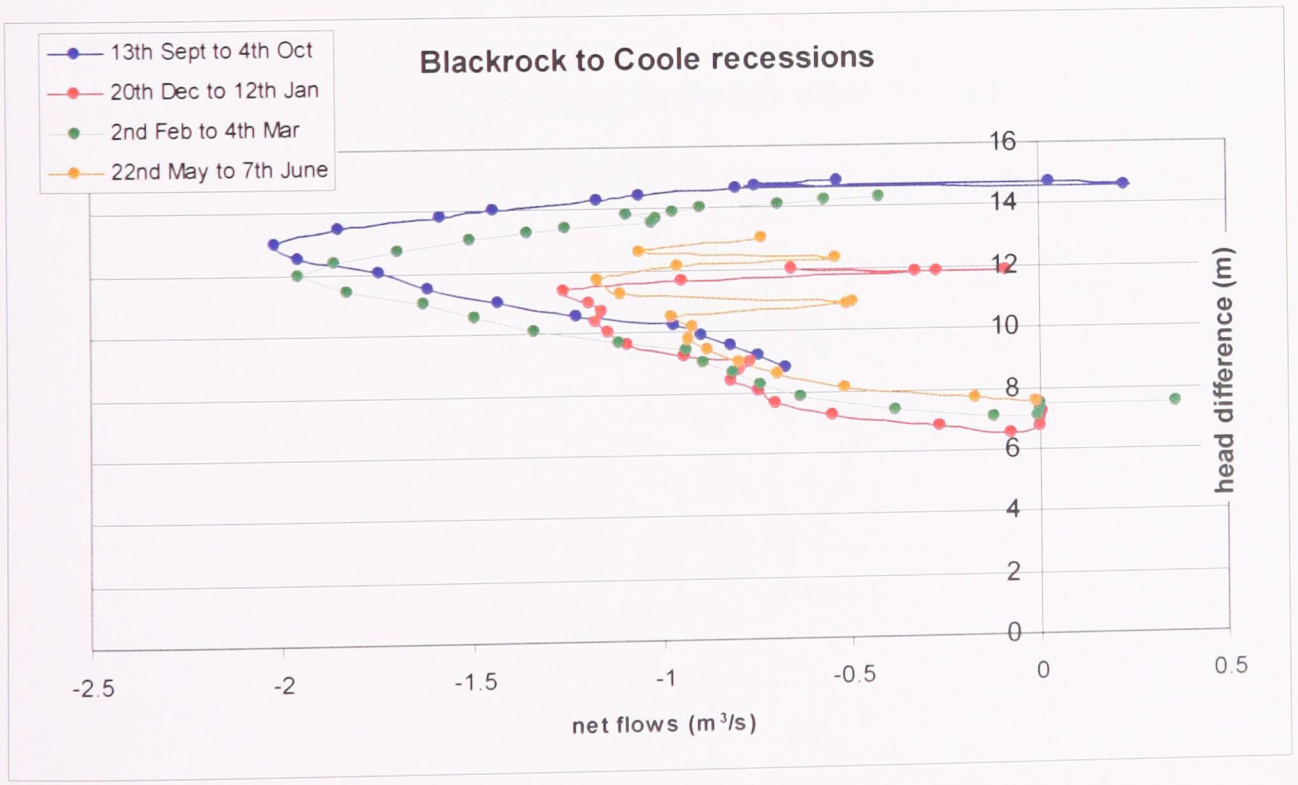


Figure 5.11 Net flows from Blackrock against head difference to Coole for four periods of turlough recession in 2008/09 season.

Similarly when looking at Coy with respect to Blackrock the data shows (Figure 5.12) that peak flows of just over 0.8 m^3/s enter the network when the relative head is less than 1 m between them. This is also indicated in a plot of flow from Blackrock vs. flows from Coy (Figure 5.13) where the flows peak at a ratio of about 5:1 (Blackrock to Coy flows) – i.e. 2 to 0.4 m^3/s respectively and 1.25:1 - i.e 1 to 0.8 m^3/s - for peak Coy flows.

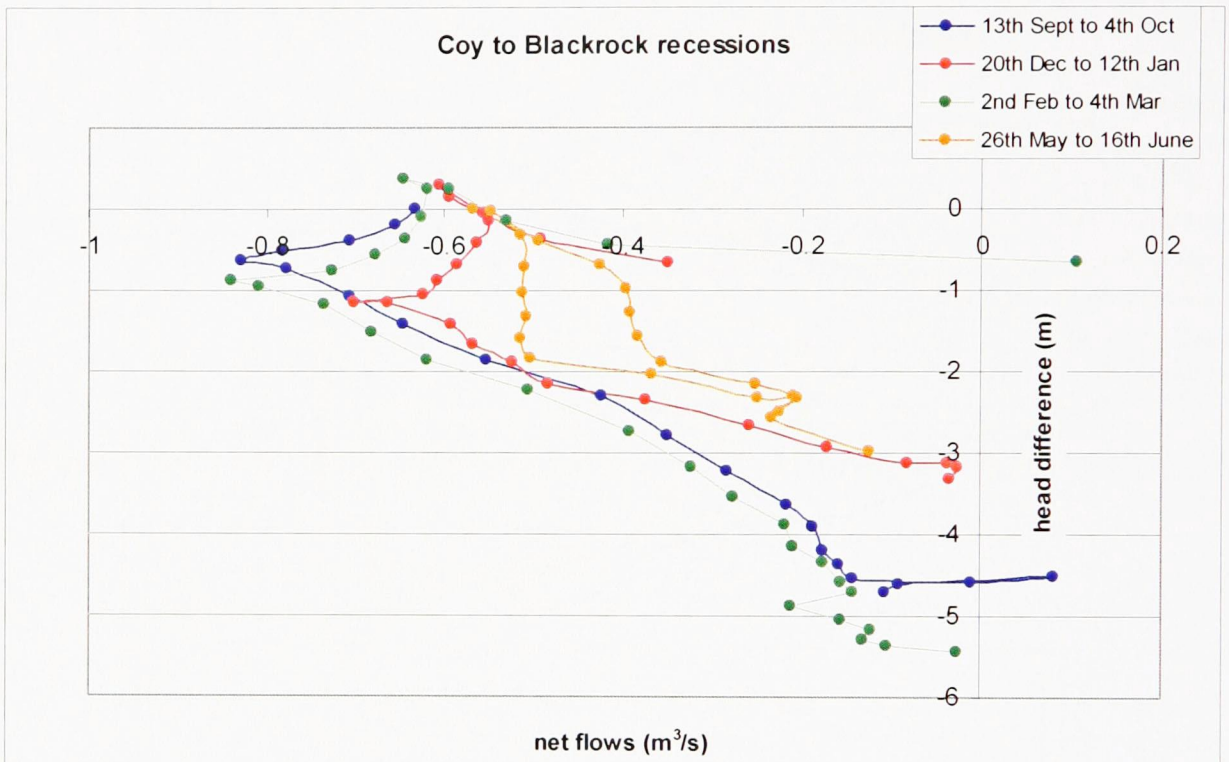


Figure 5.12 Net flows from Coy against head difference with Blackrock during recession periods.

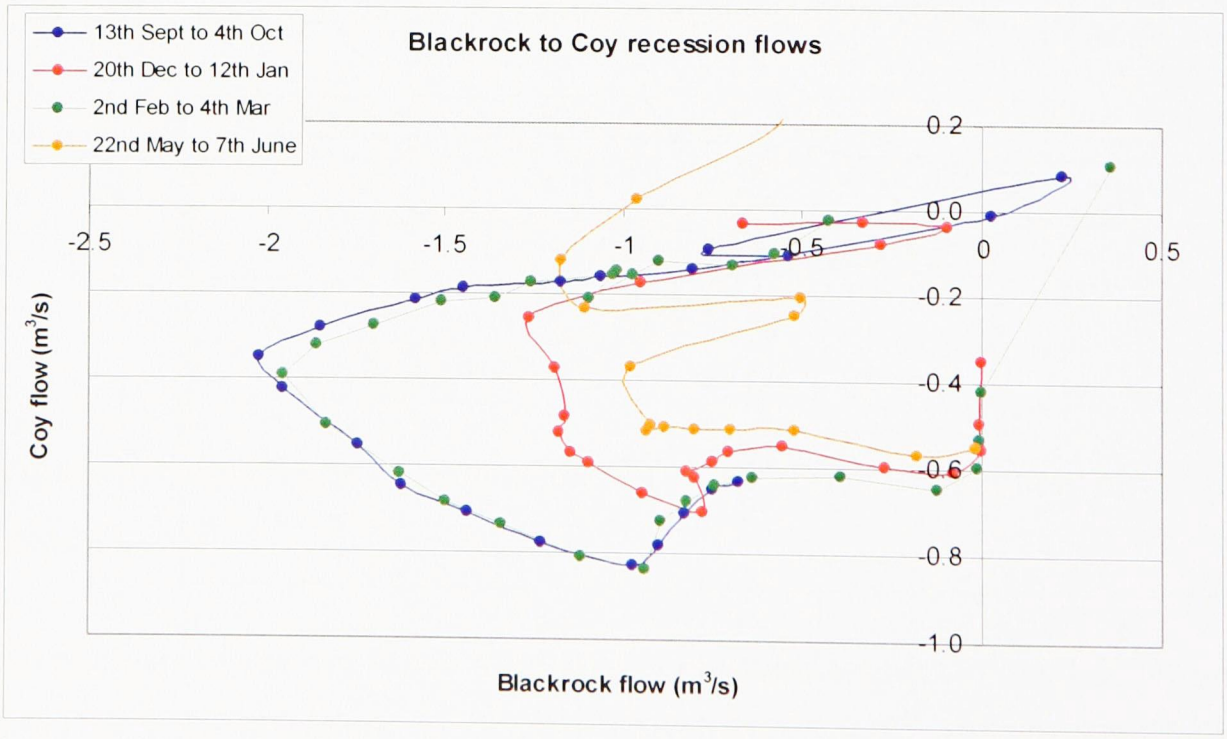


Figure 5.13 Net water leaving both Blackrock and Coy during recession periods.

For the downstream turloughs a plot of net flows from Caherglassaun with respect to head difference back up to Coole (Figure 5.14) shows little variation in flows for changes in head, reflecting a relatively unconstrained connection between the two. This is confirmed by the plot of net flows out of each turlough against each other (Figures 5.15 & 5.16) which show a linear relationship and indicate more or less proportional draining at the same time with Coole contributing just over four times the total flow into the network compared to Caherglassaun.

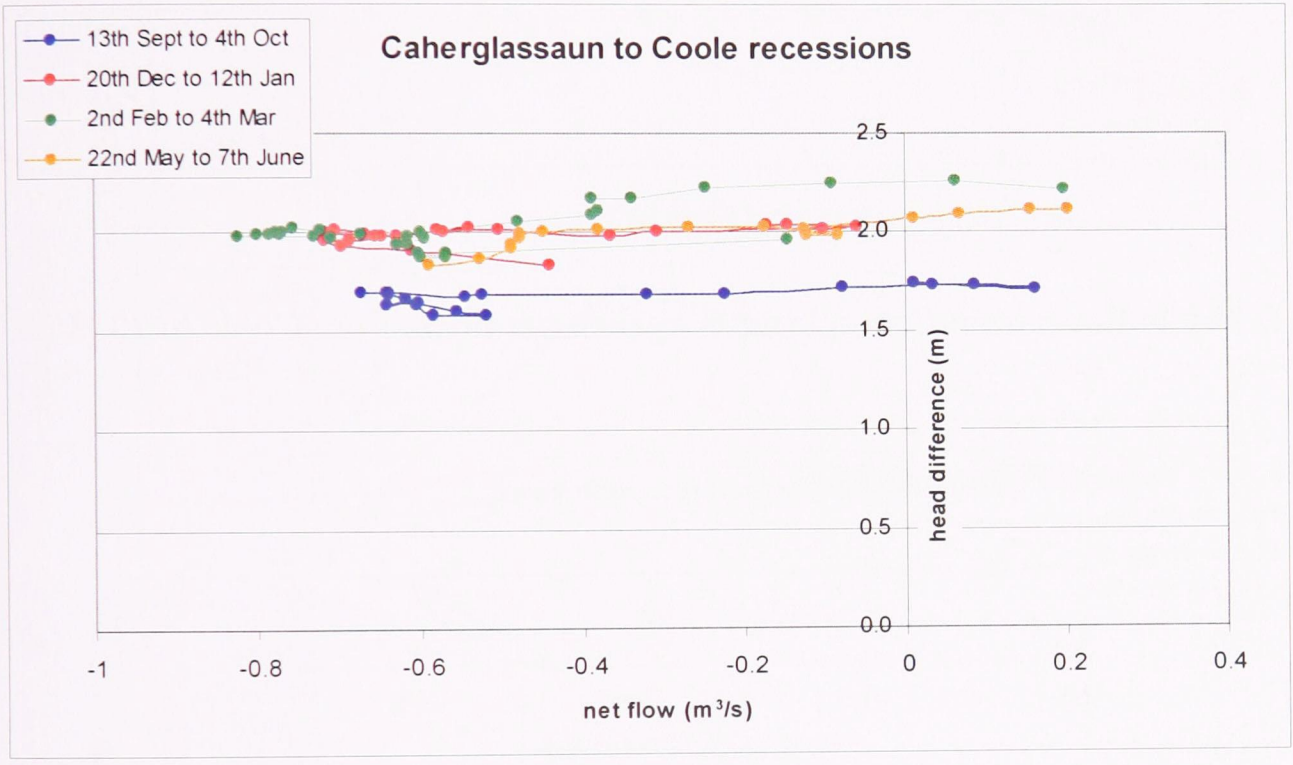


Figure 5.14 Net flows from Caherglassaun against head difference back to Coole for four periods of turlough recession in 2008/09 season.

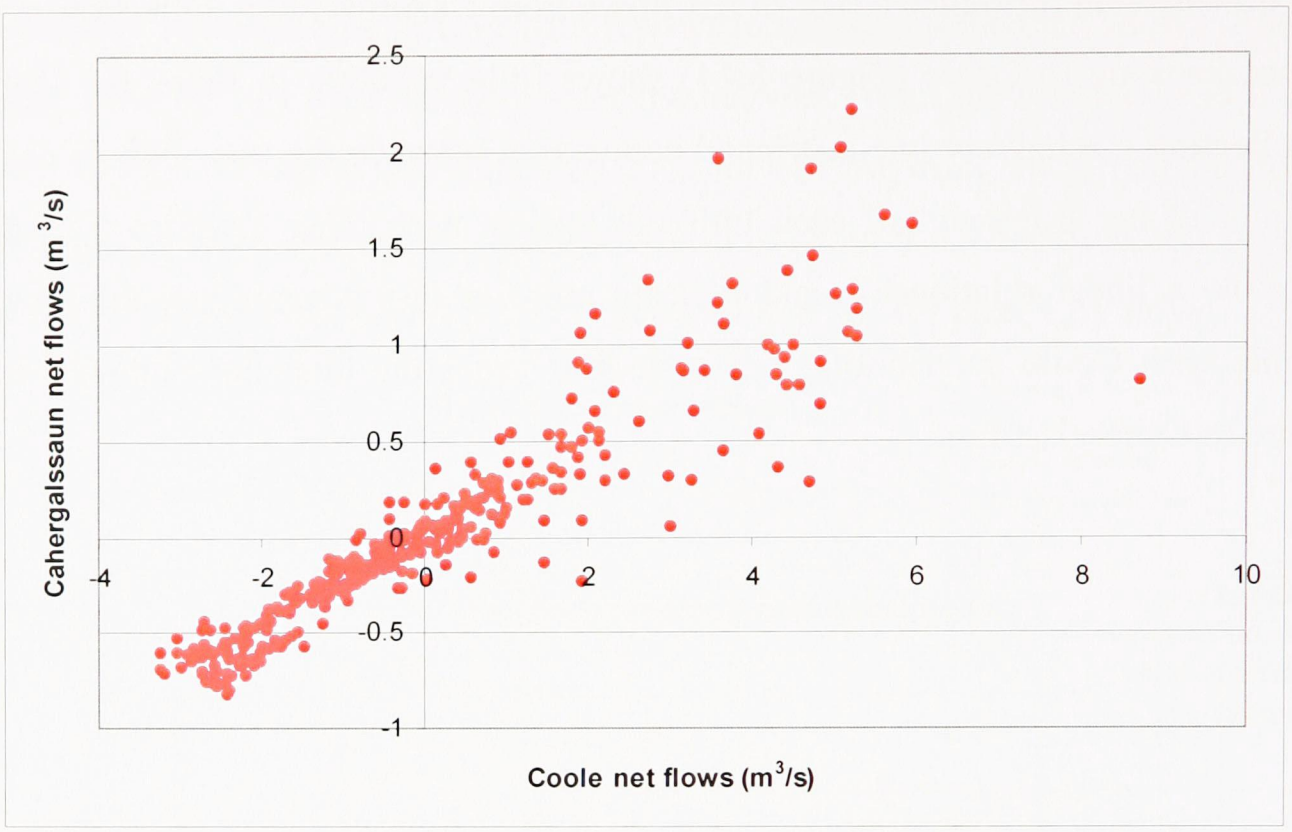


Figure 5.15 Net flows from Caherglassaun against net flows from Coole in 2008/09.

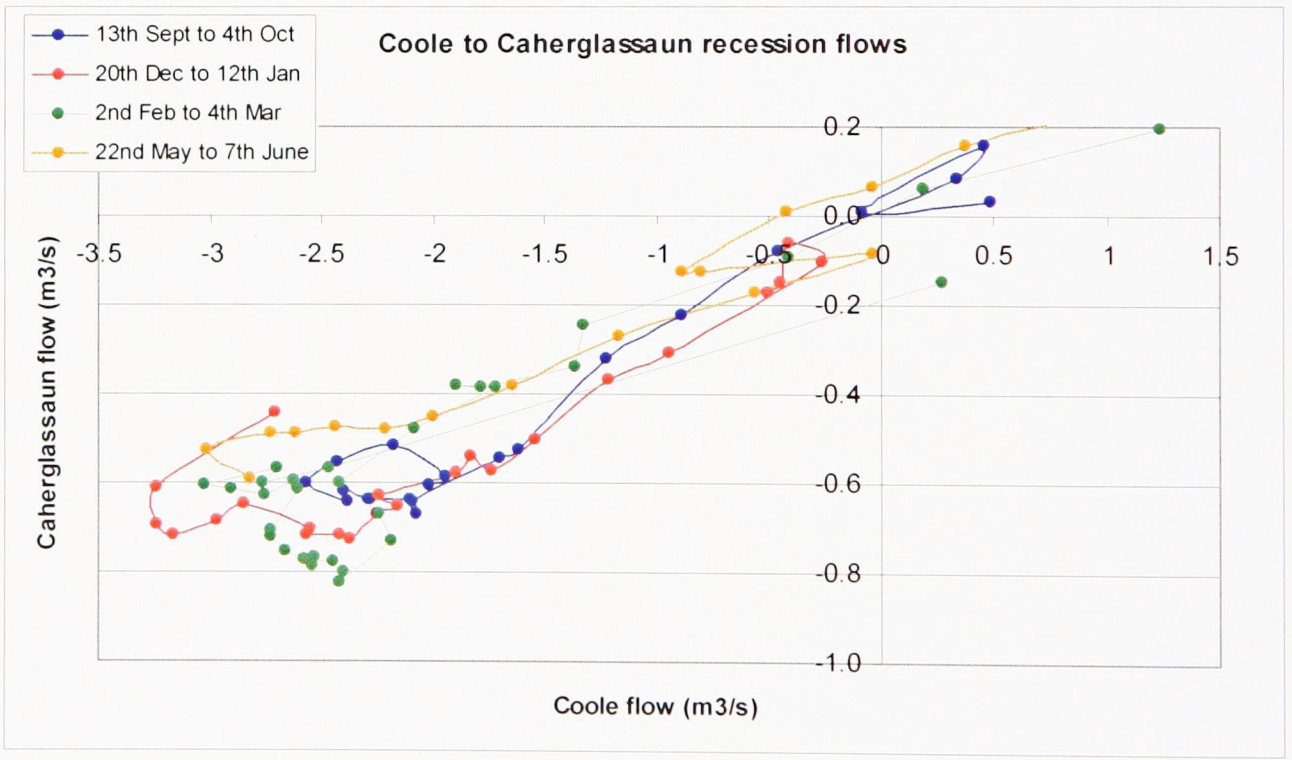
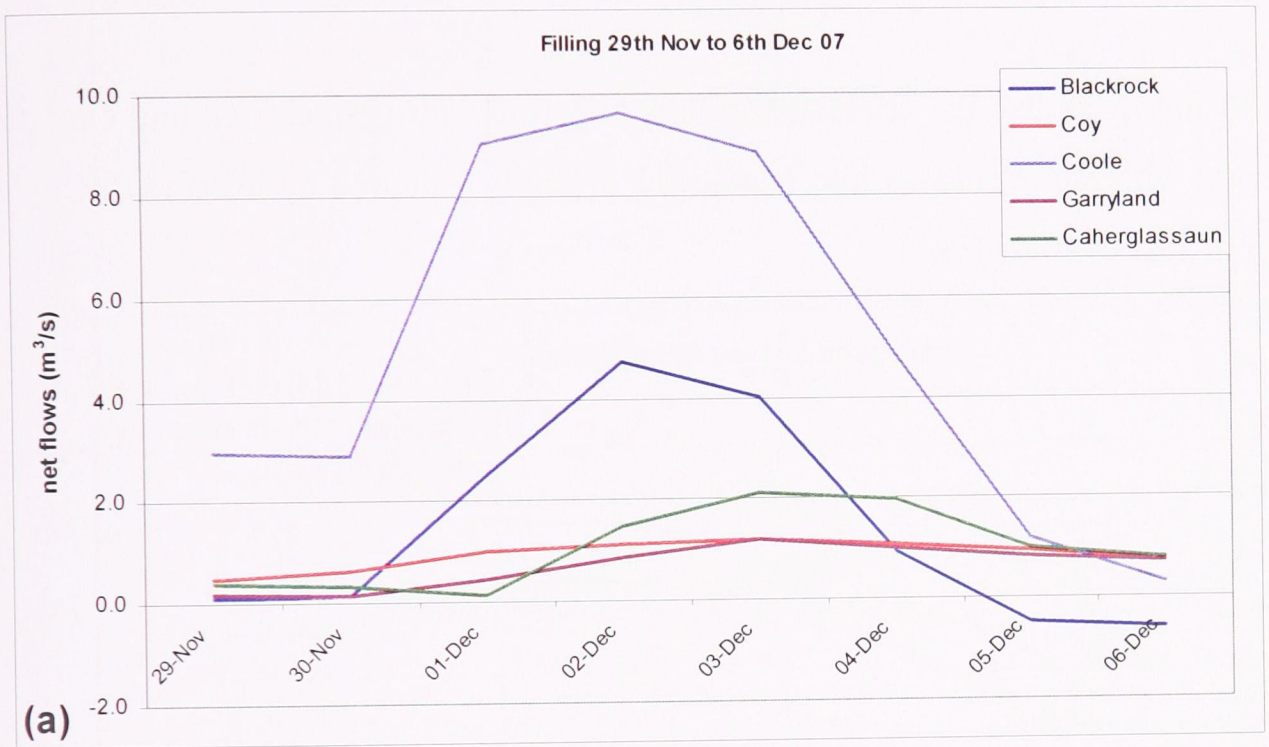


Figure 5.16 Net flows from Caherglassaun against net flows from Coole for four periods of turlough recession in 2008/09 season.

5.5.2 Filling periods

The main filling periods of the turloughs have been analysed and relative flows between the turloughs calculated. For example, two periods of sharp turlough rise in the 2008/09

season are shown in Figures 5.17 below with the rest in Appendix C. These show the sharp increase in flows in Blackrock compared to the more muted response in Coy. Peak flows of up to 10 m^3/s enter Blackrock and Coole over a daily basis (i.e. more than 0.6 million m^3 per day). It should be noted that such flow rates could not be achieved using a conceptual model of the turlough filling by epikarst type flow scenario with the typical hydraulic conductivities for matrix or fracture flow in karst as reported in Section 2.2.2 (matrix flow ~ 2 x 10^{-11} m/s; fracture flow ~ 6 x 10^{-6} to 3 x 10^{-5} m/s).



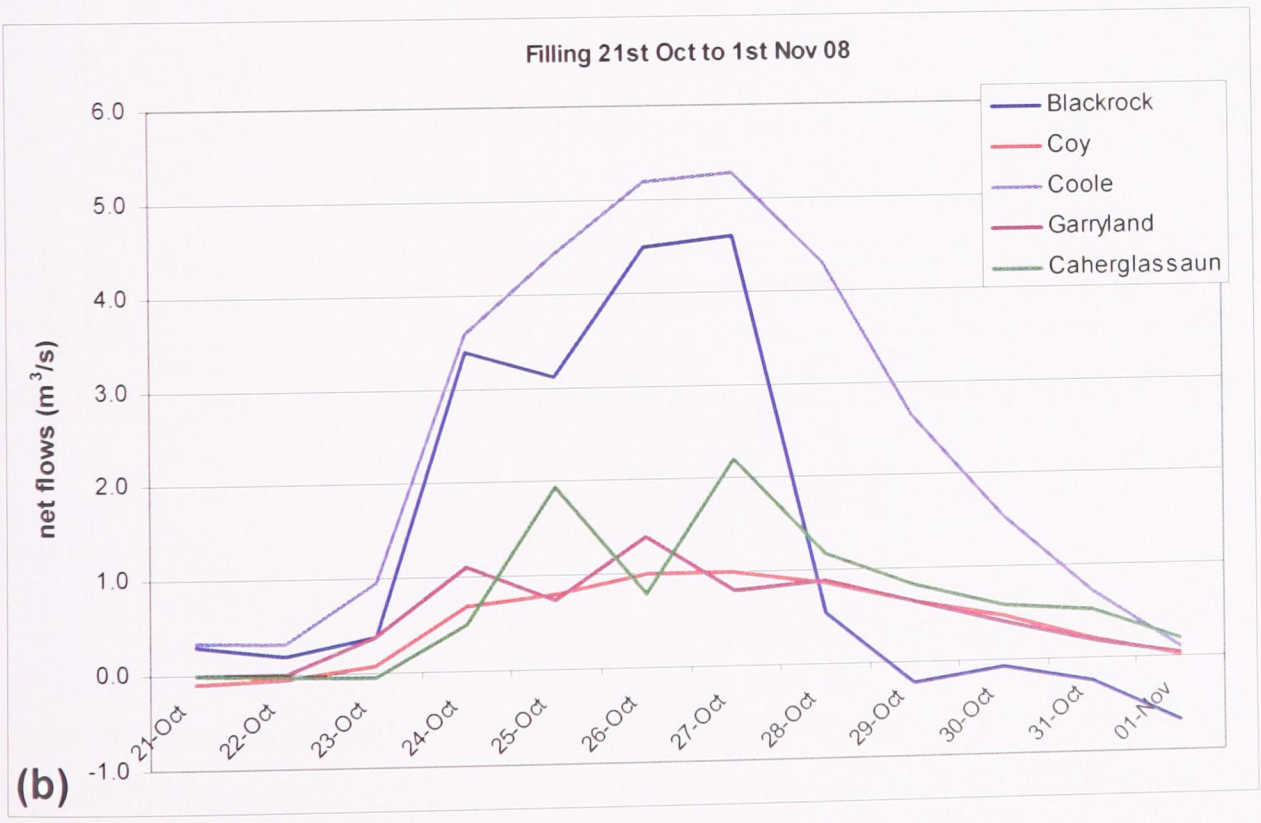


Figure 5.17 Two periods during which the turloughs filled in (a) 2007/08 season and (b) 2008/09 season.

Coy and Garryland only reach net inflows of just over 1 m^3/s which is again indicative of being off the main thrust of the conduit system. Also, it is noticeable that Coy continues to fill for several days after Blackrock has started to recede. At such times the relative head between the two turloughs is still high – hence it may indicate a more direct link between the two turloughs as opposed to two surge tanks above the main line conduit system. Caherglassaun is somewhere in-between with peak flow rates up to 2 m^3/s (indicative of a constriction between it and the sea).

Figure 5.18 below shows the relationship between flows into Blackrock and Coy during a filling period whereby increases into Blackrock are only matched by inflows to Coy up to a maximum of just over 1 m^3/s.

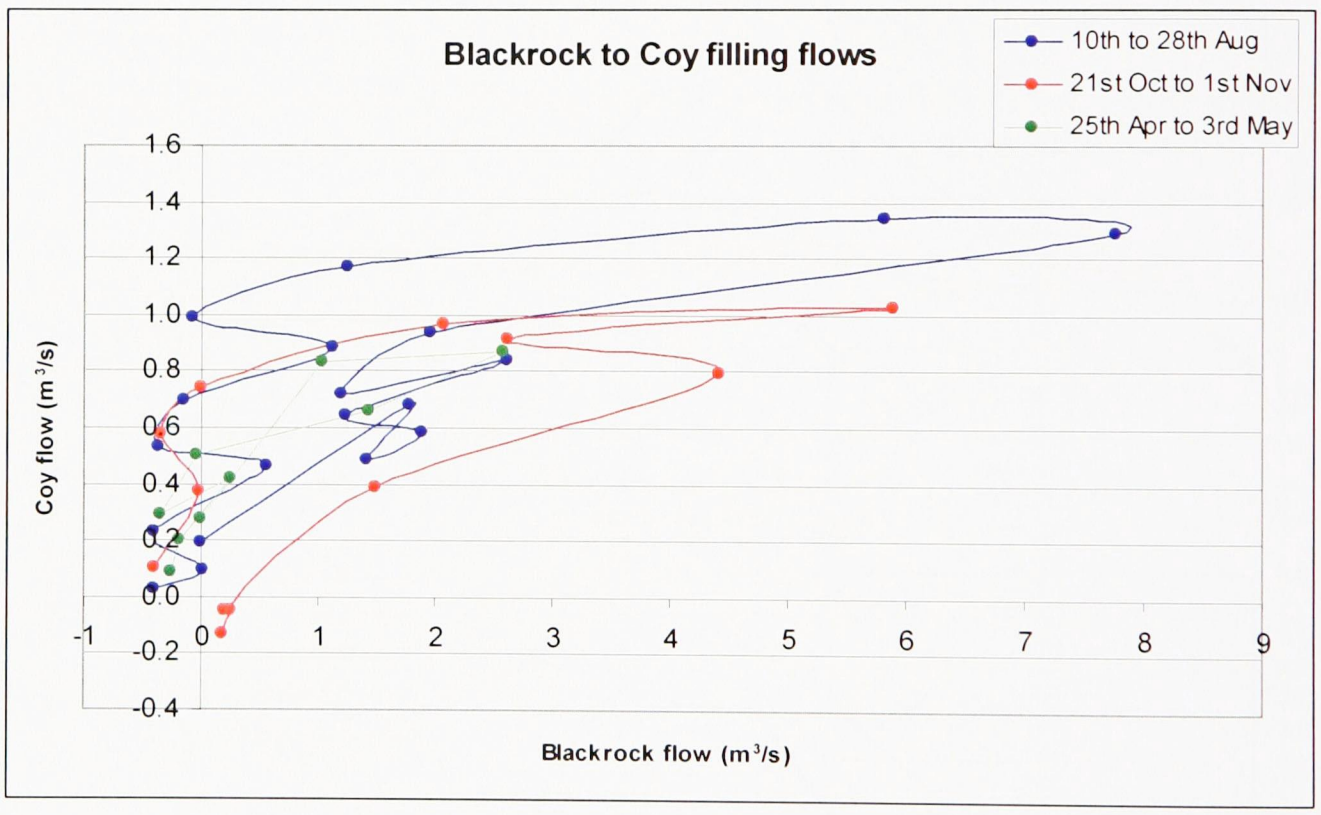
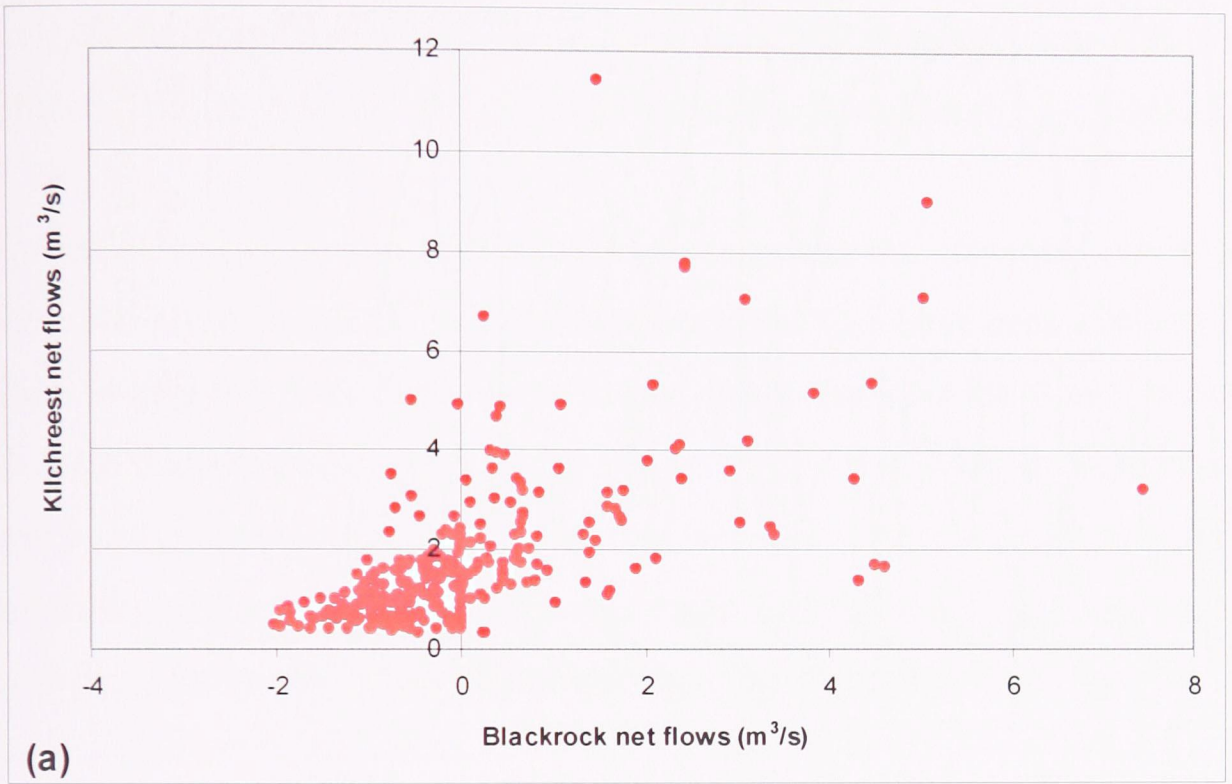


Figure 5.18 Relationship between Blackrock and Coy flows during three separate filling periods in 2009/09 season.

5.5.3 Flows into the system

The contribution of flows into the karst network from turlough and rivers at certain key confluence points have been compared. Figure 5.19 shows the comparison of net flows from Blackrock and Coy turlough with respect to Kilchreest flows. This clearly shows that net flow contribution from the turloughs starts to increase when the Kilchreest flows drop

below about 2 m^3/s with peak values occurring when Kilchreest flows are around 0.4 m^3/s for Blackrock and slightly lower (around 0.25 m^3/s) for Coy. The graphs also show the peak outflows to be 2 m^3/s from Blackrock and 0.9 m^3/s from Coy whilst in recession, as discussed earlier.



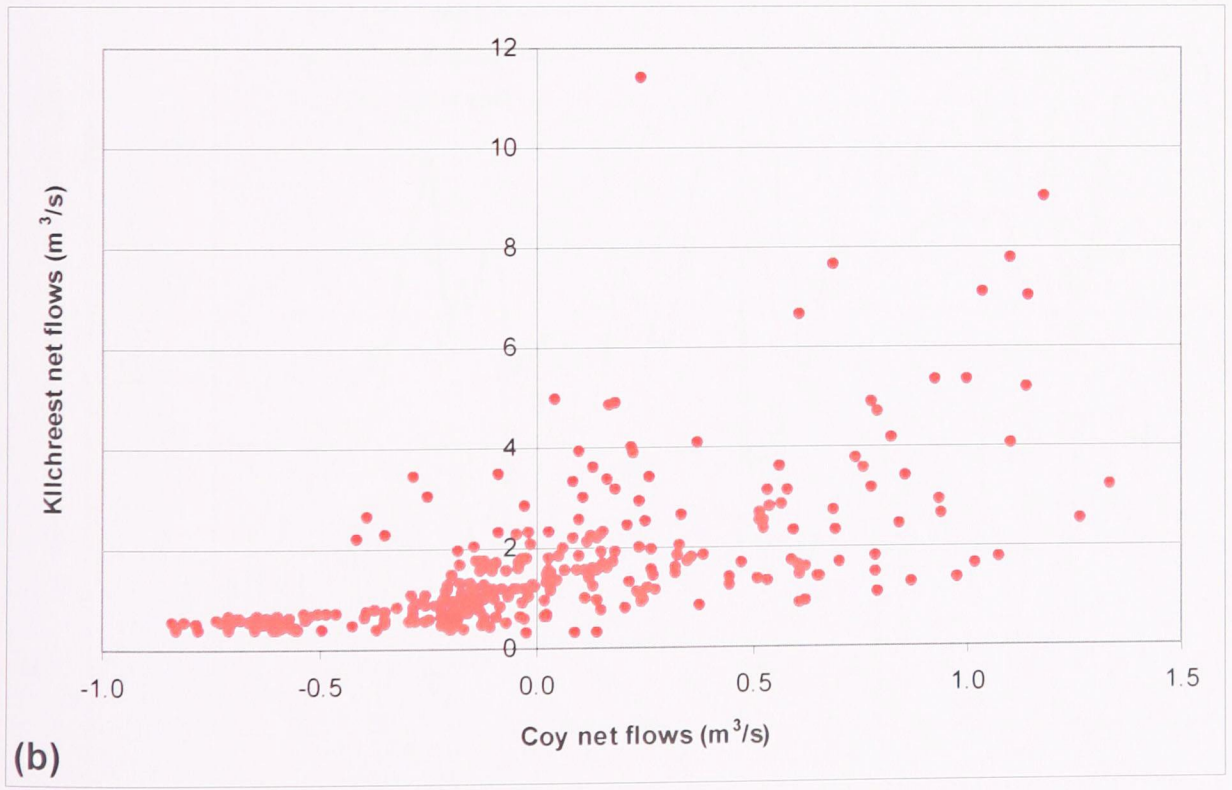
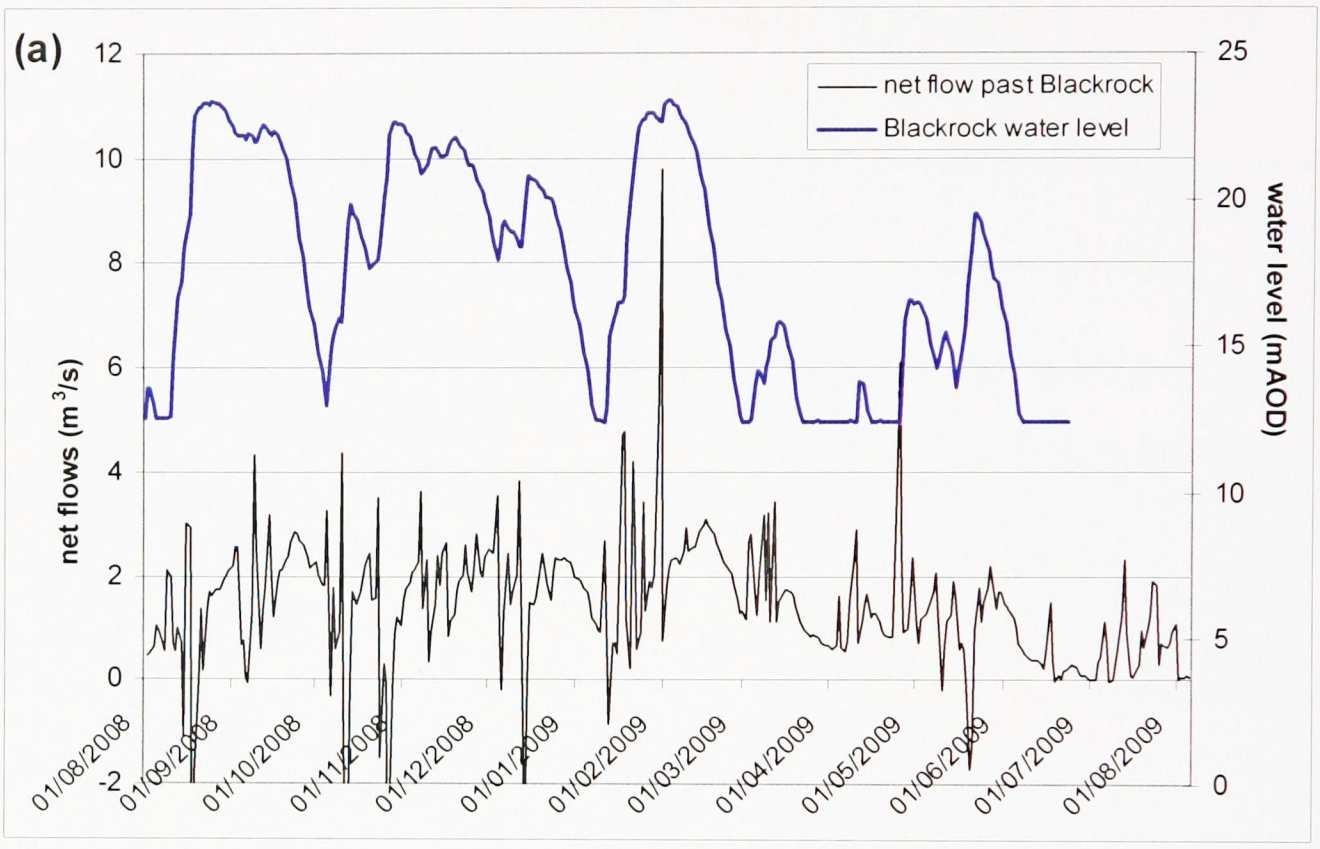


Figure 5.19 Comparison of flows in Kilchreest river to net flows into / out of **(a)** Blackrock and **(b)** Coy turloughs.

A plot of the combined flows just downstream of Blackrock (i.e. net flows from Blackrock plus flows in the Owenshree river) and downstream of Coy (i.e. net flows from Blackrock plus net flows from Coy plus flows along Kilchreest river) is shown in Figure 5.20.



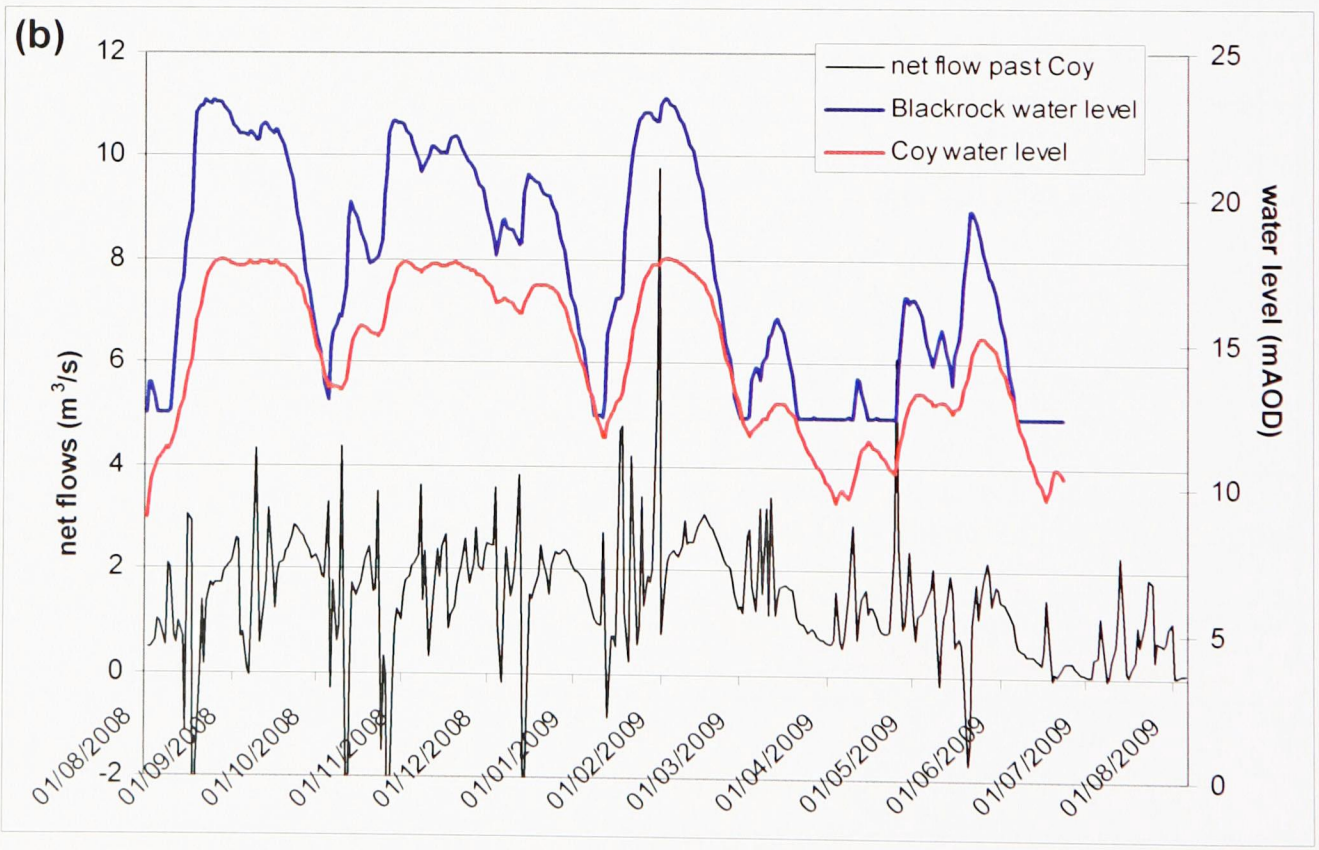
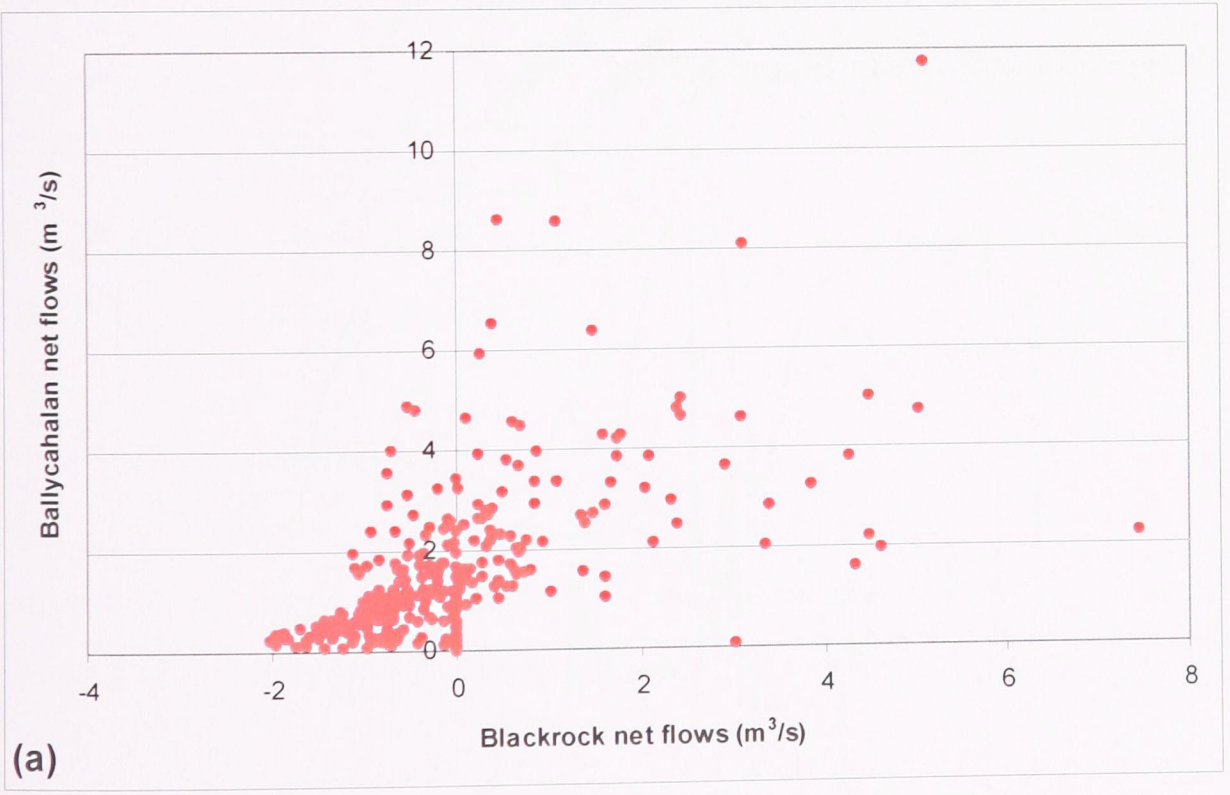


Figure 5.20 Combined flows just downstream of **(a)** Blackrock and **(b)** Coy for 2008/09 period.

Although there are a few extreme values which should be ignored due to the phase difference between the different measuring points (note these are two day averages) the network can be seen to carry a maximum of between 2 to 3 m^3/s past Blackrock and more or less the same past Coy. So, there is no significant increase in capacity downstream of Blackrock, a fact that is used later in Chapter 9 when building the network model for the area. These graphs also show how the mean flow decreases into the underlying conduit when the turlough levels are lower (for example, from March onwards in 2009).

Further downstream the Ballycahalan river meets the network (see Figure 3.1) and so similar analysis on the flows from Blackrock and Coy have been made (Figure 5.21) which again shows the peak outflows at lowest flows draining the river catchment. This might indicate that the backing up of the system is due to the downstream catchment (and not necessarily due to the capacity of the network from Kilchreest). However, the close proximity of the two river catchments mean that the same flow hydrographs are found at both places so possibly this is more likely to be the reason.



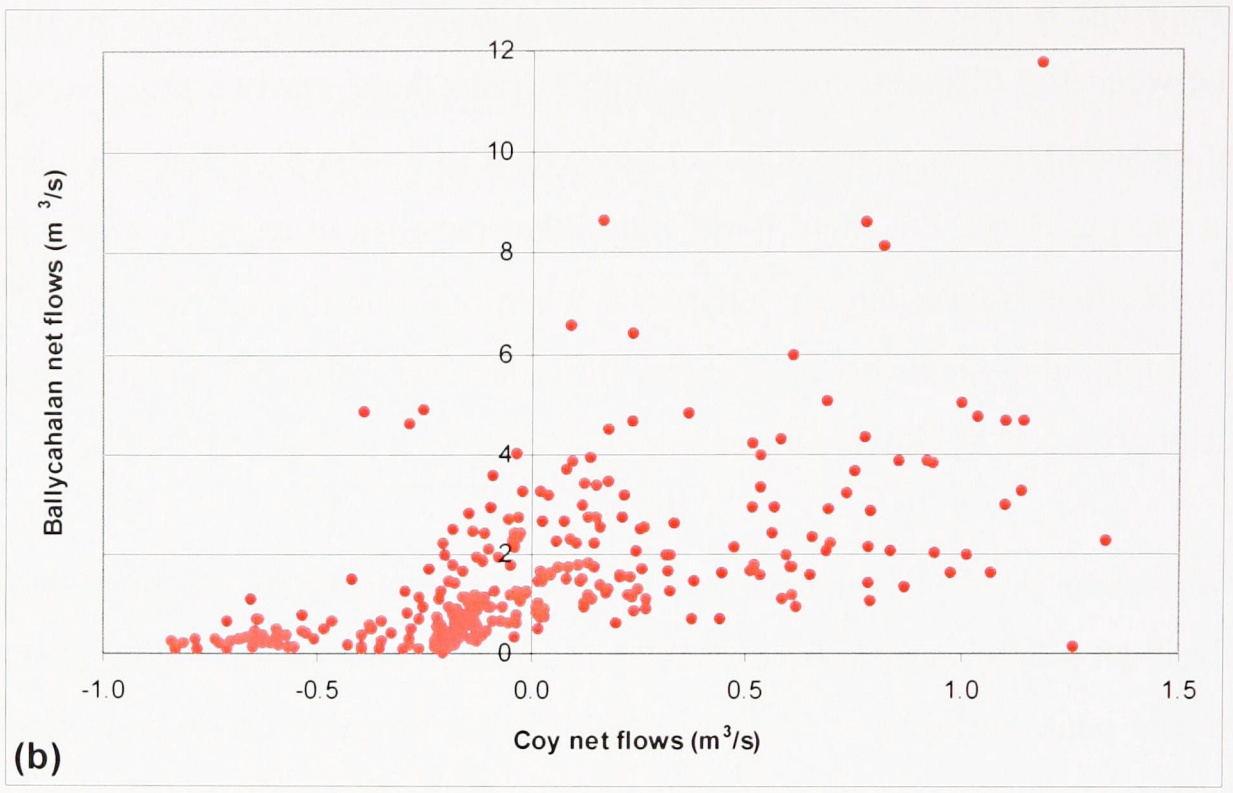


Figure 5.21 Comparison of flows in Ballycahalan river to net flows into / out of **(a)** Blackrock and **(b)** Coy turloughs.

Again the net flows have been plotted following the confluence of the Ballycahalan river flows with the conduit network in Figure 5.22.

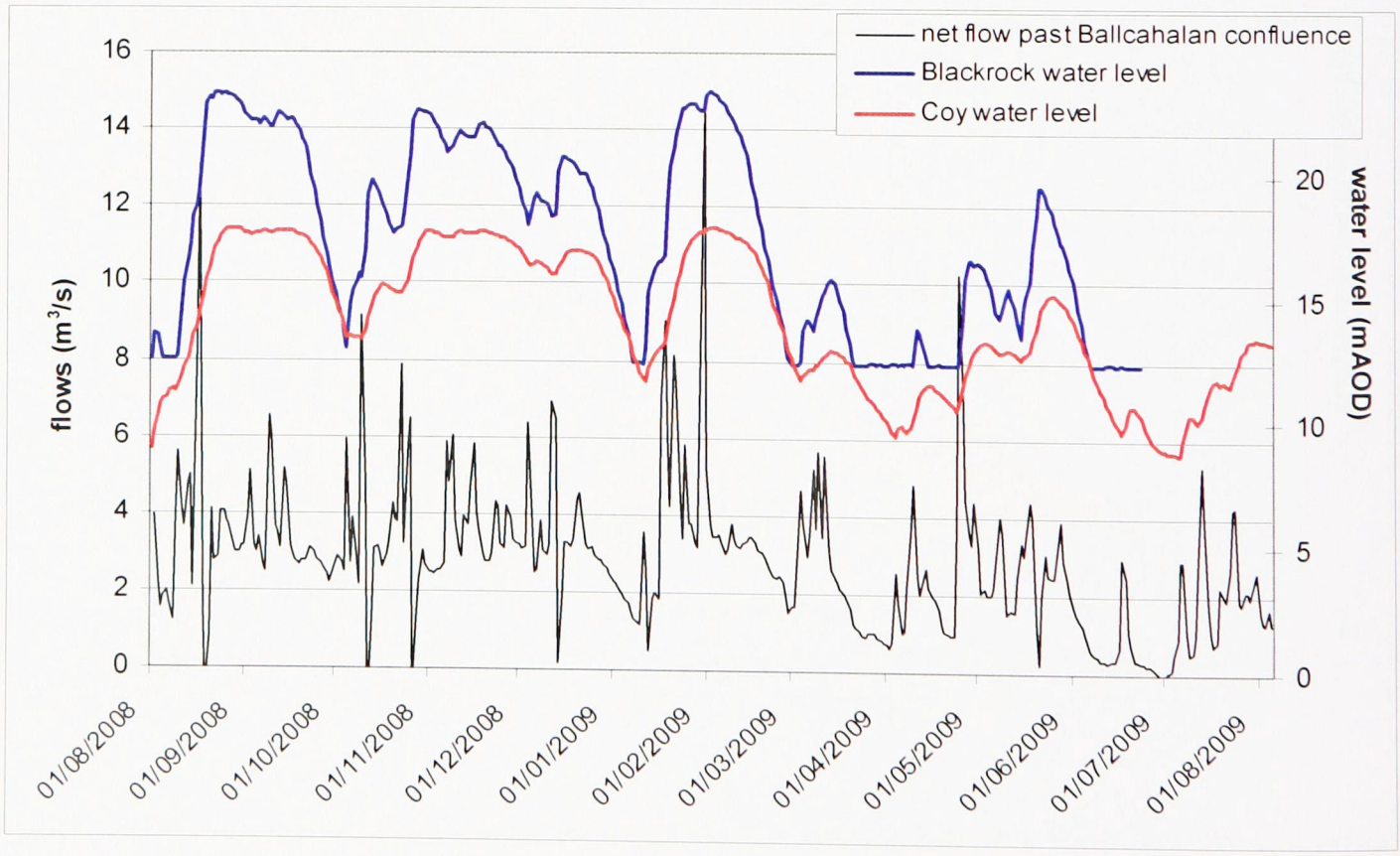


Figure 5.22 Combined flows just downstream of river Ballycahalan confluence.

Finally, the addition of flows from the River Beagh, which passes underground at the Devil's punchbowl, remerges just south of Gort and then disappears again before Coole, has been added to give the net flows into Coole as shown on Figure 5.23. The flows can be seen to be more peaky indicating less restriction compared to Figures 5.20. The mean flow levels discharging out of the network and into Coole are around 3 to 4 m^3/s.

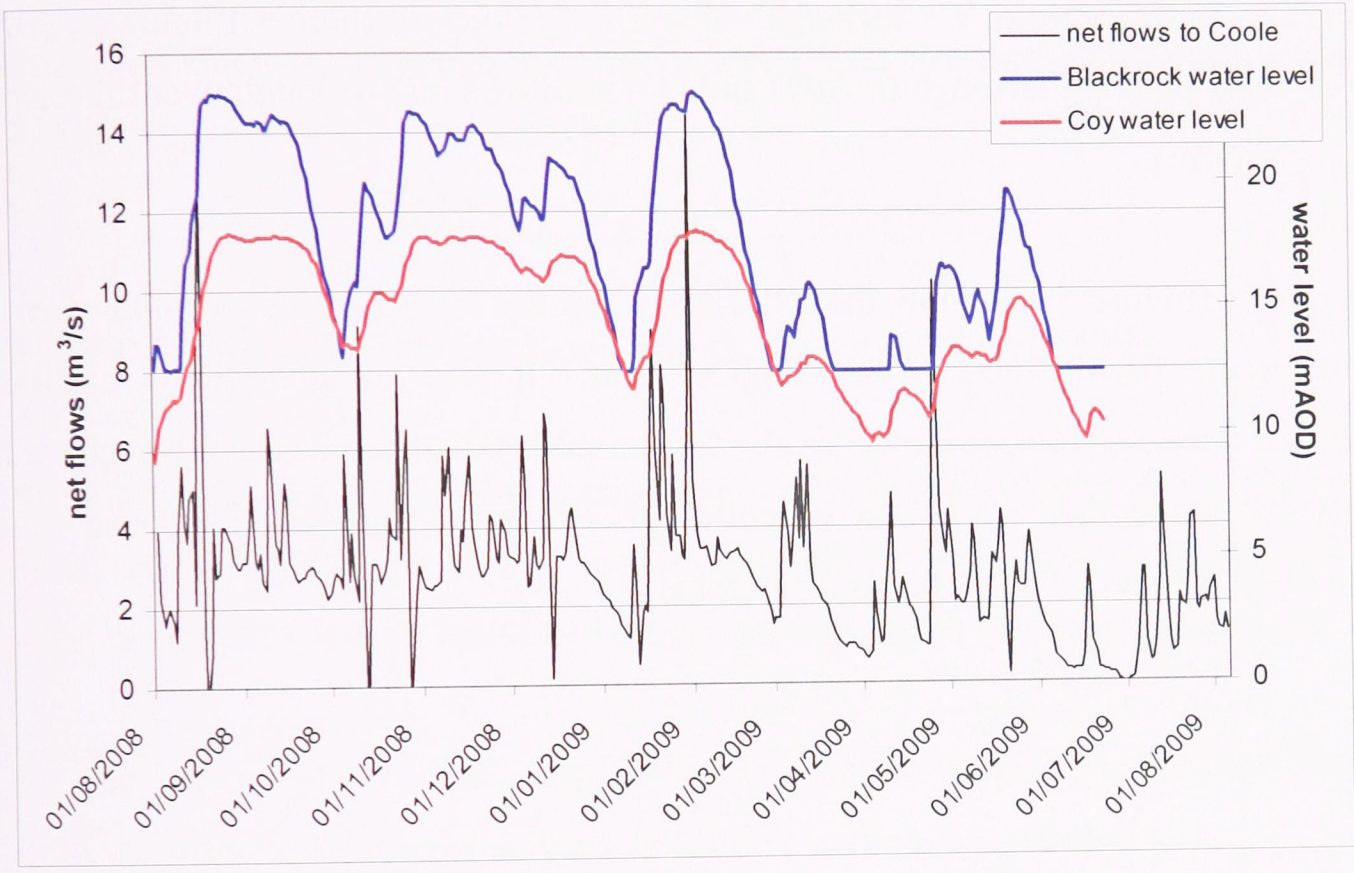


Figure 5.23 Combined flows (rivers Kilchreest, Ballycahalan and Beagh and net turlough flows) heading to the Coole basin.

5.5.4 Mean residence time

The mean residence time was calculated by assuming the following conceptual model of a surge tank as shown on Figure 5.24 and Equations 5.1 and 5.2 which assumes that the water is completely mixed at any point in time.

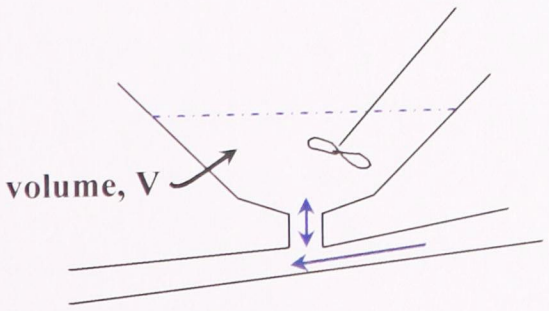


Figure 5.24 Conceptual model of turlough as a completely mixed surge tank.

when filling: $$\tau_{t+1} = \frac{V_t(\Delta t + \tau_t) + (Q_{t+1}\Delta t\,\tau_w)}{(V_t + Q_{t+1}\Delta t)}$$ Eqn. 5.1

when emptying: $$\tau_{t+1} = \tau_t + \Delta t$$ Eqn. 5.2

where τ = residence time, V = turlough volume, Δt = timestep (here = 1 hour), τ_w = mean age of water entering turlough (= $\Delta t/2$) and Q = net flows into turlough over timestep (= $(V_{t+1} - V_t)/ \Delta t$).

The results (Figure 5.25) show that Blackrock has the lowest residence time, particularly for the more flashy 2008/09 hydrological year. It was not possible to calculate the residence times for four of the turloughs for the 2006/07 period as the turloughs were not empty when the data started to be collected. However, the peak residence times are normally less than 2 months for these systems.

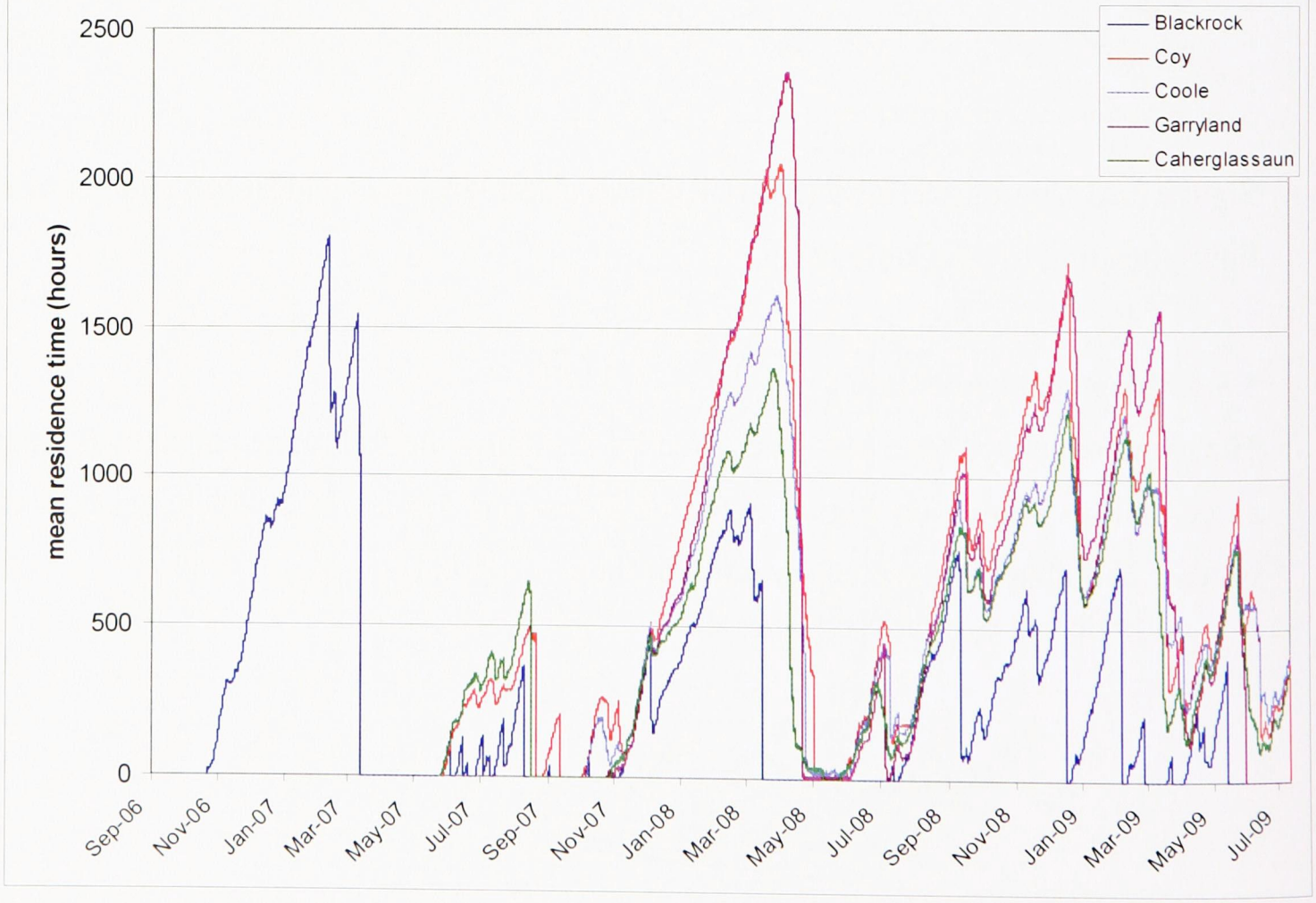


Figure 5.25 Mean residence time for water in turloughs (assuming all act as surge tanks).

If the hydraulic configuration of a turlough is not like a surge tank, then the hydraulic residence time calculation would need to be done differently. It seems (confirmed later in the thesis) that Coole operates as a river feed which drains out and Garryland more as a off-line transfer from Coole.

Hence, for Coole the equation to calculate mean residence time at any point in time (filling or emptying) needs to be modified as follows:

$$\tau_{t+1} = \frac{V_t(\Delta t + \tau_t) + (Q_{out(t+1)}\Delta t\,\tau_t - Q_{in(t+1)}\Delta t\,\tau_w)}{(V_t + Q_{t+1}\Delta t)} \qquad \text{Eqn. 5.3}$$

where Q_{in} is the river flow into Coole and Q_{out} is the flow out of Coole.

At this stage neither of these parameters are known merely from the water level measurement which only reveals the net flow into or out of the turlough. However, later when the model has been calibrated these residence times could be recalculated.

Equally, for Garryland you could make the assumption the inlet flow is flow through Coole, in which case the mean residence time equation is calculated as:

$$\tau_{t+1} = \frac{V_t(\Delta t + \tau_t) + (Q_{out(t+1)}\Delta t\,\tau_t - Q_{in(t+1)}\Delta t\,\tau_{coole(t)})}{(V_t + Q_{t+1}\Delta t)} \qquad \text{Eqn. 5.4}$$

where Q_{in} is the flow out of Coole into Garryland and τ_{coole} = mean residence time of water in Coole.

5.6 Rainfall and Evapotranspiration Analyses

5.6.1 Rainfall

The two tipping bucket gauges at Kilchreest and Francis Gap recorded rainfall every 15 minutes. A correlation between the two values on a daily basis across the winter of 2007/08 is shown on Figure 5.26, which shows a good correlation with Francis gap recording over 1.54 times the rainfall at Kilchreest which is expected due to orographic enhancement. When the data was compared on an hourly basis the correlation was much

worse with an R^2 value of only 0.59; Francis Gap showed a 2.1 times enhancement in rainfall with respect to Kilchreest at this time scale. Hence, the effects of the lag between rainfall at the two sites is evident with hourly data, although lagged correlations of between +2 to -2 hours produced worse correlations, indicating that the lag is probably less than one hour.

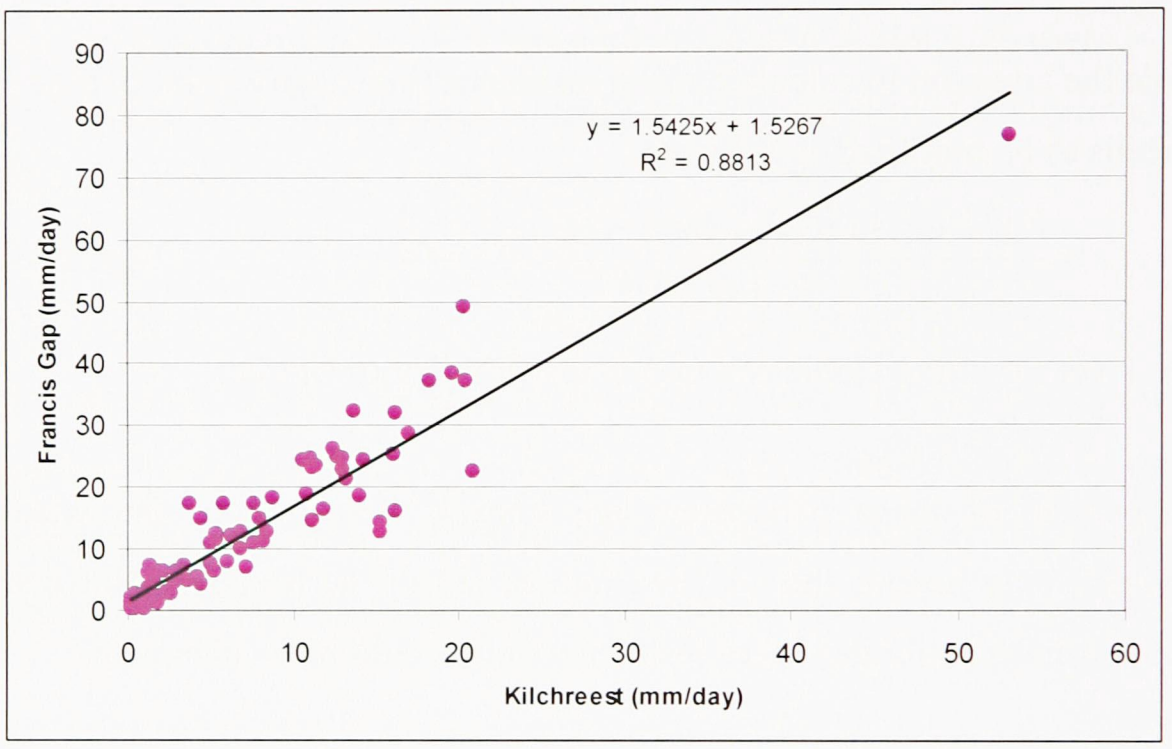


Figure 5.26 Daily rainfall correlation between Kilchreest and Francis Gap (2007/08).

The rainfall data from the nearest Met Eireann stations at Galway and Shannon (synoptic stations) and Gort, Loughrea, Carron and Ballyvaughan has been compared against the project rain gauge data on Figure 5.27. This shows an enhancement of 1.61 of Francis Gap with respect to Kilchreest, similar to the above analysis. It also shows that the cumulative rainfall at Kilchreest, Gort, Carron and Galway is very similar which is interesting from a long term perspective for the monitoring of the area. Finally, a cross-correlation matrix between the different stations on the basis of daily data is shown on Table 5.2 which again shows close correlations between Francis Gap, Kilchreest, and Galway but not with Gort.

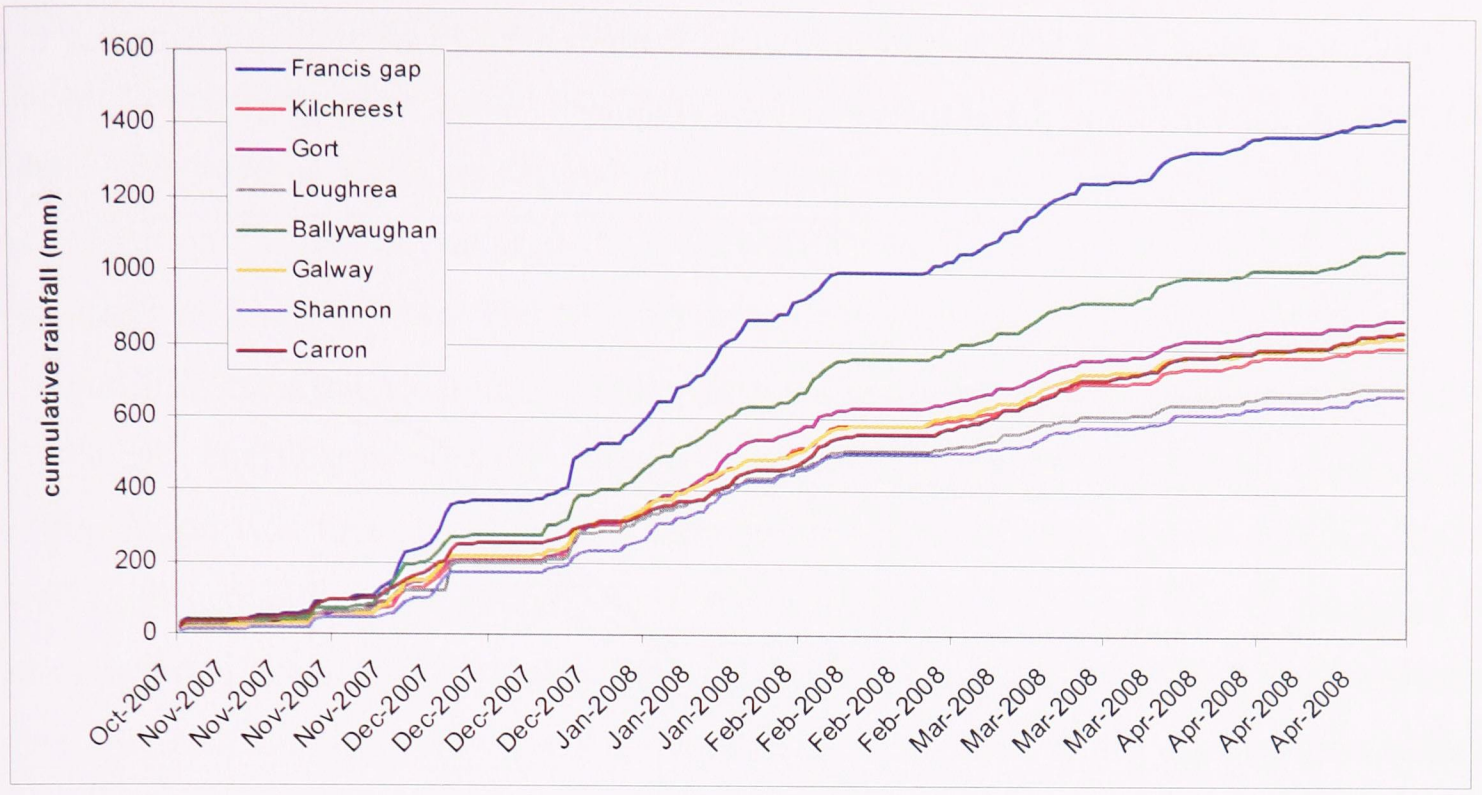


Figure 5.27 Daily rainfall cumulative correlations between rainfall stations.

Table 5.2 Cross-correlation matrix of daily rainfall measurements between stations.

	Francis Gap	**Kilch-reest**	**Gort**	**Loughrea**	**Bally-vaughan**	**Galway**	**Shannon**	**Carron**
Francis Gap	1	0.881	0.459	0.403	0.679	0.700	0.628	0.364
Kilchreest	0.881	1	0.533	0.464	0.652	0.673	0.601	0.384
Gort	0.459	0.533	1	0.386	0.377	0.430	0.406	0.259
Loughrea	0.403	0.464	0.386	1	0.384	0.312	0.213	0.377
Ballyvaughan	0.679	0.652	0.377	0.384	1	0.819	0.499	0.284
Galway	0.700	0.673	0.430	0.312	0.819	1	0.519	0.279
Shannon	0.628	0.601	0.406	0.213	0.499	0.519	1	0.347
Carron	0.364	0.384	0.259	0.377	0.284	0.279	0.347	1

5.6.2 Evapotranspiration

Potential evapotranspiration (PE) measurements are only taken at the Met Eireann synoptic weather stations and reported on a daily basis. The cumulative PE across a year for the two closest stations Shannon and Birr are shown on Figure 5.28 which reveals very close values. As the catchment is between the two stations an average daily value between the

two was taken for addition into the network model. The variation in PE across the years was shown on Figure 5.1 at the start of the chapter.

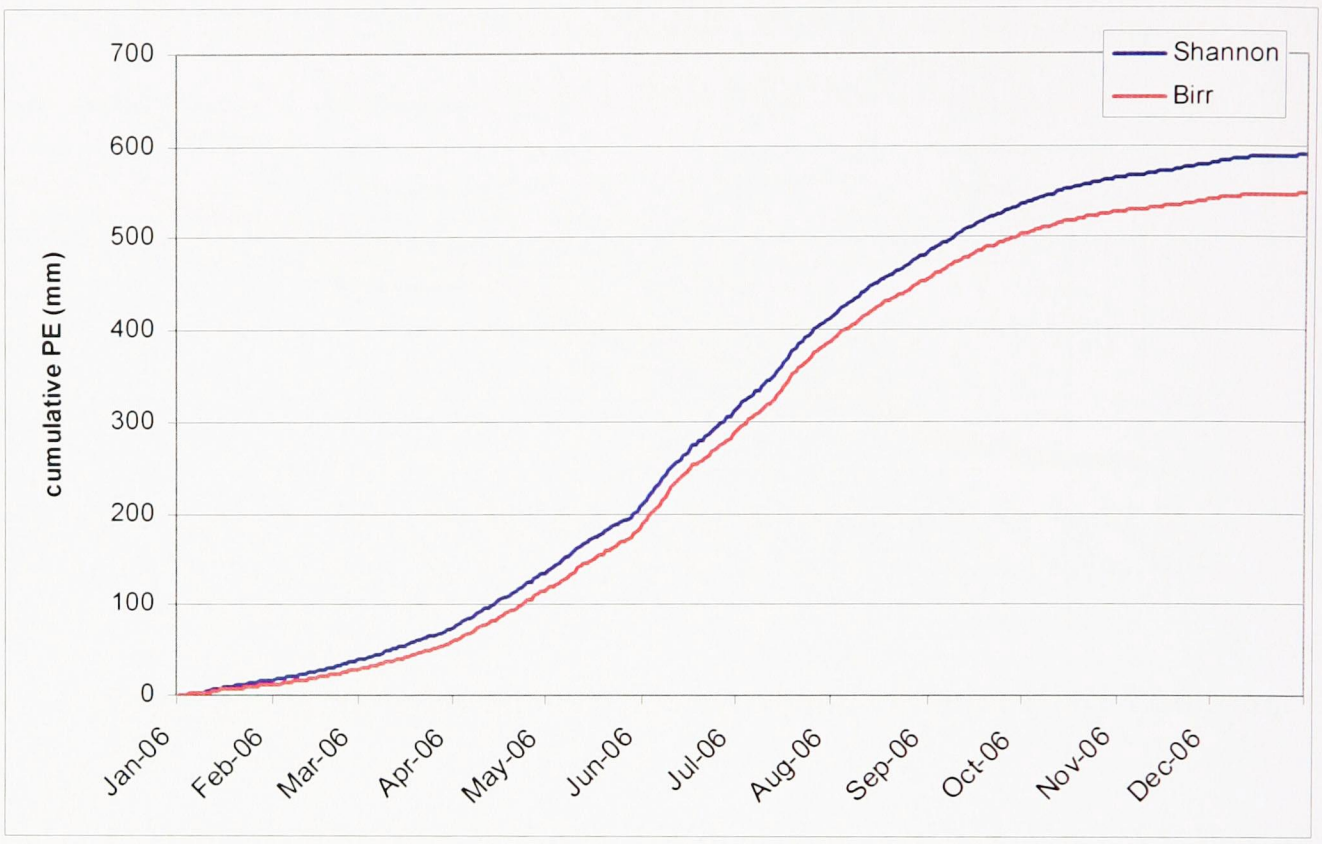


Figure 5.28 Cumulative PE over a year recorded at three synoptic stations.

5.7 River Flows

5.7.1 Rating curves

As discussed in Section 4.4, a series of depth discharge measurements were made at five locations on four different rivers (Owenshree, Ballycahalan, Owendalulleegh and Beagh) in order to produce rating curves. These were then used to calculate the flows in the rivers from the OPW depth gauges located on the four rivers and also from the pressure transducer installed approximately 12 km downstream of the Kilchreest OPW gauge at Ballynackagh (grid ref. 516 102) just before the river disappears underground to head towards Blackrock turlough. A comparison between the Owenshree river flows at Kilchreest and at Ballynackagh is presented in Section 5.7.3.

The gathered gauging data and calculated discharge enabled stage discharge curves to be plotted for the different rivers. However, the range of data did not cover the historical high flow events (as shown from the downloaded OPW gauging results) as it was both too

difficult to measure the flows during such high stages and also be present at the river during times when such events occurred – and so the rating curves had to be extended. There are several methods by which a rating curve can be extended, logarithmic extrapolation, the velocity-area method, Stevens Method or using the Manning Formula as discussed in Shaw (1994). The Stevens Method (based on the Chezy formula for open channel flow) and the Manning Formula were not used due to doubtful assumption that the roughness coefficients would remain constant at higher discharges. Logarithmic extrapolation was first attempted and although the plots of stage against flow on log-log scales did generally yield straight lines, the extrapolation required was way beyond the recommended limit of 20% higher than the highest gauged discharge; it also seemed to give unrealistically high flow rates at depths when compared to the velocity-area method. Hence, the velocity-area method was used to generate the data for the stage-discharge relationship. For this method plots of average velocity versus stage and cross-sectional area versus stage are plotted. These plots were then extended (as opposed to the rating curve) and then the higher values of discharge are calculated at specific stages from the product of the extended average velocity and extended area from the two respective graphs. An example of how this method was used is shown for the Owenshree river at Kilchreest here whilst all other data and calculations are presented for each of the rivers in Appendix D.

OWENSHREE RIVER (at Kilchreest OPW gauging station)

The results from the river gauging at Owenshree at the Kilchreest OPW gauging station are presented in Table 5.3. This data was then used to produce two graphs of stage versus velocity and stage versus cross-sectional area as shown in Figure 5.29. It should be noted that the OPW stage pressure transducer has not been set to zero at the lowest depths of the river as can be seen from Table 5.31. In fact when the gauge is zero the flow was still at 0.33 m^3/s and so an estimate had to be made of the low flows by using the recorded flow at Blackrock as discussed later.

Table 5.3 River gauging data collected for Owenshree river (at Kilchreest).

Date	Time	Mean depth (m)	Mean velocity (m/s)	Area (m^2)	Flow (m^3/s)	Stage (m)	OPW stage (m)
22/05/2009	17:30	0.283	0.298	2.635	0.785	0.09	0.09
28/05/2009	14:30	0.327	0.380	3.039	1.156	0.12	0.11
29/05/2009	10:00	0.251	0.249	2.337	0.583	0.06	0.05
04/06/2009	18:30	0.163	0.106	1.513	0.16	-0.04	0
05/06/2009	10:30	0.165	0.126	1.532	0.193	-0.04	0
12/06/2009	18:30	0.144	0.091	1.335	0.122	-0.06	0
13/06/2009	09:15	0.148	0.083	1.275	0.114	-0.06	0
17/06/2009	12:45	0.475	0.761	4.42	3.365	0.28	0.23
30/06/2009	16:00	0.123	0.068	1.145	0.077	-0.07	0
04/07/2009	17:30	0.133	0.097	1.237	0.12	-0.06	0
05/07/2009	14:00	0.143	0.094	1.33	0.125	-0.05	0
13/07/2009	14:15	0.436	0.742	4.052	3.008	0.28	0.3
14/07/2009	10:30	0.355	0.442	3.304	1.46	0.14	0.14
29/07/2009	12:30	0.274	0.316	2.547	0.805	0.09	0.09

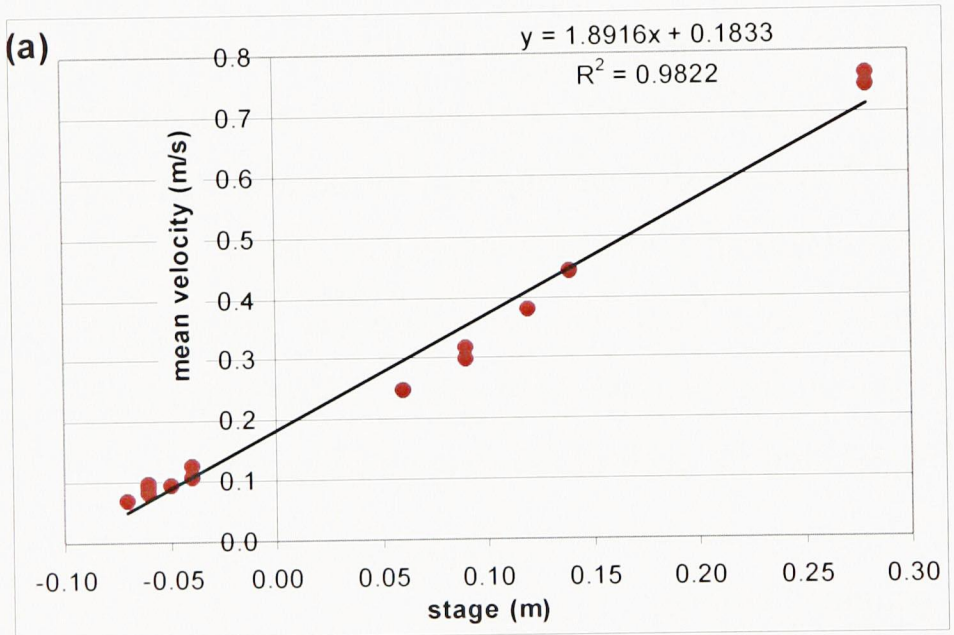


Figure 5.29 Owenshree river (at Kilchreest) **(a)** stage-velocity and **(b)** stage-cross sectional area relationships.

The equations on the trend lines on the two graphs were then used to calculate flows at higher stages, in this case from 0.4 to 0.7 m. The final rating curve was then produced (Figure 5.30) using the measured data up to stages of 0.3 m and the extrapolated stage discharge data then used from 0.4 to 0.7 m and a best fit curve added (in this case a second order polynomial) to give the final rating relationship as shown on Equation 5.5.

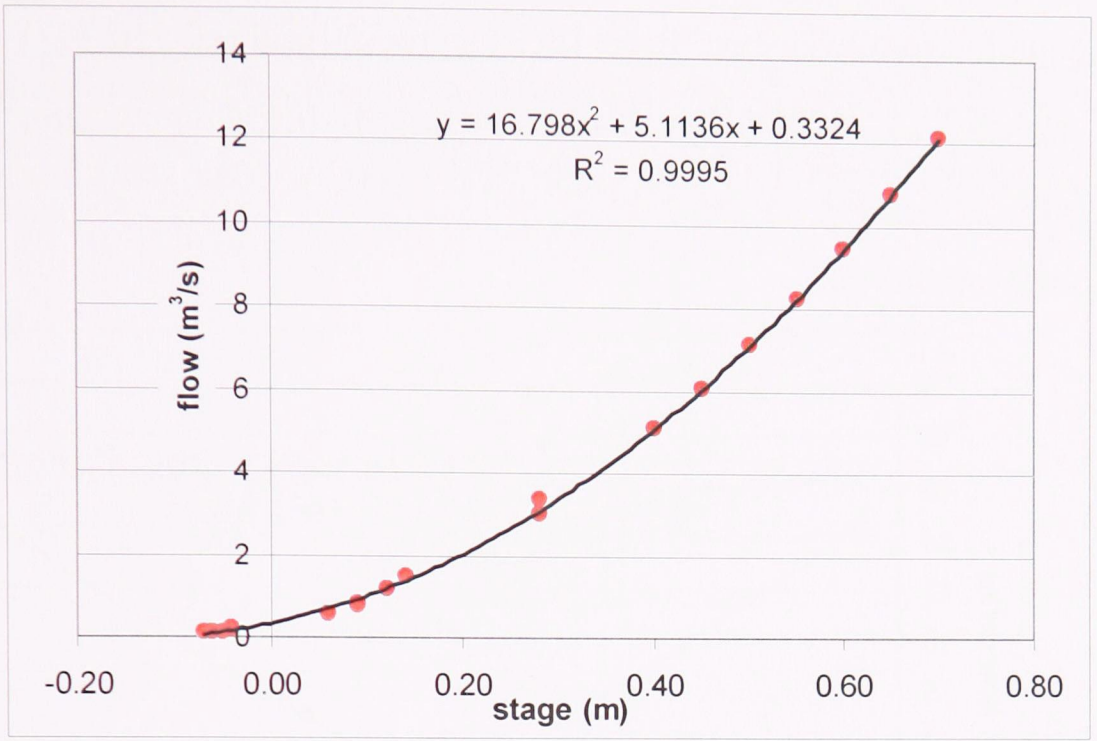


Figure 5.30 Rating curve for Owenshree River (at Kilchreest).

Rating equation for Owenshree River (at Kilchreest) [grid ref. 572 150]

$$flow\left(m^3/s\right) = 16.798\left(stage\right)^2 + 5.1136\left(stage\right) + 0.3324 \qquad \text{Eqn. 5.5}$$

OWNESHREE RIVER (before it sinks into Blackrock turlough)

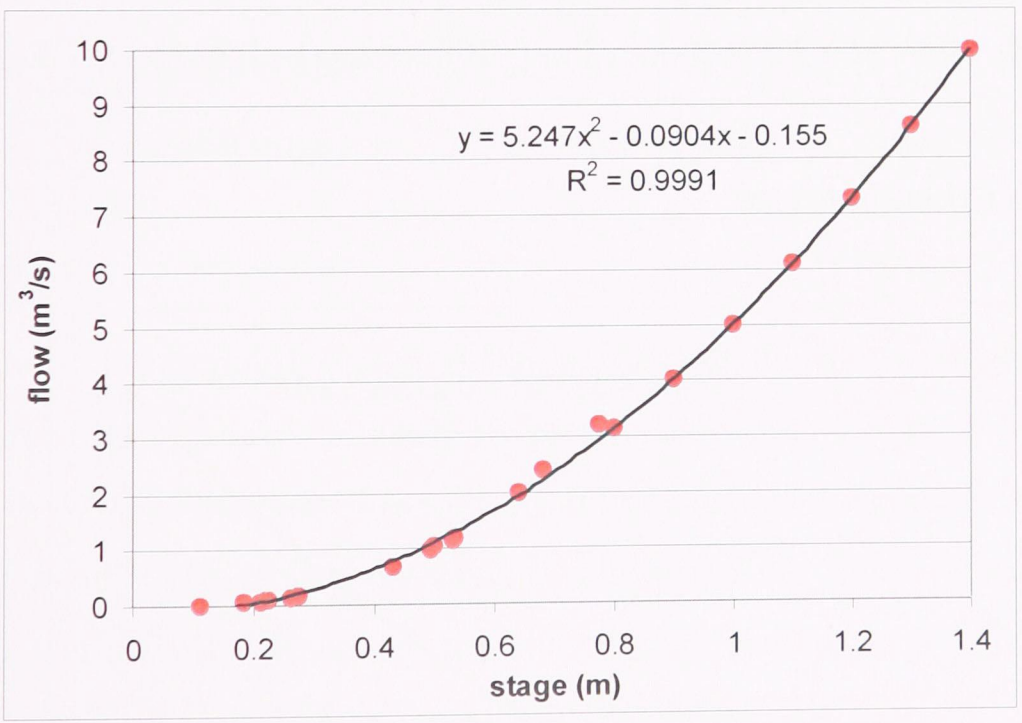


Figure 5.31 Stage-flow data and rating curve for Owenshree River (at Blackrock).

Rating equation for Owenshree River (at Blackrock) [grid ref. 516 102]

$$flow\left(m^3/s\right) = 5.247(stage)^2 - 0.0904(stage) - 0.155 \qquad \text{Eqn. 5.6}$$

BALLYCAHALAN RIVER

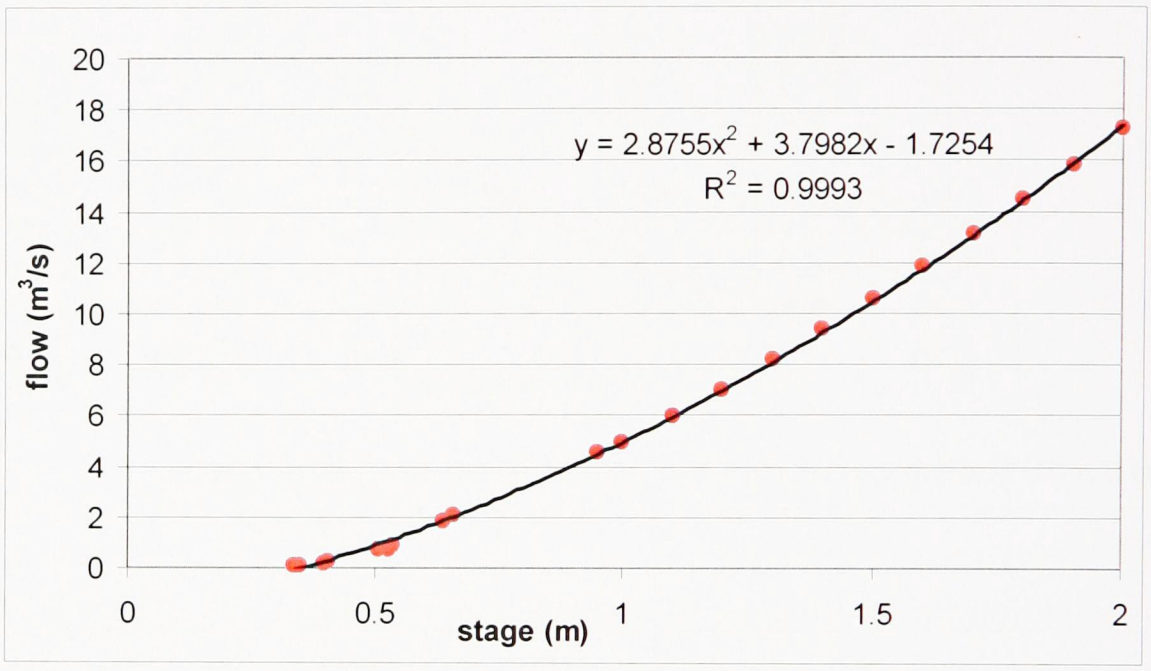


Figure 5.32 Stage-flow data and rating curve for Ballycahalan River.

Rating equation for Ballycahalan River [grid ref. 496 057]

$$flow\left(m^3/s\right) = 2.8755(stage)^2 + 3.7982(stage) - 1.7254 \qquad \text{Eqn. 5.7}$$

OWENDALULLEEGH RIVER

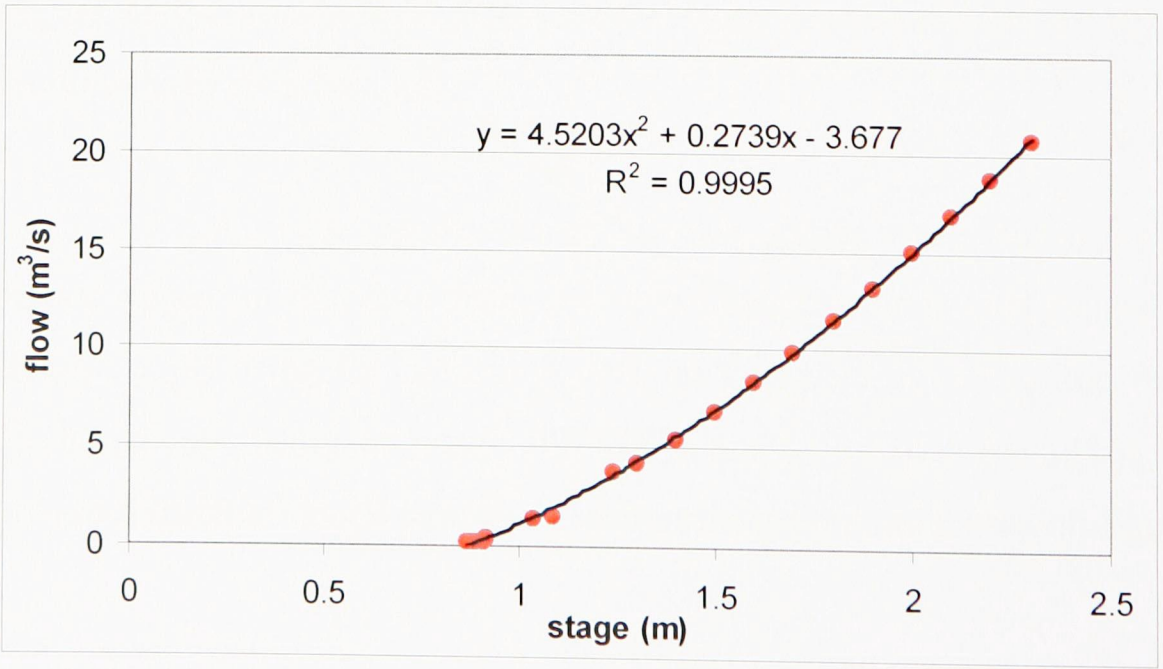


Figure 5.33 Stage-flow data and rating curve for Owendalulleegh River.

Rating equation for Owendalulleegh River [grid ref. 484 972]

$$flow\left(m^3/s\right) = 4.5203\left(stage\right)^2 + 0.2739\left(stage\right) - 3.677 \qquad \text{Eqn. 5.8}$$

BEAGH RIVER

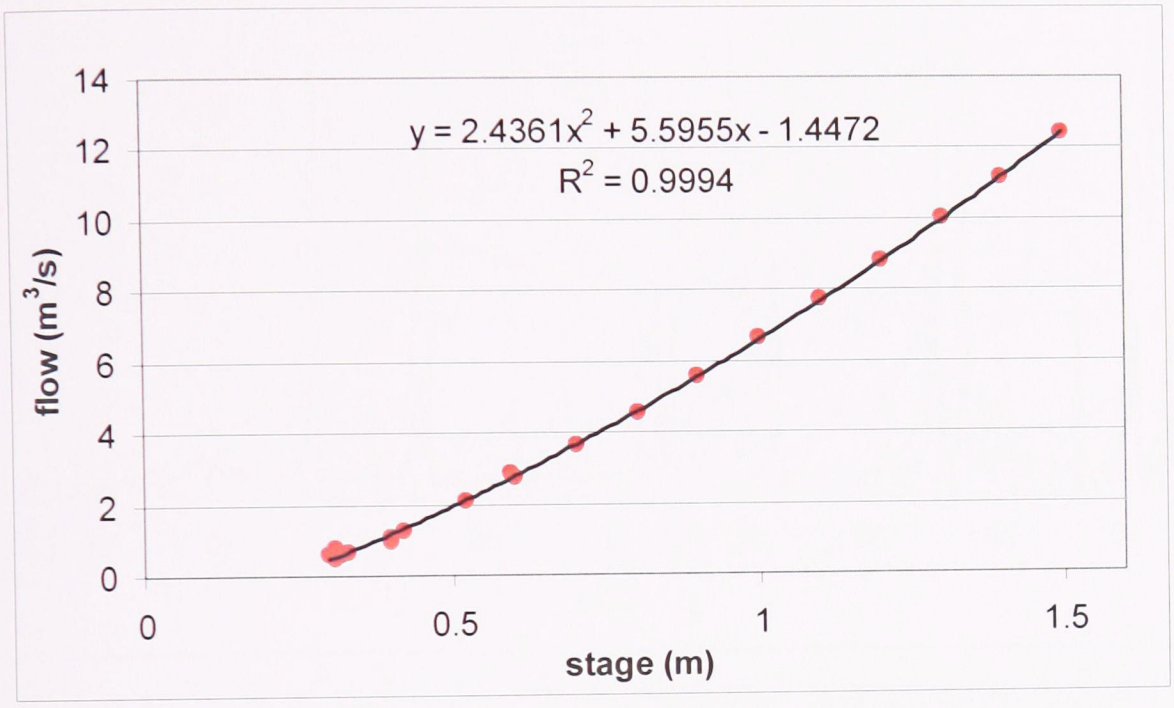


Figure 5.34 Stage-flow data and rating curve for Beagh River.

Rating equation for Beagh River [grid ref. 482 005]

$$flow\left(m^3/s\right) = 2.4361\left(stage\right)^2 + 5.5955\left(stage\right) - 1.4472 \qquad \text{Eqn. 5.9}$$

5.7.2 River flows

The flows in the rivers draining off the different sides of the Slieve Aughty Mountains - rivers Owenshree, Ballycahalan and Owendalluleegh - are shown on Figure 5.35 for 2008/09. This shows that the peak flows are from the Owendalluleegh catchment (which is to be expected as it is the largest catchment). However, the flows from this river pass through Lough Cutra which drains by the river Beagh before they drain into the karst catchment. The graph clearly shows the attenuating effect that the lake has on the peak flows which is discussed later in Section 8.4. The other two rivers draining directly into the karst network show peaks coinciding. The river flows for the other years are in Appendix D.

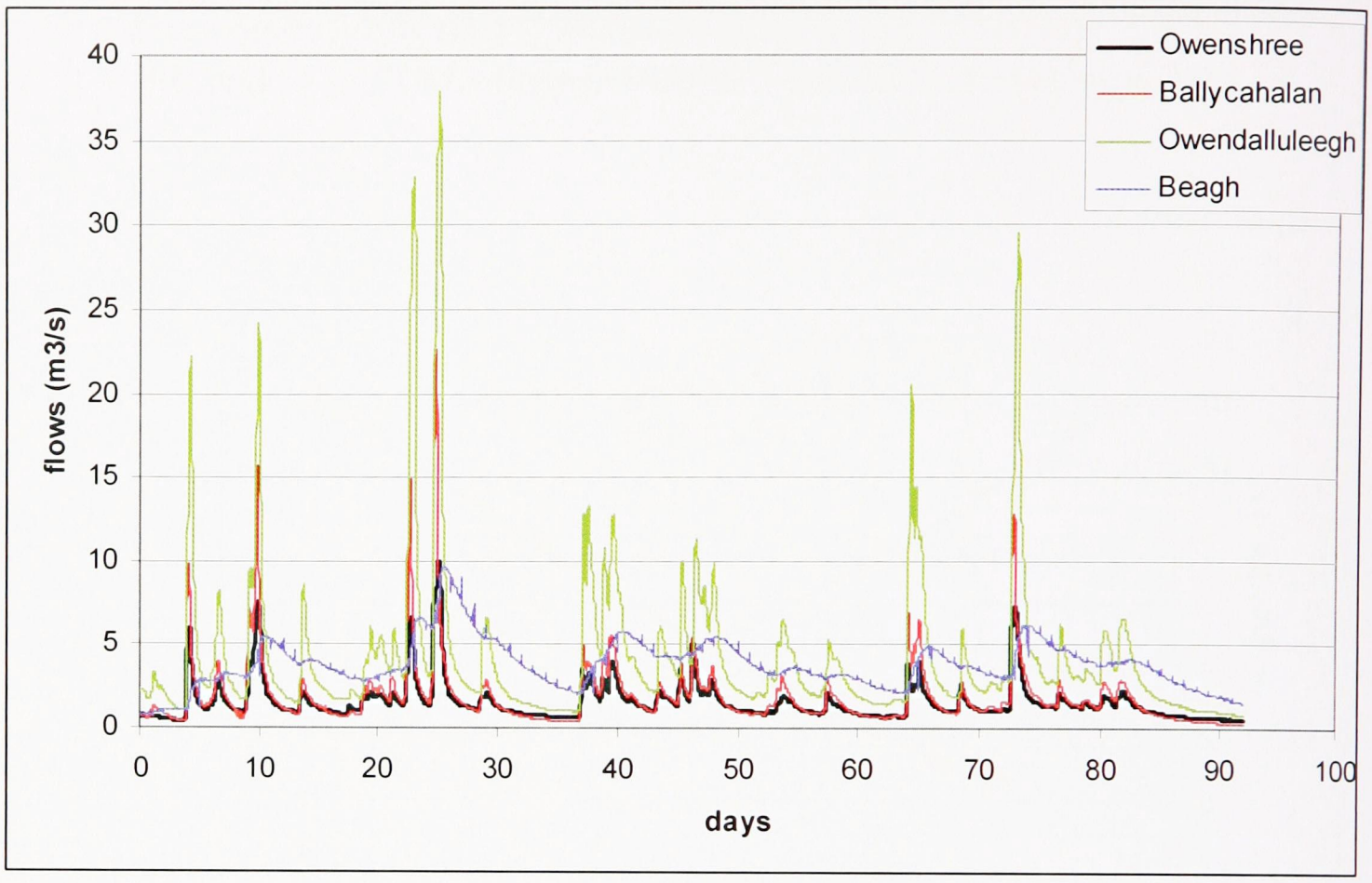


Figure 5.35 The flows at the gauging stations for rivers Owenshree, Ballycahalan, Owendalluleegh and Beagh (Sept to December 2008).

5.7.3 Calculating diffuse recharge from epikarst

Owenshree river flow increase downstream

The difference between the flows measured at the two gauging stations on the Owenshree river (at Kilchreest and just upstream of Blackrock turlough) has been compared in order to establish the enhancement in flows due to runoff and epikarst flow (via fractures etc) over this length of river flowing over the karst. This information has then been used in order to calibrate the numerical model (see Section 7.6) with respect to modelling the diffuse flows into the network system. Data was collected at Blackrock gauging station for a period of three months (10th May to 1st August 2009), as shown on Figure 5.36. In general the peak flows at Blackrock lag behind the peak flows at Kilchreest by about 6 hours.

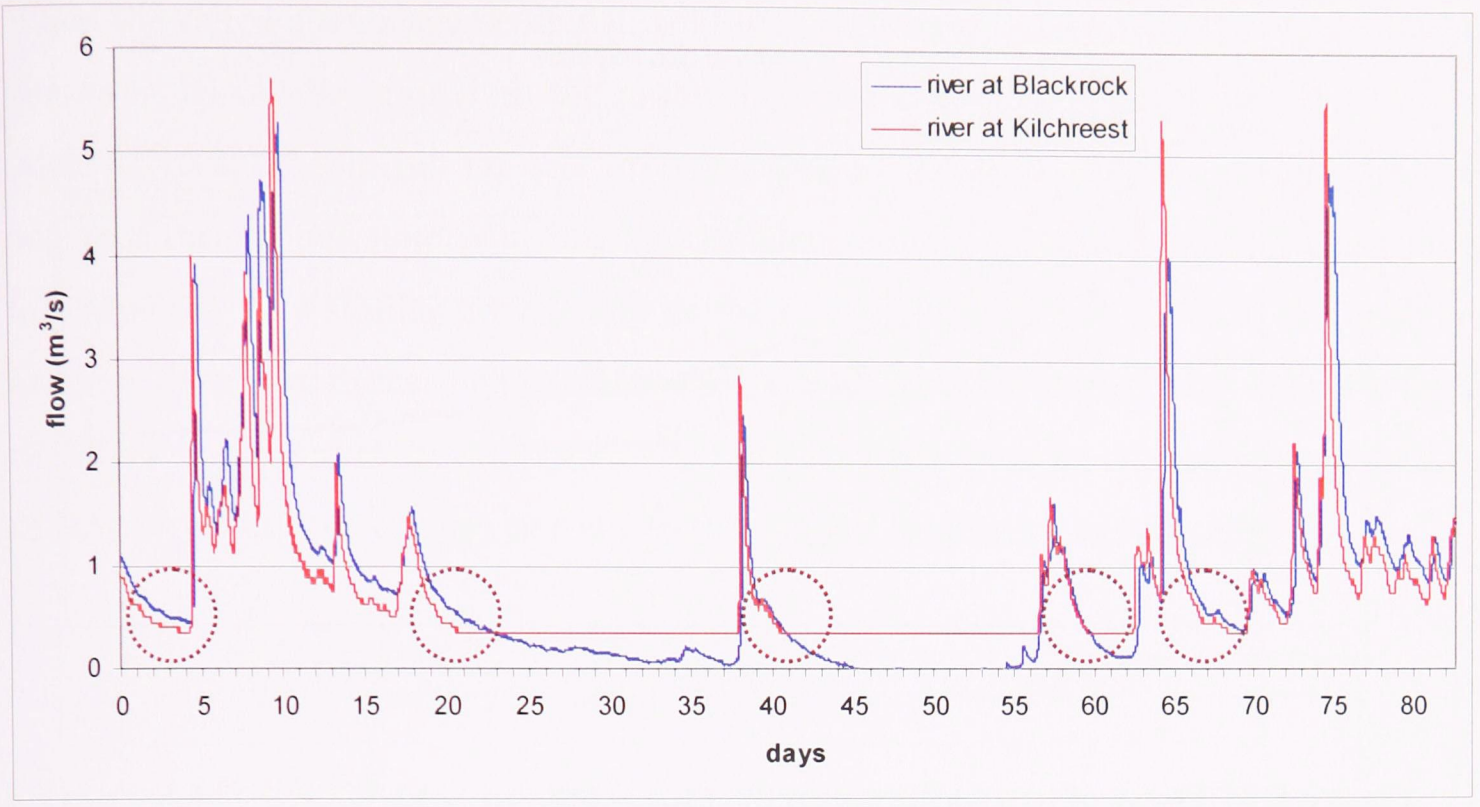


Figure 5.36 Flows at two locations on the Owneshree river between 10th May to 1st August 2009.

First an analysis of the low flows at Blackrock was compared with Kilchreest in order to get a low flow relationship for the periods when the Kilchreest gauge was recording a depth of zero. Five separate periods were compared when the flows at Kilchreest receded below 0.33 m^3/s, as shown ringed on Figure 5.36, and the mean ratio of flows at Kilchreest to flows at Blackrock calculated from every time step for each period. A close up of the first period is shown on Figure 5.37. The mean of these five mean ratios was then calculated as 0.78. It could be noted that the ratio was lower after more prolonged rain but higher (i.e. the flows were more similar) following rainfall after the long antecedent dry period (indicative of much lower recharge from the karst aquifer with high conductivities). The Blackrock flows were then used to augment the Kilchreest data at low flows when the depth gauge was reading zero to provide an adjusted data set for Kilchreest.

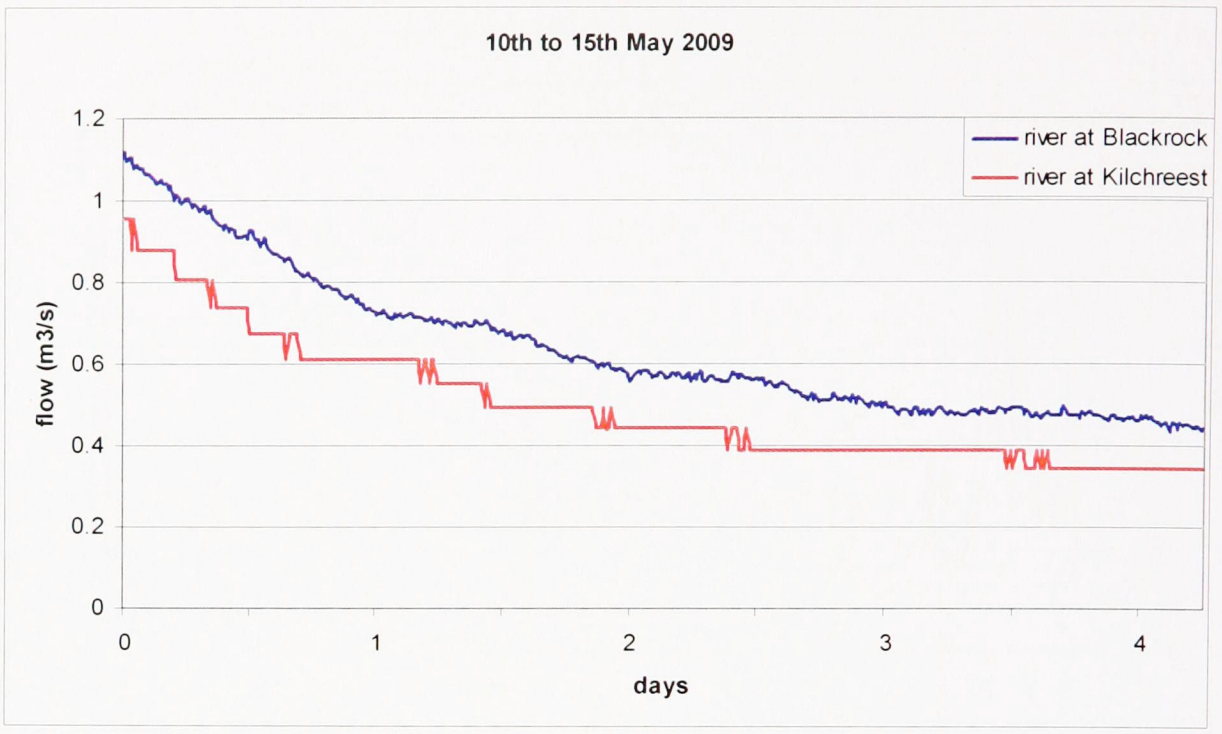


Figure 5.37 Flows at two locations on the Owneshree river between 10th May to 1st August 2009.

The overall addition to the Owenshree river flows from the karst catchment area between Kilchreest and Blackrock was assessed by comparing the cumulative volume to have passed each gauging station over the period as shown on Figure 5.38.

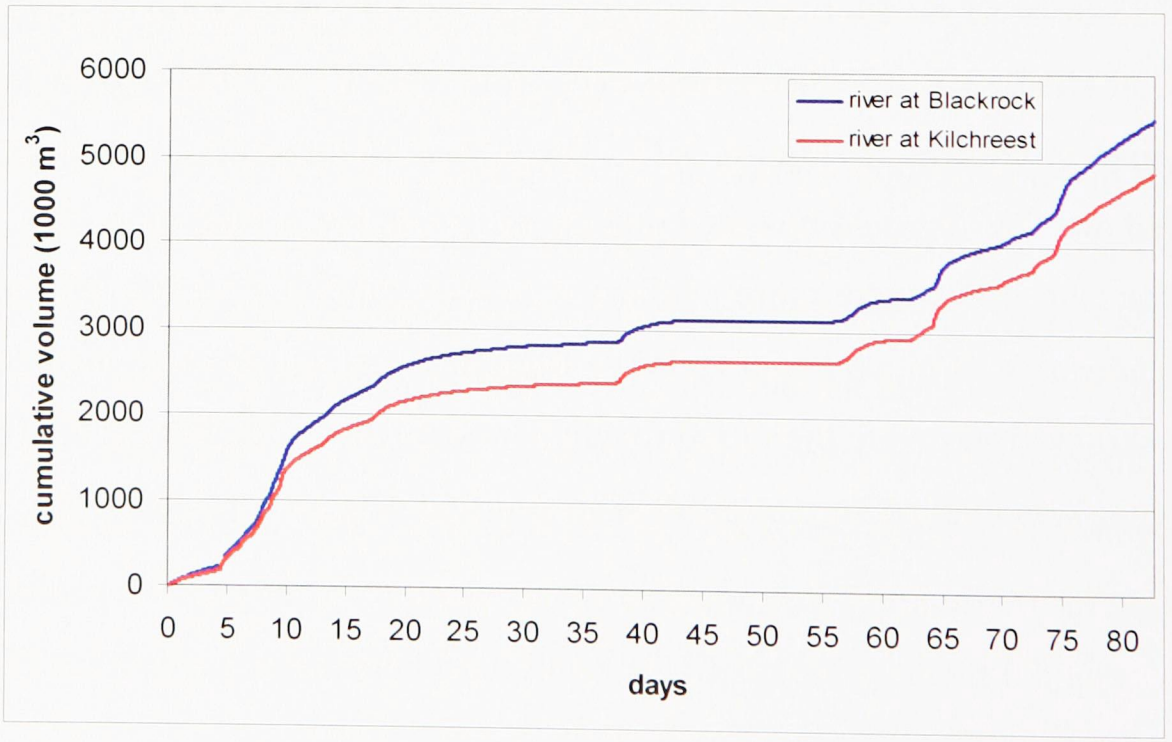


Figure 5.38 Cumulative volumes to flow past the two Owenshree river gauging stations between 10th May and 1st August 2009.

When the ratios are compared statistically the mean ratio is 1.16 with median value 1.17. However, as can be seen from the graph there are two clear peaks, one at 1.12 and the other at 1.18. The lower ratio is probably due to the slightly unusual dry period that occurred throughout June with just one isolated rainfall event. The baseflows at the two locations are very similar presumably as the river is losing some water to the underlying karst in these situations. Note, that when the flows were under 0.06 m^3/s during this extended dry period at the Blackrock location, the river could be seen to disappear 10 – 15 m downstream of the bridge (en route to the conduit leading to the turlough).

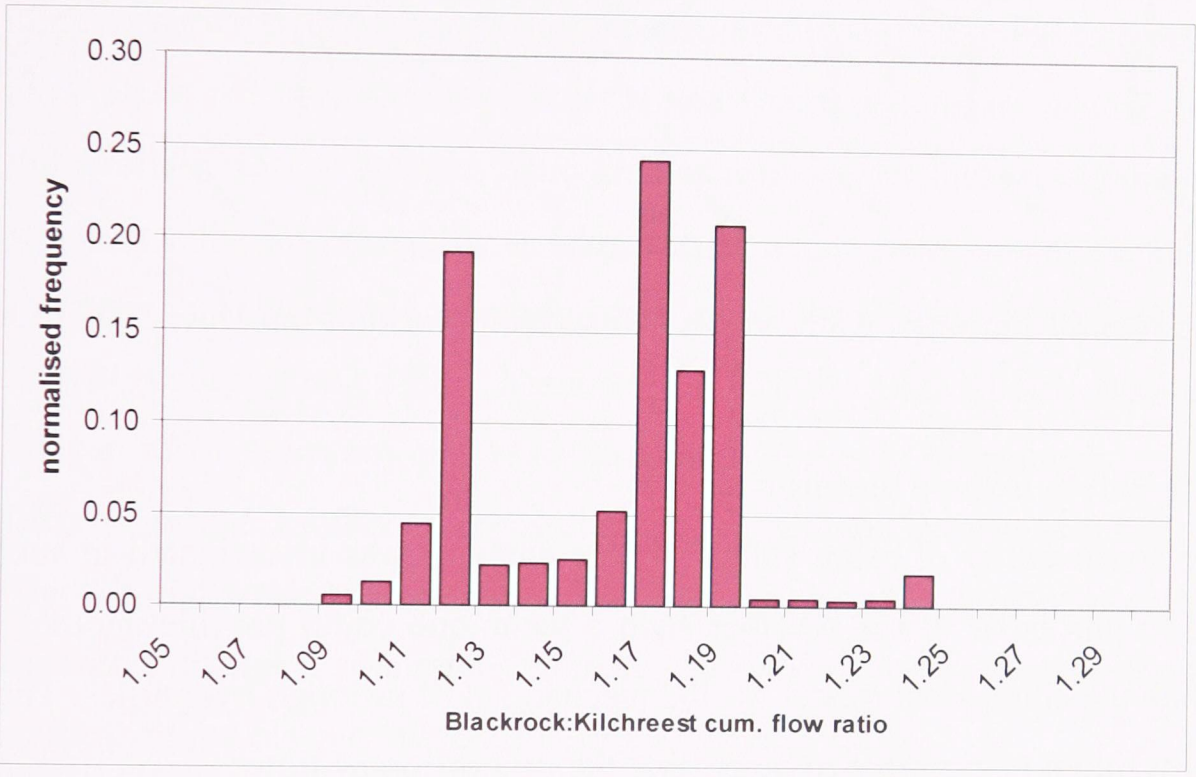


Figure 5.39 Frequency distribution of cumulative flow ratios, Blackrock to Kilchreest.

5.8 Turlough Water Quality Analyses

Water samples were analysed for the stable isotope $\delta^{18}O$ at different stages of the hydrological season from December 2008 until June 2009. The sampling times are indicated on Figure 5.40 by the grey arrows against the relative water levels of the five turloughs. This shows samples were taken before and during major filling periods and also at different stages of recession. At the same time, samples were taken for the analysis of the water's nutrient quality (nitrogen and phosphorus) and temperature and conductivity measurements were recorded.

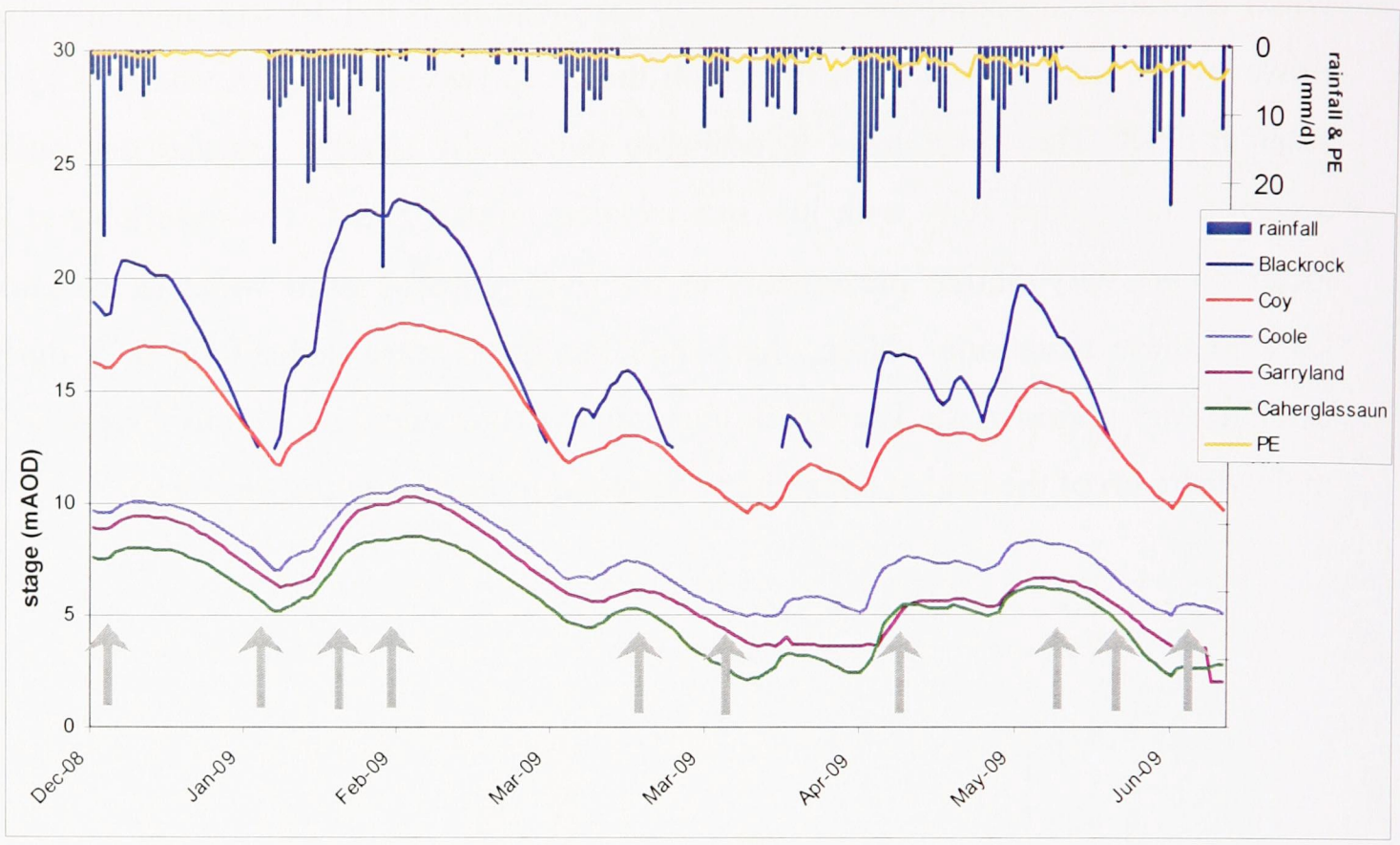


Figure 5.40 Turlough water levels and sampling visits from Dec. 2008 to June 2009.

5.8.1 Stable isotope monitoring

The applicability of using stable isotope analysis was investigated in such a karst system and in particular to see whether such a technique could provide another angle to help to define the conceptual model for the mechanism of turlough hydraulics. The hypothesis was that it might be possible to determine the proportion of flows from different sources, i.e. to what extent each turlough was fed by diffuse flow from the fracture system in epikarst with continual inflow or outflow, compared to the more variable point input flows from the sinking rivers flowing along major conduits with turloughs operating as surge tanks as discussed later in Chapter 9.

$\delta^{18}O$ isotope theory

The isotope signature of rainfall - the input signal to most hydrological systems - varies relative to the initial isotope composition of atmospheric vapour from which it originates.

$$\alpha^{18}O_{water-vapour} = \frac{\left({}^{18}O/{}^{16}O\right)_{water}}{\left({}^{18}O/{}^{16}O\right)_{vapour}} \qquad \text{Eqn. 5.10 (Clark and Fritz, 1997)}$$

where α is the equilibrium isotopic fractionation factor.

Isotopic concentrations of ^{18}O are reported in units per mil (‰) relative to the Vienna Standard Mean Ocean Water (VSMOW). So, for water with a $\delta^{18}O$ of 0 ‰ VSMOW and vapour with a $\delta^{18}O$ of -9.3‰ VSMOW, the $\alpha^{18}O_{water\text{-}vapour}$ = 1.0093. The equilibrium isotopic fraction of hydrogen differs from that of oxygen by about 8 times but maintains a fixed relationship. Hence, if a graph of δH^2 is plotted against $\delta^{18}O$ this gives a straight line with a gradient of 8 – the so called the Global Meteoric Water Line (GMWL) (Craig, 1961). If water samples analysed for both δH^2 (deuterium δD) and $\delta^{18}O$ are plotted on such a graph and lie below the line (i.e. a relative increase in $\delta^{18}O$ with respect to δH^2), this generally indicates the water has undergone evaporation. Evaporation affects surface waters leading to enrichment of heavy isotope species (^2H and ^{18}O) due to kinetic isotope fractionation – i.e. it is easier for the lighter ^1H and ^{16}O molecules to change state and so they are preferentially lost as vapour. This gradual enrichment includes both equilibrium and kinetic effects. So, for example, a lake during a dry period with no inflows will gradually become enriched until a steady state is reached whereby no further isotope enrichment will occur (Gat, 1995; Mayr *et al.*, 2007; Gat, 2010). Stable isotopic fractionation can result from any processes that cause the ratio of isotopes in a particular phase to differ from one another, such as evaporation, as well as chemical and biological reactions. Geothermal waters for example have been shown to be enriched in terms of $\delta^{18}O$ source waters due to high temperature exchange between rock and groundwater, whilst maintaining the original δH^2 - $\delta^{18}O$ ratios (Clark and Fritz, 1997).

Stable isotopes of water (δD and $\delta^{18}O$) have been used to identify multiple recharge areas and to understand flow paths and mixing in regional groundwater studies. For example, isotopes of water and chloride concentrations were used on volcanic rocks in Oregon (basalts, andesites and rhyolites) to distinguish between waters originating from different surface recharge areas (Palmer *et al.*, 2007). Water that had been used for irrigation showed enrichment of $\delta^{18}O$ isotope indicative of fractionation by evaporation. Another study (Chowdhury *et al.*, 2008) was able to differentiate between surface water recharge through stream beds and groundwater signals in alluvium as rainfall and surface runoff had much heavier $\delta^{18}O$ signals. Of particular relevance to this study is research using stable isotopes to analyse desiccating lakes in a comparison of deep crater lakes against more

ephemeral lakes (Mayr *et al.*, 2007). This showed that ratios for both (^{2}H and ^{18}O) were similar throughout the drying period and that the lakes showed highest isotopic enrichment towards the end of the dry season. The isotopic compositions were demonstrated to be affected by variable ratios of surface area to volume and by different mixing patterns.

Both ^{2}H and ^{18}O stable isotopes have been used as tracers for studying carbonate aquifers (Gat *et al.*, 2001; Vandenschrick *et al.*, 2002) which generally show low $\delta^{18}O$ values. For example, the Madison aquifer in North Dakota was studied using naturally occurring $\delta^{18}O$ to examine the dynamics of transient fluid interchange between conduit and diffusive networks (Long and Putnam, 2004). A mass balance approach was developed using the ^{18}O isotopic signatures from conduit, intermediate and diffuse flows to derive the relative flow proportions from each in the karstic aquifer. In another study the infiltration of water through 1000 m of limestone was picked up in an underground laboratory which could show the origin of the water from a much higher altitude (i.e. precipitation close to the snow line) compared to less negative signatures associated with dolomite outcropping over a much wider area of recharge (Falcone *et al.*, 2008). This was able to conclude that there was a dual-velocity groundwater circulation system.

The results of the $\delta^{18}O$ (‰) samples on turloughs, springs and rivers are contained in Appendix E and plotted for the turloughs and Kinvara springs on Figure 5.42. Three samples of rainfall were also analysed (20th January, 17th March and 6th June) which gave $\delta^{18}O$ of rainfall values of -10.98, -9.20 and -8.28 ‰ respectively, much lighter than the surface water samples as expected. Groundwater samples from two wells in the area were also analysed (values – 7.78 and -8.39 ‰) in order to see whether the groundwater held in the matrix and fractures could be differentiated from the surface water derived flows in the karst system. The more negative values from the well samples were indicative of rainfall recharge that had had little time to evaporate before percolating into the karst aquifer system compared to the surface water (river) derived samples in the rivers and turloughs. Hence, the different isotopic signatures between the generic water sources could potentially be used to proportion the net contribution of flow from each into the main karst and turlough system. The results from the turloughs (Figure 5.41) indicate a slight trend of

increasing enrichment from February onwards with Blackrock slightly more enriched than the others in general. This could be due to the fact that as it is at the top of the hydraulic system is less affected by the cumulative addition of diffuse recharge from the karst than the lower turloughs.

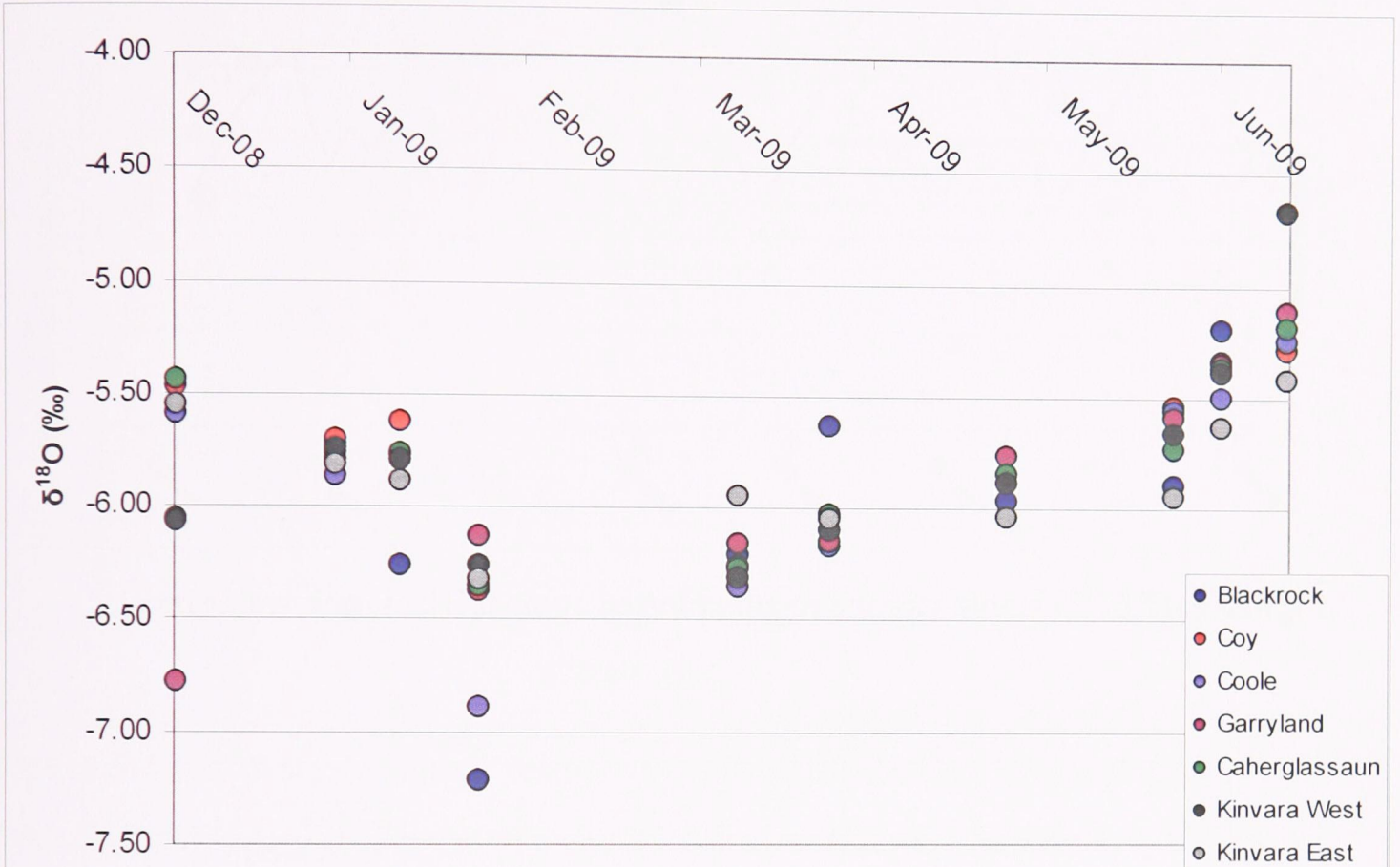


Figure 5.41 ^{18}O stable isotope sampling results from turloughs and springs.

The results for Blackrock and Coole turloughs are plotted relative to their respective water levels (Figures 5.42 and 5.43) which clearly show the values becoming more enriched (i.e. more positive) during the major recession period in the summer. This reflects that evaporation is the major process and also might suggest the turloughs are behaving as draining tanks at this time of year with no significant additional inflows from the major conduit system or through-flow from the epikarst. The lower three turloughs and Coy all show the same pattern (see Appendix E) with isotopic enrichment occurring from February onwards – and these four turloughs never fully dried out during the year – compared to Blackrock which shows more erratic results due to the fact that it did totally dry out several times over this period (Figure 5.41) although is does demonstrate enrichment at times of recession and decreasing $\delta^{18}O$ values during turlough filling periods.

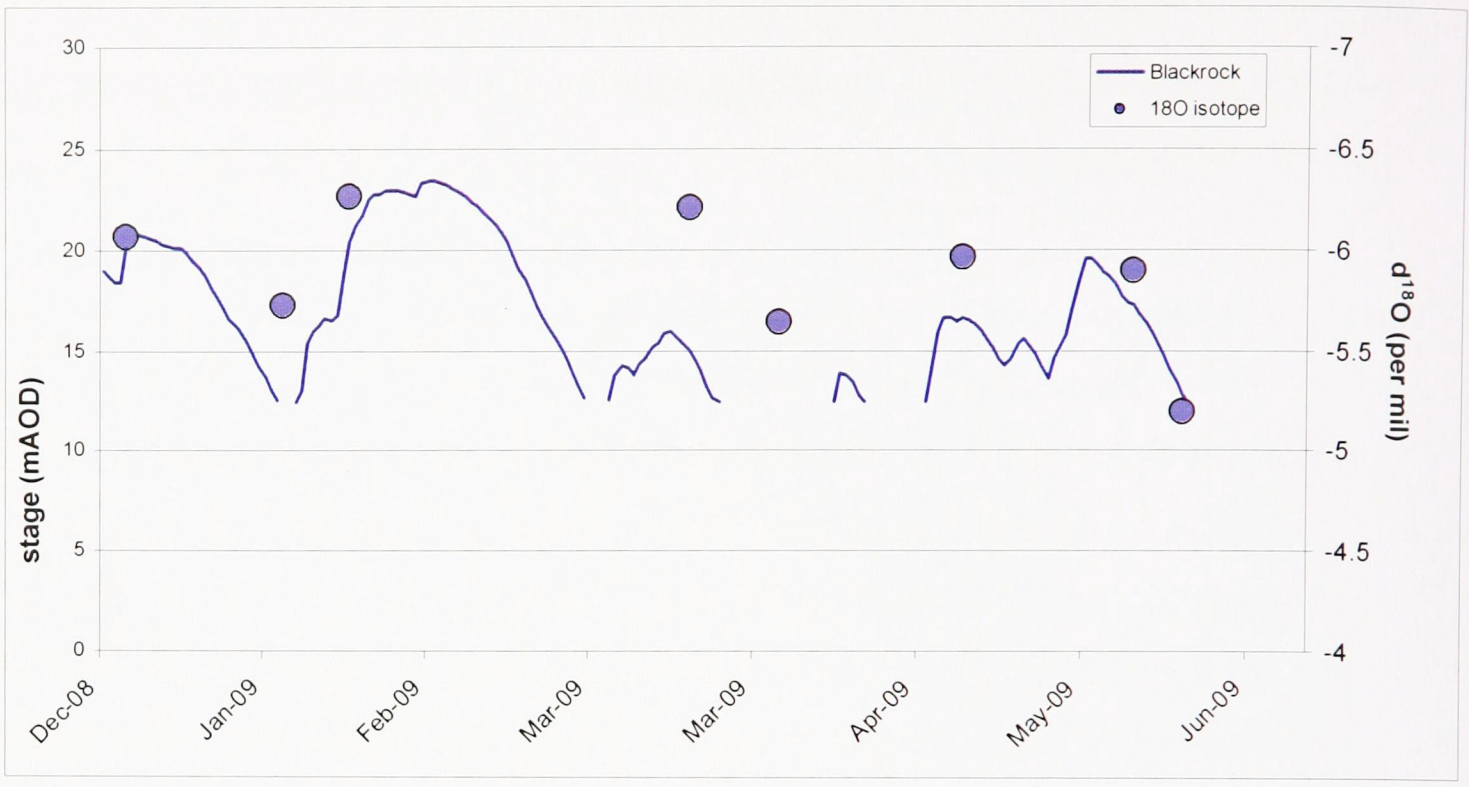


Figure 5.42 $\delta^{18}O$ stable isotope results plotted against Blackrock water level.

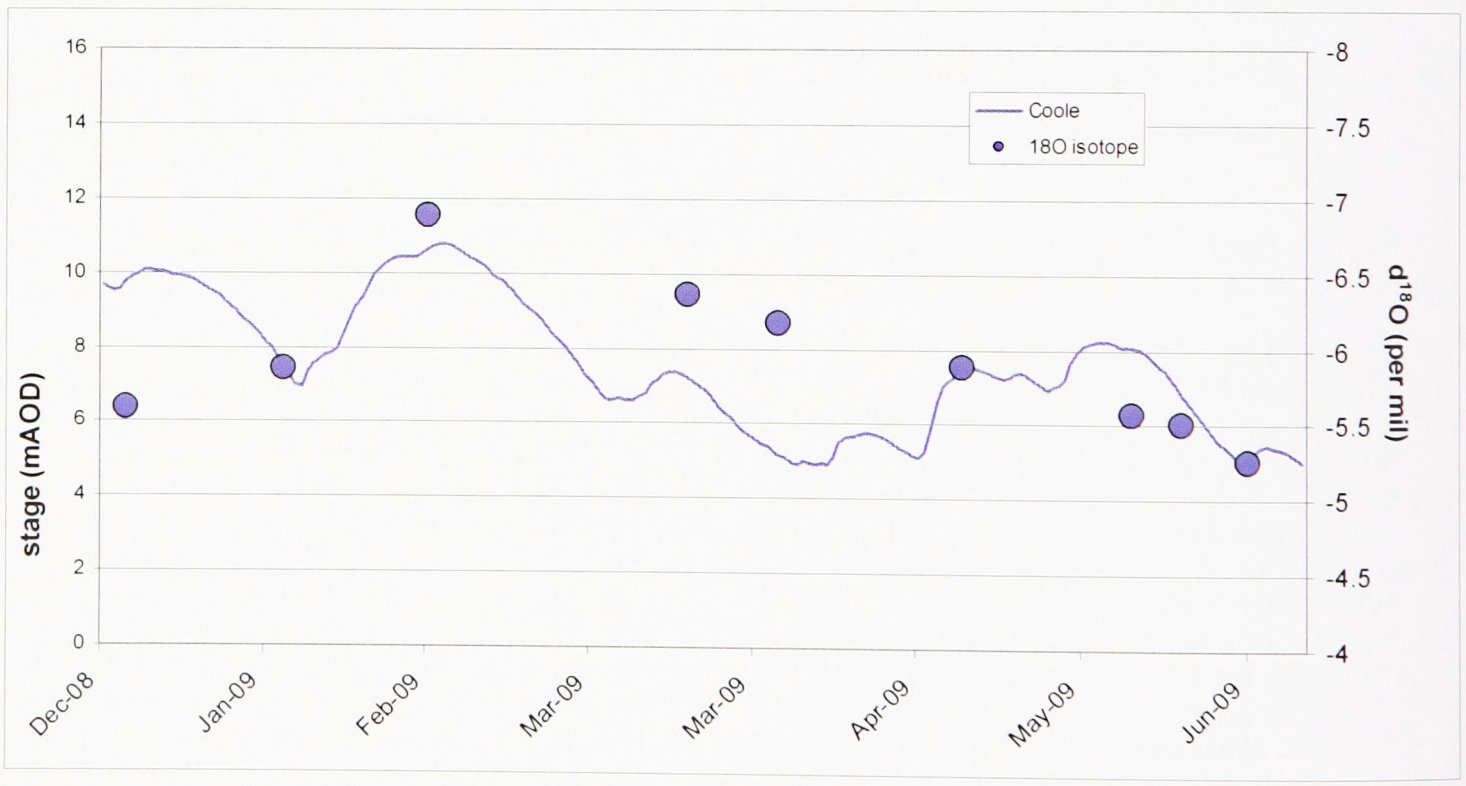


Figure 5.43 $\delta^{18}O$ stable isotope results plotted against Coole water level.

A comparison of $\delta^{18}O$ values was also made in each turlough with respect to mean residence time (as calculated in Section 5.5.4). This is shown for Coy in Figure 5.44 which does not show a clear pattern. However, for the final main recession of the year from April

onwards (points coloured purple) it does reflect the expected pattern whereby the water is becoming more enriched with ^{18}O, the longer the mean residence time.

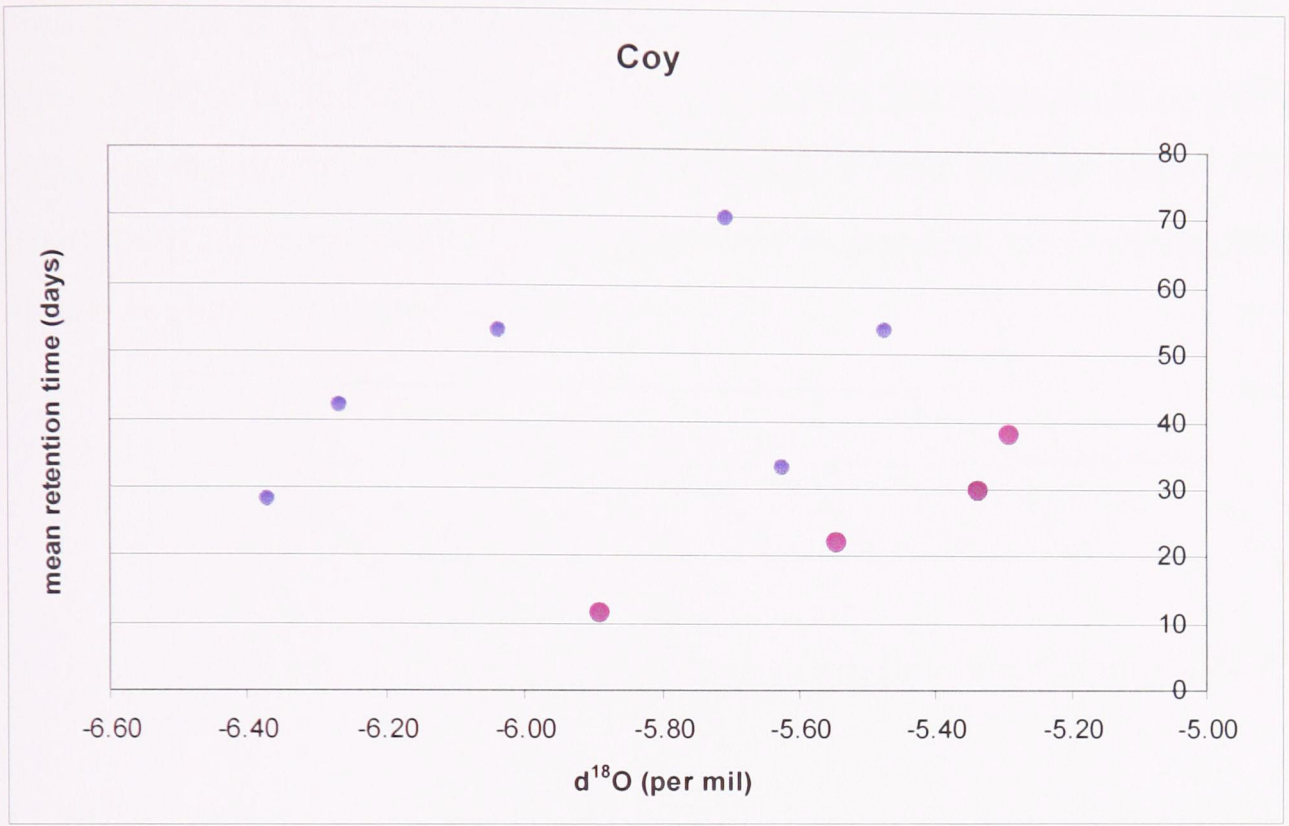


Figure 5.44 $\delta^{18}O$ stable isotope results vs mean residence time of water for Coy [Note, final main recession of the year from April 2009 onwards coloured purple].

The net addition / loss from direct rainfall and evaporation on each turlough has been calculated (Figure 5.45) taking into account the changing surface areas per hourly time step. Although Coole shows a net increase due to direct rainfall there is a distinct slow down from February onwards which correlates well with the start of the enrichment in ^{18}O isotope as shown above. Blackrock shows much lower net increases from rainfall as a result of its more highly fluctuating surface area during this period but again shows a distinct change from February onwards.

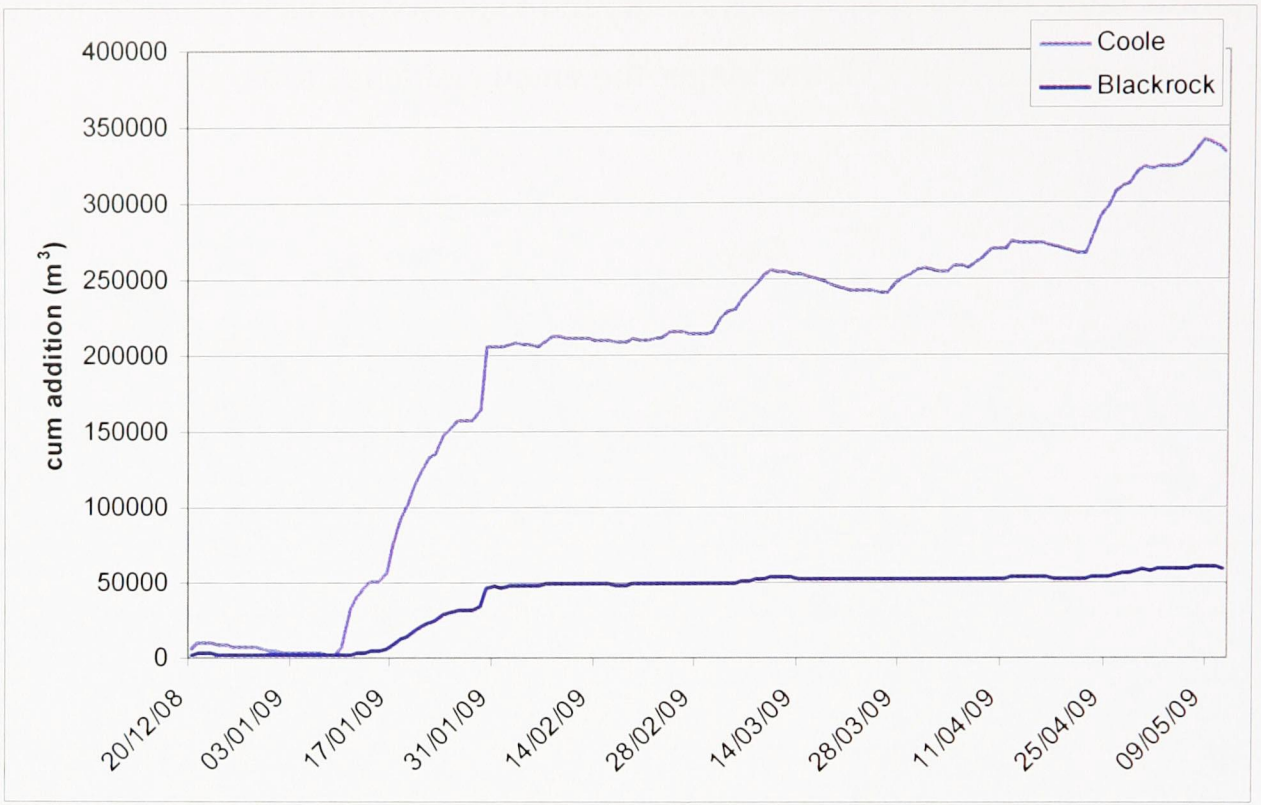


Figure 5.45 Cumulative rainfall minus evaporation on turloughs for 2009.

A full analysis of the system could be carried out on the basis of a mass balance of ^{18}O, using known inflows from the river, known rainfall inputs and evaporation due to fluctuating lake surface areas and the turlough values, which should allow the missing input (i.e. diffuse inflows from the epikarst) to be quantified using the ^{18}O signature from the wells. This also needs to take account of the flows calculated in the final network model, particularly for the downstream turloughs which receive some water that has already spent time in the upper turloughs.

5.8.2 Turlough water quality

The robustness of taking single samples of water from a turlough as representative of its water quality on the assumption that they act as fully mixed volumes was assessed by an intensive survey of an individual turlough, whereby several samples were taken both across the area of Coy turlough and also at three different depths to provide a three-dimensional profile (Figure 5.46). The samples were taken using a Discrete Interval Sampler (*Solinst*) which allowed samples to be taken at specific depths (surface, 2 m and 4 m depth). Note, the maximum depth of water in the turlough was 6 m on this date (29th May 2009) and the main estavelle in the turlough corresponds to sampling position 19, 20,

21. The results of this (and all other water quality analysis) are contained in Appendix E and summarised in Table 5.3 which show fairly good consistency between the samples with no particular spatial gradients picked up across the area of the lake. However, there does seem to be a trend of decreasing P with depth of water sample. The samples were taken during a period of recession in the summer so this trend could be due to the warmer water conditions in shallower water releasing P into soluble form. Alternatively (or additionally) it might be linked to evidence of increased algae in the upper layers as they require sunlight for photosynthesis.

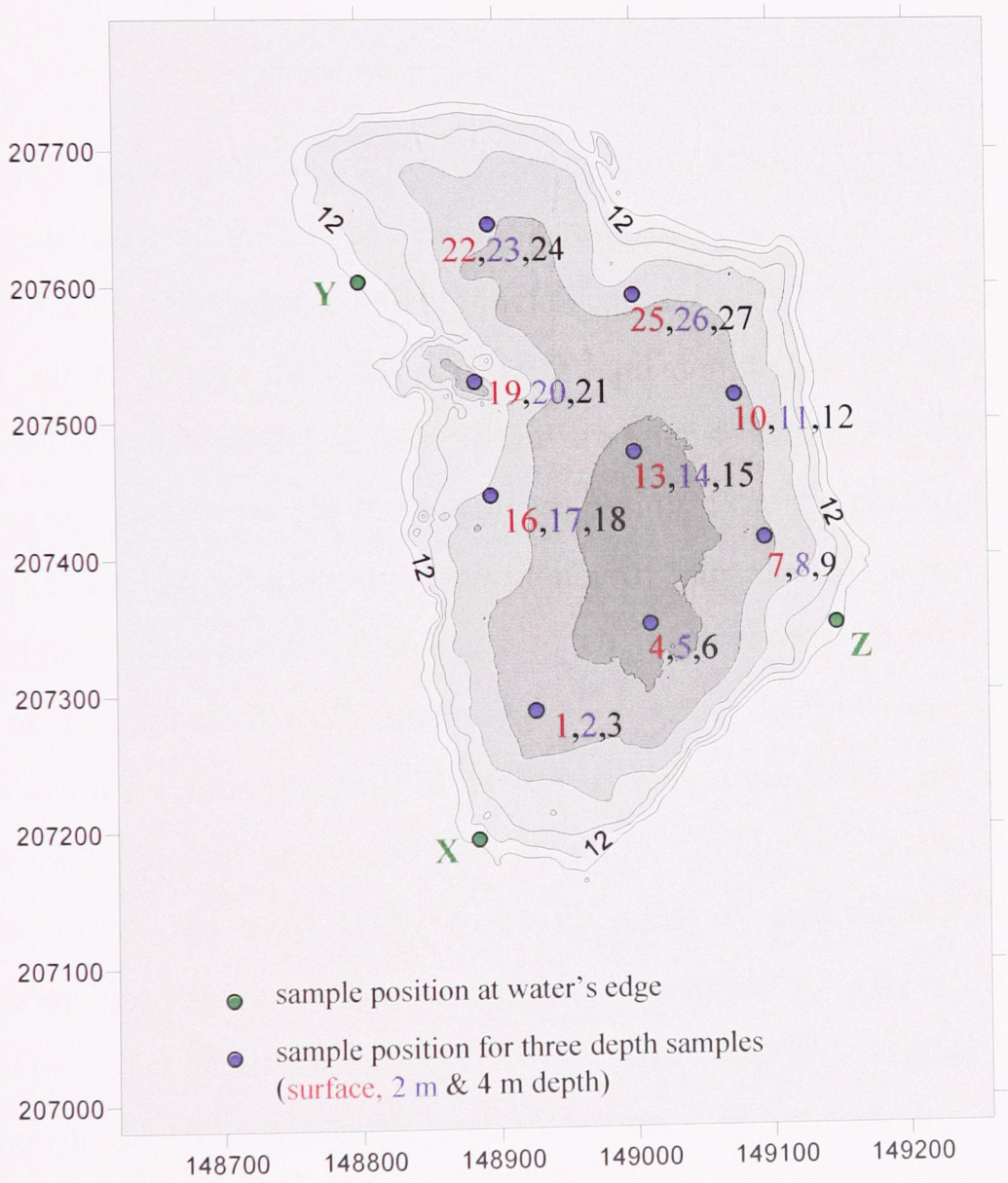


Figure 5.46 Plan view of sampling positions on Coy turlough for intensive sampling foray on 29th May 2009.

Table 5.3 Average water quality results from intensive sampling foray on Coy.

Position	Total P (µg/l)		Total P (µg/l)
1,2,3	43.2	Mean at edge	66.3
4,5,6	46.2	Mean at surface	58.7
7,8,9	57.5	Mean at 2m depth	57.9
10,11,12	66.0	Mean at 4m depth	41.2
13,14,15	43.5		
16,17,18	69.7		
19,20,21	49.0		
22,23,24	34.6		
25,26,27	63.9		

The results from measuring the conductivity of the turloughs and springs for each sampling event are shown on Figure 5.47. This shows a high correlation between the turloughs and Kinvara West, whereas the Kinvara East spring plots a relatively constant profile over time. This confirms (as stated in Chapter 3) that the main outlet of the Gort lowland conduit system must be at the Kinvara West spring and that Kinvara East is probably receiving more diffuse epikarst fracture-type flow from the area to the east that has had a longer residence time in the aquifer. The peak conductivity values displayed at the beginning of April for all turloughs correspond to a period when the turloughs were almost empty. This is probably indicative that the proportional flow from the diffuse flow into the main conduit line was relatively higher compared to the river sourced flows at such times. It is also interesting that the conductivities of the lower three turloughs are slightly lower than Coy and Blackrock due to the addition of water from two extra sources (rivers Ballycahalan and Beagh). The extremely high result (off the graph) registered for Kinvara West spring was attributed to the timing of the sample which was taken on the ebb of the tide which also coincided during a period of low flows from the karst conduit system. Hence, the sea water had mixed back into the spring at high tide before being flushed out as the tide started to fall. This also might be evidence of a significant storage volume in the area, which is known from the deep caves in the vicinity as discussed previously in Chapter 3.

The temperature profiles in the turloughs (Figure 5.48) show a rising trend with time as they move into the summer, as expected. Again the Kinvara West spring apes this trend as it is discharging water from the turlough system whereas the temperature of water from Kinvara East is more constant.



Figure 5.47 Turlough and outlet spring conductivity.

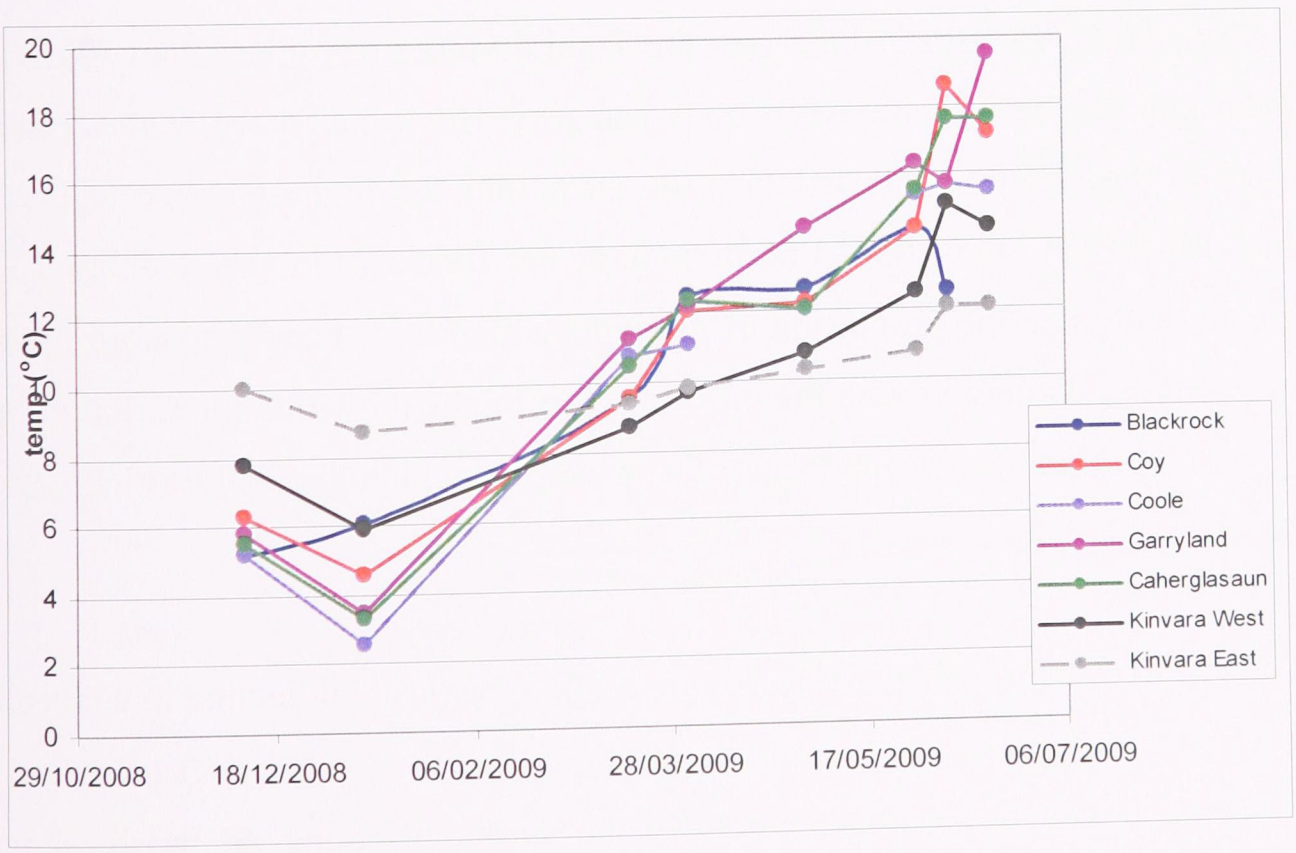


Figure 5.48 Turlough and outlet spring water temperature.

The results from phosphorus and nitrogen samples are shown in Figure 5.49 and 5.50. The P results are fairly erratic although there does seem to be a uniform rise in concentrations from the beginning of May onwards as the turloughs were in significant recession and the water temperatures rising. Hence, this increase may be a result of more soluble phosphates being released from the sediments due to the warmer temperatures in conjunction with the fact that there is no flushing effect through the lake. Another cause could be livestock which started to repopulate the fields forming the turloughs as the water levels receded – the increase in P being due to faeces etc getting washed down into the water. The P concentrations of the main rivers showed no particular trend and the average values were fairly similar with the turlough results - Owenshree, 12 µg/l, Ballycahalan 26 µg/l and Beagh 11 µg/l. The forest drainage and river samples in the Slieve Aughty gave higher values of 45 and 26 µg/l respectively. Strangely, the Kinvara East spring showed a similar profile to the turloughs in terms of P which is hard to explain, although might tentatively suggest another hypothesis that the increase in P measured in the turloughs is due to an increased contribution from the epikarst. The question as to whether turloughs act as sinks or producers for nutrients in groundwater is an interesting one for such GWDTEs, particularly with respect to the Water Framework Directive (WFD). If the values of P are compared against their trophic status according to the Water Framework Directive (see Tynan, *et al.*, 2007), for much of the year the Total P values being less than 20 µg/l would place them into the mesotrophic water body category. But with Total P values peaking up to 60 µg/l in the summer, this would push them into the highest risk category, 1a. A recommended further study would be to look at net fluxes from the rivers and into the turloughs to determine the proportion of nutrients which have been generated in-turlough compared to those coming in with the inflows – this might show that the turloughs act as a net source of nutrient to groundwater for example, which has interesting legislative connotations.

The results from the nitrogen analysis (Figure 5.50) show a small decline in concentrations as the turloughs were filling in the middle of winter and then slight rises as they empty – again possibly linked to grazing animals in the spring urinating on the local turlough catchment. This rise occurs earlier compared to the rise in phosphorus concentrations due

to the more mobile nature of nitrogen in the environment. The Total-N concentrations in the rivers during this period did not rise. Interestingly, the presumed epikarst flow at Kinvara East shows much higher levels of Total-N presumably due to diffuse nitrate contamination of groundwater from agriculture.

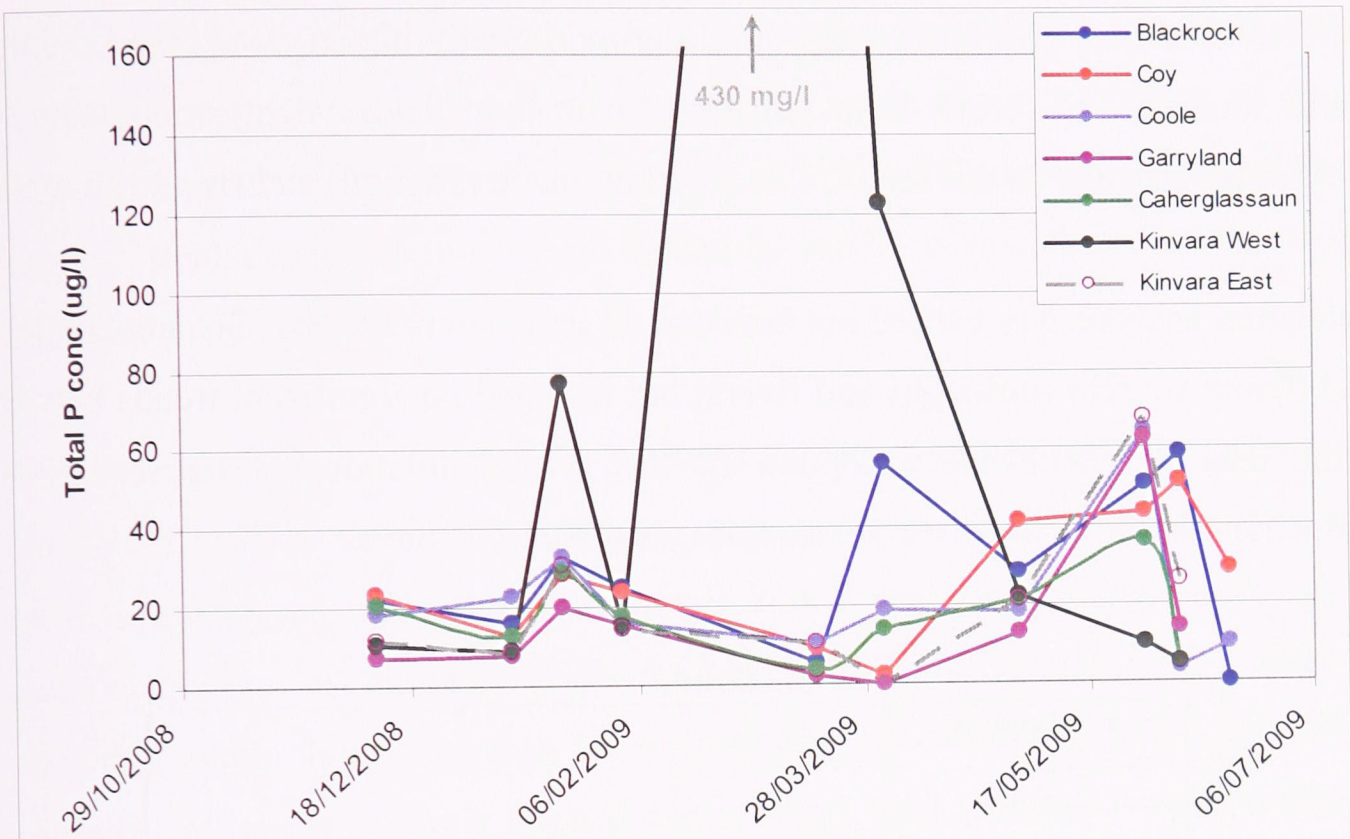


Figure 5.49 Turlough and outlet spring total phosphorus concentration.

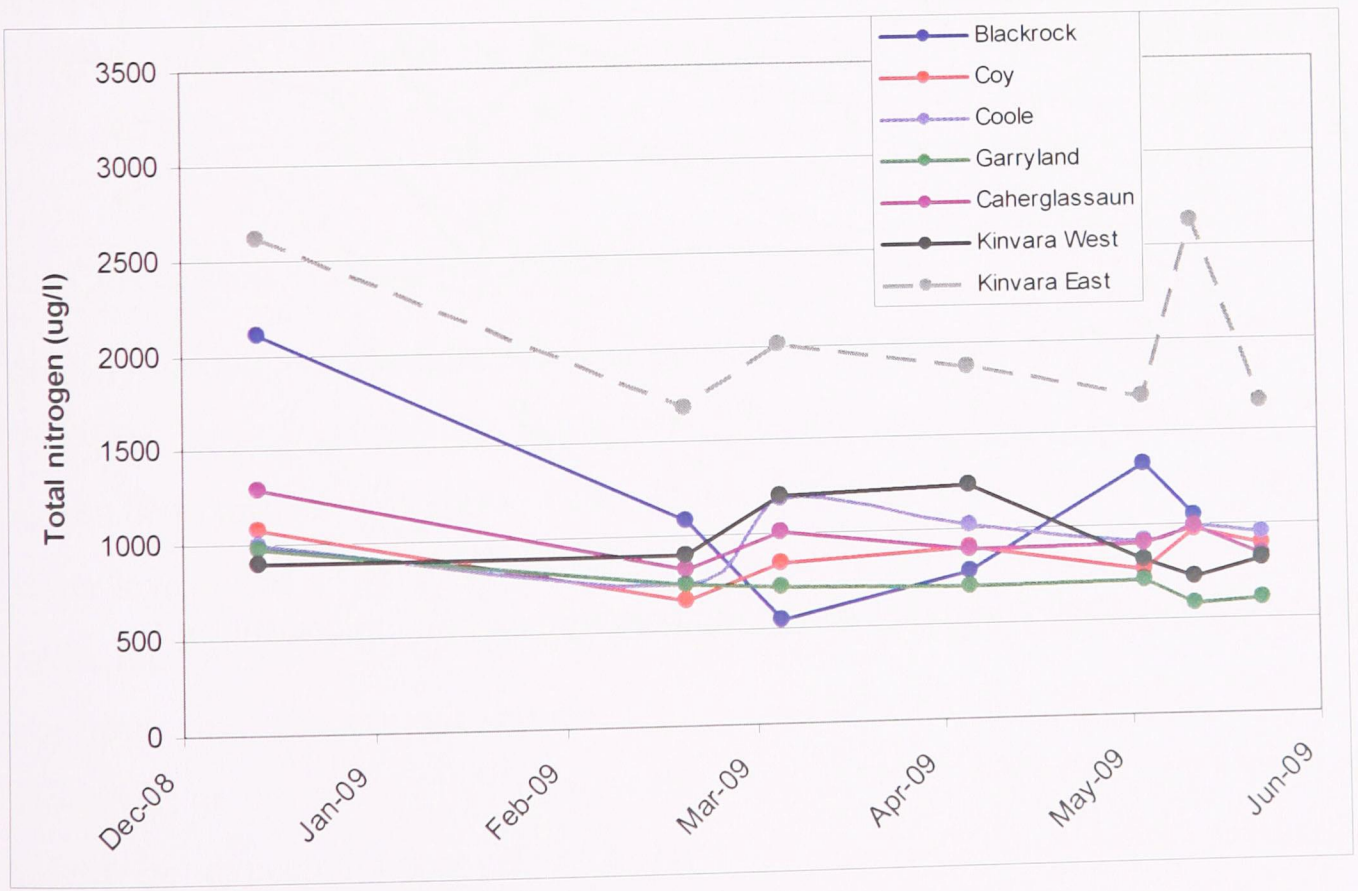


Figure 5.50 Turlough and outlet spring total nitrogen concentration.

Finally, the results from the TOC analysis (Figure 5.51) showed more or less the inverse patterns to the conductivity results: higher values indicating more conduit-borne, river-derived flow compared to the lower values coming for the epikarst. Again, this is picked up in the drop in concentrations at the beginning of April (mirroring the increase in conductivity shown on Figure 5.47) due to proportionally higher flow contributions from diffuse sources. The results from sampling up in the Slieve Aughty mountains showed much higher average values for TOC in forest drainage (37 mg/l) and rivers (26 mg/l).

Correlation analysis was carried out between all parameters (P, N, TOC and conductivity) for different sources (turloughs and rivers) but revealed no significant trends between any of the data sets with the exception of the inverse relationship between TOC and conductivity in the turloughs water samples, as discussed above.

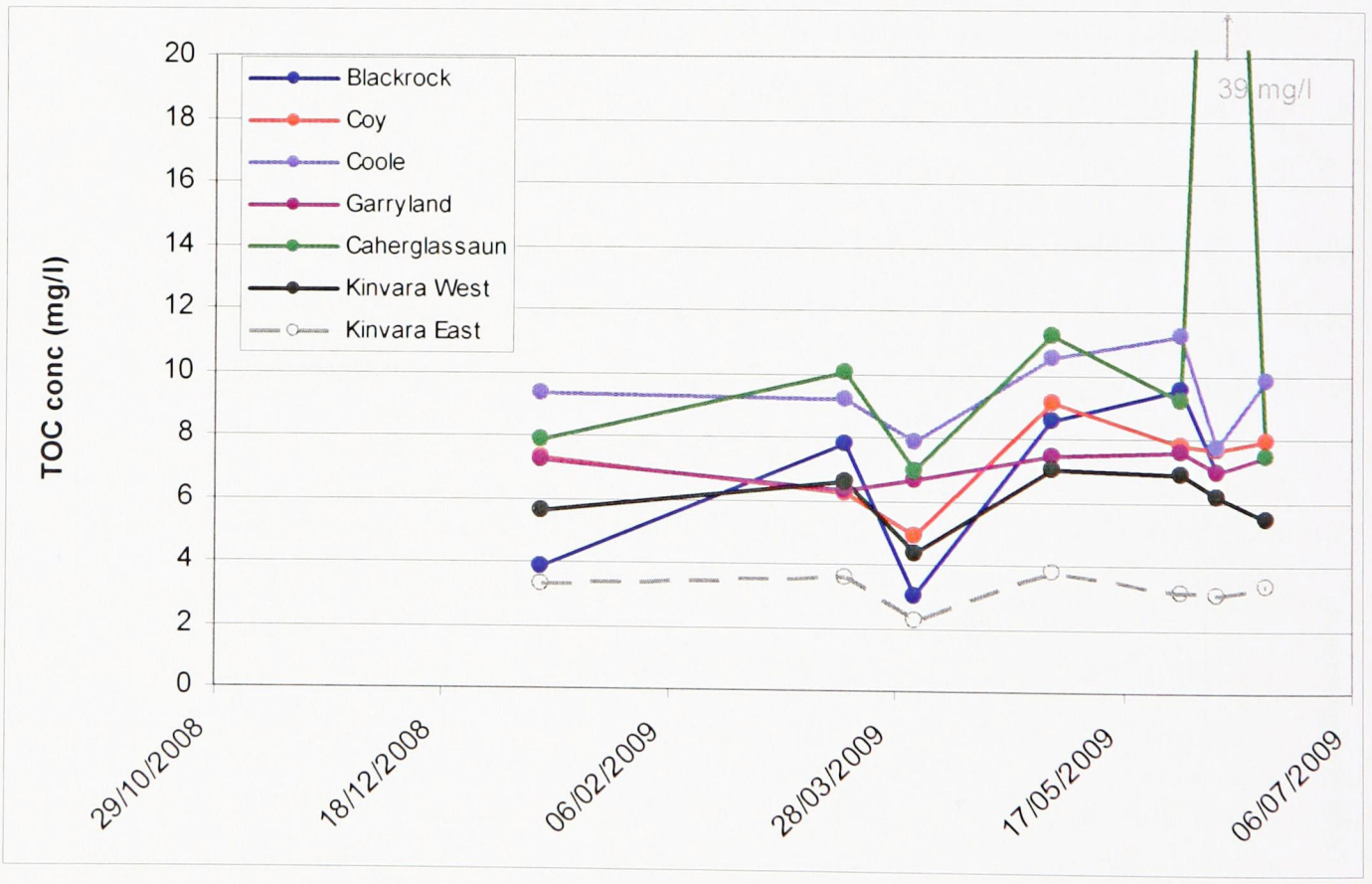


Figure 5.51 Turlough and outlet spring total organic carbon concentration.

6 TIME SERIES ANALYSIS

6.1 Introduction

The continuous time series data of turlough water levels detailed in Section 5 were investigated using different time series techniques in order to elucidate any patterns between them from which deductions could be made about the nature of the hydraulic network (conduit sizes, directions, linkages etc). This information was then incorporated into the final design of the overall hydraulic model of the linked turlough system (as discussed in Chapter 9).

Initially, some correlation analyses between the five turlough level data sets were carried out before moving on to non-stationary time series analyses. The individual time series were first analysed using the Fast Fourier Transform to see if there were any dominant patterns and to see around which frequency band any patterns of interest might be operating within. Following this, Short Term Fourier Transform (STFT analysis) was used – basically Fourier analysis applied across short time intervals – to investigate further. Finally, continuous and discrete wavelet transforms were then applied to achieve a complete timescale representation of localized and transient phenomena occurring at different time scales. All the time series analyses were carried out using MATLAB® version 7.6.0 (R2008a).

6.2 Correlation analysis of turlough water levels

Initially, simple correlations between the different turlough water levels were carried out. The five data sets were first normalized and then compared (Figure 6.1) which clearly shows that there is some form of correlation (probably time-lagged) between the individual water levels. The correlation coefficients between the hourly average water levels of all the lakes for the period September to end of December 2008 are shown on Table 6.1. This confirms that the average hourly water levels in all the lakes are highly correlated. However, as the area is likely to receive similar rainfall patterns, such close correlations might be expected, even if each turlough operated in isolation. The results show particularly close correlations between Coole, Garryland and Caherglassaun.

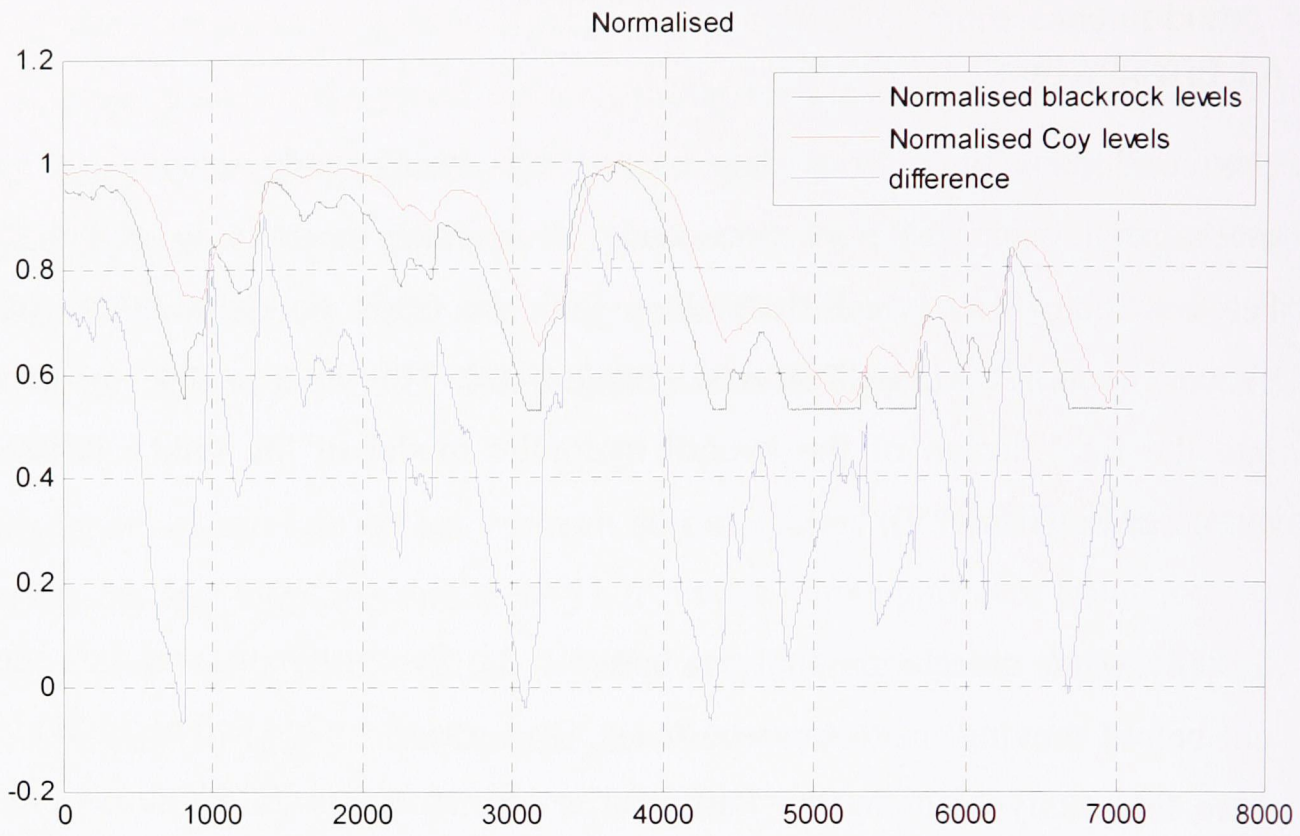


Figure 6.1 Normalized data of Blackrock and Coy water levels.

Table 6.1 Cross correlation matrix using hourly data.

	Blackrock	Coy	Coole	Garryland	Caherglassaun
Blackrock	1	0.895	0.814	0.809	0.841
Coy	0.895	1	0.925	0.948	0.951
Coole	0.814	0.925	1	0.984	0.988
Garryland	0.809	0.948	0.984	1	0.994
Caherglassaun	0.841	0.951	0.988	0.994	1

The data was also analysed using average daily water levels with the correlation results shown on Table 6.2. From the daily data, it can be inferred that the daily average water level of Blackrock has a significant influence on the water level in Coy and to a lesser extent on the water levels of Coole, Garryland and Caherglassaun. The daily average water levels of Coy also seem to be correlated with the change of water levels of the three lower lakes (Coole, Garryland and Caherglassaun). Again, the correlations between the three lower turloughs show extremely high values which would indicate that their water levels change practically simultaneously (as was seen in Figure 5.1). As such, it was not deemed necessary to check the time-lag correlation between these three lakes as they show a contemporaneous behaviour.

Table 6.2 Cross correlation matrix using daily average data.

	Blackrock	Coy	Coole	Garryland	Caherglassaun
Blackrock	1	0.844	0.680	0.676	0.729
Coy	0.844	1	0.858	0.899	0.906
Coole	0.680	0.858	1	0.973	0.983
Garryland	0.676	0.899	0.973	1	0.991
Caherglassaun	0.729	0.906	0.983	0.991	1

Time-lagged correlations were then applied to explore the relationship between the water levels of Coole, Garryland and Caherglassaun with respect to that of Blackrock and Coy as shown on the Figures 6.2.

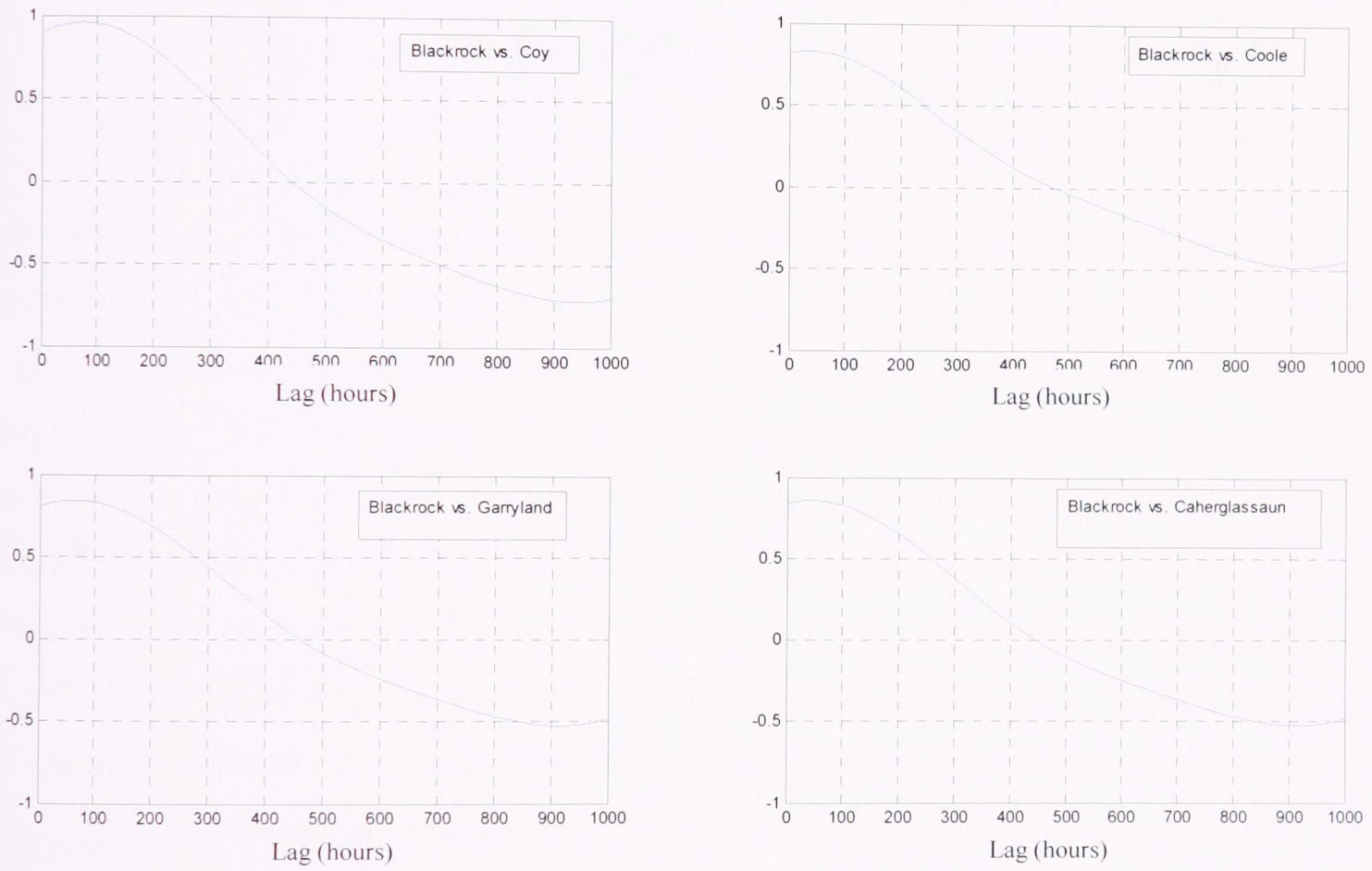


Figure 6.2 Time lagged correlations for Blackrock vs. all other turloughs (hourly data).

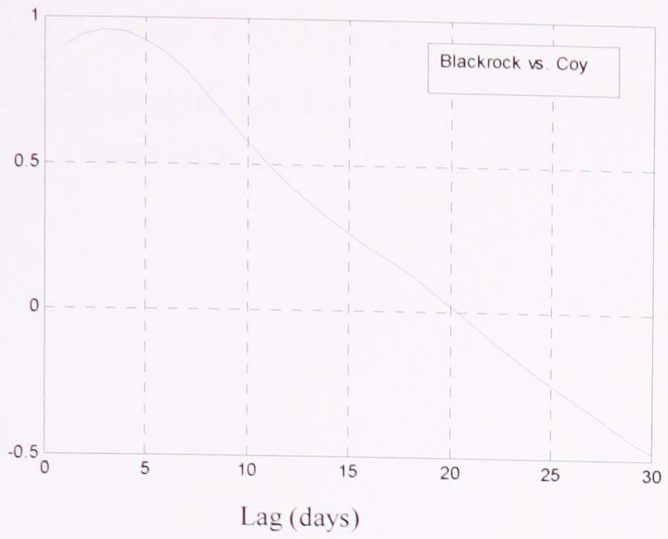
The results from these correlations using hourly data are summarised in Table 6.3 which again shows the potential influence that Blackrock turlough has on the water level changes in Coy. The three lower turloughs are also correlated with the water levels in Blackrock, but to a lesser extent. The time lags show that the water level in Coy has a damped or slower reaction to the water levels in Blackrock, even though the actual correlation value is

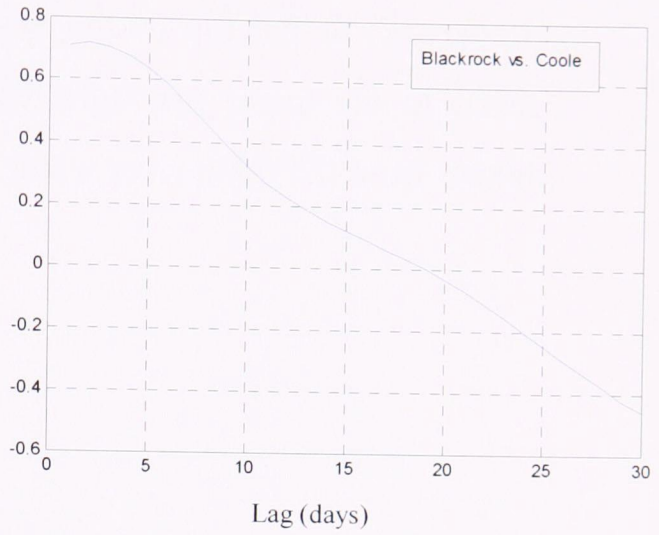
very high, i.e. the water levels in Coy seem to be controlled by the water levels in Blackrock, but it takes 76 hours to have an impact. However, the water levels in Coole, Garryland and Caherglassaun also appear to be affected by the changes in the water levels in Blackrock more promptly even though these lakes are situated further downstream than Coy. This is indicative that Coy must be somewhat off the main conduit line and mainly fed by waters from Blackrock.

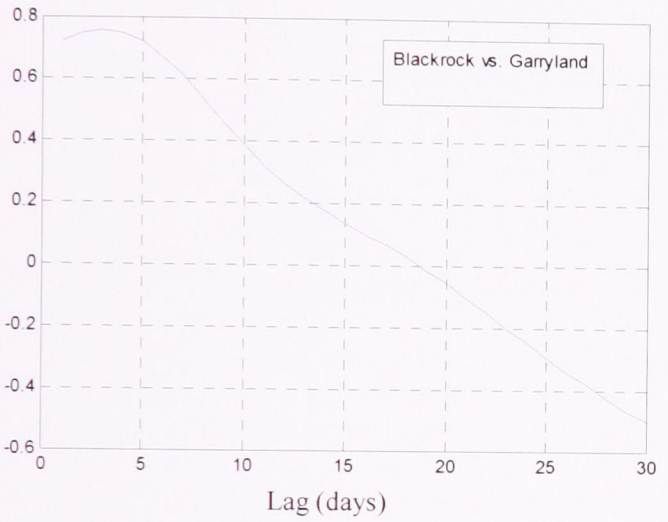
Table 6.3 Results from time-lagged correlation using hourly data.

	peak correlation coeff.	time lag
Blackrock vs. Coy	0.96018	76 hours
Blackrock vs. Coole	0.82804	36 hours
Blackrock vs. Garryland	0.84558	63 hours
Blackrock vs. Caherglassaun	0.85764	42 hours

The same time-lagged correlation was carried out using the daily average data as shown in Figure 6.3 and Table 6.4 with results that are very similar to the hourly water-level correlation plots. This shows that there is a short–term effect with respect to water levels between the turloughs. The longer lag between Blackrock and Garryland (compared to Coole and Caherglassaun) indicates that Garryland is perhaps slightly off the main conduit route to the sea. This discrepancy is also picked up between Coy and the other turloughs. Also of interest is the fact that Coy is much closer in terms of lag to the lower turloughs than Blackrock (considering they are only 1 km apart) which demonstrates the lagged drainage from the turlough due to the flows from Blackrock preferentially draining into the underlying conduit at the start of the recession (as discussed in Section 5.5).







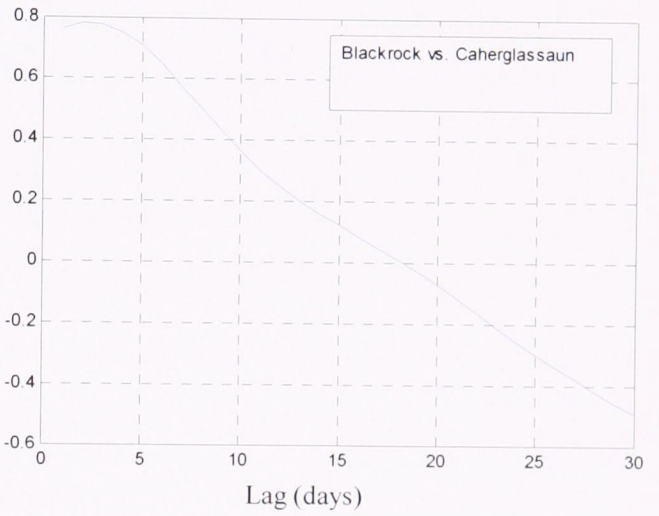


Figure 6.2 Time lagged correlations for Blackrock vs. all other turloughs (daily data).

Table 6.4 Results from time-lagged correlation using daily data.

	peak correlation coeff.	time lag
Blackrock vs. Coy	0.95461	3 days
Blackrock vs. Coole	0.71395	2 days
Blackrock vs. Garryland	0.75655	3 days
Blackrock vs. Caherglassaun	0.77879	2 days

Finally, the water-levels of Coole, Garryland and Caherglassaun have been compared with the water-levels of Coy as the previous cross-correlation matrix (Table 6.1) indicated a close match. Figure 6.3 and Table 6.5 show the time lag relationships which show only a 1 hour lag between the lower lakes and Coy. Hence, it can be inferred that Coy, Coole, Garryland and Caherglassaun all react almost contemporaneously to the rainfall. This

behaviour may be somewhat coincidental in that the extra lag at Coy (with respect to Blackrock) at the top of the system would inevitably push Coy's water level dynamics closer to the lower turloughs which are naturally lagged behind Blackrock, being more distant from the main river water inputs.

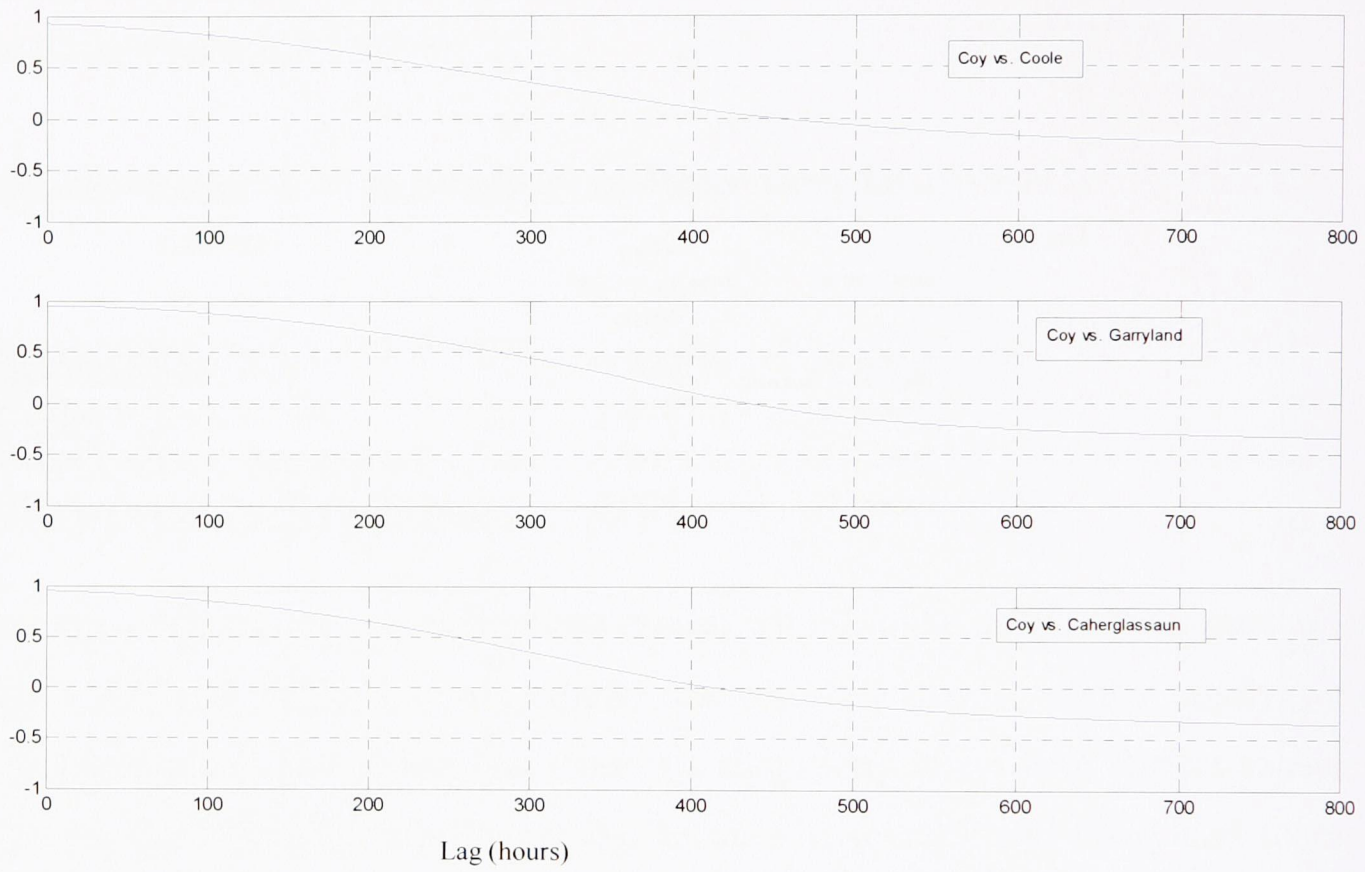


Figure 6.3 Time lagged correlations for Coy vs. lower turloughs (hourly data)

Table 6.5 Results from time-lagged correlation using hourly data.

	peak correlation coeff.	**time lag**
Coy vs. Coole	0.92462	1hr
Coy vs. Garryland	0.94762	1hr
Coy vs. Caherglassaun	0.95075	1hr

6.3 Fourier analysis

The principle of Fourier methods is that every signal can be expressed as a sum (superposition) of pure frequency terms. In the Fourier domain the building blocks are sinusoids – hence a signal can be expressed as a continuous sum of sinusoids at different amplitudes, frequencies and phases. The Fast Fourier Transform (FFT) uses an algorithm

that dramatically improves the computational time for the Discrete Fourier Transform (DFT).

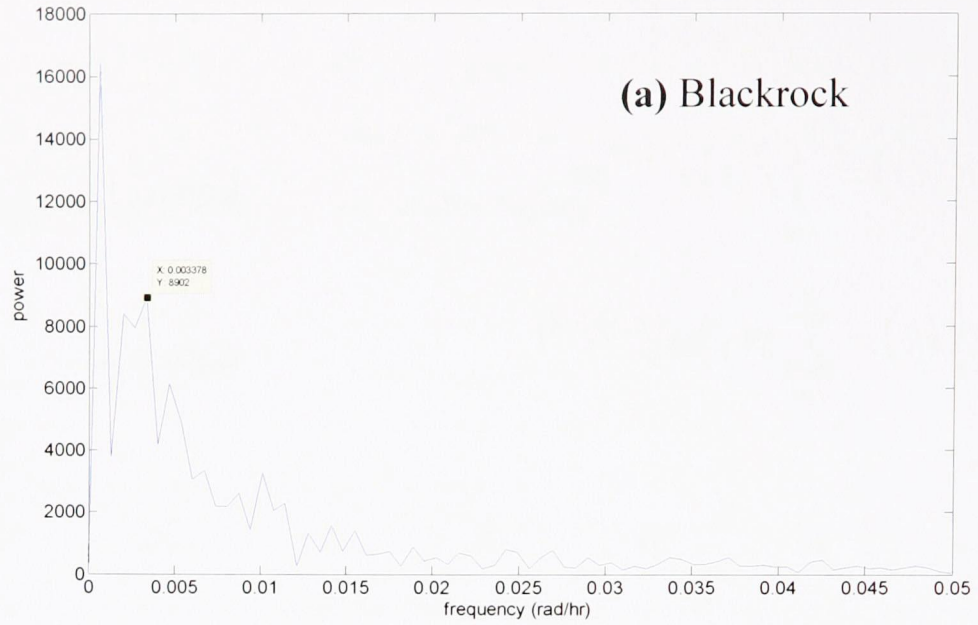
Fourier Transform: $$F(\omega) = \int_{-\infty}^{\infty} f(t) e^{-j\omega t} dt$$ Eqn. 6.1

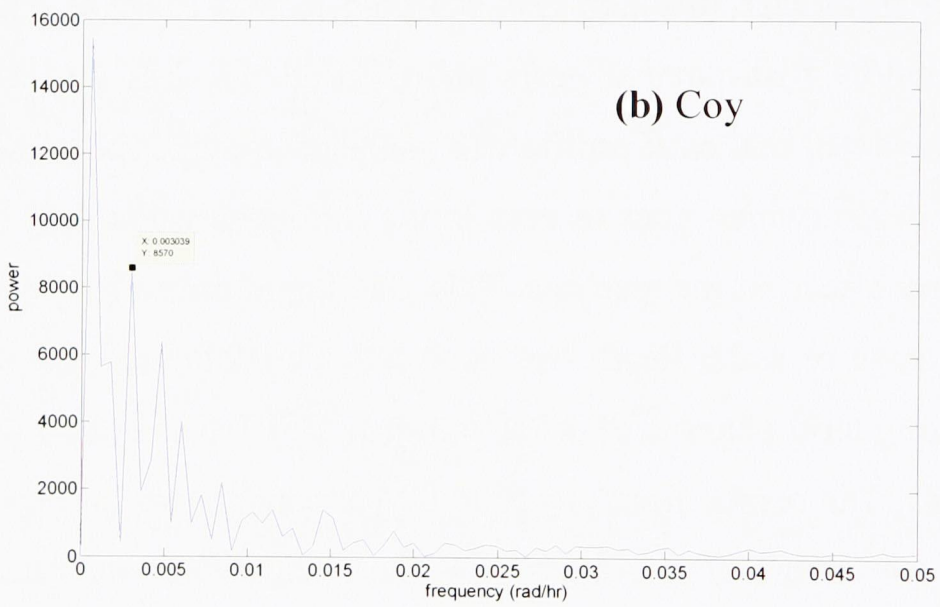
$$X(k) = \sum_{j=1}^{N} x(j) \omega_N^{(j-1)(k-1)}$$ Eqn. 6.2

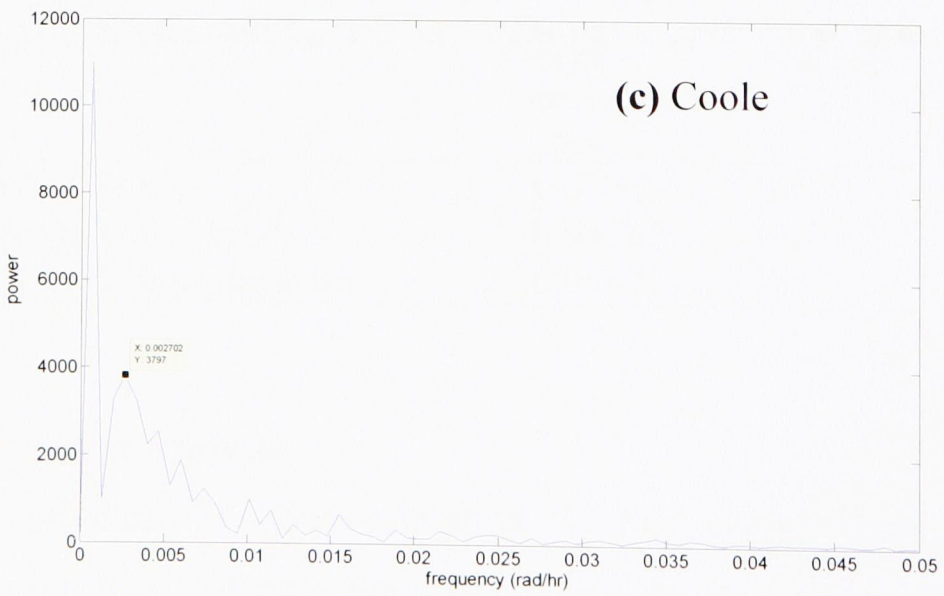
where, $\omega_N = e^{(-2\pi i)/N}$

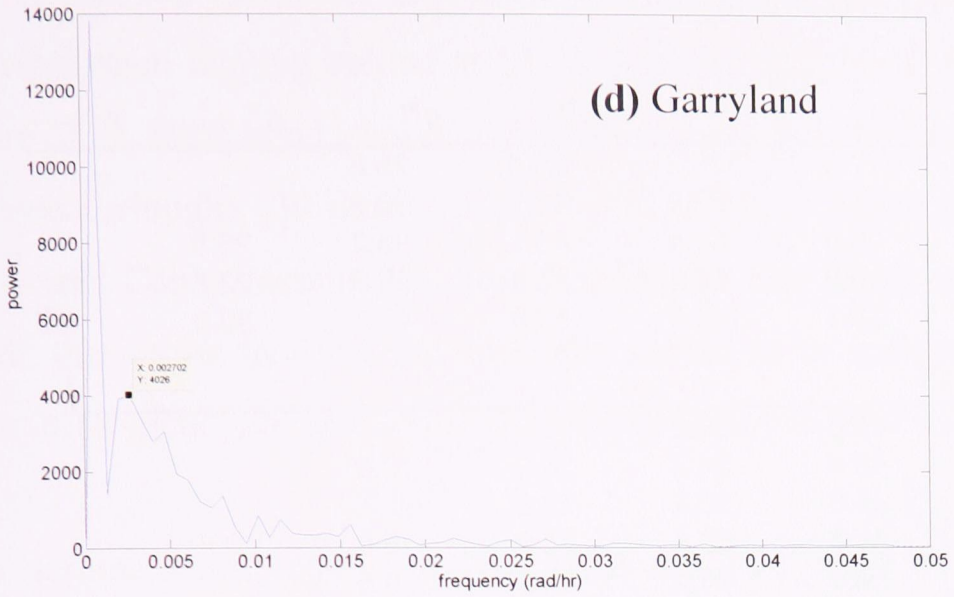
6.3.1 Fast Fourier Transform analysis

The level time series data from each turlough was analysed in four separate batches: the 2006/07, 2007/08 and 2008/09 hydrological years and then all the data together in one continuous set. It should be noted that each profile was analysed as stage (i.e. metres above sea level) and also water depth (which goes to zero in the turloughs when they empty) to check whether this had any effect on the analysis. This was found not to be the case with identical results whether stage or water depth was analysed. The data was first *detrended* (in order to remove any long term patterns of drift) and then a FFT was run on the data to look for frequency patterns. The results from the 2008/09 year are shown in Figure 6.4 for the 5 turloughs, the rest are contained in Appendix F. The peaks were then analysed in descending order of energy and the frequency (in radians/hour) converted into time periods (i.e. $2\pi/\omega$) as shown in Table 6.6. Note, a summary of the frequencies is also given in Appendix F.


(a) Blackrock
power
frequency (rad/hr)
X: 0.003378
Y: 8902
18000
16000
14000
12000
10000
8000
6000
4000
2000
0
0
0.005
0.01
0.015
0.02
0.025
0.03
0.035
0.04
0.045
0.05


(b) Coy
power
frequency (rad/hr)
X: 0.003039
Y: 8570
16000
14000
12000
10000
8000
6000
4000
2000
0
0
0.005
0.01
0.015
0.02
0.025
0.03
0.035
0.04
0.045
0.05


(c) Coole
power
frequency (rad/hr)
X: 0.002702
Y: 3797
12000
10000
8000
6000
4000
2000
0
0
0.005
0.01
0.015
0.02
0.025
0.03
0.035
0.04
0.045
0.05



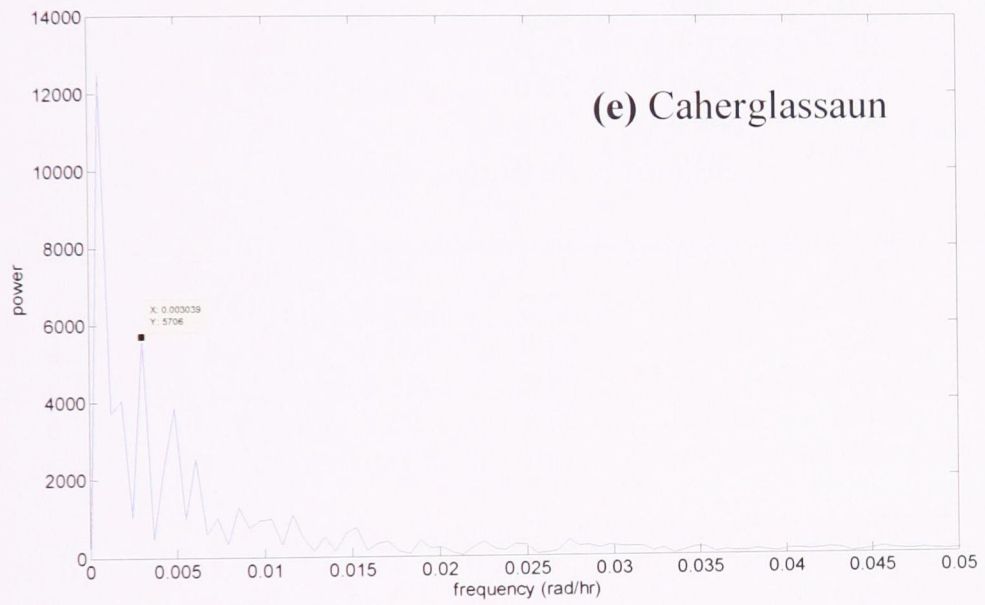


Figure 6.4 FFT results for 2008/09 for **(a)** Blackrock, **(b)** Coy, **(c)** Coole, **(d)** Garryland and **(e)** Caherglassaun water levels.

Table 6.6 Results from FFT for 5 turloughs.

2008/09	period (days)						
order of energy	***1 st***	***2 nd***	***3 rd***	***4 th***	***5 th***	***6 th***	***7 th***
Blackrock	387.5	77.5	129.2	55.4	25.8		
Coy	430.7	86.1	53.8	43.1	30.8		
Coole	387.5	96.9	55.4	43.1	35.2	25.8	
Garryland	387.6	96.9	55.4	32.3	25.8	22.8	0.5
Caherglassaun	430.7	86.1	143.5	53.8	43.1	30.8	0.5
2007/08							
Blackrock	273.9	45.6	34.2				
Coy	273.9	45.6	34.2	24.9	19.6		
Coole	273.9	45.6	30.4	19.6			
Garryland	273.9	45.6	30.4	24.9	19.6	0.5	
Caherglassaun	273.9	54.8	30.4	24.9	0.5		
2006/07							
Blackrock	300.1	50.0	75.0	30.0	23.1		
Coy	300.1	50.0	75.0	30.0	16.7		
Coole	150.0	75.0	50.0	30.0	18.8		
Garryland	233.3	46.7	25.9	0.5			
Caherglassaun	300.1	75.0	50.0	30.0	0.5		
All years							
Blackrock	320.6	192.4	961.8	87.4	53.4	120.2	
Coy	335.0	200.9	1005.0	52.9	91.3	41.9	67.0
Coole	334.9	200.9	1004.6	52.9	100.5	77.3	41.9
Garryland	298.3	178.9	52.6	74.6	63.9	40.7	0.5
Caherglassaun	335.0	200.9	1005.0	52.9	83.7	67.0	41.9

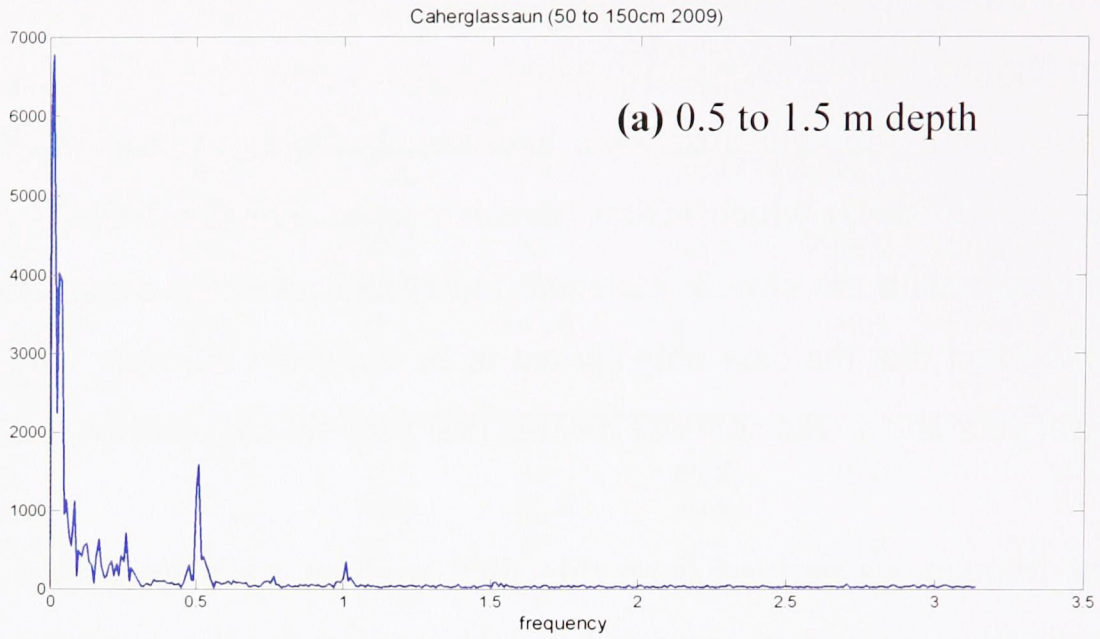
The results from the five turloughs show similar structure as might be expected for broadly the same rainfall input signature onto the system but some distinctions can be made. The first peak at high energy for the single years is really just picking up the length of the data set – although for the three year continuous data set (*all years*) the annual flooding pattern has clearly been picked up. The second peaks (in order of size) give more interesting patterns from the point of view of possible turlough linkage and dynamics. During the highly fluctuating 2008/09 year Coole and Garryland show identical periods which suggest an intimate, uninhibited connection. Equally, Coy and Caherglassaun show identical periods to each other which might indicate a similar type of hydraulic connection to the network (for example, a surge tank above the main conduit). Blackrock, however, demonstrates a significantly different pattern presumably due to it being the first to receive flows as it is much more responsive to fluctuating inflow levels. Again this indicates some isolation from the rest of the system - via a downstream throttle perhaps. The 2007/8 year shows a different pattern, where the filling and emptying cycle was much slower across the

year. Here, the turloughs are showing some energy at 45 days with the exception of Caherglassaun lagging behind at 54 days, which is again indicative of its slightly different nature. The third band shows a difference between the upland turloughs (34 days) and lowland turloughs (30 days) which makes intuitive sense. For the 2006/07 season, again Coole and Caherglassaun are closely matched. Garryland reveals a considerably different result, due to the fact that the data only started to be collected this year half way through the hydrological year and so the analysis for this first year should be disregarded.

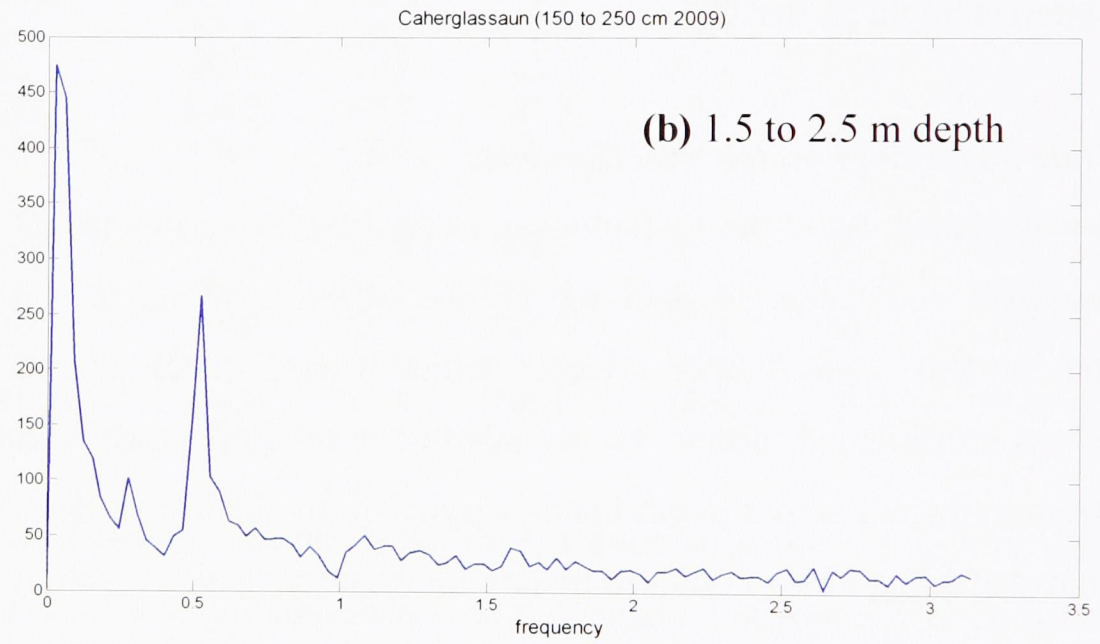
The dominant frequencies derived from this FFT analyses have been used later for the wavelet analysis (Section 6.4) in order to hone the wavelet to the signal at relevant scales where some interest might be derived.

Effect of the tide on turlough water level dynamics

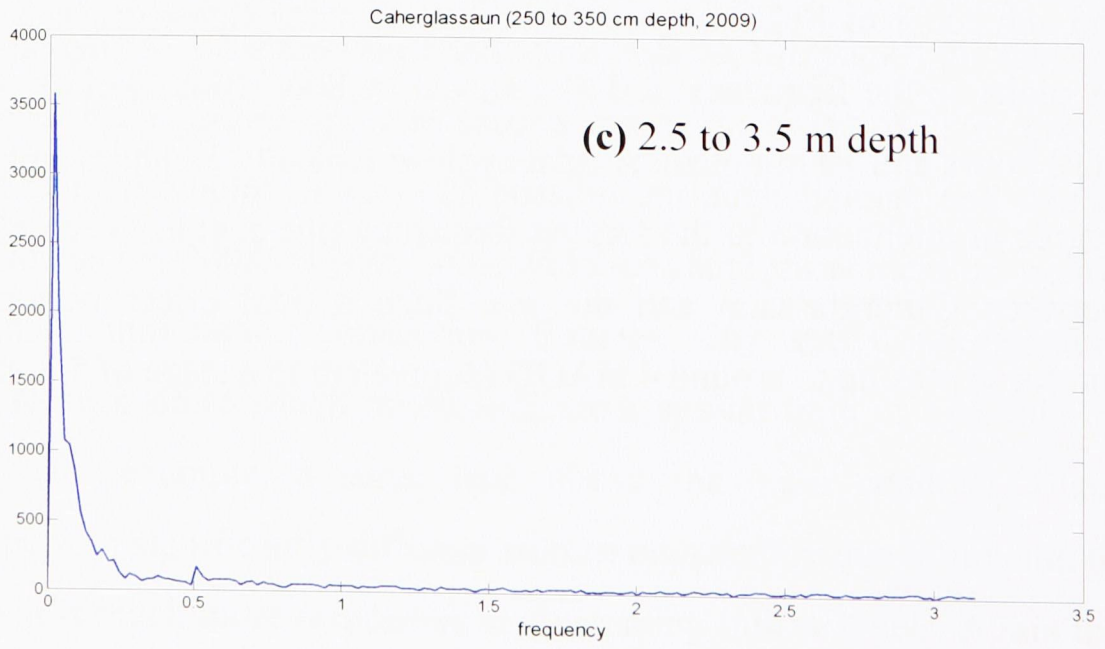
A slight blip was picked up on the FFT plots at a very high frequency (low period) of 0.5 days for Garryland and Caherglassaun for all the different years. It was known that Caherglassaun, at least, was tidally affected which would match this period so this phenomenon was investigated further. To investigate the tidal effect, different parts of the time signal were extracted across depth bands varying from shallow to deep and this data was then reanalysed using FFT in order to determine the depth bands across which the tidal effect was operating. The data from the various extracted depth sections were again detrended and subjected to FFT analysis. This is shown for Caherglassaun (Figure 6.5) which clearly picks up the frequency at 0.51 radians per hour, (time period $= 2\pi/0.51$) or 12.31 hours (12 hours and 19 minutes). A tidal cycle is typically 12 hours and 26 mins and so a slight degree of attenuation to the forcing frequency (the sea) has been observed over the 8 km between Caherglassaun and the sea. Such a tidal effect was picked up at Caherglassaun for depths up to around 4 mAOD (equivalent to a stage of 5.3. mAOD).



(a) 0.5 to 1.5 m depth



(b) 1.5 to 2.5 m depth



(c) 2.5 to 3.5 m depth

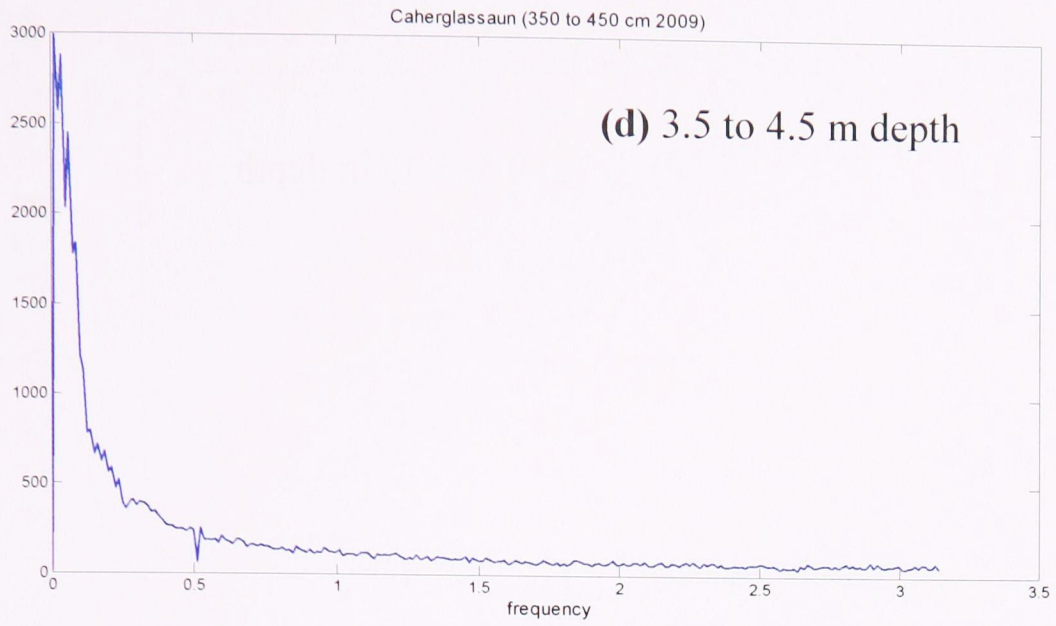


Figure 6.5 FFT on Caherglassaun level data 2009, **(a)** 50 to 150 cm depth range, **(b)** 150 to 250 cm **(c)** 250 to 350 cm **(d)** 350 to 450 cm depth ranges.

The same analysis was carried out for Garryland (Figure 6.6) which also reveals a slight tidal influence at depths up to around 1.5 m (equivalent to a stage of 5.3 mAOD). Interestingly a strong peak is also picked up at slightly deeper water levels (1.5 to 2.5 m depth) at 0.2715 radians/hour, equivalent to a time period 23.14 hours. This daily variation might be evidence of a diurnal evaporation pattern as Garryland is quite a shallow lake with a large surface area at such depths. No peak was picked up to indicate the tidal effects at these depths however.

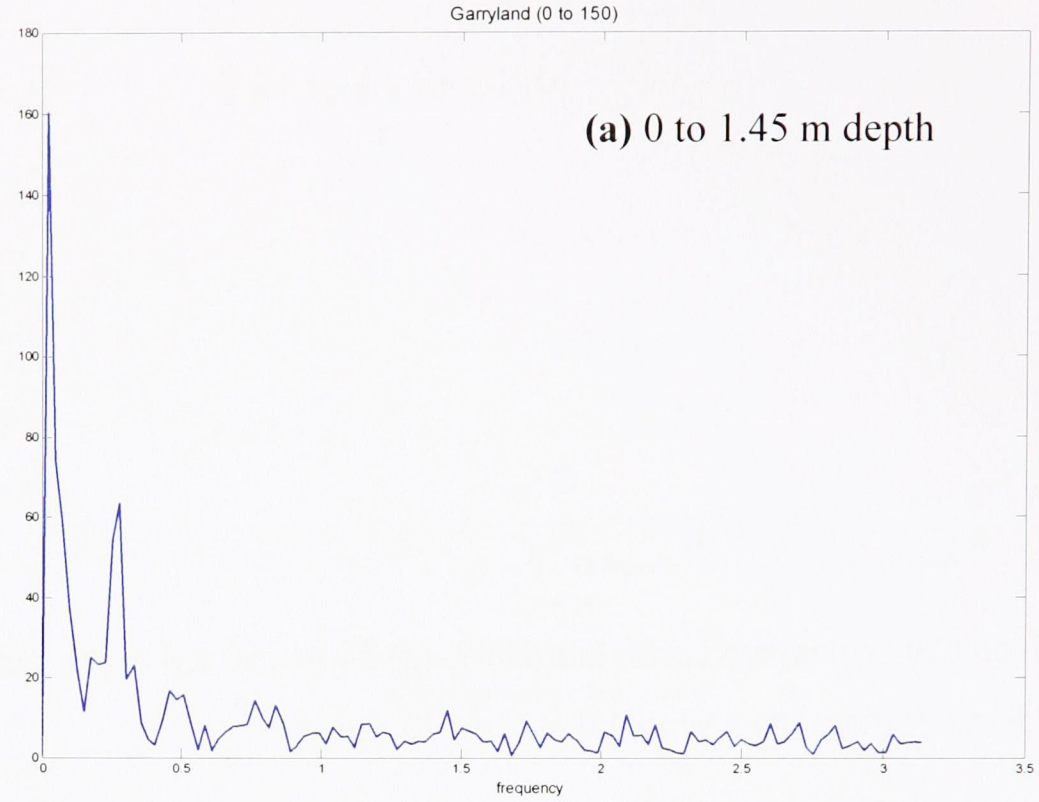
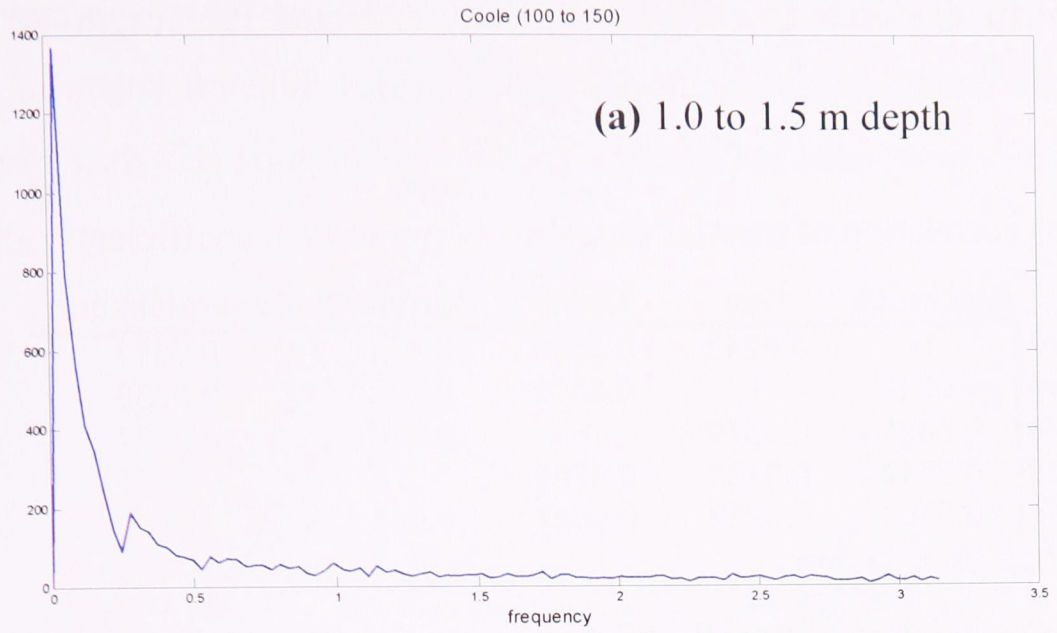


Figure 6.6 FFT on Garryland level data 2009, **(a)** 0 to 150 cm **(b)** 150 to 250 cm depth ranges.

Equally at Coole, a slight tidal influence was picked up at shallow depths up to around 1.5 m depth (stage 4.9 mAOD) as shown on Figure 6.7. Again, as found at Garryland, signs of daily fluctuation were revealed at low depths possibly indicative of evaporation for such a shallow lake with a large surface area at these depths. For example, the surface areas for Coole and Garryland at 2 m depths are 43 and 8 ha respectively.



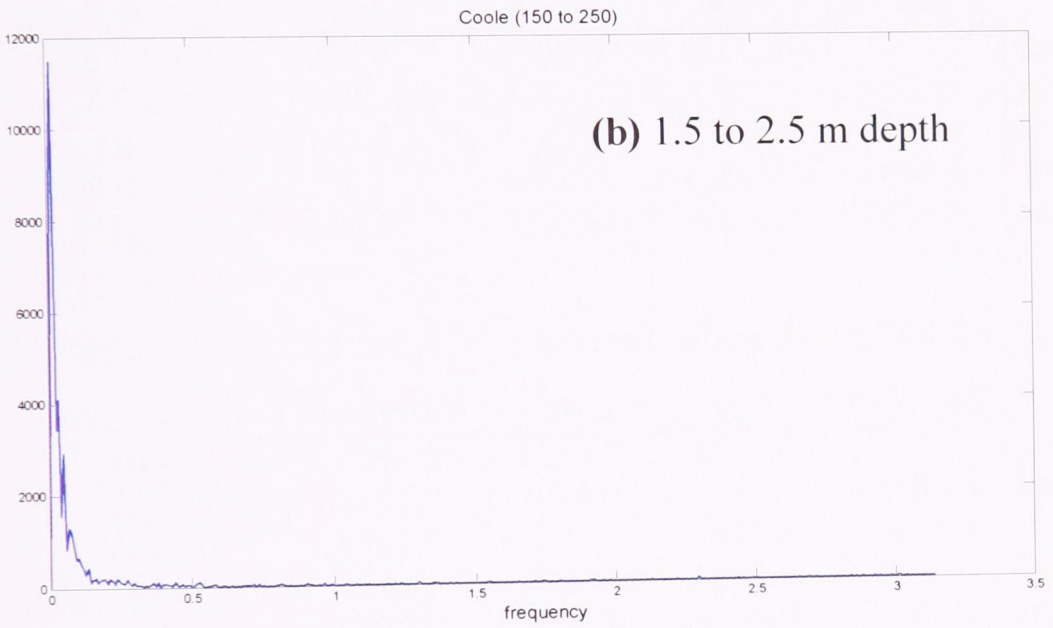


Figure 6.7 FFT on Coole level data 2009, **(a)** 100 to 150 cm depth range, **(b)** 150 to 250 cm depth ranges.

In summary, a close match was found for the three lower turloughs showing the tidal effect at 4.9, 5.3 and 5.3 mAOD for Coole, Garryland and Caherglassaun respectively. Similar plots for Coy and Blackrock turloughs (see Appendix F) show no sign of any tidal influence at any depths which is not surprising given the remoteness from the sea in terms of distance (>15 km) and altitudes of 20 to 30 m above sea level.

Transfer function analysis

Finally, the FFT coefficients from each turlough analysis were cross-correlated against each other as shown on Tables 6.7 to 6.10. The first main FFT coefficient peaks were

removed from all data sets (as they really only reflected the length of the data sets analysed) and the resultant coefficients cross-correlated.

Table 6.7 Cross correlation of transfer functions between FFT coefficients (all data).

	Blackrock	Coy	Coole	Garryland	Caherglassaun
Blackrock	1	0.6242	0.8821	0.9512	0.9353
Coy	0.6242	1	0.5379	0.6134	0.6232
Coole	0.8821	0.5379	1	0.8769	0.9627
Garryland	0.9512	0.6134	0.8769	1	0.9441
Caherglassaun	0.9353	0.6232	0.9627	0.9441	1

Table 6.8 Cross correlation of transfer functions between FFT coefficients (08/09).

	Blackrock	Coy	Coole	Garryland	Caherglassaun
Blackrock	1	0.7123	0.8810	0.9694	0.8798
Coy	0.7123	1	0.8128	0.6361	0.8213
Coole	0.8810	0.8128	1	0.8919	0.7417
Garryland	0.9694	0.6361	0.8919	1	0.8042
Caherglassaun	0.8798	0.8213	0.7417	0.8042	1

Table 6.9 Cross correlation of transfer functions between FFT coefficients (07/08).

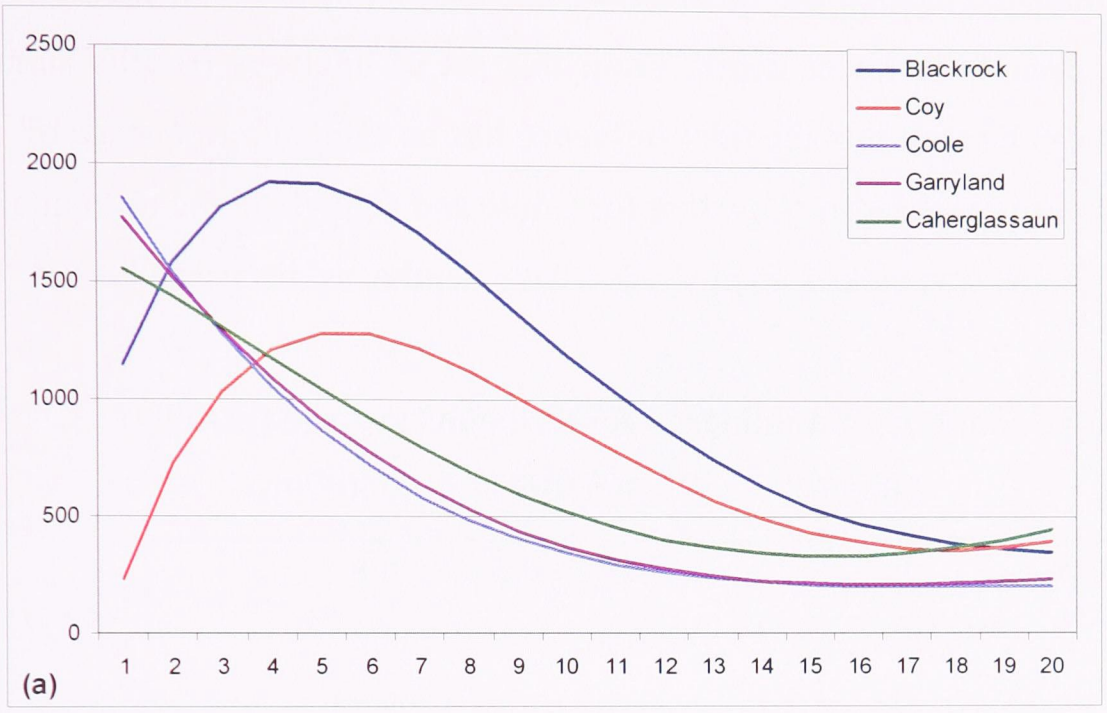
	Blackrock	Coy	Coole	Garryland	Caherglassaun
Blackrock	1	0.8878	0.8724	0.8760	0.9004
Coy	0.8878	1	0.9191	0.9233	0.8896
Coole	0.8724	0.9191	1	0.9983	0.9033
Garryland	0.8760	0.9233	0.9983	1	0.8992
Caherglassaun	0.9004	0.8896	0.9033	0.8992	1

Table 6.10 Cross correlation of transfer functions between FFT coefficients (06/07).

	Blackrock	Coy	Coole	Garryland	Caherglassaun
Blackrock	1	0.7437	0.7717	0.6732	0.7809
Coy	0.7437	1	0.8707	0.6318	0.8962
Coole	0.7717	0.8707	1	0.8742	0.9887
Garryland	0.6732	0.6318	0.8742	1	0.8599
Caherglassaun	0.7809	0.8962	0.9887	0.8599	1

These show close matches between Coole and Caherglassaun for most years and equally between Coole and Garryland. Coy and Garryland are in general not well matched indicating a degree of remoteness for both off the main system. Surprisingly Blackrock and Garryland come out to be very close for the 2008/09 highly fluctuating year but not for the other years. Best fit curves (6^{th} order polynomials) were also plotted to the resultant FFT

coefficient results (Figure 6.8) which clearly show the high correlation between the three lower turloughs for both types of hydrological year. Blackrock and Coy show different responses with Coy lagging behind Blackrock, as has been shown with previous analyses.



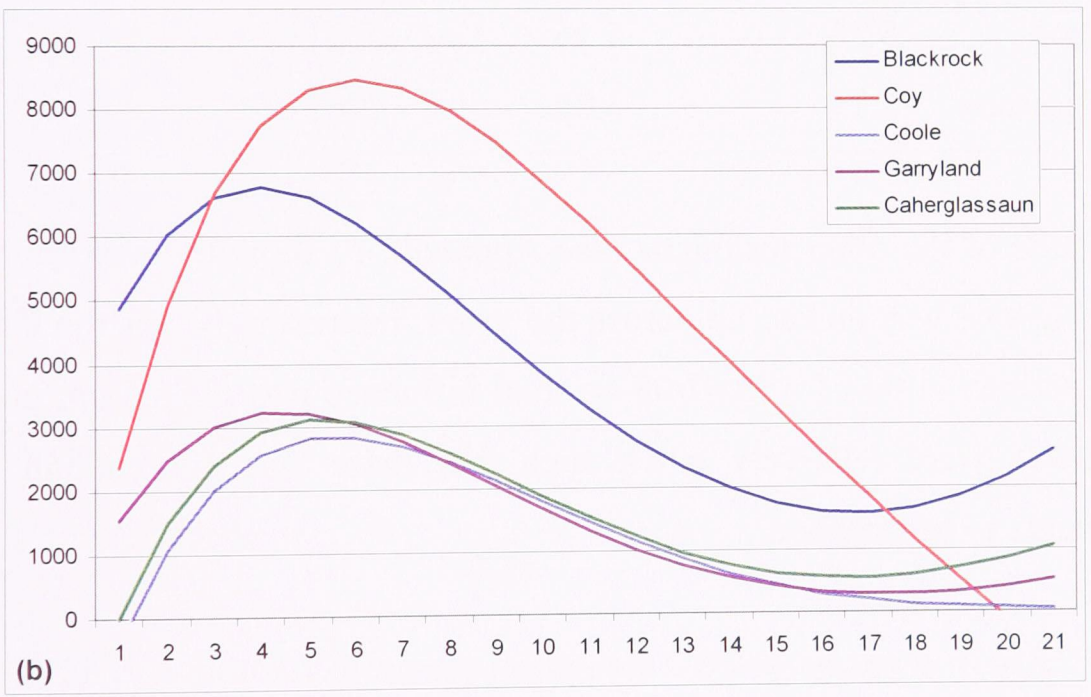


Figure 6.8 Best fit curves to FFT coefficients for **(a)** 2007/08 **(b)** 2008/09.

6.3.2 Short Term Fourier Transform analysis

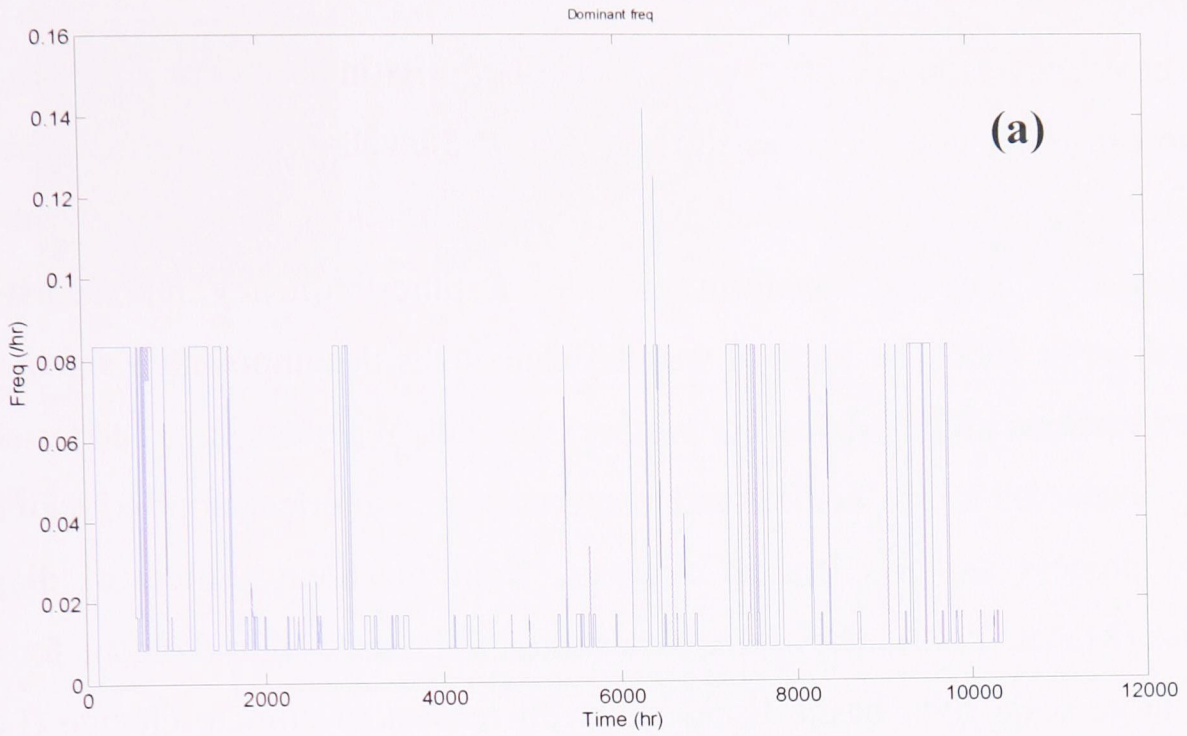
Another technique, Short Term Fourier Transform (STFT) analysis, was applied to the data sets which effectively applies Fourier analysis across small time windows. The window chosen was 120 hours (5 days) in order to see whether this technique would pick up the localised tidal effect. This proved to be the case with STFT strongly detecting the tidal

fluctuations at Caherglassaun, Garryland and Coole at low depths. For example, when the Caherglassaun 08/09 STFT results are compared against the time series in Figure 6.9, the strong frequency at 0.0833 /hour is equivalent to the tidal period of just over 12 hours. When matched against the time series of water depth the tidal period is clearly correlated against periods of lower depth. From this set of analyses (results summarised on Table 6.11) it can be seen that the tidal influence has an effect up to a stage of between 5.3 to 5.6 mAOD. The graphs also show that for Coole and Garryland the diurnal effect (frequency at 0.0833 /hour) was picked up at shallow lake depths, as discussed before.

Table 6.11 Limit of tidal influence for turloughs in stage (mAOD)

	2006/07	2007/08	2008/09
Blackrock	n/a	n/a	n/a
Coy	n/a	n/a	n/a
Coole	n/a (or 0.4)	n/a	5.34
Garryland	5.26	5.16	5.21
Caherglassaun	3.11	3.88	5.62

The results of the other turloughs (see Appendix F) show the maximum depth at which a tidal influence was picked up across the years. Interestingly, for the Coole recessions and filling periods in 06/07 and 07/08 no tidal influence was picked up, possibly as the water movements were relatively quick such that there was not enough time for the tidal movements to be revealed.



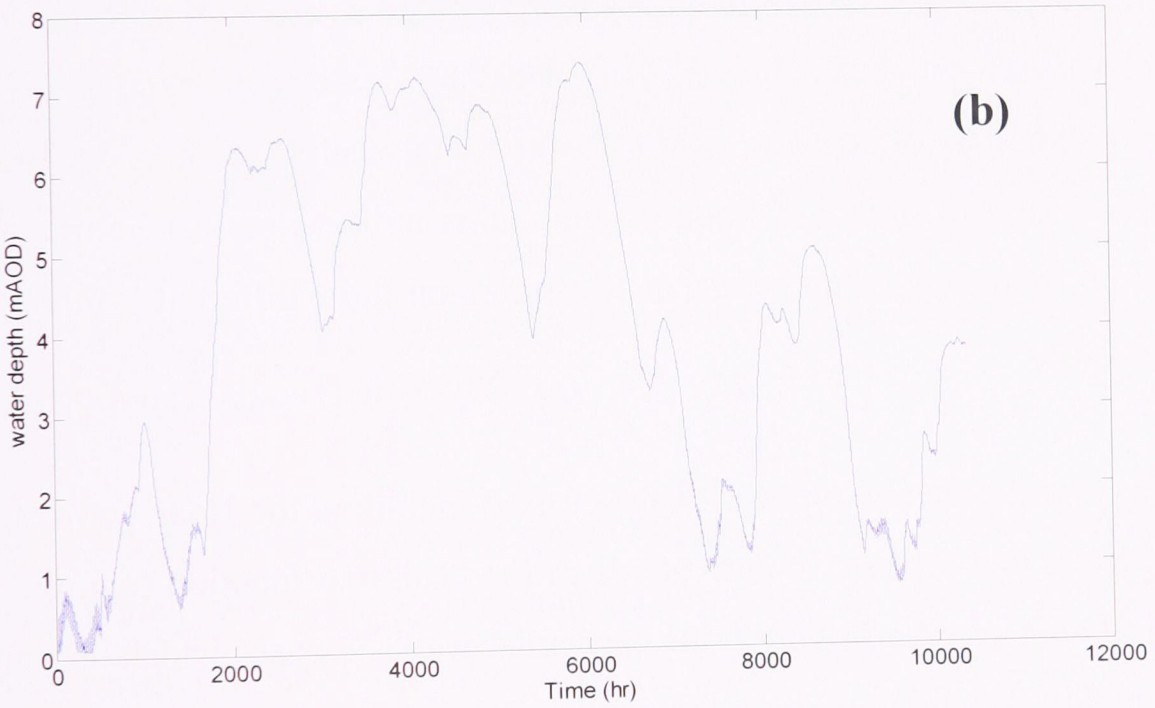


Figure 6.9 (a) STFT (window 120 hours) results for Caherglassaun turlough 2008/09 period and **(b)** corresponding depth time series.

Hence, STFT is a much quicker technique than using screened data and applying the FFT, although the time window does have to be predetermined. However, surprisingly the STFT analysis did not pick up the tidal effect as late compared to FFT for the slower filling years for Caherglassaun.

6.4 Wavelet analysis

Wavelet analysis was applied to the data sets due to its inherent capability to account for non-stationary time-series, such as fluctuating water levels in turloughs. Wavelet analysis has emerged as a powerful tool to analyse temporal variations in frequency content of time series signals. A wavelet transform provides a time-frequency representation of any signal/time series data. The basis of wavelet analysis is decomposing a signal into shifted and scaled versions of the original (or *mother*) wavelet. Wavelets have been used in several fields for example: image coding and compression, numerical approximation methods, stochastic process analysis, fractal analysis, fluid mechanics, medical diagnosis and geophysics (Mallat, 1998). They have also started to be used in hydrology, for example to compare large scale river basin discharges with respect to climate change (Labat *et al.*, 2005), to analyse and transform rainfall statistics (Kim and Valdés, 2003) and have also been applied to a karstic system in the Pyrénées (Labat *et al.*, 2001). The basic objective of the wavelet transform is to achieve a complete time-scale representation of localized and transient phenomena occurring at different time scales. Hence, wavelets must be characterised in both time and frequency domains unlike classical Fourier spectra which only pick up frequency components, as illustrated on three different synthetic time signals on Figure 6.10.

There are several different types of wavelet used including the Haar wavelet, the complex Morlet wavelet and successive derivatives of the Gaussian function (e.g. the Mexican Hat function) (Labat *et al.*, 2000b). The particular wavelet basis which is suitable for the application will depend upon both the application and the characteristics of the function to be analysed (Basu and Gupta, 1998); for example, whether the desire is to have a good localization in time (such as the Daubechies wavelet) or whether more precision is required in terms of localization in frequency (such as the Morlet).

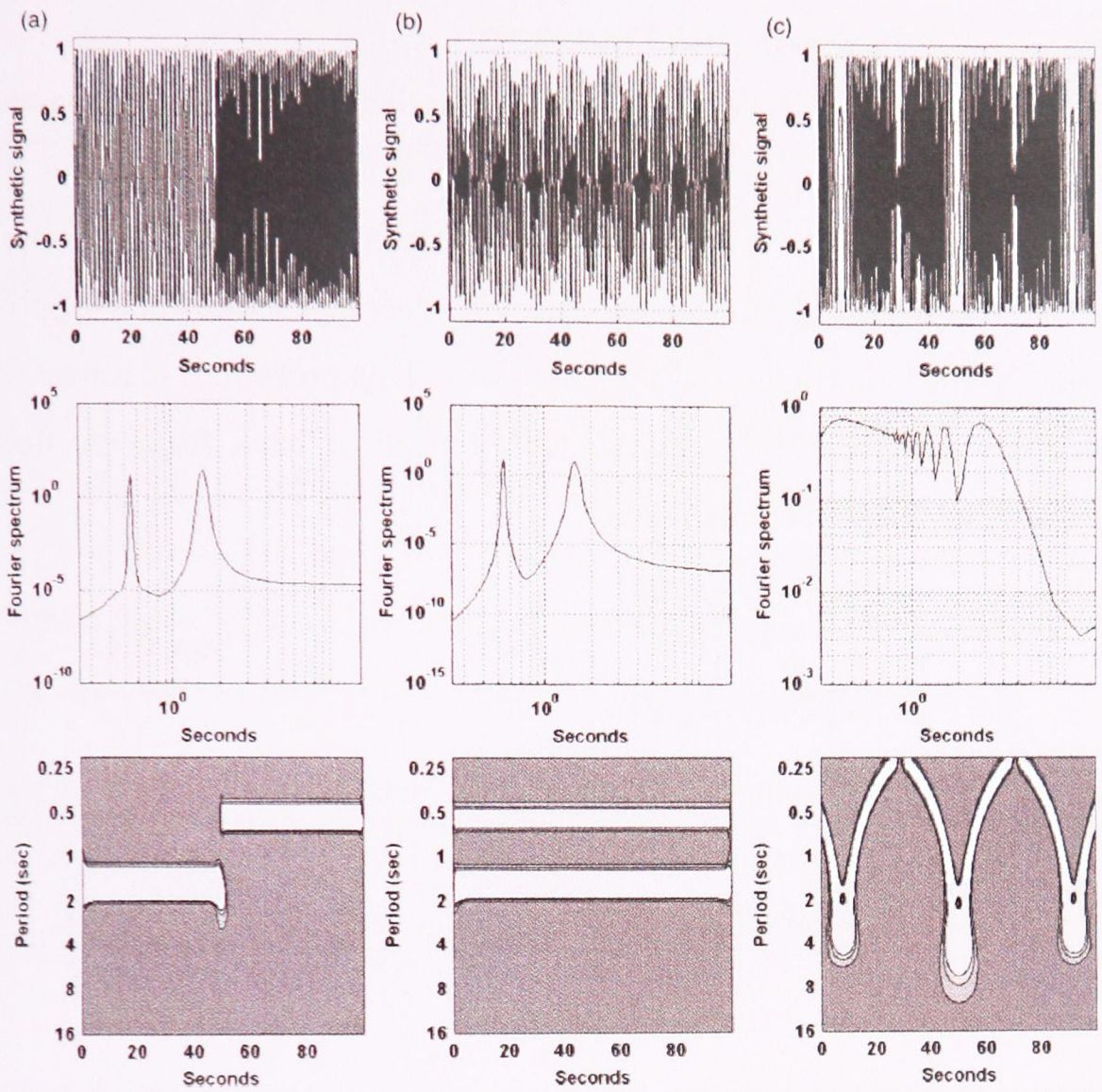


Figure 6.10 Comparison of Fourier and continuous (Morlet) wavelet transforms on three different synthetic signals (Labat, 2005).

Wavelets analysis can be *discrete* which allows one to rebuild the signal later, or *continuous* which gives more information but some of this can be redundant. The continuous wavelet transform is defined as the sum over all time of the signal multiplied by scaled, shifted versions of the wavelet function ψ.

$$C(scale, position) = \int_{-\infty}^{\infty} f(t)\psi(scale, position, t)dt \qquad \text{Eqn. 6.3}$$

where, ψ is the mother wavelet.

The characteristic frequencies for the time series signals were picked up by the FFT analyses. This knowledge was then used to refine the wavelet analysis in order to investigate these frequency bands in more detail.

6.4.1 Discrete wavelet transform (DWT) analysis

The discrete wavelet transform (DWT) consists of detailed and approximation coefficients (Equation 6.4). The DWT decomposes a signal into a large timescale (low frequency) approximation and a collection of detail at different smaller timescales (higher frequencies). The approximation coefficients are then decomposed again to approximation coefficients and detailed coefficients at the next level. This procedure is repeated for each level. The original signal can be reconstructed (if needed) back from the decomposed approximation and the detailed components.

$$\left\{\begin{array}{l} c_j(k) = < X, \varphi_{jk}(t) > \\ \\ d_j(k) = < X, \varphi_{jk}(t) > \end{array}\right\} j,k \in Z \qquad \text{Eqn. 6.4}$$

where <*,*> denotes inner product, (d_j (k)) are the detailed coefficients at level j (j = 1,2…J) and (c_j (k)) are the approximate coefficients at level j. The signal X for analysis is integrally transformed with a set of basis functions.

$$\varphi_{jk}(t) = 2^{-j/2}\varphi(2^{-j}t - k) \qquad \text{Eqn. 6.5}$$

Which is constructed from the mother wavelet ψ(t) by a time-shift operation and a dilation operation.

The Daubechies 4 (db4) wavelet was used for this DWT analysis as show on Figure 6.11.

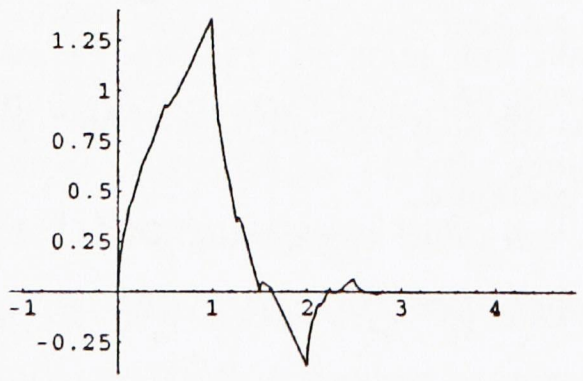


Figure 6.11 The Daubechies (db4) discrete wavelet scaling function.

Different wavelet functions correspond to different pseudo-frequencies at different scales with the relationship given in Equation 6.6. The central frequency for the Daubechies 4 (db4) wavelet is 0.7143 Hz which is needed to scale the wavelet.

$$F_a = \frac{F_c}{a\Delta} \qquad \text{Eqn. 6.6}$$

where F_a is the pseudo-frequency of a wavelet (in Hz) having a central frequency, F_c (Hz) at a scale, *a* and sampling period, Δ. So, for a 1 hour sampling period (for the water level data) a scale of unity (a=1), $F_a = 1.984 \times 10^{-4}$ Hz i.e. a sampling period of 1.40 hours.

The DWT had to be tuned to a scale corresponding to the results from the FFT analysis (Table 6.6 before) which showed the main areas of interest in the regions from 20 to 90 days. The equivalent scale to frequency for a 1 hour data sampled set using the db4 is shown in Table 6.12. So, the areas of interest from the FFT analyses of the water level time series correspond to db4 scales between 343 to 1543 (levels 8 to 11).

Table 6.12 Frequency to scale for db4 for data set at 1 hour sampling.

db4 scale	level	period (days)
171	7.4	10
343	8.4	20
514	9.0	30
686	9.4	40
857	9.7	50
1029	10.0	60
1200	10.2	70
1371	10.4	80
1543	10.6	90
1714	10.7	100
1886	10.9	110
2057	11.0	120

All the results from the DWT analysis for the different years and different time scales are in Appendix F. One of the key observations from this is that there is a considerable difference in the results between the years 2007/08 and 2008/09 when analysed at level 9 which corresponds to a time period of around 30 days. Since, the turlough response was very different between these years, this suggests that the main process governing this difference occurs on a 30 day cycle. An example of this difference is shown in Figure 6.12 for Coole but the same difference is there for all turloughs. At the other scales the difference is less marked. This may be a reflection of the timing of intense rainfall events or more intriguingly, such a 30 day cycle would also tie in with spring tides. Hence, this

suggests that the synchronicity of heavy rainfall and spring tides might be a key factor in terms of the duration of turlough flooding – a concept that should be the subject of more research, particularly with regards to the historic flooding events of the 1990s.

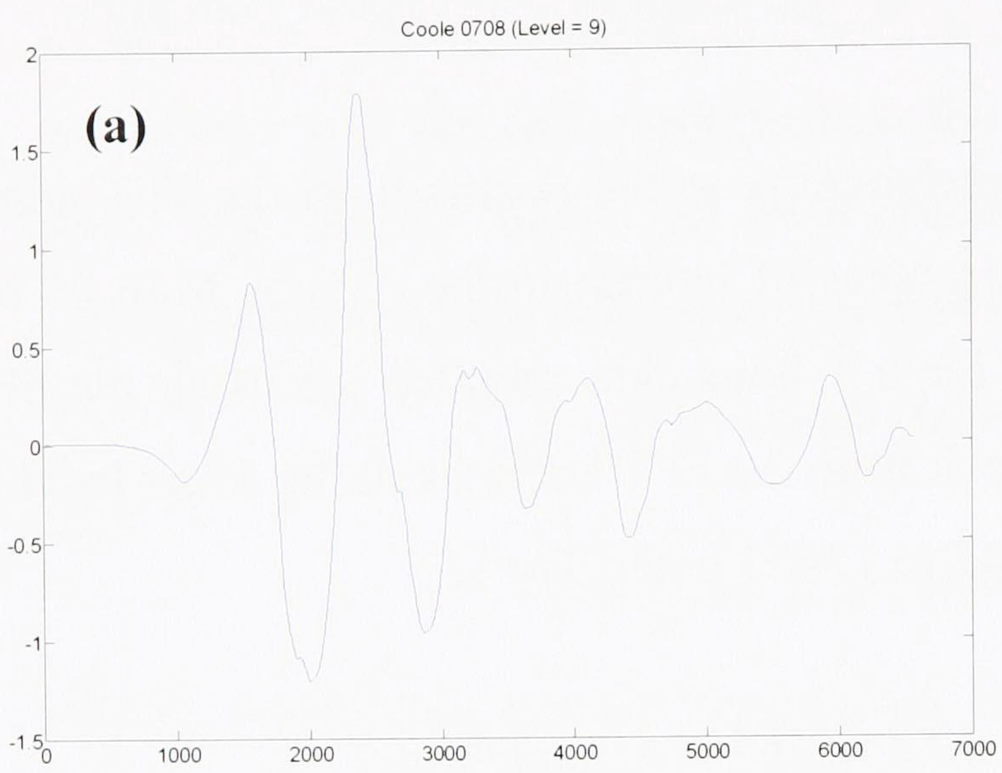
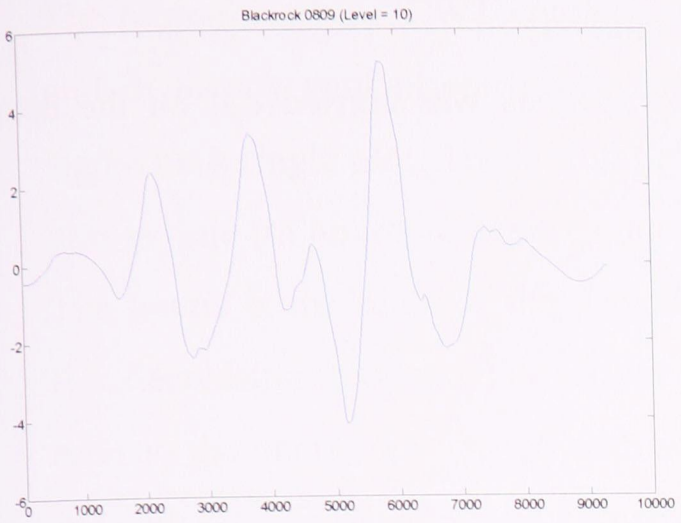
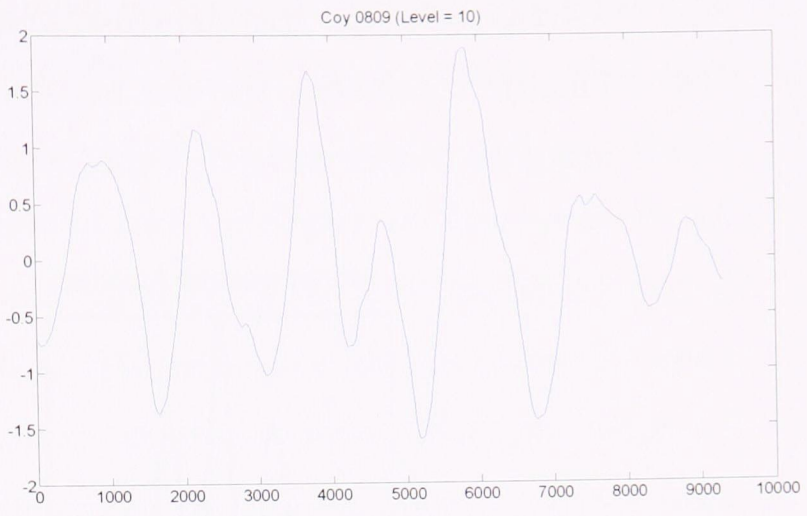


Figure 6.12 DWT (db4) results for Coole at level 9 (period 30 days) **(a)** 2007/08 **(b)** 2008/09.

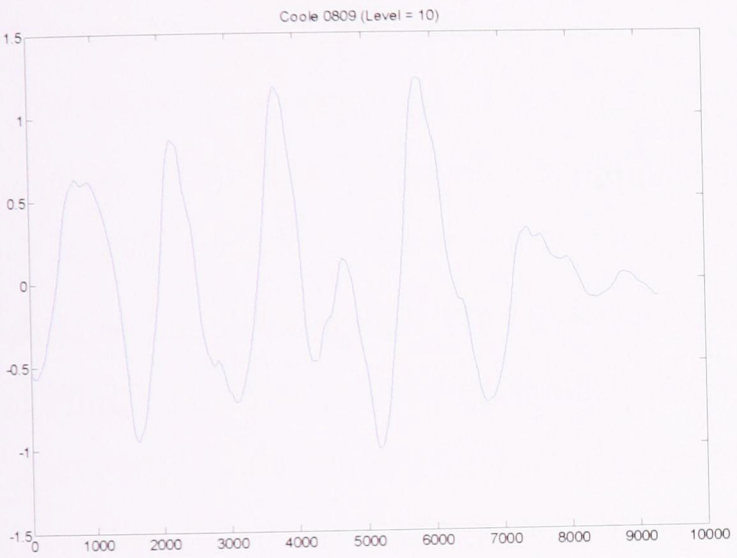
Other differences picked up between the turloughs for the same years show a different filling period for Coole and Garryland at a time period of 14 and 30 days. It shows close matches between Coole and Caherglassaun and also that Coy and Caherglassaun are very similar. At 120 days all the turloughs show very similar coefficients as expected. At a 60 day time period for the 2007/08 year, Coy differs from the other turloughs during the time of peak inundation to the start of the recession. There is an incongruous peak for Blackrock at the beginning of 08/09 compared to the other turloughs which might be indicative of a suspected instrumentation (Diver) problem during that period.



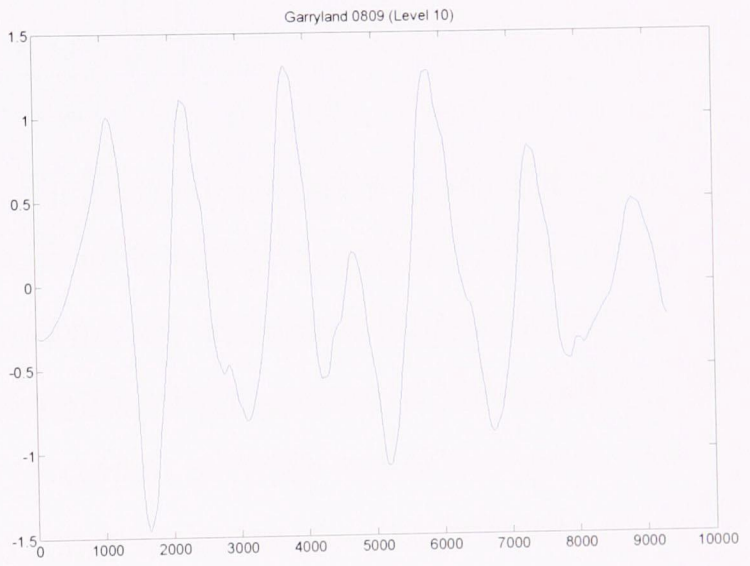
Blackrock



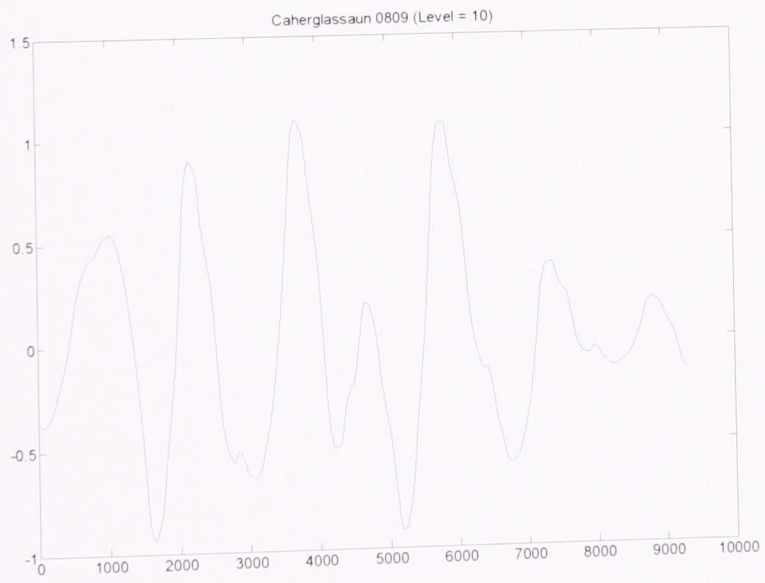
Coy



Coole



Garryland



Caherglassaun

Figure 6.13 DWT (db4) results for all turloughs 2008/09 at level 10 (period 60 days).

6.4.2 Continuous wavelet transform (CWT) analysis

Finally, continuous wavelet transform (CWT) analysis was carried out on the data set using the Morlet wavelet as shown in Figure 6.14.

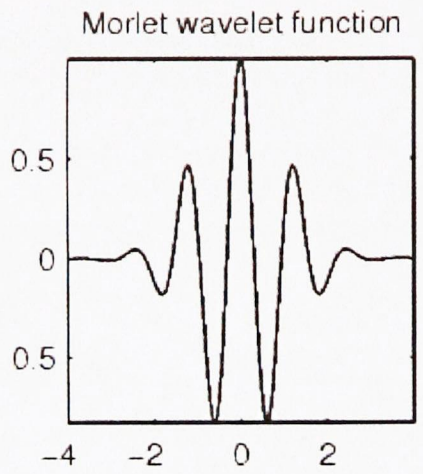


Figure 6.14 The Morlet continuous wavelet function.

The central frequency for the Morlet wavelet is 0.8125 Hz which is needed to scale the wavelet. Hence, using Equation 6.6 for a 1 hour sampling period, a scale of unity (a=1) represents $F_a = 2.257 \times 10^{-4}$ Hz - i.e. a sampling period of 1.23 hours. As for the DWT, the CWT had to be tuned to a scale corresponding to the results from the FFT analysis (Table 6.13) which showed the main areas of interest in the regions from 20 to 90 days. The equivalent scale to frequency for a 1 hour data sampled set using the Morlet CWT is shown in Table 6.13. The analyses were carried out at scales from 195 to 2340.

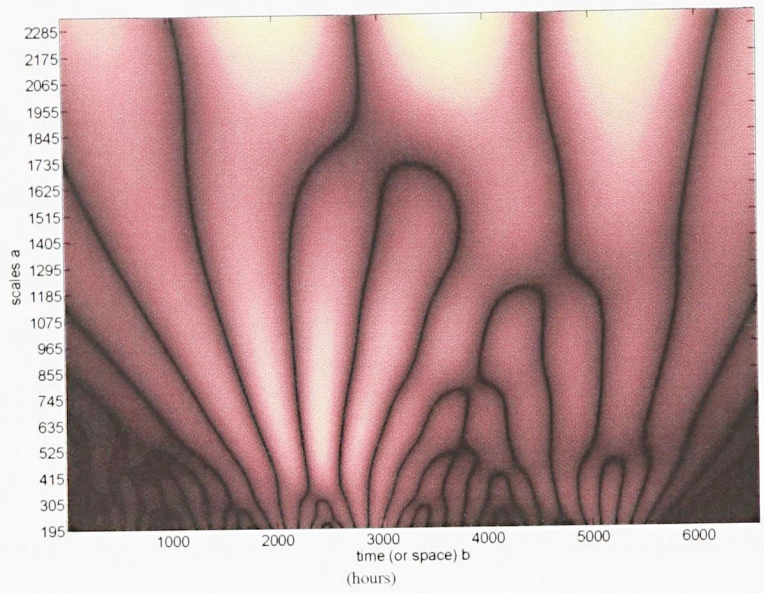
Table 6.13 Frequency to scale for Morlet wavelet at 1 hour sampling frequency.

db4 scale	level	period (days)
195	7.6	10
390	8.6	20
585	9.2	30
780	9.6	40
975	9.9	50
1170	10.2	60
1365	10.4	70
1560	10.6	80
1755	10.8	90
1950	10.9	100
2145	11.1	110
2340	11.2	120

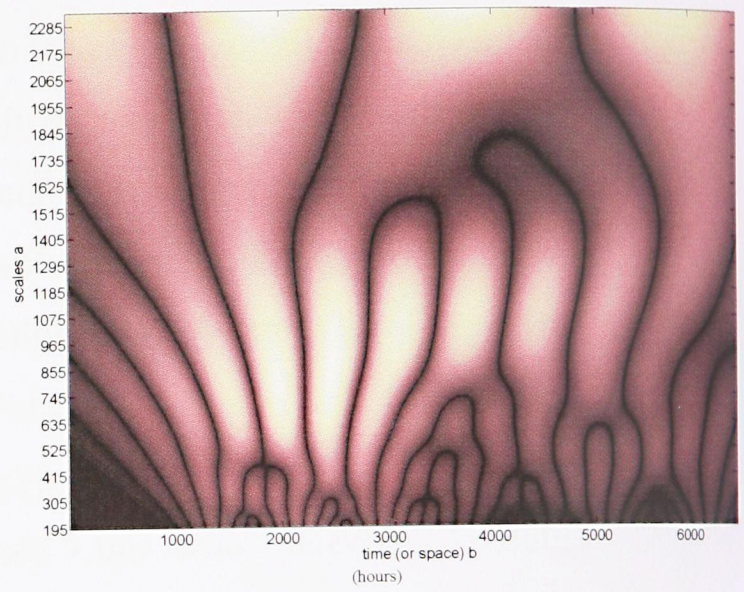
The plots for all the CWT coefficients are included in Appendix F which show the time and frequency content across the chosen scale range for each turlough water level time signal on a single plot. These slightly esoteric figures can be interpreted as follows. The x-axis is time (in hours) corresponding to the length of each turlough level data set analysed. The y-axis is the scale of the wavelet corresponding across a range of increasing period (i.e. decreasing frequency) as set out in Table 6.13. The peaks and troughs on the plot then refer to the energy associated with such frequencies at specific times across the length of the data set. For example, on Figure 6.15(b) the high peaks (shaded white) occurring from about 1500 to 3000 hours (on the x-axis) are showing that there is some pattern in the turlough level data corresponding to a scale of about 600 to 1000 (y-axis) which corresponds to a period of between approximately 30 to 60 days. At first appearance the plots comparing the same yearly data between all turloughs look very similar. For the 2006/07 analysis, Coole and Caherglassaun show similar results during the main filling cycle but different patterns during the main recession. Coy and Caherglassaun however, show similar patterns during the recession indicating the similar nature of their hydraulic connection to the network i.e. surge tanks above the main network which lag behind an upstream turlough. Again, for the 2006/07 data Garryland is out of kilter with the other turloughs of the 2006/07 season due to the different length of data set.

In the 2007/08 plots Coole, Garryland and Caherglassaun all show a high energy content at the 700 to 800 scale region which equates to a period of 30 to 40 days although Garryland exhibits slightly lower intensities reflecting its off-line connection from the main system. As shown in Figures 6.15(a and b) Blackrock and Coole have significantly different patterns, indicative of the different positions and different hydraulic connections to the main network. The 2008/09 plots however, show very similar traces between all turloughs, even Blackrock and Coole (Figure 6.15(c and d). As was found by the DWT analysis, the main difference between the two hydrological years is also clearly picked up at high energy areas corresponding to a period of 30 days.

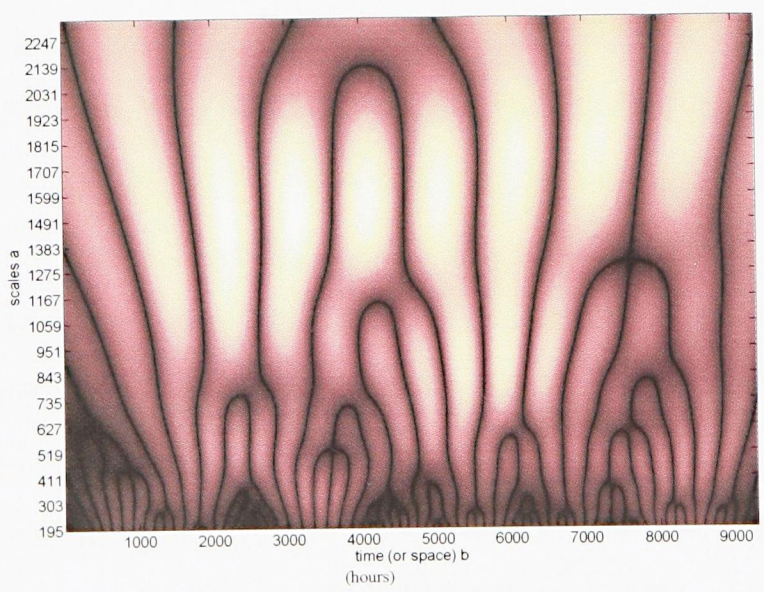
Hence, the CWT technique has picked up some of the detail from the previous time series techniques but would be more difficult to interpret and draw conclusions from, without having carried out the FFT and DWT analyses previously.



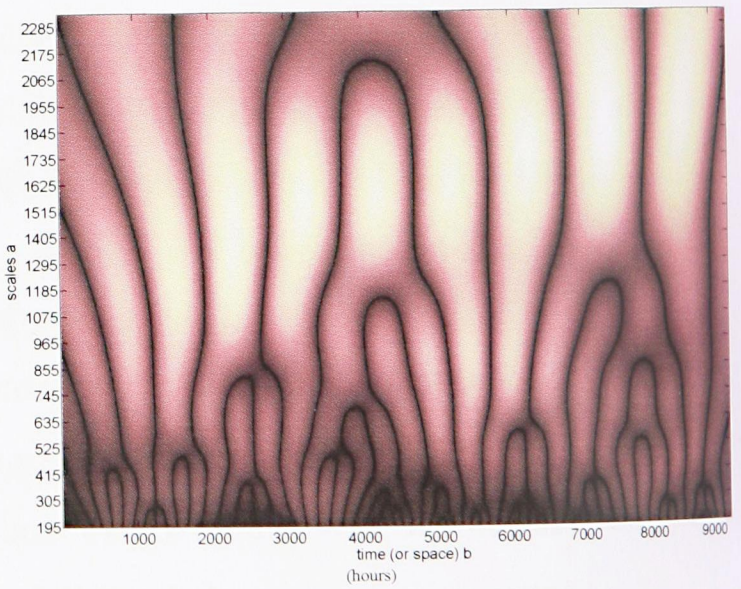
(a) Blackrock 07/08



(b) Coole 07/08



(c) Blackrock 08/09



(d) Coole 08/09

Figure 6.15 CWT (Morlet) coefficients for **(a)** Blackrock 0708 **(b)** Coole 0708 **(c)** Blackrock 0809 and **(d)** Coole 0809.

7 PIPE NETWORK MODELLING

7.1 Introduction

The inputs to the model are river flows and precipitation whilst the model will be calibrated against the five turlough water levels. Unlike most models that have been applied to karst systems, there are no discharge data available for the Gort lowlands system as it has not been possible to measure the spring discharge at Kilchreest since it is just below sea level. Therefore it is difficult to employ cross correlation type analyses etc. between the input and output of the system. The inlet and outlet flows for individual turloughs can be calculated (as done in Chapter 5) but this still does not allow the by-pass flow underneath the turloughs to be determined. So, some basic principles of modelling a pipe and tank network have been investigated which have then been assimilated to help to build the main karst network model of the Gort lowlands in Chapter 9.

7.2 Hydraulic Principles of the Pipe-Network Model

The hydraulic model was built using *Infoworks* CS version 8.5 (Wallingford Software) which is a system for the management of urban drainage networks. *Infoworks* CS incorporates the *Hydroworks* modelling engine for simulating the hydraulic behaviour of an urban drainage network under different conditions of rainfall, land use, population, inflows etc. Such a package is able to model both open channel and pressurised flow hydraulic conditions on the network of pipes and nodes (manholes, ponds etc) which is why it has been employed for the modelling of such a karst network.

A conduit is represented as a link in the network of defined length between two nodes. The boundary condition between the link and a node is either of the outfall or headloss type. The gradient of a conduit is defined by invert levels at each end of the link; this does not preclude discontinuities in level at nodes or negative gradients.

A variety of pre-defined cross-sectional shapes may be selected for both closed pipes and open channels. Circular pipes are defined by one dimension - the diameter - and all others by the height and width; in the case of open channels the height will be to the top of the

channel lining. Non-standard cross-sectional shapes (such as elliptical cross-sections) may be modeled by defining a non-dimensional height/width relationship, as dealt with later.

Two different values of hydraulic roughness may be assigned; one for the bottom third of the conduit and one for the remainder. A permanent depth of sediment may be defined in the invert of the conduit; no erosion or deposition is considered. This is useful for modeling sewer systems when the exact size of the physical infrastructure is known prior to modeling – however, this is not a relevant parameter for this research as the dimensions of the physical infrastructure is unknown and therefore such a parameter is unnecessary from a calibration point of view.

The governing model equations are the Saint-Venant equations which are a pair of conservation equations of mass and momentum:

$$\frac{\delta A}{\delta t} + \frac{\delta Q}{\delta x} = 0 \qquad \text{Eqn. 7.1}$$

$$\frac{\delta Q}{\delta t}\frac{\delta}{\delta x}\left(\frac{Q^2}{A}\right) + gA\left(\cos\theta\frac{\delta y}{\delta x} - S_o + \frac{Q|Q|}{K^2}\right) = 0 \qquad \text{Eqn. 7.2}$$

where, Q = discharge (m^3/s) A = cross-sectional area (m^2)
S_o = bed slope θ = angle of bed to horizontal (°)
K = conveyance

The conveyance function is based either on the Colebrook-White or Manning expressions - the Colebrook-White equation was used for modelling in this research.

Pressurised pipe flow can be modeled in one of two ways.

- Solving the Saint-Venant equations but introducing the elegant concept of a *Preissmann slot* into the pipe soffit. This is a conceptual vertical and narrow slot (Figure 7.1) providing a free surface condition for the flow when the water level is above the top of a closed conduit. A smooth transition between the free surface and surcharged conditions is thus enabled.

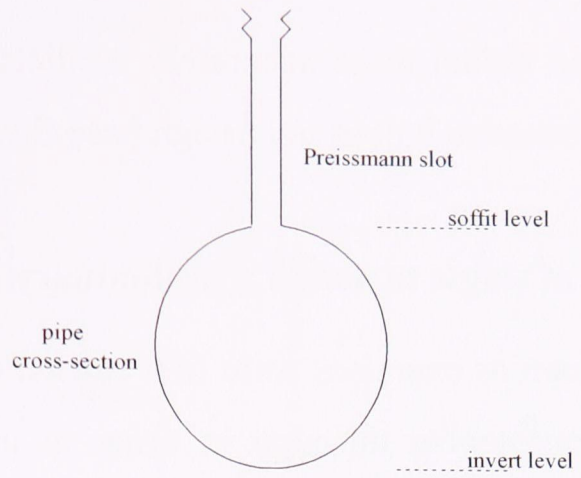


Figure 7.1 The *Preissmann slot* concept for modeling pressurised flows.

The effect of placing the Preissmann slot directly onto the pipe soffit may be an abrupt change in surface width derivative and wave celerity in the transition to pressurised conditions. A transition region is included within the model defined by a monotonic cubic between the true pipe geometry and the width of the Preissmann slot. The slot width itself is defined such that the wave celerity in the slot is ten times that at half the conduit height. This allows accurate modelling of pressurised flow and results in a slot width that is 2% of the conduit width.

The model equations for pressurised flow differ in that the free surface width is replaced conceptually by the term:

$$B = \frac{gA_f}{C_P^2} \qquad \text{Eqn. 7.3}$$

where, B = free surface width (m) A_f = pipe full area (m^2)

C_p = pipe full velocity of pressure wave (m/s)

- Alternatively a pressurised pipe model can be used on selected pipelines. The model equations for pressurised pipe flow are:

$$\frac{\delta Q}{\delta x} = 0 \qquad \text{Eqn. 7.4}$$

$$\frac{\delta Q}{\delta t} + gA\left(\frac{\delta h}{\delta x} - S_o + \frac{Q|Q|}{K^2}\right) = 0 \qquad \text{Eqn. 7.5}$$

where, A = pipe full area (m^2) K = pipe full conveyance

The pressurised pipe model more accurately predicts velocities and storage than the full (St. Venant) model because it does not assign base flow or a Preissman slot to a pipe.

7.3 Generic model of single turlough – preliminary investigations

Some modeling dynamics exercises were first carried out on a simplified generic model of a single pond to represent a turlough in order to investigate the sensitivity of such a hydraulic system to different parameters using a stepped inflow profile and tidal outflow level profile. The parameters investigated were as follows:

- Effect of pond volume (dimensions)
- Different flow rates (step input at different increasing flow levels)
- Effect of downstream pipe diameter
- Diameter of constriction (throttle) downstream of pond
- Effect of tidal cycle back up the system
- Effect of roughness coefficient (k_s) for pipes on dynamics
- Difference between two methods of modeling pressurised flows

A single turlough was modeled as a pond defined by depth, surface area and perimeters (discussed in more detail in Section 7.4) to investigate the sensitivity of the system to parameters such as pipe size and roughness coefficients and the effect of a partially submerged tidal outfall. The dimensions of the network are shown on Figure 7.2. The stepped inflow was input into the network at node 1 whilst the outfall at node 6 was a tidal response between -1.56 and 2.02 mAOD to simulate the sea (Figure 7.3).

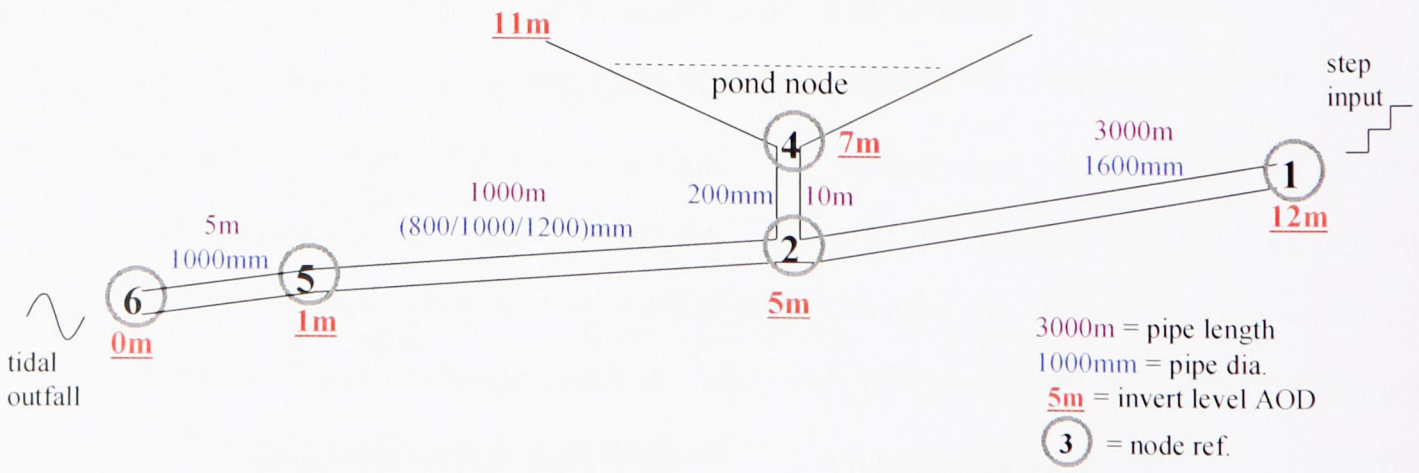


Figure 7.2 Schematic cross-section of single turlough Network Model 1.

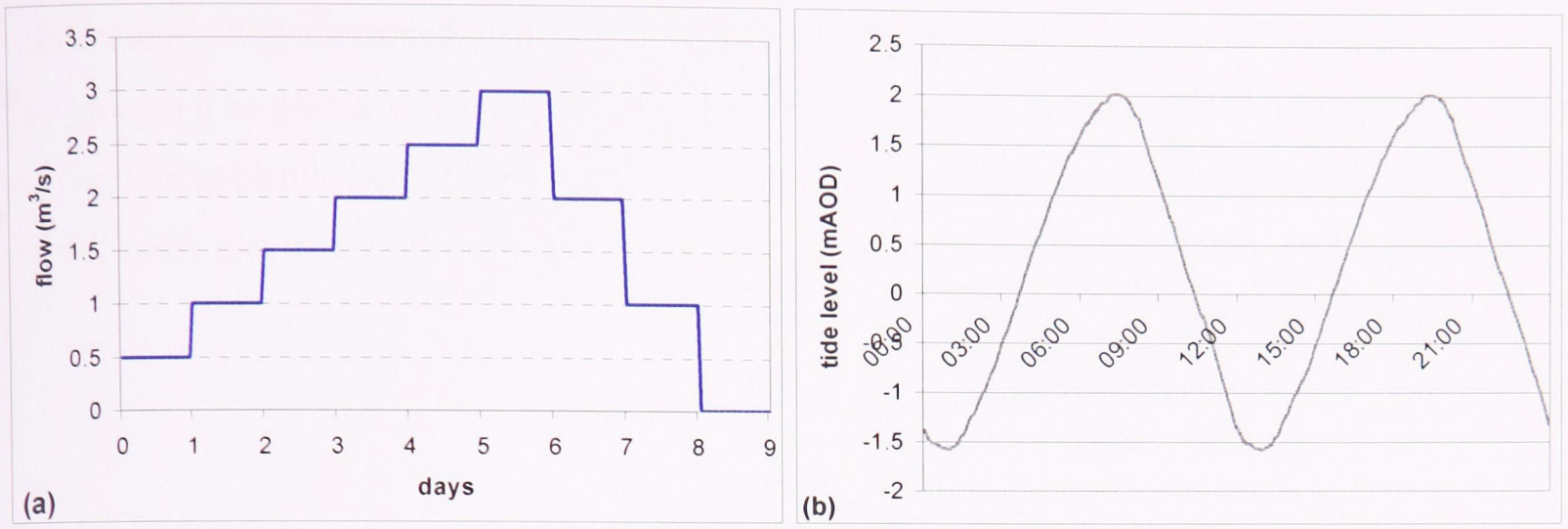


Figure 7.3 (a) stepped input at node 1 and **(b)** tidal outfall at node 6.

7.3.1 Change in pond volume

The effect of changing the dimensions of the pond was first investigated by comparing three different sizes (small, medium and large) as shown in cross-section in Figure 7.4.

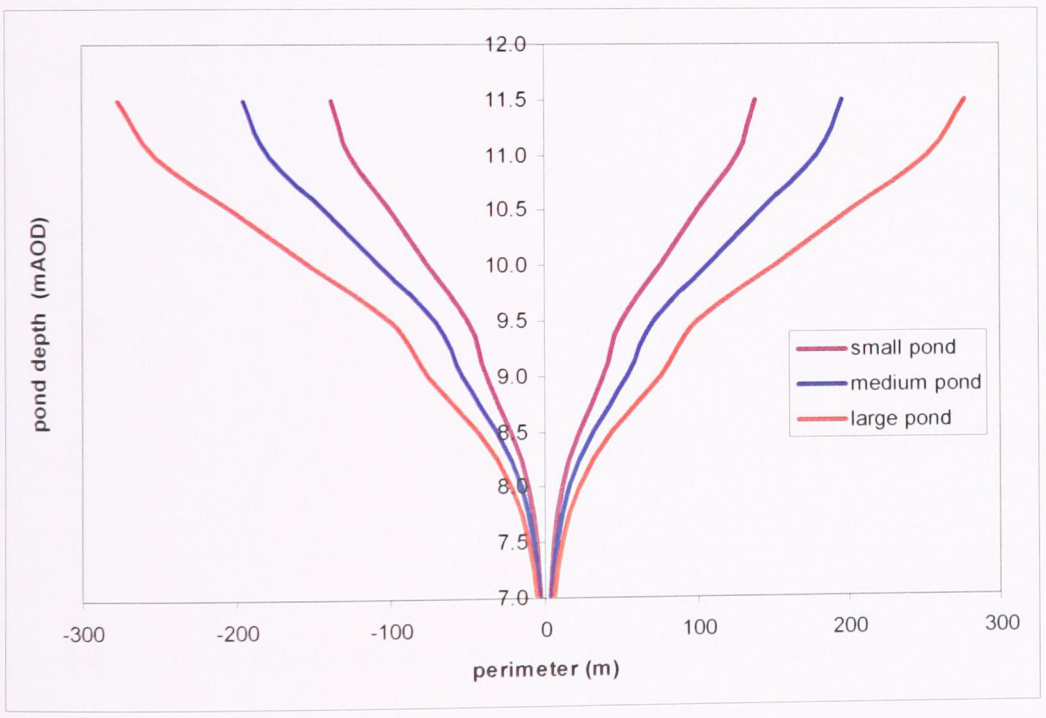
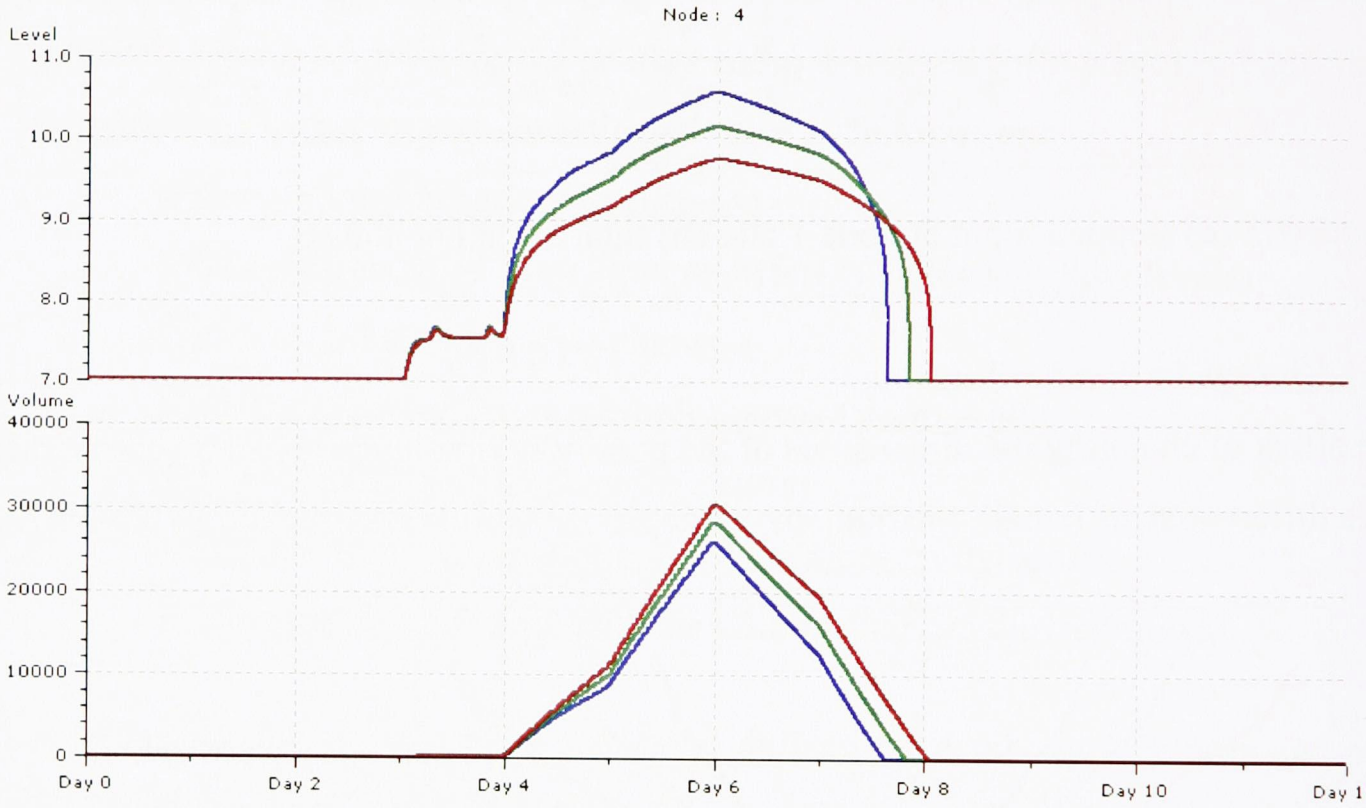


Figure 7.4 Cross-sectional profiles of three different pond sizes.

The response in the level and flooding of the pond behaved as expected as shown in Figure 7.5. The smaller pond filled to a higher level during the high inflow periods to the system compared to the larger ponds. In terms of volume, however, this represented smaller amounts of stored water compared to the larger ponds. Once the flows through the network had started to subside the smaller pond drained more quickly, initially due to the higher

head and then due to the fact that for the same head level, the same drop in level equated to a smaller flow out of the turlough. This therefore also indicates that the short 200 mm diameter (Ø) pipe linking the main base conduit to the pond was acting as a throttle on the outflows from the pond after the flows along the main conduit had subsided and had spare capacity - otherwise all three ponds would have drained at the same rate from the same head conditions.

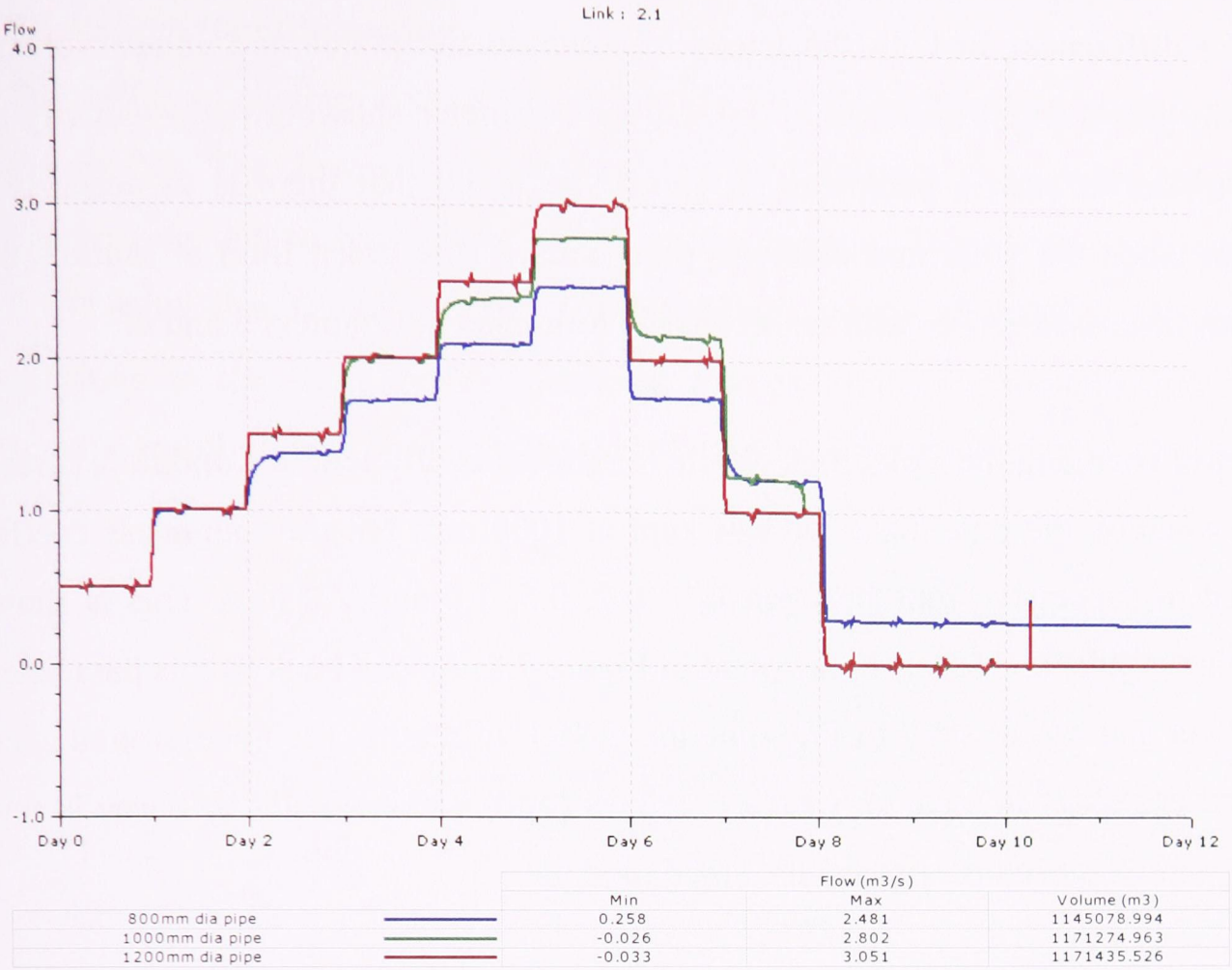


	Level (m AD)		Volume	
	Min	Max	Min	Max
small pond	7.020	10.566	0.520	25948.824
medium pond	7.020	10.137	1.041	28283.715
large pond	7.020	9.745	2.081	30363.445

Figure 7.5 Effect of changing pond size (level and volume).

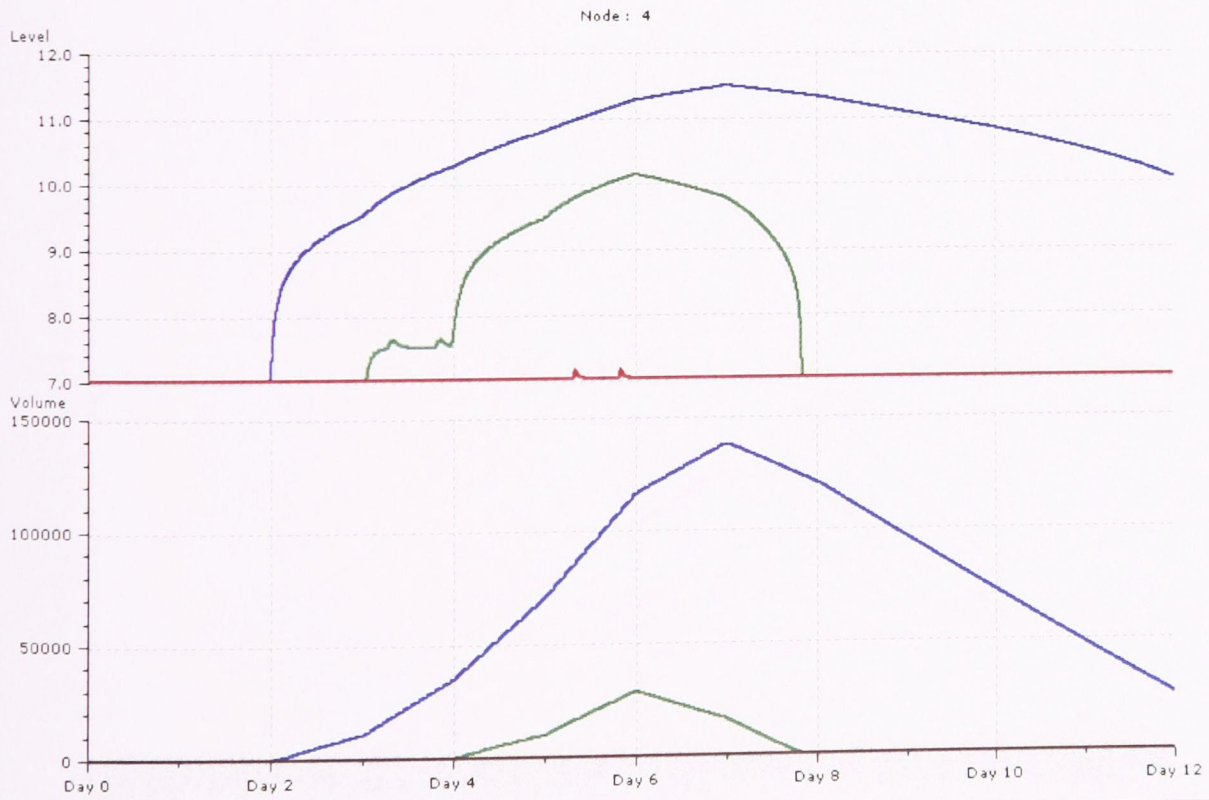
7.3.2 Downstream pipe diameter

The effect of changing the downstream pipe diameter (between node 2 to 5) from 800 to 1000 and 1200 mm Ø was investigated and is shown in terms of the flows through the pipe (Figure 7.6) and also the water levels in the pond (Figure 7.7). As shown, the 1200 mm diameter pipe can take the full flow and shows evidence of tidal influence upstream just below the pond entrance. The smaller diameter pipes show more limited flows (above 2.5 m^3/s for the 1000 mm Ø pipe and above 1.3 m^3/s for the 1000 mm Ø pipe) which cause the difference to be discharged up into the pond.



		Flow (m3/s)		
		Min	Max	Volume (m3)
800mm dia pipe		0.258	2.481	1145078.994
1000mm dia pipe		-0.026	2.802	1171274.963
1200mm dia pipe		-0.033	3.051	1171435.526

Figure 7.6 Effect of changing diameter of Conduit 2.1 (flows).

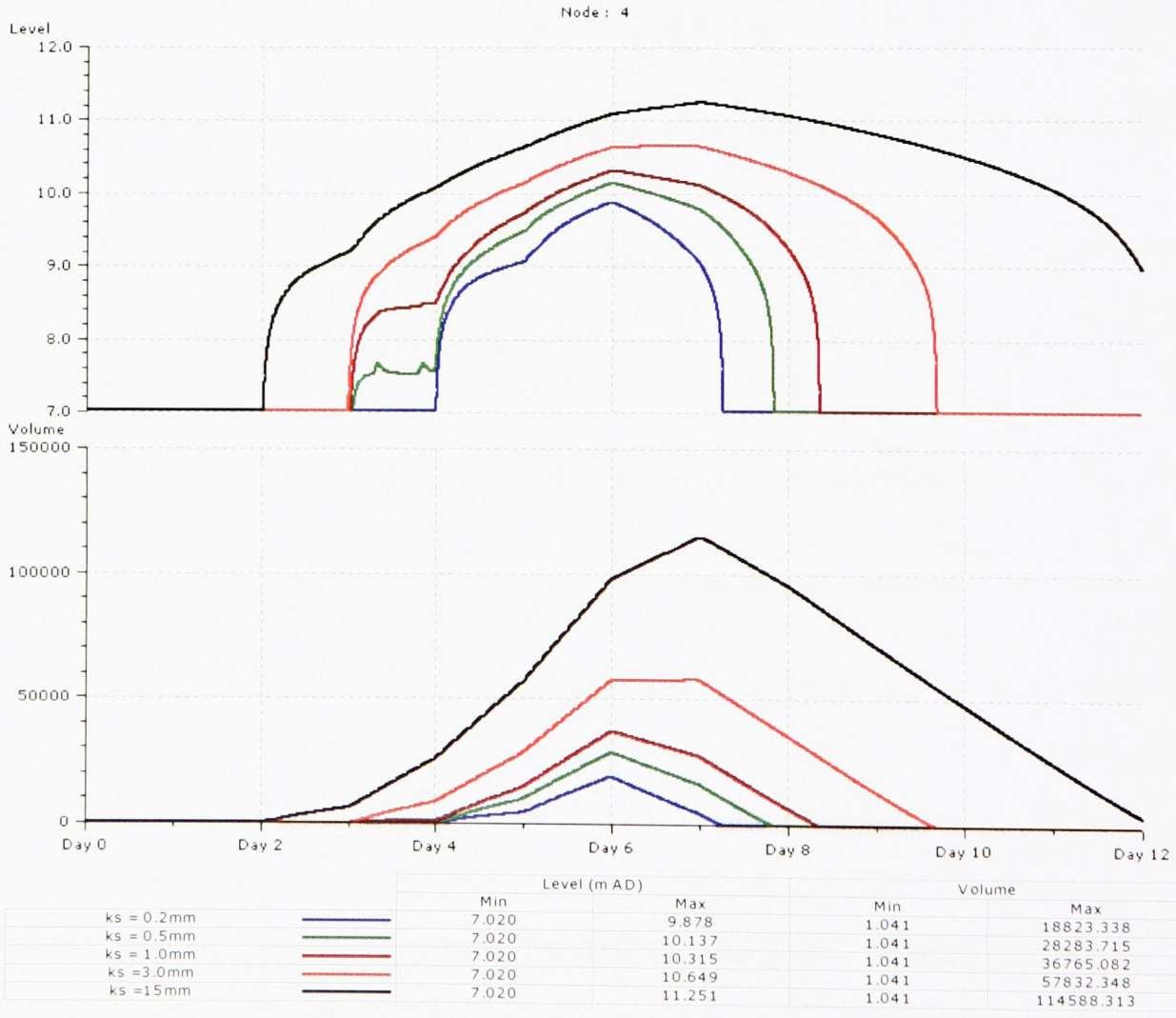


		Level (m AD)		Volume	
		Min	Max	Min	Max
800mm pipe dia		7.020	11.496	1.041	137804.766
1000mm pipe dia		7.020	10.137	1.041	28283.715
1200mm pipe dia		7.020	7.139	1.041	9.035

Figure 7.7 Pond (turlough) effect of changing downstream conduit 2.1 diameter.

Significant differences in both the levels of water in the ponds and stored volume are obtained by just a small decrease in downstream diameter showing the sensitivity of the network model to such a parameter. It should be noted that there is evidence of tidal fluctuation when the 1000 mm diameter pipe is used (the green line) at shallow depths (~0.5m), as discussed earlier with respect to the turloughs in Chapters 5 and 6.

The effect of changing the Colebrook-White roughness coefficient in Conduit 2.1 was then analysed whereby the pipe diameter was kept at 1000 mm but the roughness coefficient was varied in successive runs between k_s = 0.2, 0.5, 1.0 and 2.0 mm. This is shown in terms of the volume and levels in the pond in Figure 7.8. As can be seen this parameter has a large effect and can be used to fine tune the model. In reality, the underground conduits in the karst are likely to have very high k_s values (>60) which should be borne in mind if the objective is to develop a physically-based model.



	Level (m AD)		Volume	
	Min	Max	Min	Max
ks = 0.2mm	7.020	9.878	1.041	18823.338
ks = 0.5mm	7.020	10.137	1.041	28283.715
ks = 1.0mm	7.020	10.315	1.041	36765.082
ks =3.0mm	7.020	10.649	1.041	57832.348
ks =15mm	7.020	11.251	1.041	114588.313

Figure 7.8 Effect of changing downstream conduit roughness coefficient.

7.3.3 Short throttle section

The effect of adding a short 20 m throttle was investigated as shown schematically in Figure 7.9. The downstream pipe was set at 1200 mm Ø in order not to provide any constriction due to backwater effects on the throttle. The results in pond levels (Figure 7.10) show that flows into and corresponding storage of water in the pond are highly sensitive to the short throttle diameter. For example, a three-fold difference in stored volume resulted from changing the throttle from a 400 mm to 500mm Ø pipe.

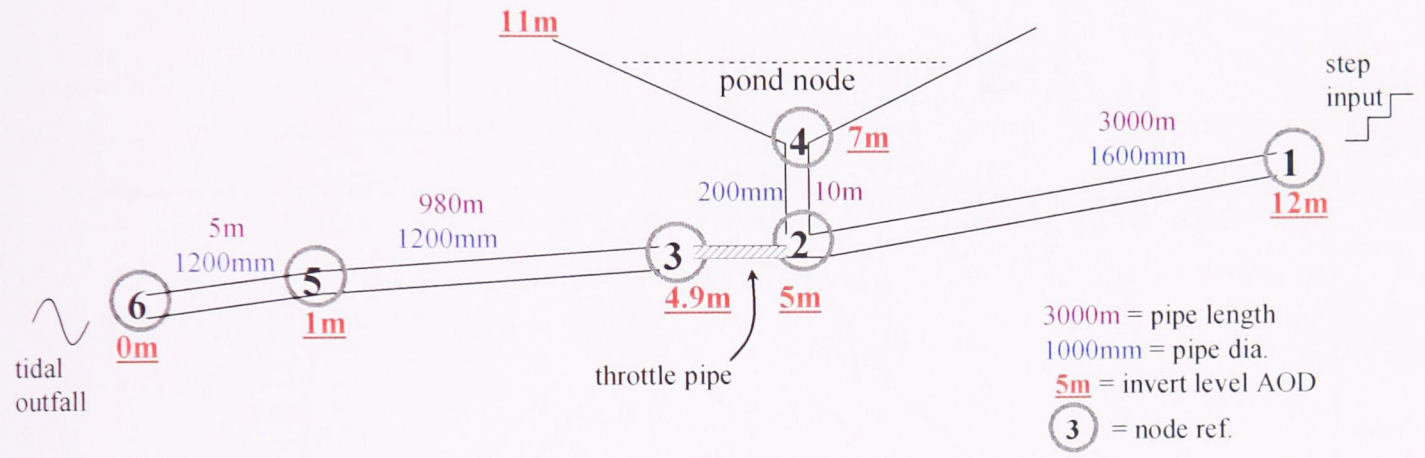
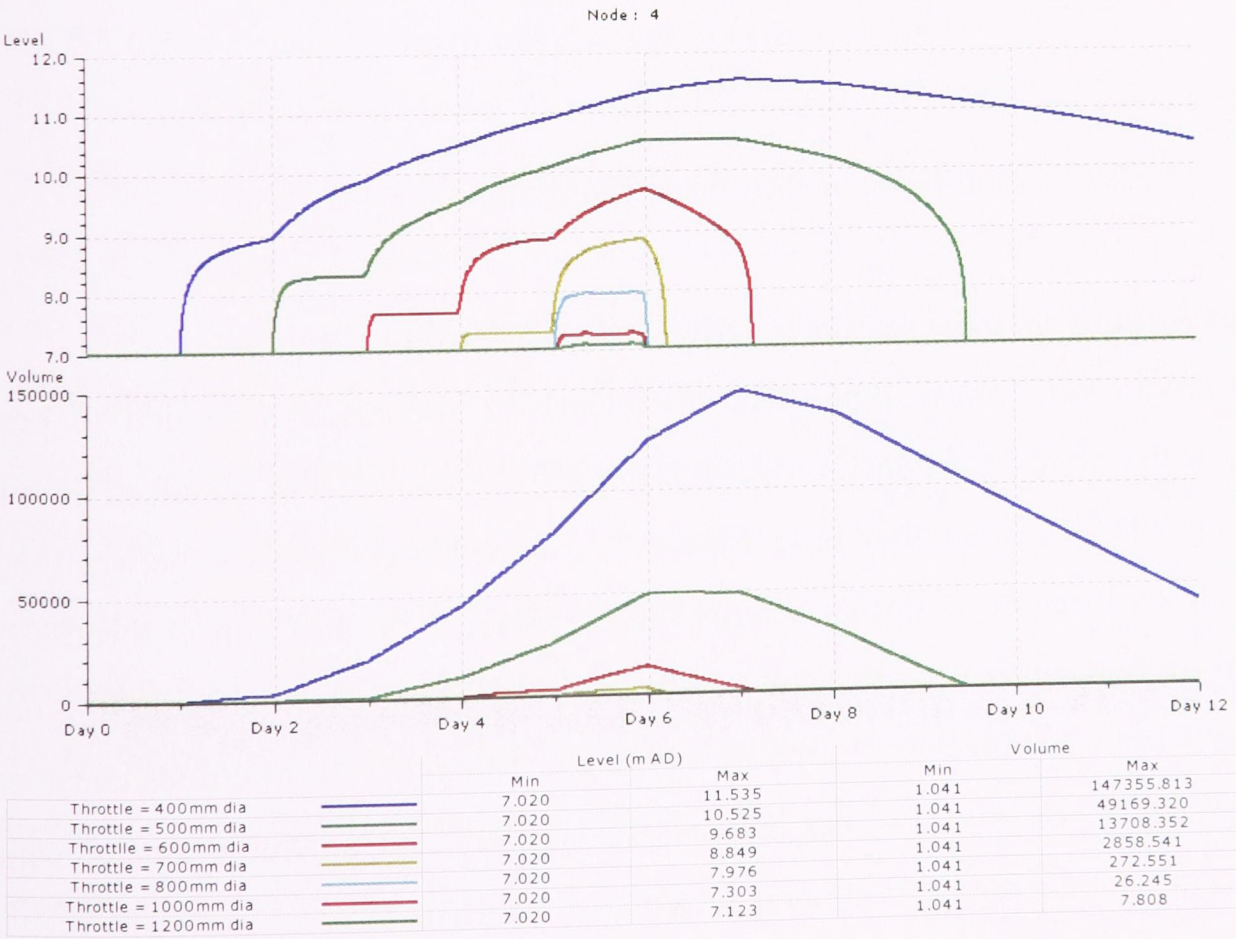


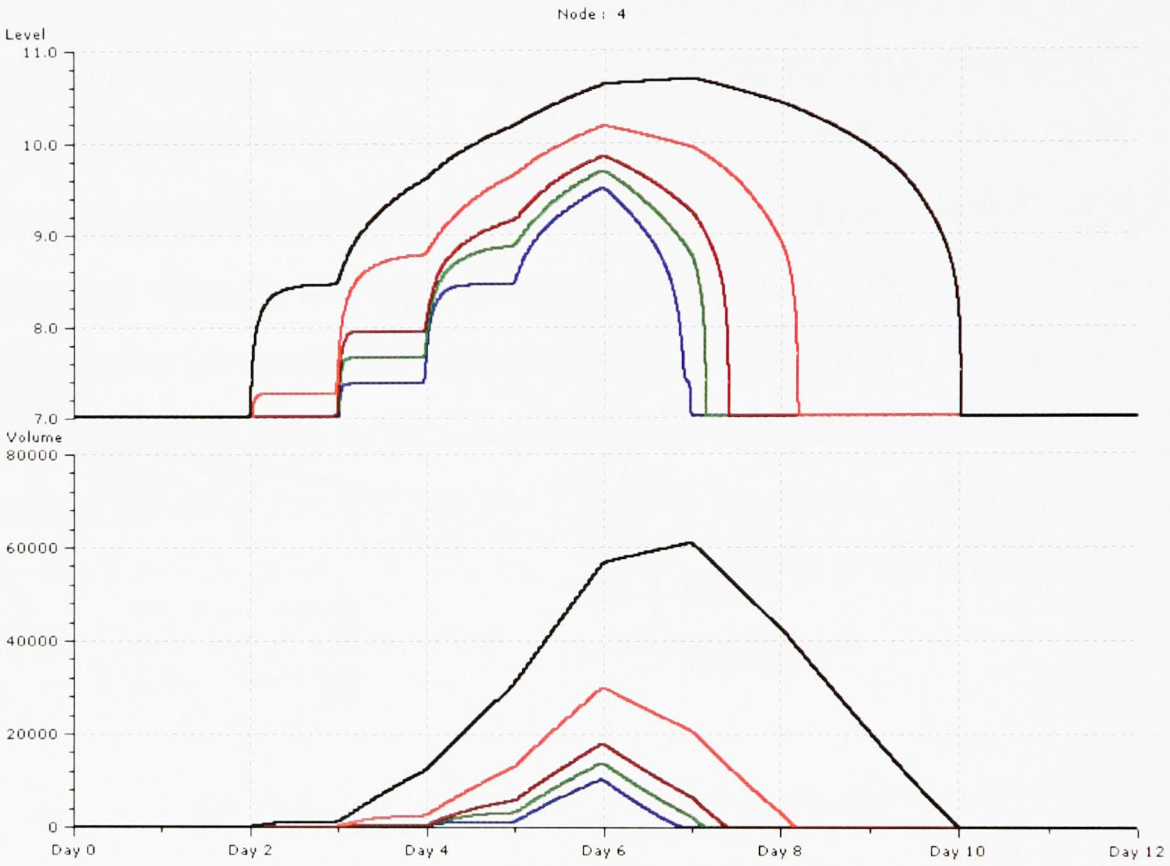
Figure 7.9 Schematic cross-section of single turlough Network Model 2.



	Level (m AD)		Volume	
	Min	Max	Min	Max
Throttle = 400mm dia	7.020	11.535	1.041	147355.813
Throttle = 500mm dia	7.020	10.525	1.041	49169.320
Throttle = 600mm dia	7.020	9.683	1.041	13708.352
Throttle = 700mm dia	7.020	8.849	1.041	2858.541
Throttle = 800mm dia	7.020	7.976	1.041	272.551
Throttle = 1000mm dia	7.020	7.303	1.041	26.245
Throttle = 1200mm dia	7.020	7.123	1.041	7.808

Figure 7.10 Effect of changing downstream throttle diameter (level and volume).

Equally, the effect of changing roughness coefficient of throttle was investigated using the 20 m throttle fixed at 600 mm Ø which shows (Figure 7.11) a more moderate effect due to short length of pipe but again can be used as a parameter to fine tune the system.

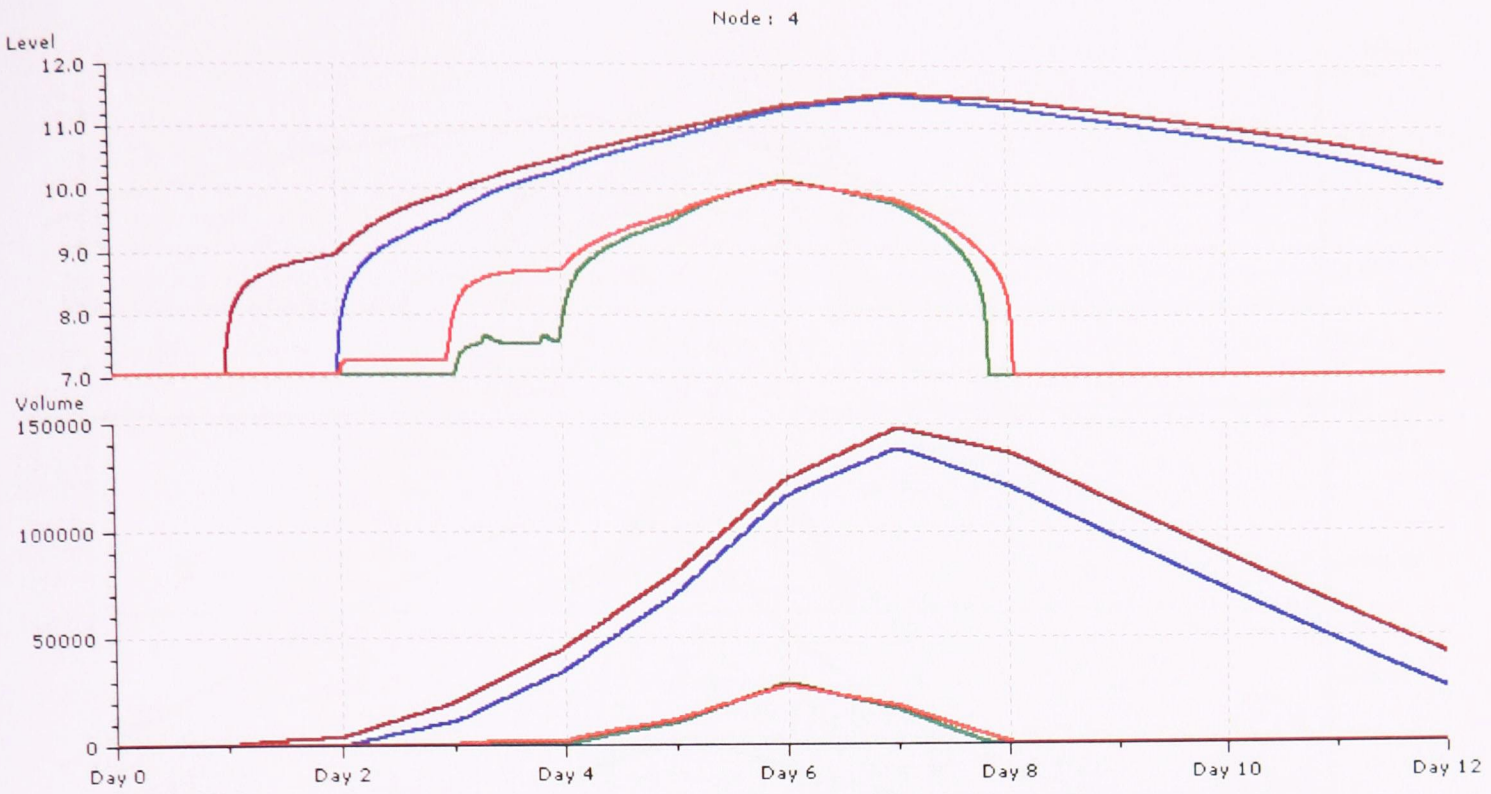


	Level (m AD)		Volume	
	Min	Max	Min	Max
ks=0.2mm	7.020	9.498	1.041	10182.239
ks=0.5mm	7.020	9.683	1.041	13708.352
ks=1.0mm	7.020	9.842	1.041	17780.369
ks=3.0mm	7.020	10.172	1.041	29792.150
ks=15mm	7.020	10.691	1.041	60940.781

Figure 7.11 Effect of changing k_s of throttle of fixed diameter = 600mm.

7.3.4 Comparison of throttle versus smaller downstream pipe

The above model runs show that there are clearly 2 scenarios in which to promote surcharging of the pond (and hence model a turlough) – either a short length to throttle the flow or a longer length of smaller pipe. Figure 7.12 shows a comparison between the two different methods to achieve similar results on the pond. The 400 mm Ø throttle (20 m long) is more or less equivalent to 1 km of 800 mm Ø pipe whilst a 550 mm Ø throttle is equivalent to 1 km of 1000 mm Ø pipe downstream. The short throttle does cause earlier onset of flooding (even though peak values are similar) and slower drainage which is interesting from a model calibration perspective.

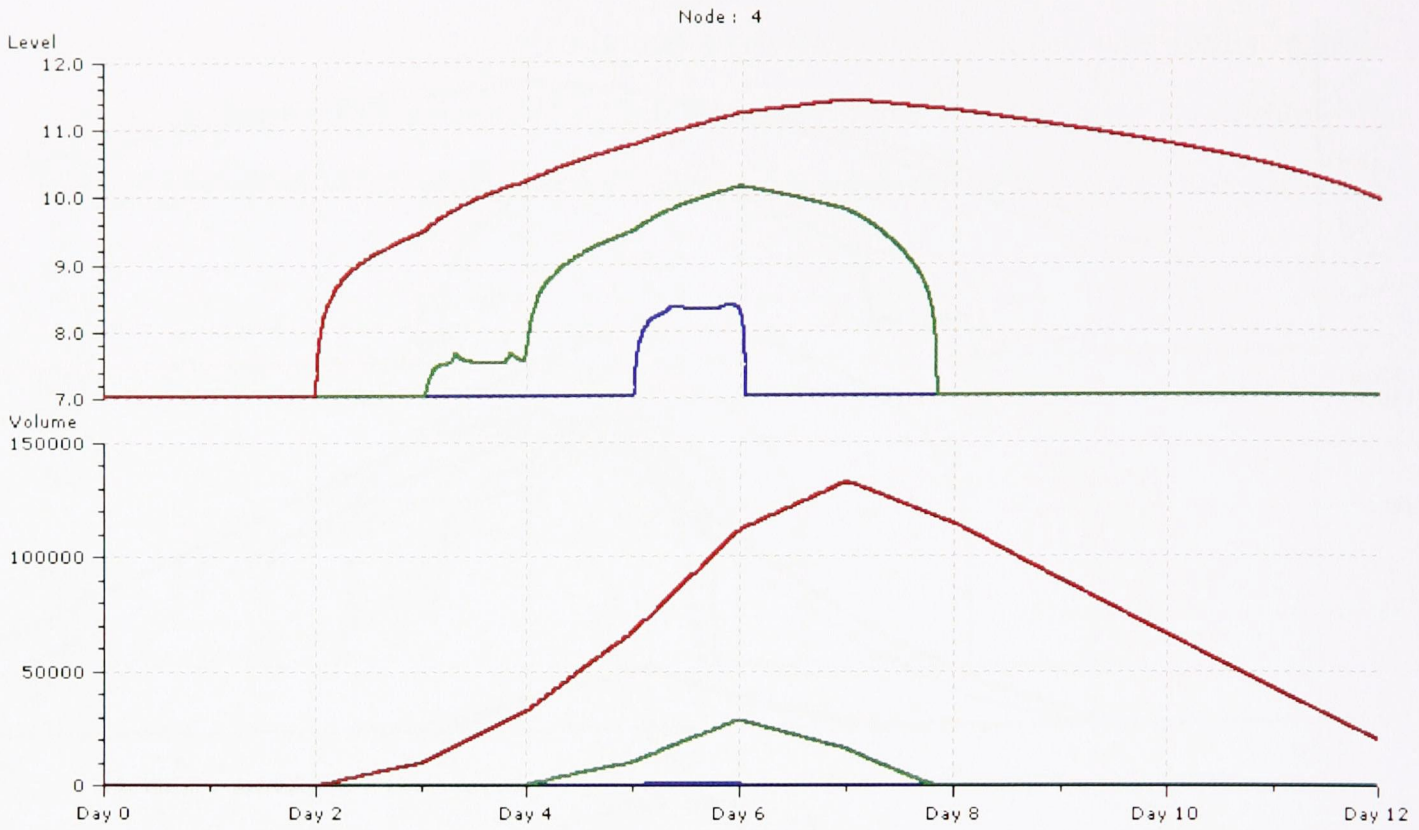


	Level (m AD)		Volume	
	Min	Max	Min	Max
800mm dia pipe ks = 0.5	7.020	11.496	1.041	137804.766
1000mm pipe ks = 0.5	7.020	10.137	1.041	28283.715
400mm dia throttle ks=0.5	7.020	11.535	1.041	147355.813
550mm dia throttle ks=0.5	7.020	10.111	1.041	27201.352

Figure 7.12 Pond levels comparing d/s pipe Ø to changing throttle (k_s = 0.5 in all cases).

7.3.5 Comparison of length of pipe versus tidal effect

The turlough Network Model 1 (Figure 7.2) was used with the downstream conduit set to 1000 mm Ø (k_s = 0.5 in all cases) but the length to the sea was varied from 500, 1000 and 3000 m. This shows (Figure 7.13) the backing up effect of the longer pipe which swamps any tidal effects. The downstream pipe was then sized such that it can take the flow (i.e. to 1600 mm Ø), to study the effect of the tide on different distances. This showed that there was no effect upstream with that pipe length with a head level at 5 m. However, when the head was reduced to 3 and 4 m it shows that it is only when the level is down around the high tide mark (i.e. at 2 m AOD invert) that any sort of tidal impact is felt 1000 m upstream on the pipe and then at high flows. Hence, from the point of view of the low lying turloughs it shows that system obviously needs to be surcharged for any tidal influence to be felt, but there is a critical depth range within which the fluctuations will be evident.



	Level (m AD)		Volume	
	Min	Max	Min	Max
500m long pipe	7.020	8.393	1.041	894.232
1000m long pipe	7.020	10.137	1.041	28283.715
3000m long pipe	7.020	11.406	1.041	132056.063

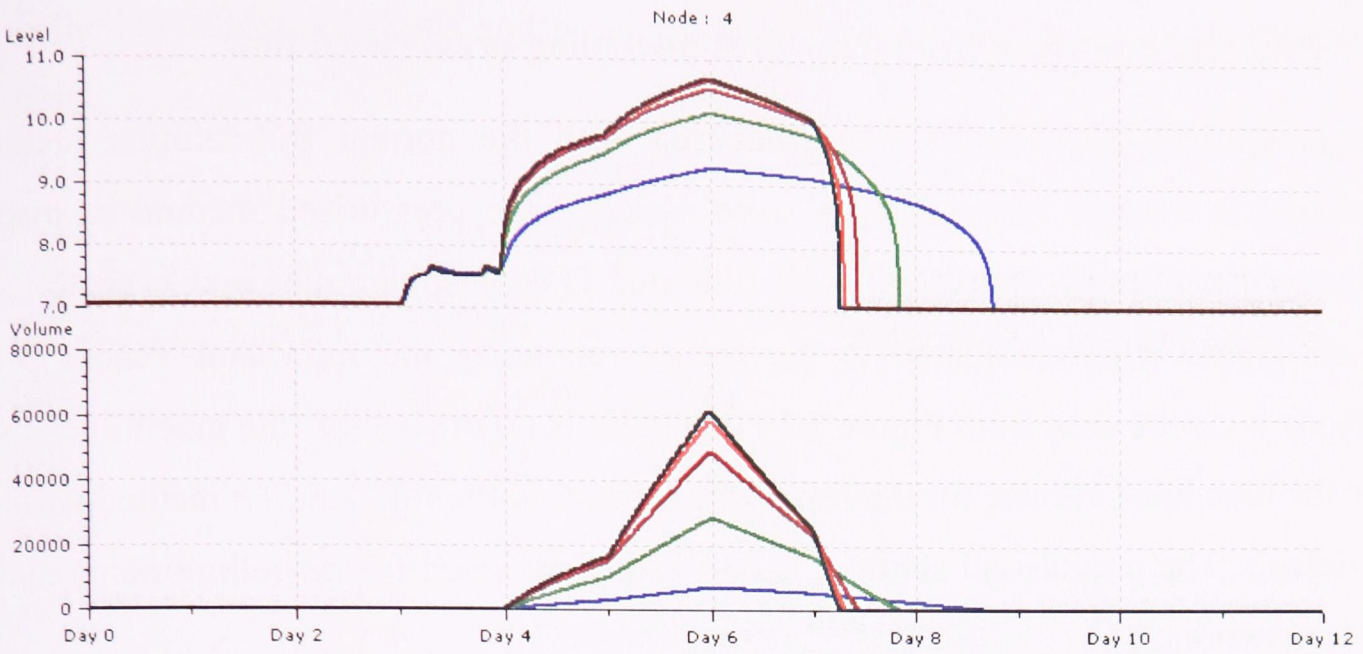
Figure 7.13 Pond levels different length of d/s pipe diameter to the sea.

7.3.6 Comparison of different entry pipe diameters into pond

The effect of the entry pipe into the pond was also evaluated as shown in Figure 7.14. The turlough Network Model 1 was used with downstream pipes at 100 mm Ø and all roughness coefficient set to k_s = 0.5 mm. Interestingly, the diameter of the entry pipe seems to have most effect on the draining of the turlough, smaller diameters delaying the draining – which makes it a useful control parameter. Once the diameter has reached 300 mm Ø or more then fairly similar level profiles in the pond are attained.

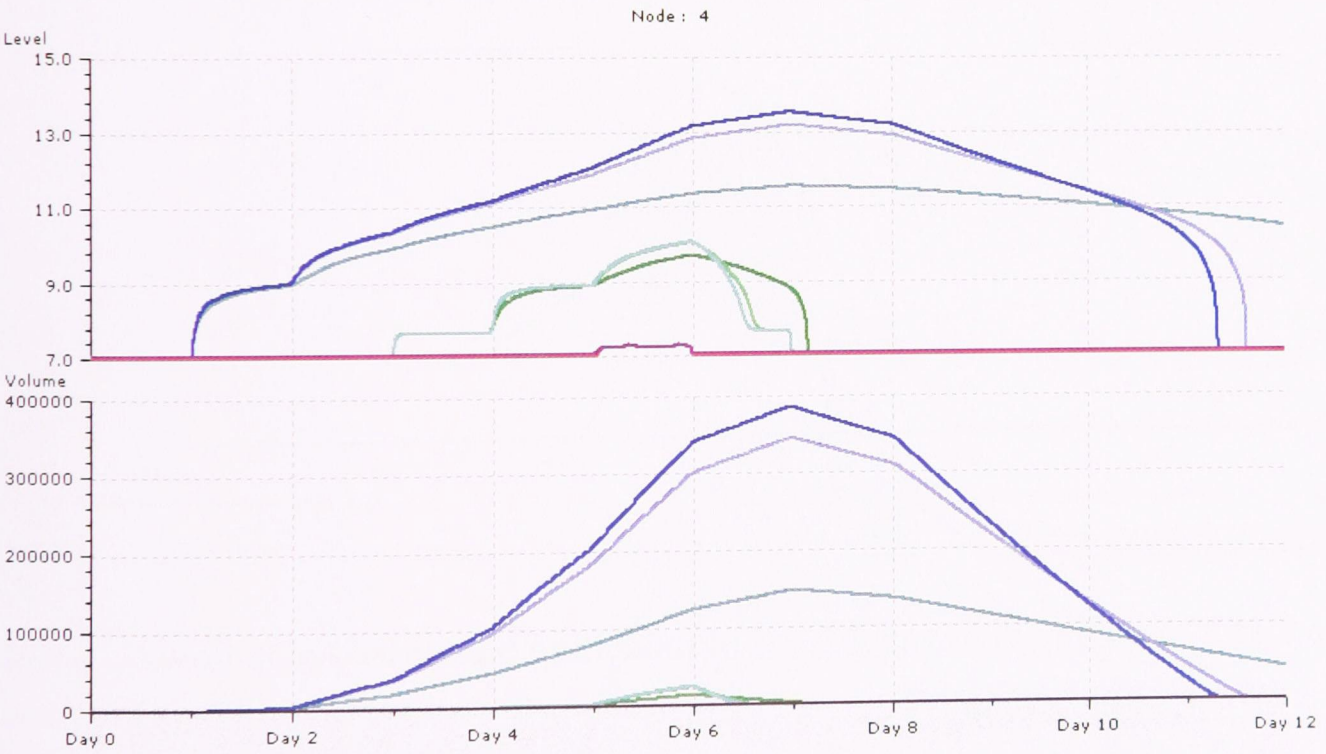
7.3.7 Balance between throttle pipe and pond entry pipe diameters

The influence of throttle pipe diameter to pond entry pipe diameter has been investigated which shows (Figure 7.15) the overriding influence of the throttle pipe diameter on the pond level. The curves for 400 mm Ø throttle are all fairly similar, as are the 600 mm Ø throttle, as are the 1000 mm Ø throttle demonstrating only small effects due to inlet pipe diameter. Note, the inlet pipe length is only 10 m long compared to 20 m long throttle.



	Level (m AD)		Volume	
	Min	Max	Min	Max
100mm dia inlet	7.020	9.258	1.041	6795.785
200mm dia inlet	7.020	10.137	1.041	28283.715
300mm dia inlet	7.030	10.517	1.592	48676.504
400mm dia inlet	7.040	10.655	2.164	58265.285
500mm dia inlet	7.050	10.699	2.758	61590.117

Figure 7.14 Effect of comparing different inlet diameter pipes (pond level and volume).

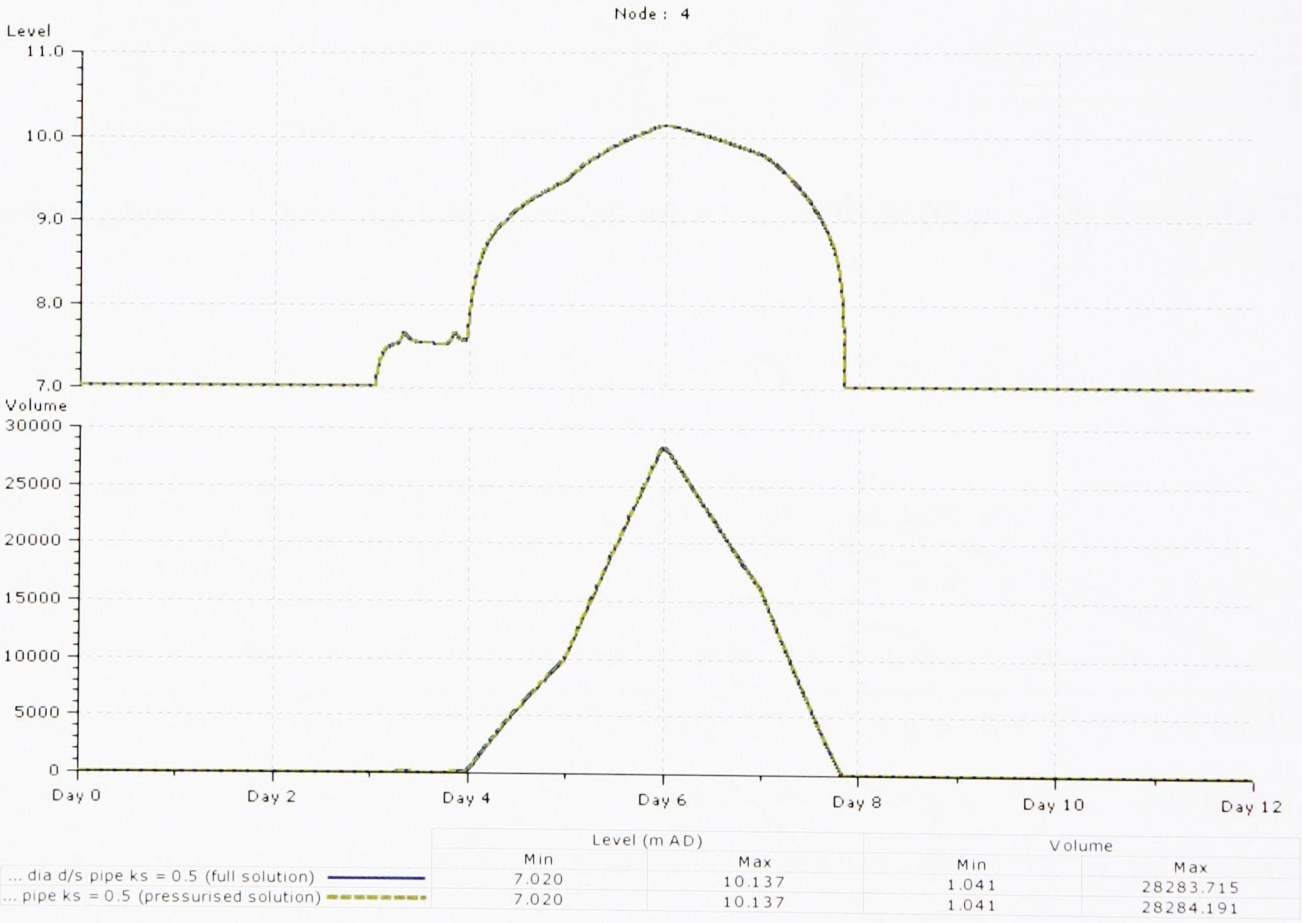


	Level (m AD)		Volume	
	Min	Max	Min	Max
400mm dia throttle, 200mm dia inlet	7.020	11.535	1.041	147355.813
400mm dia throttle, 400mm dia inlet	7.040	13.179	2.164	344652.219
400mm dia throttle, 600mm dia inlet	7.060	13.517	3.374	385123.875
600mm dia throttle, 200mm dia inlet	7.020	9.683	1.041	13708.352
600mm dia throttle, 400mm dia inlet	7.040	10.027	2.164	23875.846
600mm dia throttle, 600mm dia inlet	7.060	10.058	3.374	25055.918
...00mm dia throttle, 200mm dia inlet	7.020	7.303	1.041	26.245
...00mm dia throttle, 400mm dia inlet	7.040	7.304	2.164	26.258
...00mm dia throttle, 600mm dia inlet	7.060	7.304	3.374	26.344

Figure 7.15 Different throttle pipe and pond entry pipe diameters.

7.3.8 Difference between two methods of modelling pressurised flow

The pressurised pipe model was compared with the normal full-solution method as discussed in Section 7.2. All pipes were assigned the pressurised method as discussed earlier on the turlough Network 1 with 1000 mm Ø downstream pipe and k_s set to 0.5 mm for all pipes. When compared to the earlier run using the full Saint-Venant solution methods it can be seen from Figure 7.16 that there is no difference (the green line is sitting over the blue line). Hence, for the rest of the modelling the full solution method was left as the default. The pressurised solution is only really designed for modelling rising mains in sewer networks.



	Level (m AD)		Volume	
	Min	Max	Min	Max
... dia d/s pipe ks = 0.5 (full solution)	7.020	10.137	1.041	28283.715
... pipe ks = 0.5 (pressurised solution)	7.020	10.137	1.041	28284.191

Figure 7.16 Comparing the two methods of modelling pressurised pipe flow.

7.3.9 Comparing elliptical pipes to circular pipes

Finally, a comparison was made by using elliptical conduits as a *user defined shape* instead of circular cross-sections. As discussed in Section 2.2.2 the typical shapes of karstic conduits are elliptical. The turlough Network 1 with 1000 mm Ø downstream pipe and k_s set to 0.5 mm was used to compare both pipe shapes. The shape of the ellipse was as shown in Figure 7.17 was defined according to coordinate geometry Equation 7.6, where *a*

is the horizontal semi-axis and b the vertical semi-axis and the origin is the ellipse centre point.

$$\frac{x^2}{a^2} + \frac{y^2}{b^2} = 1 \qquad \text{Eqn. 7.6}$$

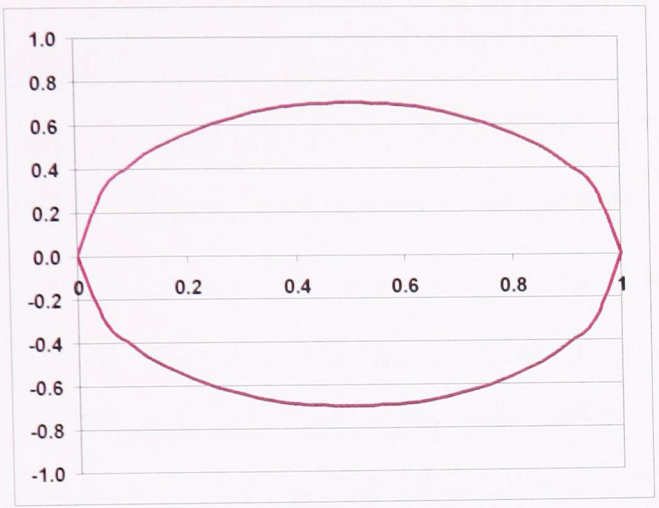


Figure 7.17 Normalised ellipse dimensions (a = 1, b = 0.7).

The results show (Figure 7.18) that to get the same flow depths and volume as a 1000 mm Ø pipe, the downstream pipe needed to be a 1220 mm width ellipse and throttle pipe 240 mm width.

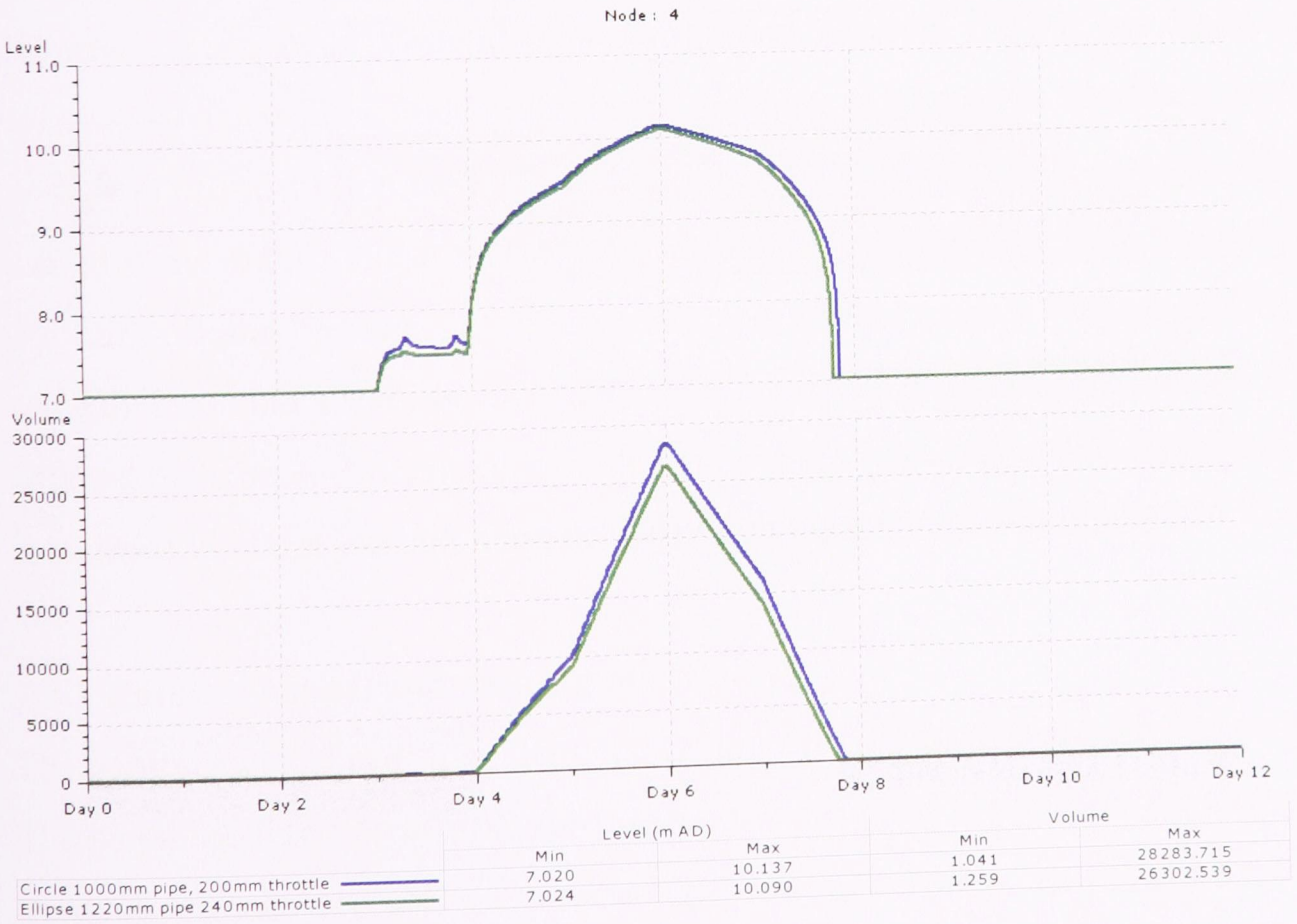


Figure 7.18 Comparison of circular pipe vs. elliptical pipe.

7.4 Representing surveyed turlough by ponds in *Infoworks*

The detailed survey of the turloughs was changed into a depth volume relationship as discussed earlier in Section 4.6. The ponds in *Infoworks* are specified in terms of a series of planes defined by depth, surface area and perimeter. Hence, the conceptual shape for each layer is actually a frustum of square based pyramid (tetrahedron). The actual geometry of each turlough has to be represented in this pond format, so it behaves in the correct manner critically in terms of depth-volume relationship. The surveying and Surfer® manipulation yields the depth and volume for the turlough. So, if each layer was represented by the pond geometry then it would conceptually look like Figure 7.19 in 3-dimensions. Hence, the volume difference between each depth layer, h, needs to be the volume enclosed by the shape defined by solid black lines. The equivalent volume to this over that depth, h is the shape of the box outlined by dashed red lines whereby the plan area is set by a plane a height of $h/\sqrt{2}$ from the base (i.e. previous depth plane) by geometry. Hence, for each enclosed volume, an equivalent depth and surface area has been defined for the turlough 3-D profile, the details of which are contained in Appendix G.

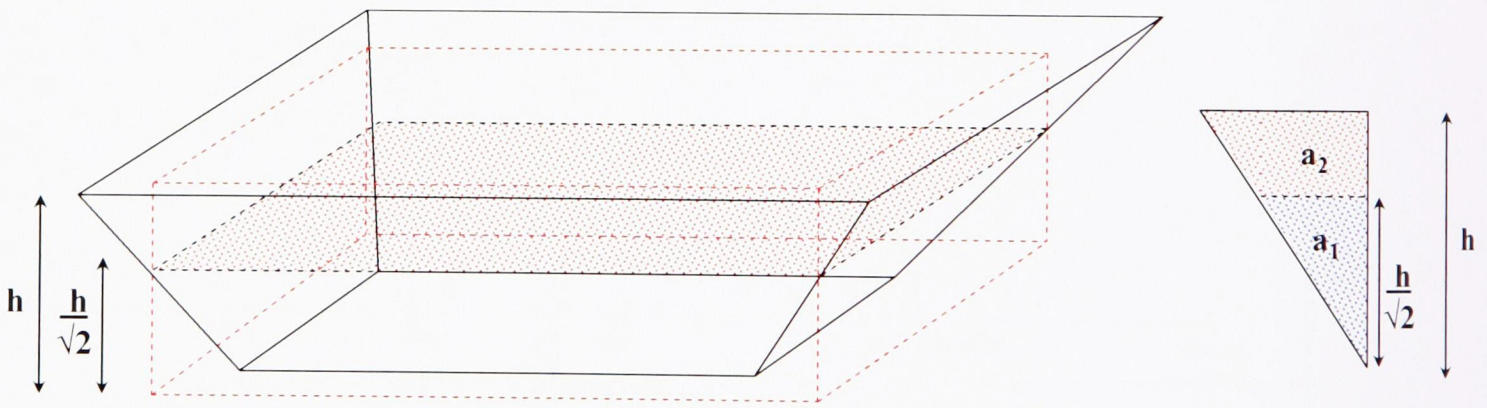


Figure 7.19 Method of changing turlough levels into pond dimensions.

7.5 Modelling Diffuse Infiltration into the Network

The contribution of the rainfall falling on the lowland karst limestone area that will ultimately end up in the main conduit system feeding the turloughs also needed to be taken into account. Hence, for this modelling scenario any infiltration / aquifer recharge from rainfall on the catchment needs to find its way into the epikarst and fracture network. This was achieved by a combination of a runoff-routing model, groundwater infiltration module and the use of SUDS (sustainable urban drainage) applications in the *Infoworks* modelling suite.

The rainfall hitting the catchment was first subjected to evapotranspiration losses and initial wetting and storage losses. Then the water had to be routed down through the soil into the conceptual epikarst fracture system which was represented by a pipe network. In *Infoworks* infiltration into the soil etc can be modelled fairly accurately (as discussed later) but this is normally from the perspective of generating the right amount of runoff which will make its way into the pipe network. The infiltration is therefore normally water lost to the pipe network system – not what is desired for this non-standard application of model. However, recently a Groundwater Infiltration Module (GIM) has been developed for *Infoworks* to provide a highly attenuated response to rainfall to represent the below-ground processes of infiltration through the soil into a pipe network and also the contribution from a high water table. These facets have been used to mimic the slow infiltration of rainfall into the soil and through the epikarst before it starts to move through the fracture network towards the main conduits. Once the runoff reaches the pipe network the fractures in the epikarst have been conceptually modelled as pipes with permeable characteristics (i.e. flow calculated via Darcy's Law), available as one of the SUDS options.

7.5.1 Rainfall runoff and routing models

The components of runoff as depicted by the *Infoworks* software are shown in Figure 7.20. The so-called fixed or Wallingford method is designed to simulate the fast direct response from impermeable areas such as roofs and roads. (Note, in practice, there are several combinations of different runoff and routing models available in *Infoworks* that will provide this fast runoff response, as detailed later). The new PR equation is for the medium

direct response from permeable areas such as lawns and grass verges which contribute overland flow to the nearest manhole. The soil store is to model the slow indirect response through the soil and into cracks in the pipes (typically of the order of 6 hours to 1 day). The ground water store is a very slow indirect response (typically in the order of days to weeks) and finally, a constant baseflow can be added which is independent of rainfall.

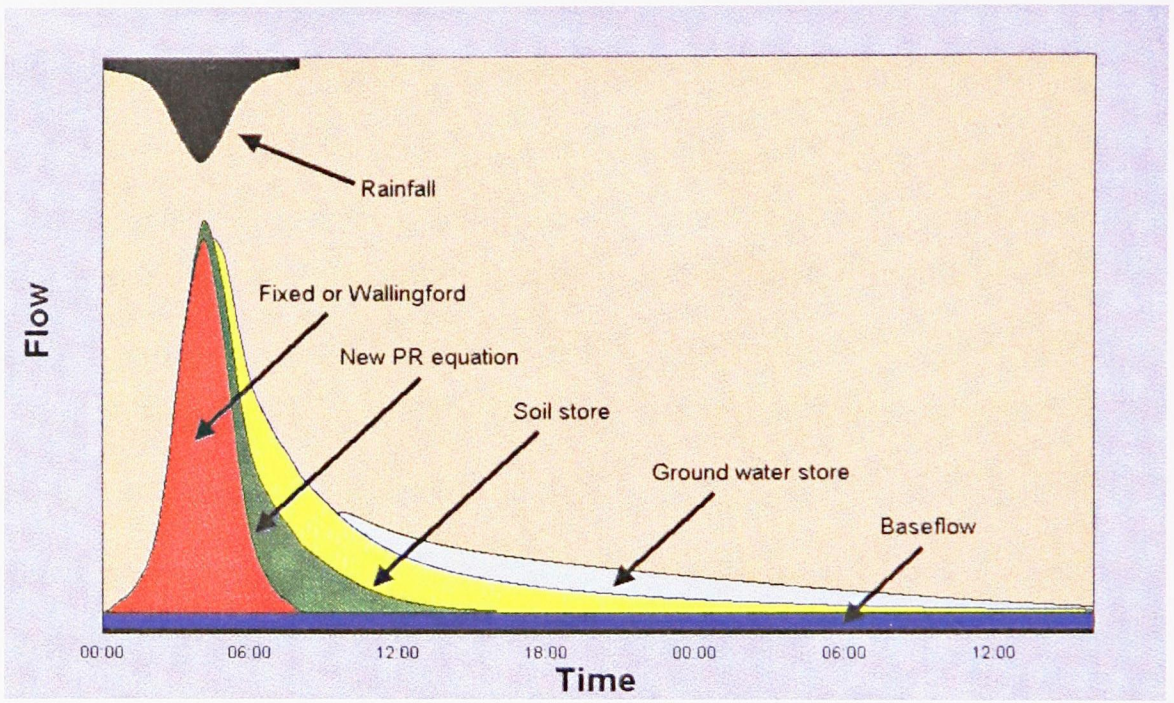


Figure 7.20 Components of runoff (Wallingford, 2006).

The three fundamental components to runoff are the runoff volume, the routing and the initial losses. The runoff volume defines the amount of rainfall falling on the ground surface that will end up in the pipe network; the routing defines the speed at which it will enter the sewer; and the initial losses represent the effect of the first few mm of water falling on the catchment surface which could be lost due to damping and cooling the catchment and filling up small surface depressions. It should be noted that evapotranspiration is applied to surface area of stored water in the ponds (turloughs) and is also applied to the GIM (see Section 7.6.4.2).

The conceptual framework for runoff is shown in Figure 7.21 below. The different sections of the model are now presented, starting with the process of runoff.

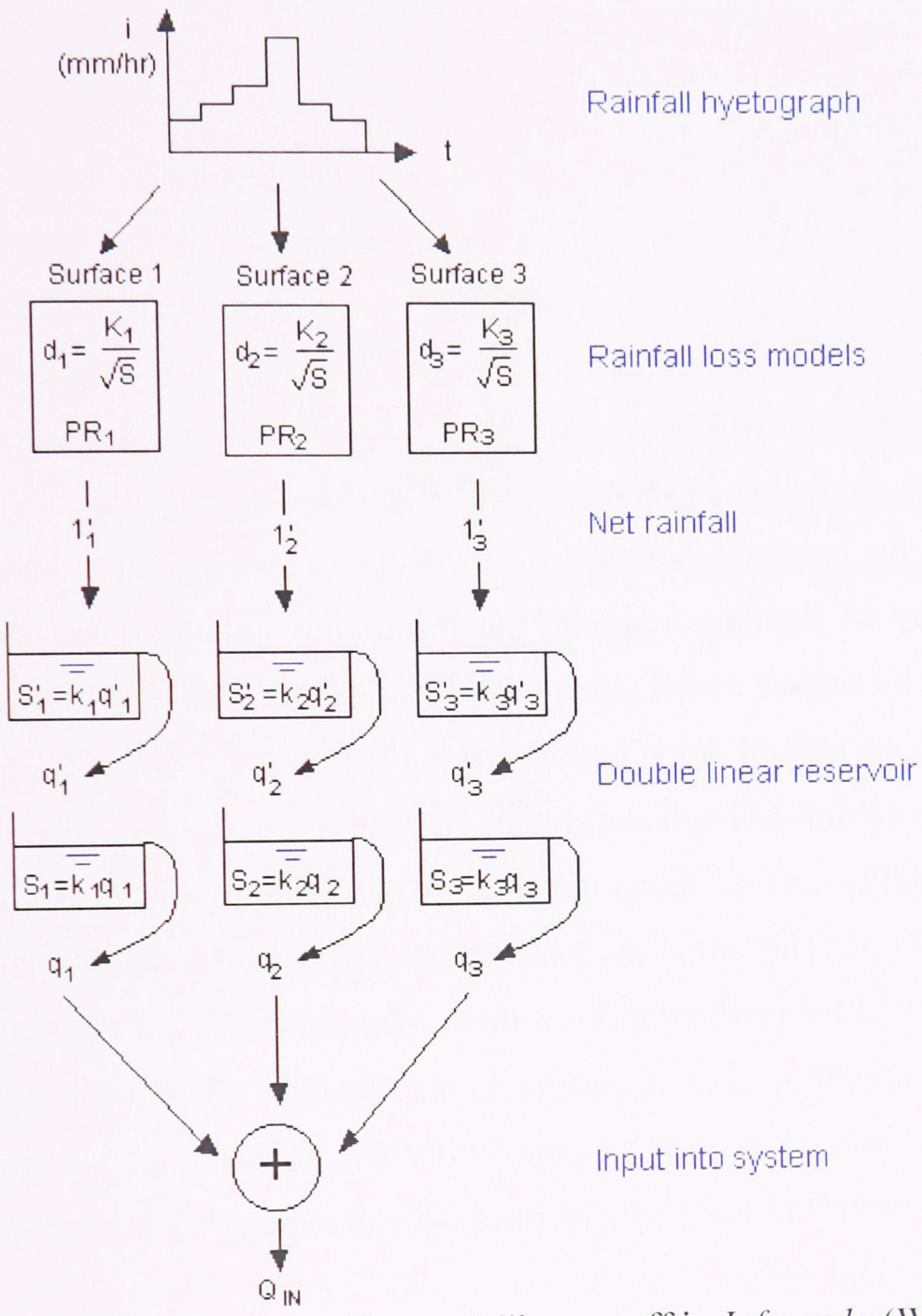


Figure 7.21 Conceptual framework for modelling runoff in *Infoworks* (Wallingford, 2009).

7.5.1.1 Runoff surfaces

Runoff surfaces are defined within each subcatchment and have a number of parameters that determine how the runoff of rainfall occurs on that surface, the volume of runoff and the rate at which it enters the drainage system. For this model each subcatchment only had one runoff surface defined. The following suite of parameters need to be specified.

- ***Runoff volume model***

The following runoff volume models are available in *Infoworks*, the advantages and disadvantages of each are covered in Appendix G.

  - Fixed
  - Wallingford

- NewUK
- SCS
- Horton
- Green-Ampt
- Constinf
- Horner

A lot of research could go into looking at the use of these different applications for this karst modeling, particularly if more targeted field data was available. Initially the overall concept for modelling infiltration adopted was to use only the runoff volume model for flows into the network (before the knowledge of the GIM was known). This required a reverse way of thinking whereby the infiltration into the karst network was modeled effectively by surface runoff (and modeled infiltration was kept to a minimum). The runoff then had to be slowed down before making it into the network (to mimic the infiltration through the subsoil and epikarst) before making it into the main fracture network whereby the permeability was modelled using the SUDS permeability coefficient in the pipes (see Section 7.5.1.3). The initial model chosen really was the SCS model which is a widely accepted model for predicting storm flow volumes from rural catchments and was chosen due to its simplicity (see Appendix G for details). The antecedent conditions has a corollary to infiltration into the karst in that the higher this value (catchment index) the higher the runoff into the pipe (fracture) which is similar to the higher the rain, the faster its pushed through the soil.

However, when running simulations over long time periods (i.e. months) it was found that the percentage runoff kept increasing as the soil got wetter until it reached 100%, a plateau at which it remained, which is not realistic. Consultation with Wallingford confirmed this and so the model was changed to the Fixed runoff model. This was chosen as the runoff fraction was going to be very small in reality (as most water was percolating in) and so not that critical as a parameter.

Other parameters that need to be defined for the runoff model are the ***Runoff routing type*** (Relative or absolute i.e. the routing factor); the ***Surface type*** (Impervious, Pervious or unknown) and the ***Ground slope*** (taken as the mean slope from OS maps for that subcatchment area).

- **Routing model**

Overland runoff on catchment surfaces is often represented by the kinematic wave equation. The direct solution of this equation in combination with the continuity equation is too time consuming for applications with distributed catchment models with a large number of contributing subcatchments and so the *Infoworks* modelling suite uses simpler reservoir-based models, which are less onerous computationally, and represent the physical processes as accurately as the more complex physically based approaches. The following routing models are available in *Infoworks*, the details of which are given in Appendix G.

- Wallingford Procedure
- Large catchment model
- Sprint
- Desbordes
- SWMM
- Unit

The large contributing area model was chosen initially as it was developed for larger contributing areas up to 100 ha; the standard Wallingford runoff routing model was designed for small catchments (up to 1 ha). The modified runoff routing takes into account the flow characteristics of the catchment and represents them using one pipe. This model contains two elements that attenuate the peak discharge from the single pipes: routing coefficient multiplier and runoff shift time. However, after several different pilot simulations it seemed that neither the routing coefficient multiplier nor runoff shift time coefficients had any effect at the scale to which the karst model was formulated (i.e. for simulations of several months). Following consultations with Wallingford software it was felt that it offered no advantage over the Wallingford procedure and therefore the Wallingford Procedure model was the routing model used.

The Wallingford storage routing model is based on the use of a double quasi-linear reservoir model (see Figure 7.21 above). Two reservoirs are applied in series for each surface type with an equivalent storage-output relationship for each reservoir. This relationship is given by:

$$S = kq \qquad \text{Eqn. 7.7}$$

where $k = Ci^{*-0.39}$ and $i^* = 0.5(1 + i_{10})$

where i_{10} is the running 10 minute average of rainfall intensity.

Combination of the two storage relationships with the continuity equation leads to a second-order ordinary differential equation of the form:

$$k^2 \frac{d^2q}{dt^2} + 2k\frac{dq}{dt} + q = i_n \qquad \text{Eqn. 7.8}$$

An overall relationship relating the coefficient C to catchment characteristics has been developed with the final relationship:

$$C = 0.117S^{-0.13}A^{0.24} \qquad \text{Eqn. 7.9}$$

where, S - slope (m/m), A – area of surface (m^2).

The runoff can be controlled by the following parameters.

Runoff routing value – the larger the value (k) the quicker the response to rainfall.

Fixed Runoff Coefficient - the proportion of runoff from this surface, for example, 0.1 indicates 10%. For the first modelling concept (i.e. without the GIM) this was set very high in order to capture all the flow into the network (to mimic infiltration across the catchment). However, later when the GIM was used, this figure was set low (at 5%) which meant that most of the rainfall would percolate into the soil and ground water stores and from there could infiltrate into the network controlled by the specific GIM parameters (see Section 7.6.1.2).

SCS Depth - the storage depth is the maximum potential storage depth, S (in metres), for this surface (see previously).

Infiltration Loss Coefficient - used to calculate the infiltration loss to groundwater when using the *ConstInf* runoff volume type – therefore this was not relevant.

- **Initial losses**

The initial losses from the catchment can be controlled by three key parameters.

Initial loss type – determines nature of initial loss value field [Abs, Slope or SCS].

Initial loss value - the quantity of rainfall just required to cause overland flow is termed the initial loss. The initial part of a rainstorm is assumed to cause no runoff because it is lost in wetting the ground surface and in forming puddles. The *initial loss porosity* parameter can be used to represent a runoff surface where the initial storage volume contains some sort of fill material such as sand, gravel or rocks. The fill material reduces the potential capacity for water storage. An Initial Loss Porosity of 0.3 represents 30% air volume in the structure (70% of the volume is taken up by fill material). This was left at 1.0 as there was no physical basis for using another figure and other coefficients could be used in place of this to gain the response so it was felt to be rather redundant for use in this modelling scenario.

Initial Abstraction Factor - the proportion of the storage depth that is retained on the surface before runoff occurs. The original SCS approach recommended k = 0.2. However other studies suggest k values between 0.05 and 0.1 may be more appropriate. This parameter is not needed however, when using the Fixed runoff volume model.

7.5.1.2 Groundwater infiltration module

The below ground processes can be simulated using the Groundwater Infiltration module (GIM) which allows two additional mechanisms for water to get into the pipe network via the soil storage reservoir and/or the groundwater store reservoir. A conceptual model of how the runoff model, soil storage reservoir and groundwater store reservoir are linked and interact is presented in Figure 7.22. The soil storage and groundwater reservoir act in a similar way to runoff whereby they have processes closely resembling volume, routing and initial losses.

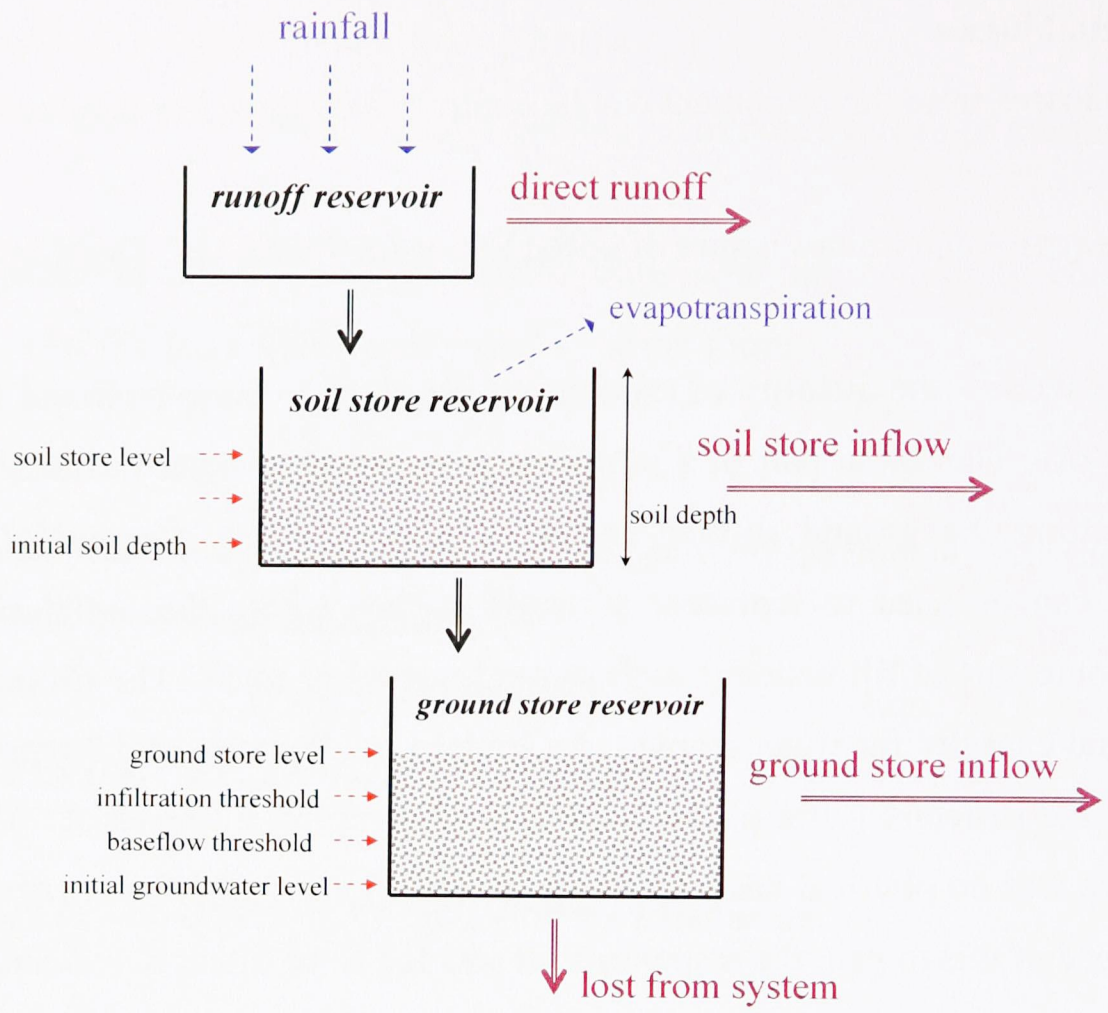


Figure 7.22 Conceptual model the runoff model, soil storage reservoir and groundwater store reservoir.

The following assumptions are made in the GIM:

- reservoirs act independently (i.e. groundwater level could be higher than the soil store level).
- the GIM takes no account of the flow depth in the pipes (i.e. there could be infiltration inflow into a surcharged pipe).
- there is no interaction between ground water levels in subcatchments.

- ***Soil store reservoir***

The soil store is modelled conceptually as a reservoir filled with a media (of certain porosity) with one outfall from it as shown in Figure 7.22 above. The height of the reservoir is the soil depth and the area is the same as the total runoff area. The initial soil depth (defined in the groundwater infiltration event) is calculated as a percentage of the soil depth. Equally, the percolation threshold (defined in the GIM) is defined as a

percentage of the soil depth. When the rainfall enters the soil store the level start to rise (the rate of which is inversely proportional to the soil porosity). Once, the level reaches the percolation threshold there is a contribution of flow into the pipe network. The proportion of flow which enters the pipe network is defined by the percolation percent infiltrating – if this is set at 10% then 10% of the flow enters the network and 90% goes down to the next layer, the groundwater store. The rate of flow into the pipe network is thus defined by the following equation:

$$\text{soil store inflow} = \frac{\text{volume above percolation threshold x perc \% infilt.}}{\text{percolation coefficient}} \qquad \text{Eqn. 7.10}$$

The soil store is also drained by evaporation linearly interpolated from 100% (when the soil store is full) down to 0% when the soil store is empty.

- ***Ground store reservoir***

The ground store is modelled conceptually as a reservoir filled with a media (of certain porosity) with two outfalls from it: one goes into the pipe network and the other leaves the system providing no contribution to the network. The infiltration threshold defines the level at which there is contribution to the network and the baseflow threshold defines the level at which flow is lost to the system, as shown on Figure 7.22 above. The infiltration level is generally higher for a sewer network. However, for this use the baseflow threshold was set to be at a higher level than the infiltration level which would ensure that most flow ended up in the network system (i.e. the karstic groundwater contribution in this scenario – which requires thinking in reverse). The starting point for the level in the groundwater store is defined as the initial groundwater level (in the groundwater infiltration event). The excess flow from the soil store (i.e. percolation percent infiltrating) starts to fill up the groundwater reservoir and the rate of flow from the groundwater store infiltrating into the pipe network is defined by:

$$\text{ground store inflow} = \frac{(\text{volume above infiltration threshold})^{1/2}}{\text{infiltration coefficient}} \qquad \text{Eqn. 7.11}$$

Equally, the rate of flow lost from the system is defined by the baseflow coefficient as follows:

$$\text{water lost to system} = \frac{\text{volume above baseflow threshold}}{\text{baseflow coefficient}} \qquad \text{Eqn. 7.12}$$

7.5.1.3 Contributing catchment area and pipe network

Sub-catchments were delineated across all of the areas which could provide diffuse flow into the main conduit network linking the turloughs. Individual links (conduits) were then extended out into each catchment area. The link has an associated catchment area with it courtesy of the "drains to link" feature and this option was used to associate a lateral inflow along the length of the link, as opposed to all the flow entering at a node. This provides the temporal balance to rainfall moving towards the main conduit system in the karst.

Permeable pipe model

One of the key concepts of the diffuse flow modelling solution for the karst area was that this could be modelled using the permeable media pipe model. For this the pipes running up the sub-catchments were modelled as rectangular pipes filled with a porous media as shown on Figure 7.23. The advantage of such a modelling approach is that the flow along the pipes is calculated using Darcy's Law which is the more appropriate flow regime for flow through fractures as would be the case in the epikarst, as discussed in Section 2.2.2

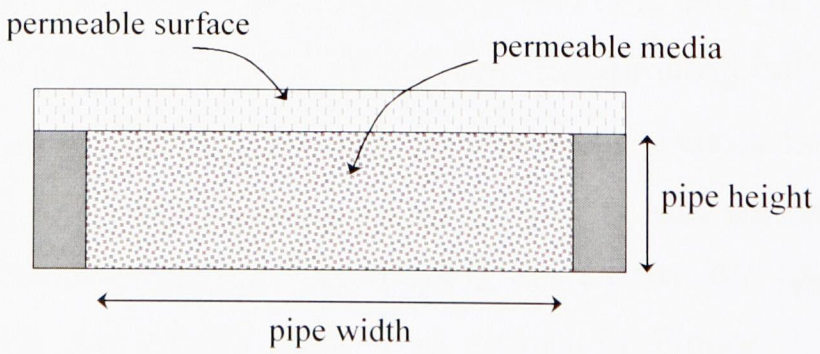


Figure 7.23 Geometric aspects of permeable pipe model for links

The use of such permeable pipes means that two parameters (media conductivity and porosity) can be used to control the rate flow and therefore conceptually control the rate of diffuse inflow through the fractures into the main karst network.

Fill material conductivity (m/s)

This is defined as the ability of the material to transmit the water. The discharge along the pipe is calculated using Darcy's Law as shown in Figure 7.24 and Equation 7.13.

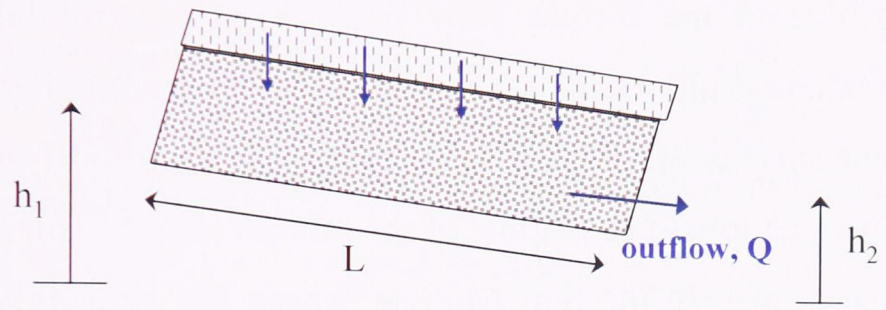


Figure 7.24 Schematic long-section of permeable pipe.

$$Q = -KA\left(\Delta h / L\right) \qquad \text{Eq. 7.13}$$

where, K = hydraulic conductivity, A = cross-sectional area of permeable formation

Δh =difference in head ($h_1 - h_2$)

Porosity (%)

The porosity affects the water level in the structure and is equivalent to reducing the plan area of the node. A porosity of 30% means 30% air volume and 70% taken up by fill.

As part of the SUDS model for permeable pipes there is the option to define infiltration losses through the base and sides of the pipe to model permeable pavement type solutions. However, for this karst modelling exercise the infiltration coefficients on base and sides were set to zero so that all the water would infiltrate into the network.

Other pertinent aspects of the model with respect to the diffuse flow are as follows

- ***Contributing catchment area*** – the whole of the defined karst subcatchment areas were considered to contribute runoff into network and so this value was set to

100%. The maximum area of each subcatchment was 150 ha (and for most cases the sub-catchments joined into the main conduit network at every node located every 750 m along the network) to suit the runoff model and match the parameters established during the calibration exercise as discussed later in Section 7.6).

- ***Runoff area (%)*** – defines how much of the subcatchment land is impermeable (the model is very sensitive to this). For this use of the model, effectively all the land should contribute to the diffuse flow network as any rainfall landing on the catchment area could ultimately make it into the karst groundwater system and so this coefficient was set at 100%. The next stage is the runoff model whereby the fixed runoff was set low to send most of the rainfall into the soil store and therefore into the Groundwater Infiltration Module where the slow infiltration processes could be modelled more accurately.

- ***Runoff slope*** – defined by the mean topography of each subcatchment area.

- ***Inflows & Dry weather flow*** – although a fixed inflow could be defined for each catchment area in order to model conceptually diffuse flow, it was decided not to use this as a significant parameter as it would be invariant with respect to rainfall. Hence, the diffuse flow was simulated by a combination of the runoff-routing model and permeable pipe solution. However, in practice it was found that a very small baseflow was necessary for the network (0.001 $m^3/s/km^2$) in order for the model to initialise before each simulation as it needed some small dry weather flow. The dry weather flow (used for diurnal wastewater profiles into the sewer network) was effectively set to zero as the population was zero for all subcatchments.

- ***SOIL class*** – defines runoff of rainfall. A soil class 3 was used in the modelling denoting a *wet* soil.

To illustrate the use of the permeable pipe solution a hypothetical catchment was built with contributing sub-catchments into a pipe network as shown on Figure 7.25. All catchments were of the same size - 10 hectares each - but had different conduits running down the centre as follows:

- Catchment 1 – normal circular pipe diameter 600 mm, length 300 m.
- Catchment 2 – permeable solution K = $1x10^{-2}$ m/s - rectangular pipe 1 m width, 2 m depth, length 300 m.
- Catchment 3 – permeable solution K = $1x10^{-3}$ m/s - rectangular pipe 1 m width, 2 m depth, length 300 m.

The SCS runoff volume model was used with pervious routing type and SCS depth set to 0.176 m.

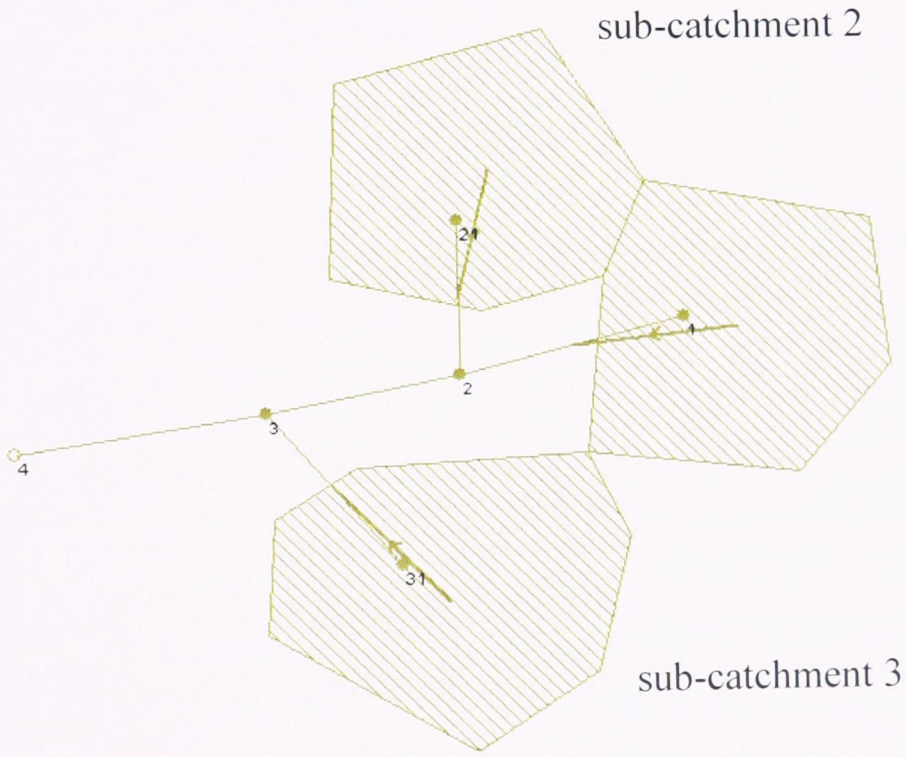
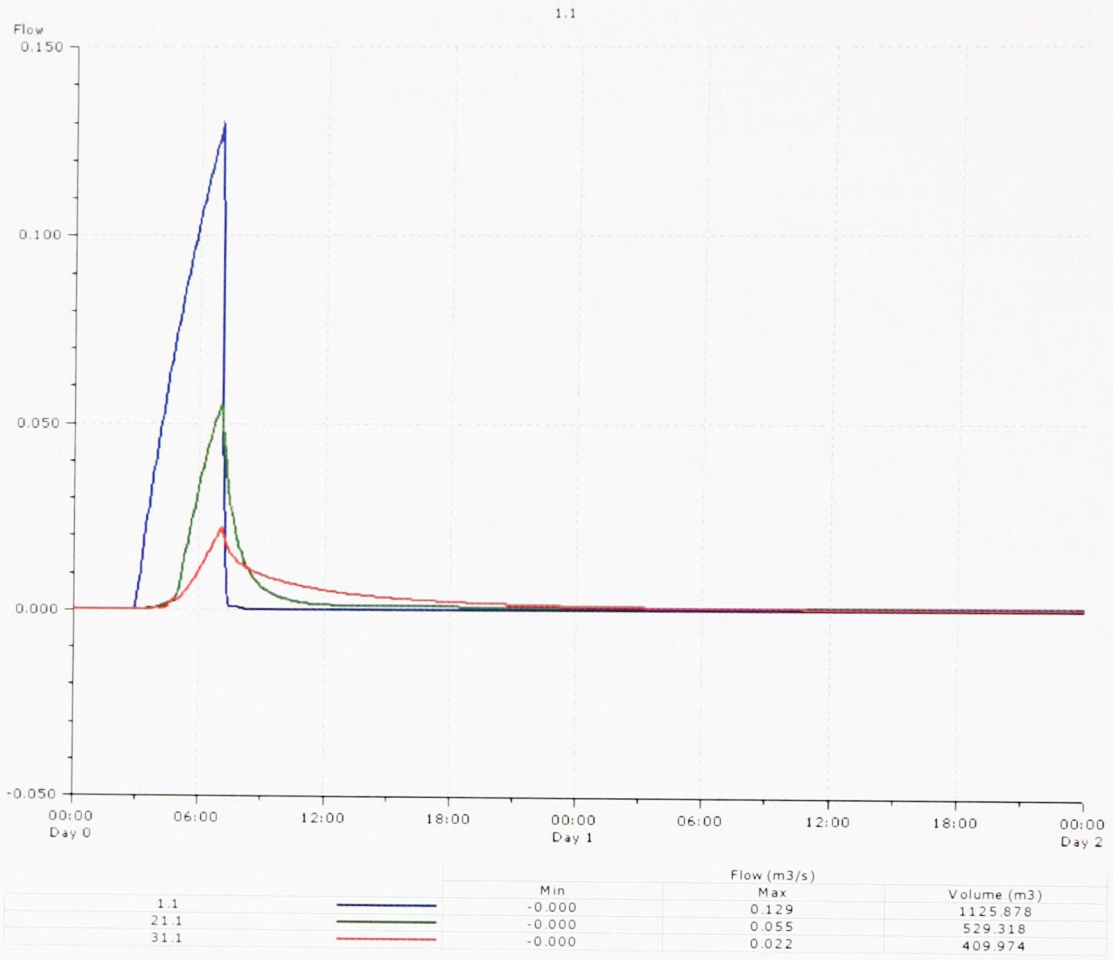


Figure 7.25 *Infoworks* layout of test network.

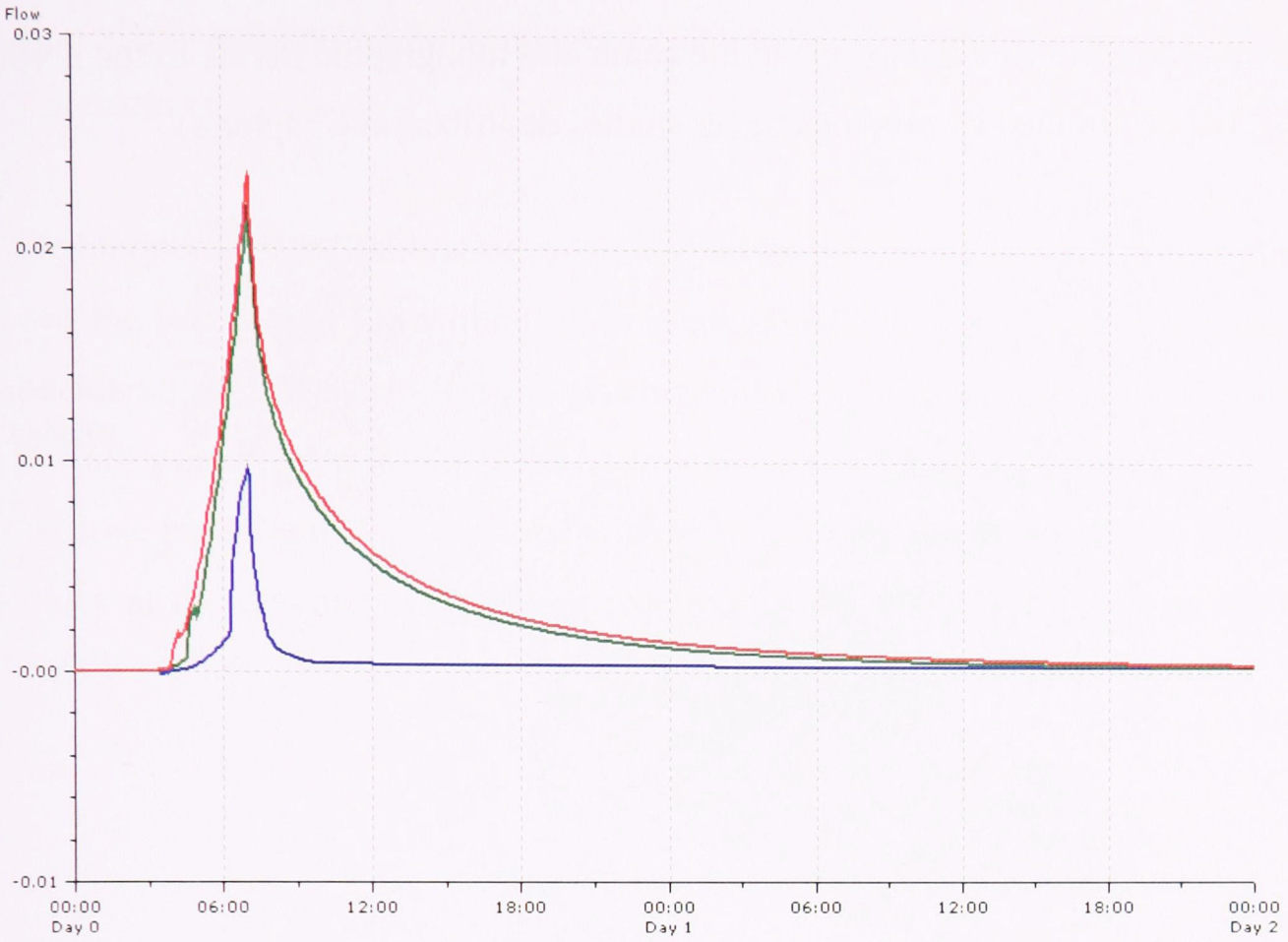
A simple 6 hour rain storm was applied to the catchment (5 mm/hr for the first two hours up to 12 mm/hr for the last 3 hours) and the response from each subcatchment compared. The flows at the downstream end of pipes 1.1, 2.1 and 3.1 are plotted on Figure 7.26 across a 2 day period. (Note, there are no other inflows associated with the network). This clearly shows the faster response from the open pipe to the permeable pipe which give a much delayed response and longer time for the water to drain the network – with Conduit 2.1 faster than Conduit 3.1 as expected due to the difference in K value for the media.



	Flow (m3/s)		
	Min	Max	Volume (m3)
1.1	-0.000	0.129	1125.878
21.1	-0.000	0.055	529.318
31.1	-0.000	0.022	409.974

Figure 7.26 Comparison of flows draining the three sub-catchments (pipes with different permeabilities).

The difference between permeable pipe sizes was also investigated. The comparison in resultant flows are shown in Figure 7.27 for sub-catchment 3 with 1000 mm Ø pipe, sub-catchment 2 with a 1 m width by 2 m depth rectangular section and sub-catchment 1 with a 4 m depth by 2 m depth pipe section. This shows little difference between the 1000 mm Ø pipe and 1000 x 2000 mm rectangular channel. However, for the larger pipe (4000 x 2000 mm) this shows a significantly smaller flow through the pipe due to the lower head as explained by Darcy's Law equation (Eqn. 7.13).



	Flow (m3/s)		
	Min	Max	Volume (m3)
...el 4m wide pipes>Test rain (50mm 6 hours)	-0.000	0.010	80.964
...el 1m wide pipes>Test rain (50mm 6 hours)	-0.000	0.022	409.974
...del 1m dia pipes>Test rain (50mm 6 hours)	-0.000	0.023	472.736

Figure 7.26 Comparison of flows draining the three sub-catchments (different cross-section permeable pipes).

7.6 Calibration of diffuse flow component of network model

The river Owenshree was gauged at two locations, as it runs off the Old Red Sandstone at Kilchreest and then approximately 13 km further downstream having run over the karst limestone at the point just before the river disappears underground before Blackrock turlough. The difference between the flows at the two positions was thus used to quantify the typical amount of diffuse infiltration draining into the network from the karst. This was also used to calibrate the *Infoworks* model in terms of modelling such diffuse flows using the techniques set out in the previous Section 7.5.

A network of this section of the river was built in *Infoworks*, as shown on Figure 7.27. The subcatchments were defined based upon the known physical boundaries to the karst

catchment area - Old Red Sandstone to the south and topographic divide to the north along the ridge (as determined by previous tracer studies described in Chapter 3).

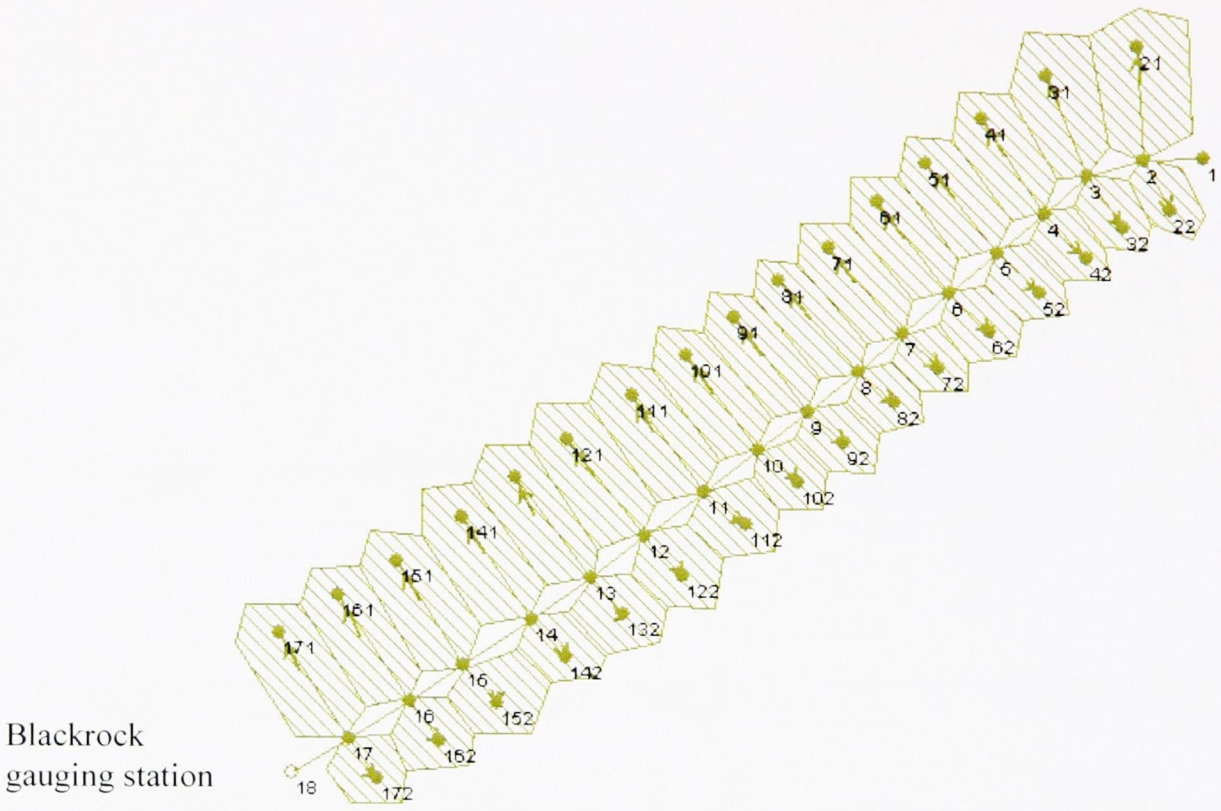
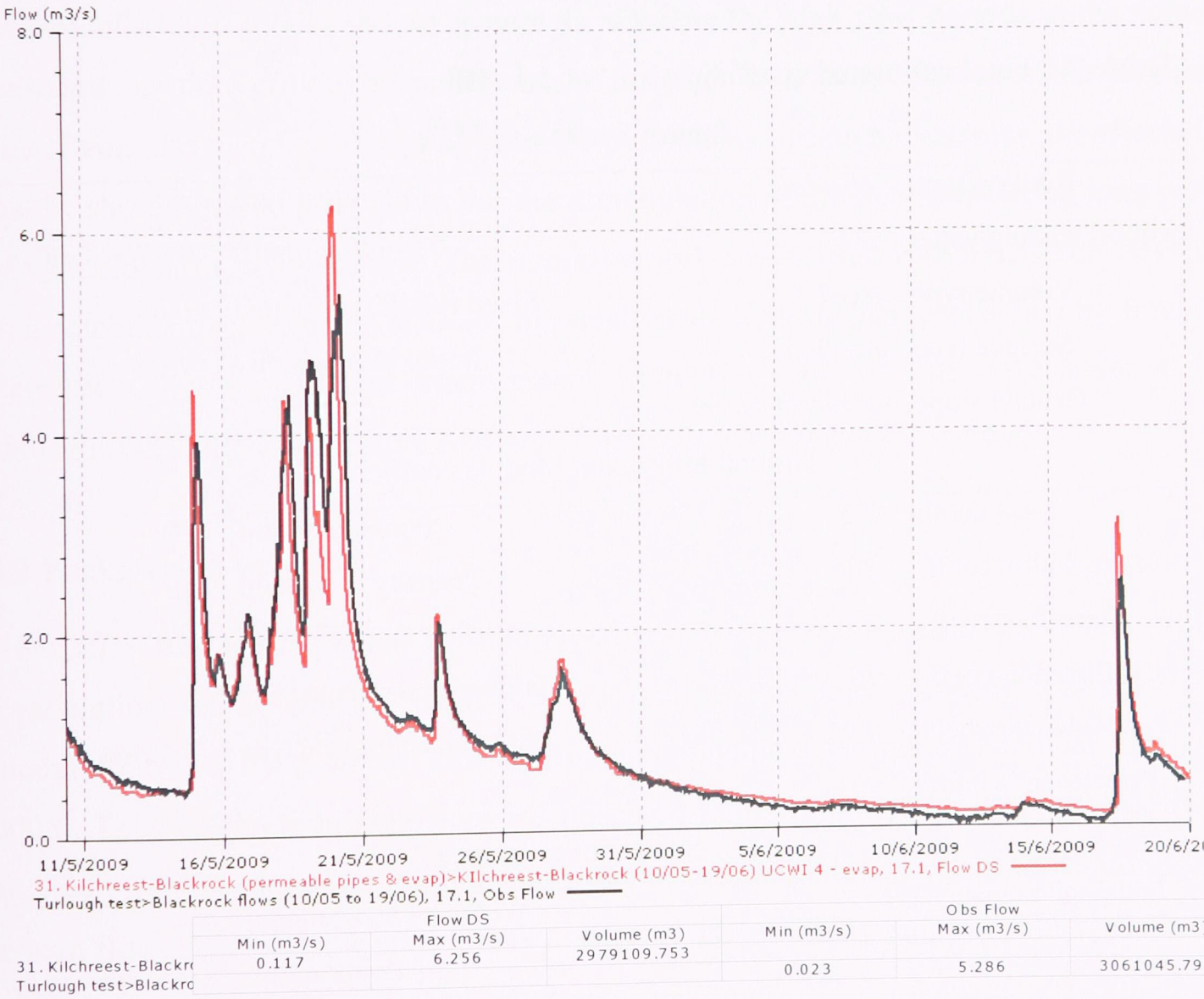


Figure 7.27 *Infoworks* network of Owneshree river from Kilchreest to Blackrock turlough.

The main river channel was modeled as a trapezoidal open channel of dimensions 8 m width by 2 m depth. It was separated into 17 equal length conduits of 750 m (separated by nodes) to give an overall river length of 12.75 km. At each node the contributing catchment area on either side of the river on the karst was covered with subcatchments to represent the total area of land up to the catchment boundary. Each subcatchment has a single permeable pipe running up the middle to represent the fracture system in the epikarst. All permeable pipes were rectangular of fixed depth 2 m and variable width scaled according to the size of the subcatchment. For example, most subcatchments on the southern side of the river were 25 ha and were served by a pipe of 2 m depth by 1 m width; subcatchments of 100 ha had pipes of 2 m depth by 2 m width. The pipes serving each subcatchment were set at an invert of 4 m depth (to give 2 m of subsoil cover as assumed from the GSI Vulnerability maps – see Appendix A. The gradients and ground levels of the subcatchments were taken from the Ordnance Survey levels (1:50 000 map). A table of

pipe sizes, lengths, invert levels and subcatchment details for this model is included in Appendix G.

The period used for calibration was 10th May to the 19th June 2009. It was decided that this was the best period for calibration as it contained a couple of heavy rainfall-runoff events but also a significant dry period which enabled the diffuse system to be compared against the full range of conditions. The calibration was an iterative process which took over 50 separate model runs to attain the optimum match between the measured flows and modeled flows at the downstream gauging location on the Owenshree river as shown on Figure 7.28.



	Flow DS			Obs Flow		
	Min (m3/s)	Max (m3/s)	Volume (m3)	Min (m3/s)	Max (m3/s)	Volume (m3)
31. Kilchreest-Blackr	0.117	6.256	2979109.753			
Turlough test>Blackro				0.023	5.286	3061045.795

Figure 7.28 Final calibrated model results for Owneshree river section (10th May to the 19th June 2009).

It proved difficult to match the early recession from the initial rainfall events against the much slower release diffuse flow following longer dry periods. The best fit was eventually attained by a balance between the various parameters used to define the Runoff Surface, Ground Infiltration and permeable pipes - in particular the soil depth and percolation coefficients in the GIM and the pipe permeability coefficients. It can be seen that although the model (the red line on Figure 7.28) gives a good fit to the observed flows (black line), it does slightly underestimate the flows in recession following a rain storm and slightly overestimates the much slower diffuse contribution. The final calibration parameters to model diffuse flow from the subcatchments are listed in Table 7.1 as follows. These have been set for all subcatchments in the final model as described in Section 9.

Table 7.1 Final calibrated coefficients to model diffuse flow.

Runoff Surface coefficients			
Routing type	*Absolute*	Initial loss type	*Slope*
Runoff routing value	*24*	Routing model	*Wallingford*
Volume type	*fixed*	Fixed runoff coefficient	*0.05*
Surface type	*pervious*	Initial loss porosity	*1.0*
Ground slope	*as subcatchment*		
Ground Infiltration Module coefficients			
Soil depth	*1.5*	Porosity of soil	*30*
Percolation coeff.	*200*	Porosity of ground	*50*
Baseflow coeff.	*2.0*	Baseflow threshold level	*-1.0*
Infiltration coeff.	*30*	Infiltration threshold level	*1.0*
Percolation threshold	*0.9*	Infiltration threshold type	*Relative*
Percolation % infilt.	*90*		
Sub-event properties			
Initial soil saturation	*65%*	Wetness (SCS) model	*3*
UCWI	*50*	Evaporation	*User defined per Δt*
Permeable pipe & catchment parameters			
Media conductivity	*0.005 m/s*	Baseflow	0.001 $m^3/s/km^2$

8 RAINFALL RUNOFF MODELLING

8.1 Introduction

An additional modelling activity undertaken in the project was to develop a rainfall-runoff model in order to simulate the three main river flows draining off the Slieve Aughty mountains which act as inputs into the karst pipe-network system. The idea was that such a model could then be used on the basis of rainfall and temperature records alone to predict the river inputs into the karstic pipe network model. It would then be possible to use the linked models to investigate historical turlough dynamics from times before when the rivers were gauged or the turloughs were monitored. It was considered most important that the rainfall-runoff model should accurately simulate the high flow periods in the winter as these are the more critical times in terms of turlough inundation. However, the cumulative runoff volumes also need to be as accurate possible as turlough dynamics are affected not just by short duration peak flows but the accumulation of groundwater during long periods of variable surface water flow. The rainfall-runoff model used was IHACRES developed as a catchment scale model (i.e. not for small-scale hydrological processes) by Integrated Catchment Assessment and Management (iCAM) Centre of The Australian National University and the Cooperative Research Centre for Catchment Hydrology.

8.2 Background to model

IHACRES v2 (Identification of unit Hydrographs And Component flow from Rainfall Evaporation and Streamflow data) is based upon two modules in series: a non-linear loss model followed by a linear unit hydrograph module (Australian National University, 2005). The non-linear module converts observed rainfall into effective (or excess) rainfall and then the linear routing module takes this excess rainfall and converts it into observed stream flow. The model is conceptually based upon a spatially lumped basis (i.e. processes are not spatially distributed) and requires a maximum of 12 parameters (6 for the non-linear loss model and 6 for the linear unit hydrograph). However, for many simulations it only requires 8 parameters to gain a good fit and has been deliberately designed that way as it was not deemed appropriate to over-parameterise such a model in relation to the fairly straightforward model structure (Jakeman and Hornberger, 1993).

Non-linear loss model

The non-linear model is an adaptation of the non-linear module by Ye *et al.*, (1997) which supposes that the proportion of rainfall, *r* that becomes effective rainfall, *u* at each discrete time step, *k* is directly proportional to the catchment wetness index as follows,

$$u_k = \left[c\left(\phi_k - l\right)\right]^p r_k \qquad \text{Eqn. 8.1}$$

where r_k is observed rainfall, c, l and p are parameters [(mass balance, soil moisture threshold index and non-linear response (or power on soil moisture)].

ϕ_k is a soil moisture index ,

$$\phi_k = r_k + \left(1 - {}^{1}\!/_{\tau_k}\right)\phi_{k+1} \qquad \text{Eqn. 8.2}$$

with the drying rate τ_k given by,

$$\tau_k = \tau_w e^{(0.62 f(T_r - T_k))} \qquad \text{Eqn. 8.3}$$

where τ_w, f and T_r are parameters – reference drying rate at reference temperature, temperature modulation (temp dependence of drying rate) and reference temperature respectively.

Linear routing model

Once the effective rainfall has been calculated it is input into a parallel linear store model of quick and slow flow as follows,

$$Q_k = Qq_k + Qs_k \qquad \text{Eqn. 8.4}$$

$$\text{where, } \textit{quick flow } Qq_k = \beta_q u_{k-\delta} + \alpha_q Qq_{k-1} \qquad \text{Eqn. 8.5}$$

$$\textit{slow flow } Qs_k = \beta_s u_{k-\delta} + \alpha_s Qs_{k-1} \qquad \text{Eqn. 8.6}$$

$x.q_k$ is the quickflow component and $s.q_k$ is the slowflow component.

α_q β_q α_s β_s are the model parameters estimated by least squares estimation and δ is the number of time samples (again estimated as part of the model identification process). As these equations are linear stores then the residence time can be calculated from,

$$\tau_s = -\frac{\Delta t}{\ln(\alpha_s)} \qquad \text{Eqn. 8.7}$$

where Δt is the time step (1 hour used here).

There are five options with regards to the conceptual model used for calibration:

- Single exponential store (1, 0)
- 2 exponential stores in series (2, 0)
- 2 exponential stores and 2 instantaneous stores in parallel (2, 2)
- 1 exponential stores and 1 instantaneous store in parallel (1, 1)
- 2 exponential stores in parallel (2, 1)

The main two performance statistics for goodness of fit are model efficiency (or R^2) and bias. R^2 is calculated according to Eqn. 8.8,

$$R^2 = 1 - \frac{\sum (Q_o - Q_{sim})^2}{\sum (Q_o - \overline{Q}_o)^2} \qquad \text{Eqn. 8.8}$$

where Q_o is the observed flow and Q_m is the modelled flow at each timestep.

Bias is the overall error in volume (in mm/year) calculated as,

$$bias = \frac{\sum (Q_o - Q_{sim})}{n} \qquad \text{Eqn. 8.9}$$

Other statistics are also available which give weight to different aspects of the goodness-of-fit such as $\sqrt{R^2}$, log R^2 and inv R^2.

$\sqrt{R^2}$, the variation of R^2, gives less weight to the peak flows.

$$\sqrt{R^2} = 1 - \frac{\sum \left(\sqrt{Q_0} - \sqrt{Q_m}\right)^2}{\sum \left(\sqrt{Q_o} - \overline{\sqrt{Q_o}}\right)^2} \qquad \text{Eqn. 8.10}$$

Log R^2 gives more equal weight to all flow percentiles.

$$\log R^2 = 1 - \frac{\sum \left(\ln(Q_o + \varepsilon) - \ln(Q_m + \varepsilon)\right)^2}{\sum \left(\ln(Q_o + \varepsilon) - \overline{\ln(Q_o + \varepsilon)}\right)^2} \qquad \text{Eqn. 8.11}$$

Inv R^2 gives more weight to low flows.

$$invR^2 = 1 - \frac{\sum\left(\frac{1}{Q_o + \varepsilon} - \frac{1}{Q_m + \varepsilon}\right)^2}{\sum\left(\frac{1}{Q_o + \varepsilon} - \frac{\overline{1}}{Q_o + \varepsilon}\right)^2} \qquad \text{Eqn. 8.12}$$

All of these were reviewed at the end of every simulation run in an iterative process to gauge the effect of the different parameters on the quality of calibration at different parts of the hydrograph.

The use of the model is split into 3 distinct phases: Data, Calibration and Simulation.

8.3 Data

As discussed in Section 4.4 a continuous record of river flows at was calculated from the gauging stations. In addition the flow out of Lough Cutra was gauged which shows the attenuation effect of the reservoir (as discussed later in Section 8.5). IHACRES requires three sets of input data: rainfall, temperature (or evapotranspiration) and observed river flows at the bottom of the catchment. The data was converted to mean hourly figures which is the appropriate time step for catchments under 100 km^2 according to IHACRES. The catchment areas for the three river systems were delineated topographically and measured to be the following sizes:

River Owenshree	38 km^2
River Ballycahalan	46 km^2
River Owendalullagh	89 km^2

The areal rainfall on each catchment was compiled using Theissen polygons (but with areas weighted against altitude) between the rain gauge at Kilchreest, Francis Gap and Gort. The results of this were that the three catchments were weighted on an areal basis as follows.

- River Owenshree catchment [Kilchreest 38%, Francis Gap 62%]
- River Ballycahalan catchment [Kilchreest 8%, Francis Gap 78%, Gort 14%]
- River Owendalulleegh catchment [Francis Gap 68%, Gort 33%]

The calibration periods for the model was taken as the 2007/08 hydrological year used for the simulation of the main pipe-network model as discussed in Chapter 9 (i.e. 20/11/07 to 30/04/08). This period across the winter was chosen for primary calibration as this was the main period when all the turloughs were flooded to a high level.

The air temperature data used was based upon the hourly profiles recorded by the BaroDiver® at Coy (Section 4.2) which were slightly modified according to mean altitude for the catchments according to the general rule that temperature decreases by 0.65°C for every 100 m increase in altitude.

8.4 Model calibration

The IHACRES software automatically optimises the model for every run according to the parameter boundaries set for the coefficients by the user. The wider the boundaries set the longer the computational time and so an iterative process was adopted whereby individual parameters were optimised one at a time. For each run the model produces several different options with the respective performance statistic listed. The results can be ordered on the basis of whichever performance statistic is deemed the most appropriate. For this research the goodness of fit (R^2) was chosen as the best parameter to rank the model's suitability as it disproportionately matches the higher flow values which are the more crucial periods of river flow from the point of view of the turlough water levels – i.e. the turloughs do not surcharge during low flow periods and so matching the baseflow was not of particular concern.

The final calibration coefficients for the three catchments are shown on Table 8.1 with the plots of the simulated flows against observed flows for two of the rivers during the 2007/08 year shown on Figures 8.1 and 8.2.

Table 8.1 Rainfall-runoff model calibration results

	Owenshree	Ballycahalan	Owendalulleegh
Linear coefficients			
recession rate 1, α_s	-0.952	-0.950	-0.935
peak response 1, β_q	0.043	0.044	0.058
peak response 2, β_s	0.099	0.113	0.105
time constant 1, τ_s	20.303	19.53	14.91
volume proportion 1, v_s	0.901	0.887	0.895
volume proportion 1, v_q	0.099	0.113	0.105
Non-linear coefficients			
mass balance, c	0.003121	0.003294	0.003685
drying rate at ref. temp., τ_w	33.0	27.0	27.5
temp. dependence of drying rate, f	1.5	2.5	1.5
reference temp., tref	29.0	20.0	20.0
Soil moisture threshold index, l	0.1	0.1	0.1
non-linear response (power on soil moisture), p	1.0	1.0	1.0
Model performance			
Efficiency (R^2)	0.72	0.73	0.68
bias	183	172	203

For all three catchments the exponential store and instantaneous store in parallel (1, 1) configuration proved to give the best results. The goodness-of-fit (R^2) values for the three catchments however, are not particularly impressive and it can be seen from Figures 8.1 and 8.2 that the model failed to simulate the low flow periods adequately. However, the size and timing of the peak flows are well matched, which was deemed to be the primary objective for the models. It is also interesting to note that all three catchments yielded fairly similar linear and non-linear coefficients which should be expected given that the catchments are so close together draining the same mountains and with similar rainfall patterns, antecedent conditions, soil type, vegetation and gradients.

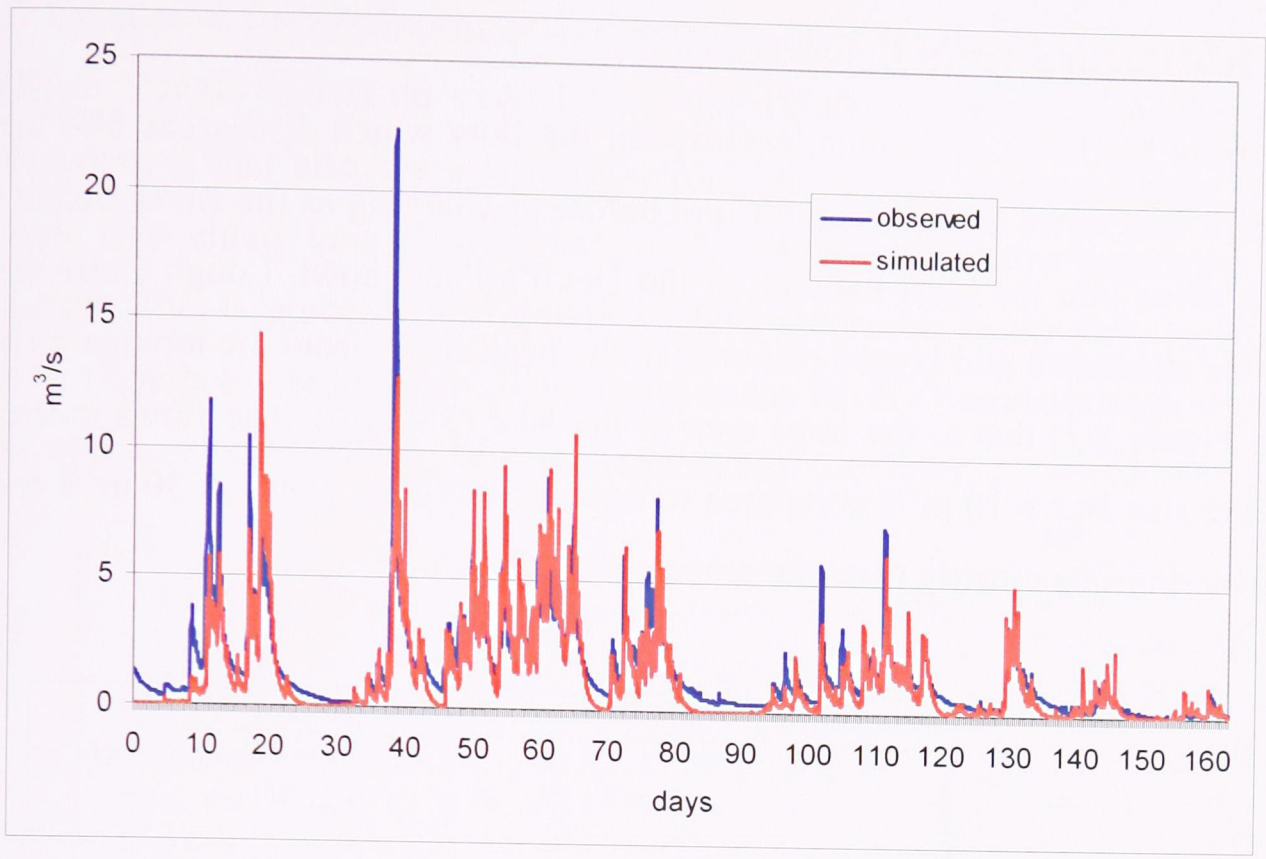


Figure 8.1 Observed and simulated flows from the River Ballycahalan catchment using IHACRES.

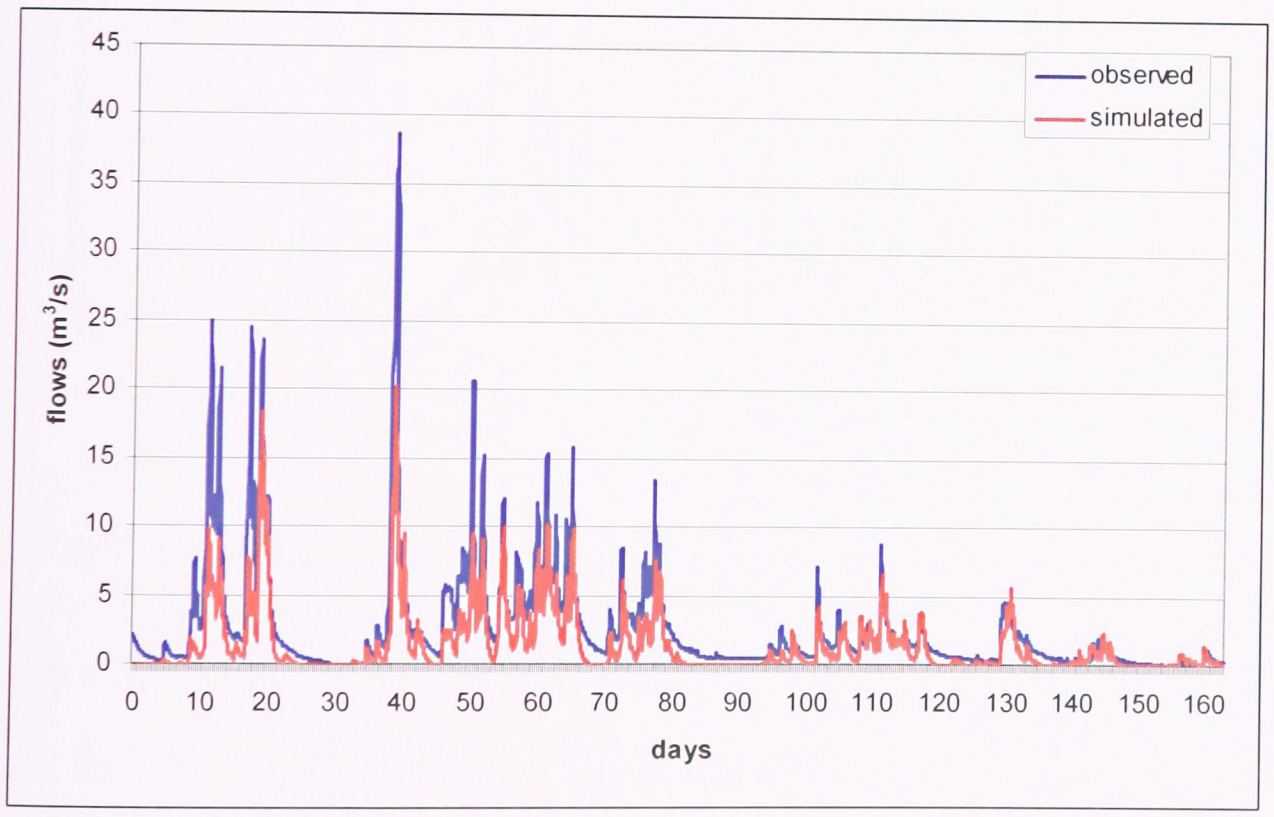


Figure 8.2 Observed and simulated flows from the River Owendallulleegh catchment using IHACRES.

The results from these optimised calibrations were then saved and input as lows into the main *Infoworks* pipe-network model as discussed later in Section 9.3.

8.5 Reservoir Routing across Lough Cutra

The flow from the River Owendalulleegh is not the flow which discharges into the karst network as it first flows though Lough Cutra before discharging as the River Beagh which then down dives into the karst network at the Devil's Punchbowl. Lough Cutra causes a considerable attenuated and lagged response to the peak flows from the mountain river (as shown on Figure 8.3) due to the large area of the lake (3.9 km^2). The flows in the River Beagh never rise above 10 m^3/s compared to some of the large peaks at 30 m^3/s and over for the River draining directly from the mountain catchment.

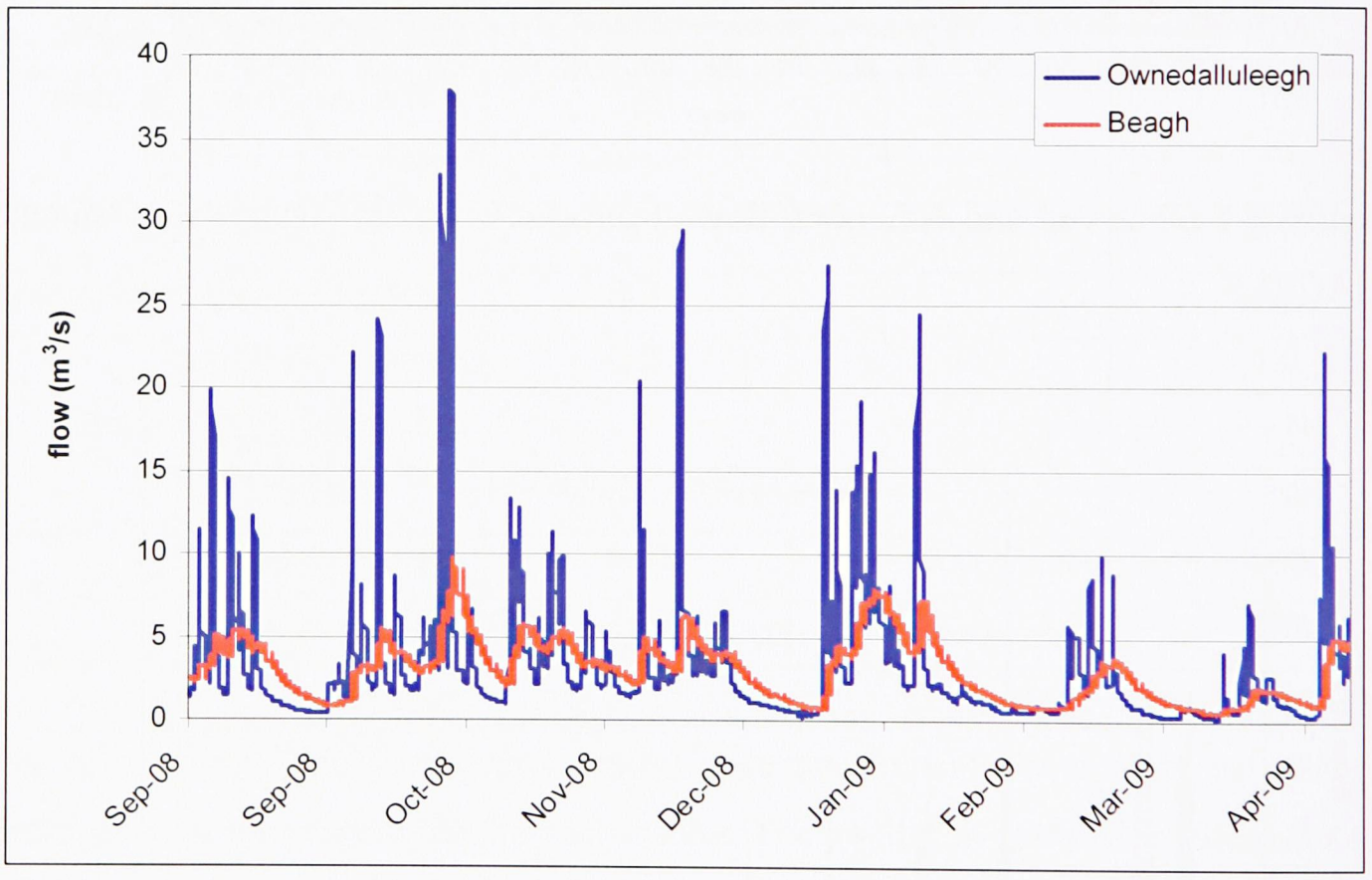


Figure 8.3 Time series of flows into (Owendalulleegh) and out of (Beagh) Lough Cutra for year 2008/09.

It should be noted that there is an additional small catchment feeding into Lough Cutra (via the river Tarry) of 8.2 km^2. As this river was not gauged, a simple judgement was made to increase the Owendalulleegh's flows by a factor relative to the catchment (equivalent to 9%) to take account for this extra volume, although it is acknowledged that the relative timing of this flow into the lake may not be accurate.

A cumulative flow plot (Figure 8.4) between the inlet (River Owendalulleegh) and outlet (River Beagh) shows an overall loss, the difference being accounted for by rainfall / evaporation and also the extra flows from the smaller catchment area. This shows that more flow enters Lough Cutra than leaves which is somewhat surprising over the winter period. This is probably also due to slight inaccuracies in the river gauging, particularly with regards to the higher peaking flows in the River Owendalluleegh which are likely to be open to more error (probably overestimating) the flows.

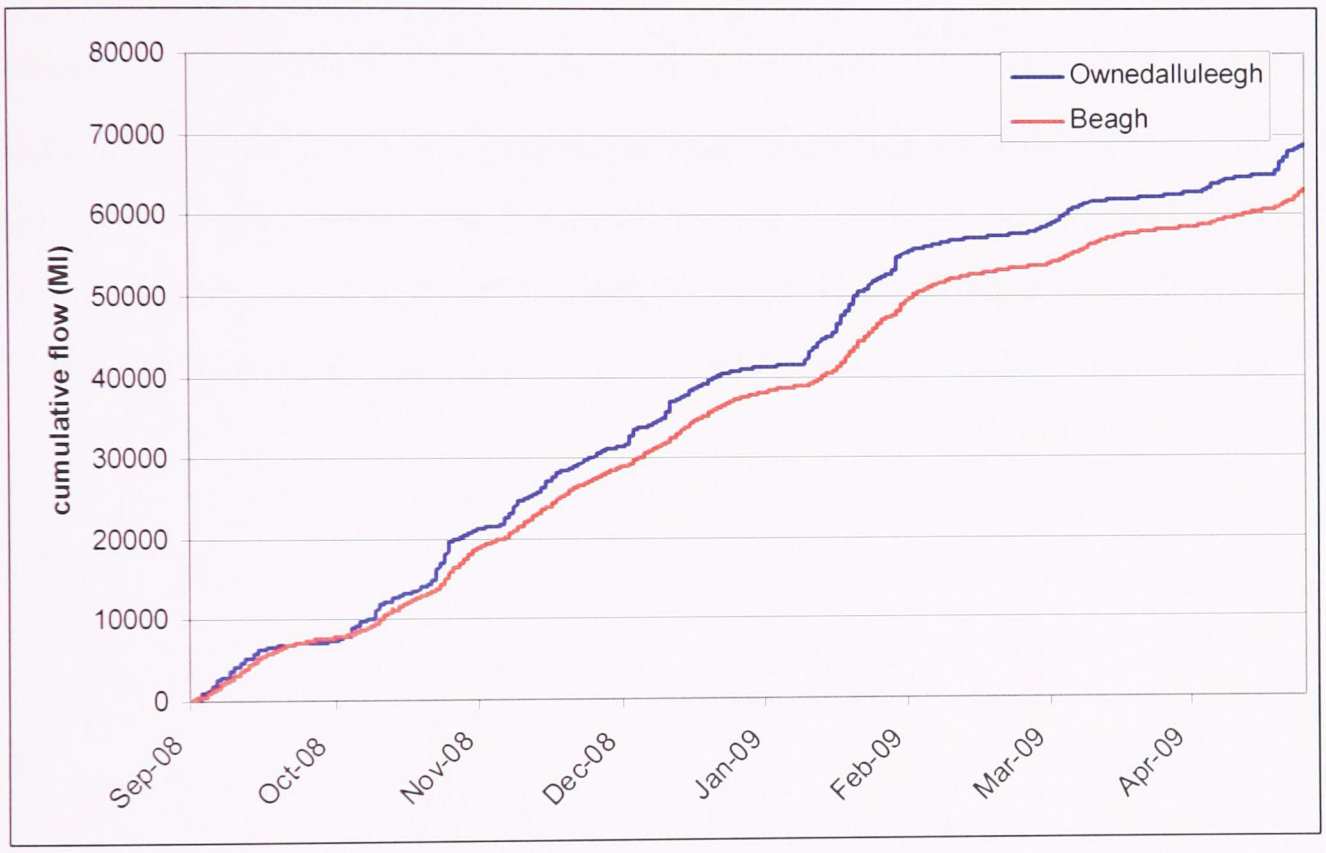


Figure 8.4 Cumulative inflow and outflows from Lough Cutra for year 2008/09.

The reservoir (or level–pool) routing method was chosen to route the flows across Lough Cutra. The reservoir routing method is based on a combination of the continuity equation with a non-linear storage discharge equation (Bedient and Huber, 1992; Shaw, 1994). For this, a stage-discharge and stage-storage relationship needs to be defined – the so-called auxiliary curve, which is a plot of G vs Q_{out} according to the following relationships.

$$G_2 = G_1 + \frac{\left(Q_{in(1)} + Q_{in(2)}\right)}{2} - Q_{out(1)} \qquad \text{Eqn. 8.13}$$

$$Q_{out(2)} = x_2 G_2^2 + x_1 G_2 + x_0 \qquad \text{Eqn. 8.14}$$

$$G_t = S_t + \frac{Q_{out(t)}}{2} \qquad \text{Eqn. 8.15}$$

The outflow (Q_{out}) at each time step is thus calculated sequentially through the data. The parameters were optimised using the Solver macro function in Excel in order to minimise the sum of the difference squared (least squared) between the observed and simulated data at each time step.

The final optimised parameters were:

$x_0 = 0.0422$ $x_1 = -0.1834$ $x_2 = 0.6214$

The comparison between the routed flow through Lough Cutra and the flows from the river Beagh for the period 2008/09 is shown on Figure 8.5 which shows a good match (peaks and timing), again particularly at the more critical high flow events. This routed flow through Lough Cutra was then used as the input into the final *Infoworks* model as described in Section 9.3.

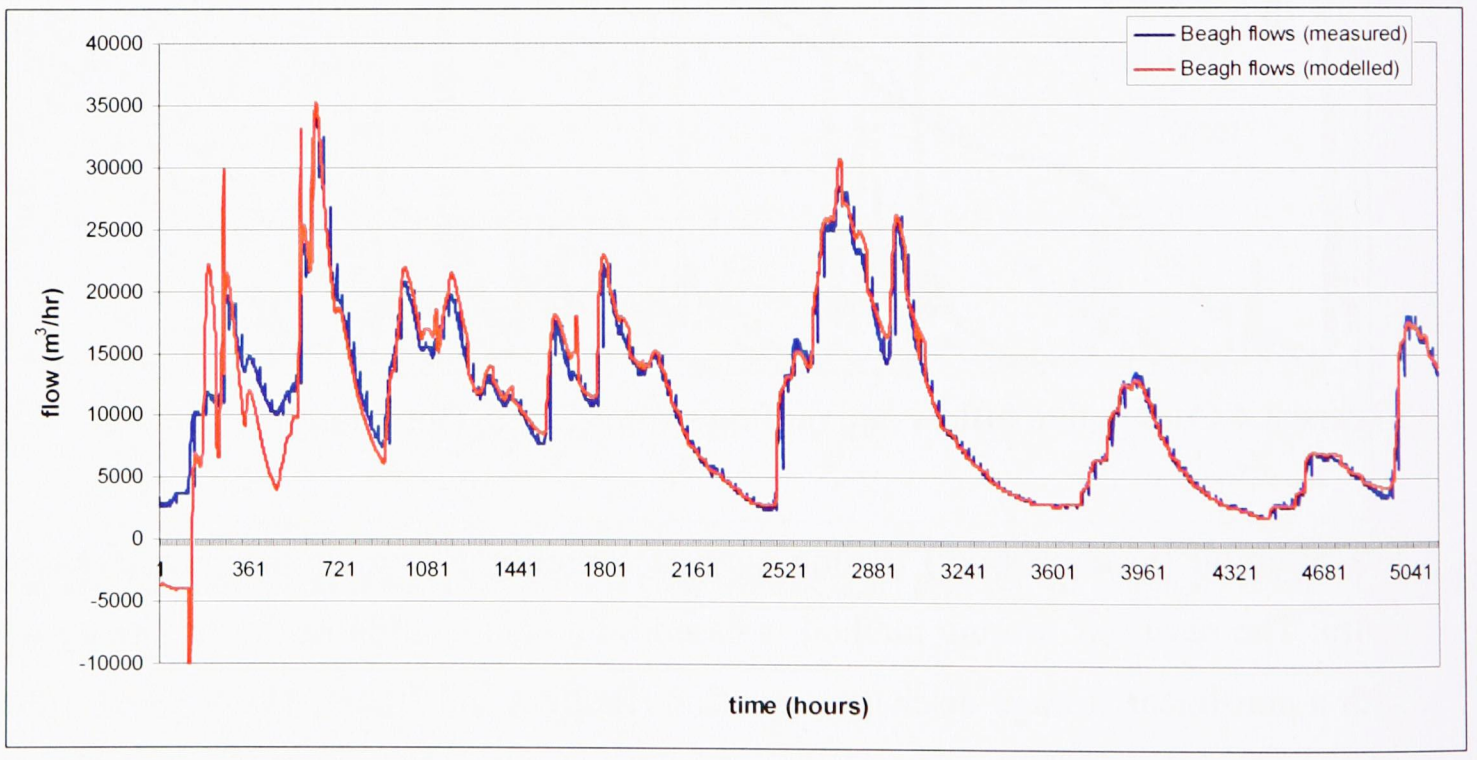


Figure 8.5 River Neagh flows compared to routed flows through Lough Cutra for year 2008/09.

9 OVERALL MODEL OF LINKED TURLOUGH SYSTEM

9.1 Overall Turlough Conceptual Model

The final model was developed as an integration of all the previous work: the flows and hydro-chemical analysis from the collected field data (Chapter 5); time series analysis of the dynamics of turlough water levels (Chapter 6); and investigations into network systems using pipes and ponds (Chapter 7); in addition to the knowledge gained from previous studies in the area, as collated in Chapter 3. The development of the pipe-network model of the karst system is detailed in this chapter. Once built, the model was then calibrated using the gauged inflows from the Owenshree, Ballycahalan and Owendalluleegh rivers. Finally, the calibrated network model was run using the flow results from the rainfall-runoff model simulations (Chapter 8) as the river flows (as opposed to the actual measured flows), to assess the overall performance of the two models linked together.

In general, the modelling process can be split into four main stages, although in practice this is an iterative process and these stages often become blurred.

- Model construction
- Model calibration
- Model validation
- *Predictive simulation (not undertaken in this study)*

As discussed in Section 7.2, an objective of the research was to provide a linked model which reacts to a known rainfall input. Rainfall is converted into river runoff for the streams coming off the Slieve Aughty sandstone mountains. These rivers are then entered as inflows into the *Infoworks* pipe network model. The rainfall is also entered into the *Infoworks* pipe network model as diffuse rainfall onto the limestone and will also contribute directly onto the turloughs. The *Infoworks* model then predicts the levels in the ponds which can be calibrated against the turloughs. The conceptual structure is shown in Figure 9.1 which shows the main rainfall input and other parameters required in purple.

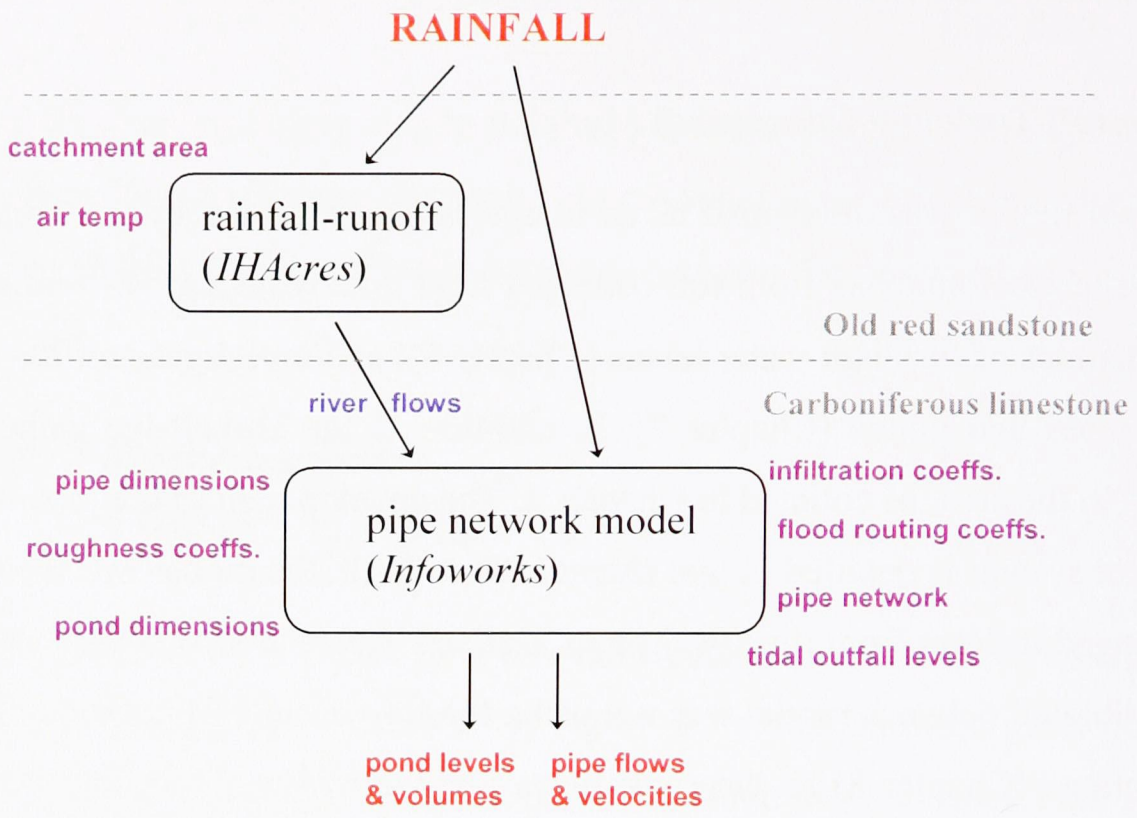


Figure 9.1 The conceptual structure of the overall turlough model.

9.2 Linked pipe network model

The pipe network model was built using the gauged river inflows for the years 2007 to 2009 as inflow inputs into the system. The period from 1st August 2008 to 10th October 2008 was chosen to make the initial calibration against, before simulations were carried out across the full hydrological years 2007/08 and 2008/09. Rainfall onto the karst catchment was taken as the hourly rainfall recorded at the Kilchreest rain gauge. Once the preliminary calibration had been completed, the model was then run for the yearly simulations. The results of these revealed some longer term effects that had not been picked up in the shorter calibration period and so the model was adjusted (finely recalibrated) again to provide the best overall fit to annual water level fluctuations of the five turloughs.

In principle there are three main ways in which a turlough could operate hydraulically as shown in Figure 9.2. However, on the basis of all the information gathered, analysed and discussed in the previous Chapters, a reasonable idea of the generic hydraulic connection of the five turloughs to the main network had already been formed.

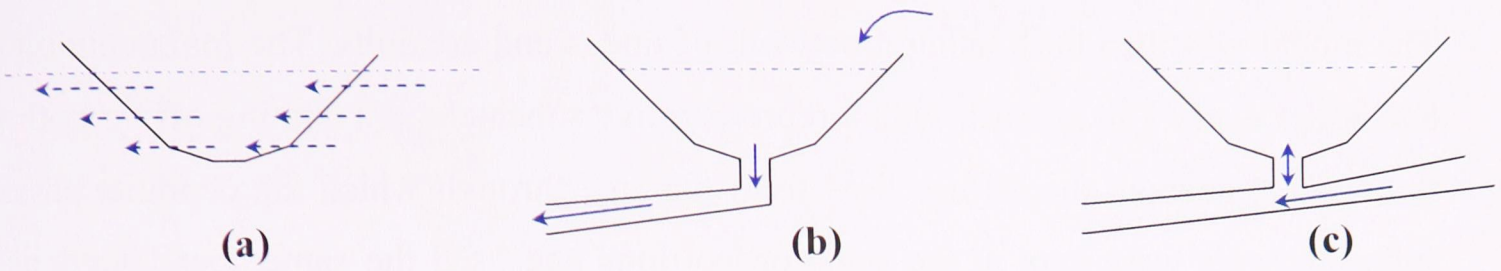


Figure 9.2 Conceptual model for hydraulic mechanism of turlough **(a)** epikarst diffuse flow, **(b)** river input and point drain and **(c)** surcharge tank.

9.2.1 Initial network development

The model was first developed with estimates of the pipe sizes. The study of the net flows into the karst at different points allowed the capacity of the pipe network to be gained and hence the maximum pipe sizes carrying the flow. As shown in Figures 5.20, 5.22 and 5.23 in Chapter 5, net flows into the main conduit network were calculated just downstream of Blackrock, just downstream of Coy and after the input from the Ballycahalan and Beagh rivers. These showed that the network could carry just over 2 m^3/s maximum in the Blackrock-Coy region and then flows from 3 to 4 m^3/s after the Ballycahalan river sinks into the karst and heads to the Coole basin.

The time series analysis indicated that Blackrock and Coy probably operated as surcharge tanks (as per Figure 9.2(c)), with Coy's level highly influenced by the water level in Blackrock. Therefore it was likely that the two turloughs had some direct conduit link. During recession periods the analysis has shown that the overall system was able to take just over 2 m^3/s of water draining from both the turloughs and the sinking river. The discharge of the river into the north-east end of Coole indicated that this must be the main entry of water into this, the largest turlough. Hence, Coole has been modelled as the conceptual scenario shown in Figure 9.2(b) whereby the water enters in the form of an open channel at atmospheric pressure. Garryland has been shown to act as a somewhat off-line tank to Coole and so was modelled as a side-link with little restriction. Finally, Caherglassaun has been shown to have similar dynamics to Coy and is closely correlated to the water level in Coole and so has been modelled as a surge tank off the main discharge conduit between Coole and the sea.

The model was then built using a network of nodes and conduits. The main conduit lines had nodes every 750 m, each with a representative subcatchment coming off on both sides to take into account the diffuse flow from the area through which the conduits pass. The subcatchments were kept at the same proportions and used the same coefficients as was defined in the calibration of diffuse flows in Section 7.6 (see Table 7.1). The final network configuration is shown in Figure 7.3 with the points of entry of the main river inflows into the system and the five turloughs highlighted. All details of the conduit sizes and lengths for the final model are contained in Appendix G.

9.2.2 Model calibration

The model was built and it was decided to calibrate against a period with relatively rapid fluctuation - 1st August 2008 to 10th October 2008. Using knowledge gained from the theoretical turloughs (Section 7.3) throttle pipe diameters and lengths were iteratively adjusted to balance the system. The model was run at a time step of 1 minute for the calibration period. River inflows and rainfall were input as hourly values, evapotranspiration was on a daily basis and tidal levels at the Kinvara outfall were defined every 6 minutes.

Although it proved relatively quick to get the turloughs peaking to the right time and balanced with respect to each other, Blackrock and Coy proved to be more complex than the original conceptual model that had been assumed. However, the fact the results from even the first simulation correlated well with, not only the overall trend in the observed data for all turloughs but also more subtle transitory water level movements was very heartening as it showed that the pipe-network modelling approach was obviously the right conceptual mechanism for this chain of turloughs.

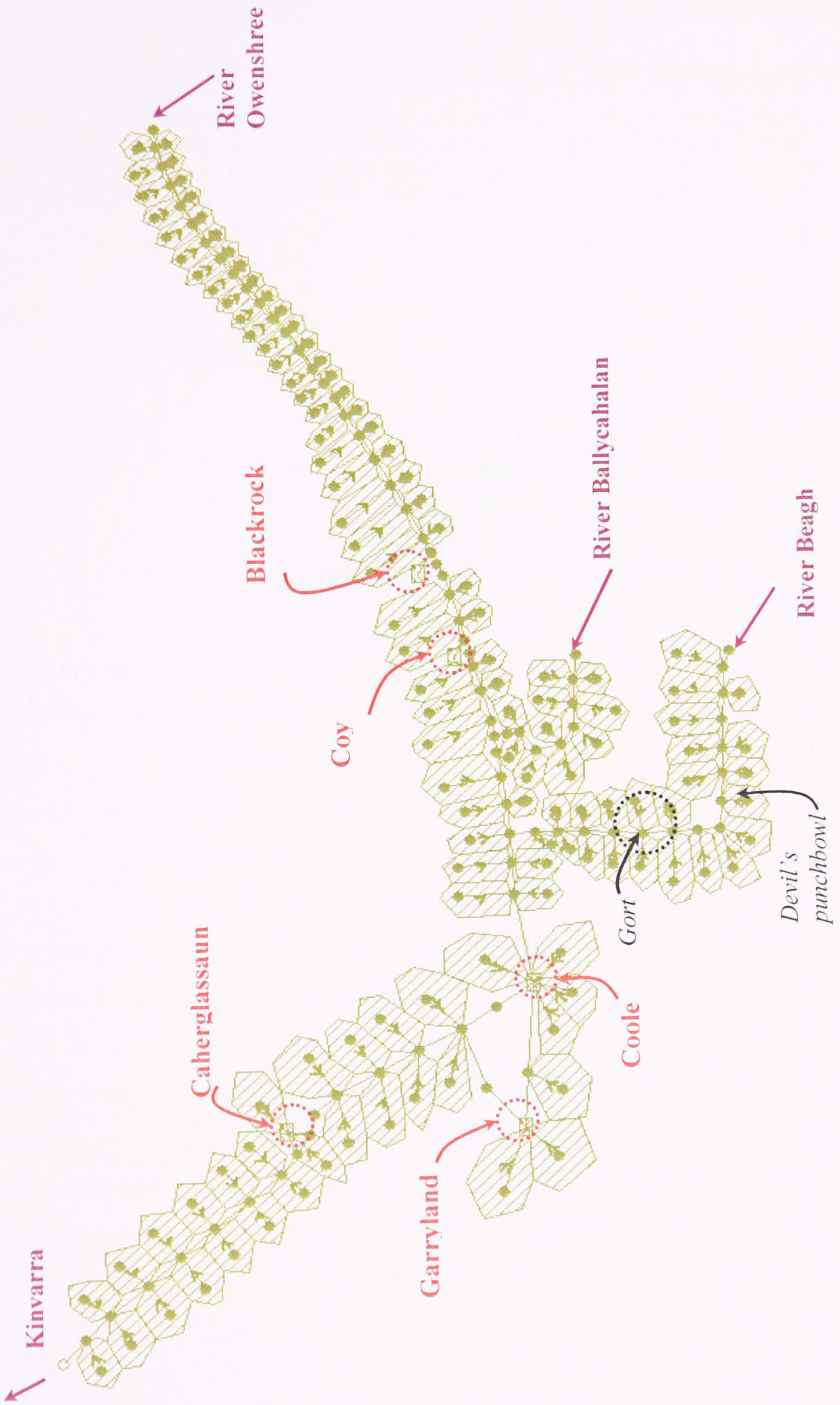


Figure 9.3 *Infoworks* plot of overall pipe-network model.

Blackrock and Coy – configuration 1

The first set of calibrations were run with the local network around Blackrock and Coy linked together as shown in Figure 9.4 – two surge tanks above the main conduit line, each one throttled downstream.

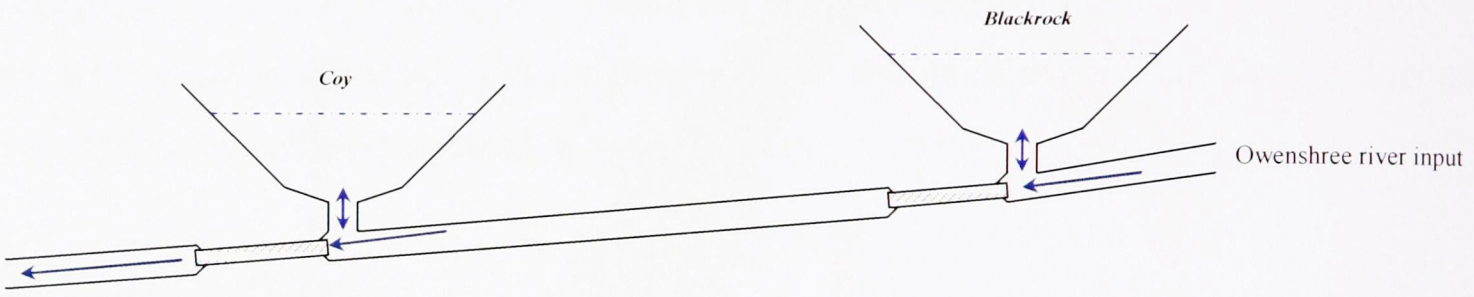


Figure 9.4 Blackrock-Coy hydraulic network – configuration 1.

It was relatively simple task to get both turloughs surcharging to the observed levels at the right timing and also mimicking the observed fluctuations. However, the recession from both turloughs proved difficult to model using this first configuration. More than 80 separate permutations of downstream throttle sizes, diameters, lengths etc were tried without success. For example, successively longer and larger pipes were trialled to generate the throttle instead of shorter narrower pipes (as discussed in Section 7.3.4) to gain a faster recession. It was finally concluded that the type of network needed to back up the flows enough in order to surcharge the ponds to the observed levels could not then let out the water at a fast enough rate during periods of recession using this hydraulic configuration. Equally, the model was making both turloughs start to fill too soon. This is shown on Figure 9.5 where both Blackrock and Coy have been modelled to get the correct peaks but the recessions are too slow. *Note, for all plots the red line is the simulated levels from the model and black line is the observed data.* It can be seen however, that the shape of both the simulated levels is very good. For this scenario the throttle downstream of Blackrock was 180 m long and 800 mm Ø and the throttle downstream of Coy was 110 m long and 820 mm Ø.

The difference between using the downstream network to surcharge the system as a result of the flows from the Ballycahalan and Beagh rivers was also investigated as shown on

configuration 2 (Figure 9.6). The theory was that the pipes passing Blackrock and Coy could be larger but still generate the same peak surcharge levels but to little effect – the water levels could not be made to recede fast enough and they were again starting to rise too soon.

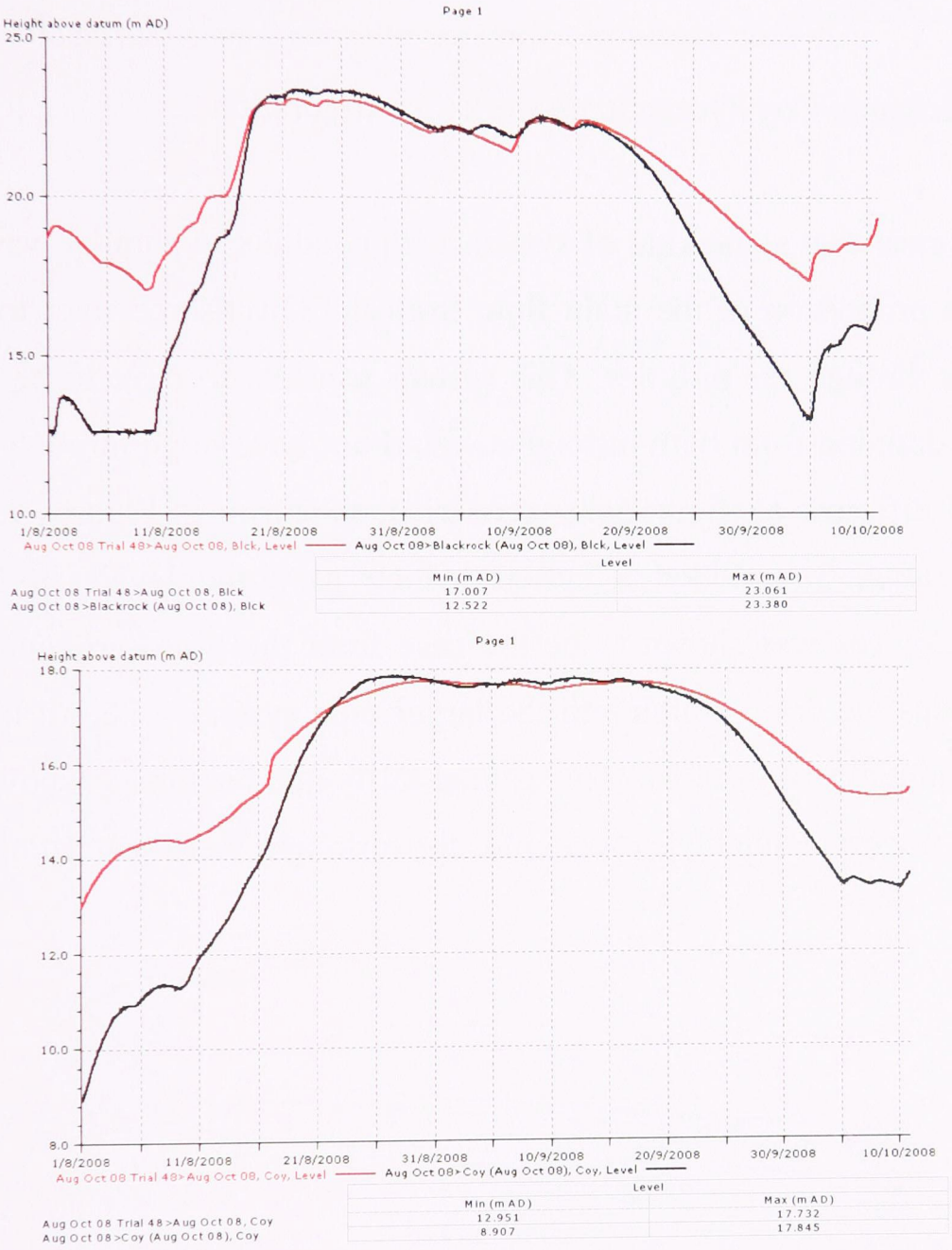


Figure 9.5 Results from model calibration at **(a)** Blackrock and **(b)** Coy using configuration 1 (red line is model, black line observed level).

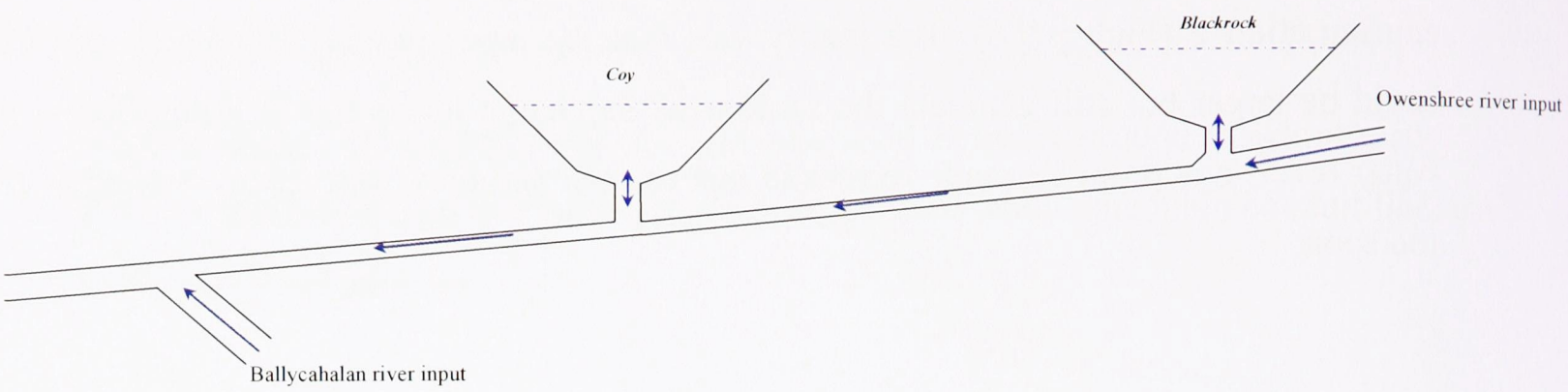


Figure 9.6 Blackrock-Coy hydraulic network – configuration 2.

Hence, it was clear that some kind of system with conduits in parallel was required which would allow a proportion of the main flow from the Owenshree river to bypass without having to pass through the throttles. This system would also have to be configured such that the water draining from both turloughs would not have to go through both throttles in series. Several different configurations were tried, as shown in Figures 9.7, 9.8, 9.10 and 9.11. Configuration 3 provided a system which gave the levels in Blackrock more influence on Coy (as was shown to be the case from the time series analysis) and also allowed two separate drain points into the larger pipe system – i.e. all the water doesn't have to pass through two throttles. This gained fairly good results as shown on Figure 9.9 but still would not drain quickly enough, plus the turloughs were still filling too fast.

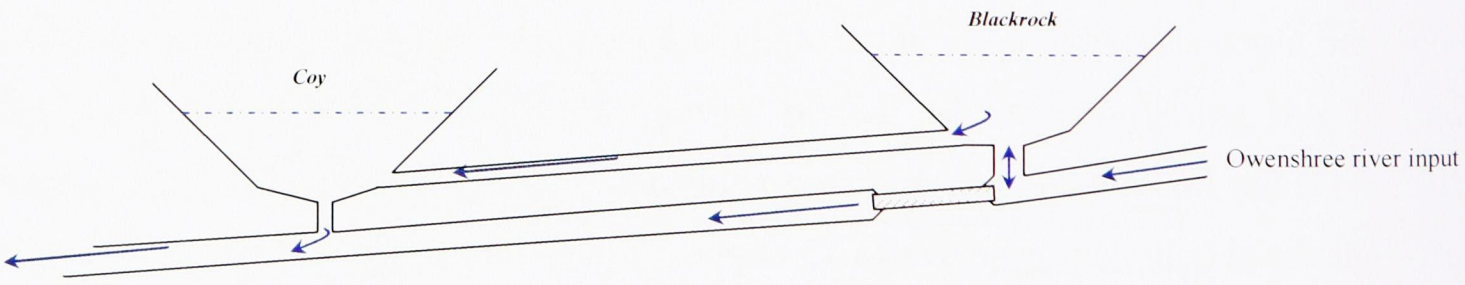


Figure 9.7 Blackrock-Coy hydraulic network – configuration 3.

Configuration 4 (Figure 9.8) followed on from this which allowed slightly more control of the water levels with the throttles and entry pipes into both turloughs all able to produce different effects. This proved a slight improvement but still fundamentally had the same problems of surcharging too soon and receding too slowly (i.e. more or less the same as Figure 9.9).

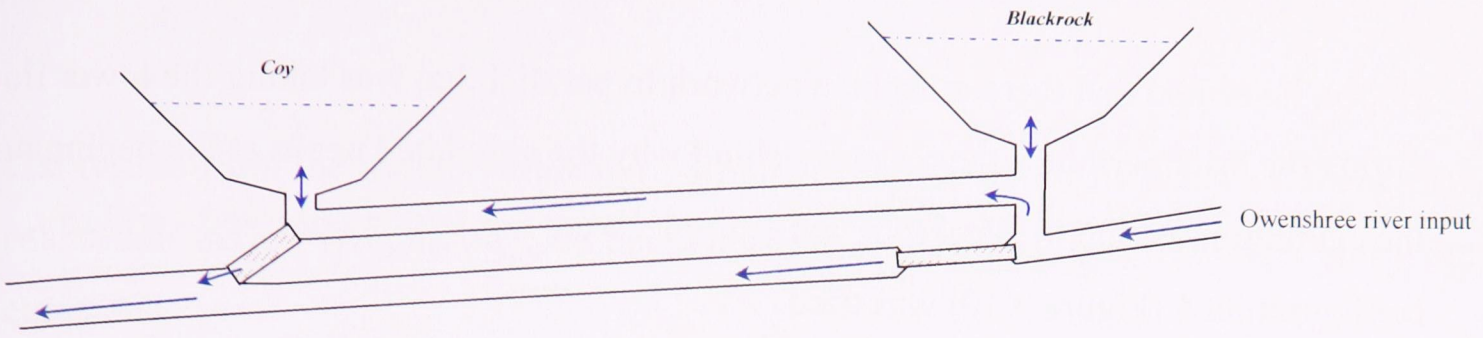
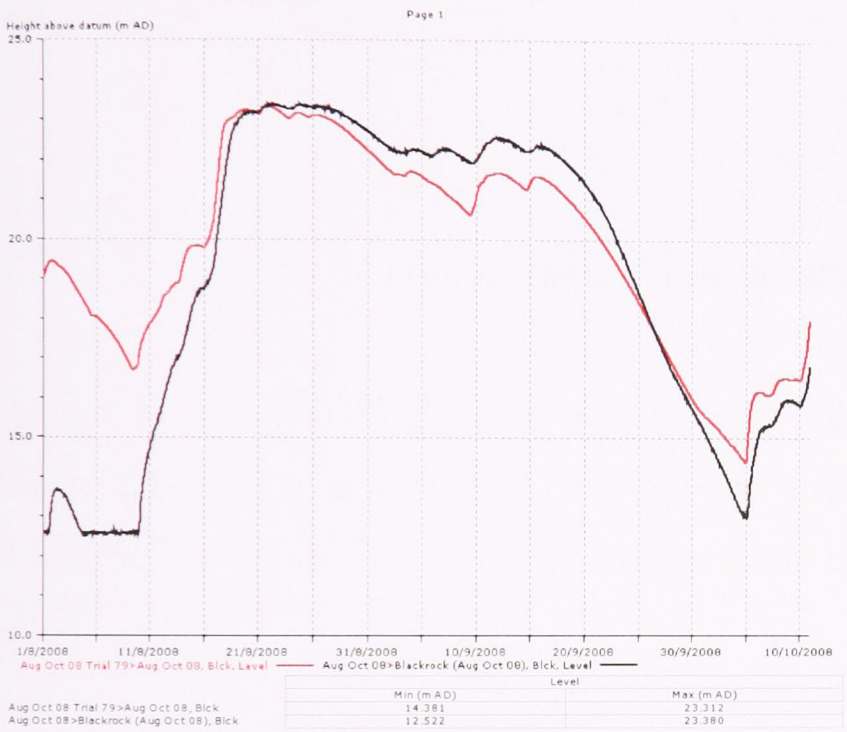


Figure 9.8 Blackrock-Coy hydraulic network – configuration 4.



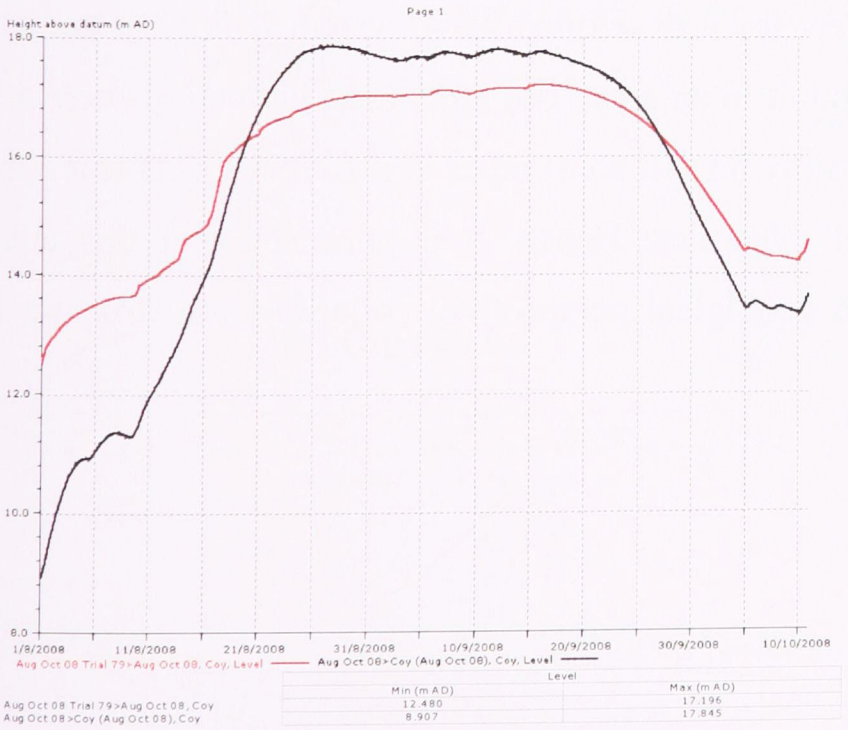


Figure 9.9 Results from model calibration at **(a)** Blackrock and **(b)** Coy using configuration 3 (red line is model, black line observed level).

Hence, it seemed that there must be a network in parallel that was taking the lower flows during the drier periods – the reasons behind why the simulated peaks at the beginning of the calibration period in Blackrock for example, were not in fact observed - and so configuration 5 (Figure 9.10) was tried.

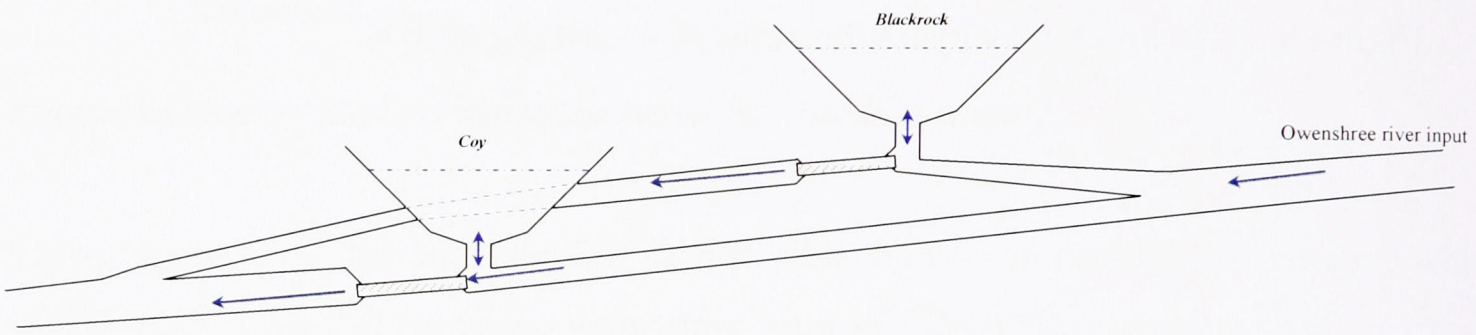


Figure 9.10 Blackrock-Coy hydraulic network – configuration 5.

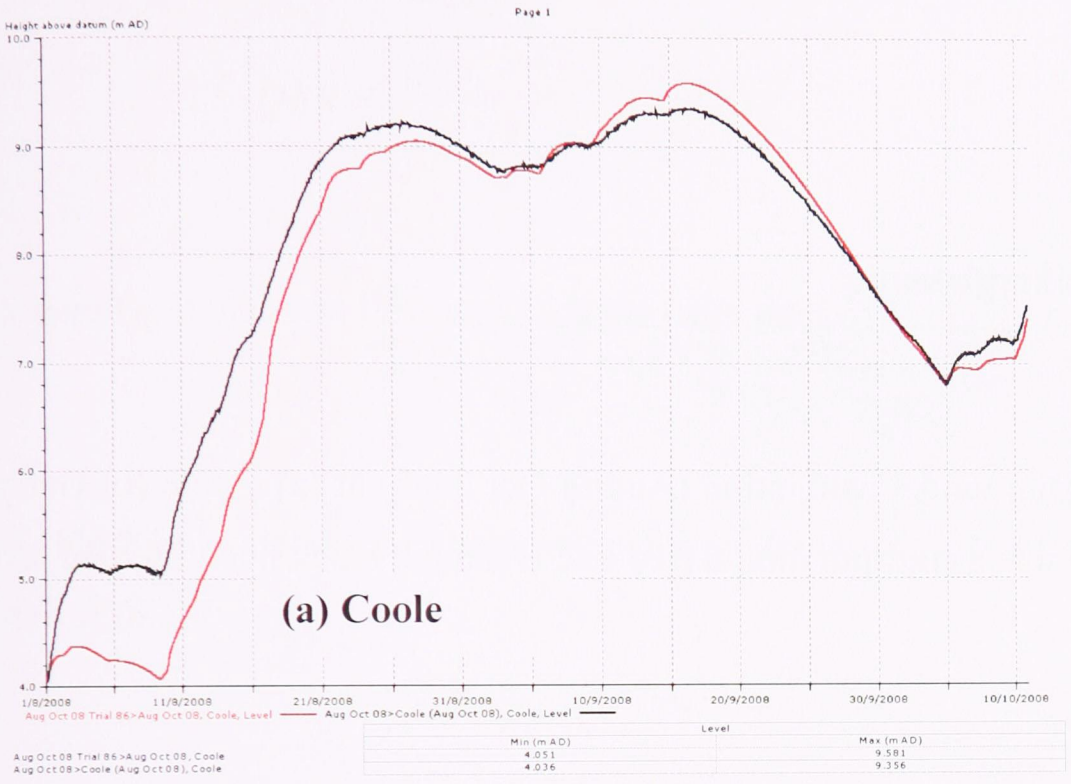
However, this parallel configuration proved very difficult to control and so the final configuration 6 was tried, as shown in Figure 9.11. This was slightly better but still suffered the same short-comings to some extent. This was the configuration used for all subsequent annual simulations.

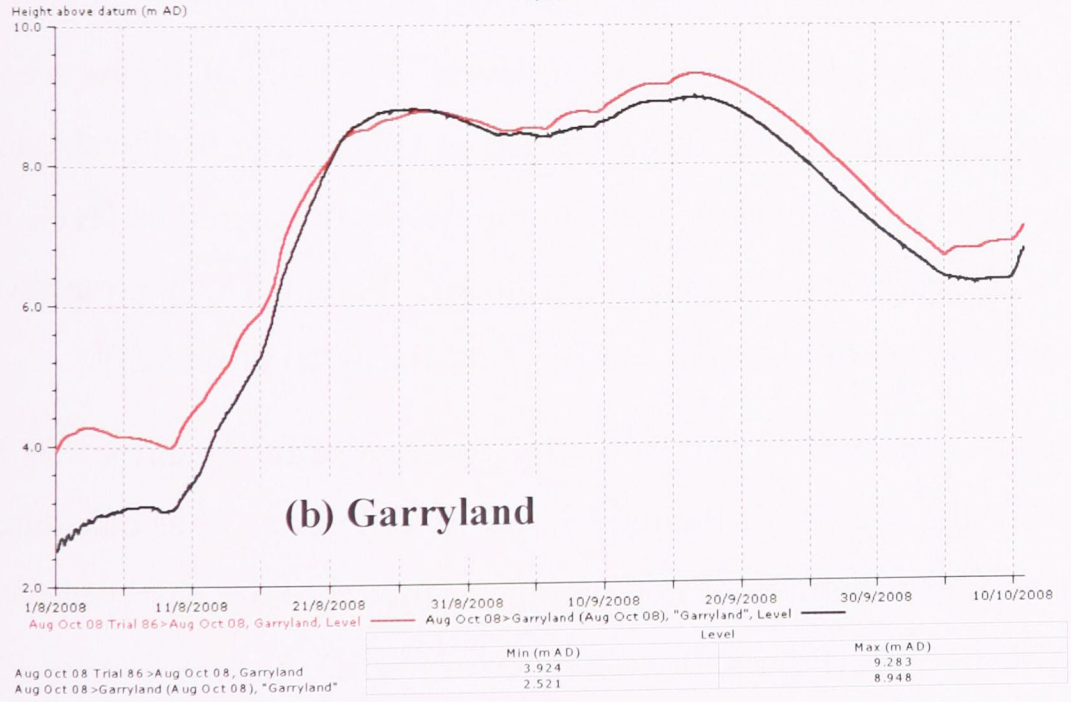
As detailed in the Literature Review for a developed karst system it is very unusual for there to be more than one main conduit in an area. The modelling indications here are that a complex network of parallel (possibly inter-linked) pipes at different levels is required to promote the observed water level dynamics. Hence, it is surmised that this could be evidence of a fairly recent (from a geological perspective) collapse karst structure in the area between Blackrock and Coy.



Figure 9.11 Blackrock-Coy hydraulic network – configuration 6 (chosen configuration).

The results from the model validation periods for the three downstream turloughs for the calibration period (August to October 2008) are shown in Figure 9.12 and show much closer fits.





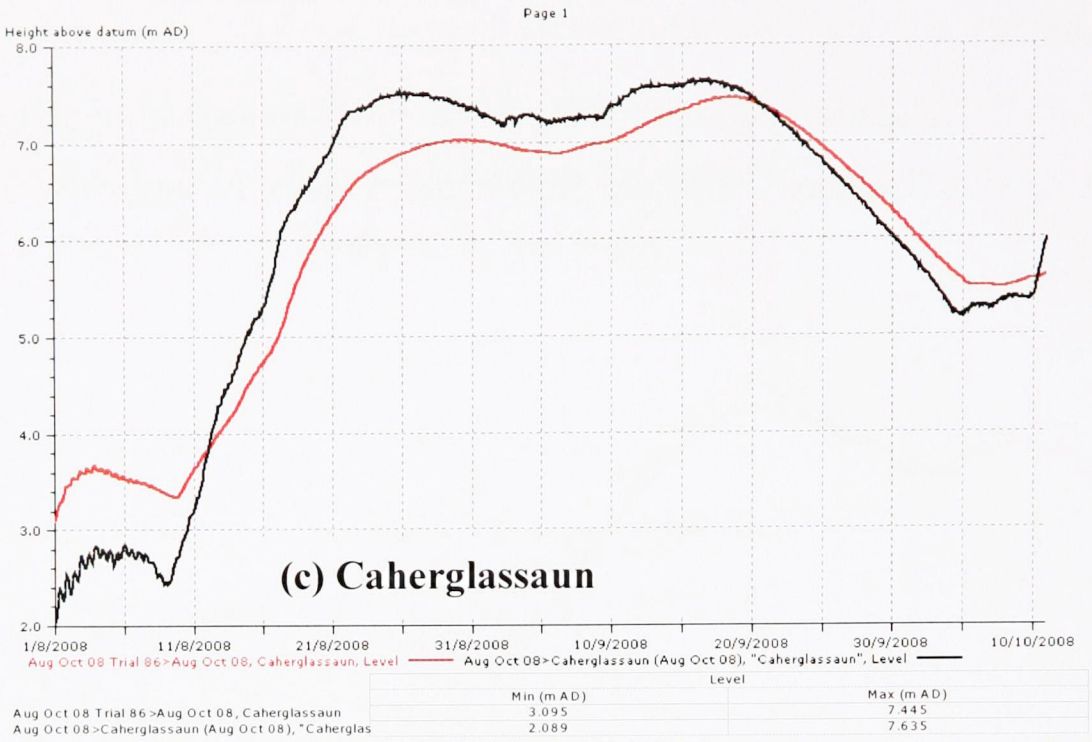


Figure 9.12 Results from model calibration (Aug to Oct 2008) at **(a)** Coole **(b)** Garryland and **(c)** Caherglassaun using configuration 6 (red line is model, black line observed level).

9.2.3 Model validation

The calibrated model was then run for two years, 2007/08 and 2008/09 using hourly data and compared against the observed turloughs water levels. The rainfall inputs were the hourly data at Kilchreest and hourly river flows gauged at Owenshree, Ballycahalan and Beagh. The Galway Bay tidal measurements every 6 minutes were entered as levels at the bottom of the system at Kinvarra (the system outlet node). Potential evapotranspiration was entered as daily data (average of Shannon and Birr), as discussed previously.

The results are presented in Figures 9.13 and 9.14 and goodness of fit parameters in Table 9.2. The main criterion for the success of the model was its efficiency, E as calculated by Equation. 8.8 (Chapter 8). Other methods of comparing the model to the observed data are the mean square error (MSE), bias (Eqn. 8.9), volume error (VER), peak flow error (QER) and peak time error (TER) (Lee and Singh, 1999). Peak flow and time error were not calculated as it is difficult to distinguish true peak times in either the observed data or the model with many of the turlough signals – however the plots show excellent timing.

$$MSE = \left[\frac{\sum (Q_{obs} - Q_{sim})^2}{n} \right]^{0.5} \quad \text{Eqn. 9.1}$$

$$VER = \frac{\sum Q_{obs} - \sum Q_{sim}}{\sum Q_{obs}} \times 100 \quad \text{Eqn. 9.2}$$

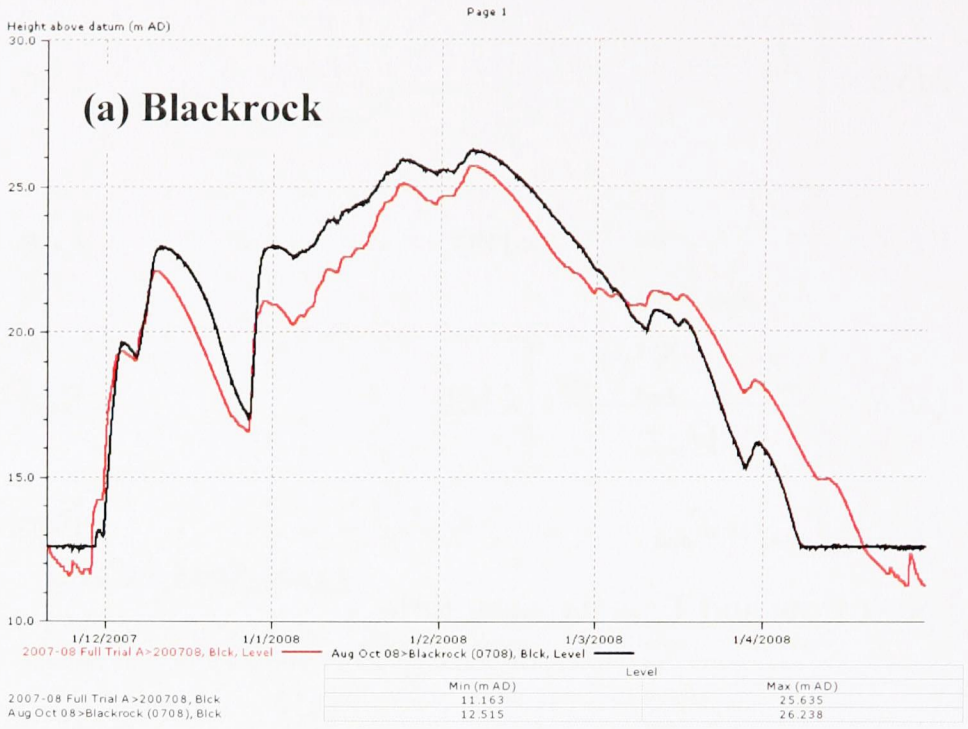
$$QER = \left[\frac{Q_{pobs} - \sum Q_{pest}}{Q_{pobs}} \right] \times 100 \quad \text{Eqn. 9.3}$$

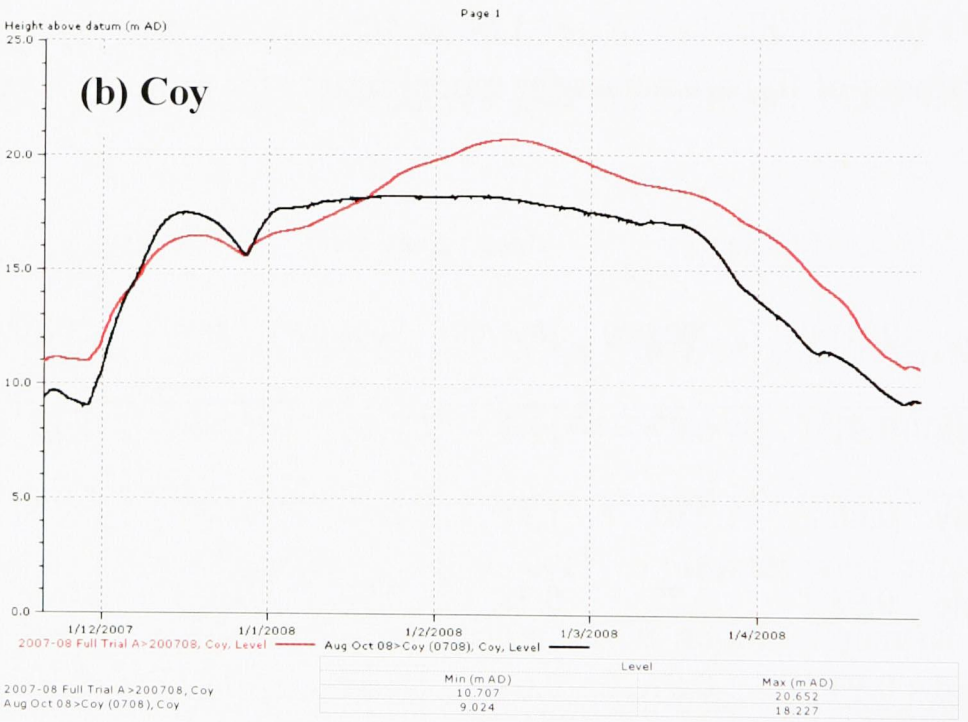
$$TER = T_{pobs} - T_{pest} \quad \text{Eqn. 9.4}$$

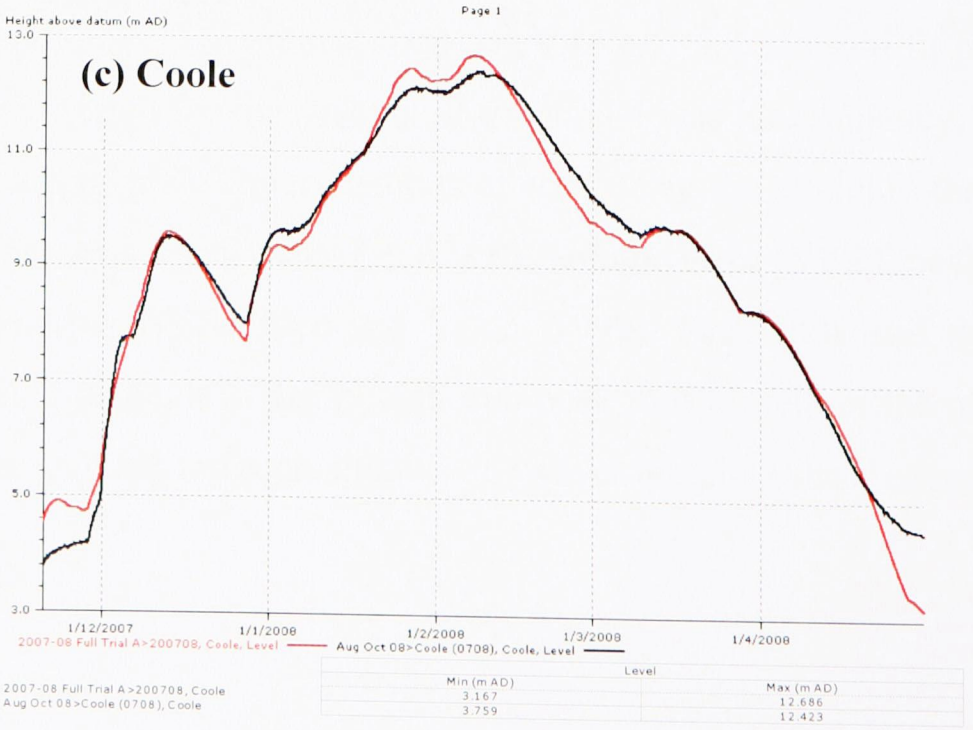
where Q_p is the peak flow and T_p is the peak time.

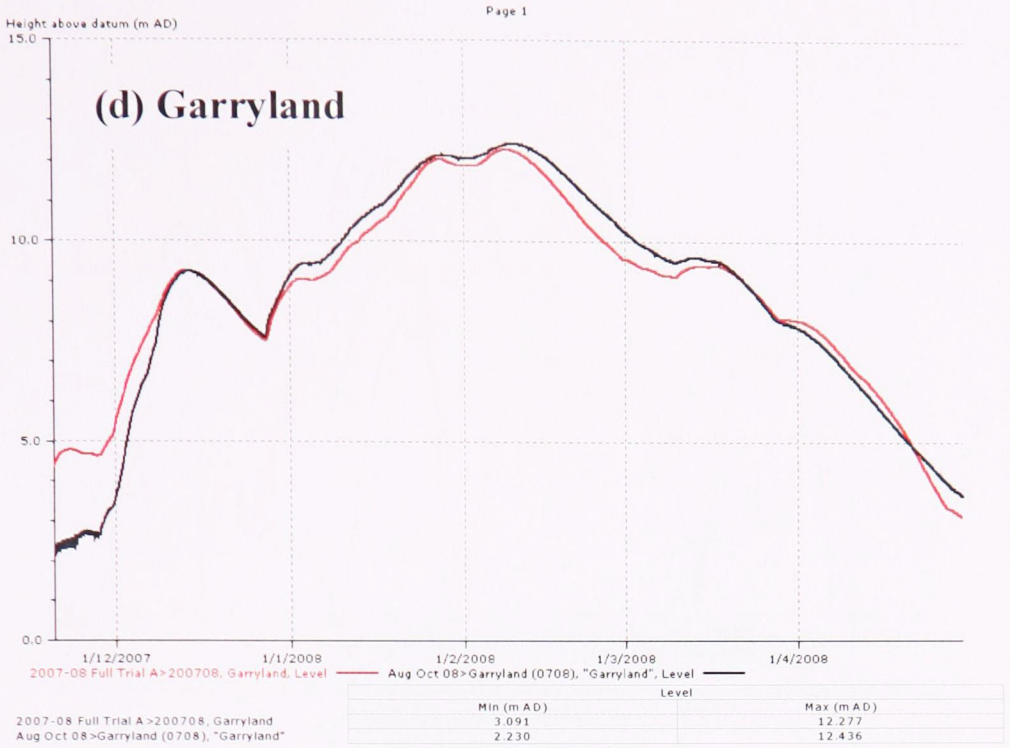
Table 9.2 Goodness-of fit parameters for model results for turlough level data (2007/08 and 2008/09).

	Efficiency		Mean square error		Bias		Volume error	
	2007/08	2008/09	2007/08	2008/09	2007/08	2008/09	2007/08	2008/09
Blackrock	0.91	0.27	1.41	3.26	0.27	-1.75	0.014	-0.100
Coy	0.66	0.02	1.81	2.57	-1.23	-1.55	-0.079	-0.106
Coole	0.98	0.72	0.35	0.90	0.034	0.697	0.004	0.087
Garryland	0.94	0.97	0.68	0.38	-0.017	-0.107	-0.002	-0.015
Caherglassaun	0.58	0.91	1.58	0.56	1.372	0.225	0.191	0.038


Page 1
Height above datum (m AD)
(a) Blackrock
30.0
25.0
20.0
15.0
10.0
1/12/2007
1/1/2008
1/2/2008
1/3/2008
1/4/2008
2007-08 Full Trial A>200708, Blck, Level
Aug Oct 08>Blackrock (0708), Blck, Level
Level
Min (m AD)
Max (m AD)
2007-08 Full Trial A>200708, Blck
11.163
25.635
Aug Oct 08>Blackrock (0708), Blck
12.515
26.238


Page 1
Height above datum (m AD)
(b) Coy
25.0
20.0
15.0
10.0
5.0
0.0
1/12/2007
1/1/2008
1/2/2008
1/3/2008
1/4/2008
2007-08 Full Trial A>200708, Coy, Level
Aug Oct 08>Coy (0708), Coy, Level
Level
Min (m AD)
Max (m AD)
2007-08 Full Trial A>200708, Coy
10.707
20.652
Aug Oct 08>Coy (0708), Coy
9.024
18.227


Page 1
Height above datum (m AD)
(c) Coole
13.0
11.0
9.0
7.0
5.0
3.0
1/12/2007
1/1/2008
1/2/2008
1/3/2008
1/4/2008
2007-08 Full Trial A>200708, Coole, Level
Aug Oct 08>Coole (0708), Coole, Level
Level
Min (m AD)
Max (m AD)
2007-08 Full Trial A>200708, Coole
3.167
12.686
Aug Oct 08>Coole (0708), Coole
3.759
12.423



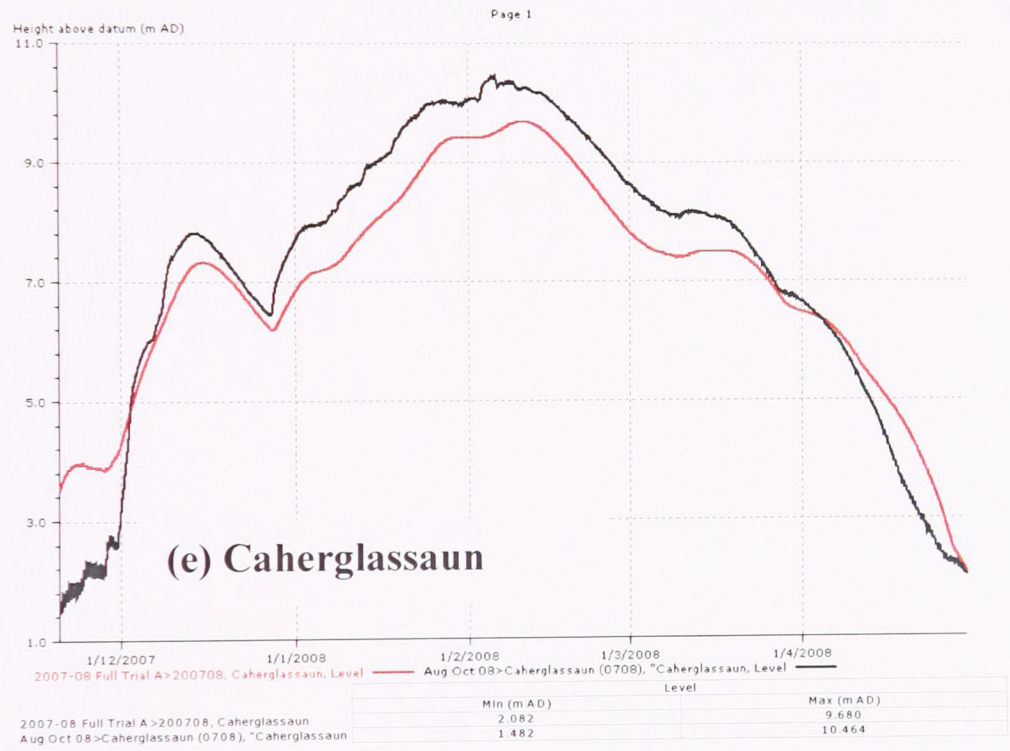
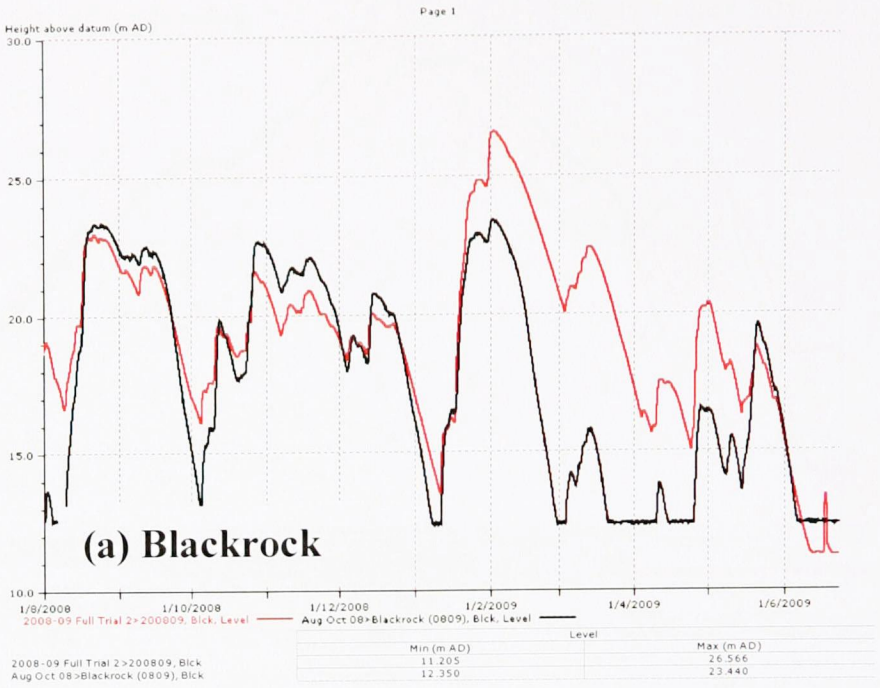
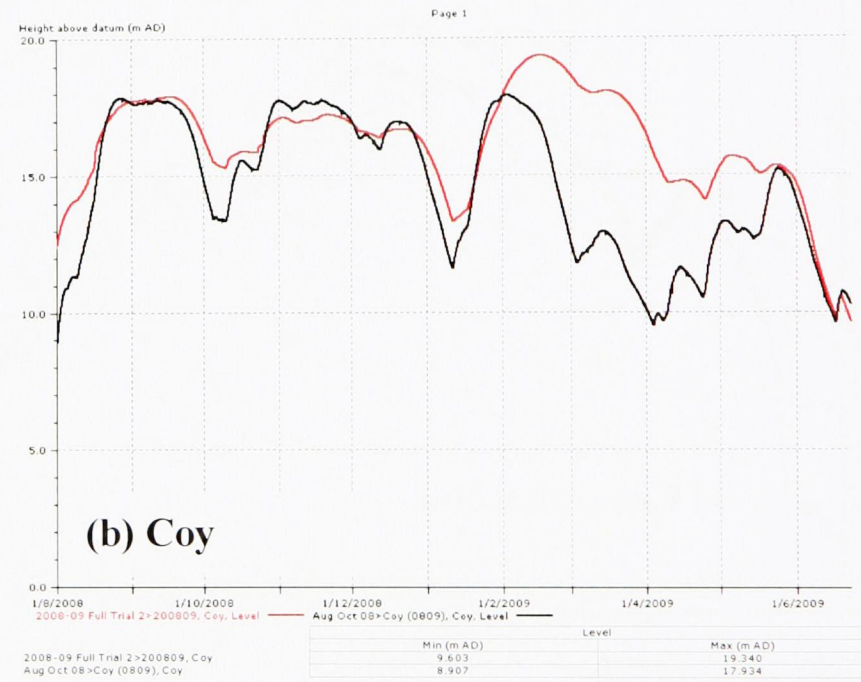
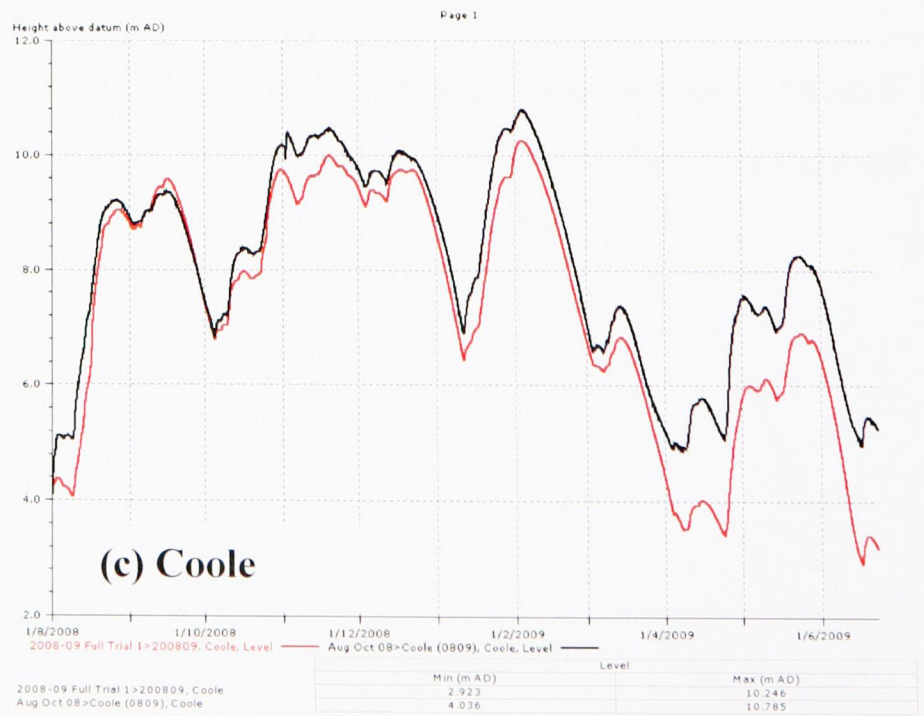
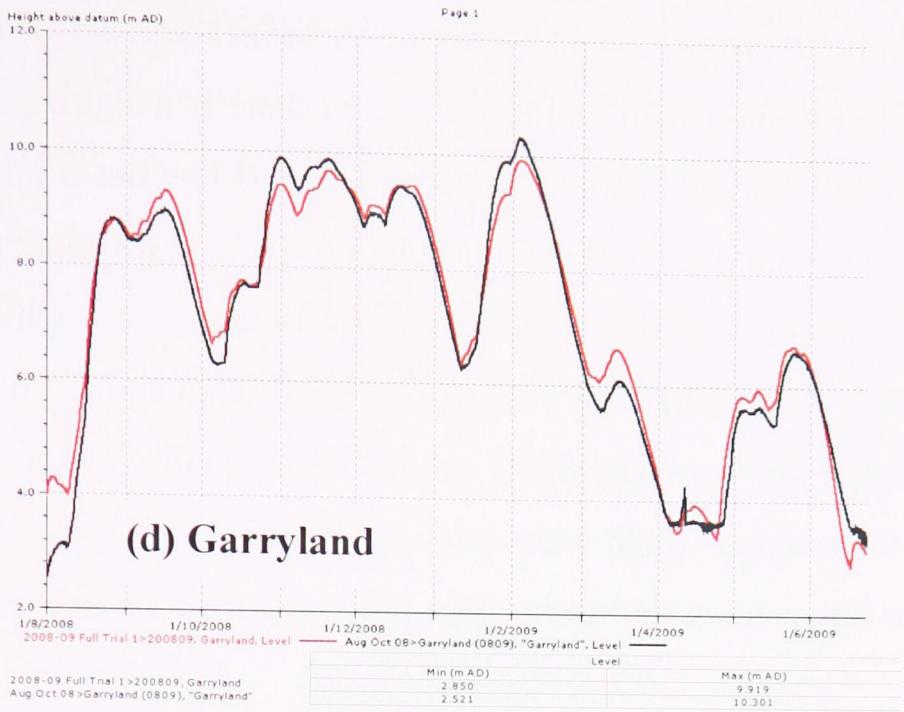


Figure 9.13 Results from model calibration (2007/08) using the measured river flows as inflows into the karst network model.


Page 1
Height above datum (m AD)
30.0
25.0
20.0
15.0
10.0
1/8/2008
1/10/2008
1/12/2008
1/2/2009
1/4/2009
1/6/2009
(a) Blackrock
2008-09 Full Trial 2>200809, Blck, Level
Aug Oct 08>Blackrock (0809), Blck, Level
Level
Min (m AD)
Max (m AD)
2008-09 Full Trial 2>200809, Blck
11.205
26.566
Aug Oct 08>Blackrock (0809), Blck
12.350
23.440


Page 1
Height above datum (m AD)
20.0
15.0
10.0
5.0
0.0
1/8/2008
1/10/2008
1/12/2008
1/2/2009
1/4/2009
1/6/2009
(b) Coy
2008-09 Full Trial 2>200809, Coy, Level
Aug Oct 08>Coy (0809), Coy, Level
Level
Min (m AD)
Max (m AD)
2008-09 Full Trial 2>200809, Coy
9.603
19.340
Aug Oct 08>Coy (0809), Coy
8.907
17.934


Page 1
Height above datum (m AD)
12.0
10.0
8.0
6.0
4.0
2.0
1/8/2008
1/10/2008
1/12/2008
1/2/2009
1/4/2009
1/6/2009
(c) Coole
2008-09 Full Trial 1>200809, Coole, Level
Aug Oct 08>Coole (0809), Coole, Level
Level
Min (m AD)
Max (m AD)
2008-09 Full Trial 1>200809, Coole
2.923
10.246
Aug Oct 08>Coole (0809), Coole
4.036
10.785



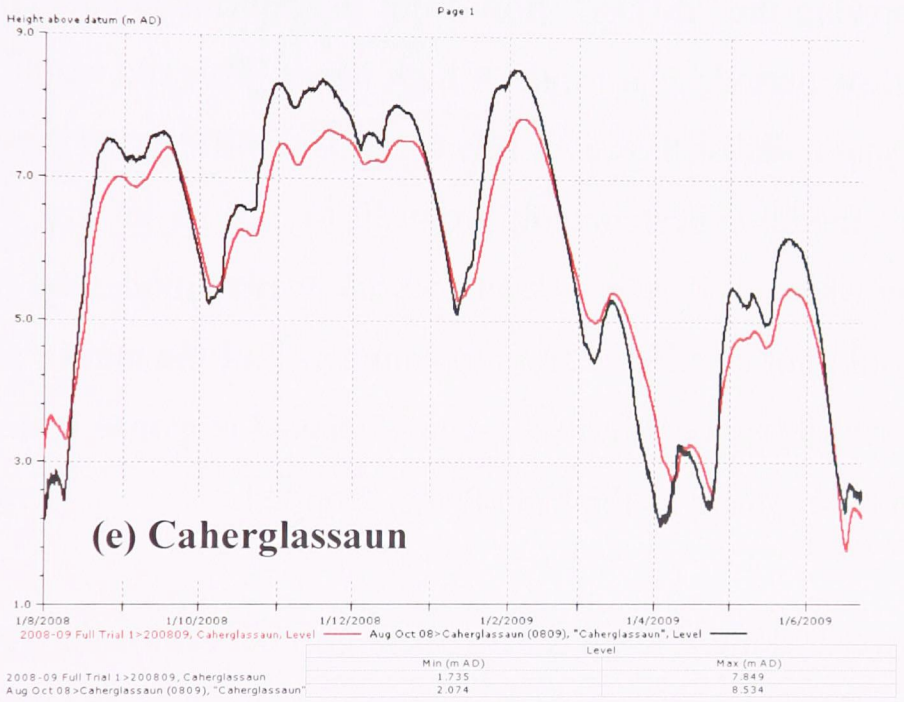


Figure 9.14 Results from model calibration (2008/09) using the measured river flows as inflows into the karst network model.

The results from 2007/08 show fairly good (and in the case of Garryland and Coole excellent) correlations. However, Coy significantly overshoots compared to the observed data which may indicate that there is some form of high level drain acting as a weir for this turlough – the peak levels certainly plateau off every year as discussed in Chapter 5. The more highly fluctuating 2008/09 simulation however, reveals an area of concern for both Blackrock and Coy, whereby later in the year (after February) the model is predicting high

water levels in both turloughs which were never in fact realised. This period corresponds to a drier time of year and might be indicative that there is a significant volume of storage in the epikarst that the model is not taking account of. When the whole network is surcharged in the winter this is not too much of a problem as there is no spare capacity in the epikarst. However, for the situation of a high flow event in the system which follows a significant dry period, there does seem to be a route for a significant amount of water which the model is not accounting for. Another, factor might be the quality of the gauging curves derived for the river Owenshree which were extended for high flows and therefore might be over-predicting the flows down into the system following heavy rain events.

The pipes carrying the "diffuse" flow from the subcatchments could be seen to back up during high flow periods as a result of high heads. This did result in some loss of volume into the notional epikarst, however this was not significant as the model was only using a single pipe to model subcatchments from 30 to 120 ha in size. Although the permeable pipes solution was considered to be an accurate way to model the flow characteristics from the area, it could not mimic the storage volume of all the matrix and fractures across such areas. The permeable pipes showed a much delayed response in draining water back down into the main pipe system as the head levels dropped.

Again the lower turloughs show an excellent correlation for the 2008/09 hydrological year although Caherglassaun does not surcharge enough. It is also interesting to see that the model is clearly simulating the tidal effects at Caherglassaun, Garryland and Coole at shallow depths as observed and picked up in the time series analyses. It should be noted that the model is much more sensitive at lower depths due to the bowl shaped topography of the turloughs and so what might appear to be significant differences in level only represents relatively small volumes of water.

Finally, it would be interesting to run the model using daily data input values (river flows, and rainfall in particular) to see the sensitivity of the results to the coarseness of the input data.

9.2.4 Gort lowland system statistics

A plot of the net flows into system (rivers) and out of the system at Kinvarra West spring is shown in Figure 9.15 which shows the damping effect that the network of linked pipes and turloughs has on the input signals.

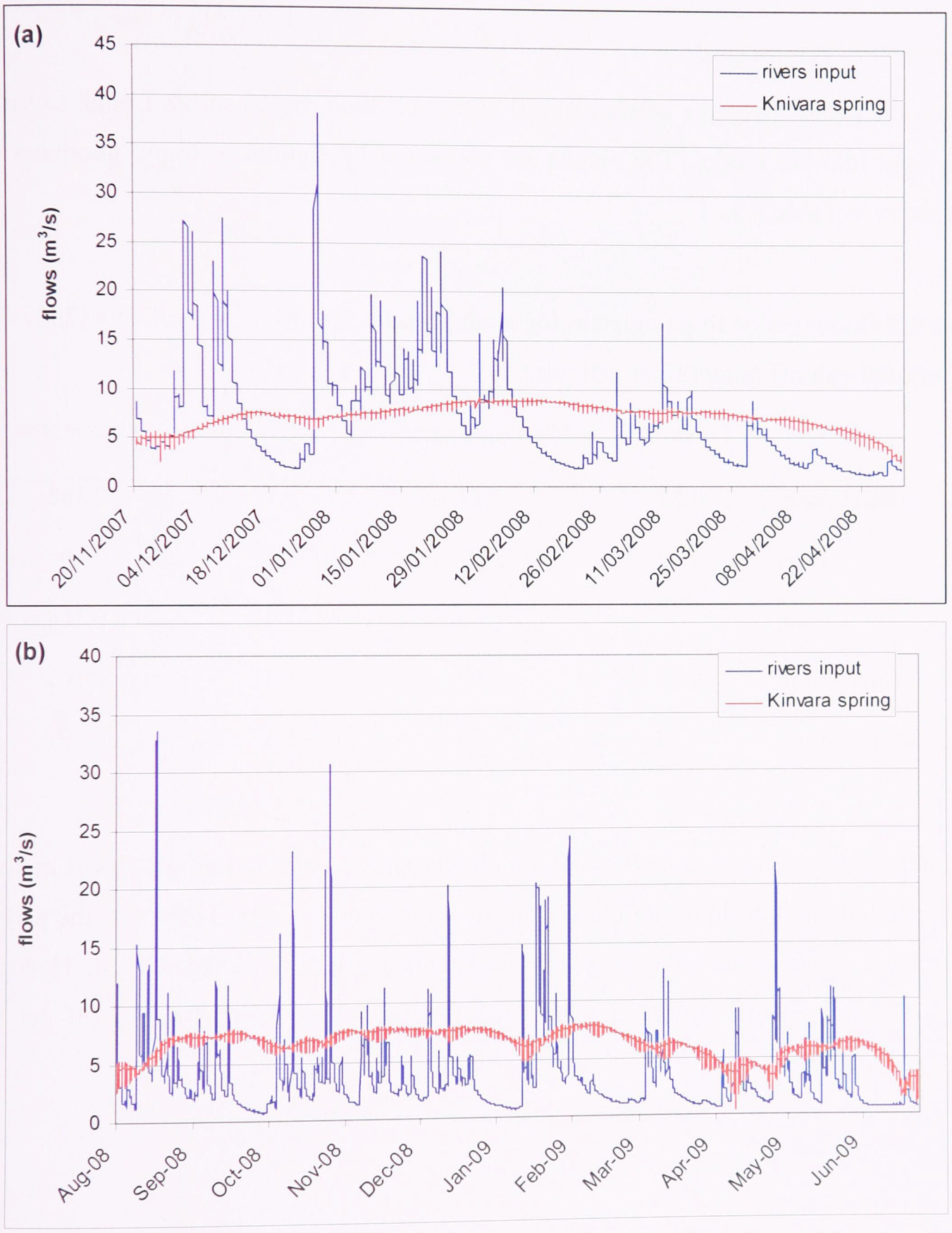


Figure 9.15 Net flows into system (rivers) plotted against flows out of the spring at Kinvara **(a)** 2007/08 and **(b)** 2008/09.

A further interesting study would be to derive a transfer function for the whole Gort lowland karst system – a black box model – for comparison with this physically based model.

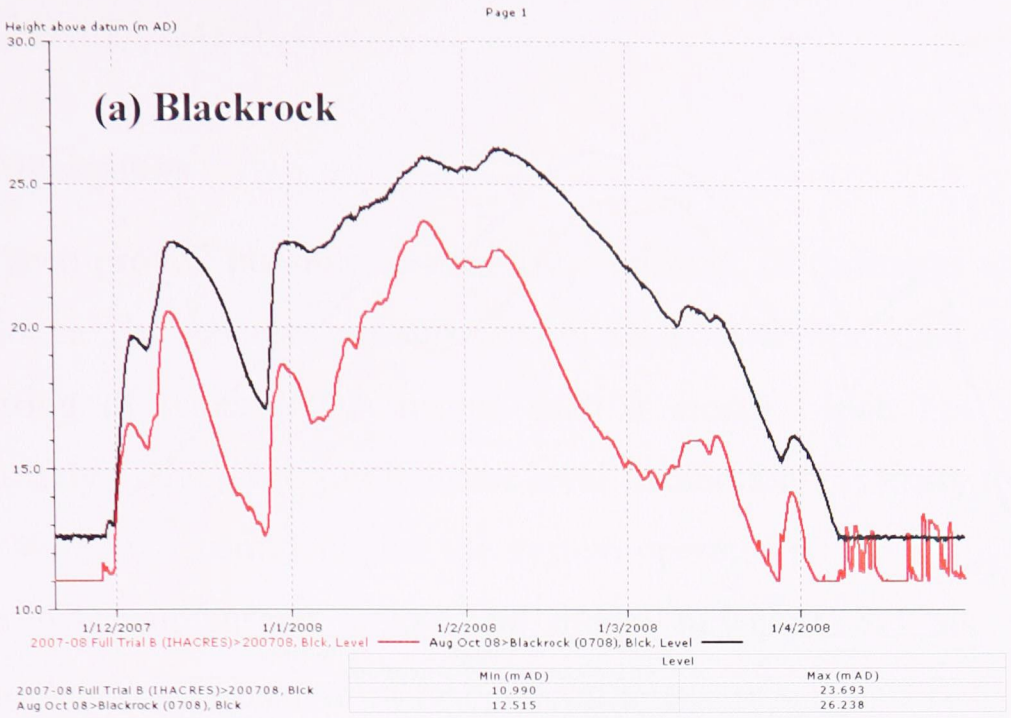
9.3 Linked Model validation

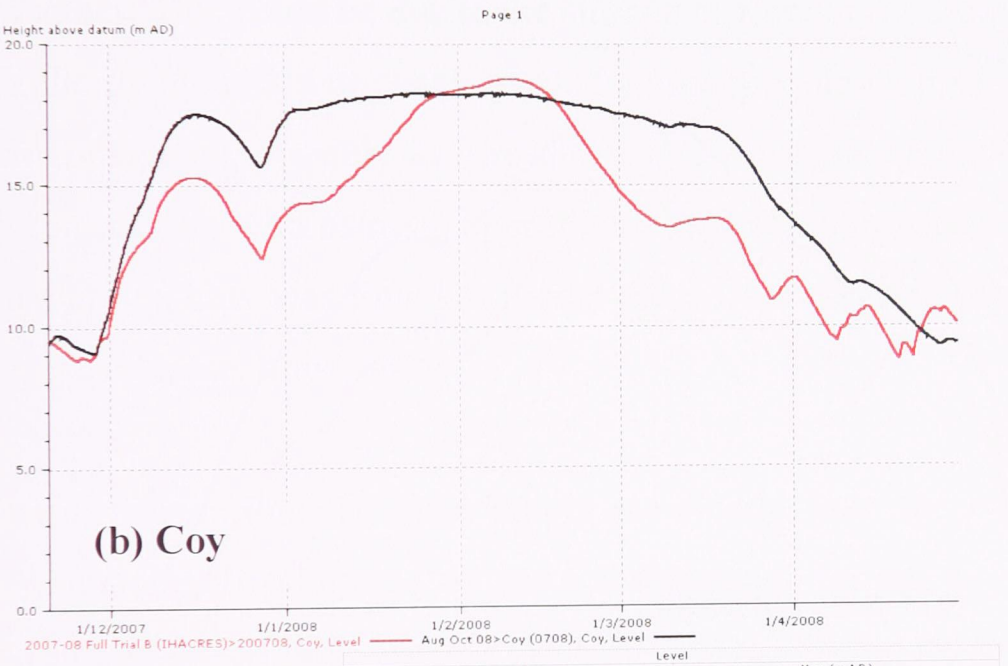
Finally, the results from the rainfall-runoff and river flood routed across Lough Cutra have been input into the model. The results are presented in Figures 9.16 and goodness of fit parameters in Table 9.3.

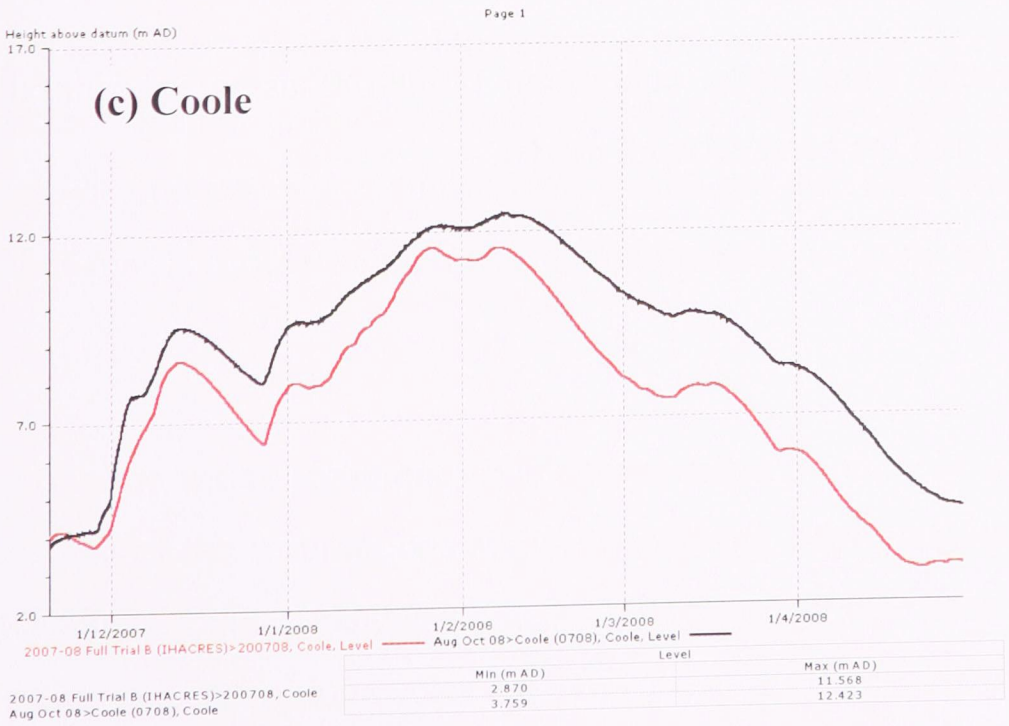
Table 9.3 Goodness-of fit parameters for model results for turlough level data (2007/08) with rainfall-ruinoff model river inflows.

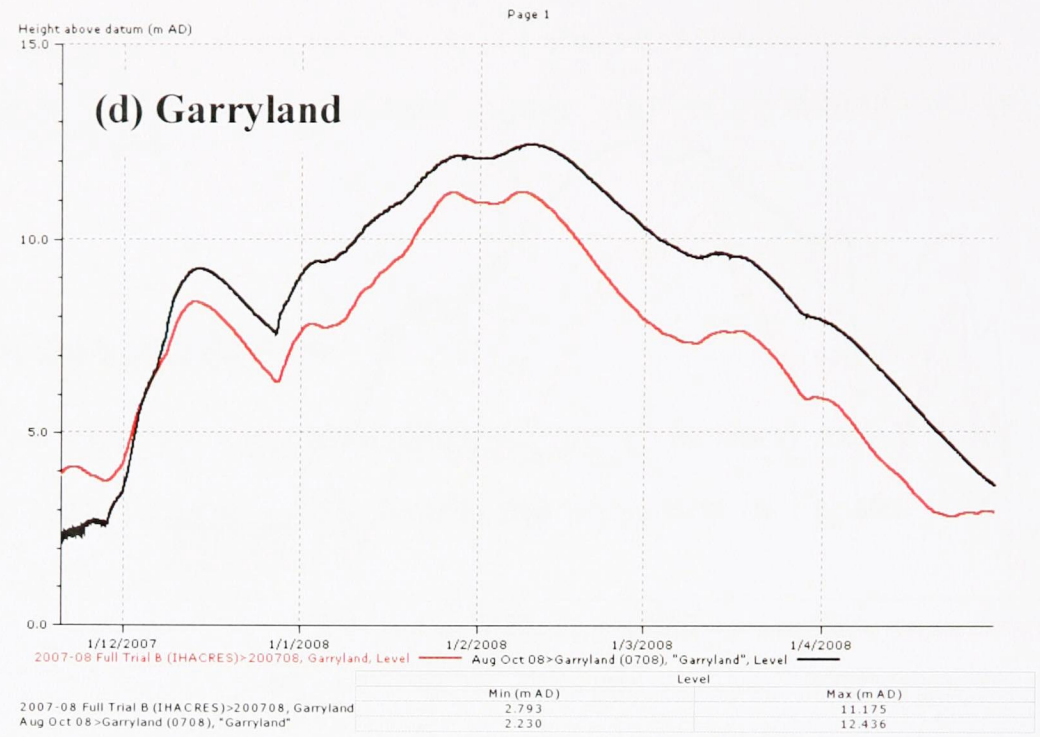
	Efficiency	Mean square error	Bias	Volume error
Blackrock	0.23	4.17	3.72	0.188
Coy	0.50	2.19	1.67	0.108
Coole	0.53	1.65	1.51	0.168
Garryland	0.63	1.69	1.41	0.163
Caherglassaun	0.58	1.58	1.37	0.191

The plots are shown in Figure 9.16 which clearly shows that the rainfall-runoff model has not generated enough flow into the system to surcharge the tanks. However, the pattern in water level movement and timing and fluctuations are still modeled well. Hence, this shows that more work is needed with respect to modelling rainfall-runoff off the Slieve Aughty mountains.


Page 1
Height above datum (m AD)
30.0
25.0
20.0
15.0
10.0
(a) Blackrock
1/12/2007
1/1/2008
1/2/2008
1/3/2008
1/4/2008
2007-08 Full Trial B (IHACRES)>200708, Blck, Level
Aug Oct 08>Blackrock (0708), Blck, Level
Level
Min (m AD)
Max (m AD)
2007-08 Full Trial B (IHACRES)>200708, Blck
10.990
23.693
Aug Oct 08>Blackrock (0708), Blck
12.515
26.238


Page 1
Height above datum (m AD)
20.0
15.0
10.0
5.0
0.0
(b) Coy
1/12/2007
1/1/2008
1/2/2008
1/3/2008
1/4/2008
2007-08 Full Trial B (IHACRES)>200708, Coy, Level
Aug Oct 08>Coy (0708), Coy, Level
Level
Min (m AD)
Max (m AD)
2007-08 Full Trial B (IHACRES)>200708, Coy
8.739
18.751
Aug Oct 08>Coy (0708), Coy
9.024
18.227


Page 1
Height above datum (m AD)
17.0
12.0
7.0
2.0
(c) Coole
1/12/2007
1/1/2008
1/2/2008
1/3/2008
1/4/2008
2007-08 Full Trial B (IHACRES)>200708, Coole, Level
Aug Oct 08>Coole (0708), Coole, Level
Level
Min (m AD)
Max (m AD)
2007-08 Full Trial B (IHACRES)>200708, Coole
2.870
11.568
Aug Oct 08>Coole (0708), Coole
3.759
12.423



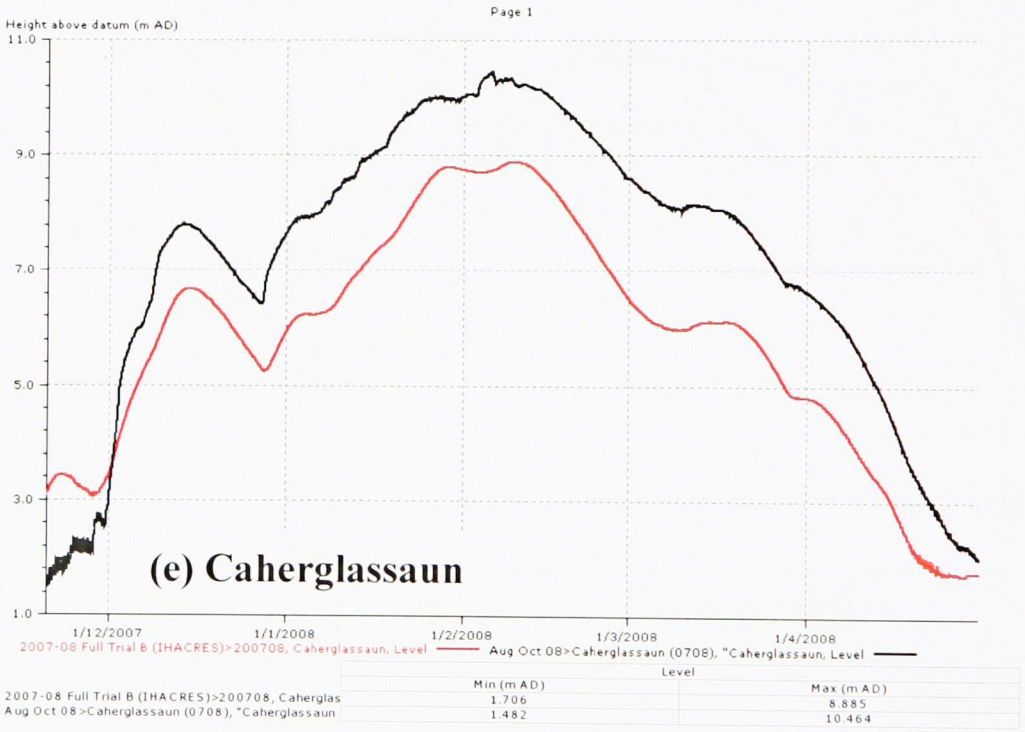


Figure 9.16 Results from model calibration (2007/08) using the rainfall-runoff model results as inflows into the karst network model.

10 CONCLUSIONS

10.1 Conclusions

It has been proved possible to model the network of turloughs using a pipe network and tank model. The accurate measurement of each of the turloughs topography and continuous monitoring of water levels means such a model which has such a closeness of fit (particularly to the more subtle water level fluctuations) is likely to be close to the physical reality – i.e. it is confident that the system operates on the basis of a significant conduits system with surcharged tanks. The model however, did not accurately simulate the Blackrock and Coy system in response to heavy rain events following significant periods of dry weather. This could be due to the storage of flow in the drained epikarst which is not being explicitly modelled or possibly due to a more complex pipe network in the area than has been considered, possibly as a result of a collapse structure. The combination of soil store in conjunction with using the permeable pipe solution which is controlled by laminar flow via Darcy's Law was found to model the diffuse flow contribution well with volume and timing of release, however.

The network shows that the main inputs are clearly from the rivers draining the Slieve Aughty mountains. Blackrock, Coy and Caherglassaun operate as surge tanks whilst Coole appears to be river fed with Garryland really just an off-line storage volume as part of the Coole complex. The combination of the rainfall-runoff model to provide inputs into the karst system did promote the right patterns of water level fluctuation in the simulated turloughs but did not provide enough flow to fill the turloughs adequately. Hence, more work is needed on both the rainfall-runoff model and also calibrating the network model to the rainfall-runoff model outputs if this combination is going to be used as a predictive tool.

The use of time series techniques has shown some promise as a tool and has helped to confirm some of the assumptions about the network configuration. The tidal effect in the lower turloughs Coole, Garryland and Caherglassaun has been picked up, as well as possible diurnal evaporation cycles in Coole and Garryland at shallow depths. The FFT has

proved to be a powerful technique and has helped to identify some of the linkages in the network. The use of wavelets has generally corroborated the findings from the FFT but the DWT (db4) technique has also suggested the hypothesis that a significant driving factor for turlough inundation in the Gort lowland might be a combination of the heavy rainfall events occurring at times of spring tides. Such a hypothesis can be checked by looking back at tidal records and rain statistics with respect to the major flooding episodes in the 1990s. The CWT technique was more difficult to interpret if used in isolation without having first done the FFT and DWT.

The water quality analyses has revealed some interesting dynamics and confirmed that the main spring for the system is Kinvara West. However, it would be interesting to look at net fluxes from the rivers and into the turloughs to determine the proportion of nutrients which have been generated in-turlough compared to those coming in with the inflows – this might show that the turloughs act as a net source of nutrient to groundwater for example, which has interesting legislative connotations. Finally, the use of $\delta^{18}O$ stable isotopes sampled at different points along the network and in the epikarst has shown some promise but more work is needed in the future to see whether the signatures can be used to source apportion the flow from the epikarst and man conduit lines into each turlough.

10.2 Further Research

Recommendations

River gauging

- The accuracy of the model is obviously susceptible to high flow events and there is some concern that the extended rating curves are overestimating the flows. Hence, there is a need to continue to improve the rating curves, especially at high flows. This will also help to clarify whether the model in the Blackrock-Coy area should include a significant storage element to model the drained epikarst following dry periods. The gauge on the Owenshree at Kilchreest also needs to be reset to read at low flow events as it is too high. In addition, the flows into Coole should also be

gauged for a period to confirm that it is mainly river fed (and matches the model simulation results).

Diffuse flow contribution

- More targeted research on the contribution of diffuse flow into the conduit network is needed. For example, monitoring the speed of response of the water table around the turloughs i.e. what is the dynamic relationship between the turlough water level and groundwater levels which can be measured by monitoring nearby boreholes / wells. Further monitoring of Owenshree river between Kilchreest and Blackrock should take place throughout the year to establish realistic epikarst input. A full analysis of the system could be carried out on the basis of a mass balance of ^{18}O, using known inflows from the river, known rainfall inputs and evaporation due to fluctuating lake surface areas and the turlough values, which should allow the missing input (i.e. diffuse inflows from the epikarst) to be quantified.

Rainfall analysis

- A much more detailed analysis of rainfall across the area needs to be carried out in order to get better input values for the model and link it to daily input rainfall data. Indeed the accuracy of the model needs to be compared in response to daily input rainfall data. Such rainfall analysis could use stochastic techniques and then be used as a predictive tool in conjunction with the model. For example, previous research into rainfall patterns in the west of Ireland (Chandler and Wheater, 2002) has used a Generalised Linear Modelling approach where potential predictors are used to forecast a probability distribution for daily values at a specified location.

Development of transfer function model

- Further use of time series techniques (in particular Discrete Wavelet Transform based techniques) should be made to compare river inflows into the Got lowlands with respect to the spring outflow at Kinvara. A back-box transfer function model could then be developed.

Hydraulic properties of karst network and future development

- There is much further research that can be done using the karst network model with respect to hydraulic properties of a karst conduit system. For example, the velocities at different points on the network could be compared against respective hydraulic gradient. Friction factors should also be determined for the system conduits and compared to other studies. The storage of water in the Gort lowlands across the hydrological year should also be calculated by taking the difference between the cumulative inflows and simulated outflows. Another interesting comparison would be to correlate simulated spring flow against estimated hydraulic conductivity (K) for the overall system (or between turloughs). This might pick up some form of hysteresis loop which could be indicative of stage dependent internal routing of the water as has been found by other researchers (e.g. Bonacci and Roje-Bonacci, 2000; Rozos and Koutsoyiannis, 2006).

Relevant hydrological parameters for vegetation and fauna (conservation)

- The model should be used to help to examine the relationship of vegetation and invertebrates to hydrological indicators / parameters. For example, depth-duration frequency curves, areal rates of change, shoreline velocities etc are all parameters that can easily be derived from the model's output. This can then be used with the results from the NPWS project with respect to vegetation and invertebrates.

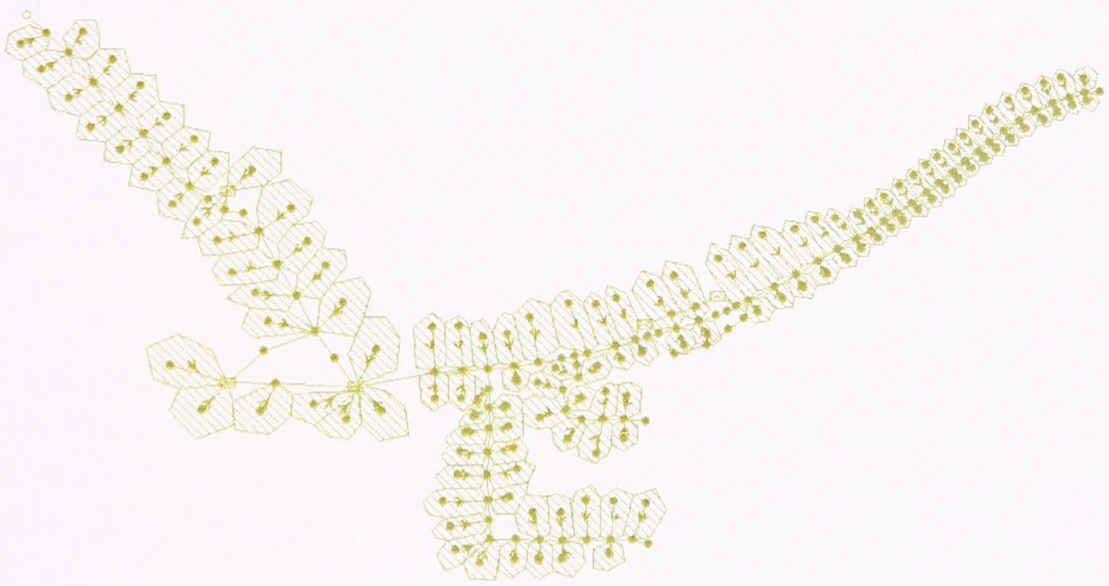
Predictive use of the model

- The model should be used with appropriate historic rainfall records to back-calculate the levels in turloughs to time before their levels were being monitored. This will be particularly interesting information for the botanical and invertebrate studies. Equally, the model should be used to make future predictions on the levels of the turloughs with regards to Climate Change predictions. For example, the C4I Project (Community Climate Change Consortium for Ireland) predicts warmer temperatures with 10-15% higher rainfall in winter (and drier in summer). It also predicts a 3.5 cm sea level rise per decade – all of which are parameters which are

obviously intimately linked to turlough water level dynamics and can be simulated using the model.

The nutrient origin and flux through turloughs

- Interesting further work should investigate whether turloughs act as sinks or producers for nutrients in groundwater. For example, the net fluxes from the rivers and into the turloughs can be determined from which conclusions can be drawn as to whether the nutrients have been generated in-turlough or from outside. Is the chemical condition of the turloughs determined largely by conditions up-gradient or by conditions (anthropogenic?) within the turlough itself – i.e. cattle grazing / manure etc? If the former then it might be very affected by the time of year when the turlough starts to fill as runoff from the catchment at certain times may be higher in nutrients than at other times due to livestock management practices. The concept of whether turloughs act as net *exporters* of nutrients to groundwater is a critical issue with respect to the Water Framework Directive for example.



REFERENCES

Adams, R. and Parkin, G. (2001). Development of a coupled surface-groundwater-pipe network model for the sustainable management of karstic groundwater. *Proceedings of the 8th Multidisciplinary Conference on Sinkholes and the Engineering and Environmental Impacts of Karst:* Louisville, Kentucky, April 1-4, 2001.

Adams, R. and Younger, P.L. (2001). A strategy for modelling ground water rebound in abandoned deep mine systems. *Ground Water* 39(2): 249-261.

Aldous P.J., Smart, P.L. and Black, J.A. (1986). Groundwater management problems in abandoned coal-mined aquifers: a case study of the Forest of Dean, England. *Quarterly Journal of Engineering Geology* 19: 375- 388.

Angelini, P. and Dragoni, W. (1997). Problem of modelling limestone springs: the case of Bagnara (North Apennines, Italy). *Ground Water* 35(4): 612-618.

Atkinson, T.C. (1977). Diffuse flow and conduit flow in limestone terrain in the Mendip Hills, Somerset (Great Britain). *Journal of Hydrology* 35: 93-11.

Ayalon, A., Bar-Mathews, M. and Sass, E. (1998). Rainfall-recharge relationships within a karstic terrain in Eastern Mediterranean semi-arid region, Israel: $\delta^{18}O$ and $\delta^{1}D$ characteristics. *Journal of Hydrology* 207: 18-31.

Australian National University (2005). *IHACRES v2 User guide*. Integrated Catchment Assessment and Management (iCAM) Centre of The Australian National University and the Cooperative Research Centre for Catchment Hydrology. The Australian National University, Australia.

Back W., Hanshaw, B.B., Pyle, T., Plummer, L.N. and Weirdie, A.E. (1979). Geochemical significance of groundwater discharge and carbonate solution to the formation of Caleta Xel Ha, Quintana Roo, Mexico. *Water Resources Research* 15(6): 1521-1545.

Baedke, S.J. and Krothe, N.C. (2000). Quantitative tracer test of the Beech Creek aquifer at the Ammunition Burning Grounds, Naval Surface Warfare Centre, Crane, Indiana. *In*, Sasowsky I.D. & Wicks C.M (eds) *Groundwater Flow and Contaminant Transport in Carbonate Aquifers.* A.A. Balkema, Rotterdam.

Bailly-Comte, V., Jourde, H., Roesch, A., Pistre, S. and Batiot-Guilhe, C. (2008). Time series analyses for karst / river interactions assessment: case of the Coulazou river (southern France). *Journal of Hydrology* 349: 98-114.

Baker, A. and Genty, D. (1999). Fluorescence wavelength and intensity variations of cave waters. *Journal of Hydrology* 217: 19-34.

Banks D., Davies, C. and Davies, W. (1995). The Chalk as a karstic aquifer: evidence from a tracer test at Stanford Dingley, Berkshire, UK. *Quarterly Journal of Engineering Geology* 28: S31- S38.

Barnes, S. (1999). Karstic groundwater flow characteristics in the Cretaceous Chalk aquifer, Northern Ireland. *Quarterly Journal of Engineering Geology* 32: 55-68.

Barrett, M.E. and Charberneau, R.J. (1997). A parsimonious model for simulating flow in a karstic aquifer. *Journal of Hydrology* 196: 47-65.

Basu, B. and Gupta, V.K. (1998). Seismic response of SDOF systems by wavelet modelling of nonstationary processes. *Journal of Engineering Mechanics* 10:1142-1150.

Beaudeau, P., Leboulanger, T. Lacroix, M. Hanneton, S. and Wang H.Q. (2001). Forecasting of turbid floods in a coastal, chalk karstic drain using an artificial neural network. *Ground Water* 39(1): 109-118.

Bedient, P.B. and Huber, W.C. (1992). *Hydrology and Floodplain Analysis* (2nd ed.). Addison-Wesley Publishing Company, Reading, MA.

Beven, K.J. (2001*). Rainfall-Runoff Modelling: The Primer*. Wiley, New York.

Binet, S., Mudry, J., Bertrand, C., Guglielmi, Y. and Cova, R. (2006). Estimation of quantitative descriptors of northeastern Mediterranean karst behaviour: multiparametric study and local validation of the Siou-Blanc massif (Toulon, France). *Hydrogeology Journal* 14: 1107-1121.

Birk, S., Liedl, R., Sauter, M. and Teutsch, G. (2005). Simulation of the development of gypsum maze caves. *Environmental Geology* 48: 296-306.

Birk, S., Liedl, R. and Sauter, M. (2006). Karst spring responses examined by process-based modelling. *Ground Water* 44(6): 832-836.

Bonacci, O. (2004). Poljes, in *Encyclopaedia of Caves and Karst Science* (ed. J. Gunn), Fitzroy Dearborn, New York, pp. 599-600.

Bonacci, O. and Bojanić, D. (1991). Rhythmic karst springs. *Hydrological Sciences* 36(1): 35-47.

Bonacci, O. and Roje-Bonacci, T. (2000). Interpretation of groundwater level monitoring results in karst aquifers: examples from the Dinaric karst. *Hydrological Processes* 14: 2423-2438.

Burke, S.P. and Younger, P.L. (2000). Groundwater rebound in the South Yorkshire coalfield: a first approximation using the GRAM model. *Quarterly Journal of Engineering Geology and Hydrogeology* 33: 149-160.

Butscher, C. and Huggenberger, P. (2007). Implications for karst hydrology from 3D geological modelling using the aquifer base gradient approach. *Journal of Hydrology* 342: 184-198.

Caballero, E., Jimenez De Cisneros, C. and Reyes, E. (1996). A stable isotope study of cave seepage waters. *Applied Geochemistry* 11: 583-587.

Carey, M.A. and Chadha, D. (1998). Modelling the hydraulic relationship between the River Derwent and the Corallian Limestone aquifer. *Quarterly Journal of Engineering Geology* 31: 63-72.

Chadwick, A., Morfett, J. and Borthwick, M. (2004). *Hydraulics in Civil and Environmental Engineering* (4th ed.). Spon, London.

Chandler, R.E. and Wheater, H.S. (2002). Analysis of rainfall variability using generalized linear models: a case study from the west of Ireland. *Water Resources Research* 18(4): 1192.

Chowdhury, A.H., Uliana, M. and Wade, S. (2008). Ground water recharge and flow characterization using multiple isotopes. Ground Water 46(3): 426-436.

Clark, I. and Fritz, P. (1997). *Environmental isotopes in Hydrogeology*. Lewis Publishers, Boca Raton, FL.

Clemens, T., Hückinghaus, D., Sauter, M., Liedl, R. and Teutsch, G. (1998). Simulation of the evolution of maze caves. *Bulletin d'Hydrogéologie* 16:201–210.

Coplen, T.B. (1994). Reporting of stable hydrogen, carbon and oxygen isotopic abundances. *Pure and Applied Chemistry* 66: 273-276.

Coxon, C. (1987). An examination of the characteristics of turloughs using multivariate statistical techniques. *Irish Geography* 20, 24-42.

Coxon, C. (1994a). Carbonate deposition in turloughs (seasonal lakes) on the western limestone lowlands of Ireland. I: Present day processes. *Irish Geography* 27: 14-27.

Coxon, C. (1994b). Carbonate deposition in turloughs (seasonal lakes) on the western limestone lowlands of Ireland. II: The sedimentary record. *Irish Geography* 27: 28-35.

Craig, H. (1961). Isotopic variation in meteoric water. *Science* 133: 1702-1703.

Curl, R.L. (1974). Deducing flow velocity in cave conduits from scallops. *National Speleological Society Bulletin* 36: 1-5.

Daly, D., Dassargues, A., Drew, D., Dunne, S., Goldscheider, N., Neale, S., Popescu, I.C. and Zwahlen, F. (2002). Main concepts of the "European approach" to karst-groundwater-vulnerability assessment and mapping. *Hydrogeology Journal* 10: 340-345.

Darcy, H. (1856). *Les fontaines publiques de la Ville de Dijon*. Dalmont, Paris, France.

Debieche, T.H., Guglielmi, Y. and Mudry, J. (2002). Modelling the hydraulic behaviour of a fissured-karstic aquifer in exploitation conditions. *Journal of Hydrology* 257: 247-255.

De Lima, M.I.P. and Grasman, J. (1999). Multifractal analysis of 15 minute daily rainfall from a semi-arid region in Portugal. *Journal of Hydrology* 220: 1-11.

Denić-Jukić V. and Jukić, D. (2003). Composite transfer functions for karst aquifers. *Journal of Hydrology* 274: 80-94.

Dreiss, S.J. (1982). Linear kernels for karst aquifers. *Water Resources Research* 38 (10): 865-876.

Dreiss, S.J. (1989a). Regional scale transport in a karst aquifer. 1.Component separation of spring flow hydrographs. *Water Resources Research* 25(4), 117-125.

Dreiss, S.J (1989b). Regional scale transport in a karst aquifer. 2.Linear systems and moment analysis. *Water Resources Research* 25(4), 126-134.

Drew, D.P. (1990). The hydrology of the Burren, Co. Clare. *Irish Geography* 23: 69-89.

Drew, D.P. and Daly, D. (1993). Groundwater and karstification in Mid Galway, South Mayo and North Clare. Geological Survey of Ireland, Report Series RS 93/3.

Drew, D.P., Doerfliger, N. and Formentin, K. (1997). The use of bacteriophages for multi-tracing in a lowland karst aquifer in western Ireland. *In:* Kranjc, A. (ed.) *Tracer Hydrology*. Balkema, Rotterdam, 33-38.

Drew, D.P. (2002). The karst environment and karst hydrogeology. In: *Proceedings of the Geotechnical and Hydrogeological Aspects of Karst in Ireland – Working Group on Karst,* Tullamore, County Offaly, Ireland.

Drew, D. P. (2008). Hydrogeology of lowland karst in Ireland. *Quarterly Journal of Engineering Geology and Hydrogeology* 41: 61-72.

Dreybrodt, W. (1990). The role of dissolutional kinetics in the development of karst aquifers in limestone: a model simulation of karst evolution. *Journal of Geology* 98: 639-655.

Dreybrodt, W. (1992). Dynamics of karstification: a model applied to hydraulic structures in karst terrains. *Hydrogeology Journal* 1(3): 20-32.

Dreybrodt, W. (1996). Principles of early development of karst conduits under natural and man-made conditions revealed by mathematical analysis of numerical models. *Water Resources Research* 32: 2923-2935.

Dufresne, D.P. and Drake, C.W. (1997). Wellfield site selection and groundwater flow model construction of the karst area in Lake City, Columbia County, Florida. *Proceedings of the 6th Multidisciplinary Conference on Sinkholes and the Engineering and Environmental Impacts of Karst*: Springfield, Missouri: April 6-9, 1997.

Einsiedl, F. (2005). Flow system dynamics and water storage of a fissured-porous karst aquifer characterized by artificial and environmental tracers. *Journal of Hydrology* 312: 312-321.

Eisenlohr L., Bouzelboudjen, M., Király, L. and Rossier, Y. (1997). Numerical versus statistical modelling of natural response of a karst hydrological system. *Journal of Hydrology* 202: 244-262.

Ellis, B.M. (1988). *An introduction to cave surveying*. British Cave Research Association, Buxton, England.

Estrela, T. and Sahuquillo, A. (1997). Modelling the response of a karstic spring at Arteta Aquifer in Spain. *Ground Water* 35(1): 18-24.

EC (2000). Council Directive 2000/60/EC establishing a framework for Community action in the field of water policy. *Official Journal no. L 321/1, 22.12.2000.*

EEC (1992). Council Directive 92/43/EEC on the conservation of natural habitats and of wild fauna and flora. *Official Journal no. 206, 27.7.92.*

EN ISO 748 (2007). *Hydrometry -Measurement of liquid flow in open channels using current meters or floats*. International Organisation for Standardization, Geneva.

Environmental Protection Agency (2004). *Guidance on the assessment of pressures and impacts on groundwater dependant terrestrial ecosystems, Risk Assessment Sheet GWDTERA2a – Risk to turloughs from phosphate*. Water Framework Directive Pressures and Impacts Assessment Methodology, Guidance Document GW9. Working Group on Groundwater, Subcommittee on Turloughs.

Ewen, J., Parkin, G. and O'Connell, P.E. (2000). SHETRAN: a coupled surface/ subsurface modelling system for 3D water flow, sediment and contaminant transport in river basins. *ASCE Journal of Hydrologic Engineering* 5(3): 250-258.

Falcone, R.A. Falgani, A., Parisse, B., Petitta, M., Spizzico, M. and Tallini, M. (2008). Chemical and isotopic ($\delta^{18}O‰$, $\delta^{2}H‰$, $\delta^{13}C‰$, ^{222}Rn) multi-tracing for groudnwater cocneptual model of carbonate aquifer (Gran Sasso INFN underground laboratory – central Italy). *Journal of Hydrology* 357: 368-388.

Field, M.S. and Pinsky, P.F. (2000). A two-region non-equilibrium model for solute transport in solution conduits in karstic aquifers. *Journal of Contaminant Hydrology* 44: 329-351.

Fitzsimons, V., Daly D., Wright, G. & Hunter-Williams, T. (2005). Rock type versus fractures – current understanding of Irish aquifers. *In: Groundwater in Ireland: Proceedings of the International Association of Hydrogeologists (Irish Group) 25th Annual Groundwater Conference, Tullamore,* International Association of Hydrogeologists (Irish Group), Dublin, 17-28.

Fleury, P., Bakalowicz, M. and de Marsily, G. (2007a). Submarine springs and coastal karst aquifers. *Journal of Hydrology* 339: 79-92.

Fleury, P., Plagnes, M. and Bakalowicz, M. (2007b). Modelling of the functioning of karst aquifers with a reservoir model: application to Fontaine de Vaucluse (south of France). *Journal of Hydrology* 345: 38-49.

Ford, D.C. and Williams, P. (2007). *Karst Geomorphology and Hydrogeology [Rev. Ed.].* John Wiley & Sons Ltd., Chichester, England.

Gale, S.J. (1984). The hydraulics of conduit flow in carbonate aquifers. *Journal of Hydrology* 70: 309-327.

Gat, J.R. (2010). *Isotope Hydrology. A Study of the Water Cycle*. Series of Environmental Science and Management – Vol. 6. Imperial College Press, London, England.

Gat, J.R., Mook, W.G. and Mejer, H.A.J. (2001). Environmental isotopes in the hydrological cycle. Principles and applications. Atmospheric water. UNESCO/IAEA Series 39(2).

Goldscheider, N. (2009). Origin, transport and monitoring of particles and microbial contaminants in karst aquifer systems. *29th Annual Groundwater Conference - International Association of Hydrogeologists (IAH) Irish Group*, Tullamore, 21st -22nd April 2009.

Goodwillie, R. and Reynolds, J.D. (2003). Turloughs. *In*, Otte, M.L. (ed.) *Wetlands of Ireland. Distribution, ecology uses and economic value.* University College Dublin Press, Dublin.

Grasso, D.A. and Jeannin, P-Y. (2002). A global experimental system approach of karst springs' hydrographs and chemographs. *Ground Water* 40(6): 608-617.

Grasso, D.A., Jeannin, P-Y. and Zwahlen, F. (2003). A deterministic approach to the coupled analysis of karst springs' hydrographs and chemographs. *Journal of Hydrology* 271: 65-76.

Groves, C.G. and Howard, A.D. (1994). Early development of karst systems. 1. Preferential flow path enlargement under laminar flow. *Water Resources Research* 30: 2837-2846.

Halihan, T., Wicks, C.M. and Engeln, J.F. (1998). Physical response of a karst drainage basin to flood pulses: an example of the Devil's Icebox cave system (Missouri, USA). *Journal of Hydrology* 204: 24-36.

Halihan, T. and Wicks, C.M. (1998). Modelling of storm response in conduit flow aquifers with reservoirs. *Journal of Hydrology* 208: 82-91.

Halihan T., Sharp, J.M. and Mace, R.E. (2000). Flow in the San Antonio segment of the Edwards aquifer: matrix, fractures or conduits? *In*, Sasowsky I.D. & Wicks C.M (eds) *Groundwater Flow and Contaminant Transport in Carbonate Aquifers.* A.A. Balkema, Rotterdam.

Hanna, R.B and Rajaram, H. (1998). Influence of aperture variability on dissolutional growth of fissures in karst formations. *Water Resources Research* 34: 2843-2853.

Hao, Y., Yeh, T.J., Wang, Y. and Zhao, Y. (2007). Analysis of karst aquifer spring flows with a gray system decomposition model. *Ground Water* 45(1): 46-52.

Hauns, M., Jeannin, P-Y. and Atteia, O. (2001). Dispersion, retardation and scale effect in tracer breakthrough curves in karst conduits. *Journal of Hydrology* 241: 177-193.

Heery, S. and Madden, B. (1997). A summer concentration of little grebes *Tachybaptus ruficollis* in south County Galway. *Irish Birds* 6: 53-54.

Herczeg, A.L., Leaney, F.W.J., Stadter, M.F., Allan, G.L. and Fifield, L.K. (1997). Chemical and isotopic indicators of point-source recharge to a karst aquifer, South Australia. *Journal of Hydrology* 192: 271-299.

Hoke, J.A. and Wicks, C.M. (1997). Contaminant transport in karst aquifers. *Proceedings of the 6th Multidisciplinary Conference on Sinkholes and the Engineering and Environmental Impacts of Karst:* Springfield, Missouri; April 6-9, 1997.

Howard A.D. and Groves, C.G. (1995). Early development of karst systems. 2. Turbulent flow. *Water Resources Research* 31: 19-26.

Howes, C. (1997). *Images Below: a manual of underground and flash photography*. Wild Places Publishing, Cardiff, Wales.

ISO 748 (2007). *ISO 748. Hydrometry - Measurement of liquid flow in open channels using current-meters or floats*. International Organization for Standardization, Geneva, Switzerland.

Jakeman, A.J. and Hornberger, G.M. (1993). How much complexity is warranted in a rainfall-runoff model? *Water Resources Research* 29(8): 2637-2649.

Jeannin, P-Y. (2001). Modeling flow in phreatic and epiphreatic karst conduits in the Holloch cave (Muotatal, Switzerland). *Water Resources Research* 37: 191-200.

Jennings O'Donovan / Southern Water Global (1997). *An investigation of the flooding problems in the Gort-Ardrahan area of South Galway.* Report to the Office of Public Works (ref: 77135).

Johannet, A., Mangin, A. and D'Hulst , D.(1994). Subterranean water infiltration modelling by Neural Networks: use of water source flow. *Proceedings of the International Conference on Artificial Neural Networks (ICANN '94)*, Sorrento – Naples, May 26-29 1994. Springer-Verlag, London (UK)

Johnston, P.M. and Peach, D. (1999). Hydrological modelling of the flows in the karst limestones of the Gort Lowlands. In: *Proceedings of the Annual Irish Association of Hydrogeologists Symposium,* Tullamore, County Offaly, Ireland.

Jukić, D. and Denić-Jukić, V. (2004). A frequency domain approach to groundwater recharge estimation in karst. *Journal of Hydrology* 289: 95-110.

Kattan, Z. (1997). Environmental isotope study of the major karst springs in Damascus limestone aquifer systems: case of the Figeh and Barada springs. *Journal of Hydrology* 193: 161-182.

Kaufmann, G. (2009). Modelling karst geomorphology on different time scales. *Geomorphology* 106: 62-77.á

Kavvadas, M.J. and Marinos, P.G. (1994). Prediction of groundwater table lowering for lignite open-cast mining in a karstic terrain in western Macedonia, Greece. *Quarterly Journal of Engineering Geology* 27: S41-S55.

Kim, T-W. and Valdés, J.B. (2003). Nonlinear model for drought forecasting based on a conjunction of wavelet transforms and neural networks. *ASCE Journal of Hydrologic Engineering* 8(6): 319-328.

Kincaid T.R. (2000). A method for producing 3-D geometric and parameter models of saturated cave systems with a discussion of applications. *In*, Sasowsky I.D. & Wicks C.M (eds) *Groundwater Flow and Contaminant Transport in Carbonate Aquifers.* A.A. Balkema, Rotterdam.

Kogovsek, J. (1981). Vertical percolation in Planina Cave in the period 1980/81. *Acta Carsologica* 10, 111-125.

Kovács, A., Perrochet, P., Király, L. and Jeannin, P-Y. (2005). A quantitative method for the characterisation of karst aquifers based on spring hydrograph analysis. *Journal of Hydrology* 303: 152-164.

Labat, D., Ababou, R. and Mangin, A. (2000a). Rainfall-runoff relations for karstic springs. Part I: convolution and spectral analyses. *Journal of Hydrology* 238: 123-148.

Labat, D., Ababou, R. and Mangin, A. (2000b) Rainfall-runoff relations for karstic springs. Part II: continuous wavelet and discrete orthogonal multiresolution analyses. *Journal of Hydrology* 238: 149-178.

Labat, D., Ababou, R. and Mangin, A. (2001). Introduction to wavelet analyses to rainfall/runoff relationship for a karstic basin: the case of Licq-Athery karstic system (France). *Ground Water* 39(4): 605-615.

Labat D., Mangin, A. and Ababou, R. (2002). Rainfall-runoff relations for karstic springs: multifractal analyses. *Journal of Hydrology* 256: 176-195.

Labat, D. (2005). Recent advances in wavelet analyses: Part 1-A review of concepts. *Journal of Hydrology* 314: 275-288.

Labat, D., Ronchail, J. and Guyot, J.L. (2005). Recent advances in wavelet analyses: Part 2-Amazon, Panama, Orinoco and Congo discharges timescale variability. *Journal of Hydrology* 314: 289-311.

Lacroque M., Mangin, A., Razack, M. and Banton, O. (1998). Contribution of correlation and spectral analyses to the regional study of a large karst aquifer (Charente, France). *Journal of Hydrology* 205: 217-231.

Lambert, D.W., Luke, B.A. and Chase, D.S. (1997). Dipole-dipole D.C resistivity surveying for exploration of karst features. *Proceedings of the 6th Multidisciplinary Conference on Sinkholes and the Engineering and Environmental Impacts of Karst: Springfield, Missouri - April 6-9, 1997.*

Lane, S.R. and Smart, C.C. (1999). A method for correction of variable background fluorescence in filter fluorometry. *Proceedings of the 7th Multidisciplinary Conference on Sinkholes and the Engineering and Environmental Impacts of Karst*: Harrisburg/Hershey, Pennsylvania: April 10-14, 1999.

Lastennet, R. and Mudry, J. (1997). Role of karstification and rainfall in the behaviour of a heterogeneous karst system. *Environmental Geology* 34(2/3): 243-250.

Lauritzen, S-E., Abbott, J., Arnesen, R., Crossley, G., Grepperud, D., Ive, A. and Johnson, S. (1985). Morphology and hydraulics of an active phreatic conduit. *Cave Science* 12(4): 139-146.

Lee, Y.H. and Singh, V.P. (1999). Tank model using Kalman filter. *ASCE Journal of Hydrologic Engineering* 4(4): 344-349.

Liedl, R., Sauter, M., Hückinghaus, D., Clemens, T. and Teutsch, G. (2003). Simulation of the development of karst aquifers using a coupled continuum pipe flow model. *Water Resources Research* 39(3): 1057-1068.

Lipson, D.S., McCray, J.E. and Thyne, G.D. (2007). Using PHREEQC to simulate solute transport in fractured bedrock. *Groundwater* 45(4): 468-472.

Long, A.J. and Derickson, R.G. (1999). Linear systems analysis in a karst aquifer. *Journal of Hydrology* 219: 206-217.

Long, A.J. and Putnam, L.D. (2004). Linear model describing three components of flow in karst aquifers using ^{18}O data. *Journal of Hydrology* 296: 254-270.

Loop, C. and White, W.B. (2001). A conceptual model for DNAPL transport in karst ground water basins. *Ground Water* 39(1): 119-127.

López-Chicano M., Bouamama, M., Vallejos, A. and Pulido-Bosch, A. (2001). Factors which determine the hydrogeochemical behaviour of karstic springs. A case study from the Betic Cordilleras, Spain. *Applied Geochemistry* 16: 1179-1192.

López-Chicano M., Calvache, M.L., Martin-Rosales, W. and Gisbert, A. (2002). Conditioning factors in flooding of karstic poljes – the case study of the Zafarraya polje (South Spain). *Catena* 49(4): 331-352.

Luke, B.A. and Chase, D.S. (1997). Detecting caves using seismic surface waves; a feasibility study. *Proceedings of the 6th Multidisciplinary Conference on Sinkholes and the Engineering and Environmental Impacts of Karst:* Springfield, Missouri - April 6-9, 1997.

Lynn, D.E. and Waldren, S. (2001). Morphological variation in population of *Ranunculus repens* from the temporary limestone lakes (turloughs) in the west of Ireland. *Annals of Botany* 87: 9-17.

Mace R.E and S.D. Hovorka (2000). Estimating porosity and permeability in a karstic aquifer using core plugs, well tests and outcrop measurements. *In*, Sasowsky I.D. &

Wicks C.M (eds) *Groundwater Flow and Contaminant Transport in Carbonate Aquifers.* A.A. Balkema, Rotterdam.

Mahler, B.J. and Lynch, F.L. (1999). Muddy waters: temporal variations in sediment discharging from a karst spring. *Journal of Hydrology* 214: 165-178.

Mahler, B.J., Personné, J-C., Lods, G.F. and Drogue, C. (2000). Transport of free and particulate-associated bacteria in karst. *Journal of Hydrology* 238: 179-193.

Maillet, E. (1905). *Essais d'hydraulique souterraine et fluviale*. Hermann, Paris.

Majone, B., Bellin, A. and Borsato, A. (2004). Runoff generation in karst catchments: multifractal analysis. *Journal of Hydrology* 294: 176-195.

Mallat, S. (1998). *A wavelet tour of signal processing*. (2^{nd} ed.). Academic Press, London.

Maloszewski, P., Stichler, W., Zuber, A. and Rank, D. (2002). Identifying the flow systems in a karstic-fissured porous aquifer, the Schneealpe, Austria, by modelling of environmental ^{18}O and ^{3}H isotopes. *Journal of Hydrology* 256: 48-59.

Mangin, A. (1984). The use of autocorrelation and spectral analysis to obtain a better understanding of hydrological systems. *Journal of Hydrology* 67: 25-43.

Maramanthas, A., Maroulis, Z. and Marinos-Kouris, D. (2003). Brackish karstic springs model: application to Almiros Spring in Crete. *Ground Water* 41(5): 608-619.

Martin, J.B. and Gordon, S.L. (2000). Surface and ground water mixing, flow paths and temporal variations in chemical compositions of karst springs. *In*, Sasowsky I.D. & Wicks C.M (eds) *Groundwater Flow and Contaminant Transport in Carbonate Aquifers.* A.A. Balkema, Rotterdam.

Martin, J.B. and Dean, R.W. (2001). Exchange of water between conduits and matrix in the Floridan aquifer. *Chemical Geology* 179: 145-165.

Massei, N., Wang, H.Q., Dupont, J.P., Rodet, J. and Laignel, B. (2003). Assessment of direct transfer and resuspension of particles during turbid floods at a karstic spring. *Journal of Hydrology* 275: 109-121.

Massei, N., Dupont, J.P., Mahler, B.J., Laignel, B., Fournier, M., Valdes, D. and Ogier, S. (2006). Investigating transport properties and turbidity dynamics of karst aquifer using correlation, spectral and wavelet analyses. *Journal of Hydrology* 329: 244-257.

Massey, B.S. (1989). *Mechanics of Fluids*. (6th ed.). Van Nostrand Reinhold, U.K.

Mayr, C., Lücke, A., Stichler, W., Trimborn, P., Ercolano, B., Oliva, G., Ohlendorf, C., Soto, J., Fey, M., Haberzettl, T., Janssen, S., Schäbitz, F., Schleser, G.H., Wille, M. and Zolitschka, B. (2007). Precipitation origin and evaporation of lakes in semi-arid Patagonia (Argentina) inferred from stable isotopes ($\delta^{18}O$, $\delta^{2}H$). *Journal of Hydrology* 334: 53-63.

MATLAB (2008). MATLAB 7.6.0 (R2008a) Help documentation.

McCarthy, C. (2002). Flooding problems in the Gort-Ardrahan area of south Galway: engineering options and modelling. *Proceedings of Karst Working Group Seminar*: Tullamore, October 4th, 2002.

Milanovic, P.T. (1976). Water regime in deep karst: case study of the Ombla spring drainage area. *In*, Yevjevich, V. (ed), *Karst Hydrology and Water Resources: Proceedings of the U.S.-Yugoslavian Symposium, Dubrovnik, June 1975:* Water Resources Publications, Fort Collins, Colorado.

Mohrlok, U. and Sauter, M. (1997). Modelling groundwater flow in a karst terrain using discrete and double-continuum approaches- importance of spatial and temporal distribution of recharge. *Proceedings of the 6th Conference on Limestone Hydrology and Fissured Media.* La Chaux-de-Fonds, Switzerland.

Morales-Juberías, T., Olazar, M., Arandes, J.M., Zafra, P., Antigüedad, I. and Basauri, F. (1997). Application of a solute transport model under variable velocity conditions in a conduit flow aquifer: Olalde karst system, Basque Country, Spain. *Environmental Geology* 30 (3/4): 143-151.

Motyka, J. (1998). A conceptual model of hydraulic networks in carbonate rocks, illustrated by examples form Poland. *Hydrogeology Journal* 6: 469-482.

Najib, J., Jourde H. and Pistre S. (2008). A methodology for extreme groundwater surge predetermination in carbonate aquifers: groundwater flood frequency analysis. *Journal of Hydrology* 352: 1-15.

Nash, J.E. and Sutcliffe, J.V. (1970). River flow forecasting through conceptual models part 1 – a discussion of principles. *Journal of Hydrology* 10(3): 282-290.

Nativ, R., Günay G., Hötzl, H., Reichart, B., Solomon, D.K. and Tezcan, L. (1999). Separation of groundwater-flow components in a karstified aquifer using environmental tracers. *Applied Geochemistry* 14: 1001-1014.

Neuman, S.P. and de Marsily, G. (1976). Identification of linear systems response by parametric programming. *Water Resources Research* 12(2): 253-262.

O'Driscoll, M.A. and DeWalle, D.R. (2006). Stream-air temperature relations to classify stream-ground water interactions in a karst setting, central Pennsylvania, USA. *Journal of Hydrology* 329: 140-153.

Olsson, J. and Niemczynowicz, J. (1996). Multifractal analysis of daily spatial rainfall distributions. *Journal of Hydrology* 187: 29-43.

Oraseanu, I. and Mather, J. (2000). Karst hydrogeology and origin of thermal waters in the Cordru Moma Mountains, Romania. *Hydrogeology Journal* 8: 379-389.

Oron, A.P. and Berkowitz, B. (1998). Flow in rock fractures : the local cubic law assumption re-examined. *Water Resources Research* 34: 2811-2825.

Ortega, R.M.V. and Espinosa, J.G. (1999). Evaluation of aquifer transmissivity in karst using geophysical well logs. *Journal of Environmental Hydrology* 7: paper 16.

Otte, M.L. (2003). *Wetlands of Ireland. Distribution, ecology uses and economic value*. Otte, M.L. *(ed)*. University College Dublin Press.

Padilla, A. and Pulido-Bosch, A. (1995). Study of hydrographs of karstic aquifers by means of correlation and cross-spectral analysis. *Journal of Hydrology* 168: 73-89.

Palmer, A.N. (1991). Origin and morphology of limestone caves. *Geological Society of America Bulletin* 103: 1-21.

Palmer, P.C., Marshall, W.G and Hinkle, S.R. (2007). Isotopic characterization of three groundwater recharge sources and inferences for slected aquifers in the upper Klamath Basin of Oregon and California, USA. *Journal of Hydrology* 336: 17-29.

Pereira, H.C., Coxon, C. and Allott, N. (2009). Turlough water quality and implications for groundwater management. *29th Annual Groundwater Conference - International Association of Hydrogeologists (IAH) Irish Group*, Tullamore, 21st -22nd April 2009.

Perrin, J., Jeannin, P-Y. and Zwahlen, F. (2003). Epikarst storage in a karst aquifer: a conceptual model based on isotopic data, Milandre test site, Switzerland. *Journal of Hydrology* 279: 106-124.

Petelet-Giraud, E., Luck, J-M., Othman, D.B. and Negrel, P. (2003). Dynamic scheme of water circulation in karstic aquifers as constrained by Sr and Pb isotopes. Application to the Hérault watershed, Southern France. *Hydrogeology Journal* 11: 560-573.

Peterson E.W., Davis, R.K. and Brahana, J.V. (2000). The use of regression analysis to predict nitrate-nitrogen concentrations in springs of north-west Arkansas. *In*, Sasowsky I.D. & Wicks C.M (eds) *Groundwater Flow and Contaminant Transport in Carbonate Aquifers.* A.A. Balkema, Rotterdam.

Peterson, E.W. and Wicks, C.M. (2003). Characterisation of the physical and hydraulic properties of the sediment in karst aquifers of the Springfield Plateau, Central Missouri, USA. *Hydrogeology Journal* 11: 357-367.

Peterson, E.W. and Wicks, C.M. (2006). Assessing the importance of conduit geometry and physical parameters in karst aquifers using the storm water management model (SWMM). *Journal of Hydrology* 329: 294-305.

Plummer, L.N., Wigley, T.M.L. and Parkhusrt, D.L. (1978). The kinetics of calcite dissolution in CO_2-water system at 5° to 50°C and 0.0 to 1.0 atm CO_2. *American Journal of Science* 278: 179-216.

Plummer, L.N. and Busenburg, E. (1982). The solubilities of calcite, aragonite and vaterite in CO_2-H_2O solutions between 0 and 90°C and an evaluation of the aqueous model for the system $CaCO_3$-CO_2-H_2O. *Geochimica et Cosmochimica Acta* 46, 1011-1040.

Plummer, L.N., Busenberg, E., McConnell, J.B., Drenkard, S., Schlosser, P. and Michel, R.L. (1998). Flow of river water into a karstic limestone aquifer. 1.Tracing the young fraction in groundwater mixtures in the Upper Floridian Aquifer near Valdosta, Georgia. *Applied Geochemistry* 13: 995-1015.

Porst, G., Naughton, O., Gill, L., Johnston, P., Irvine, K. (2009). The importance of disturbance for seasonal and inter-annual succession of macroinvertebrates in turloughs. *Freshwater Biology* (in press).

Pronk, M., Goldscheider N. and Zopfi, J. (2006). Dynamics and interaction of organic carbon, turbidity and bacteria in a karst aquifer system. *Hydrogeology Journal* 14:473-484.

Pronk, M., Goldscheider N. and Zopfi, J. (2007). Particle-size distribution as indicator for fecal bacteria contamination of drinking water from karst springs. *Environmental Science and Technology* 41: 8400-8405.

Pronk, M., Goldscheider N., Zopfi, J. and Zwahlen, F. (2009). Percolation and particle transport in the unsaturated zone of a karst aquifer. *Ground Water* 47(3): 361-369.

Quinlan, J.F. and Ray, J.A. (1995). Normalized base-flow discharge of ground water basins: a useful parameter for estimating recharge area of springs and recognizing drainage anomalies in karst terrains. *In*: B.F. Beck, Editor, *Karst Geohazards*, Balkema, Rotterdam.

Quinn, J.J. and Tomasko, D. (2000). A numerical approach to simulating mixed flow in karst aquifers. *In*, Sasowsky I.D. & Wicks C.M (eds) *Groundwater Flow and Contaminant Transport in Carbonate Aquifers.* A.A. Balkema, Rotterdam.

Quinn, J.J., Tomasko, D. and Kuiper, J.A. (2006). Modelling complex flow in karst aquifer. *Sedimentary Geology* 184: 343-351.

Rauch, H.W. and White, W.B. (1977). Dissolution kinetics of carbonate rocks. 1. Effects of lithology on dissolution rate. *Water Resources Research* 13: 381-394.

Ravbar, N. and Goldscheider, N. (2009). Comparative application of four methods of groundwater vulnerability mapping in a Slovene karst catchment. *Hydrogeology Journal* 17: 725-733.

Ray, J.A. (1997). Overflow conduit systems in Kentucky: a consequence of limited underflow capacity. *In,* Beck & Stephenson (eds) *The Engineering Geology and Hydrogeology of Karst Terranes*, A.A. Balkema, Rotterdam.

Redwine, J.C. and Howell, J.R. (2001). Geochemical methods for distinguishing surface water from groundwater in the Knox aquifer system. *Proceedings of the 8th Multidisciplinary Conference on Sinkholes and the Engineering and Environmental Impacts of Karst:* Louisville, Kentucky April 1-4, 2001.

Reynolds, J.D. (1996). Significance and conservation of turloughs. In: Reynolds, J.D. (ed.) *Conservation of aquatic systems.* Royal Irish Academy, Dublin: 38-46.

Reynolds, J.D. and Marnell, F. (1999). New records of *Eurycercus glacialis* (Cladocera, Chydoridae) in turloughs in south-east Galway. *Irish Naturalist's Journal* 26: 177-180.

Rimmer, A. and Salingar, Y. (2006). Modelling precipitation-streamflow processes in karst basin: the case of the Jordan river sources, Israel. *Journal of Hydrology* 331: 524-542.

Rovey II, C.W. (1998). Digital simulation of the scale effect in hydraulic conductivity. *Hydrogeology Journal* 6:216-225.

Rozos, E. and Koutsoyiannis, D. (2006). A multicell karstic aquifer model with alternative flow equations. *Journal of Hydrology* 325: 340-355.

Ryan, M. and Meiman, J. (1996). An examination of short-term variations in water quality at a karst spring in Kentucky. *Ground Water* 34(1): 23-40.

Sánchez-Villa, X., Carrera, J. And Girardi, J.P. (1996). Scale effects in transmissivity. *Journal of Hydrology* 183: 1-22.

Sasowsky, I.D. (2000). Carbonate aquifers: a review of thoughts and methods. *In,* Sasowsky I.D. & Wicks C.M (eds) *Groundwater Flow and Contaminant Transport in carbonate Aquifers.* A.A. Balkema, Rotterdam.

Scanlon B.R., Mace, R.E., Barrett, M.E. and Smith, B. (2003). Can we simulate regional groundwater flow in a karst system using equivalent porous media models? Case study, Barton Springs Edwards aquifer, USA. *Journal of Hydrology* 276: 137-158.

Shaw, E.M. (1994). *Hydrology in Practice (3rd edition).* Chapman and Hall, London.

Shevenell, L. (1996). Analysis of well hydrographs in a karst aquifer: estimates of specific yields and continuum transmissivities. *Journal of Hydrology* 174: 331-355.

Shuster, E.T and White, W.B. (1971). Seasonal fluctuations in the chemistry of limestone springs: a possible means for characterising carbonate aquifers. *Journal of Hydrology* 14: 93-128.

Siemers, J. and Dreybrodt, W. (1998). Early development of karst aquifers on percolation networks of fractures in limestone. *Water Resources Research* 34: 409-419.

Skeffington, M.S., Moran, J., O'Connor, Á, Regan, E., Coxon, C.E., Scott, N.E. and Gormally, M. (2006). Turloughs – Ireland's unique wetland habitat. *Biological Conservation* 133(2-3): 265-290.

Skeffington, M.S. and Scott, N.E. (2008). Do turloughs occur in Slovenia? *Acta Carsologica* 37(2-3): 291-306.

Smart, C.C. (1988). Exceedance probability distributions of steady conduit flow in karst aquifers. *Hydrological Processes* 2: 31-41.

Springer, G.S. and Wohl, E.E. (2002) Empirical and theoretical investigations of sculpted forms in Buckeye Creek Cave, West Virginia. *Journal of Geology* 110(4): 469-481.

Springer, G.S. (2004). A pipe-based, first approach to modelling closed conduit flow in caves. *Journal of Hydrology* 289: 178-189.

Simms, M.J. (2003). The geology of the Burren and Gort Lowlands. *In*, Mullan, G. (ed) *Caves of County Clare and South Galway.* University of Bristol Spelæological Society 9-14, Bristol U.K.

Svensson, U. and Dreybrodt, W. (1992). Dissolution kinetics of natural calcite minerals in CO_2 – water systems approaching calcite equilibrium. *Chemical Geology* 100: 129-145.

Svensson, C., Olsson, J. and Bernedtsson, R. (1996). Multifractal properties of daily rainfall in two different climates. *Water Resources Research* 32(8): 2463-2472.

Talarovich, S.G. and Krothe, N.C. (1998). Three component storm hydrograph separation of a karst spring contaminated by Polychlocinated Biphenyls, Central Indiana. *Environmental Geosciences*, 5(4): 162-175.

Teutsch, G. and Sauter, M. (1998). Distributed parameter modelling approaches in karst-hydrological investigations. *Bulletin d'Hydrogeologie* 16: 99-109.

Thrailkill, J. (1974). Pipe flow models of a Kentucky limestone. *Ground Water* 12(4): 202-205.

Tooth, A.F. and Fairchild, I.J. (2003). Soil and karst aquifer hydrological controls on the geochemical evolution of speleothem-forming drip waters, Crag Cave, southwest Ireland. *Journal of Hydrology* 273: 51-68.

Toran, L., Herman, E.K. and White, W.B. (2007). Comparison of flowpaths to a well and spring in a karst aquifer. *Ground Water* 45(3): 281-287.

Tranter, J., Gunn, J., Hunter, C. and Perkins, J. (1997). Bacteria in the Castleton Karst, Derbyshire, England. *Quarterly Journal of Engineering Geology* 30: 171-178.

Tucker, R.B. and Crawford, N.C. (1999). Non-linear curve-fitting analysis as a tool for identifying and quantifying multiple fluorescence tracer dyes present in samples analyzed with a spectrofluorometer and collected as part of a dye tracer study of groundwater flow. *In*, Beck, Pettit & Herring (eds) *Hydrogeology and Engineering Geology of Sinkholes and Karst*. A.A. Balkema, Rotterdam.

Tynan, S., Gill, M., Johnston, P.M. (2007). *Development of a methodology for the characterisation of a karstic groundwater body with particular emphasis on the linkage with associated ecosystems such as turlough ecosystems*. Synthesis Report - ERTDI Report Series, Wexford, Environmental Protection Agency, 2007, 62pp.

Valdes, D., Dupont, J-P., Massei, N., Laignel, B. and Rodet, J. (2006). Investigation of karst hydrodynamics and organization using autocorrelations and T-ΔC curves. *Journal of Hydrology* 329: 432-443.

Vandenschrick, G., Van Wesemael, B., Frot, E., Pulido-Bosch, A., Molina, L., Stievenard, M. and Souchez, R. (2002). Using stable isotope analysis (D-^{18}O) to characterize the regional hydrology of the Sierra de Gador, southeast Spain. *Journal of Hydrology* 265:43-55.

Vaute, L., Drogue, C., Garrelly, L. and Ghelfenstein, M. (1997). Relations between the structure of storage and the transport of chemical compounds in karstic aquifers. *Journal of Hydrology* 199: 221-238.

Verbovšek, T. (2008). Estimation of transmissivity and hydraulic conductivity from specific capacity and specific capacity index in dolomite aquifers. *ASCE Journal of Hydrologic Engineering* 13(9): 817-823.

Vesper, D.J., Loop, C. M. and White, W.B. (2003). Contaminant transport in karst aquifers. *Speleogenesis and Evolution of Karst Aquifers* 1(2): 1-11.

Vouillamoz, J.M., Legchenko, A., Albouy, Y., Bakalowicz, M., Baltassat, J.M. and Al-Fares, W. (2003). Localisation of saturated karst aquifer with Magnetic Resonance Sounding and Resistivity Imagery. *Ground Water* 41(5): 578-586.

Wallace III R.E. (1993). Dye trace and bacteriological testing of sinkholes tributary to Sulphur Spring, Tampa, Florida. *Proceedings of the 4th Multidisciplinary Conference on Sinkholes and the Engineering and Environmental Impacts of Karst:* Panama City, Florida January 25-27, 1993.

Wallingford (2006). *Groundwater Infiltration Module Technical Note 2*. Wallingford, Oxfordshire, U.K.

Wanfrang, Z., Beck, B.F. and Stephenson, B. (1999). Investigation of groundwater flow in karst areas using component separation of natural potential measurements. *Environmental Geology* 37(1/2): 19-25.

Weiss, M. and Gvirtzman, H. (2007). Estimating ground water recharge using flow models of perched karstic aquifers. *Ground Water* 46(6): 761-773.

White, W.B. (1988). *Geomorphology and Hydrology of Karst Terrains*. Oxford University Press, U.K.

White, W.B. (1999). Karst hydrology: Recent Developments and Open Questions. *Proceedings of the 7th Multidisciplinary Conference on Sinkholes and the Engineering and Environmental Impacts of Karst*: Harrisburg/Hershey, Pennsylvania April 10-14, 1999.

White, W.B. (2002). Karst hydrology: recent developments and open questions. *Engineering Geology* 65: 85-105.

White, W.B. and White, E.L. (2005). Ground water flux distribution between matrix, fractures and conduits: constraints on modelling. *Speleogenesis and Evolution of Karst Aquifers* 3(2): 6pp.

Wicks, C.M. (1997). Origins of groundwater in a fluviokarst basin: Bonne Femme Basin in Central Missouri, USA. *Hydrogeology Journal* 5: 89-96.

Wicks C.M. and Bohm, B. (2000). Application of the Unit hydrograph Technique to the discharge Record at Big Spring, Carter County, Missouri. *In*, Sasowsky I.D. & Wicks C.M (eds) *Groundwater Flow and Contaminant Transport in Carbonate Aquifers.* A.A. Balkema, Rotterdam.

Williams, P.W. (1983). The role of the subcutaneous zone in karst hydrology. *Journal of Hydrology* 61: 45-67.

Winiarski, T., Thomas, O. and Charrier, C. (1995). Analysis of the spatial and temporal variations in the water quality of a karstic aquifer using UV spectrophotometry. *Journal of Contaminant Hydrology* 19: 307-320.

Worthington, S.R.H., Ford, D.C and Davies, G.J. (2000). Matrix, fracture and channel components of storage and flow in a Paleozoic limestone aquifer. *In*, Sasowsky I.D. & Wicks C.M (eds) *Groundwater Flow and Contaminant Transport in Carbonate Aquifers.* A.A. Balkema, Rotterdam.

Ye, W., Bates, B.C., Viney, N.R., Sivapalan, N. and Jakeman, J. (1997). Performance of rainfall-runoff models in low-yielding ephemeral catchments. *Water Resources Research* 33: 153-166.

Younger, P.L. (1995). Hydrogeochemistry of minewaters flowing from abandoned coal workings in County Durham. *Quarterly Journal of Engineering Geology* 28: 101-113.

Younger, P.L. and Adams, R. (1999). *Predicting mine water rebound. Research and Development Technical Report W179*. Environment Agency, Bristol, U.K.

Younger P.L, Teutsch, G., Custodio, E., Elliot, T., Sauter, M., Manzano, M., Liedl, R., Clemens, T., Hückinghaus, D., Tore, C.S., Lambán, J. and Cardoso da Silva G. (1997). Groundwater resources and climate change effects – GRACE: Final report. EC Framework III Environment and Climate Program, Project EV5V – CT94 – 0471.

Zhang, D. (1993). Bedding karst and multi-layered groundwater flows in karstic block mountains in the northeast of Mount Xishan, Taiyuan , China. *Quarterly Journal of Engineering Geology* 26: 205-216.

Zhou, W. (2000). Studies of confluent flow in mature karst aquifers using analog models and numerical mixing cell models. *In*, Sasowsky I.D. & Wicks C.M (eds) *Groundwater Flow and Contaminant Transport in Carbonate Aquifers.* A.A. Balkema, Rotterdam.

Zuber, A. and Motyka, J. (1998). Hydraulic parameters and solute velocities in triple-porosity karstic-fissured-porous carbonate aquifers: case studies in Poland. *Environmental Geology* 34(2/3): 243-250.

Appendix A Maps

Figure A.1 Bedrock and fault map.

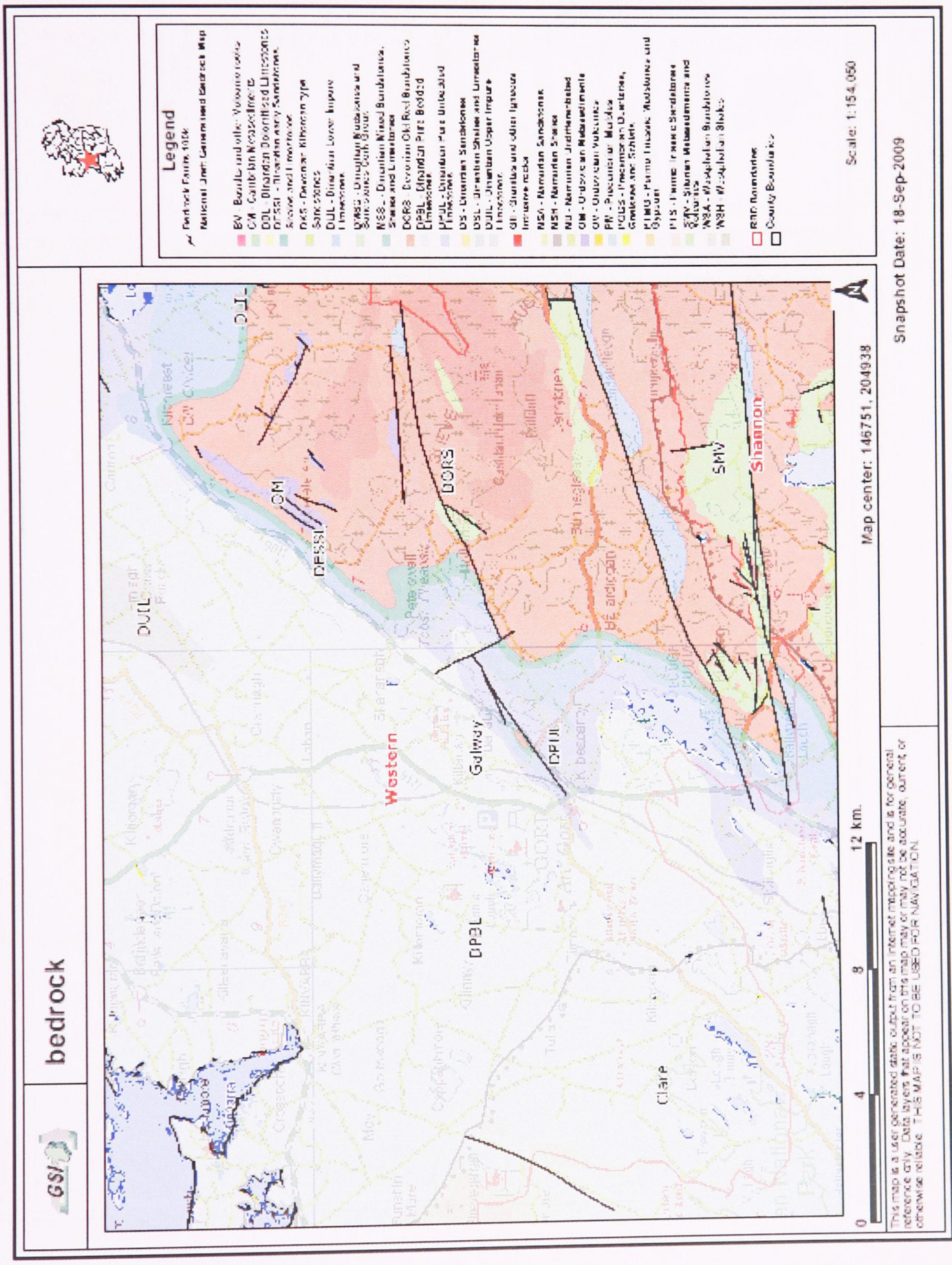


Figure A.2 Aquifer map

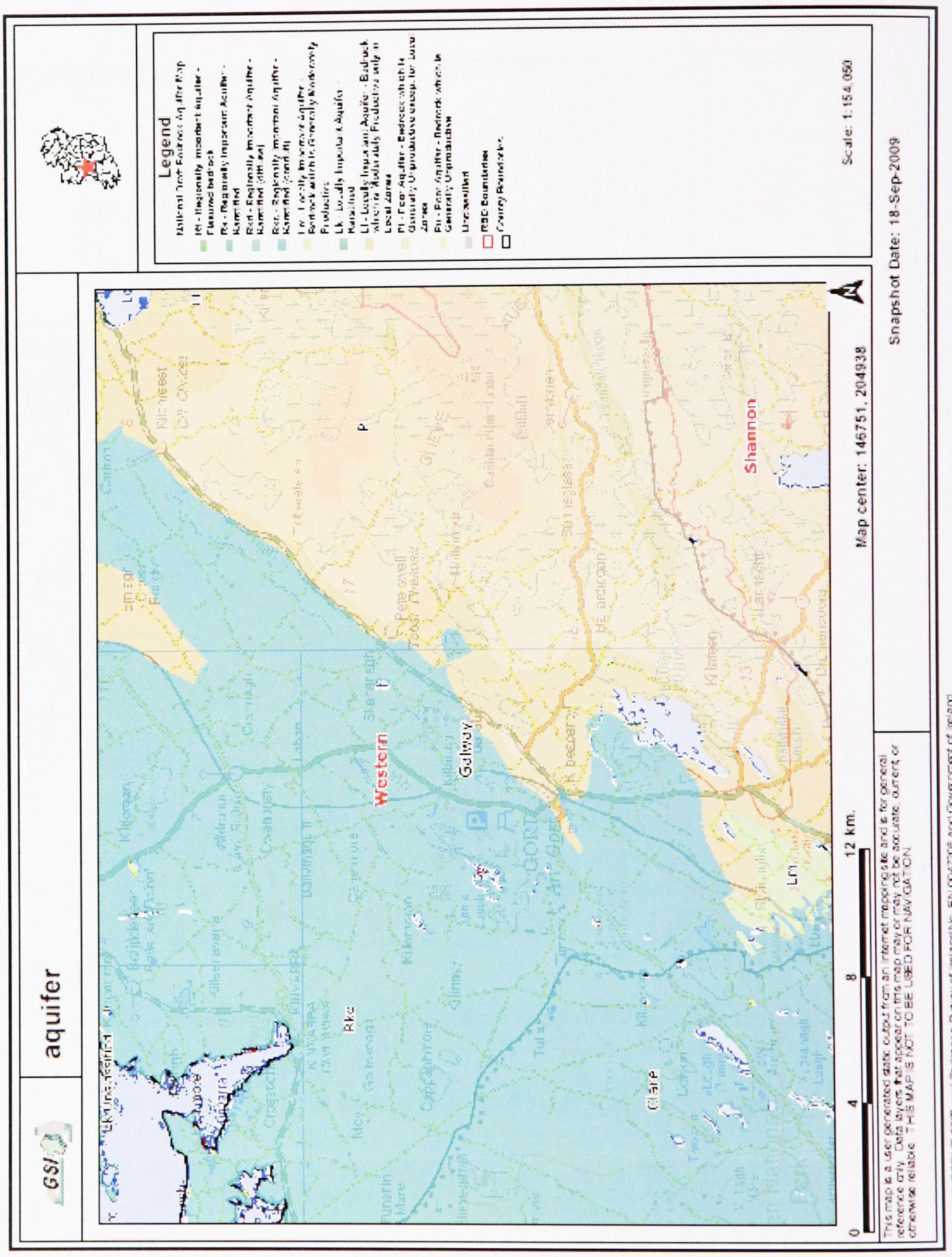


Figure A.3 Groundwater vulnerability map.

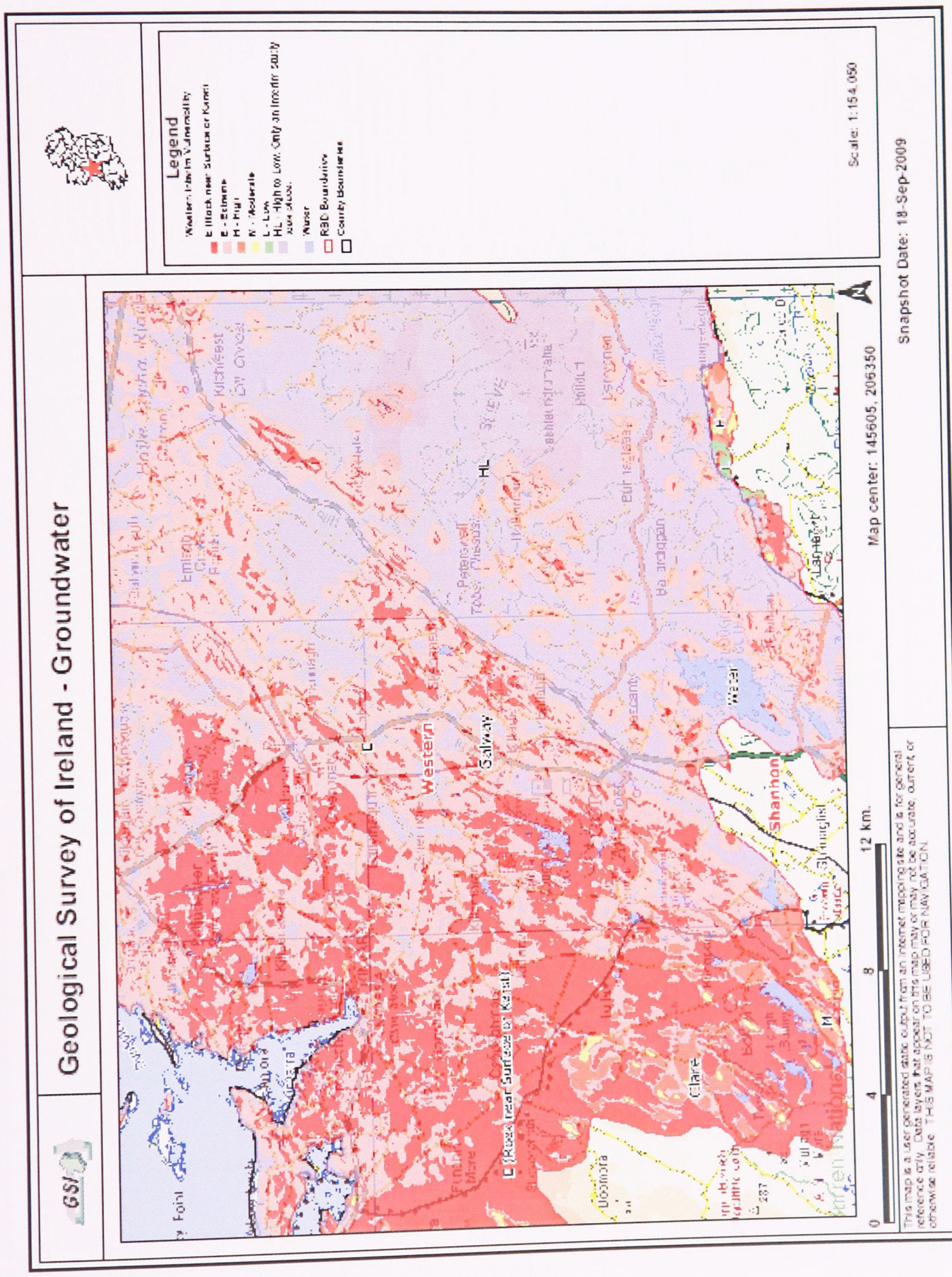


Figure A.4 Subsoils map.

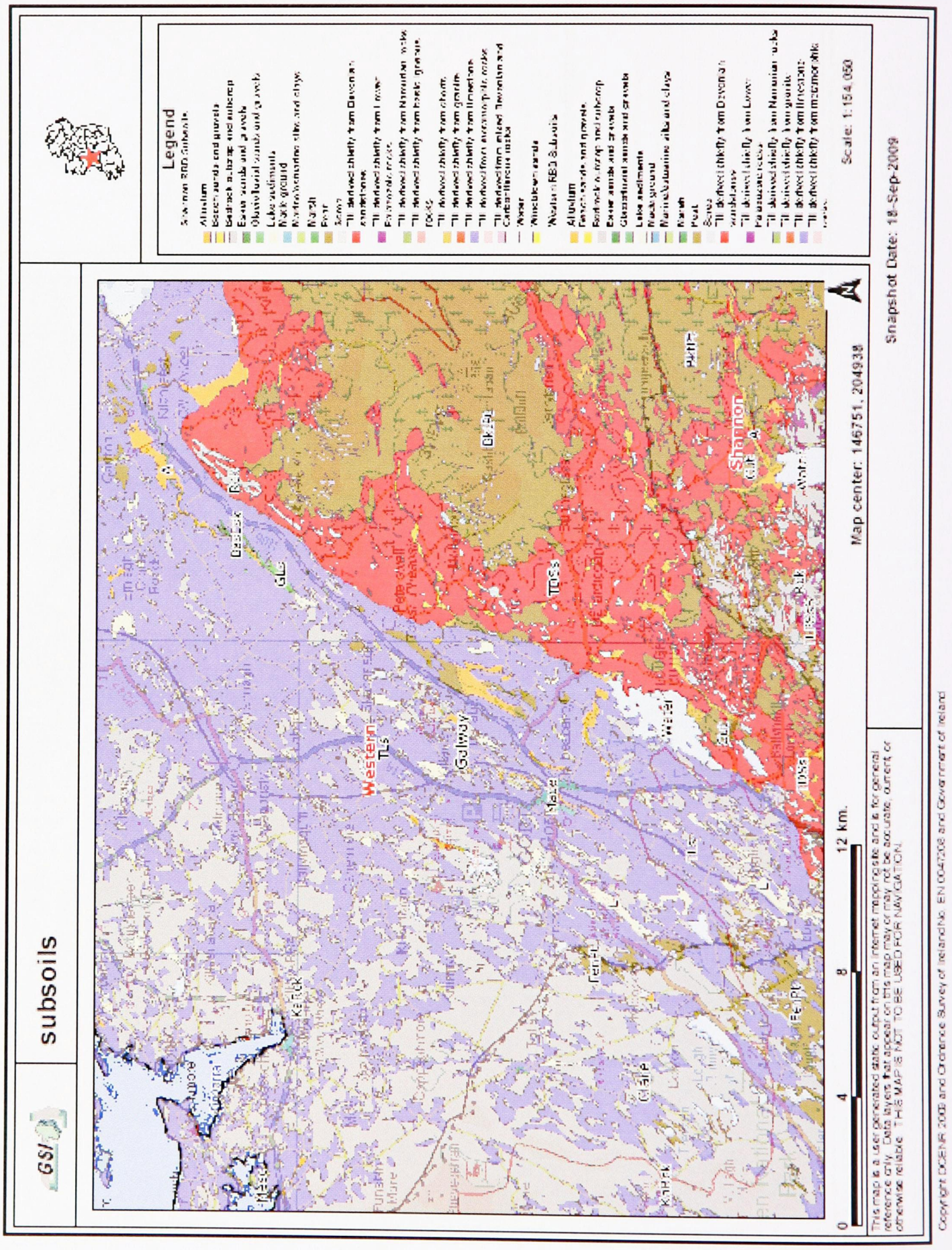


Figure A.5 Karst features map.

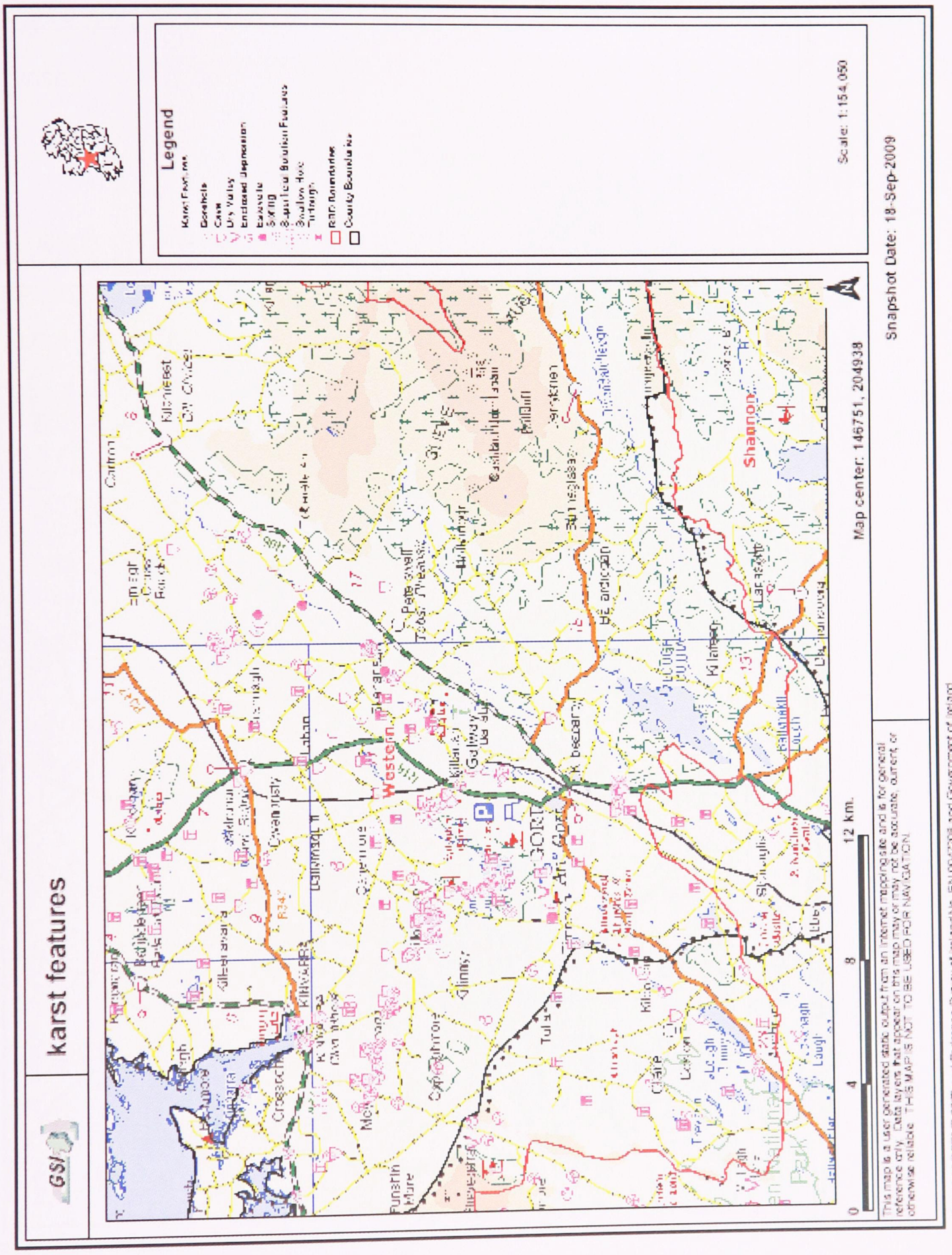
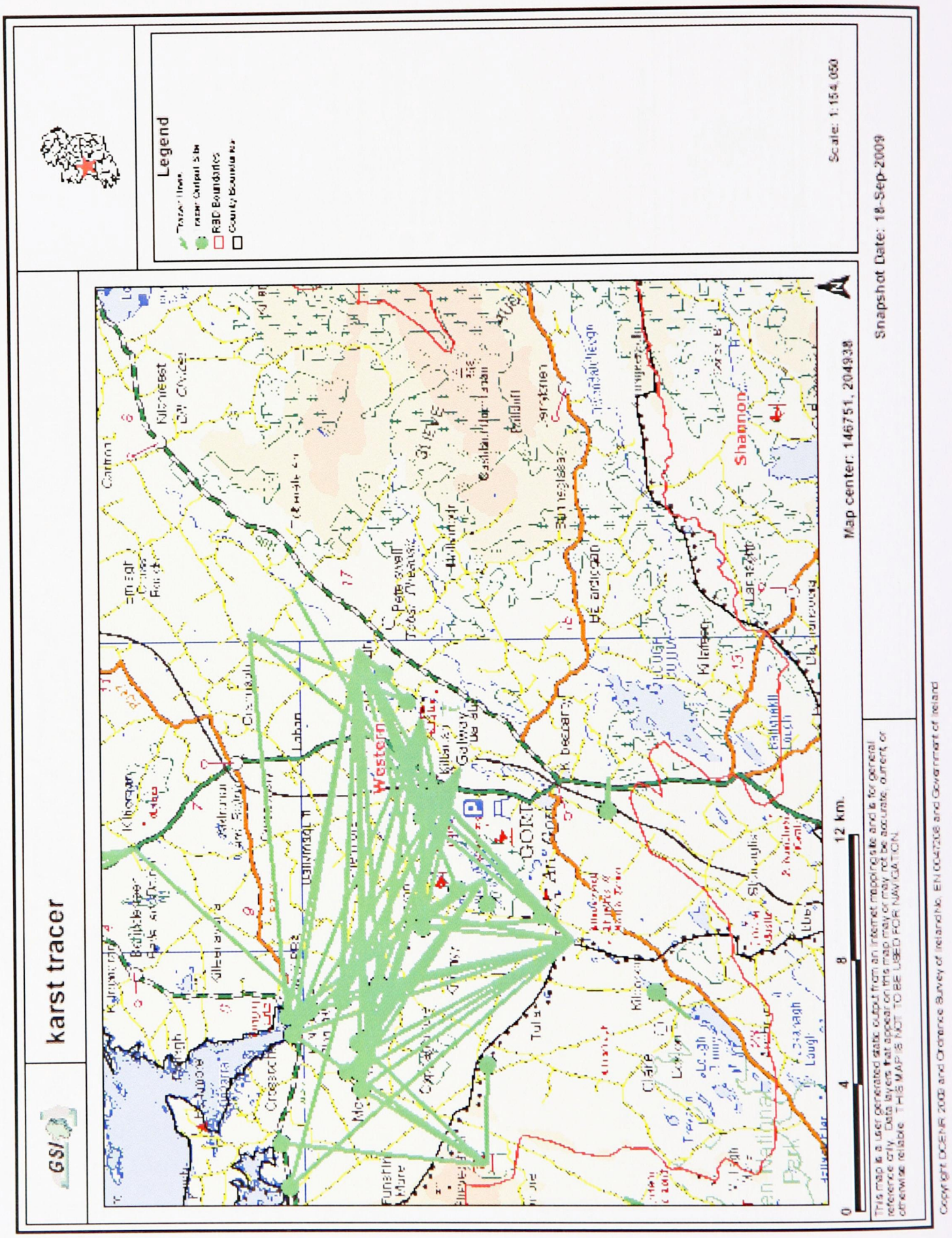


Figure A.6 Results from past karst tracer studies.



APPENDIX B TURLOUGH SURVEYS

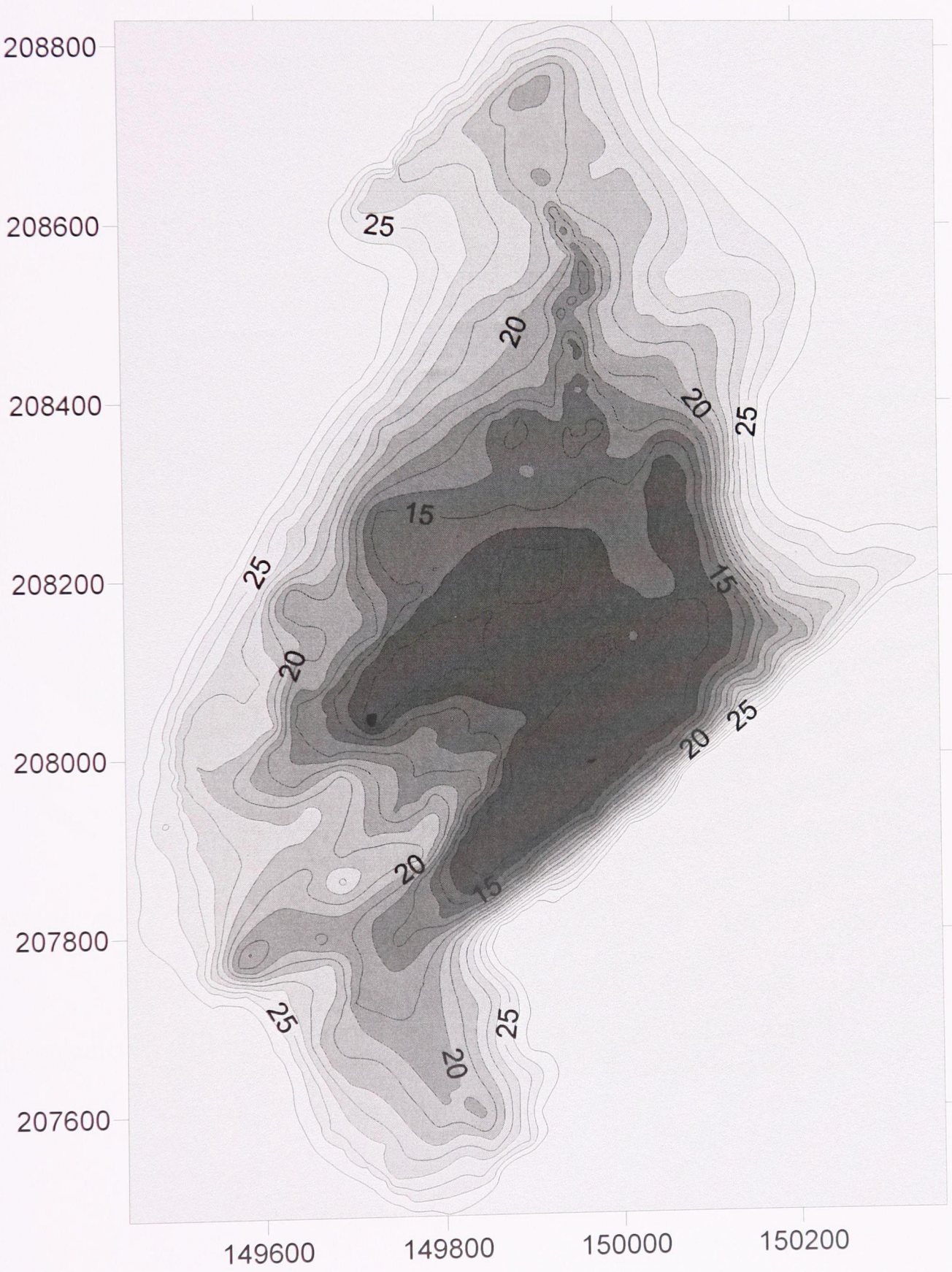


Figure B.1 Blackrock contour plot



Figure B.2 Three-dimensional surface and contour plot of Blackrock

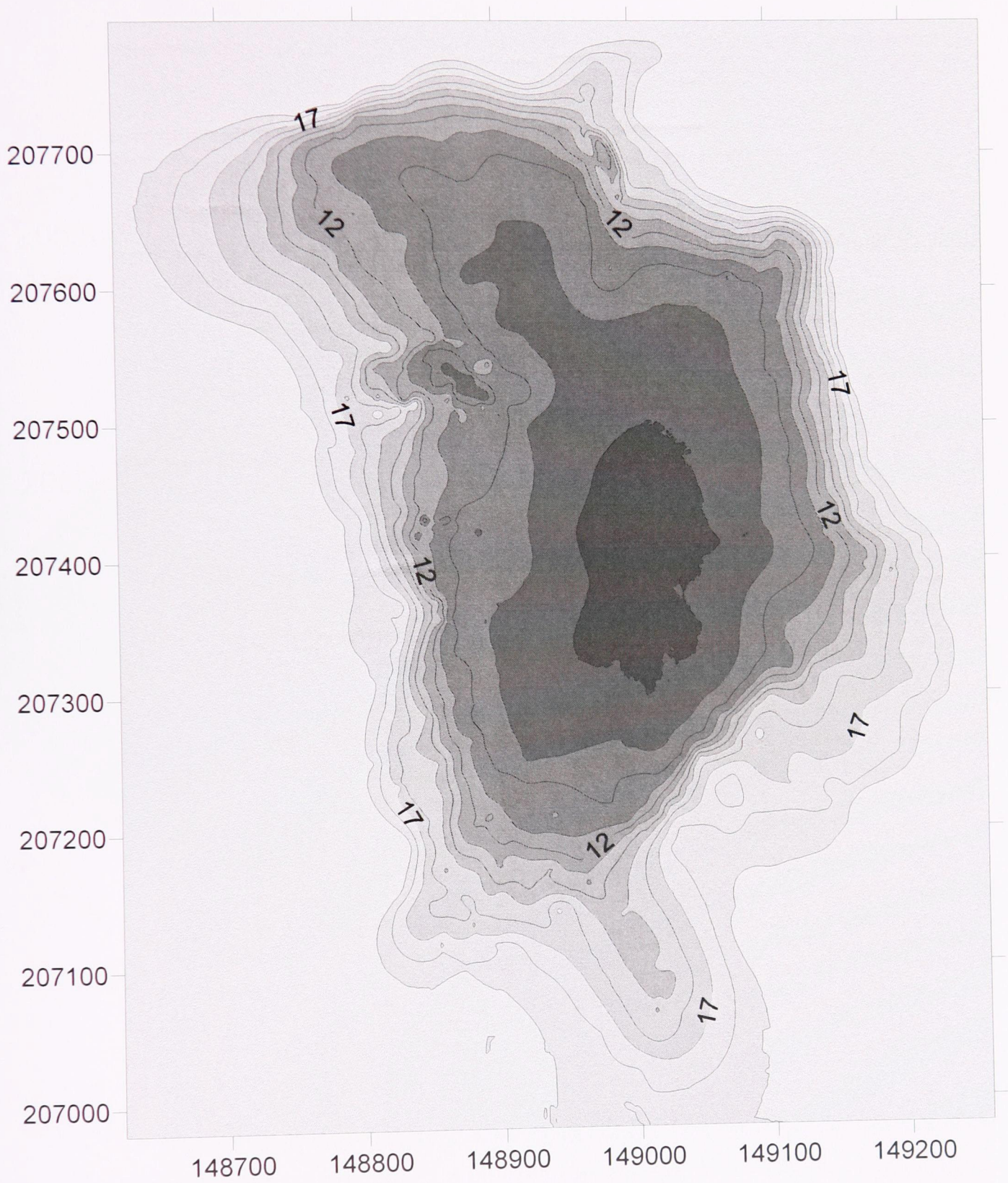


Figure B.3 Coy contour plot

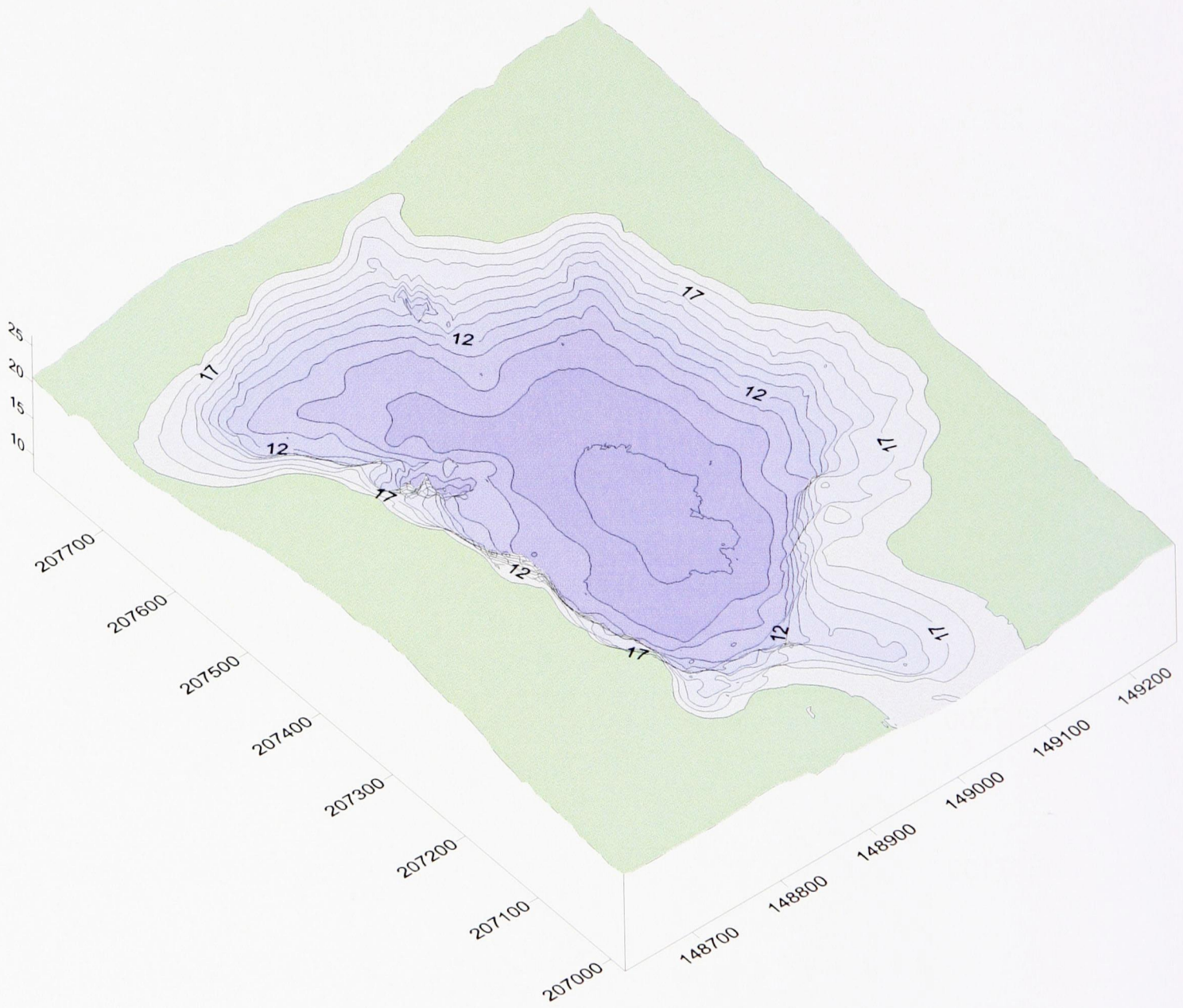


Figure B.4 Three-dimensional surface and contour plot of Coy

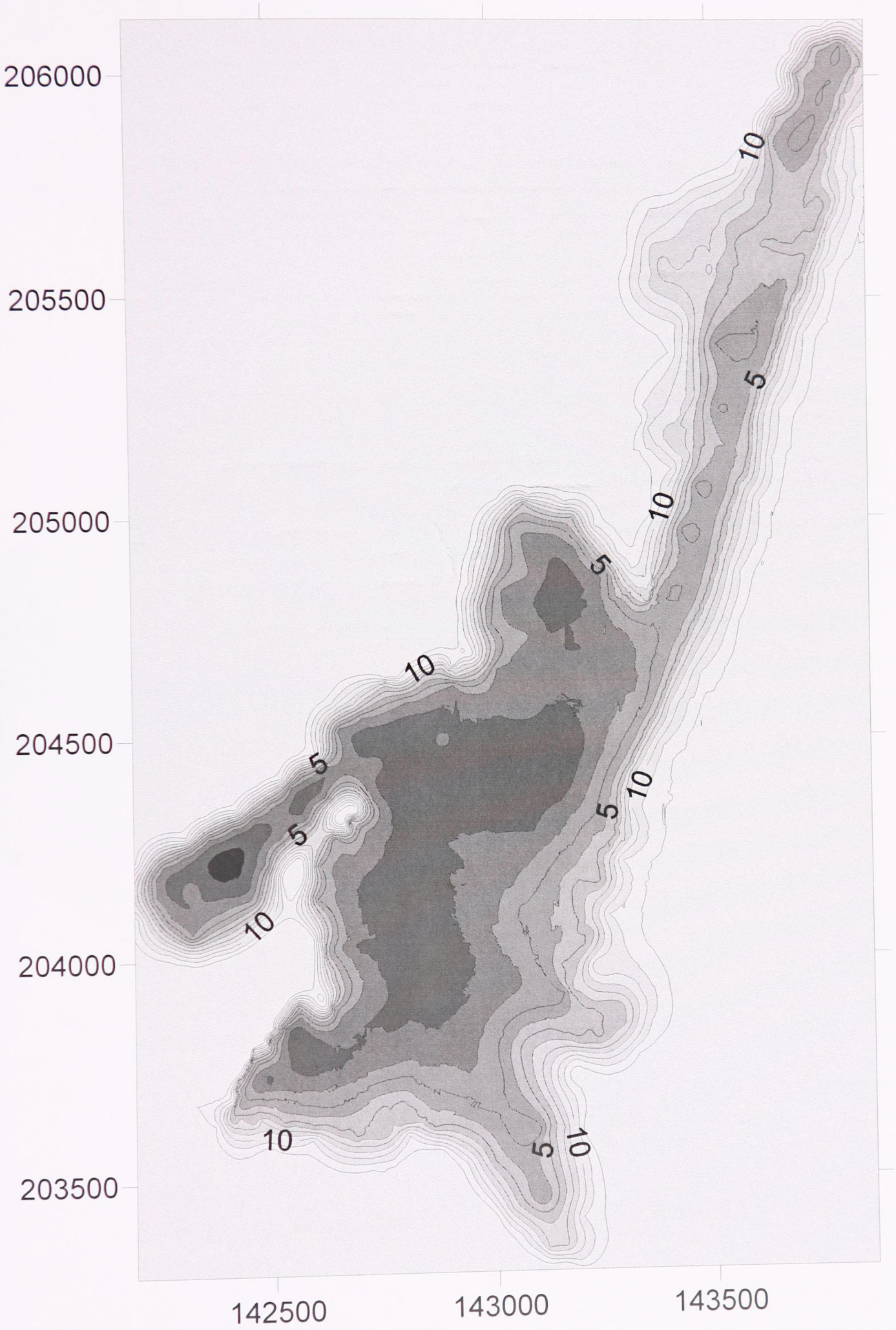


Figure B.5 Coole contour plot



Figure B.6 Three-dimensional surface and contour plot of Coole

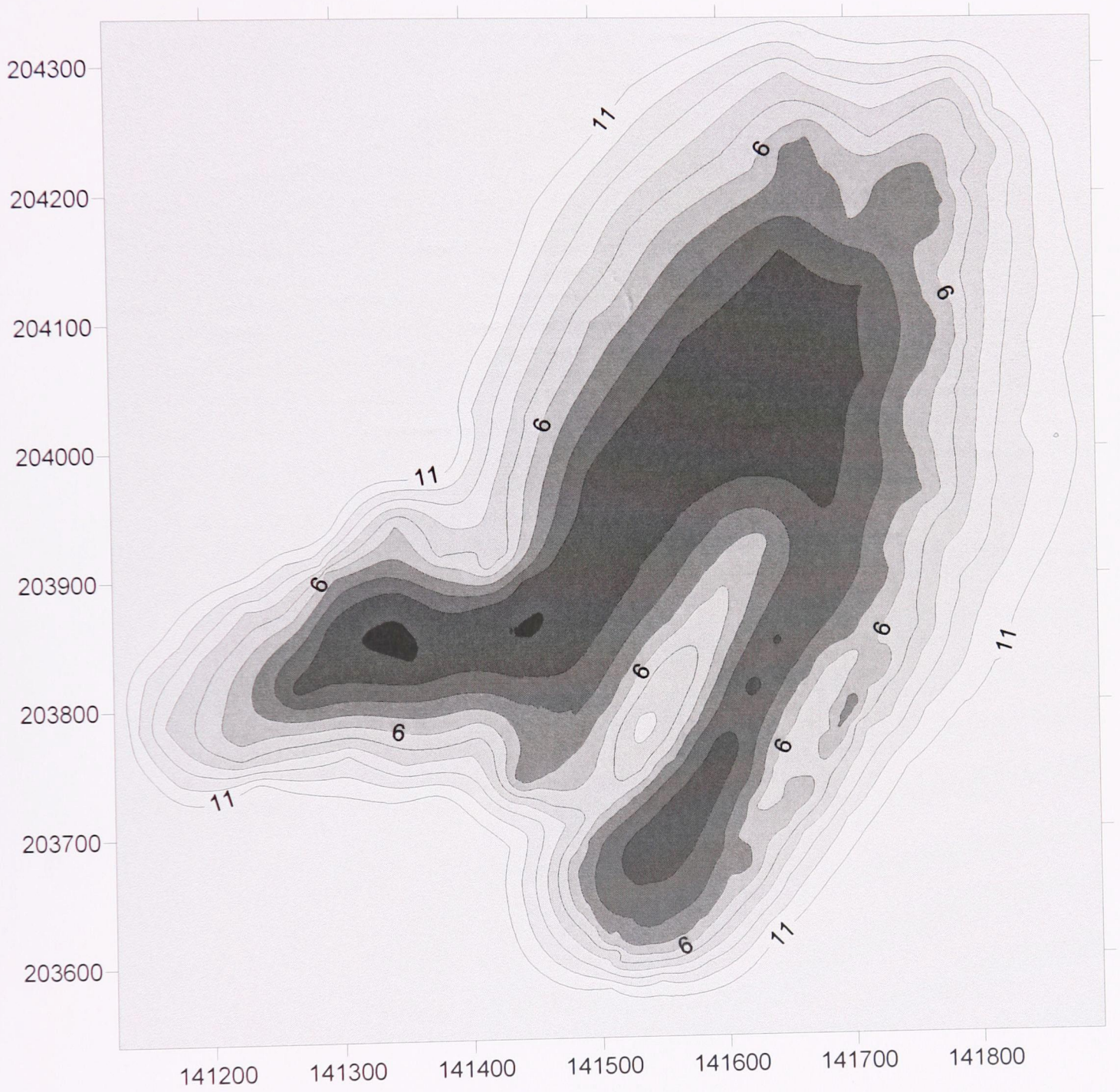


Figure B.7 Garryland contour plot



Figure B.8 Three-dimensional surface and contour plot of Garryland

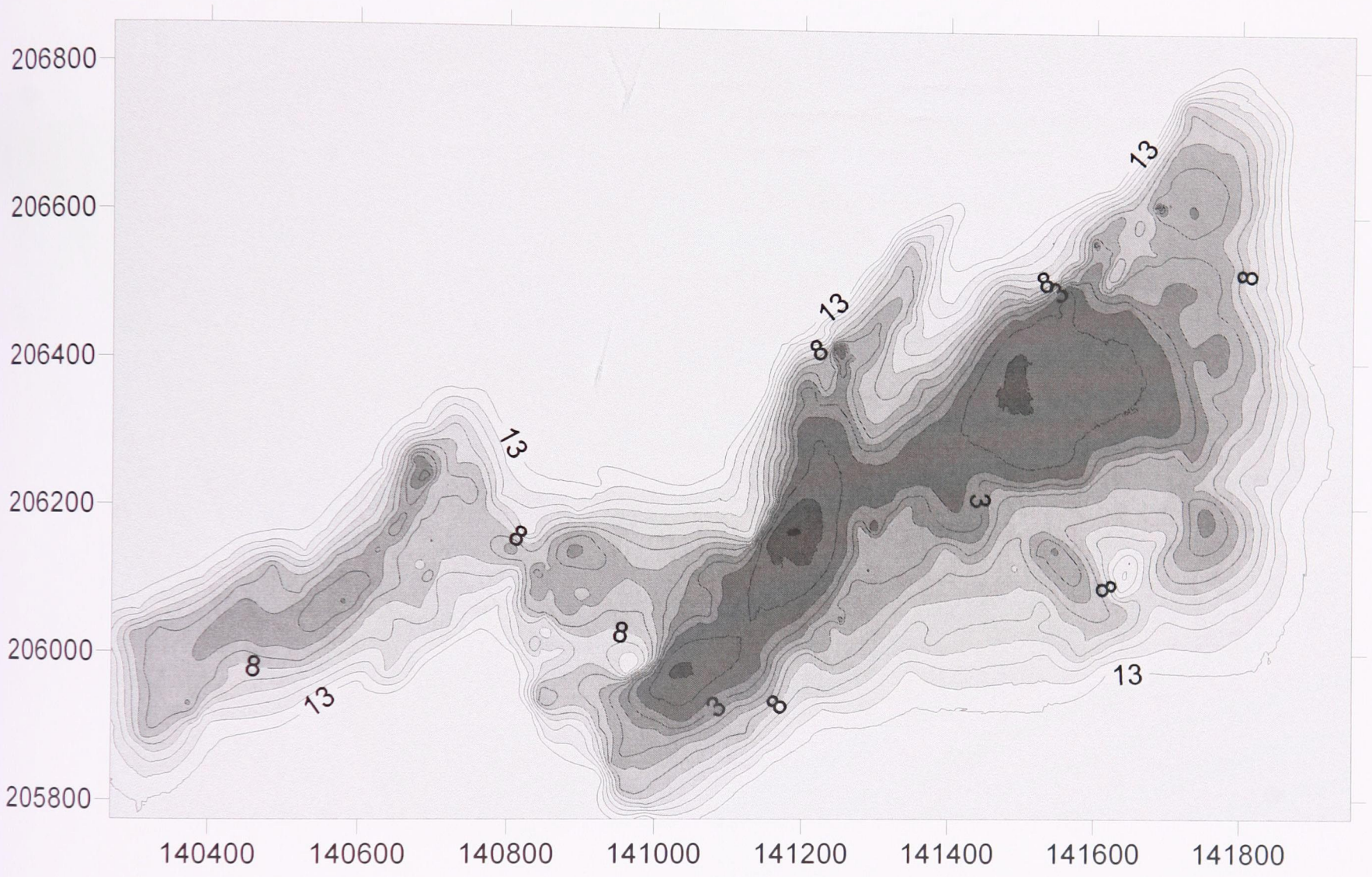


Figure B.9 Caherglassaun contour plot

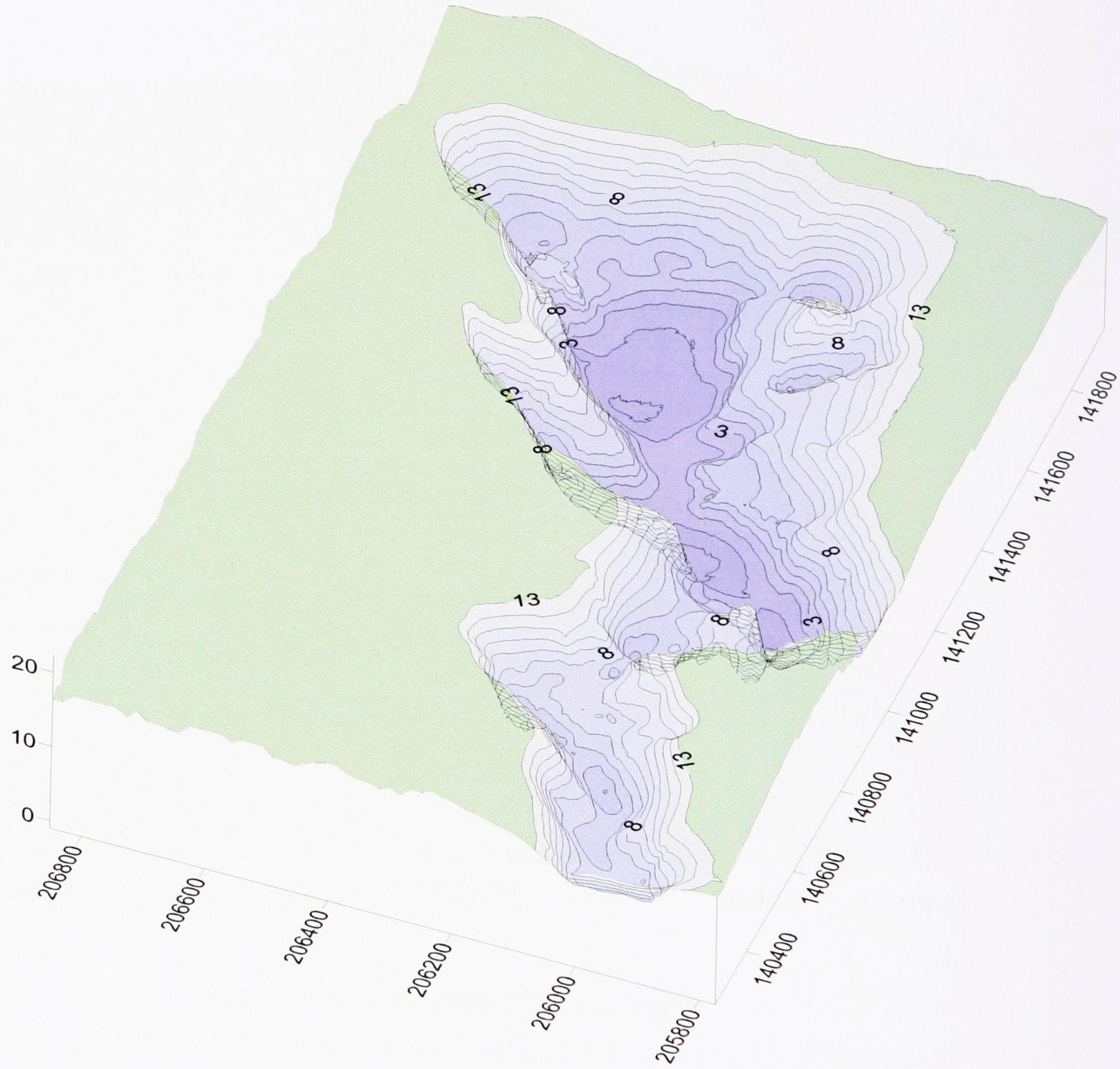


Figure B.10 Three-dimensional surface and contour plot of Caherglassaun

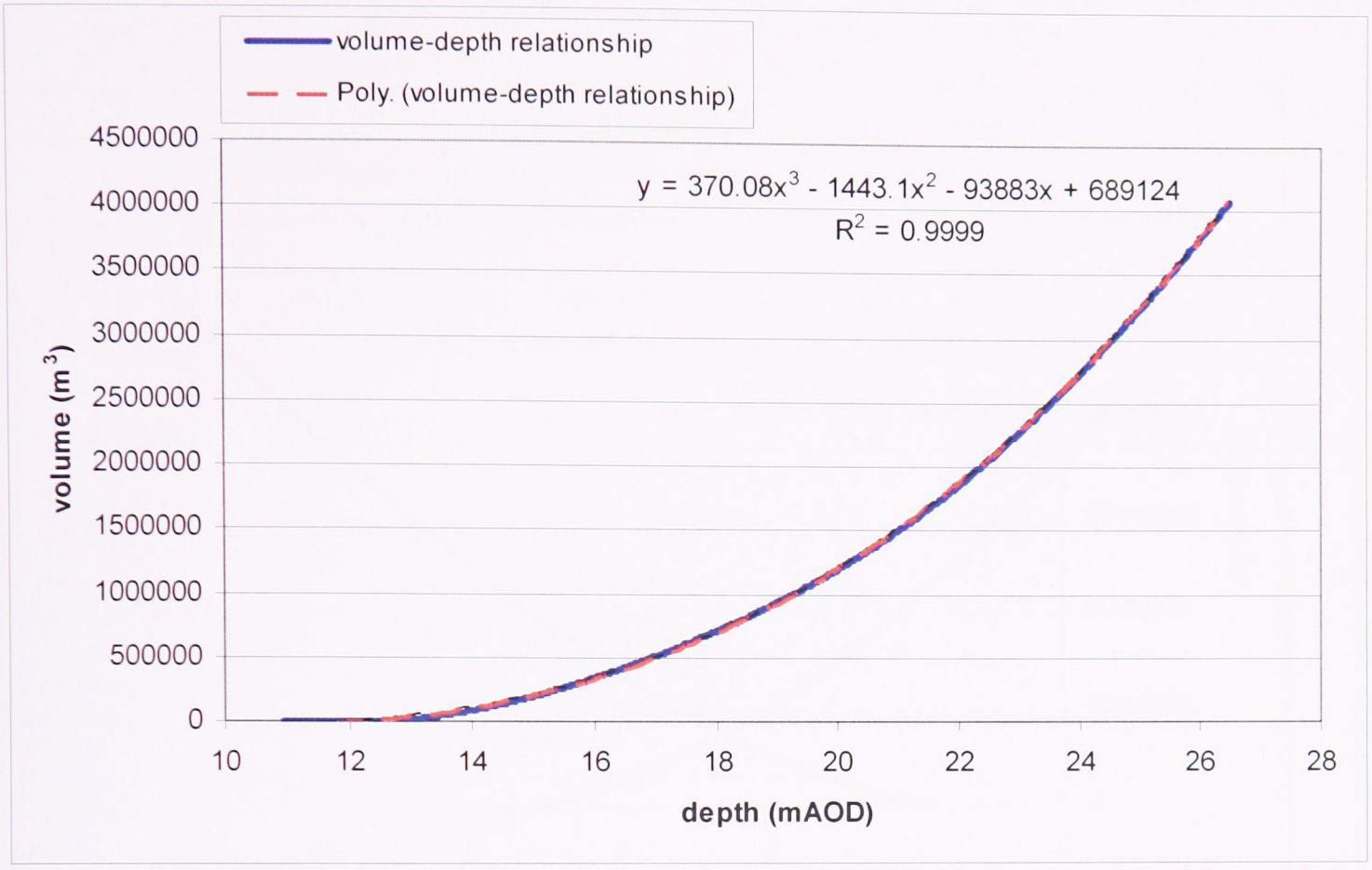


Figure B.11 Depth-volume relationship for Blackrock turlough.

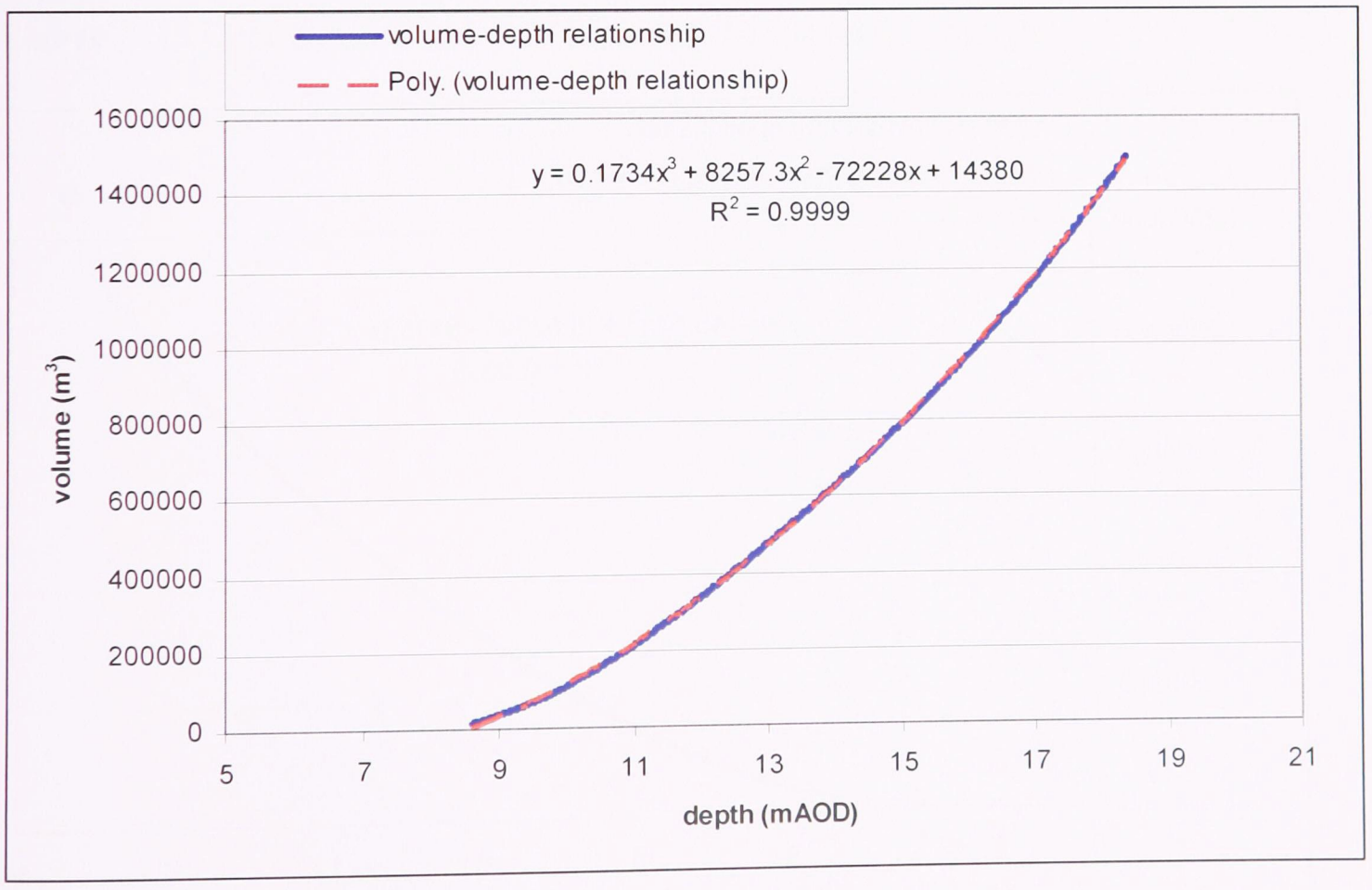


Figure B.12 Depth-volume relationship for Coy turlough.

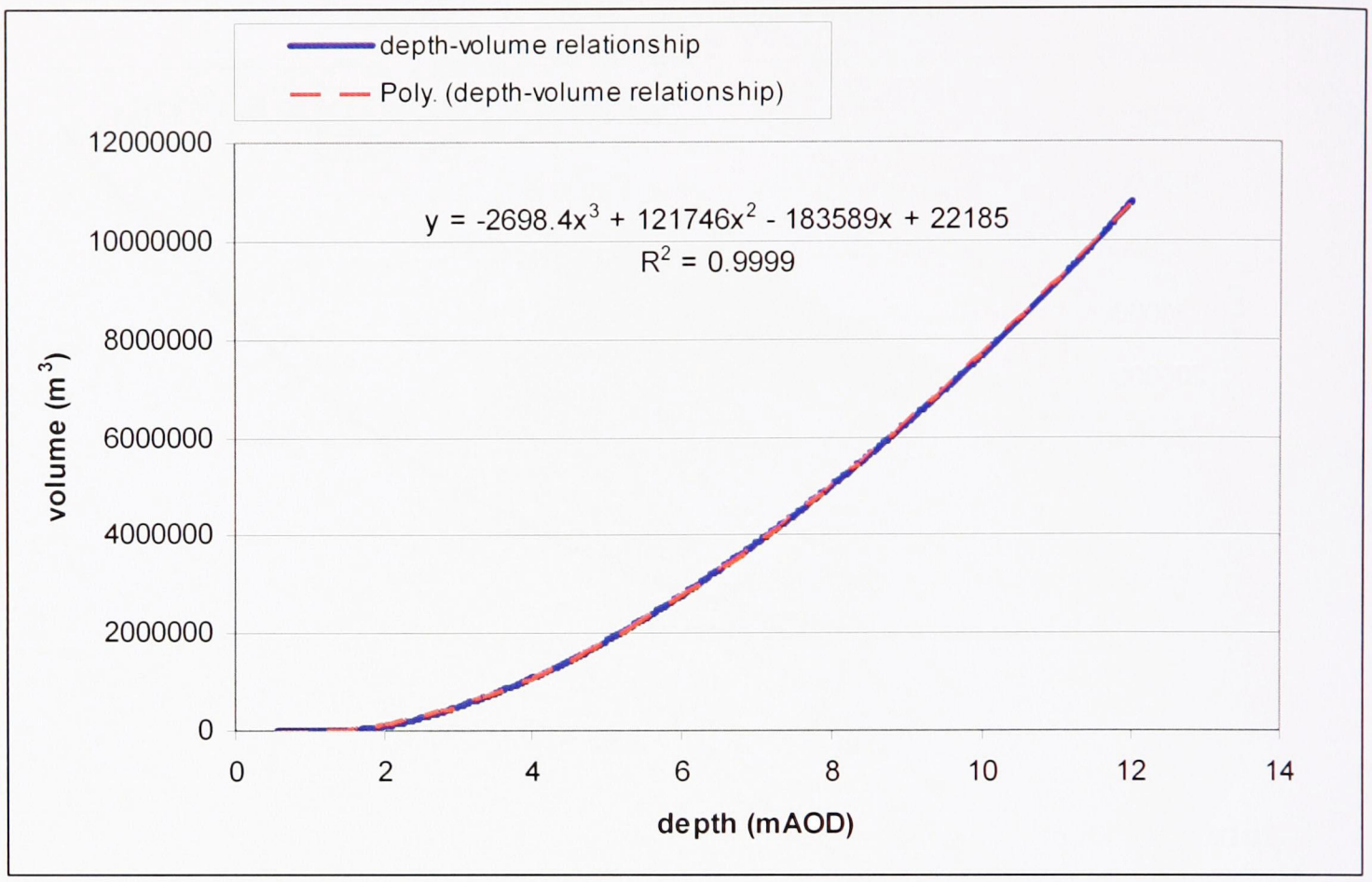


Figure B.13 Depth-volume relationship for Coole turlough.

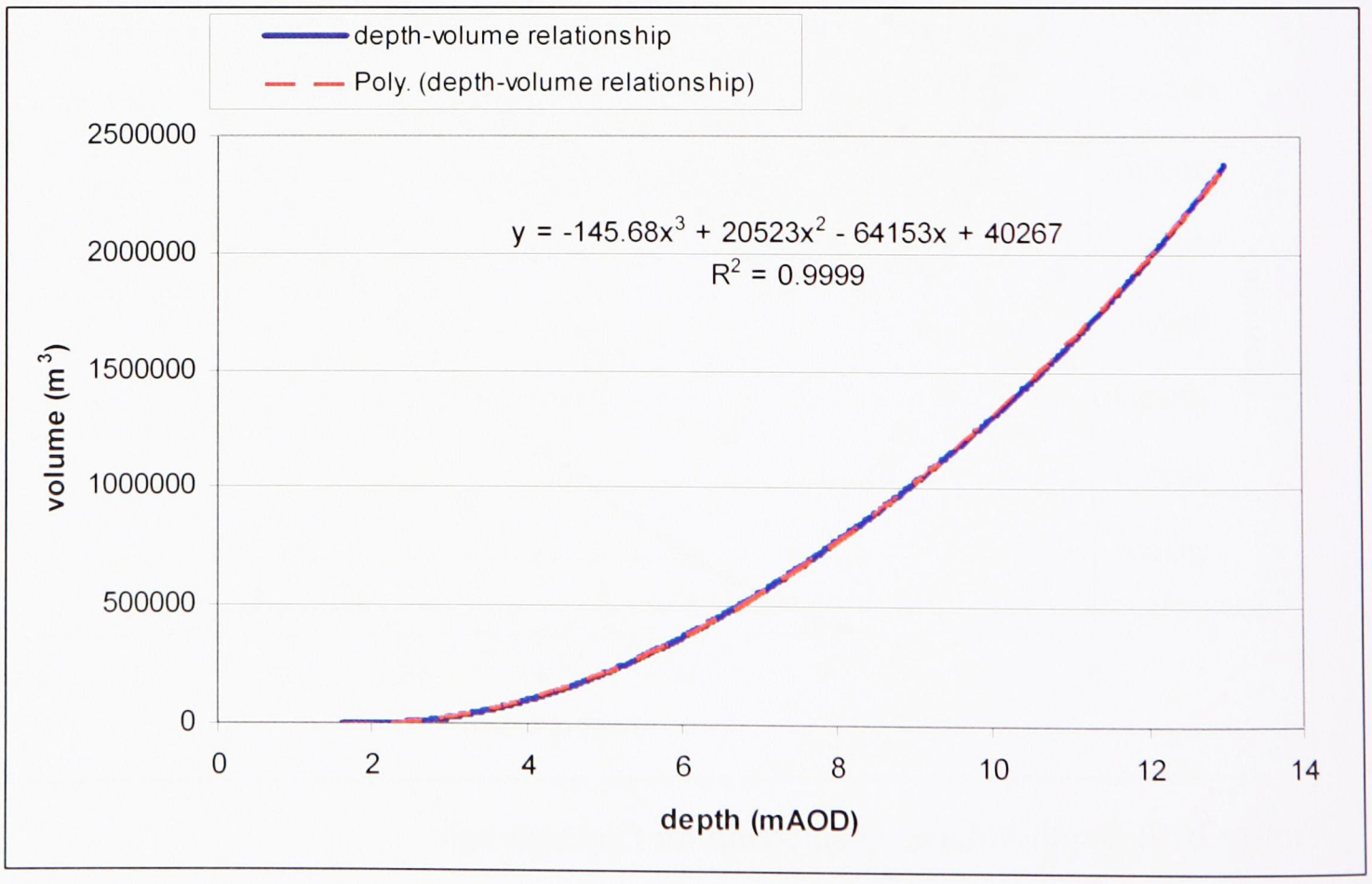


Figure B.14 Depth-volume relationship for Garryland turlough.

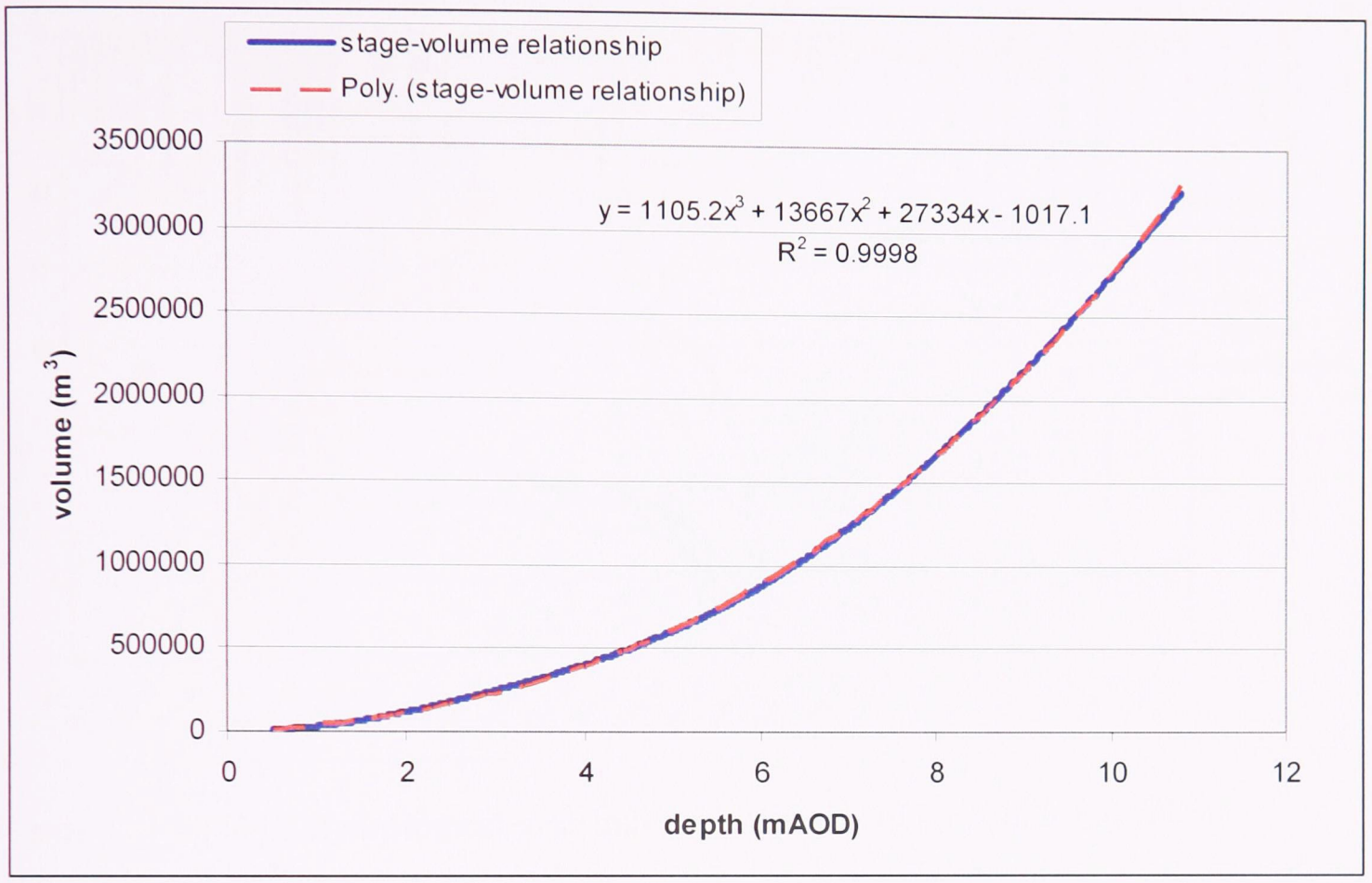


Figure B.15 Depth-volume relationship for Caherglassaun turlough.

APPENDIX C FLOW ANALYSIS

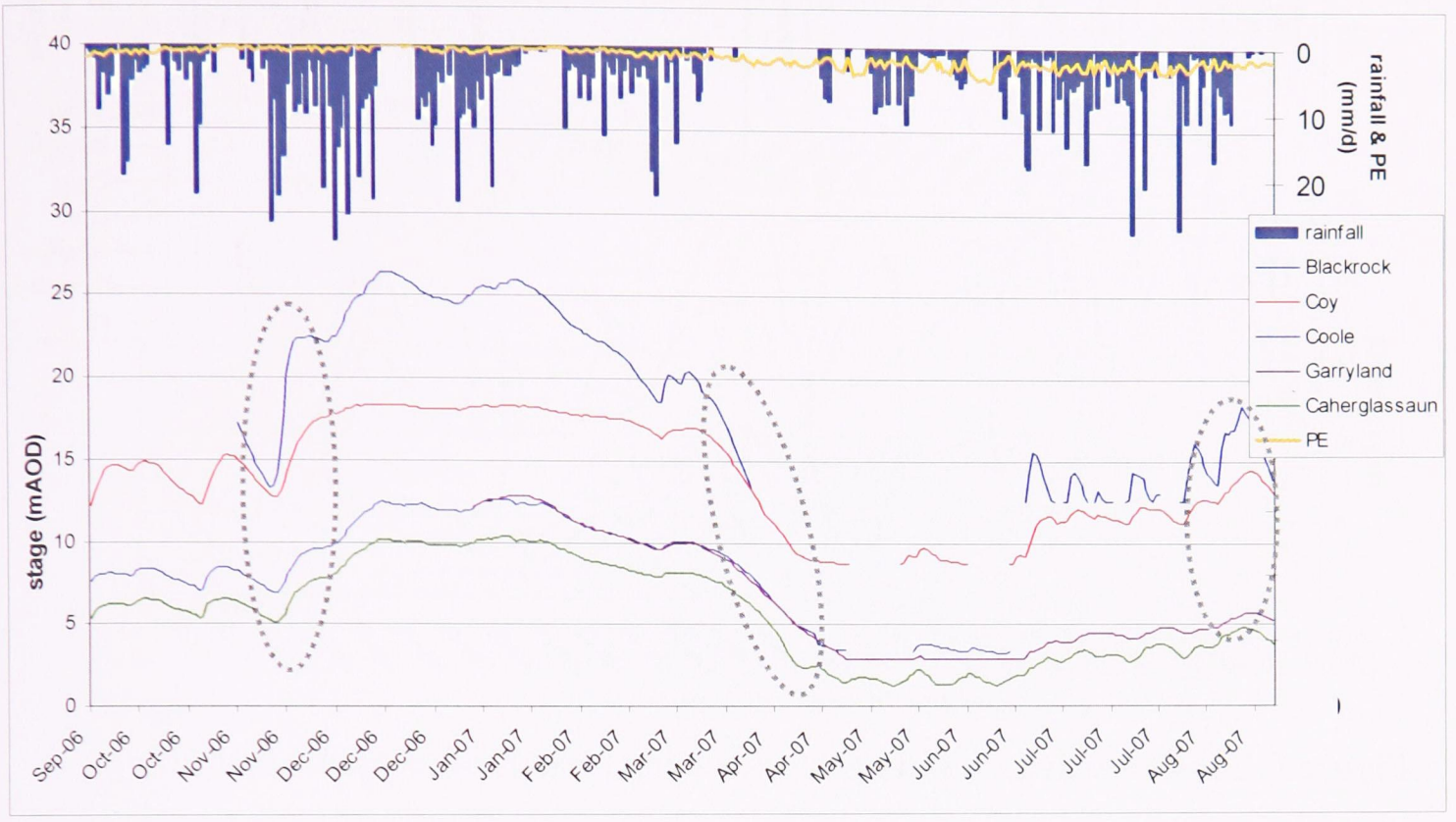


Figure C.1 2006/07 hydrological year indicating periods of recession and filling.

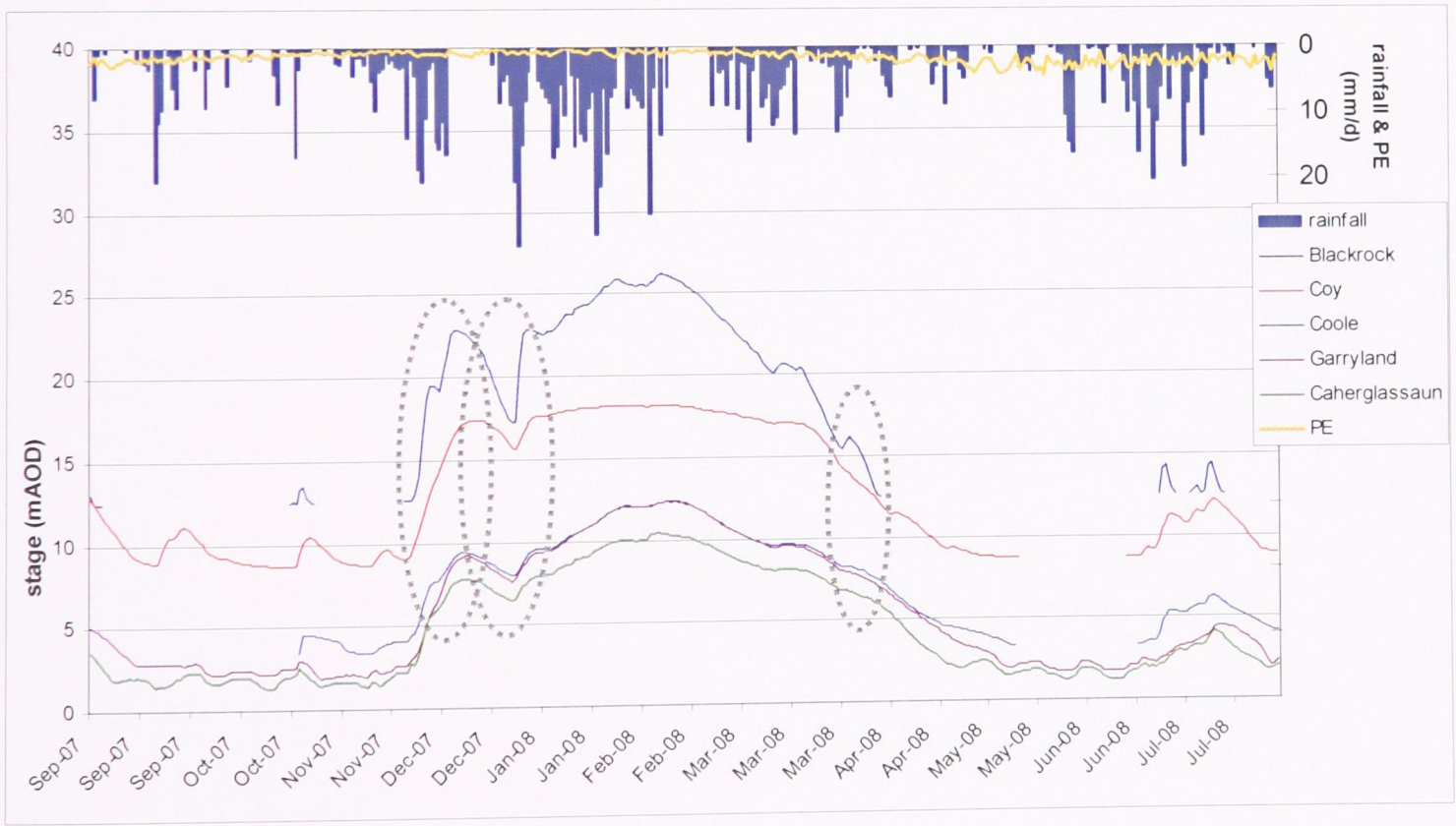


Figure C.2 2007/08 hydrological year indicating periods of recession and filling.

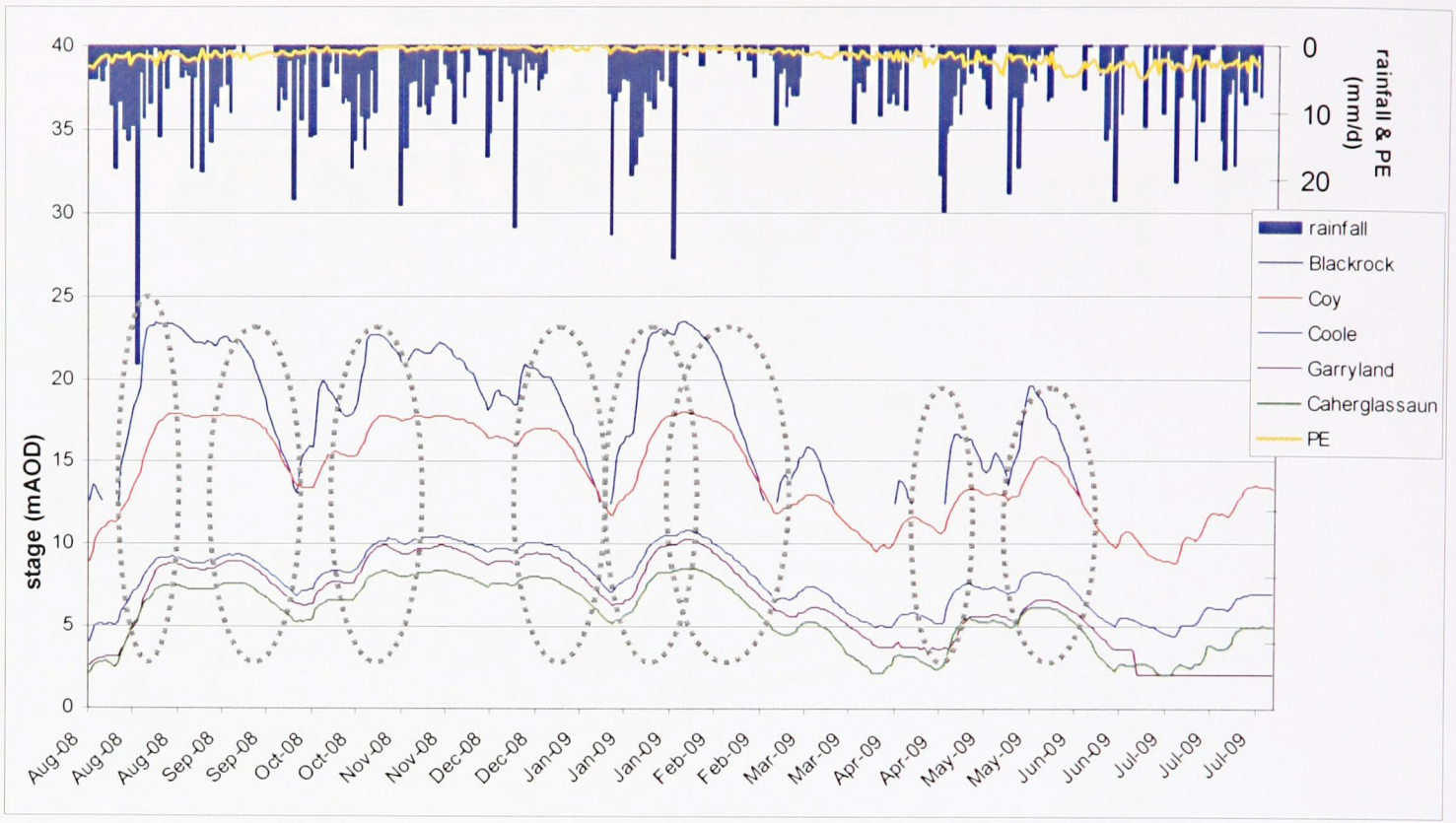
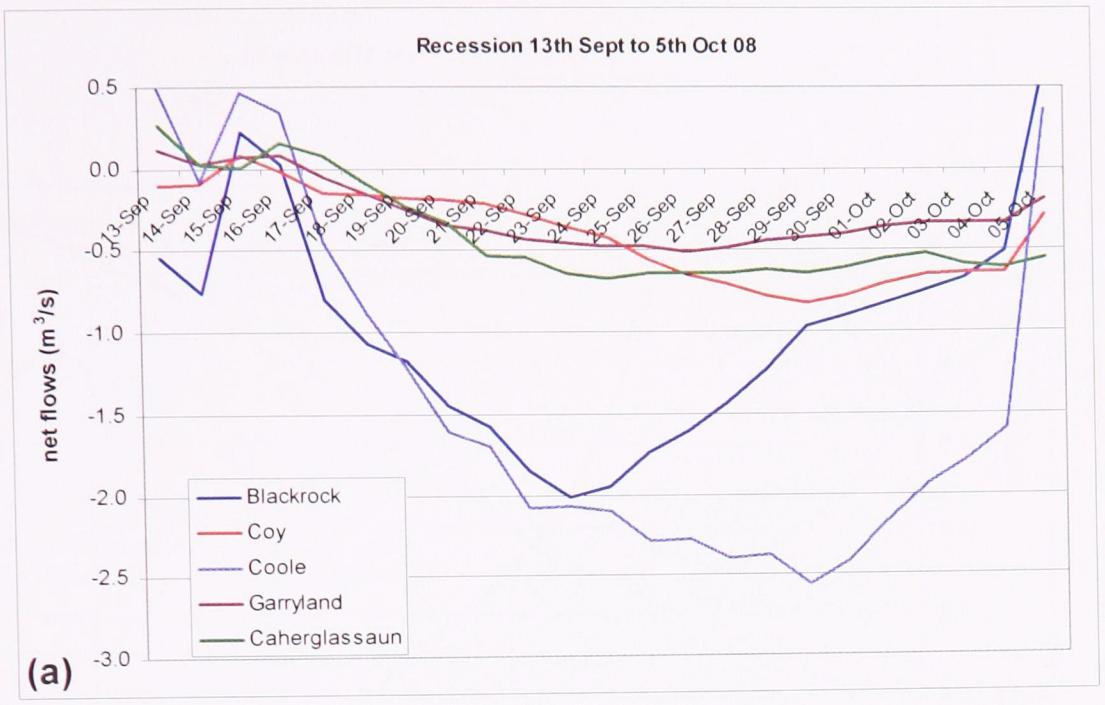
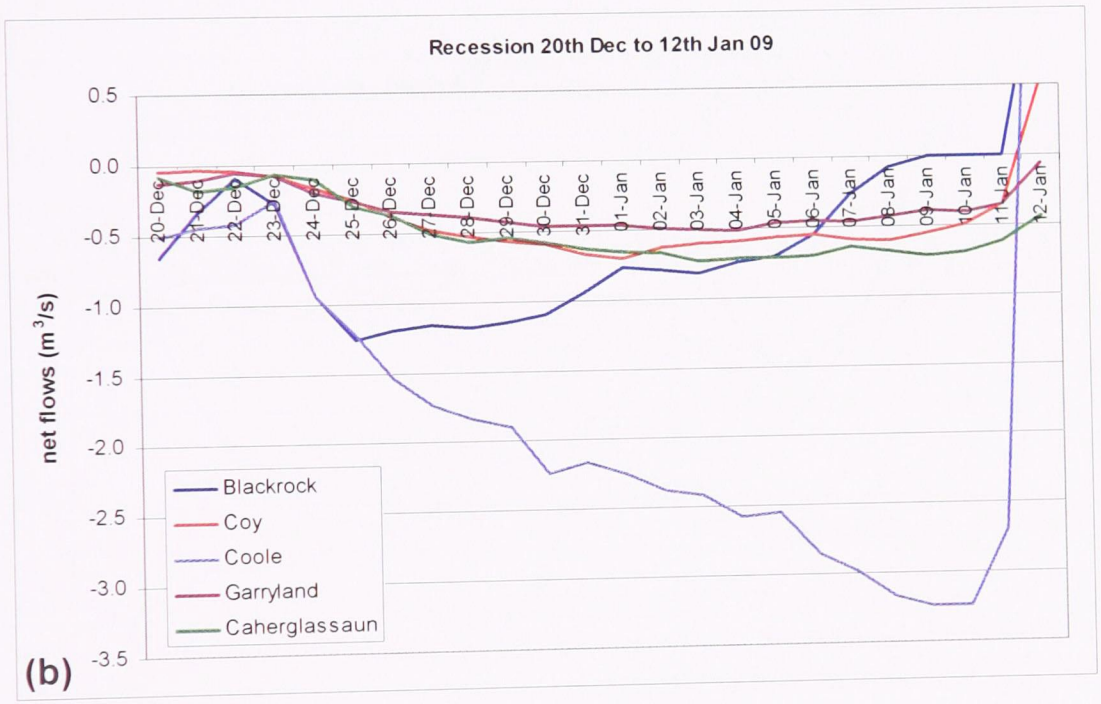
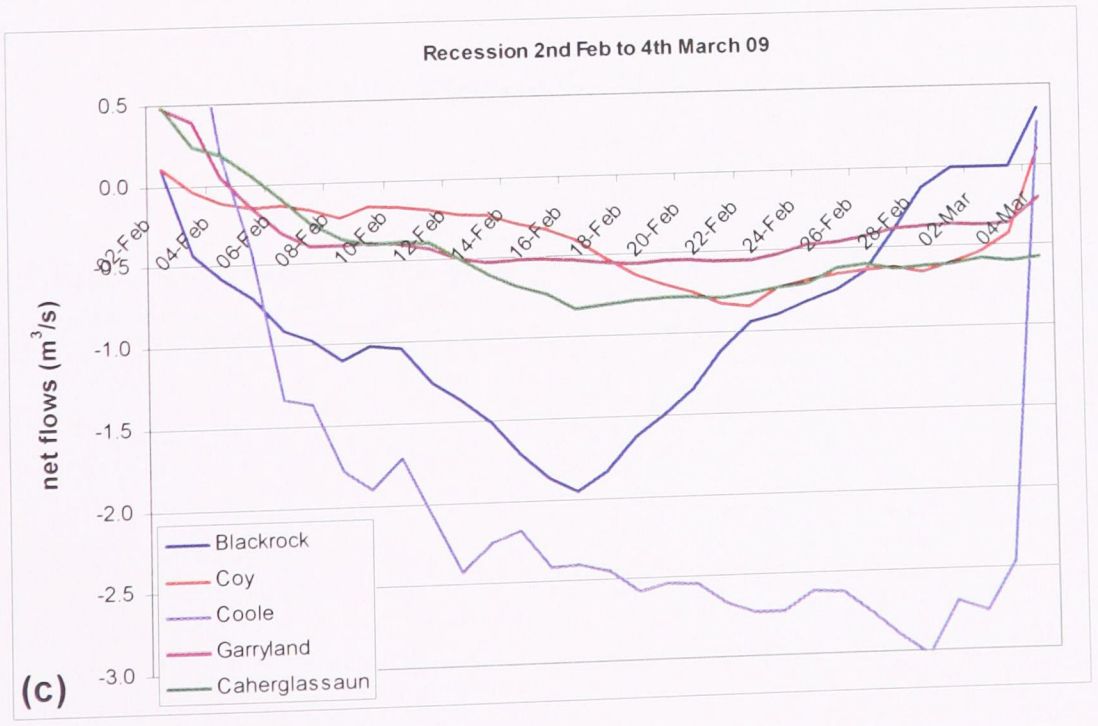


Figure C.3 2008/09 hydrological year indicating periods of recession and filling.

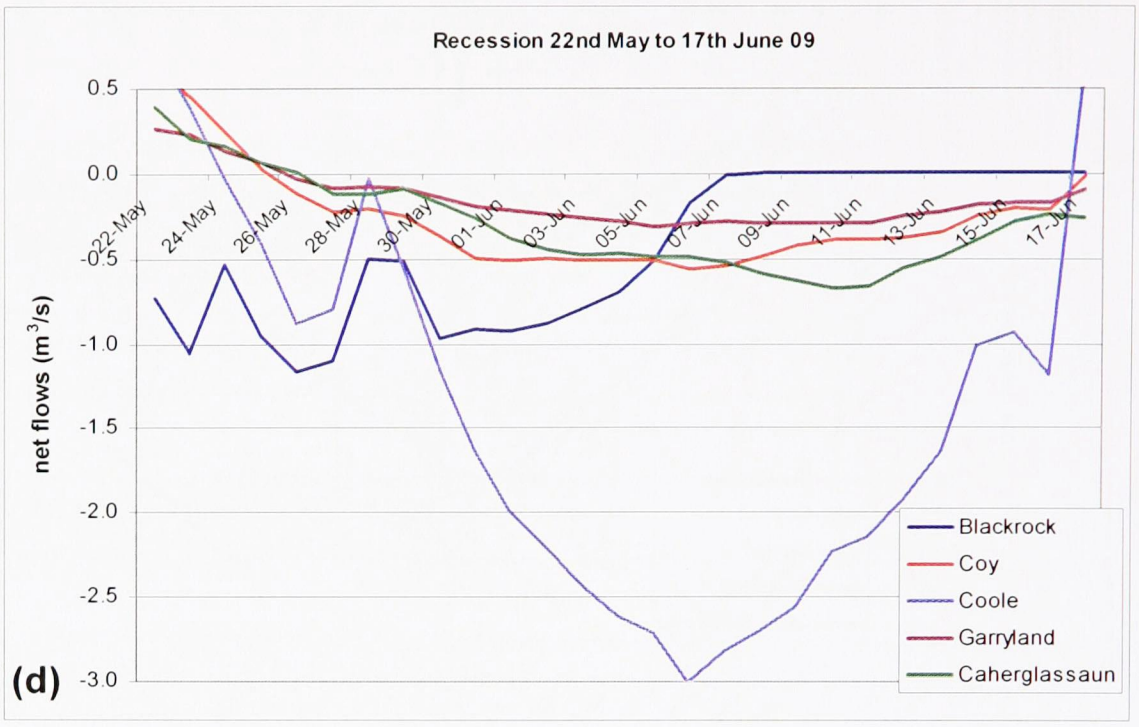
Recessions

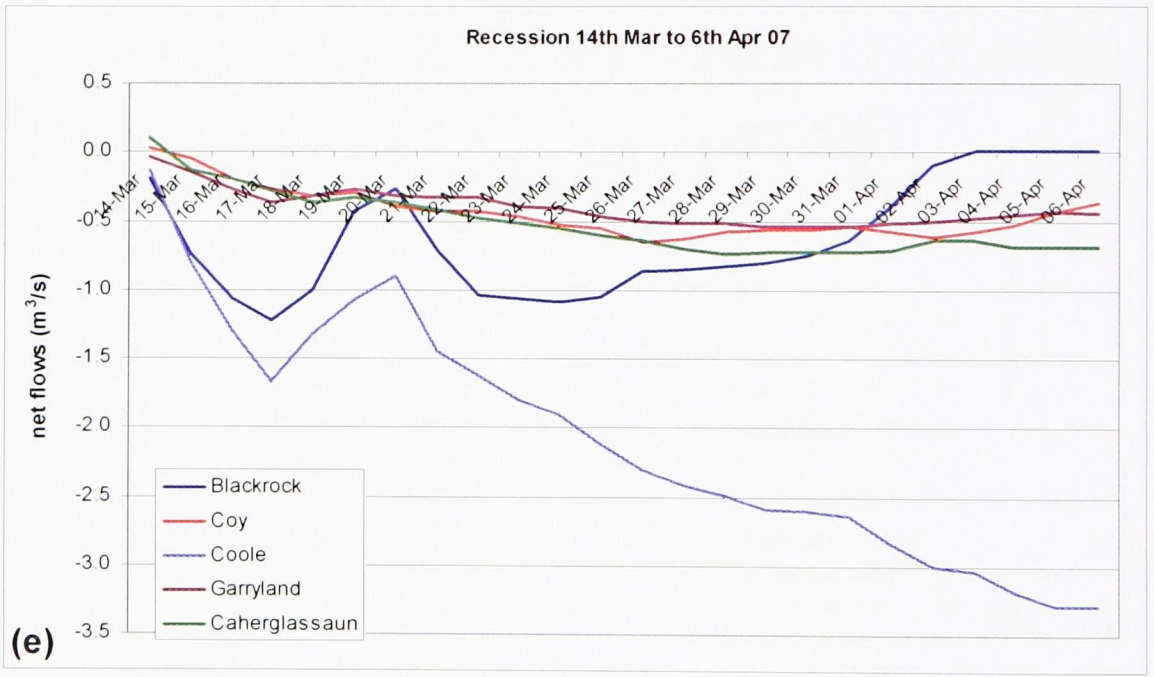

Recession 13th Sept to 5th Oct 08
net flows (m3/s)
0.5
0.0
-0.5
-1.0
-1.5
-2.0
-2.5
-3.0
13-Sep
14-Sep
15-Sep
16-Sep
17-Sep
18-Sep
19-Sep
20-Sep
21-Sep
22-Sep
23-Sep
24-Sep
25-Sep
26-Sep
27-Sep
28-Sep
29-Sep
30-Sep
01-Oct
02-Oct
03-Oct
04-Oct
05-Oct
Blackrock
Coy
Coole
Garryland
Caherglassaun
(a)

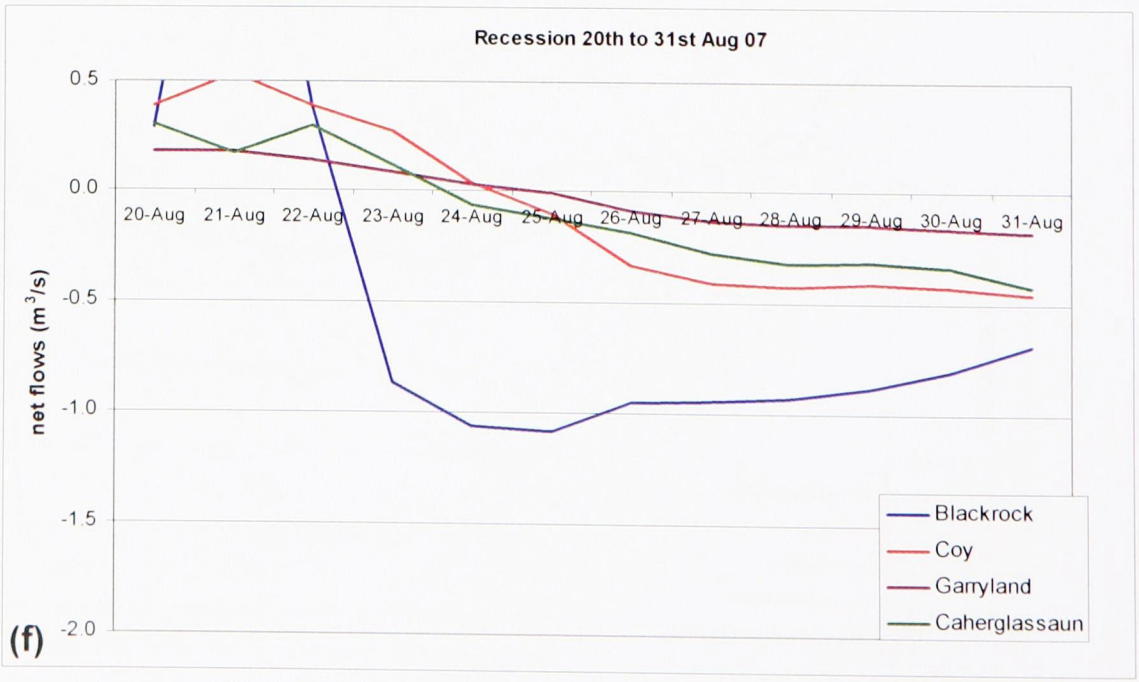

Recession 20th Dec to 12th Jan 09
net flows (m3/s)
0.5
0.0
-0.5
-1.0
-1.5
-2.0
-2.5
-3.0
-3.5
20-Dec
21-Dec
22-Dec
23-Dec
24-Dec
25-Dec
26-Dec
27-Dec
28-Dec
29-Dec
30-Dec
31-Dec
01-Jan
02-Jan
03-Jan
04-Jan
05-Jan
06-Jan
07-Jan
08-Jan
09-Jan
10-Jan
11-Jan
12-Jan
Blackrock
Coy
Coole
Garryland
Caherglassaun
(b)


Recession 2nd Feb to 4th March 09
net flows (m3/s)
0.5
0.0
-0.5
-1.0
-1.5
-2.0
-2.5
-3.0
02-Feb
04-Feb
06-Feb
08-Feb
10-Feb
12-Feb
14-Feb
16-Feb
18-Feb
20-Feb
22-Feb
24-Feb
26-Feb
28-Feb
02-Mar
04-Mar
Blackrock
Coy
Coole
Garryland
Caherglassaun
(c)

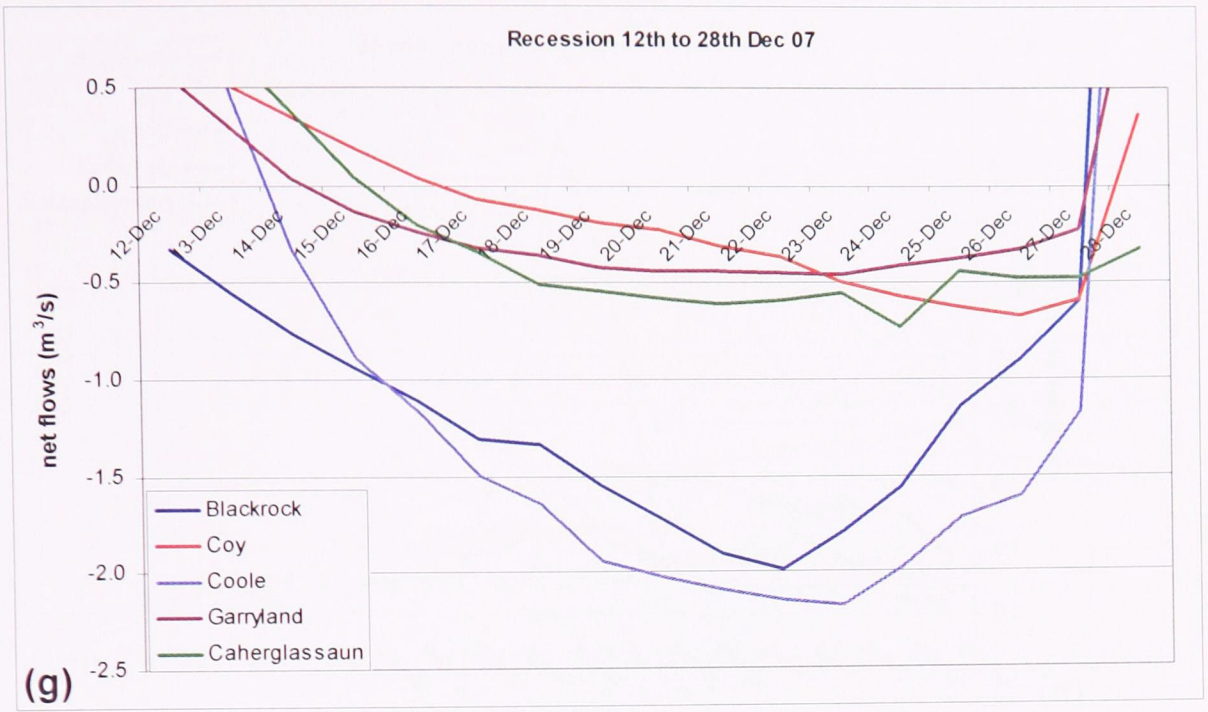
Recessions (cont.)

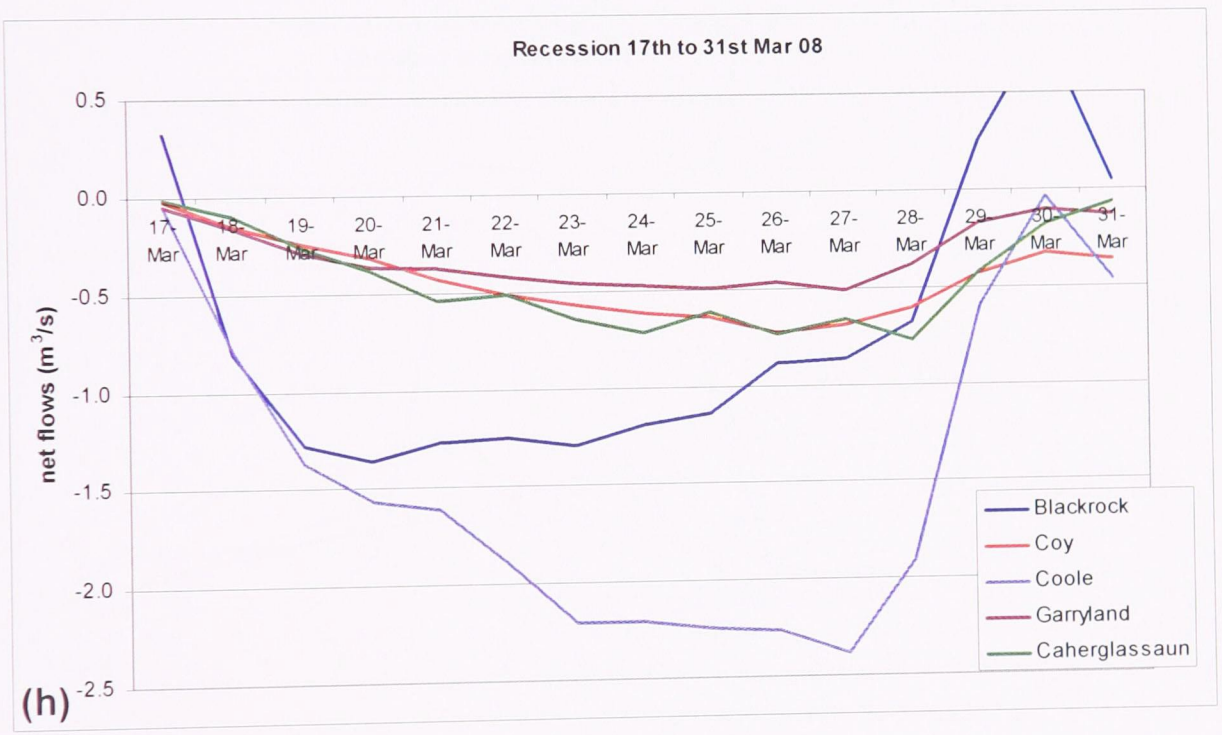




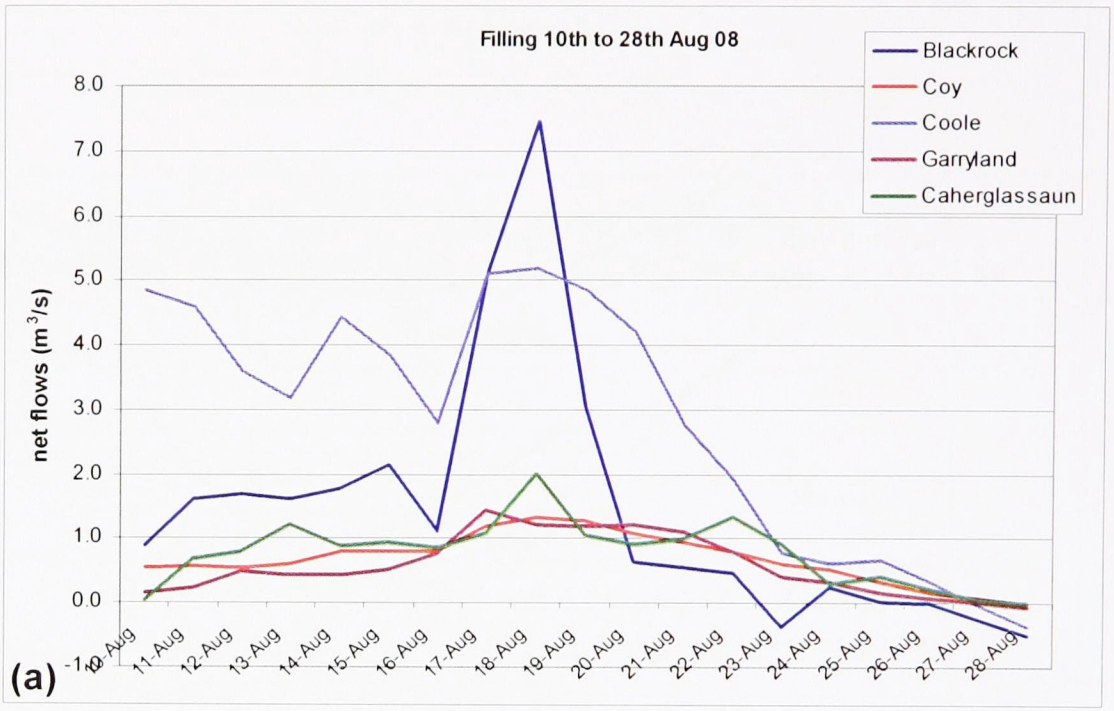


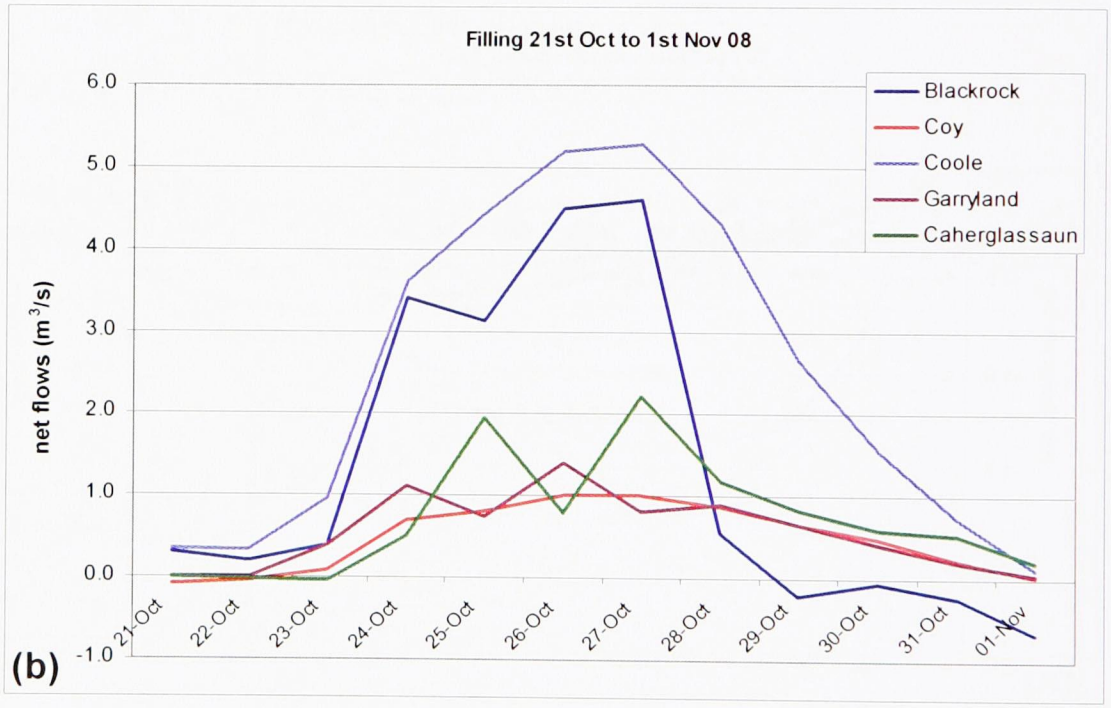
Recessions (cont.)

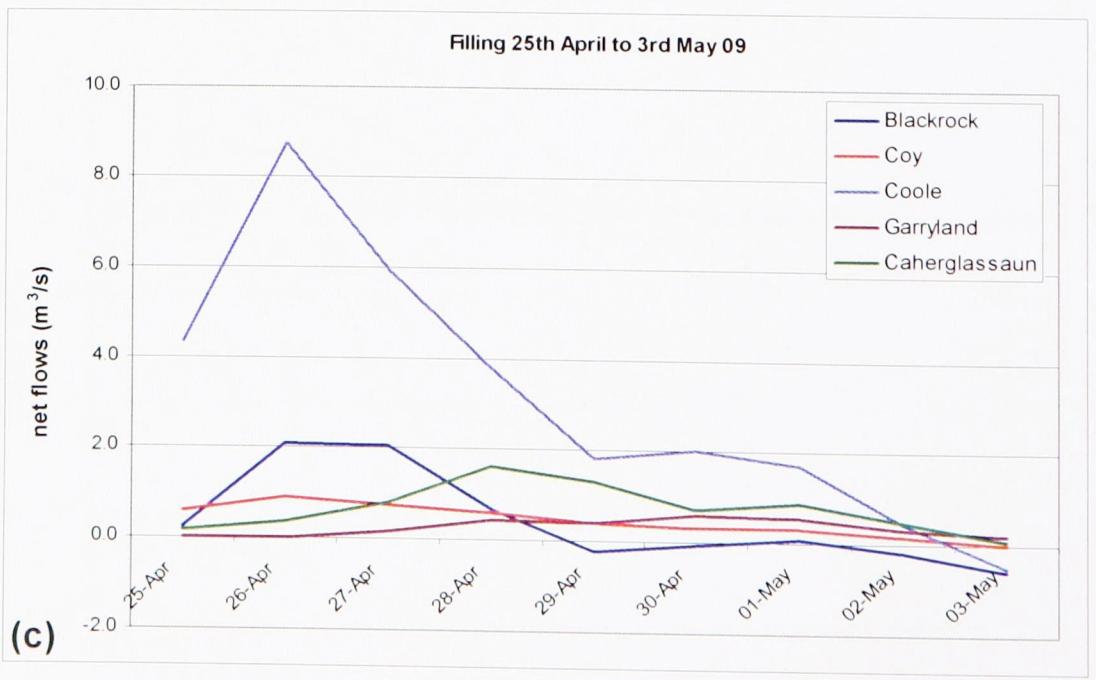




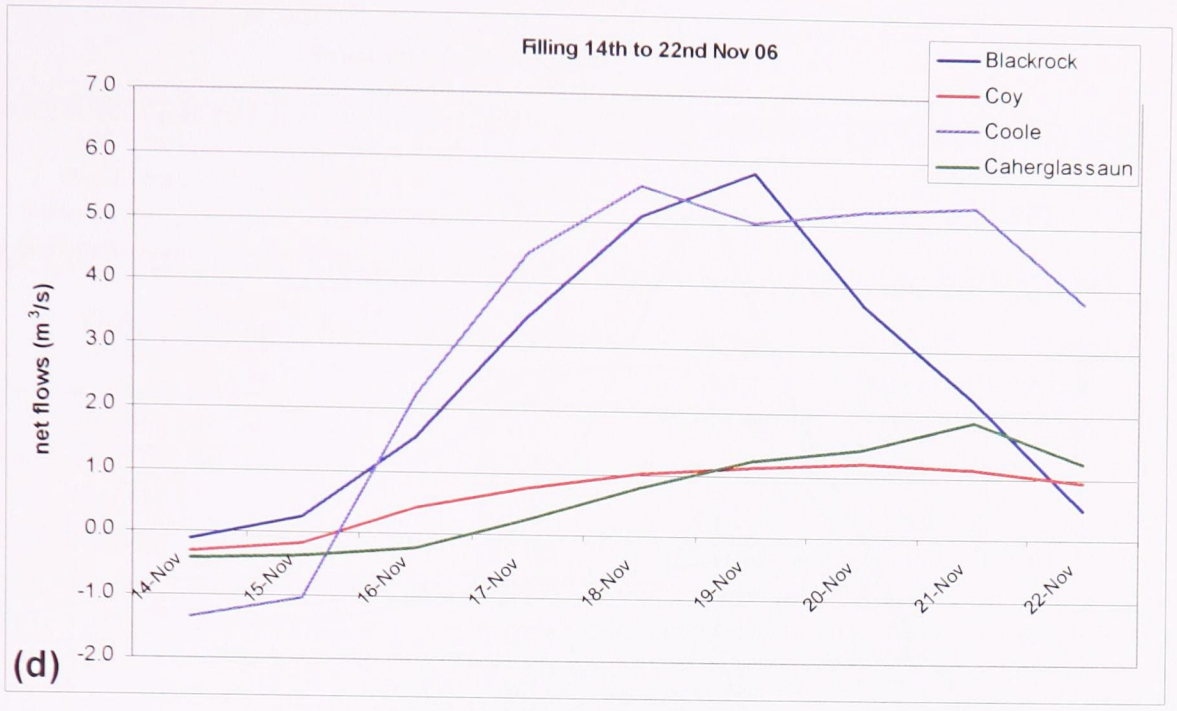
Filling periods

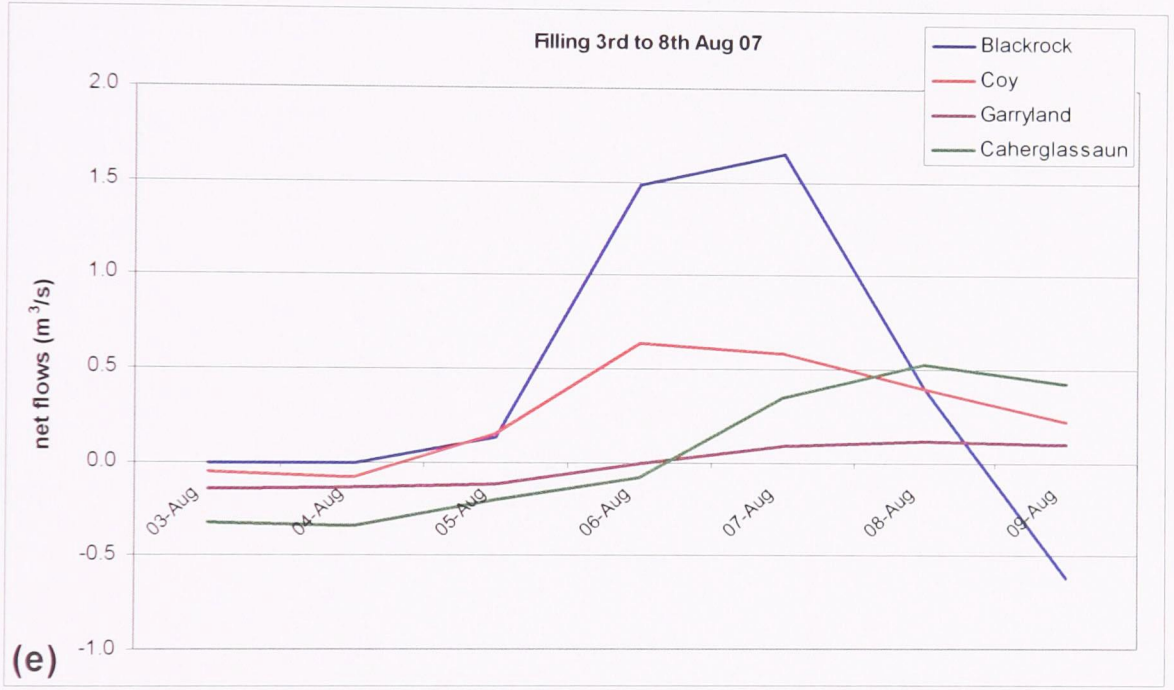


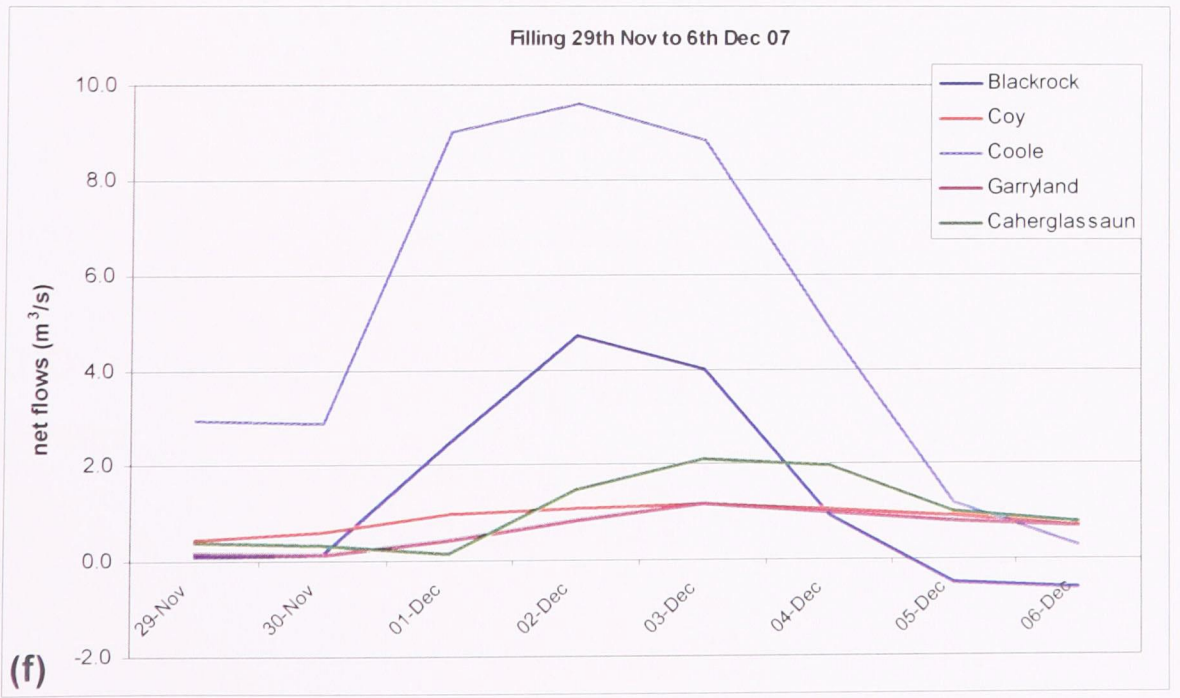




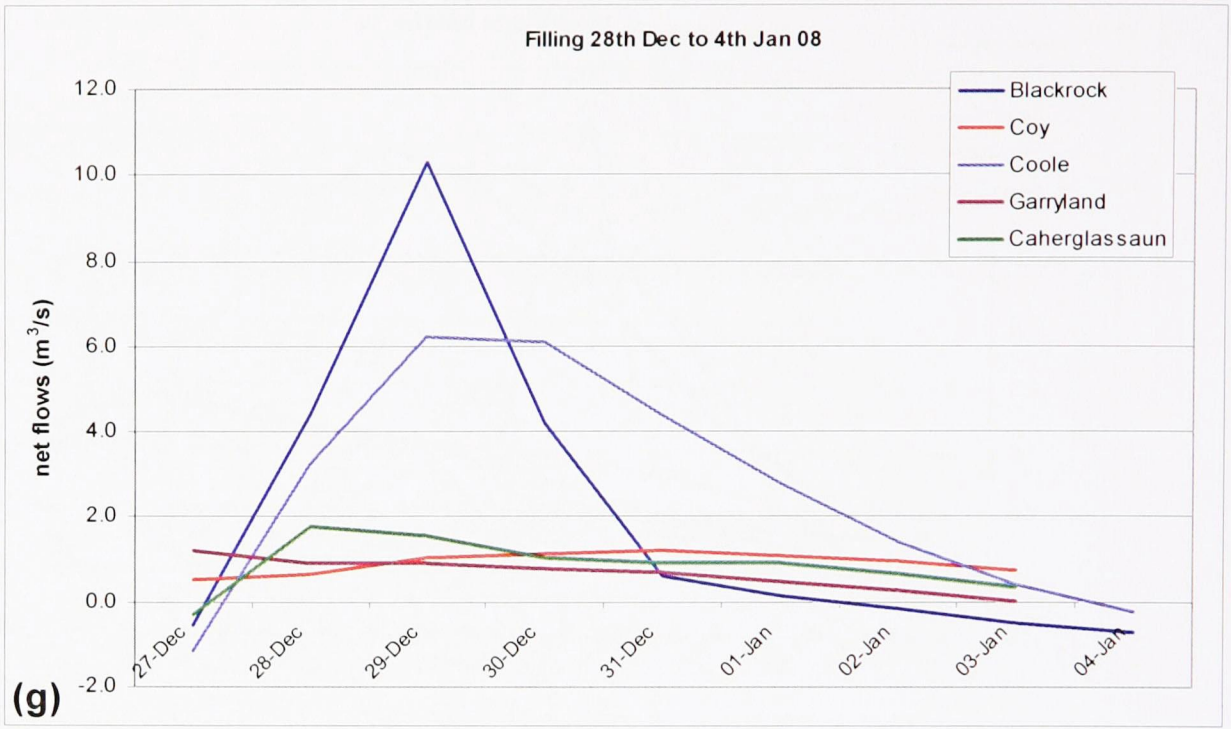
Filling periods (cont.)







Filling periods (cont.)



APPENDIX D RATING CURVES

OWNESHREE RIVER *(at Kilchreest OPW gauging station)* [grid ref. 572 150]

Table D.1 River gauging data collected for Owenshree river (at Kilchreest).

Date	Time	Mean depth (m)	Mean velocity (m/s)	Area (m^2)	Flow (m^3/s)	Stage (m)	OPW stage (m)
22/05/2009	17:30	0.283	0.298	2.635	0.785	0.09	0.09
28/05/2009	14:30	0.327	0.380	3.039	1.156	0.12	0.11
29/05/2009	10:00	0.251	0.249	2.337	0.583	0.06	0.05
04/06/2009	18:30	0.163	0.106	1.513	0.16	-0.04	0
05/06/2009	10:30	0.165	0.126	1.532	0.193	-0.04	0
12/06/2009	18:30	0.144	0.091	1.335	0.122	-0.06	0
13/06/2009	09:15	0.148	0.083	1.275	0.114	-0.06	0
17/06/2009	12:45	0.475	0.761	4.42	3.365	0.28	0.23
30/06/2009	16:00	0.123	0.068	1.145	0.077	-0.07	0
04/07/2009	17:30	0.133	0.097	1.237	0.12	-0.06	0
05/07/2009	14:00	0.143	0.094	1.33	0.125	-0.05	0
13/07/2009	14:15	0.436	0.742	4.052	3.008	0.28	0.3
14/07/2009	10:30	0.355	0.442	3.304	1.46	0.14	0.14
29/07/2009	12:30	0.274	0.316	2.547	0.805	0.09	0.09

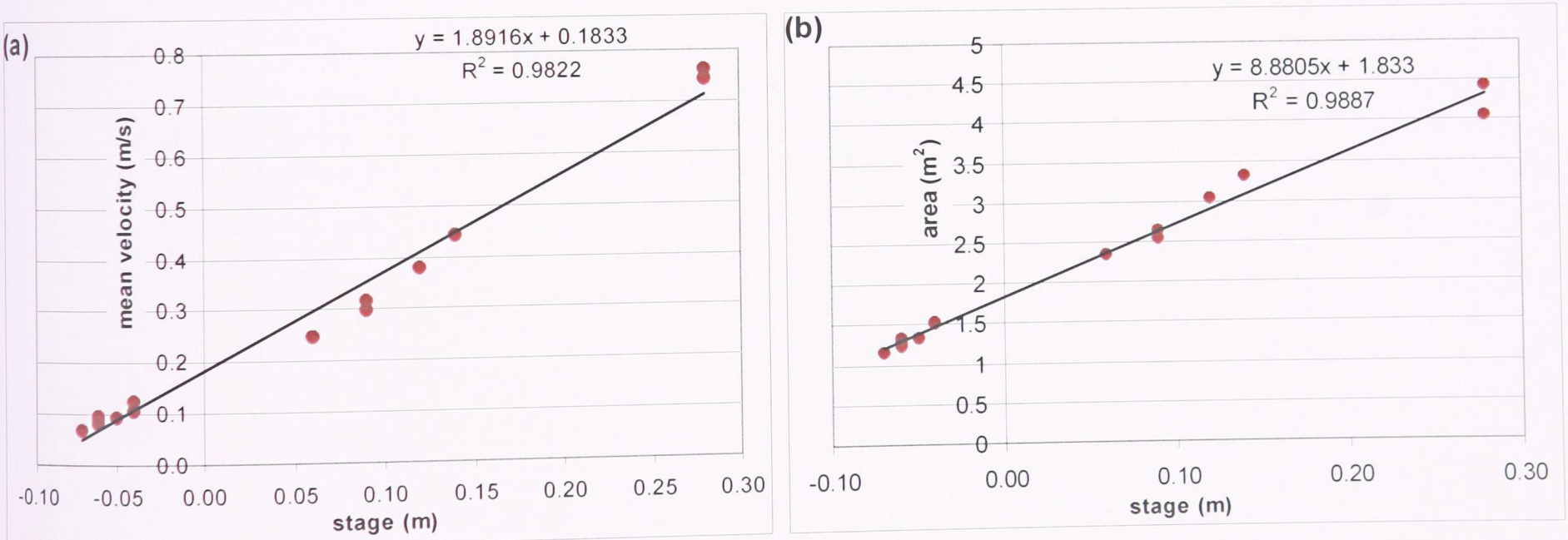


Figure D.1 Owenshree river (at Kilchreest) **(a)** stage-velocity and **(b)** stage-cross sectional area relationships.

Stage (m)	Flow (m^3/s)
-0.07	0.08
-0.06	0.12
-0.06	0.11
-0.06	0.12
-0.05	0.13
-0.04	0.16
-0.04	0.19
0.06	0.58
0.09	0.79
0.09	0.81
0.12	1.16
0.14	1.46
0.28	3.37
0.28	3.01
0.4	5.06
0.45	6.03
0.5	7.08
0.55	8.22
0.6	9.44
0.65	10.75
0.7	12.13

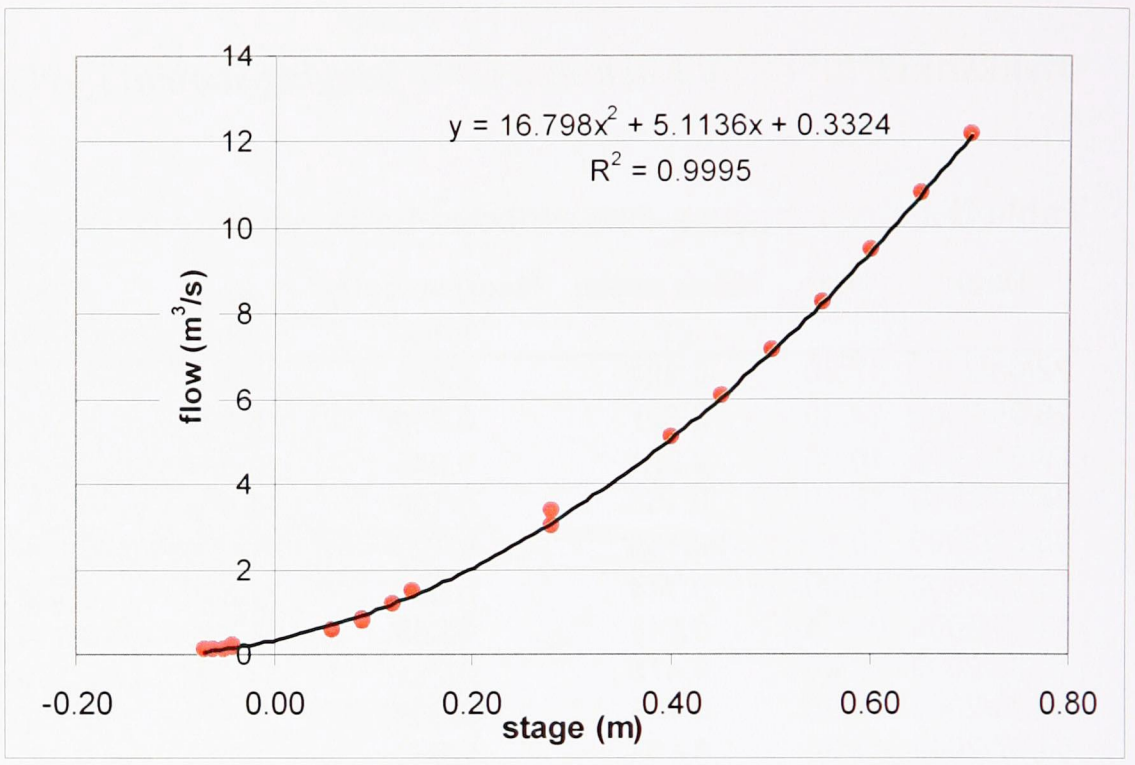


Figure D.2 Stage-flow data and rating curve for Owenshree River (at Kilchreest) – (*values in blue calculated using velocity-area method*).

Rating equation for Owenshree River (at Kilchreest) [grid ref. 572 150]

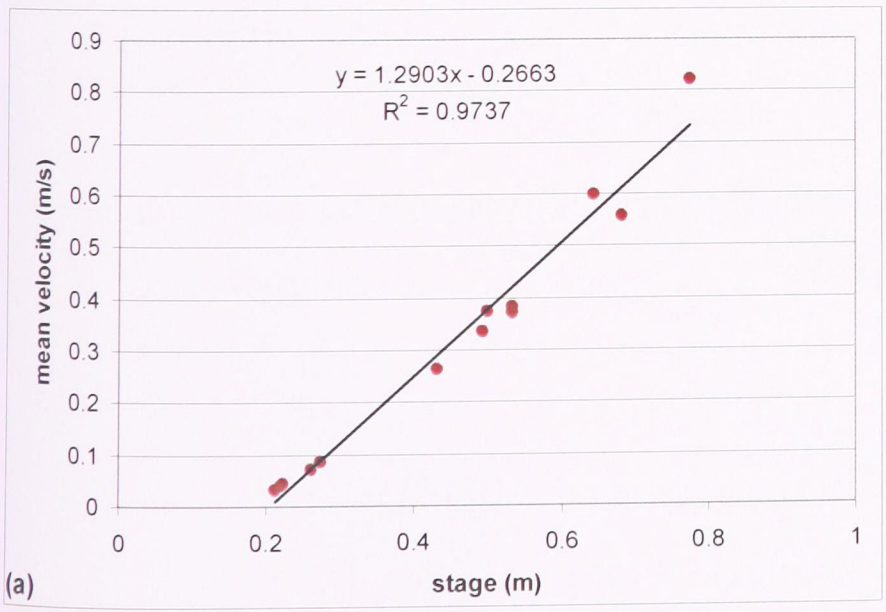
$$flow\left(m^3/s\right) = 16.798\left(stage\right)^2 + 5.1136\left(stage\right) + 0.3324 \qquad \text{Eqn. D.1}$$

OWNESHREE RIVER *(before it sinks into Blackrock turlough)* [grid ref. 516 102]

Table D.2 River gauging data collected for Owenshree river (at Blackrock).

Date	Time		Mean depth (m)	Mean velocity (m/s)	Area (m^2)	Flow (m^3/s)	Total flow (m^3/s)	stage (m)
22/05/2009	15:00	*pier 1*	0.59	0.373	1.356	0.506		
		pier 2	0.61	0.448	1.527	0.684	1.19	0.533
28/05/2009	13:30	*pier 1*	0.53	0.384	1.216	0.467		
		pier 2	0.56	0.495	1.383	0.685	1.152	0.532
29/05/2009	10:30	*pier 1*	0.45	0.264	1.037	0.274		
		pier 2	0.49	0.342	1.224	0.396	0.67	0.431
04/06/2009	17:30	*pier 1*	0.32	0.088	0.742	0.065		
		pier 2	0.36	0.125	0.894	0.112	0.177	0.274
05/06/2009	11:00	*pier 1*	0.32	0.071	0.744	0.053		
		pier 2	0.37	0.105	0.91	0.095	0.148	0.262
12/06/2009	17:30	*pier 1*	0.28	0.042	0.672	0.028		
		pier 2	0.32	0.076	0.797	0.061	0.089	0.221
13/06/2009	10:00	*pier 1*	0.28	0.034	0.676	0.023		
		pier 2	0.33	0.067	0.813	0.055	0.078	0.214
17/06/2009	13:15	*pier 1*	0.64	0.558	1.558	1.068		
		pier 2	0.78	0.689	1.715	1.332	2.4	0.681
30/06/2009	15:30	*pier 1*	0.17	-0.002	0.418	-0.001		
		pier 2	0.22	0.026	0.553	0.014	0.013	0.114
04/07/2009	15:45	*pier 1*	0.24	0.034	0.59	0.02		
		pier 2	0.29	0.05	0.723	0.036	0.056	0.184
05/07/2009	13:30	*pier 1*	0.27	0.046	0.647	0.03		
		pier 2	0.32	0.08	0.785	0.063	0.093	0.224
13/07/2009	14:50	*pier 1*	0.49	0.375	1.172	0.439		
		pier 2	0.52	0.462	1.303	0.602	1.041	0.499
13/07/2009	18:00	*pier 1*	0.71	0.823	1.721	1.417		
		pier 2	0.80	0.901	1.96	1.77	3.187	0.774
14/07/2009	11:00	*pier 1*	0.61	0.601	1.463	0.879		
		pier 2	0.64	0.688	1.602	1.102	1.981	0.642
29/07/2009	13:15	*pier 1*	0.48	0.337	1.17	0.395		
		pier 2	0.53	0.439	1.322	0.581	0.976	0.493

Pier 1 width = 2.42 m Pier 2 width = 2.49 m



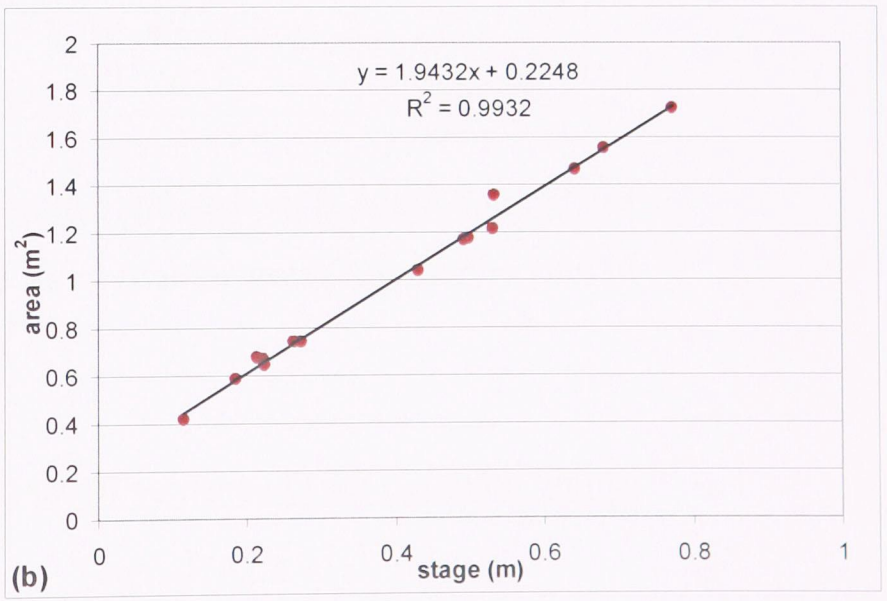
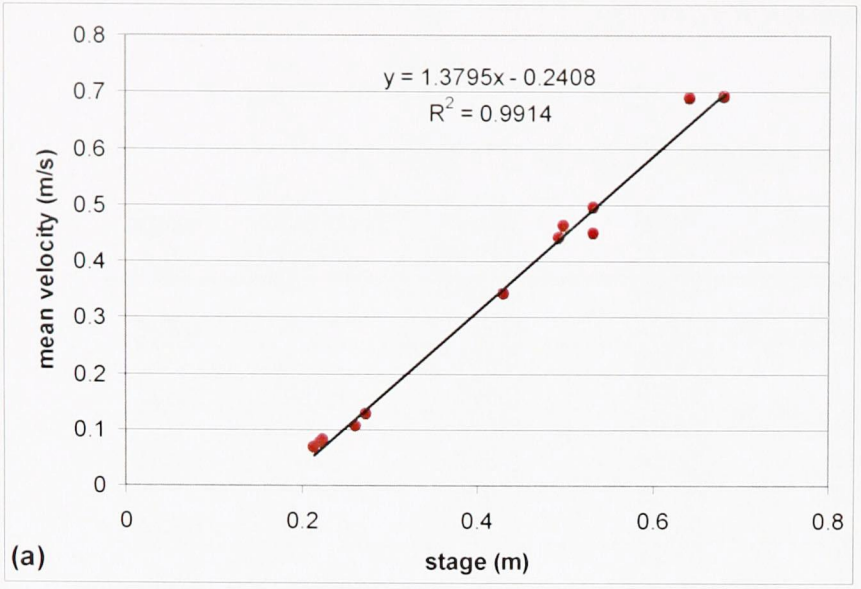


Figure D.3 Owenshree river (at Blackrock) Pier 1 **(a)** stage-velocity and **(b)** stage-cross sectional area relationships.



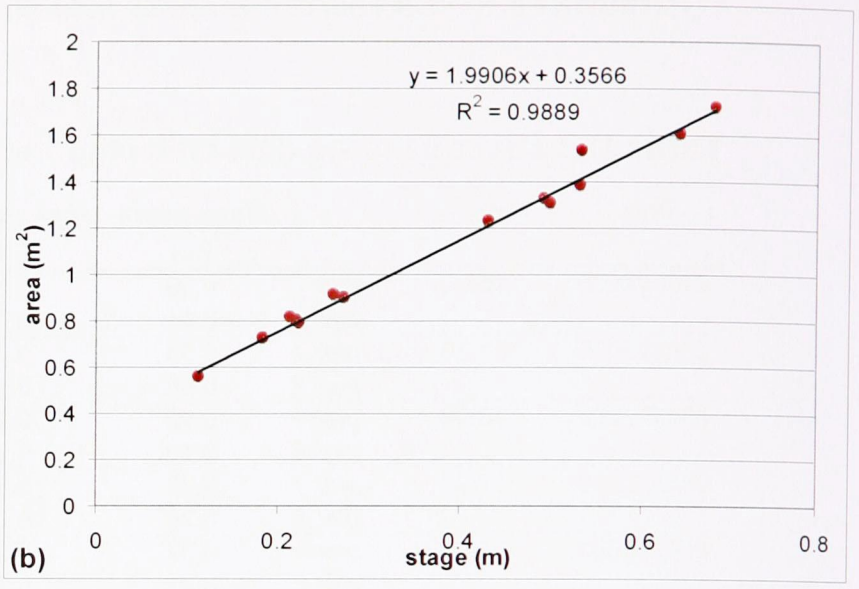


Figure D.4 Owenshree river (at Blackrock) Pier 2 **(a)** stage-velocity and **(b)** stage-cross sectional area relationships.

Stage (m)	Flow (m^3/s)
0.11	0.01
0.18	0.06
0.21	0.08
0.22	0.09
0.22	0.09
0.26	0.15
0.27	0.18
0.43	0.67
0.49	0.98
0.50	1.04
0.53	1.15
0.53	1.19
0.64	1.98
0.68	2.40
0.77	3.19
0.80	3.12
0.90	4.00
1.00	4.99
1.10	6.08
1.20	7.28
1.30	8.58
1.40	9.98

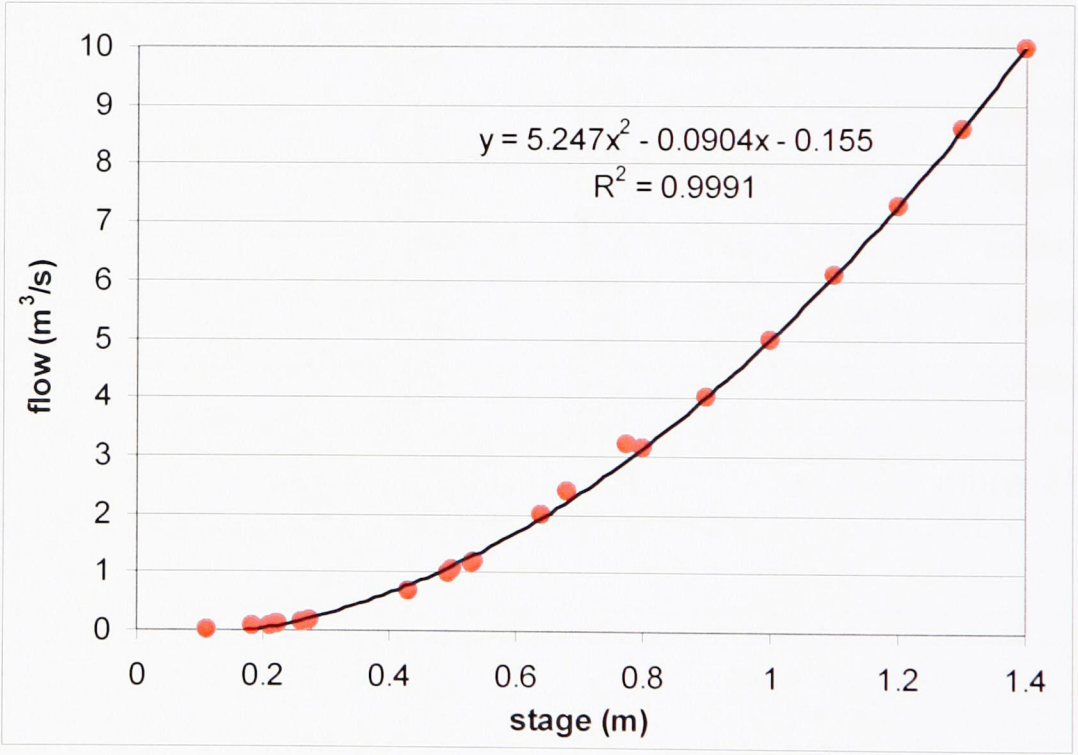


Figure D.5 Stage-flow data and rating curve for Owenshree River (at Blackrock) – (*values in blue calculated using velocity-area method*).

Rating equation for Owenshree River (at Blackrock) [grid ref. 516 102]

$$flow\left(m^3/s\right) = 5.247\left(stage\right)^2 - 0.0904\left(stage\right) - 0.155 \qquad \text{Eqn. D.2}$$

BALLYCAHALAN RIVER [grid ref. 496 057]

Table D.3 River gauging data collected for Ballycahalan river.

Date	Time	Mean depth (m)	Mean velocity (m/s)	Area (m^2)	Flow (m^3/s)	Stage (m)	OPW stage (m)
22/05/2009	16:30	0.319	0.27	2.649	0.715	0.53	0.52
28/05/2009	12:30	0.467	0.539	3.874	2.087	0.66	0.66
29/05/2009	11:30	0.323	0.276	2.678	0.74	0.51	0.51
04/06/2009	17:00	0.179	0.063	1.485	0.094	0.35	0.35
05/06/2009	11:30	0.176	0.057	1.462	0.083	0.35	0.35
12/06/2009	17:00	0.176	0.065	1.46	0.095	0.34	0.34
13/06/2009	11:00	0.181	0.05	1.504	0.075	0.34	0.35
17/06/2009	14:15	0.726	0.747	6.023	4.497	0.95	0.96
30/06/2009	15:00	0.174	0.059	1.448	0.086	0.34	0.34
04/07/2009	16:15	0.210	0.108	1.74	0.189	0.4	0.39
05/07/2009	13:00	0.247	0.105	2.051	0.215	0.41	0.41
14/07/2009	11:30	0.431	0.502	3.581	1.797	0.64	0.64
29/07/2009	13:30	0.347	0.309	2.878	0.889	0.54	0.53

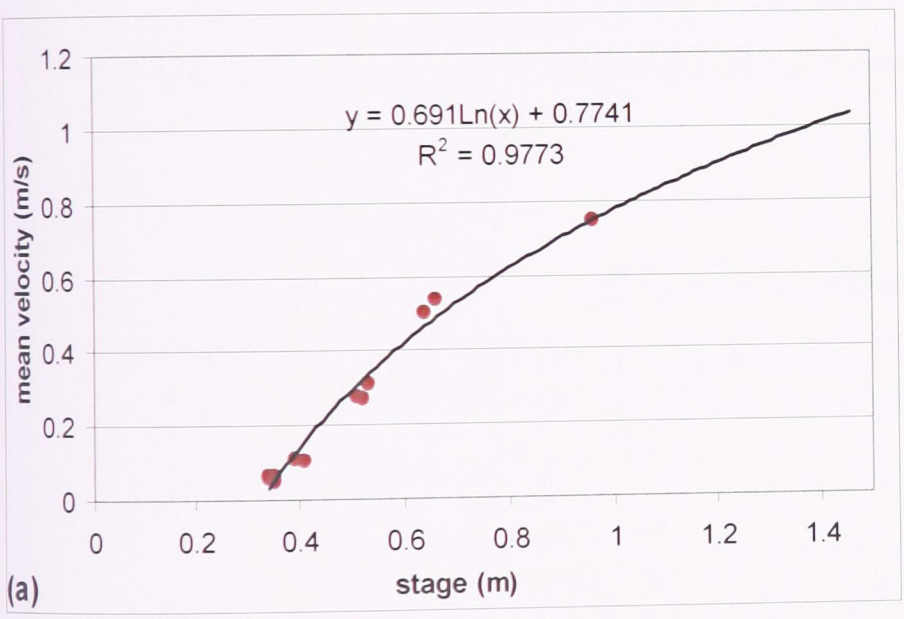


Figure D.6 Ballycahalan river **(a)** stage-velocity and **(b)** stage-cross sectional area relationships.

Stage (m)	Flow (m^3/s)
0.34	0.10
0.34	0.08
0.34	0.09
0.35	0.09
0.35	0.08
0.40	0.19
0.41	0.22
0.51	0.74
0.53	0.72
0.54	0.89
0.64	1.80
0.66	2.09
0.95	4.50
1.00	4.89
1.10	5.93
1.20	7.02
1.30	8.15
1.40	9.34
1.50	10.56
1.60	11.82
1.70	13.12
1.80	14.44
1.90	15.80
2.00	17.19

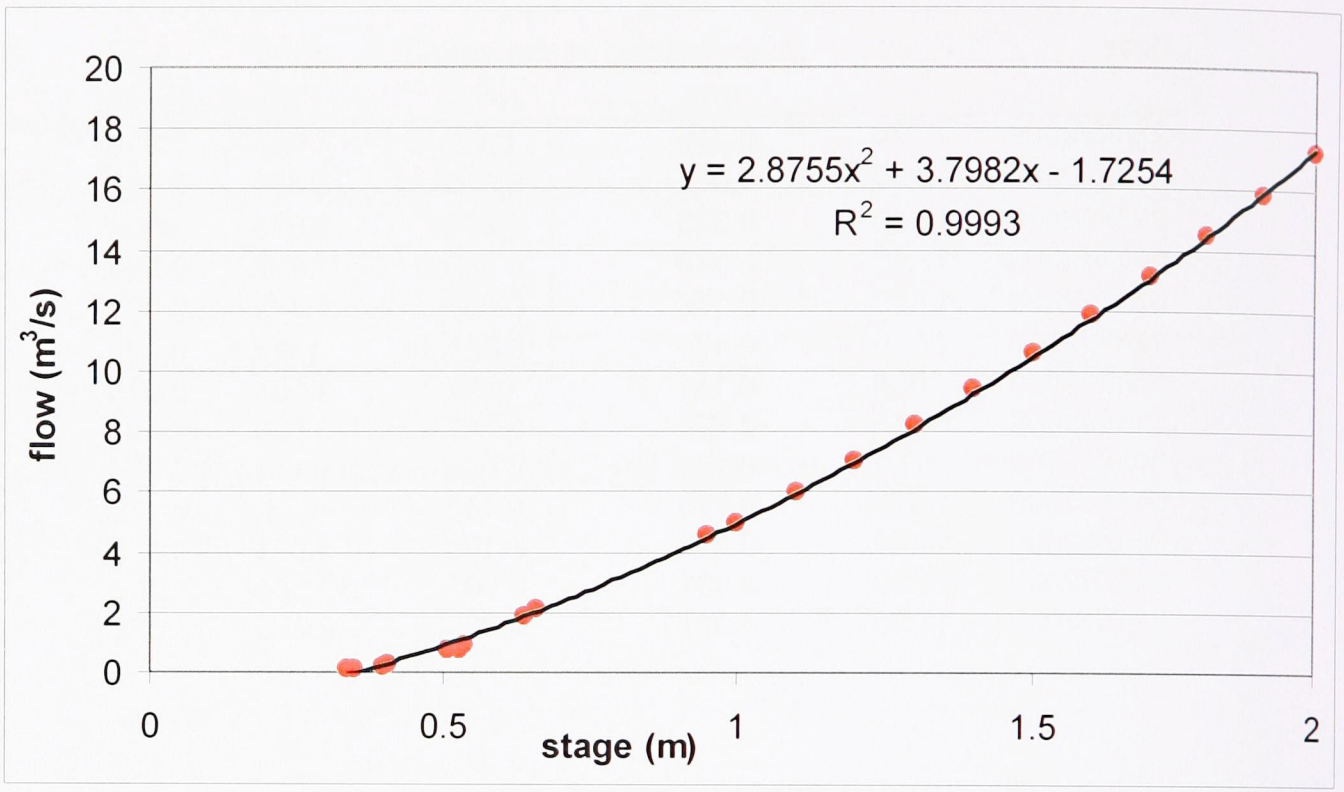


Figure D.7 Stage-flow data and rating curve for Ballycahalan River– (*values in blue calculated using velocity-area method*).

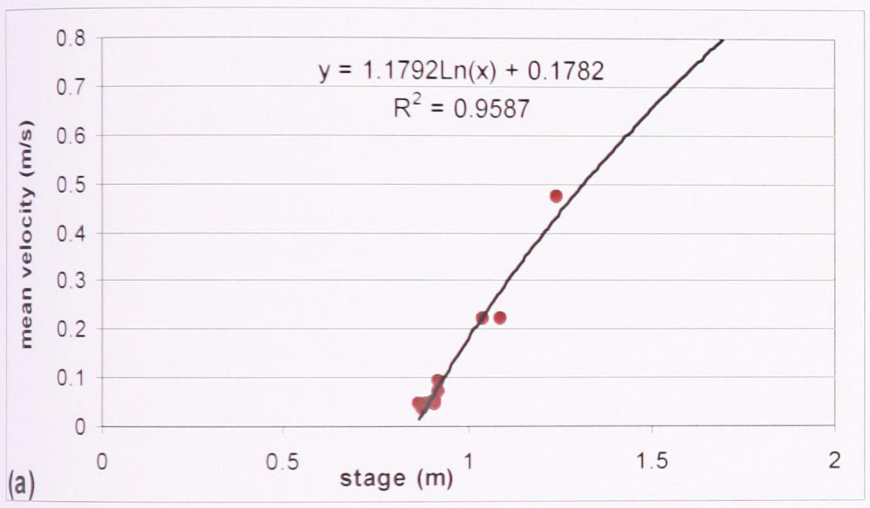
Rating equation for Ballycahalan River [grid ref. 496 057]

$$flow\left(m^3/s\right) = 2.8755\left(stage\right)^2 + 3.7982\left(stage\right) - 1.7254 \qquad \text{Eqn. D.3}$$

OWENDALULLEEGH RIVER [grid ref. 484 972]

Table D.4 River gauging data collected for Owendalulleegh river.

Date	Time	Mean depth (m)	Mean velocity (m/s)	Area (m^2)	Flow (m^3/s)	Stage (m)	OPW stage (m)
29/05/2009	12:30	0.610	0.222	6.705	1.491	1.1	1.09
04/06/2009	14:30	0.455	0.053	5.008	0.266	0.92	0.91
05/06/2009	12:30	0.460	0.046	5.06	0.233	0.92	0.91
12/06/2009	15:00	0.414	0.037	4.55	0.169	0.91	0.88
13/06/2009	11:30	0.467	0.048	5.14	0.249	0.93	0.89
30/06/2009	13:00	0.425	0.048	4.67	0.226	0.87	0.87
04/07/2009	16:45	0.455	0.071	5.003	0.355	0.905	0.92
05/07/2009	11:00	0.480	0.092	5.28	0.488	0.92	0.92
14/07/2009	12:00	0.731	0.473	8.04	3.802	1.25	1.24
29/07/2009	14:15	0.583	0.222	6.413	1.412	1.03	1.04



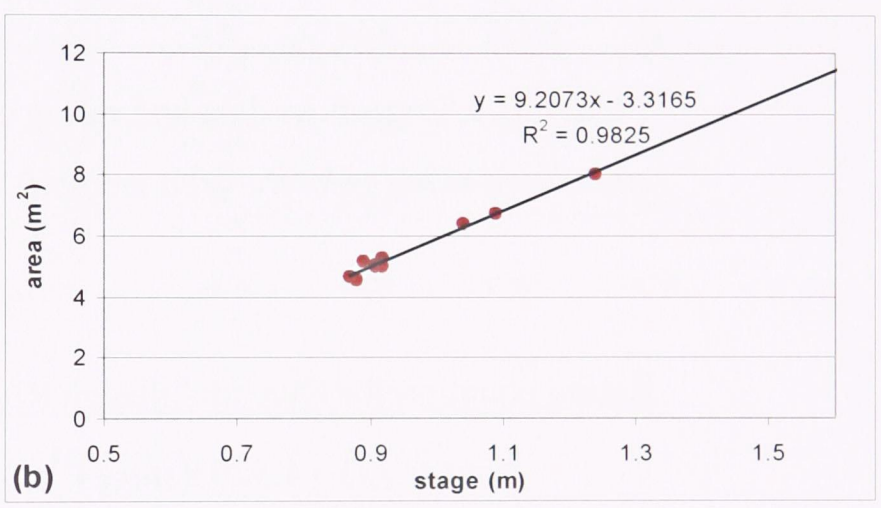


Figure D.8 Owendalulleegh river **(a)** stage-velocity and **(b)** stage-cross sectional area relationships.

Stage (m)	Flow (m^3/s)
0.87	0.23
0.88	0.17
0.89	0.25
0.91	0.27
0.91	0.23
0.92	0.36
0.92	0.49
1.04	1.41
1.09	1.49
1.24	3.80
1.30	4.22
1.40	5.50
1.50	6.89
1.60	8.36
1.70	9.92
1.80	11.55
1.90	13.26
2.00	15.03
2.10	16.87
2.20	18.77
2.30	20.72

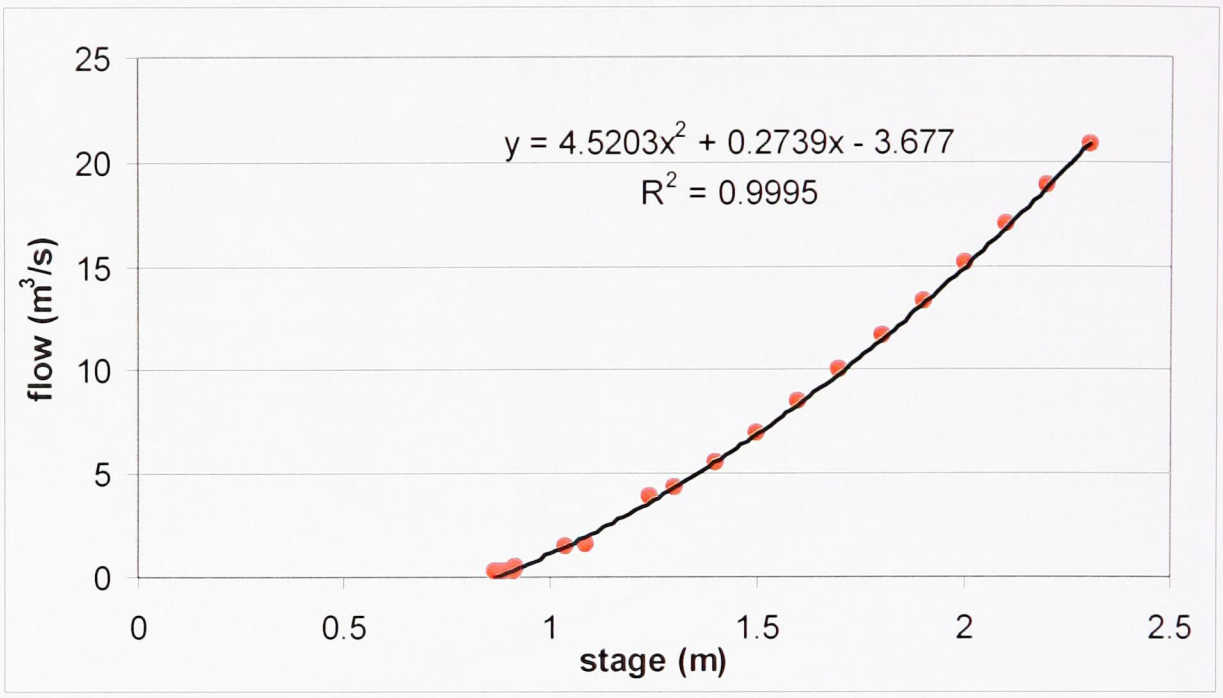


Figure D.9 Stage-flow data and rating curve for Owendalulleegh River– (*values in blue calculated using velocity-area method*).

Rating equation for Owendalulleegh River [grid ref. 484 972]

$$flow\left(m^3/s\right) = 4.5203\left(stage\right)^2 + 0.2739\left(stage\right) - 3.677 \qquad \text{Eqn. D.4}$$

BEAGH RIVER [grid ref. 482 005]

Table D.4 River gauging data collected for Beagh river.

Date	Time		Mean depth (m)	Mean velocity (m/s)	Area (m^2)	Flow (m^3/s)	Total flow (m^3/s)	Stage (m)	OPW stage (m)
04/06/2009	15:30	*pier 1*	0.188	0.144	0.452	0.052			
		pier 2	0.421	0.288	1.474	0.425			
		pier 3	0.508	0.45	1.725	0.776	1.253	0.42	0.42
05/06/2009	13:00	*pier 1*	0.159	0.095	0.382	0.036			
		pier 2	0.432	0.239	1.51	0.36			
		pier 3	0.536	0.387	1.82	0.704	1.1	0.4	0.4
12/06/2009	15:30	*pier 1*	0.070	0.025	0.168	0.004			
		pier 2	0.362	0.13	1.266	0.164			
		pier 3	0.400	0.31	1.36	0.422	0.59	0.32	0.31
13/06/2009	12:30	*pier 1*	0.070	0.028	0.166	0.005			
		pier 2	0.328	0.121	1.149	0.139			
		pier 3	0.450	0.209	1.529	0.319	0.463	0.31	0.31
17/06/2009	16:30	*pier 1*	0.164	0.125	0.393	0.049			
		pier 2	0.408	0.288	1.428	0.411			
		pier 3	0.525	0.308	1.785	0.511	0.971	0.4	0.4
30/06/2009	14:30	*pier 1*	0.100	0.06	0.2	0.009			
		pier 2	0.337	0.196	1.178	0.23			
		pier 3	0.456	0.26	1.551	0.404	0.643	0.33	0.33
04/07/2009	17:40	*pier 1*	0.090	0.05	0.19	0.008			
		pier 2	0.320	0.213	1.119	0.238			
		pier 3	0.447	0.23	1.52	0.35	0.596	0.3	0.31
05/07/2009	12:00	*pier 1*	0.100	0.06	0.2	0.1			
		pier 2	0.344	0.187	1.205	0.225			
		pier 3	0.434	0.291	1.474	0.429	0.754	0.31	0.3
13/07/2009	18:10	*pier 1*	0.216	0.285	0.518	0.149			
		pier 2	0.528	0.449	1.847	0.829			
		pier 3	0.615	0.525	2.091	1.097	2.075	0.51	0.52
29/07/2009	15:00	*pier 1*	0.282	0.318	0.677	0.215			
		pier 2	0.615	0.535	2.15	1.151			
		pier 3	0.716	0.63	2.43	1.523	2.889	0.595	0.59

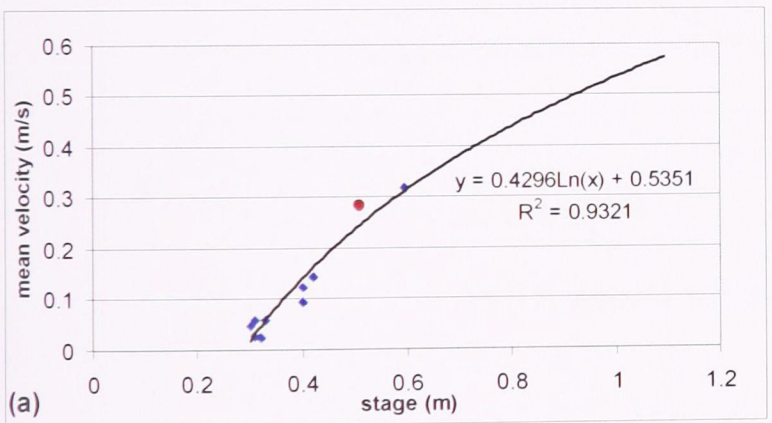


Figure D.10 Beagh river Pier 1 **(a)** stage-velocity and **(b)** stage-cross sectional area.

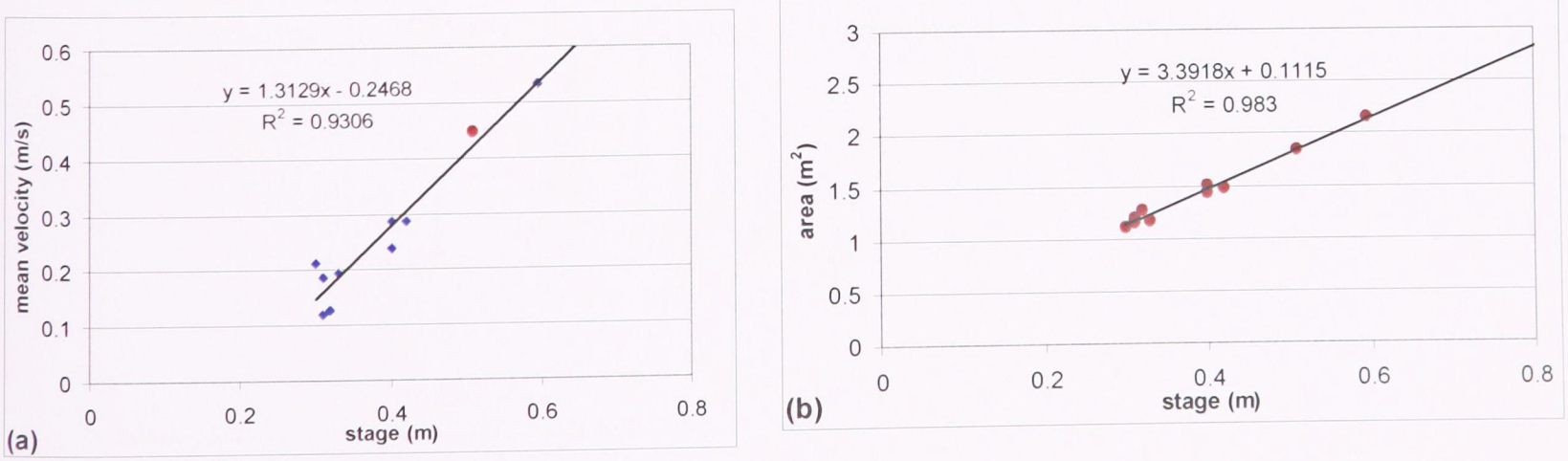


Figure D.11 Beagh river Pier 2 **(a)** stage-velocity and **(b)** stage-cross sectional area.

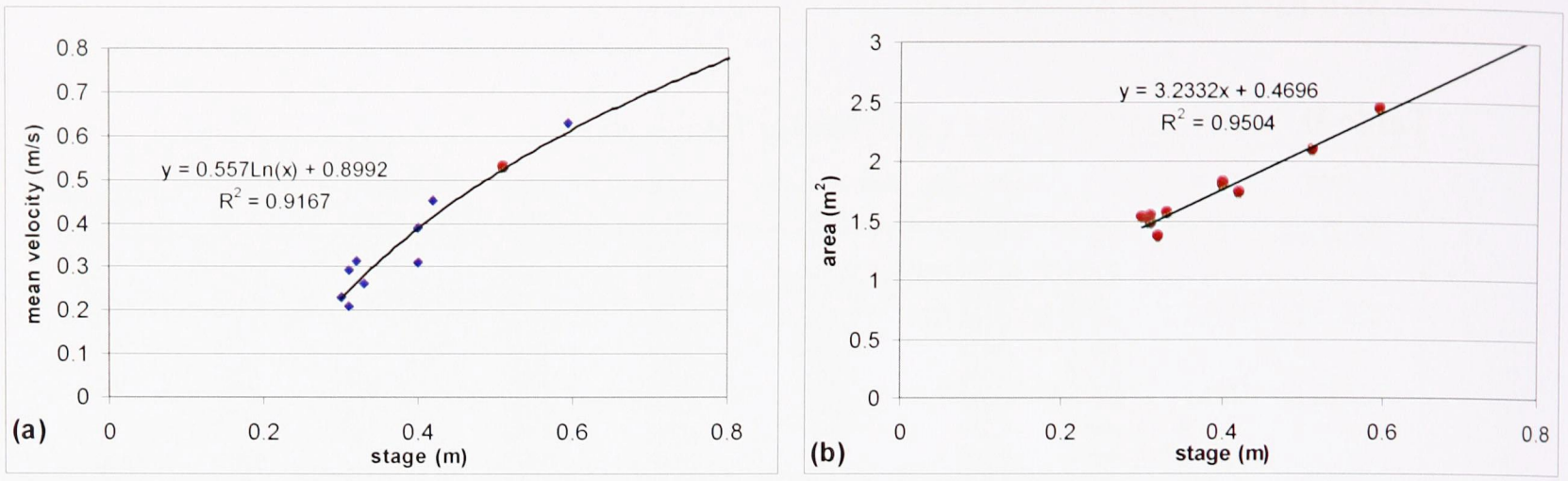


Figure D.12 Beagh river Pier 3 **(a)** stage-velocity and **(b)** stage-cross sectional area relationships.

Stage (m)	Flow (m^3/s)
0.30	0.60
0.31	0.46
0.31	0.75
0.32	0.59
0.33	0.64
0.40	1.10
0.40	0.97
0.42	1.25
0.52	2.08
0.59	2.79
0.60	2.83
0.70	3.63
0.80	4.57
0.90	5.57
1.00	6.62
1.10	7.70
1.20	8.82
1.30	9.97
1.40	11.15
1.50	12.37

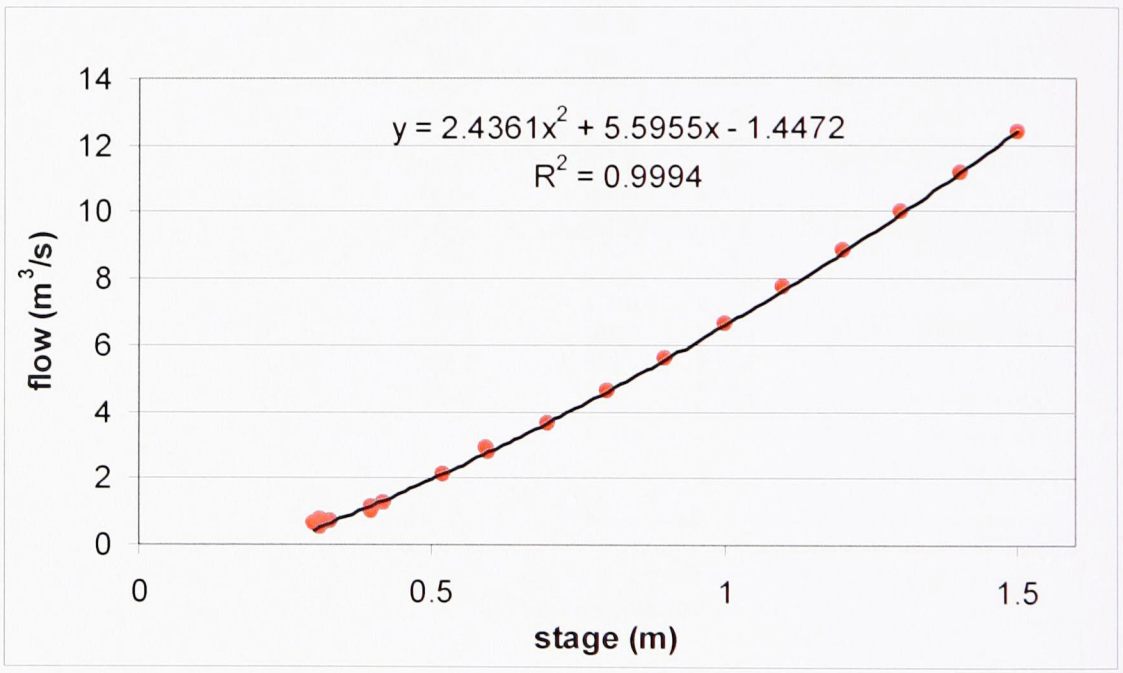


Figure D.13 Stage-flow data and rating curve for Beagh River.

Rating equation for Beagh River [grid ref. 482 005]

$$flow\left(m^3/s\right) = 2.4361(stage)^2 + 5.5955(stage) - 1.4472 \qquad \text{Eqn. D.5}$$

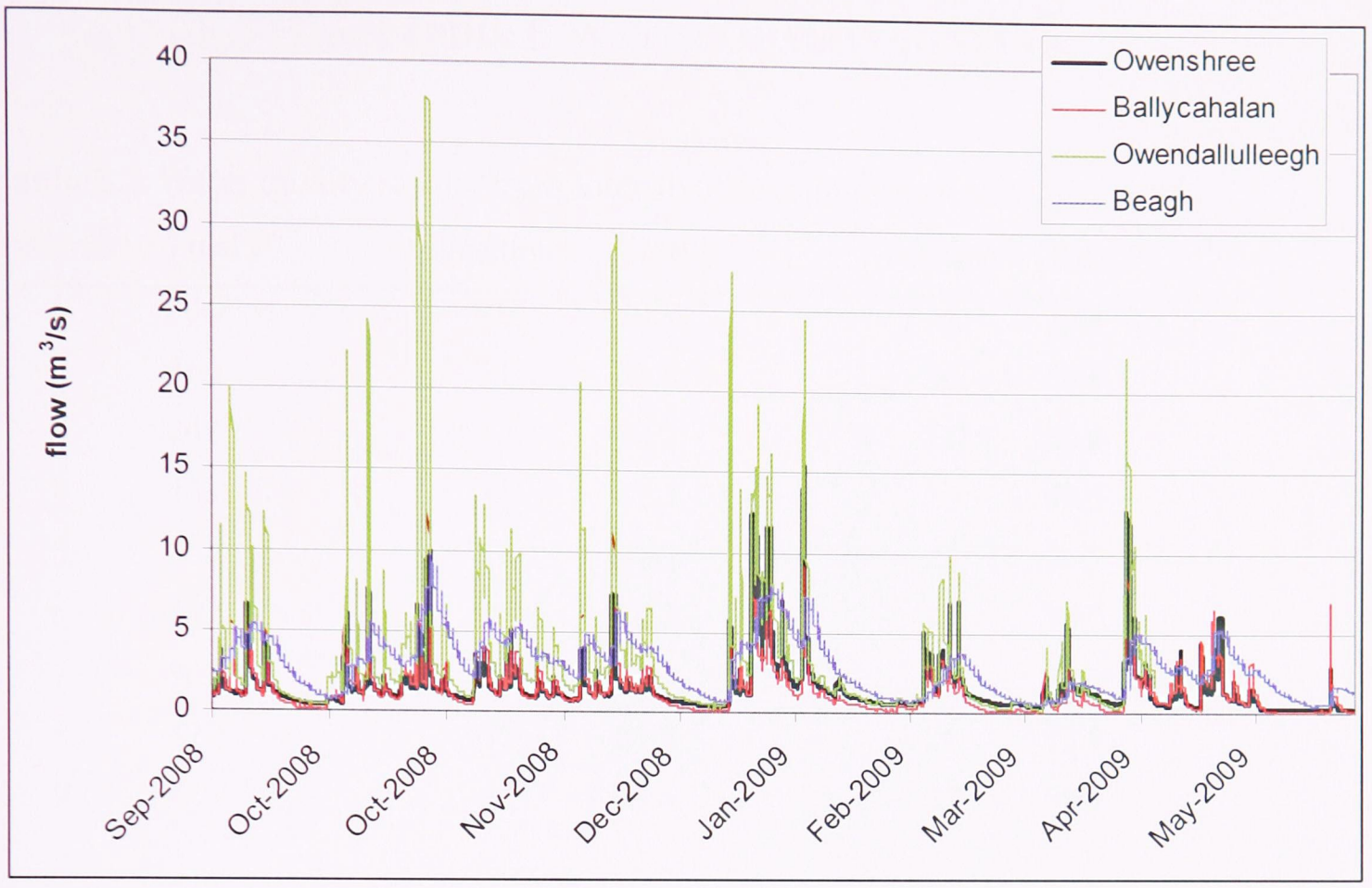


Figure D.14 River flow for 2008/09 year.

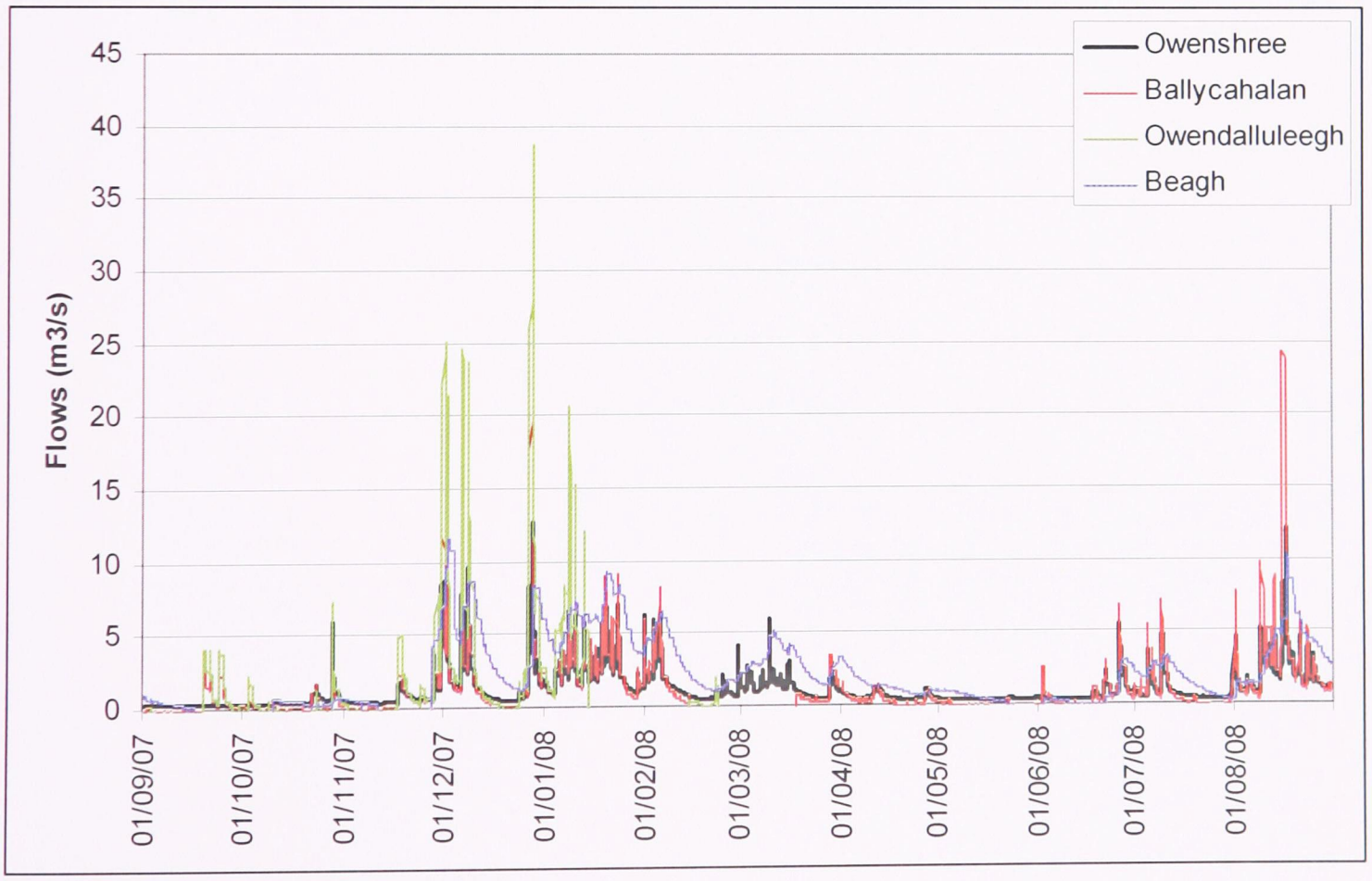


Figure D.15 River flow for 2007/08 year.

APPENDIX E WATER QUALITY RESULTS

Table E.1 Water quality results from intensive sampling foray on Coy.

Position	Total P	Position	Total P	Position	Total P
1	58.7	10	70.5	19	39.4
2	46.1	11	84.8	20	56.8
3	24.9	12	42.7	21	50.9
4	45.0	13	41.7	22	39.5
5	58.0	14	52.5	23	26.2
6	35.6	15	36.3	24	38.0
7	96.2	16	78.3	25	58.7
8	42.1	17	81.2	26	73.9
9	34.2	18	49.5	27	59.1
X	47.6	Y	96.2	Z	55.0

Table E.2 Conductivity results (µS/cm).

turloughs	10/12/2008	09/01/2009	20/01/2009	02/02/2009	17/03/2009	01/04/2009	01/05/2009	29/05/2009	06/06/2009	17/06/2009
Blackrock	372	506	x	x	393	608	291	356	512	empty
Coy	393	409	x	x	393	505	312	344	353	411
Coole	299	356	x	x	296	309	265	260	310	346
Garryland	325	358	x	290	340	335	290	290	316	333
Caherglassaun	302	385	x	x	257	373	216	275	320	359
Kinvara (east)	653	632	x	x	612	608	603	627	629	639
Kinvara (west)	384	454	x	x	390	590	389	386	469	3520
rivers										
Owenshree River (Blackrock)	494	590	382	413	563	570	413	413	618	557
Ballycahalan river (Yeat's tower)	x	x	x	236	438	439	236	281	516	365
Beagh River (Gort)	170	191	x	x	175	199	x	167	177	201
Bog	x	x	x	x	x	816	x	x	54	36
Forest Drainage	x	x	x	x	x	x	x	x	74	59
Mountain river	x	x	x	x	x	x	x	x	215	51

Table E.3 Total phosphorus sampling results (µg/l).

turloughs	10/12/2008	09/01/2009	20/01/2009	02/02/2009	17/03/2009	01/04/2009	01/05/2009	29/05/2009	06/06/2009	17/06/2009
Blackrock	22.4	16.2	32.9	25.3	5.4	56.4	28.3	50.7	58.6	x
Coy	23.7	12.9	28.3	24.2	9.7	2.0	41.5	43.7	51.1	29.2
Coole	18.2	22.7	33.0	16.2	10.6	18.8	18.3	64.2	4.1	9.8
Garryland	7.5	8.1	20.0	15.5	2.3	0.0	13.0	62.2	14.2	0.0
Caherglassaun	20.4	12.9	29.1	17.6	4.1	13.9	21.5	36.3	5.3	0.0
Kinvara (east)	11.5	8.2	30.4	14.2	10.5	0.0	21.3	67.3	26.2	0.0
Kinvara (west)	10.5	9.1	76.9	15.3	430.6	122.6	22.3	10.1	4.9	0.0
rivers										
ee River (Blackrock)	26.9	18.3	21.2	7.0	8.7	0.0	25.4	15.2	0.2	0.0
n river (Yeat's tower)	x	x	x	x	12.8	16.1	35.7	59.5	5.1	25.5
Beagh River (Gort)	21.3	6.7	15.1	17.9	19.5	0.0	16.1	0.0	12.9	0.0
Bog	x	x	x	x	x	x	x	x	3.358	1.67
Forest Drainage	x	x	x	x	x	x	x	21.565	45.006	10.159
Mountain river	x	x	x	x	x	x	x	52.191	13.014	70.322

Table E.4 Total nitrogen sampling results (µg/l).

turloughs	10/12/2008	09/01/2009	20/01/2009	02/02/2009	17/03/2009	01/04/2009	01/05/2009	29/05/2009	06/06/2009	17/06/2009
Blackrock	x	2112.4	x	x	1082.6	548.4	781.0	1324.9	1046.5	
Coy	x	1086.1	x	x	669.4	856.6	909.6	771.5	980.4	893.3
Coole	x	999.9	x	x	750.1	1190.4	1029.7	920.7	988.3	959.0
Garryland	x	979.5	x	x	749.2	725.3	702.9	706.3	586.7	604.6
Caherglassaun	x	1291.3	x	x	829.9	1018.3	903.9	913.2	997.1	835.2
Kinvara (east)	x	2617.3	x	x	1685.0	2008.5	1870.9	1694.7	2623.3	1659.6
Kinvara (west)	x	895.3	x	x	899.3	1205.2	1231.0	818.1	722.8	822.1
rivers										
Owenshree River (Blackrock)	x	1364.5		x	716.4	866.9	1020.2	842.4	938.9	1076.1
Ballycahalan river (Yeat's tower)	x	x		x	940.6	903.2	x	748.2	1064.2	948.6
Beagh River (Gort)	x	849.6		x	547.4	875.7	1181.3	x	842.2	802.4
Bog	x	x		x	x	946.5	x	x	18793.2	867.1
Forest Drainage	x	x		x	x	582.7	x	x	1070.1	730.2
Mountain river	x	x		x	x		x	x	634.0	946.8

Table E.5 Total organic carbon sampling results (mg/l).

turloughs	10/12/2008	09/01/2009	20/01/2009	02/02/2009	17/03/2009	01/04/2009	01/05/2009	29/05/2009	06/06/2009	17/06/2009
Blackrock	x	3.9	x	x	7.8	3.0	8.5	9.5	6.9	x
Coy	x	7.3	x	x	6.2	4.9	9.1	7.8	7.6	7.9
Coole	x	9.3	x	x	9.2	7.9	10.6	11.3	7.7	9.8
Garryland	x	7.2	x	x	6.3	6.7	7.4	7.6	6.9	7.4
Caherglassaun	x	7.9	x	x	10.0	7.0	11.2	9.2	39.3	7.5
Kinvara (east)	x	3.3	x	x	3.5	2.3	3.8	3.1	3.1	3.4
Kinvara (west)	x	5.6	x	x	6.6	4.4	7.0	6.9	6.2	5.4
rivers										
Owenshree River (Blackrock)	x	3.2	x	x	5.9	3.2	10.9	9.6	2.6	7.0
Ballycahalan river (Yeat's tower)	x	0.0	0.0	0.0	7.7	6.1	0.0	25.2	5.5	8.9
Beagh River (Gort)	x	12.5	x	x	12.5	10.0	13.7	0.0	10.7	12.6
Bog	x	x	x	x	x	x	x	x	40.7	21.1
Forest Drainage	x	x	x	x	x	x	x	x	46.6	28.4
Mountain river	x	x	x	x	x	x	x	x	31.0	21.2

Table E.6 $\delta^{18}O$ results.

	14/12/2008	09/01/2009	20/01/2009	02/02/2009	17/03/2009	01/04/2009	01/05/2009	29/05/2009	06/06/2009	17/06/2009
Owneshree river	-6.13	-5.95	-6.38	-6.62	-6.19	-5.89	-5.92	-5.68	-5.71	-5.90
Ballycahalan river					-6.09	-6.28		-5.80	-5.49	-5.56
Ballylee river	-5.80	-5.73	-6.16	-7.00	-6.23	-5.97	-5.99			
Beagh river	-5.43	-5.97	-5.83	-6.73	-6.35	-6.30	-5.87		-5.49	-5.18
Blackrock	-6.06	-5.72	-6.26	-7.22	-6.21	-5.63	-5.96	-5.89	-5.19	
Coy	-5.47	-5.71	-5.62	-6.37	-6.27	-6.04	-5.89	-5.54	-5.34	-5.29
Coole	-5.59	-5.86		-6.89	-6.36	-6.17	-5.88	-5.56	-5.50	-5.25
Garyland	-6.78	-5.79	-5.77	-6.13	-6.16	-6.15	-5.76	-5.59	-5.35	-5.11
Caherglassaun	-5.44	-5.77	-5.76	-6.36	-6.27	-6.02	-5.84	-5.73	-5.37	-5.18
Kinvara East	-5.55	-5.82	-5.88	-6.32	-5.94	-6.05	-6.04	-5.95	-5.63	-5.42
Kinvara West	-6.07	-5.75	-5.79	-6.26	-6.31	-6.10	-5.89	-5.66	-5.39	-4.67
Rain			-10.78		-9.2				-8.38	
				Borehole Sample 1		-7.78		Bog	-4.57	-6.29
				Borehole Sample 2		-8.39		Forest runoff	-4.72	-6.21
								Mountain river	-5.21	-6.27

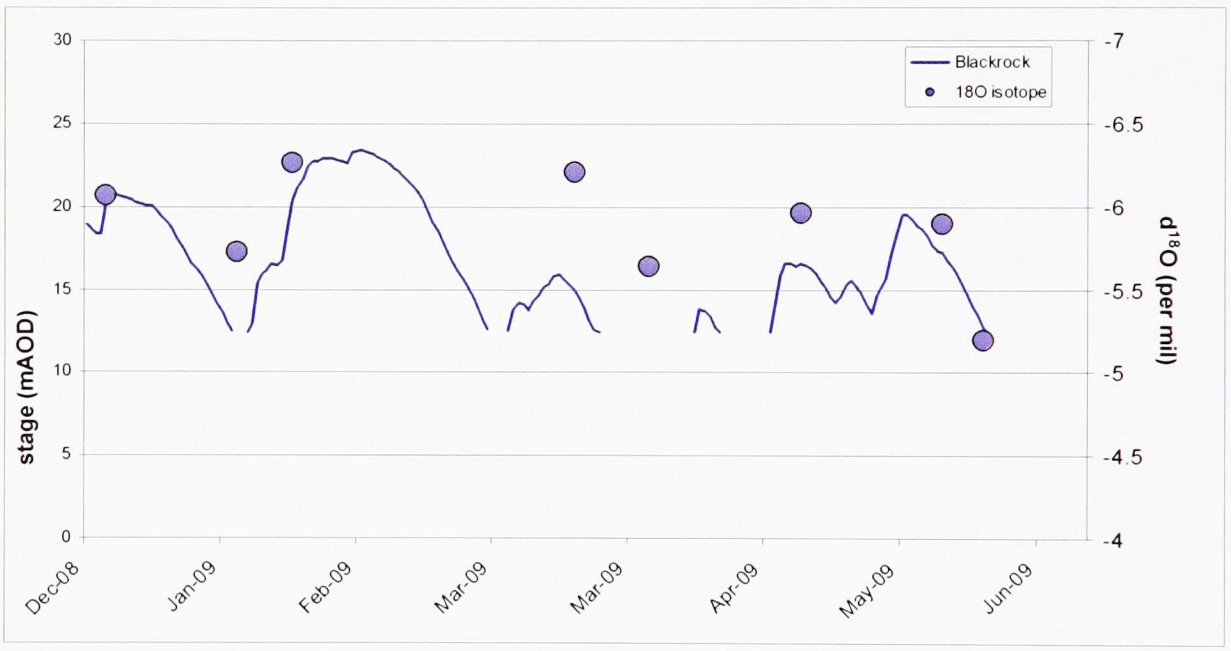


Figure E.1 $\delta^{18}O$ stable isotope results plotted against Blackrock water level.

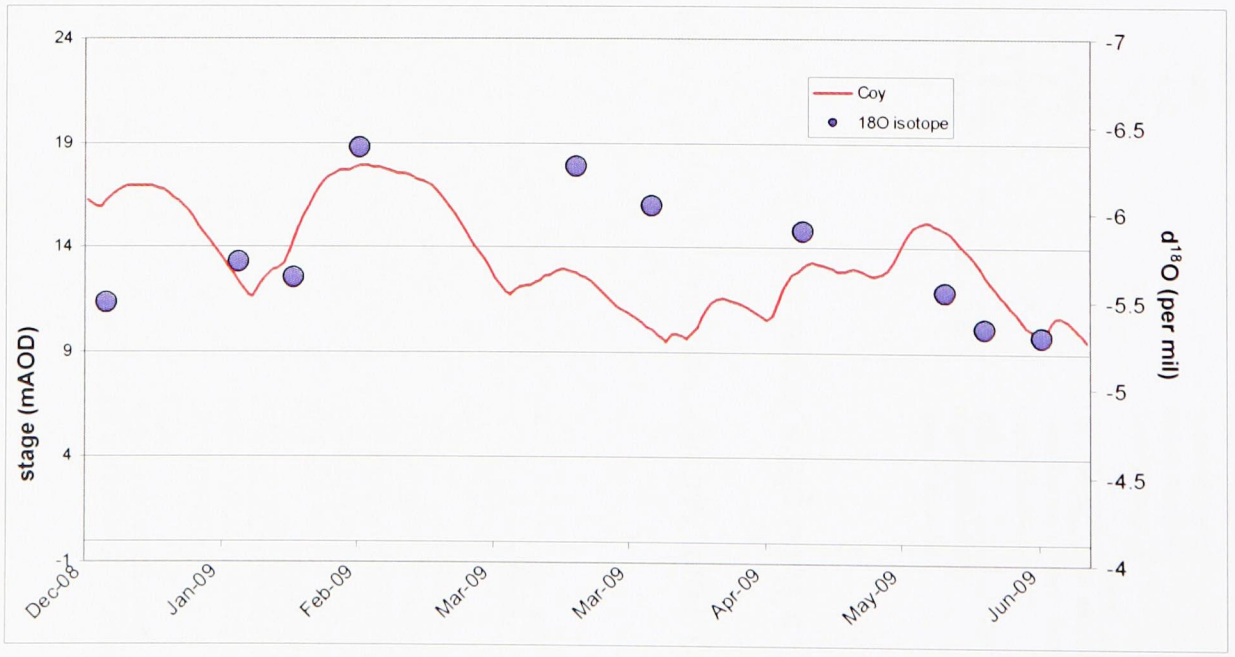


Figure E.2 $\delta^{18}O$ stable isotope results plotted against Coy water level.

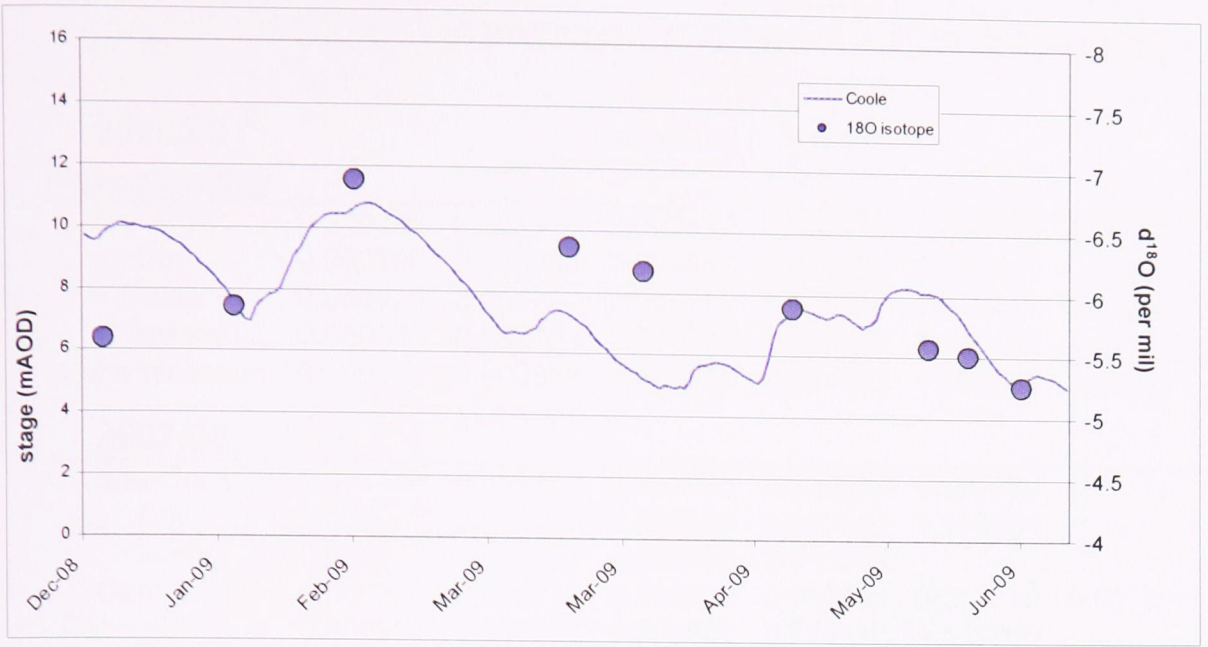


Figure E.3 $\delta^{18}O$ stable isotope results plotted against Coole water level.

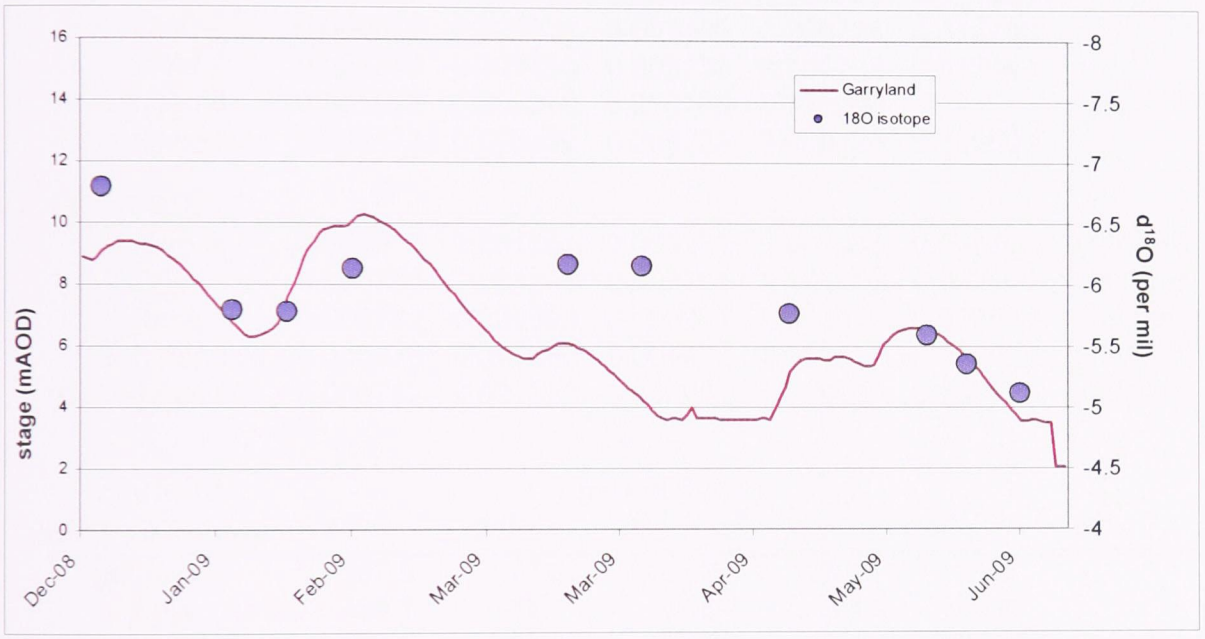


Figure E.4 $\delta^{18}O$ stable isotope results plotted against Garryland water level.

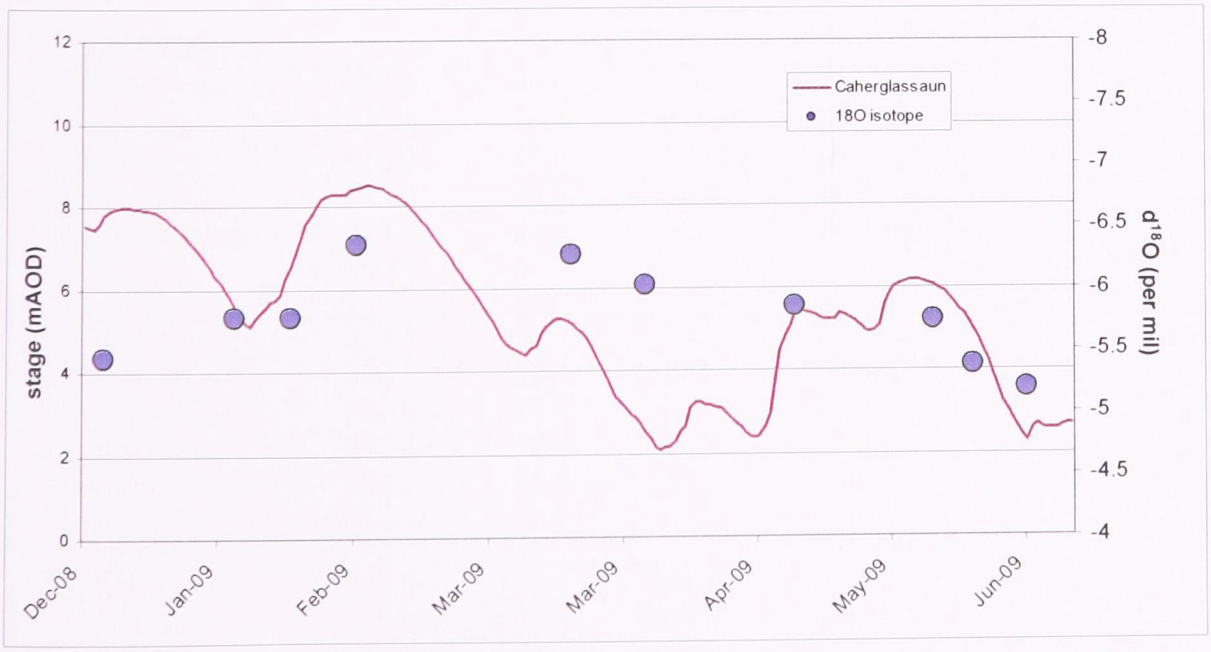


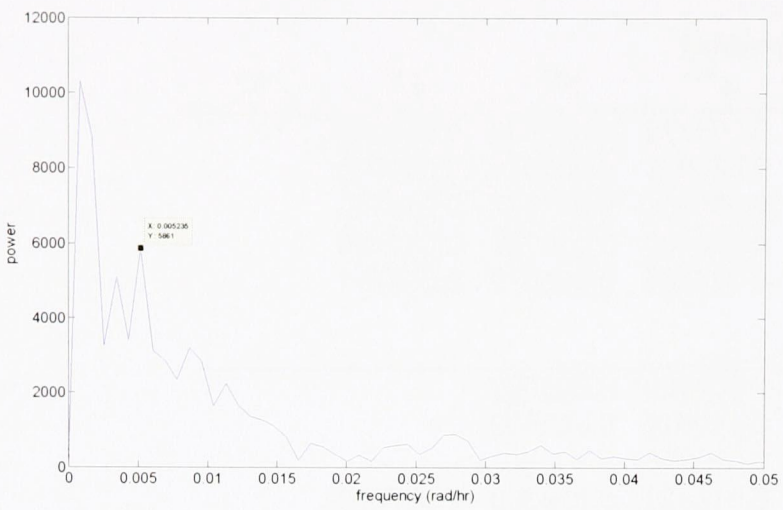
Figure E.5 $\delta^{18}O$ stable isotope results plotted against Caherglassaun water level.

APPENDIX F TIME SERIES ANALYSIS

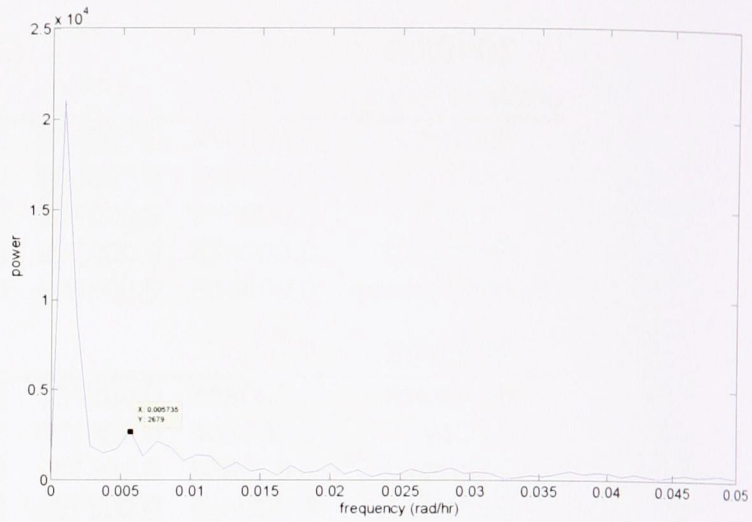
2008/09	frequency (rad/hr)						
order of energy	*1 st*	*2 nd*	*3 rd*	*4 th*	*5 th*	*6 th*	*7 th*
Blackrock	0.000676	0.003378	0.002027	0.004729	0.010130	0.000000	
Coy	0.000608	0.003039	0.004863	0.006079	0.008511	0.000000	
Coole	0.000676	0.002702	0.004729	0.006081	0.007432	0.010130	
Garryland	0.000676	0.002702	0.004728	0.008106	0.010130	0.011480	
Caherglassaun	0.000608	0.003039	0.001824	0.004863	0.006079	0.008511	
2007/08							
Blackrock	0.000956	0.005735	0.007646	0.000000	0.000000		
Coy	0.000956	0.005735	0.007646	0.010510	0.013380		
Coole	0.000956	0.005735	0.008602	0.013380			
Garryland	0.000956	0.005735	0.008604	0.010520	0.013380	0.507500	
Caherglassaun	0.000956	0.004779	0.008602	0.010510	0.507500		
2006/07							
Blackrock	0.000872	0.005235	0.003490	0.008724	0.011340		
Coy	0.000872	0.005235	0.003490	0.008724	0.015700		
Coole	0.001745	0.003490	0.005235	0.008724	0.013960		
Garryland	0.001122	0.005610	0.010100	0.506000			
Caherglassaun	0.000872	0.003490	0.005235	0.008724	0.506000		
All years							
Blackrock	0.000817	0.001361	0.000272	0.002995	0.004900	0.002178	
Coy	0.000782	0.001303	0.000261	0.004950	0.002866	0.006253	0.003908
Coole	0.000782	0.001303	0.000261	0.004951	0.002606	0.003387	0.006253
Garryland	0.000878	0.001463	0.004973	0.003510	0.004095	0.006435	0.506000
Caherglassaun	0.000782	0.001303	0.000261	0.004950	0.003126	0.003908	0.006253

2008/09	period (days)						
order of energy	*1 st*	*2 nd*	*3 rd*	*4 th*	*5 th*	*6 th*	*7 th*
Blackrock	387.5	77.5	129.2	55.4	25.8		
Coy	430.7	86.1	53.8	43.1	30.8		
Coole	387.5	96.9	55.4	43.1	35.2	25.8	
Garryland	387.6	96.9	55.4	32.3	25.8	22.8	
Caherglassaun	430.7	86.1	143.5	53.8	43.1	30.8	
2007/08							
Blackrock	273.9	45.6	34.2				
Coy	273.9	45.6	34.2	24.9	19.6		
Coole	273.9	45.6	30.4	19.6			
Garryland	273.9	45.6	30.4	24.9	19.6	0.5	
Caherglassaun	273.9	54.8	30.4	24.9	0.5		
2006/07							
Blackrock	300.1	50.0	75.0	30.0	23.1		
Coy	300.1	50.0	75.0	30.0	16.7		
Coole	150.0	75.0	50.0	30.0	18.8		
Garryland	233.3	46.7	25.9	0.5			
Caherglassaun	300.1	75.0	50.0	30.0	0.5		
All years							
Blackrock	320.6	192.4	961.8	87.4	53.4	120.2	
Coy	335.0	200.9	1005.0	52.9	91.3	41.9	67.0
Coole	334.9	200.9	1004.6	52.9	100.5	77.3	41.9
Garryland	298.3	178.9	52.6	74.6	63.9	40.7	0.5
Caherglassaun	335.0	200.9	1005.0	52.9	83.7	67.0	41.9

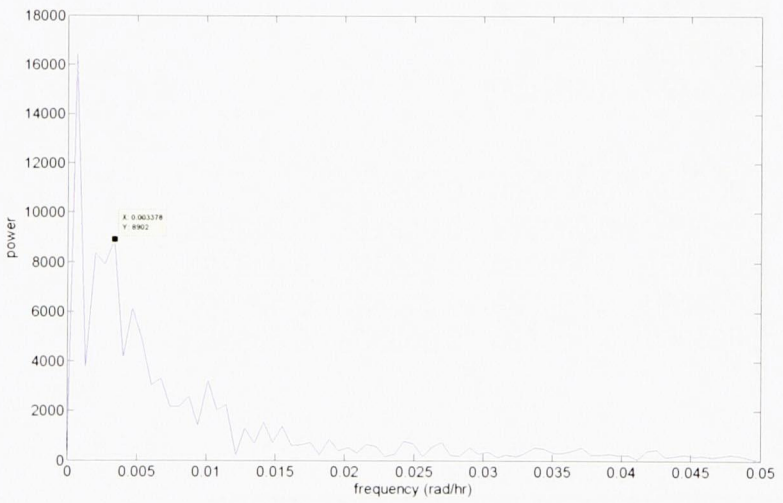
Fast Fourier Transform results



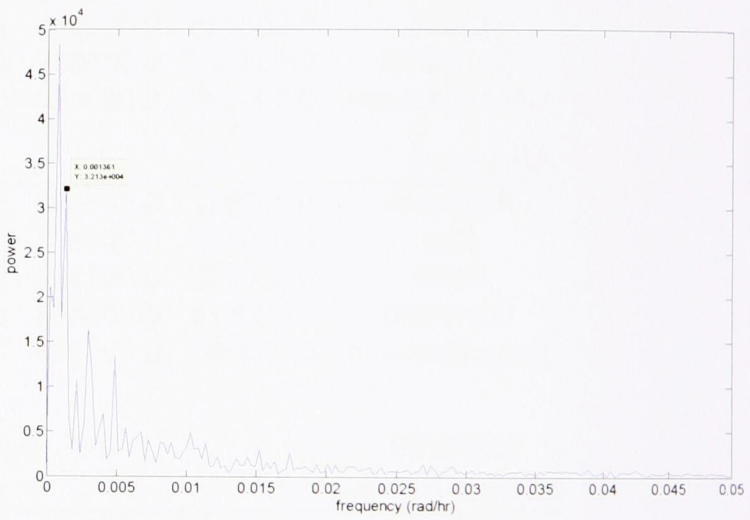
Blackrock 06/07 stage



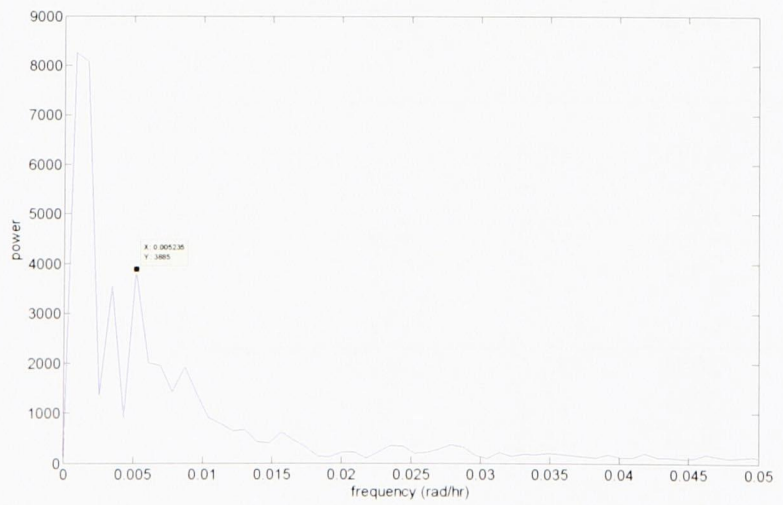
Blackrock 07/08 stage



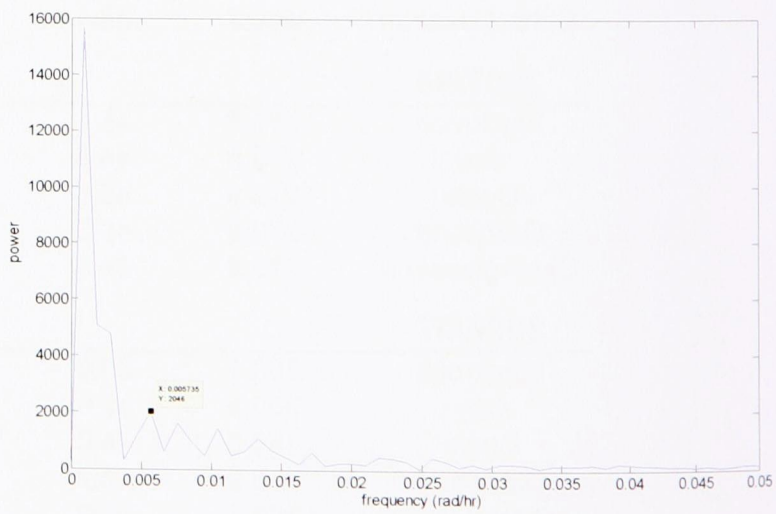
Blackrock 08/09 stage



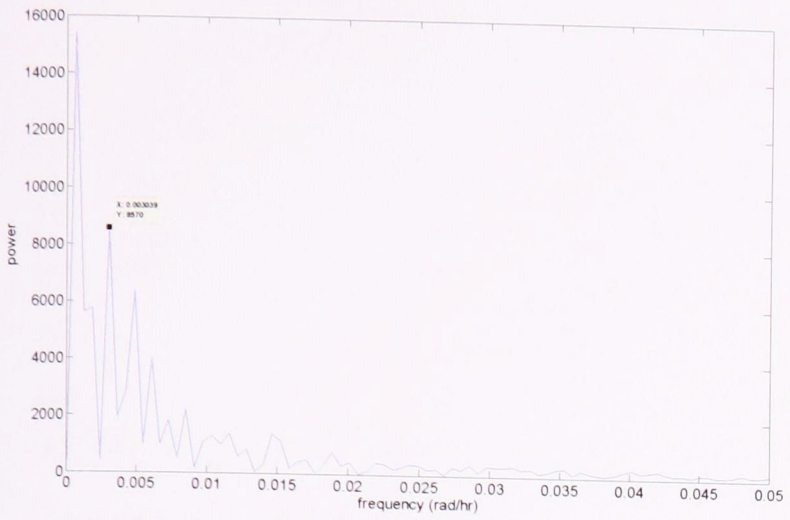
Blackrock 06 to 09 stage



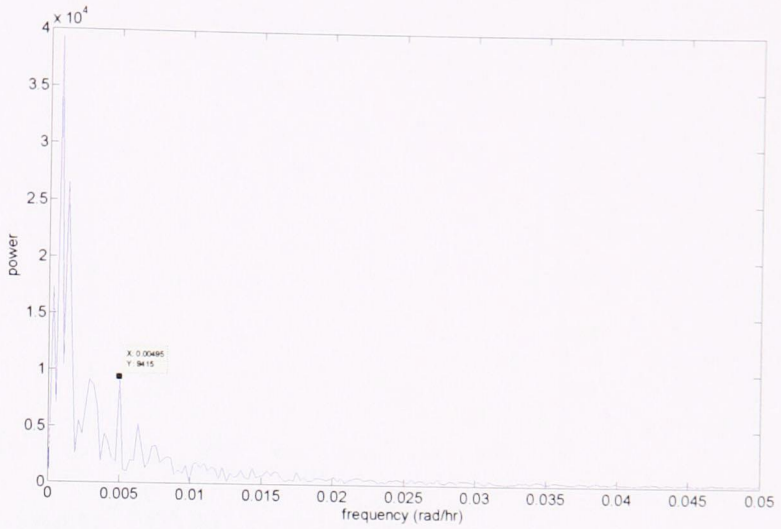
Coy 06/07 stage



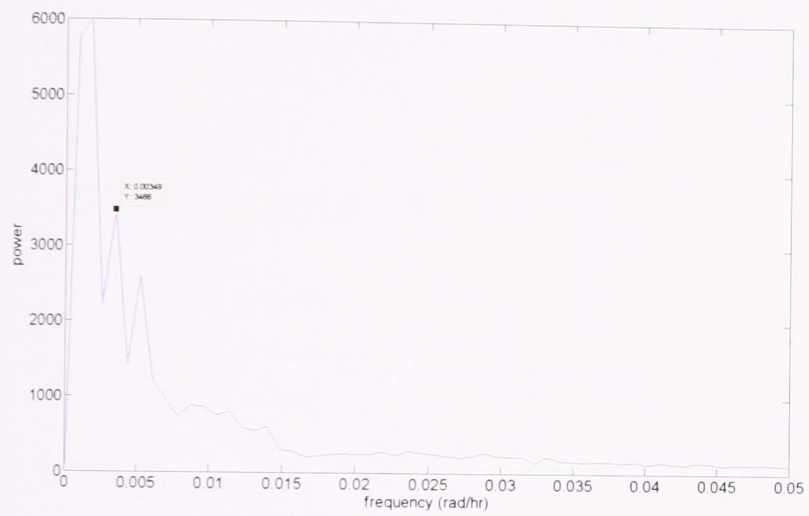
Coy 07/08 stage



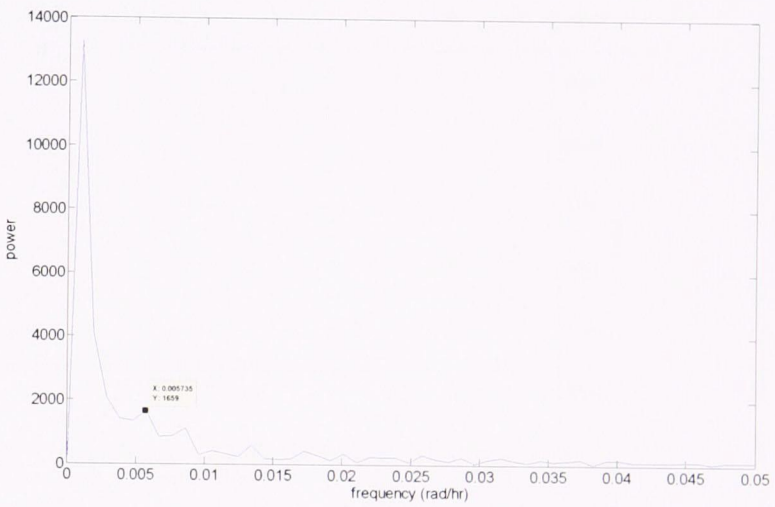
Coy 08/09 stage



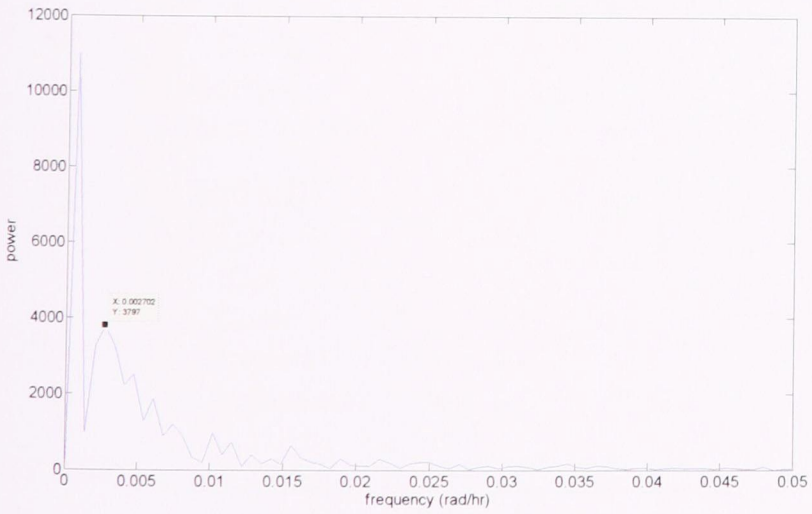
Coy 06 to 09 stage



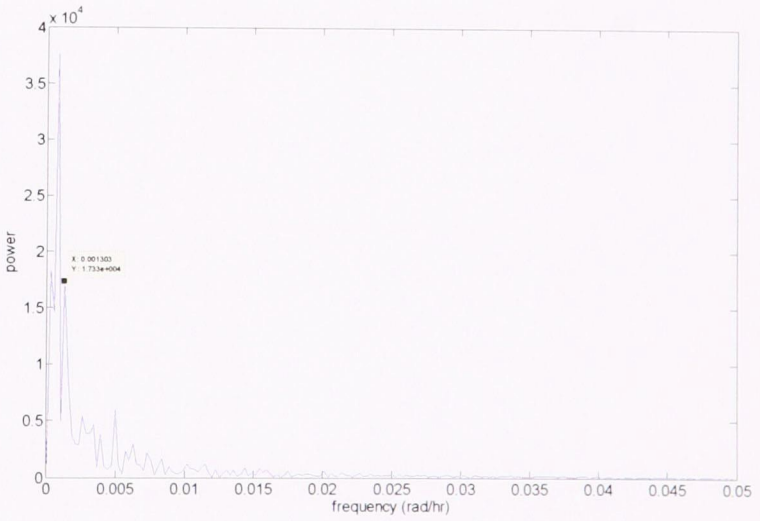
Coole 06/07 stage



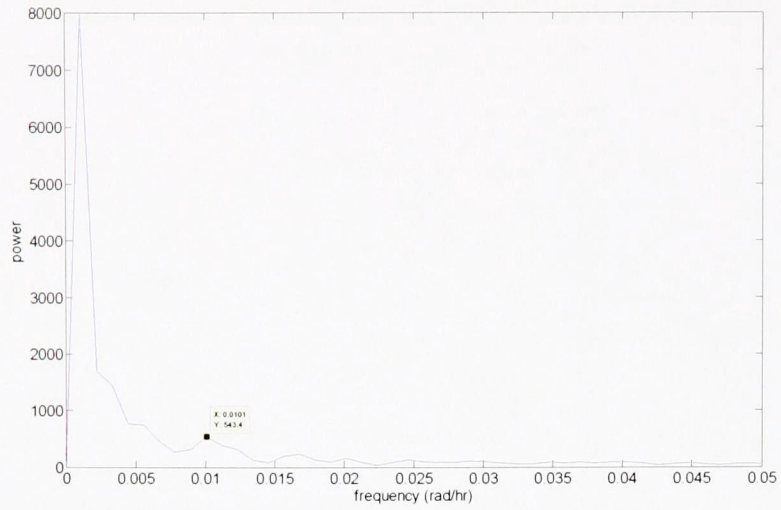
Coole 07/08 stage



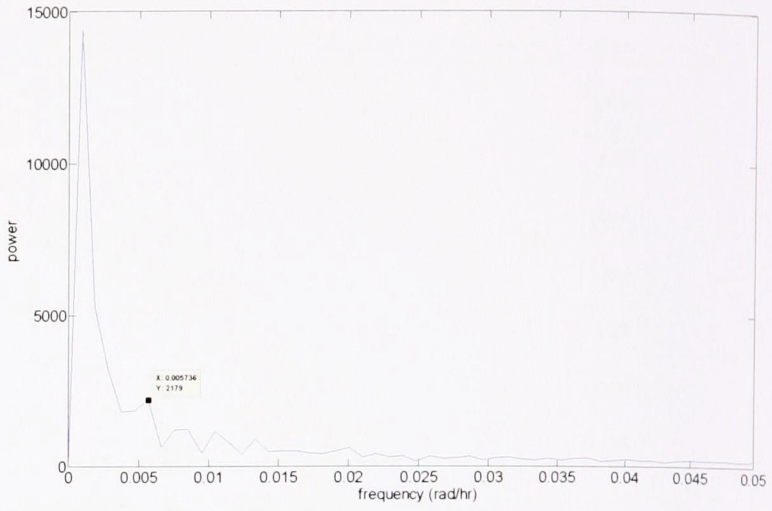
Coole 08/09 stage



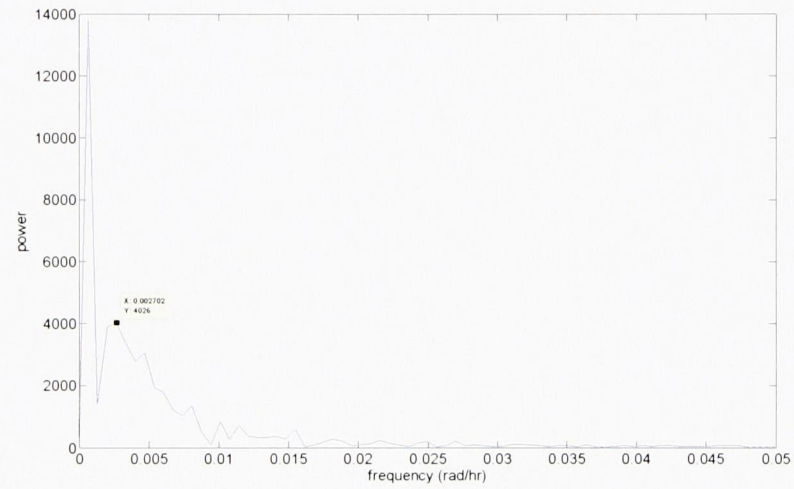
Coole 06 to 09 stage



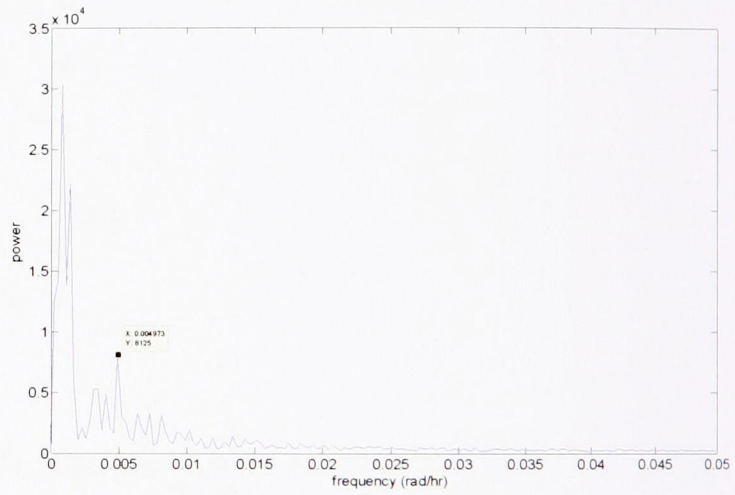
Garryland 06/07 stage



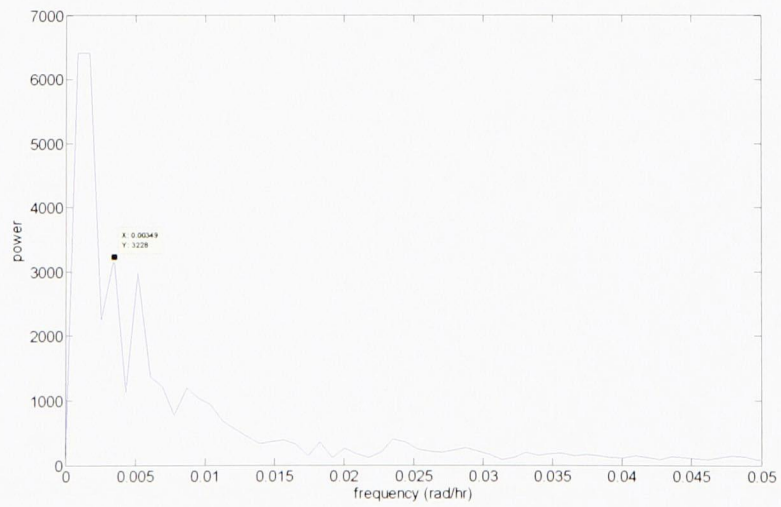
Garryland 07/08 stage



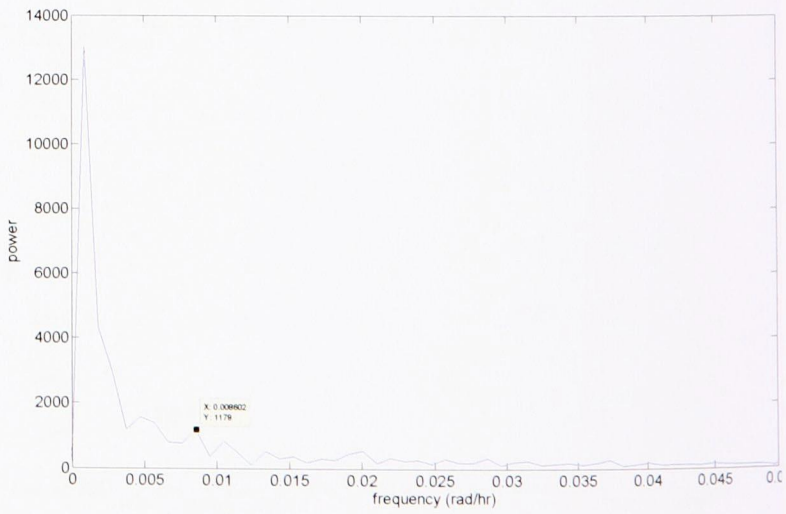
Garryland 08/09 stage



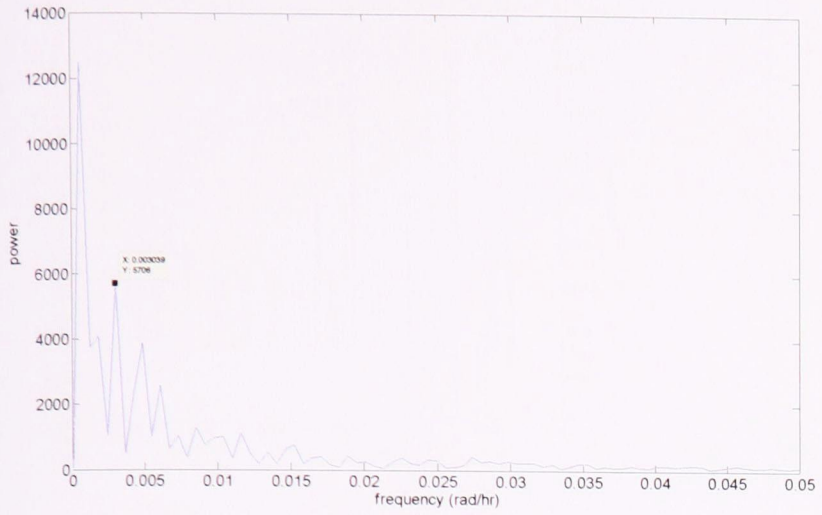
Garryland 06 to 09 stage



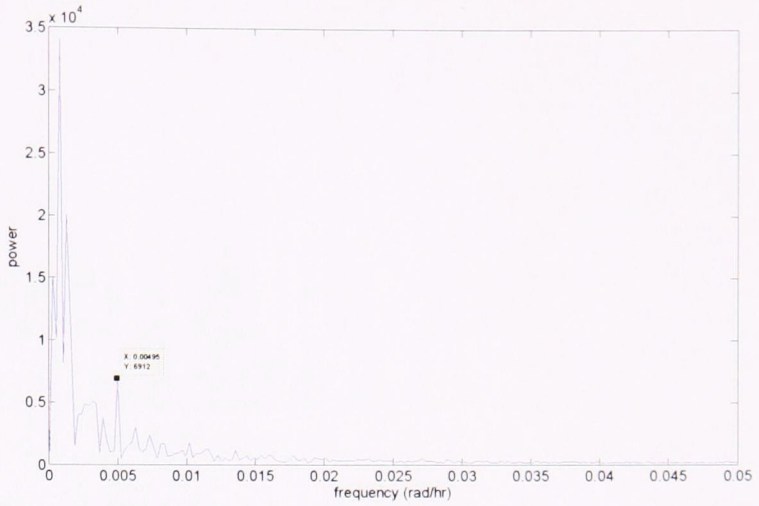
Caherglassaun 06/07 stage



Caherglassaun 07/08 stage



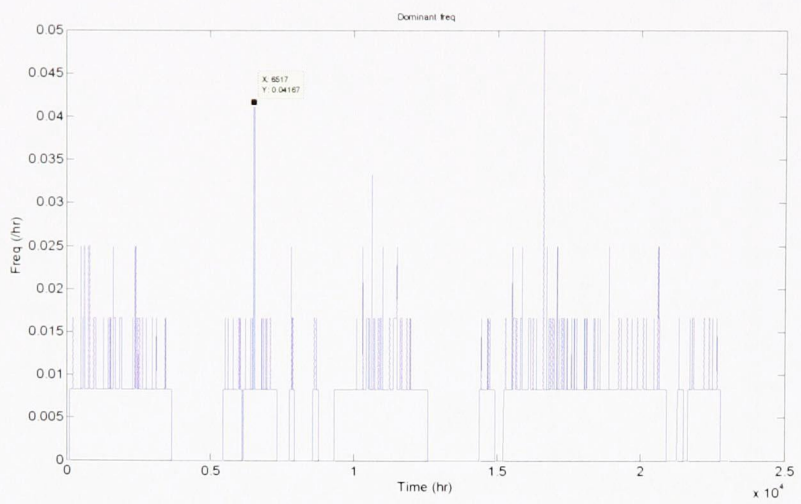
Caherglassaun 08/09 stage



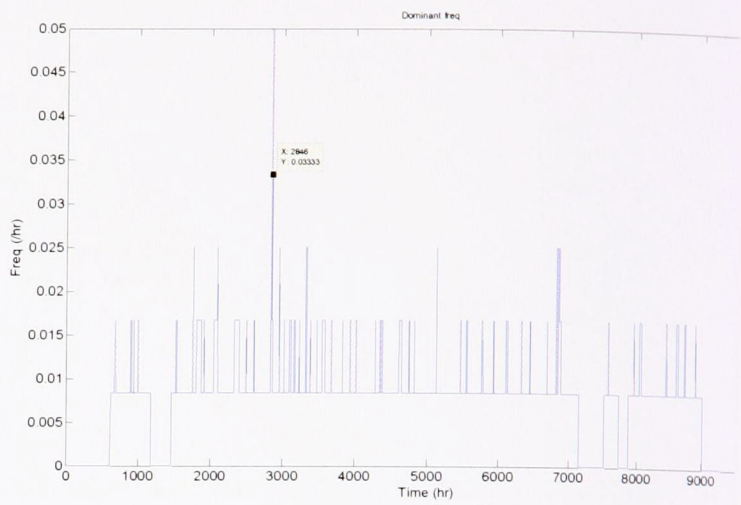
Caherglassaun 06 to 09 stage

STFT results

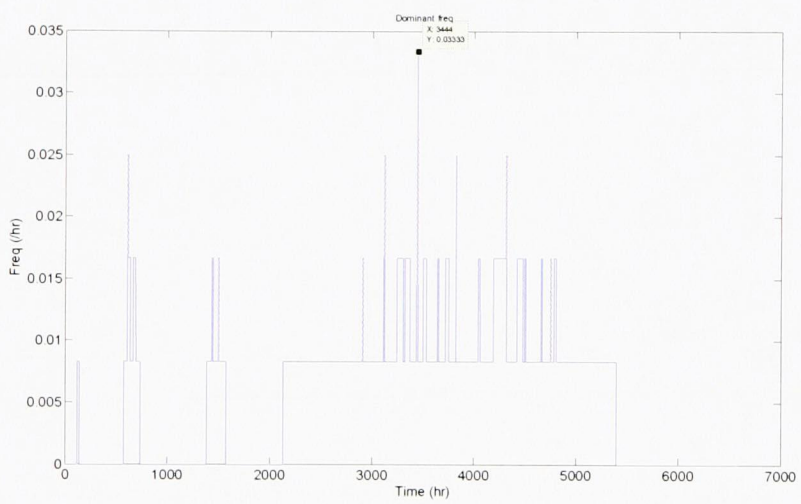
2008/09 order of energy	period (days) 1st	2nd	3rd	4th	5th	6th
Blackrock	5.0	2.5	1.7	1.3		
Coy	5.0	2.5	1.7	1.0		
Coole	5.0	2.5	1.7	1.0	0.5	0.5
Garryland	5.0	2.5	1.7	1.0	0.8	0.5
Caherglassaun	5.0	2.5	1.7	0.5	0.3	
2007/08						
Blackrock	5.0	2.5	1.7			
Coy	5.0	2.5	1.7	1.3	0.5	
Coole	5.0	2.5	1.0	0.7	0.5	
Garryland	5.0	2.5	1.7	1.0	0.5	
Caherglassaun	5.0	2.5	1.7	1.0	0.5	
2006/07						
Blackrock	5.0	2.5	1.7	1.0		
Coy	5.0	2.5	1.7	1.3	1.0	
Coole	5.0	2.5	1.7	1.3	1.0	0.8
Garryland	5.0	2.5	1.7	1.0	0.5	
Caherglassaun	5.0	2.5	1.7	1.3	1.0	0.5
All years						
Blackrock	5.0	2.5	1.7	1.3	1.0	
Coy	5.0	2.5	1.7	1.3	1.0	0.6
Coole	5.0	2.5	1.7	1.0	0.7	0.5
Garryland	5.0	2.5	1.7	1.0	0.8	0.5
Caherglassaun	5.0	2.5	1.7	1.3	1.0	0.5



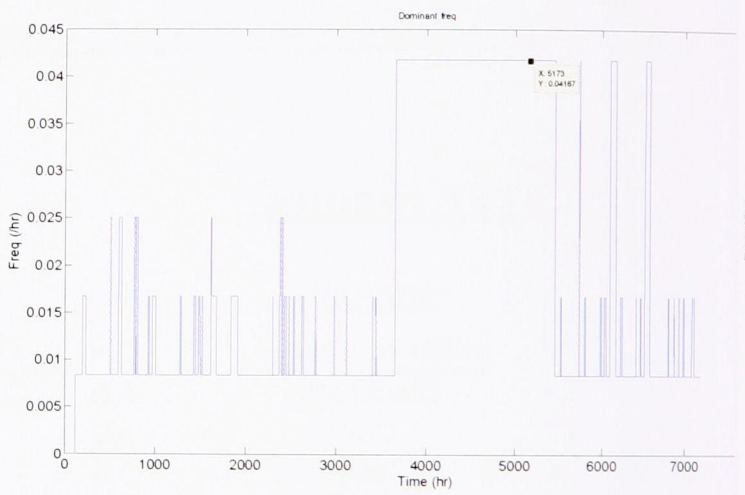
Blackrock all 06/09 (window = 120 hours)



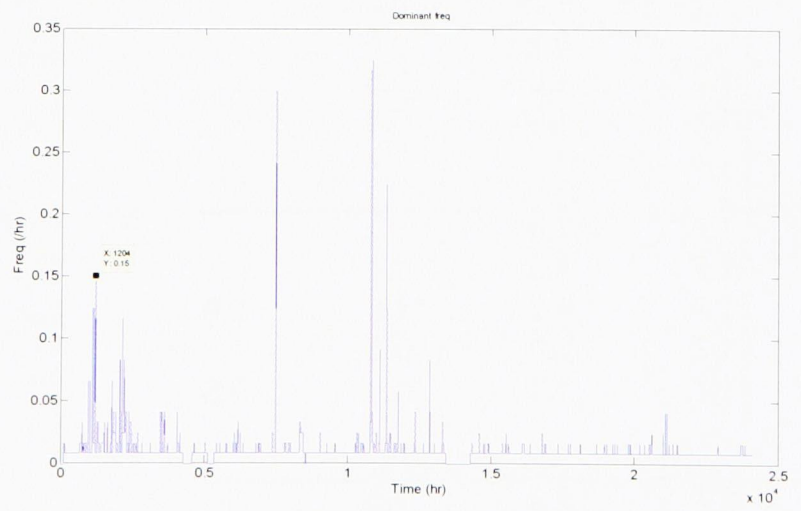
Blackrock 08/09 (window = 120 hours)



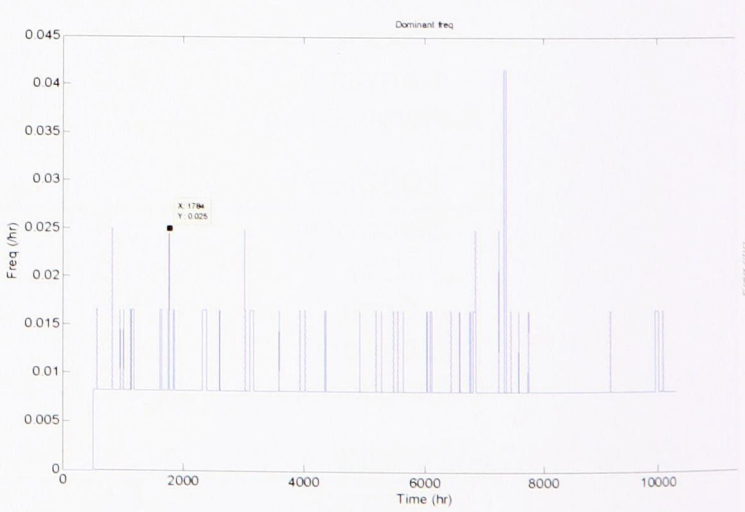
Blackrock 07/08 (window = 120 hours)



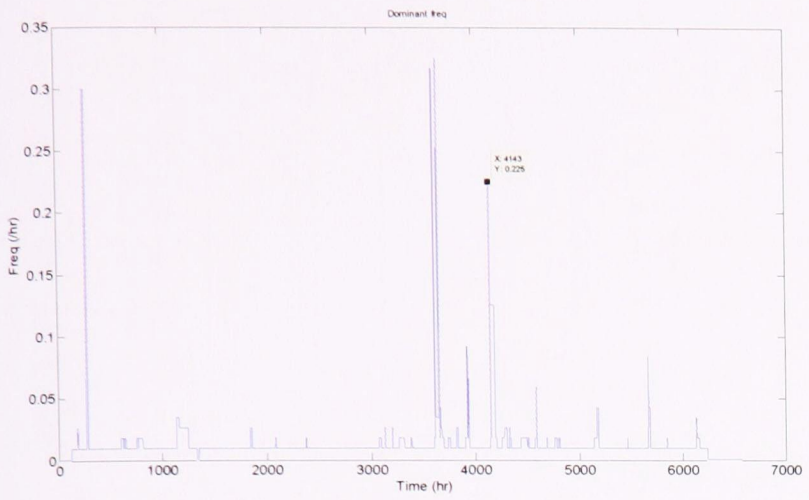
Blackrock 06/07 (window = 120 hours)



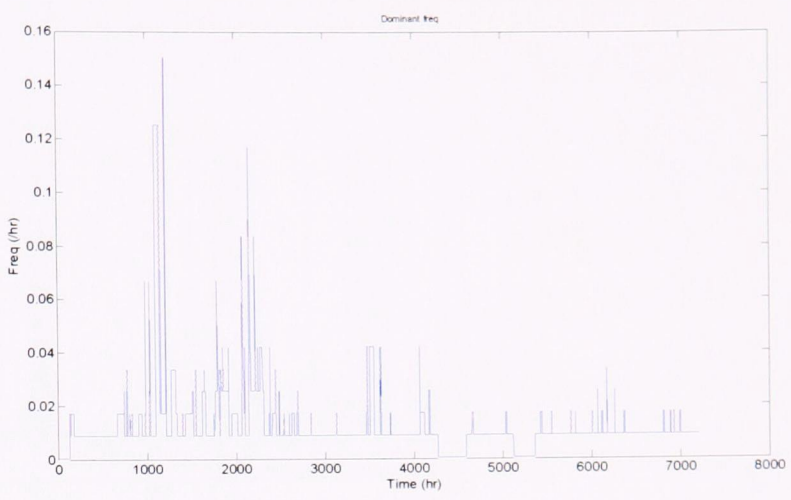
Coy all 06/09 (window = 120 hours)



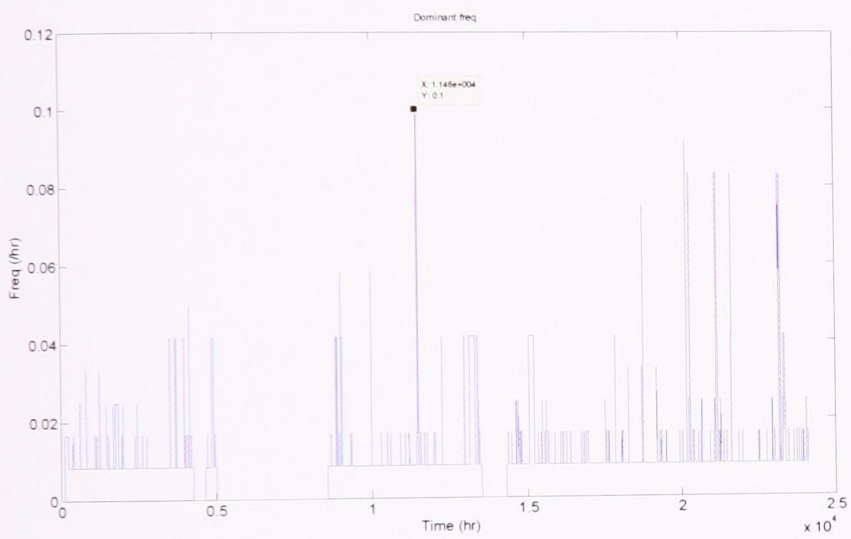
Coy 08/09 (window = 120 hours)



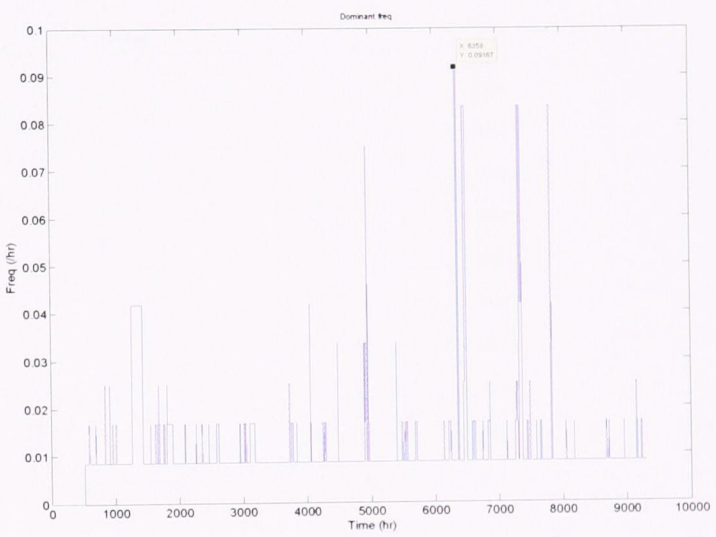
Coy 07/08 (window = 120 hours)



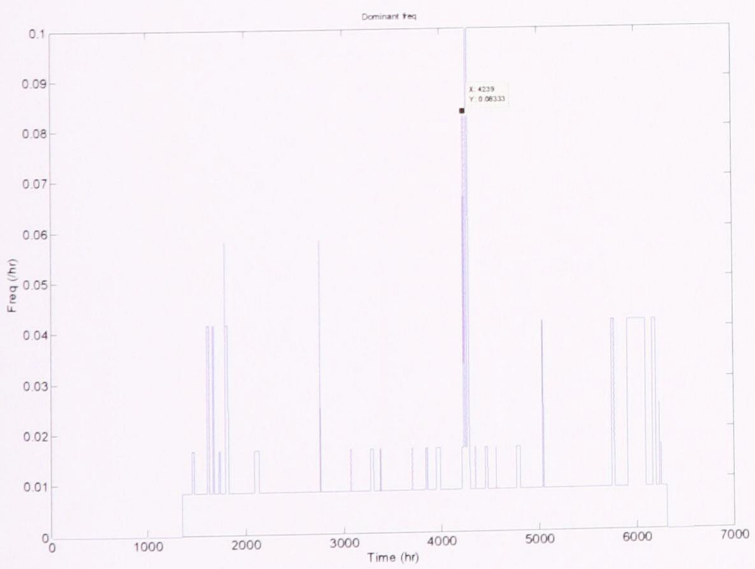
Coy 06/07 (window = 120 hours)



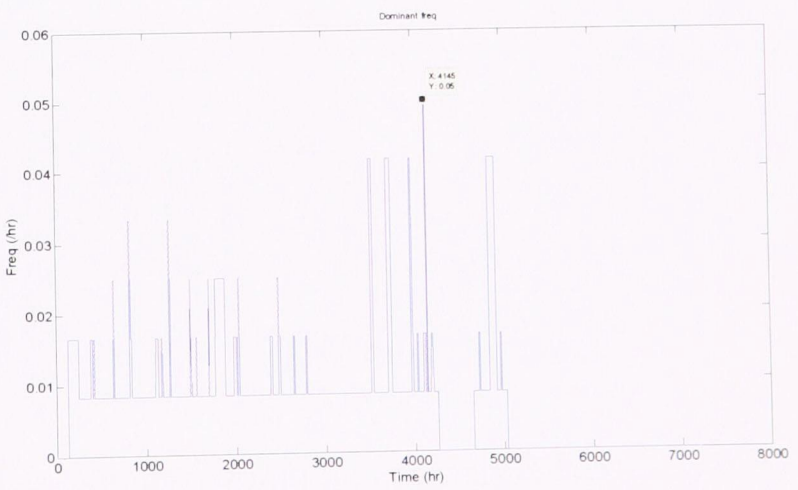
Coole all 06/09 (window = 120 hours)



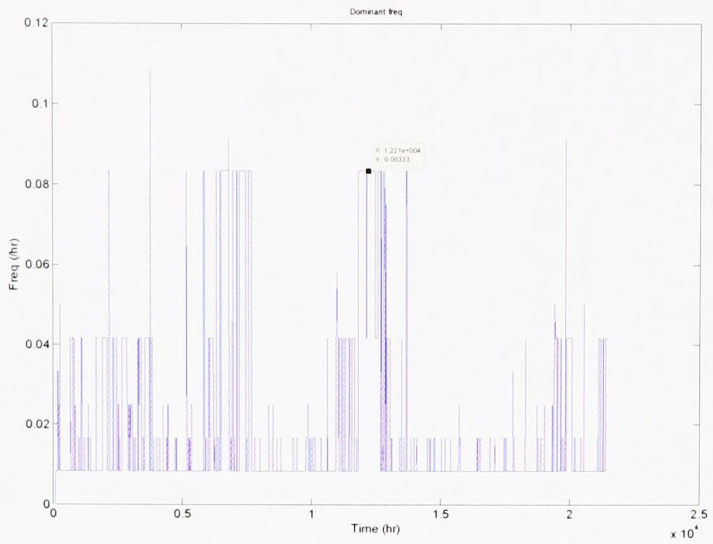
Coole 08/09 (window = 120 hours)



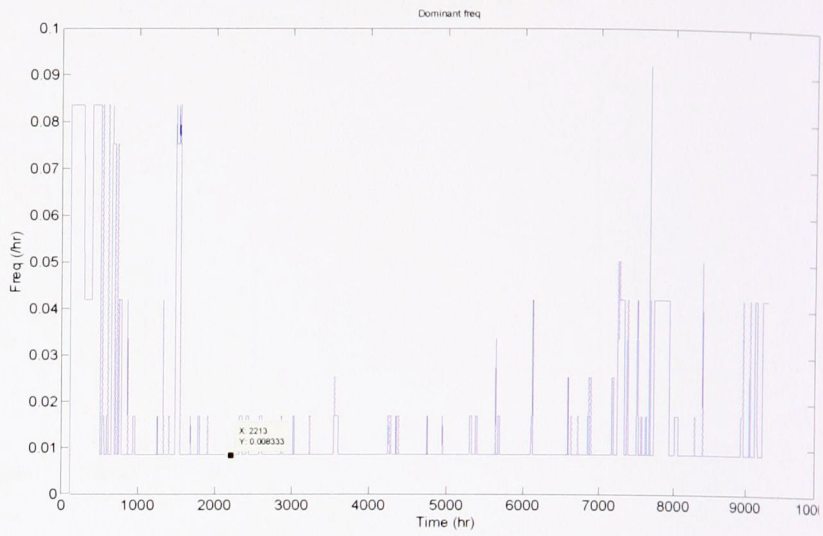
Coole 07/08 (window = 120 hours)



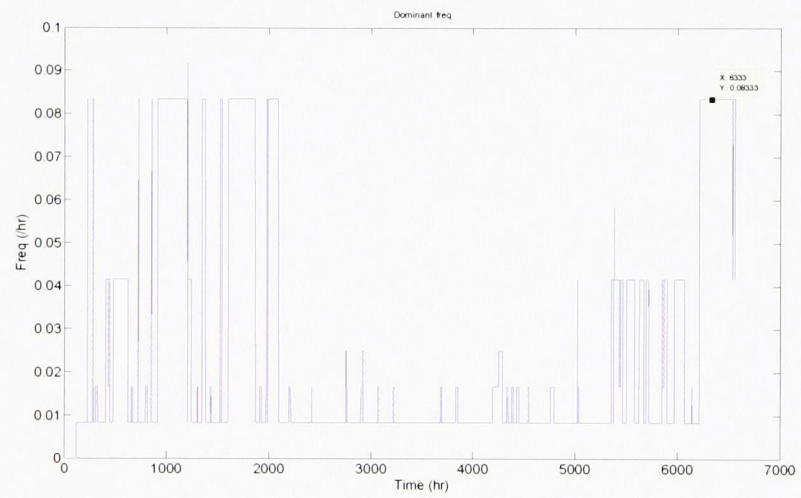
Coole 06/07 (window = 120 hours)



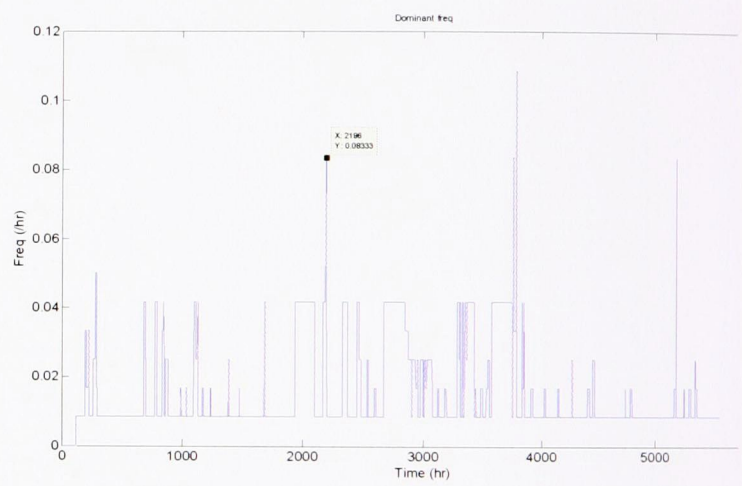
Garryland all 06/09 (window = 120 hours)



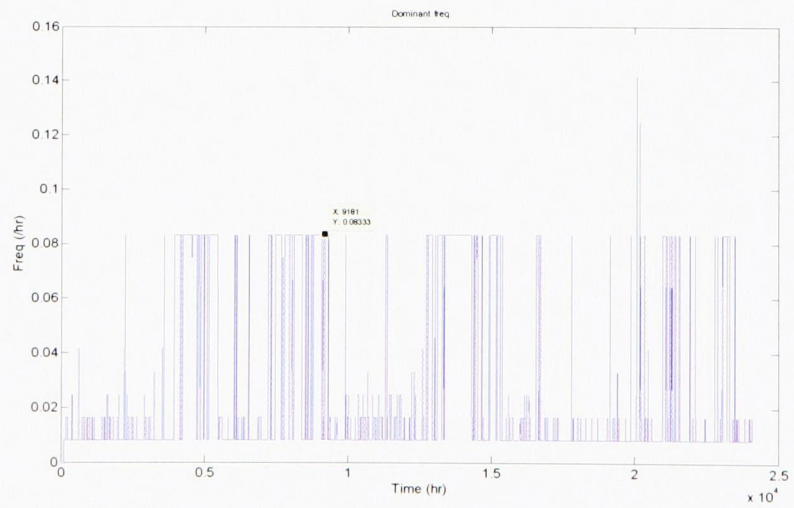
Garryland 08/09 (window = 120 hours)



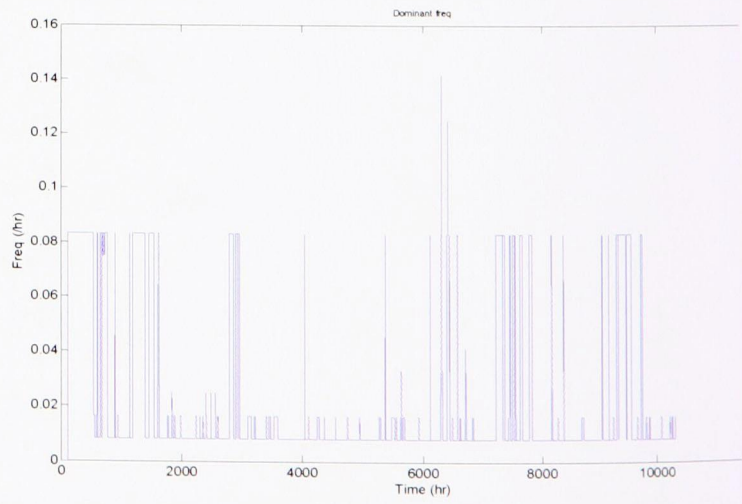
Garryland 07/08 (window = 120 hours)



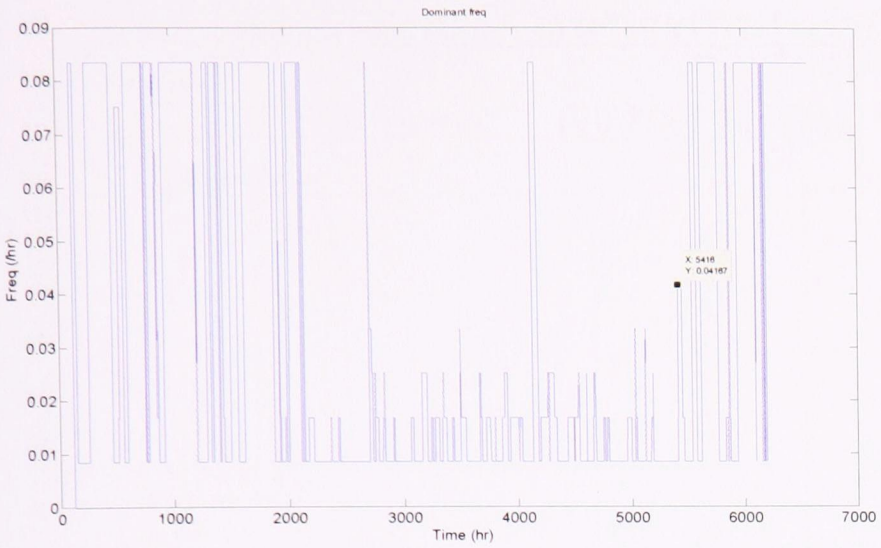
Garryland 06/07 (window = 120 hours)



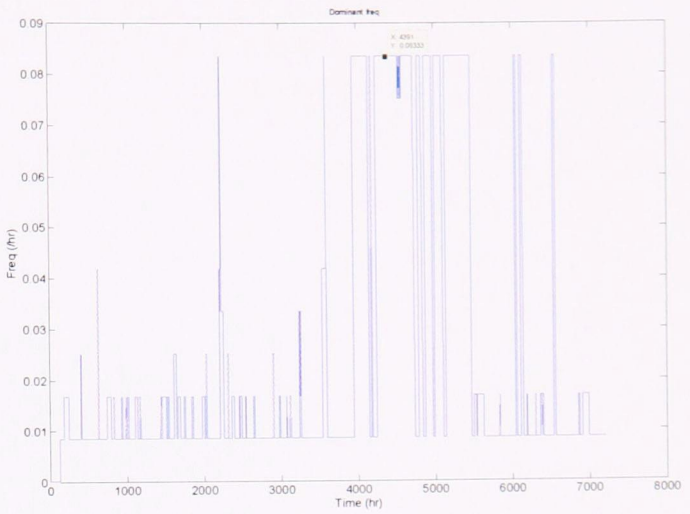
Caherglassaun all 06/09 (window = 120 hours)



Caherglassaun 08/09 (window = 120 hours)



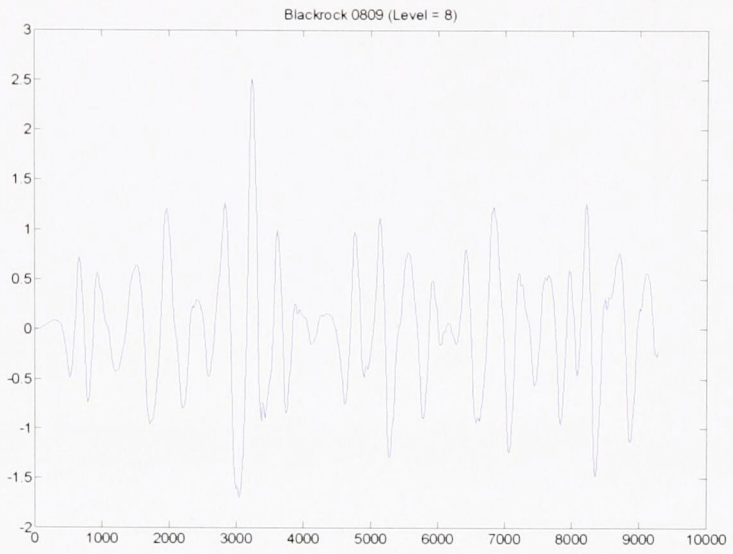
Caherglassaun 07/08 (window = 120 hours)



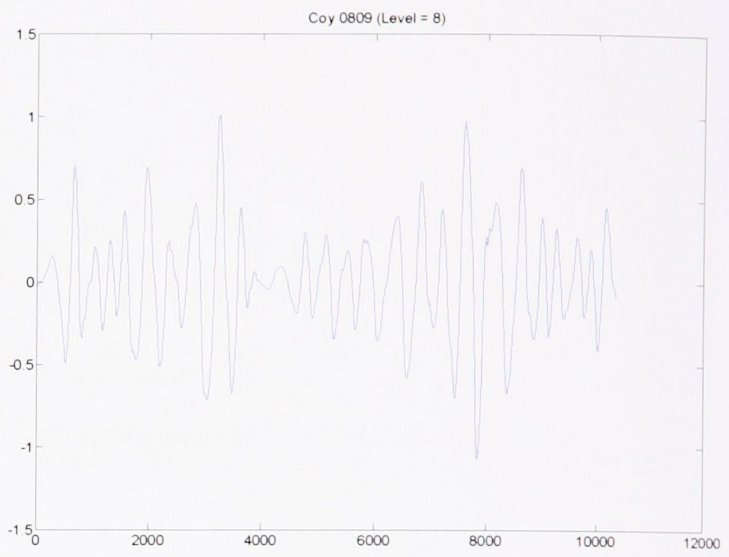
Caherglassaun 06/07 (window = 120 hours)

Discrete Wavelet Transform Analysis

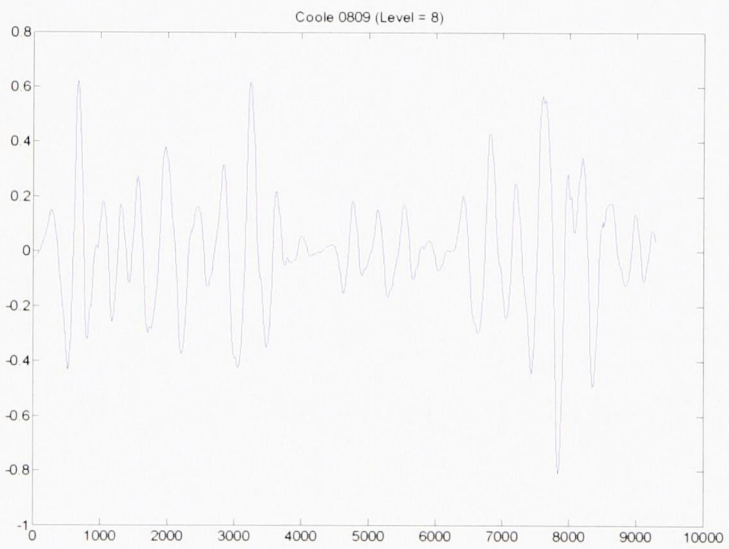
Level 8 (2008/09)



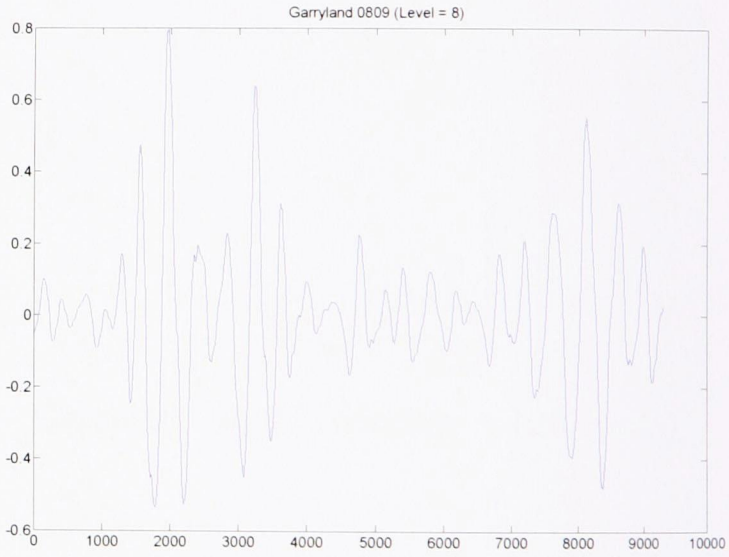
Blackrock 08/09



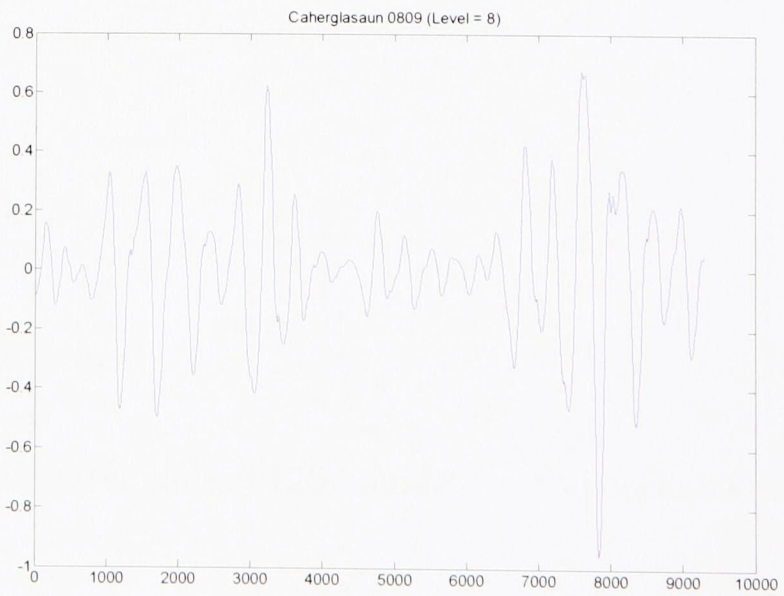
Coy 08/09



Coole 08/09

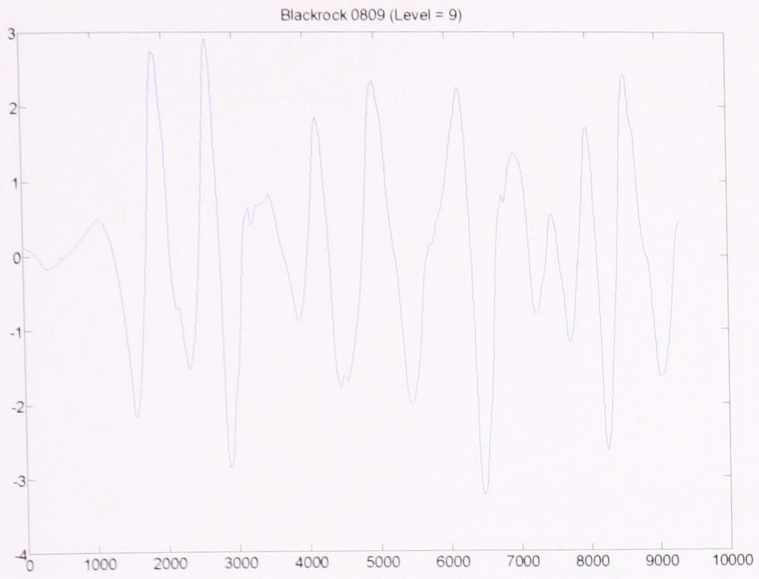


Garryland 08/09

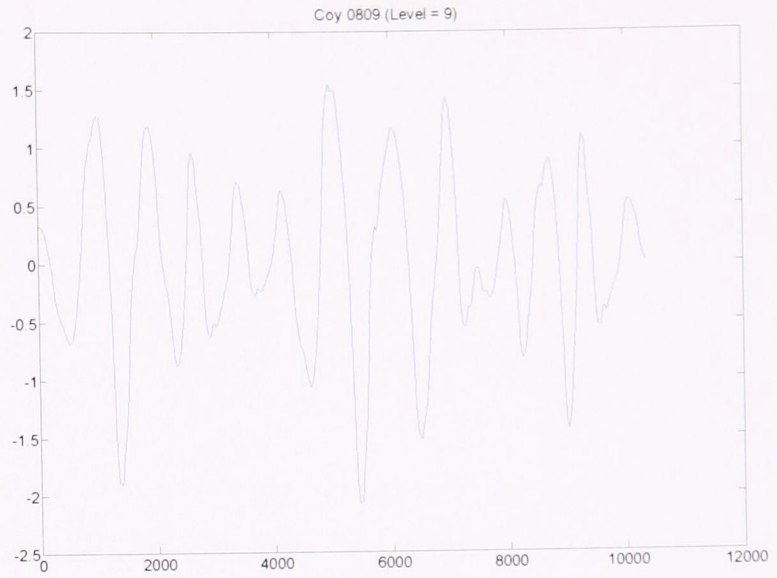


Caherglassaun 08/09

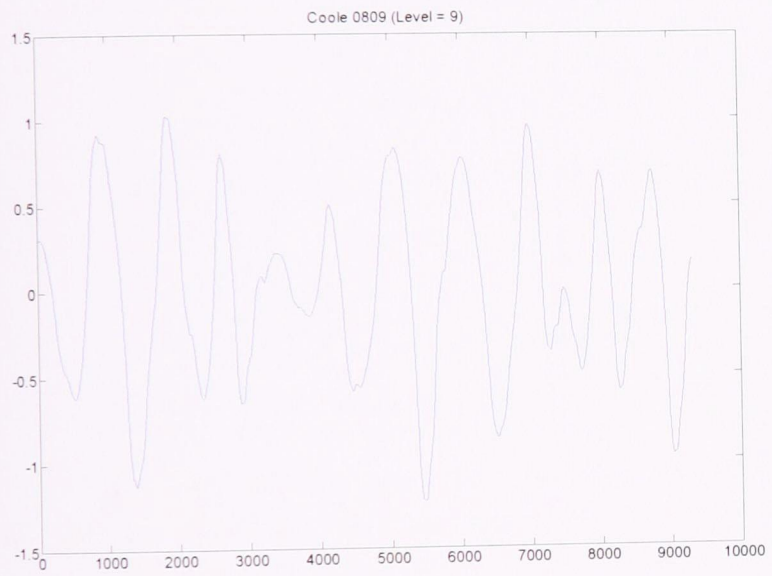
Level 9 (2008/09)



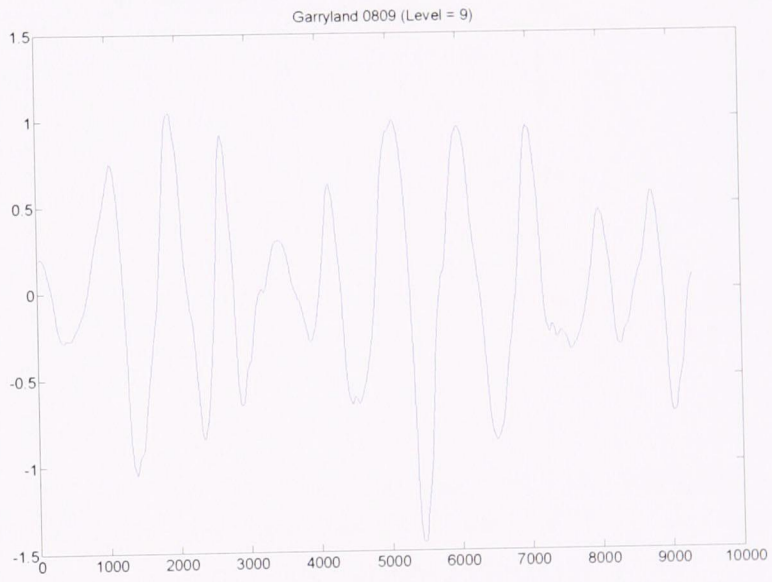
Blackrock 08/09



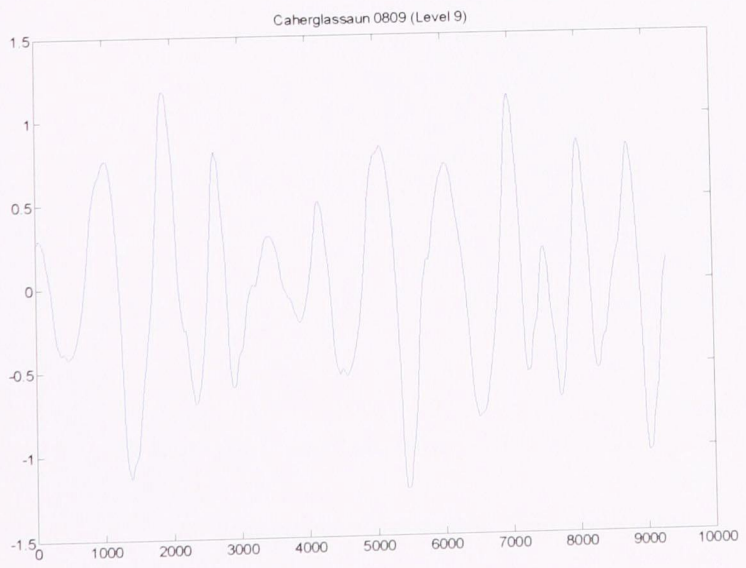
Coy 08/09



Coole 08/09

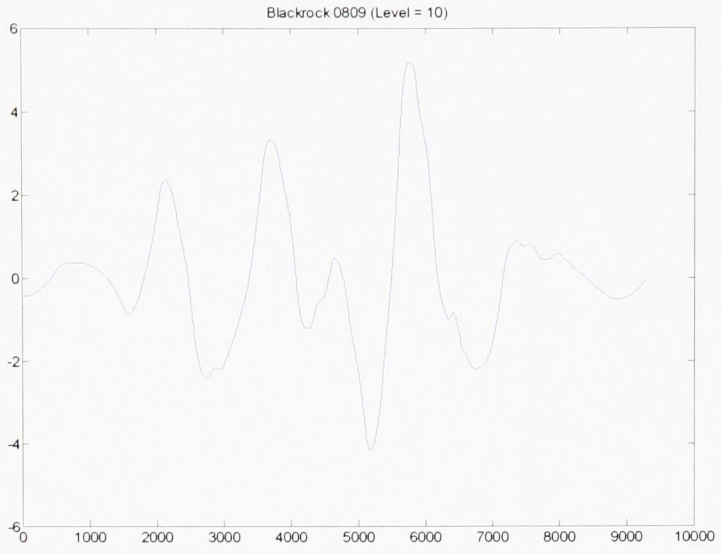


Garryland 08/09

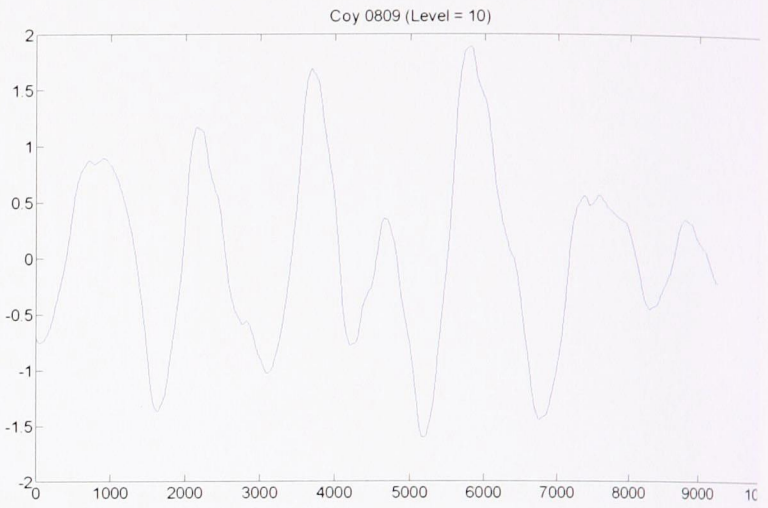


Caherglassaun 08/09

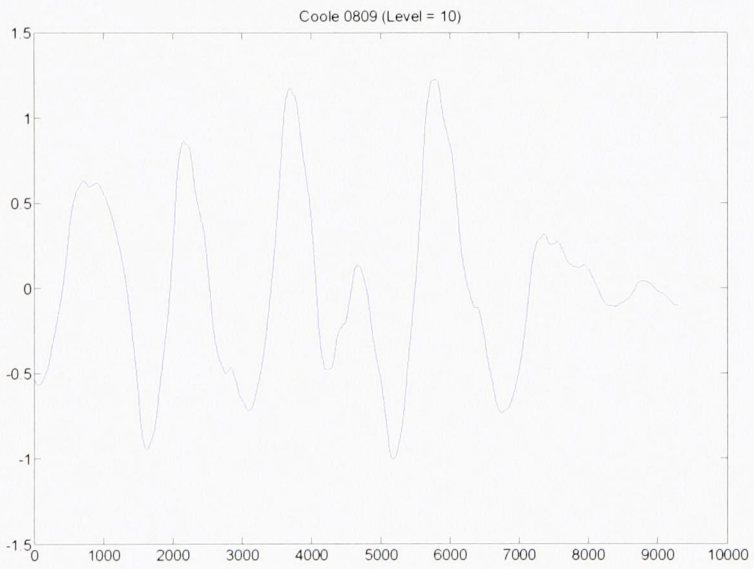
Level 10 (2008/09)



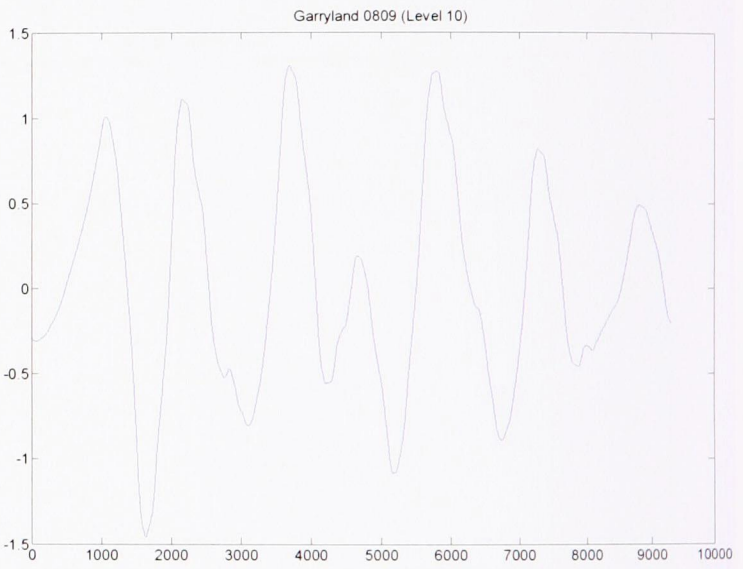
Blackrock 08/09



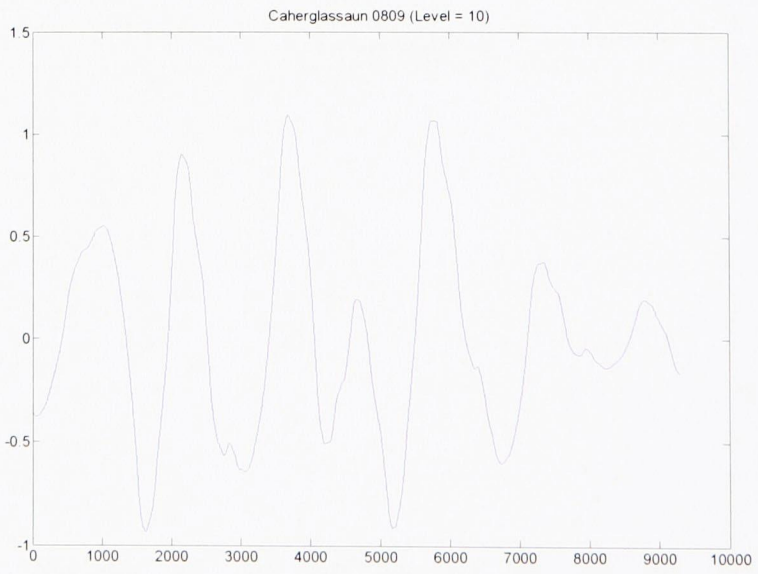
Coy 08/09



Coole 08/09

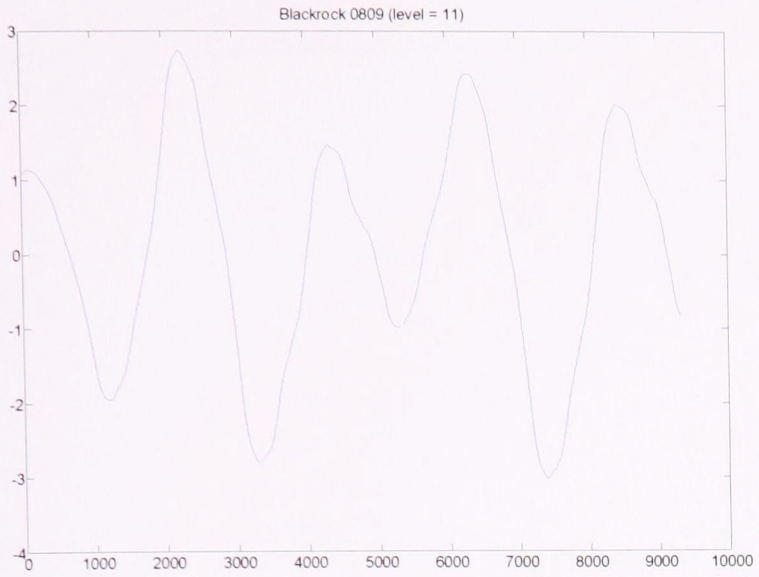


Garryland 08/09

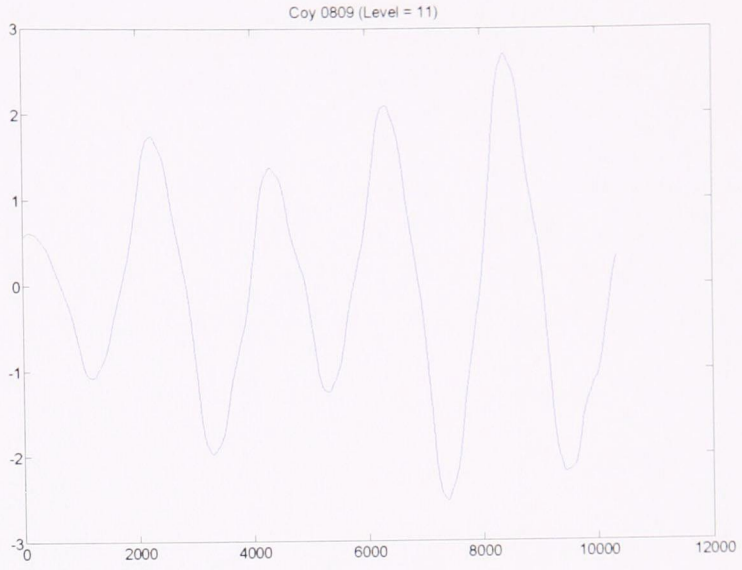


Caherglassaun 08/09

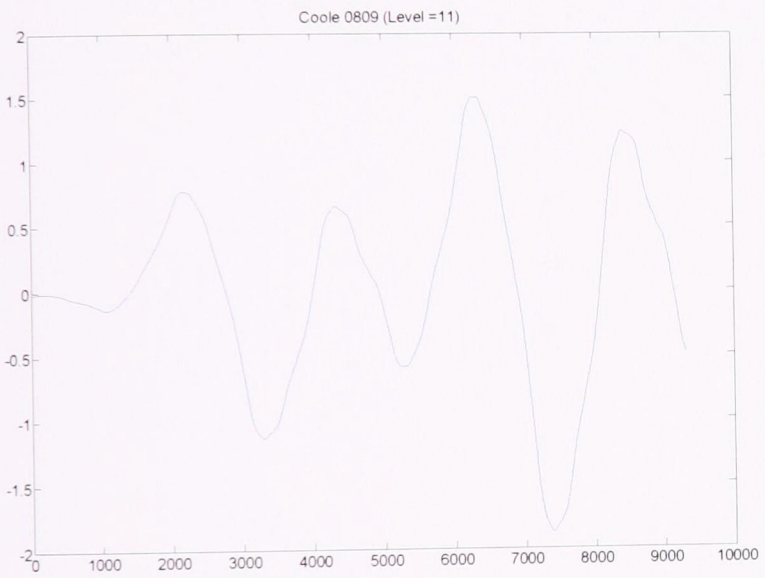
Level 11 (2008/09)



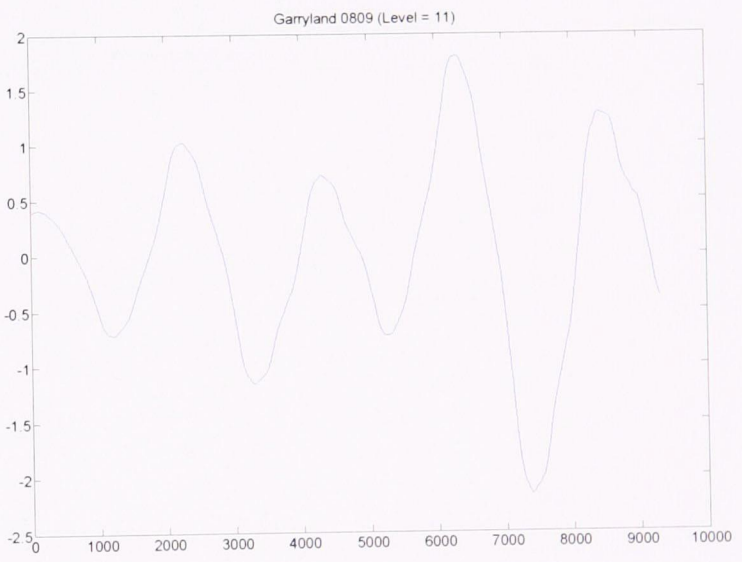
Blackrock 08/09



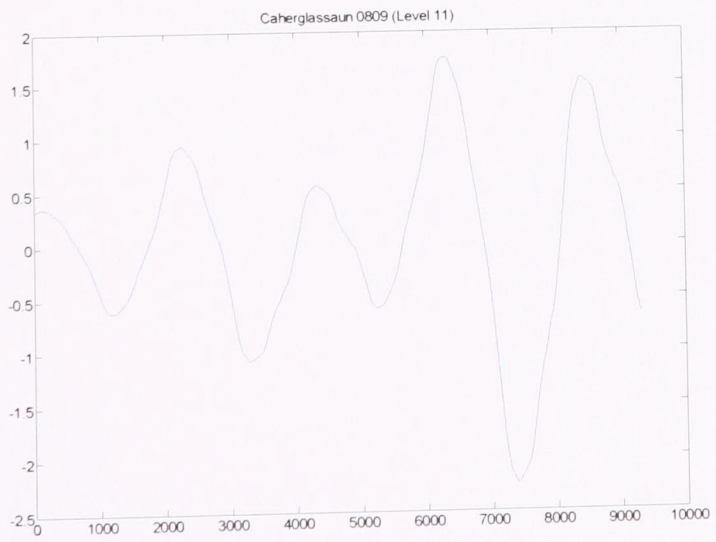
Coy 08/09



Coole 08/09

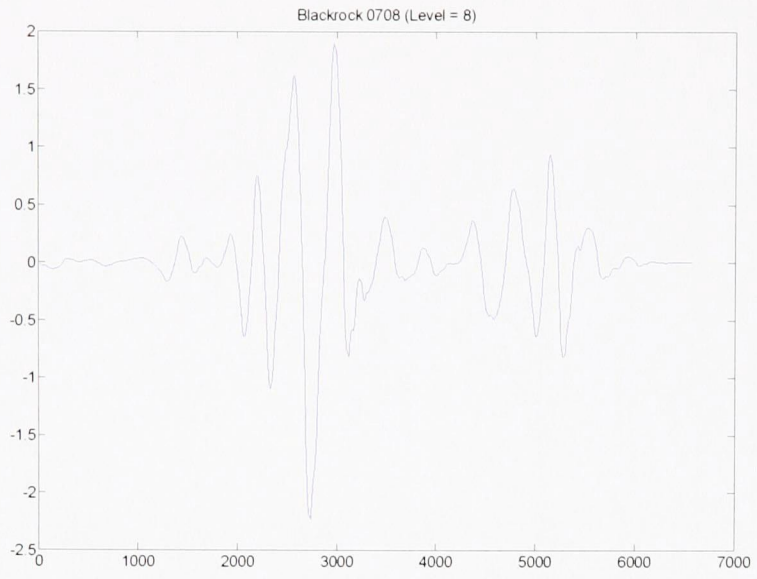


Garryland 08/09

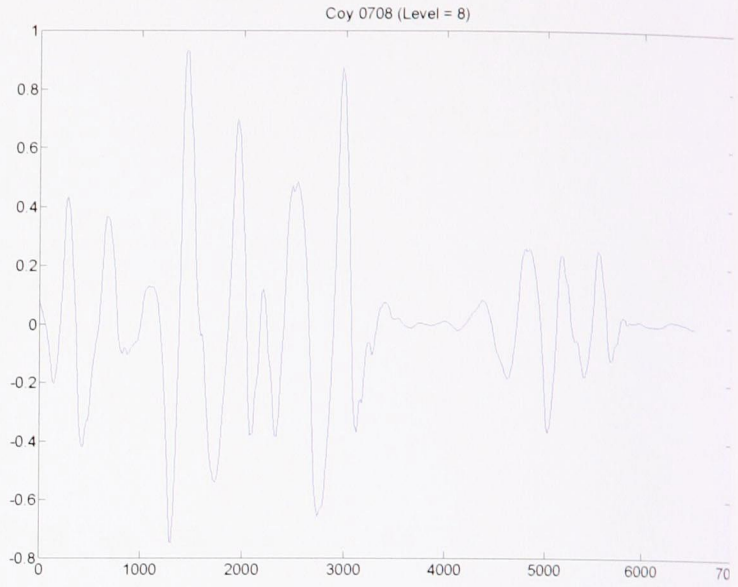


Caherglassaun 08/09

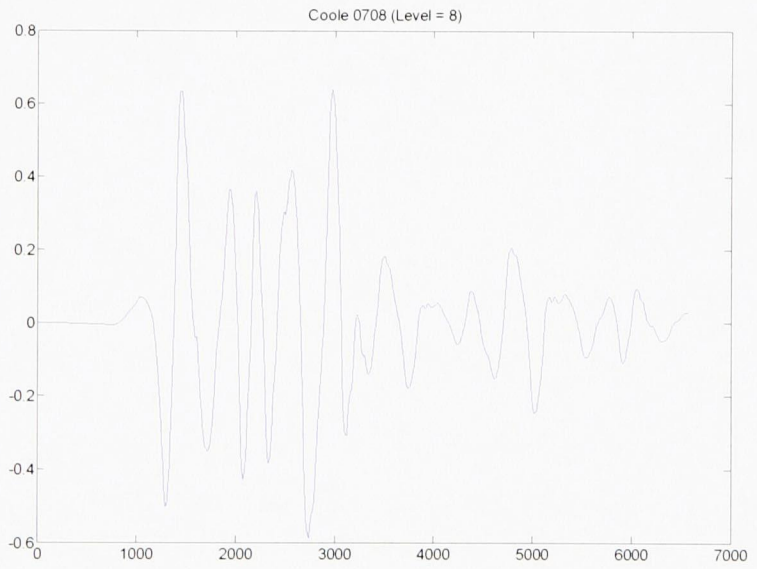
Level 8 (2007/08)



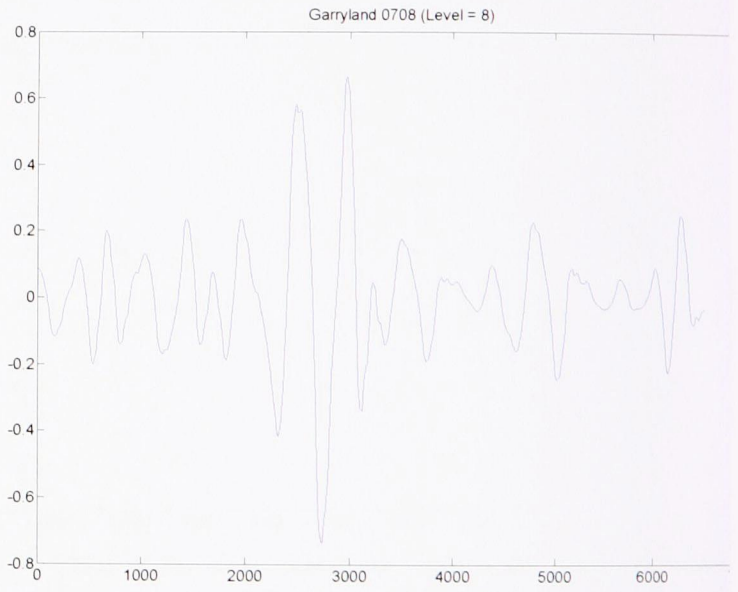
Blackrock 07/08



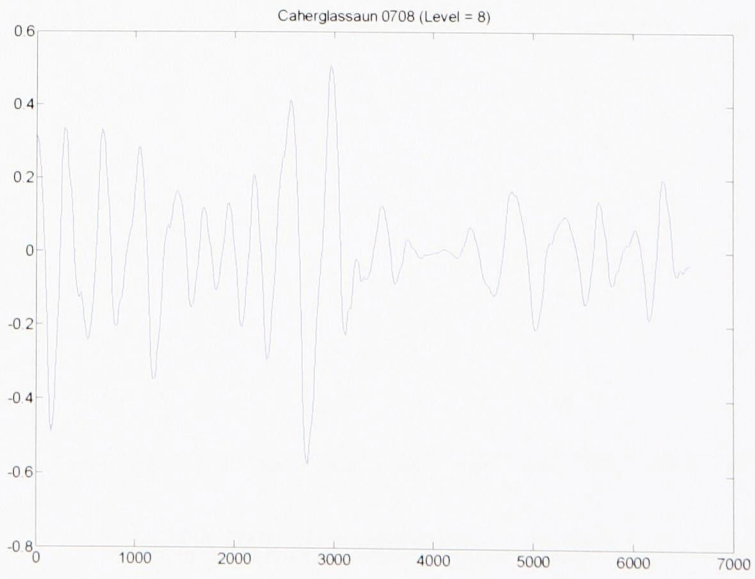
Coy 07/08



Coole 07/08

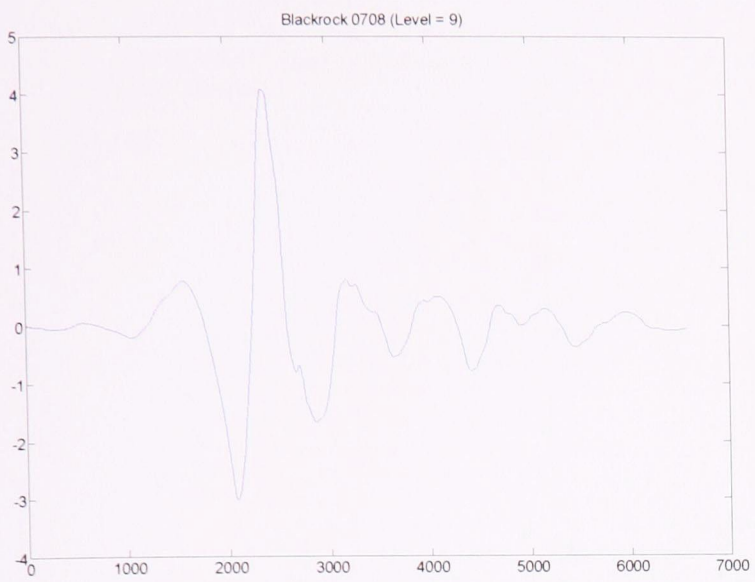


Garryland 07/08

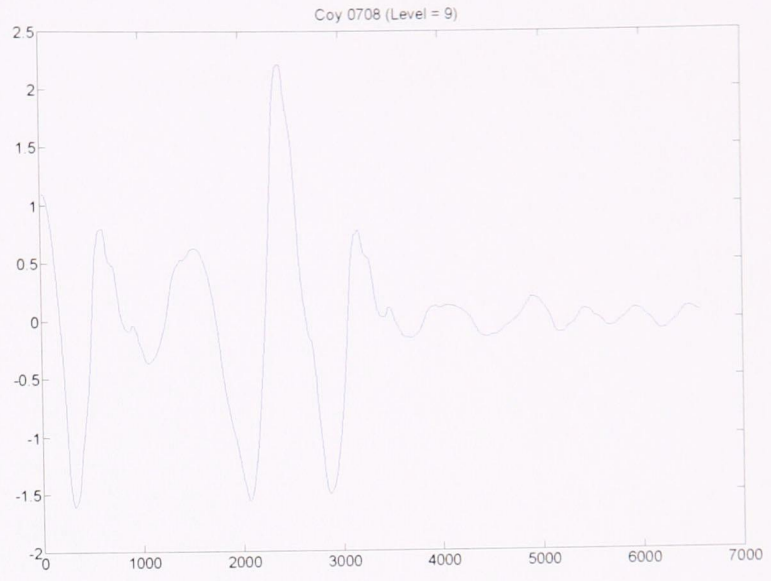


Caherglassaun 07/08

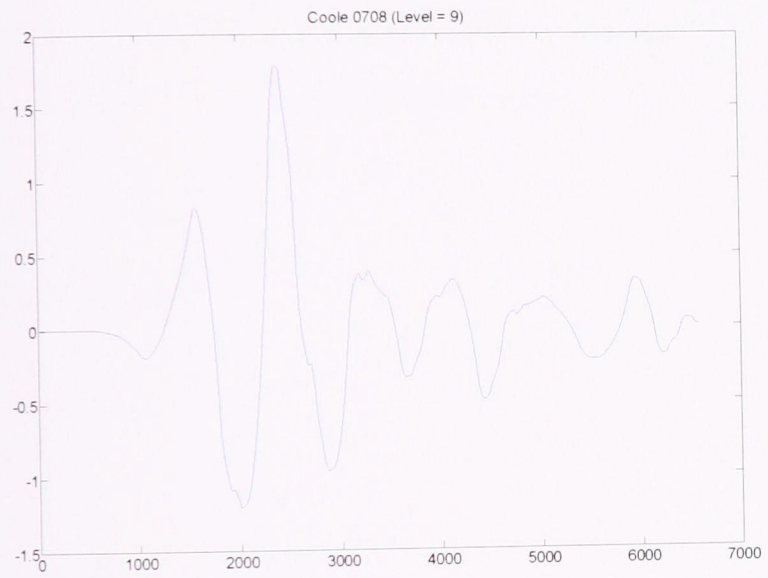
Level 9 (2007/08)



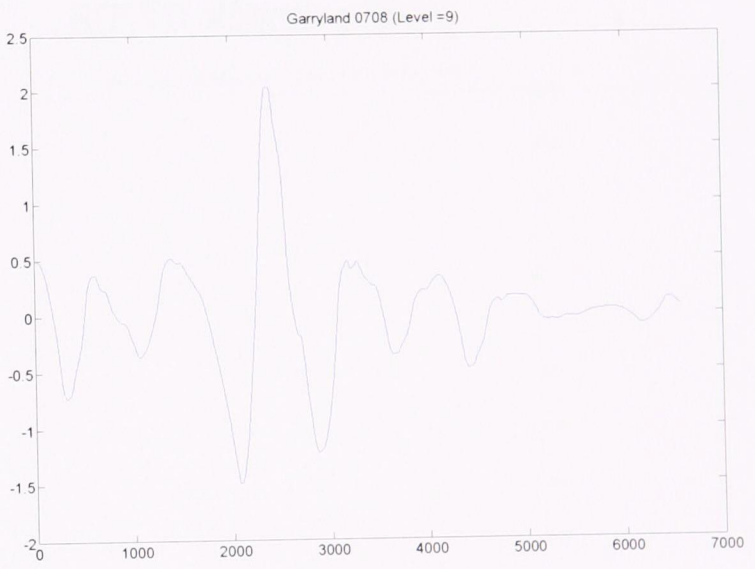
Blackrock 07/08



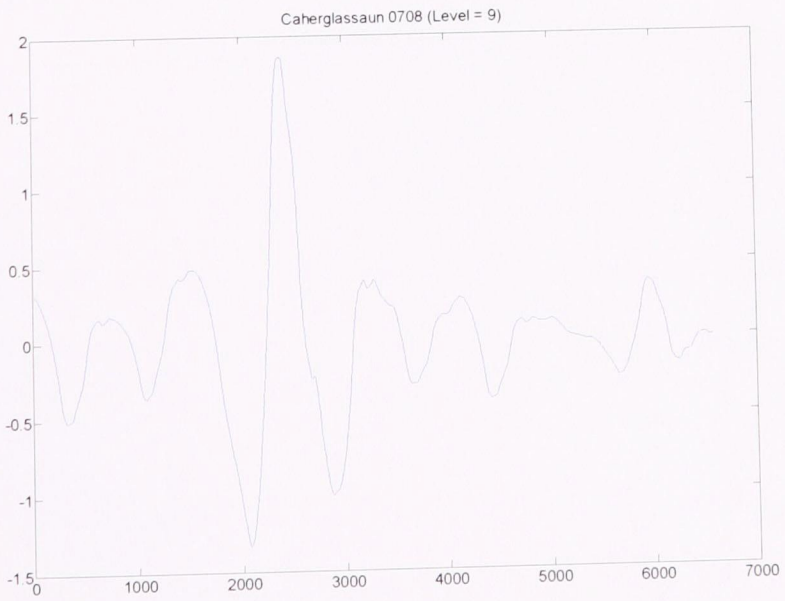
Coy 07/08



Coole 07/08

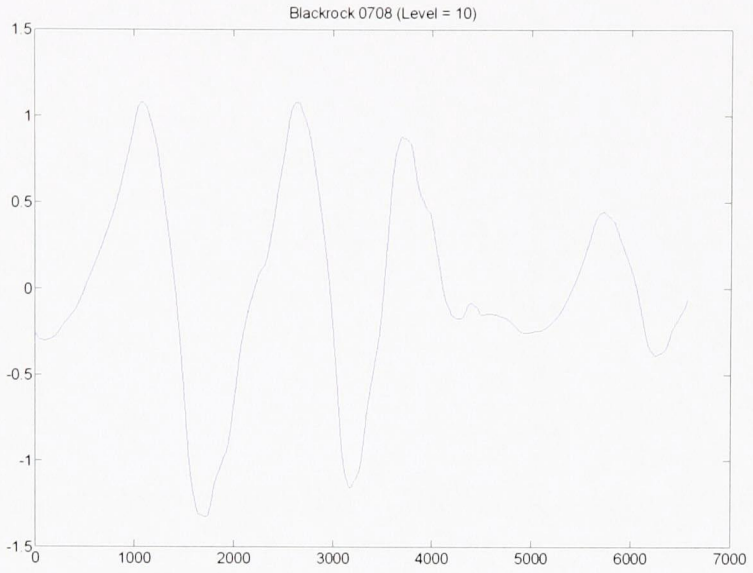


Garryland 07/08

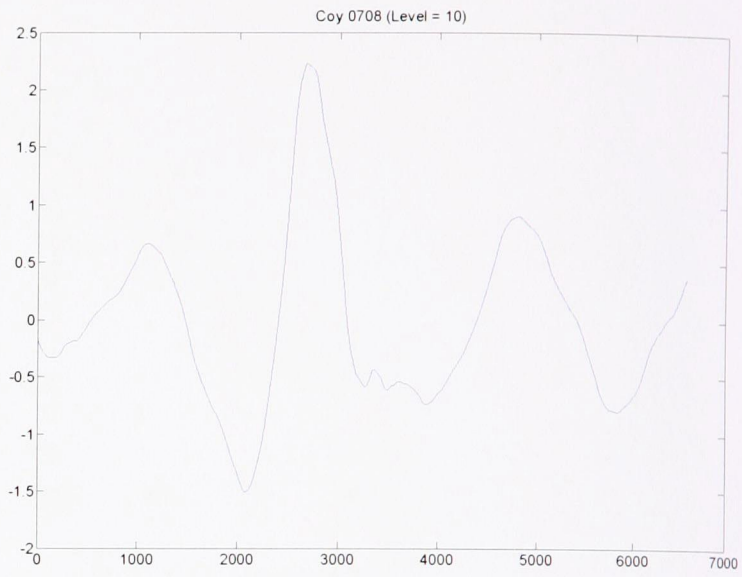


Caherglassaun 07/08

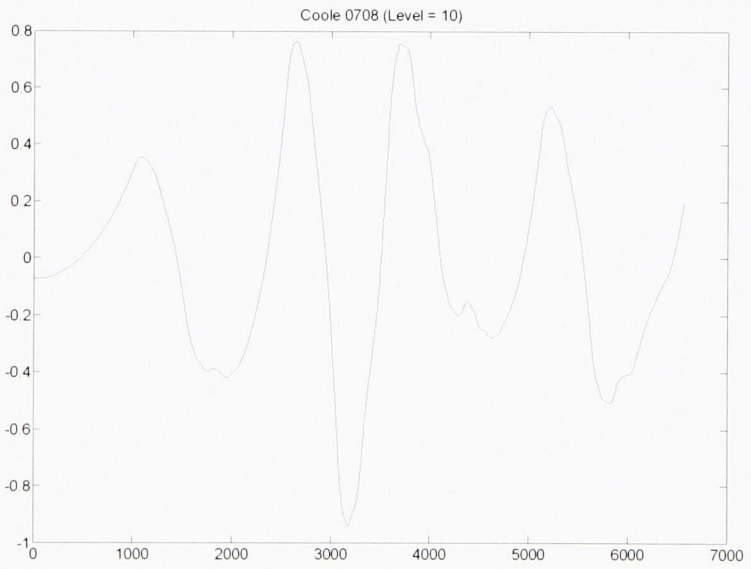
Level 10 (2007/08)



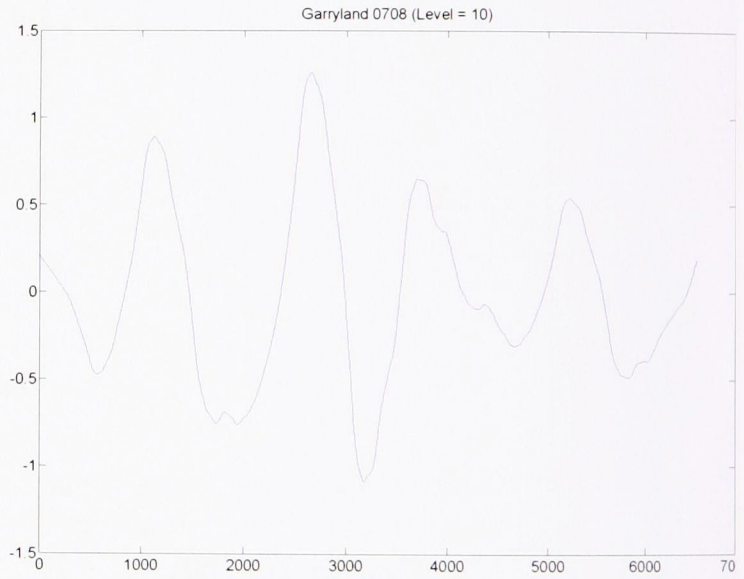
Blackrock 07/08



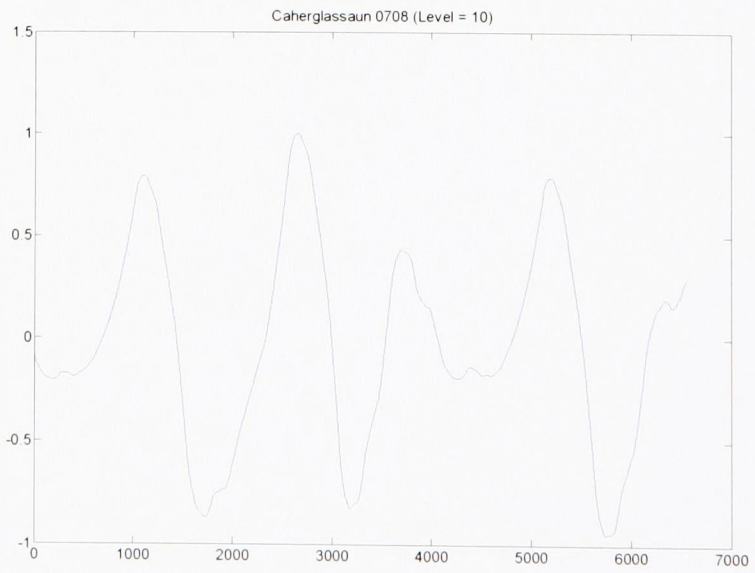
Coy 07/08



Coole 07/08

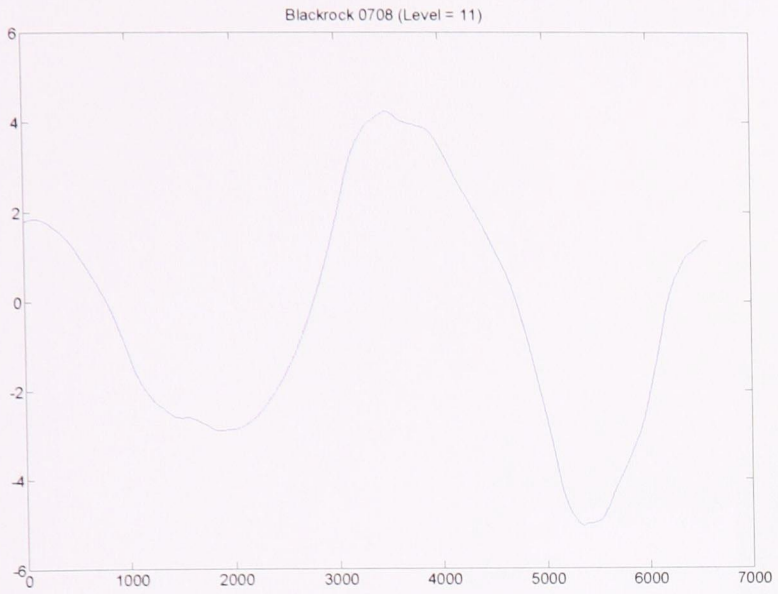


Garryland 07/08

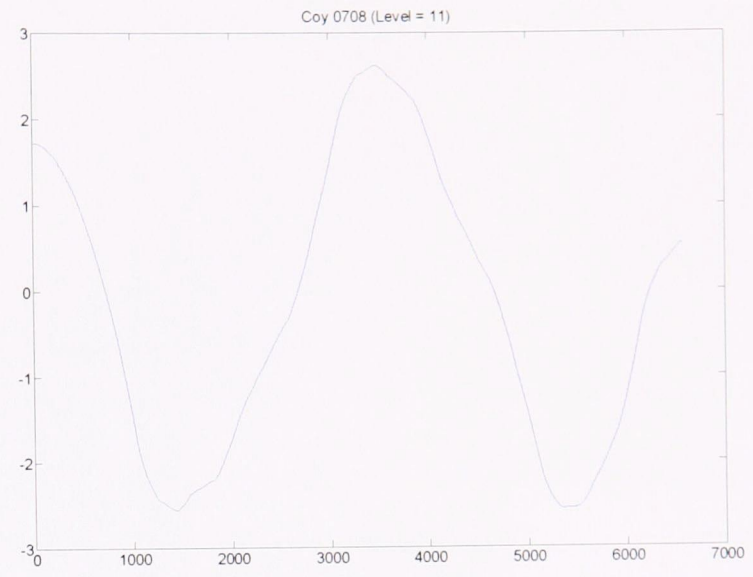


Caherglassaun 07/08

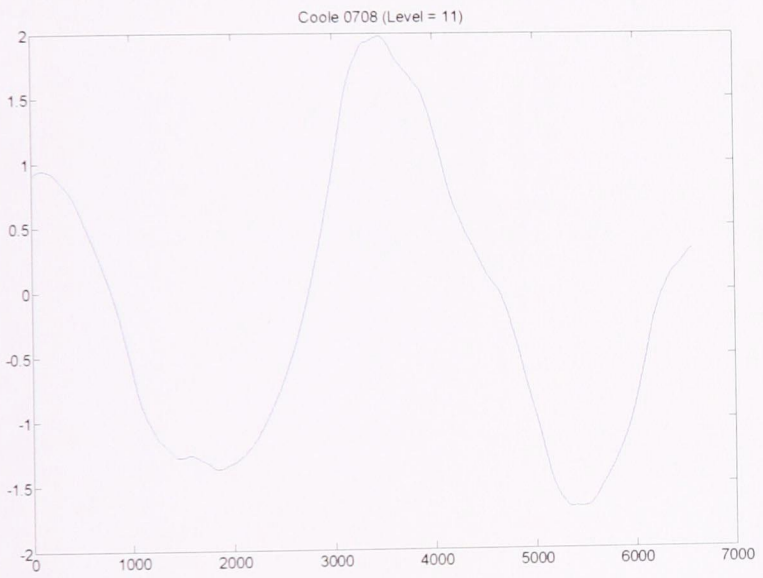
Level 11 (2007/08)



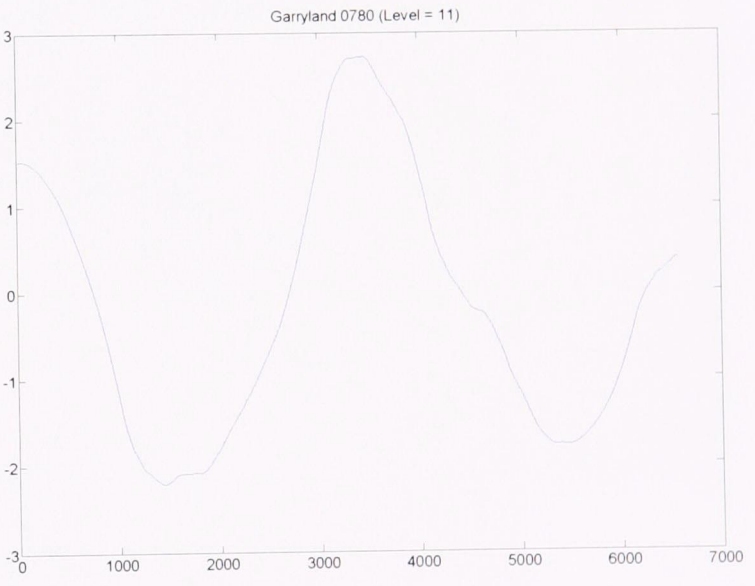
Blackrock 07/08



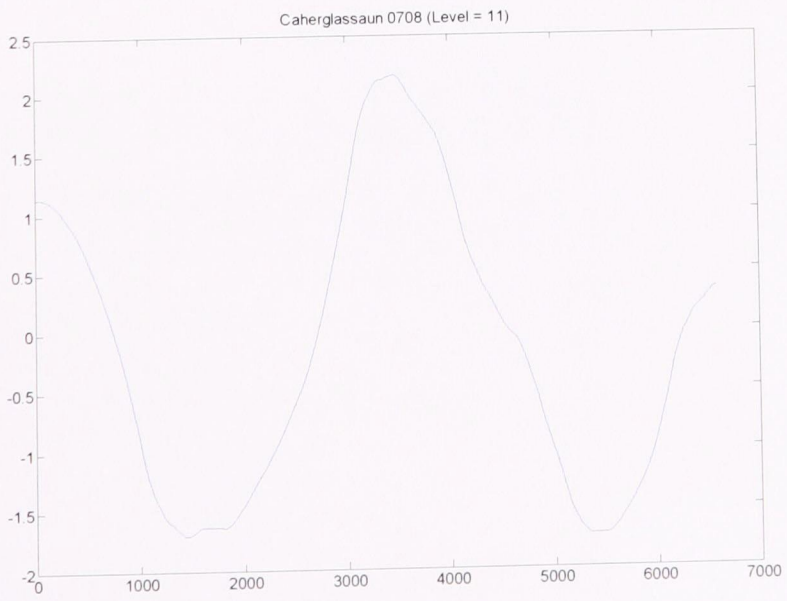
Coy 07/08



Coole 07/08



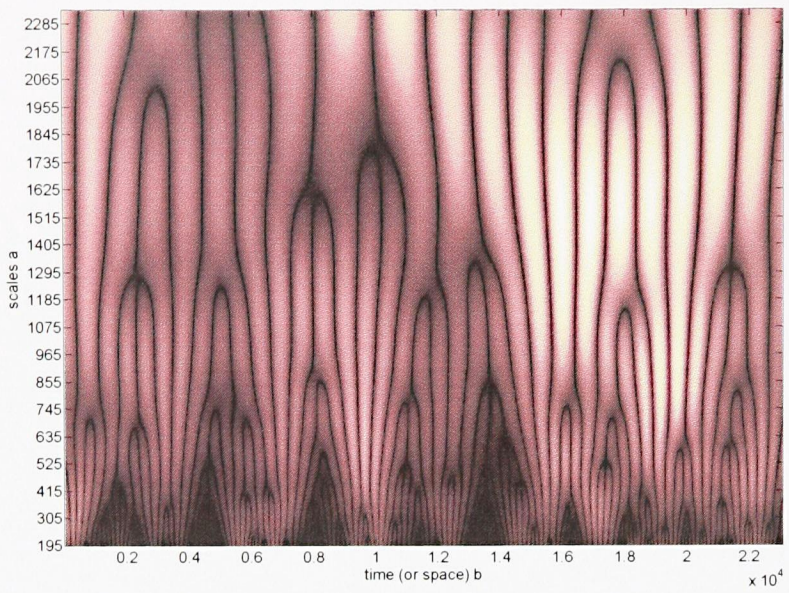
Garryland 07/08



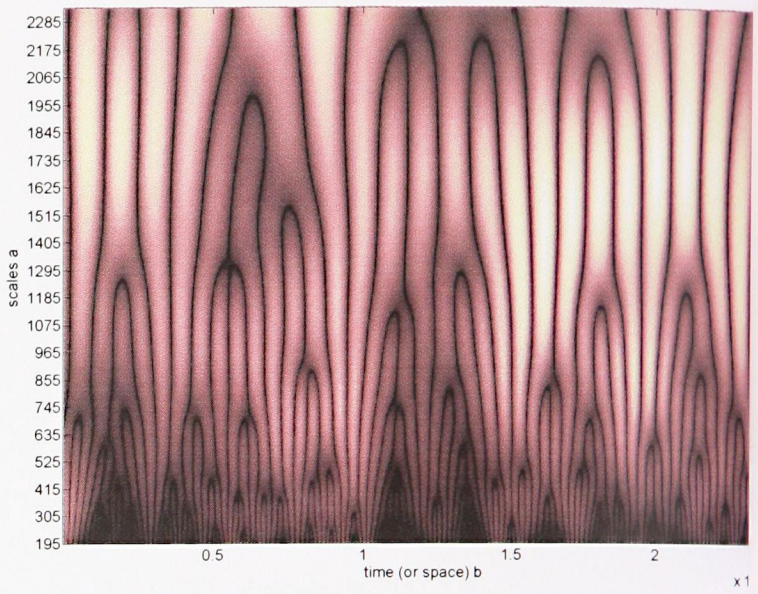
Caherglassaun 07/08

Continuous Wavelet Transform Analysis

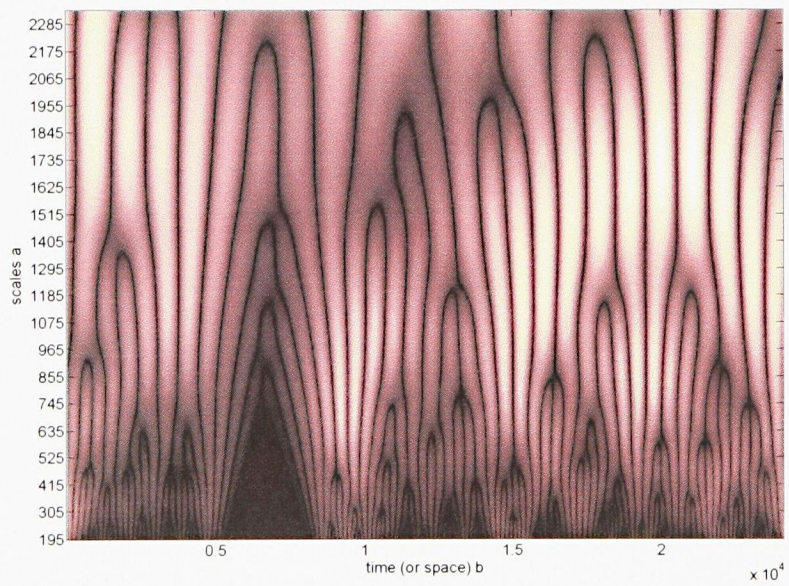
All three years



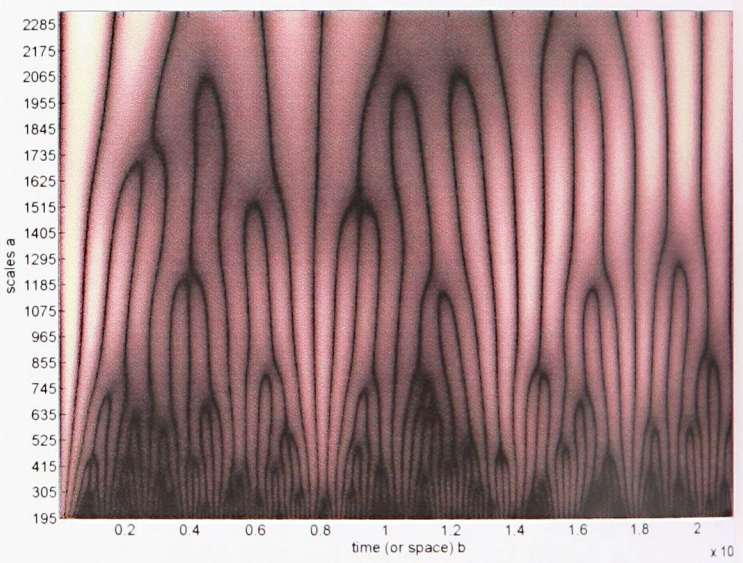
Blackrock 06/09



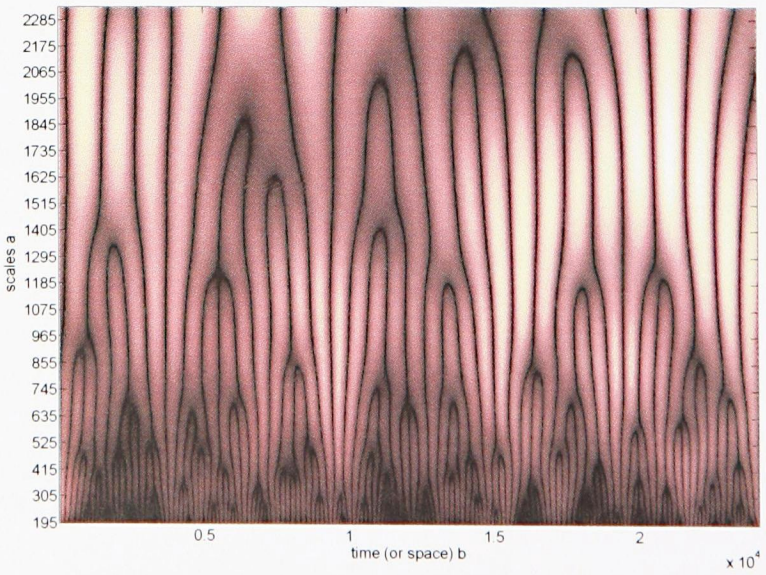
Coy 06/09



Coole 06/09

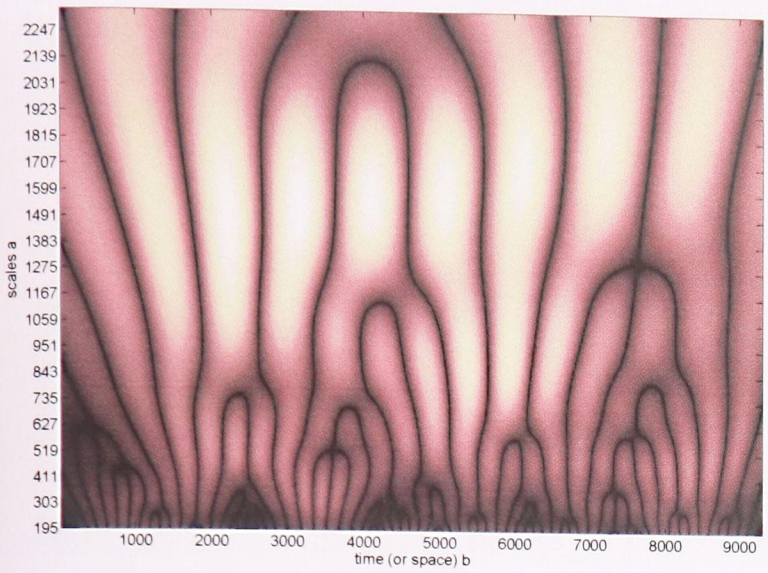


Garryland 06/09

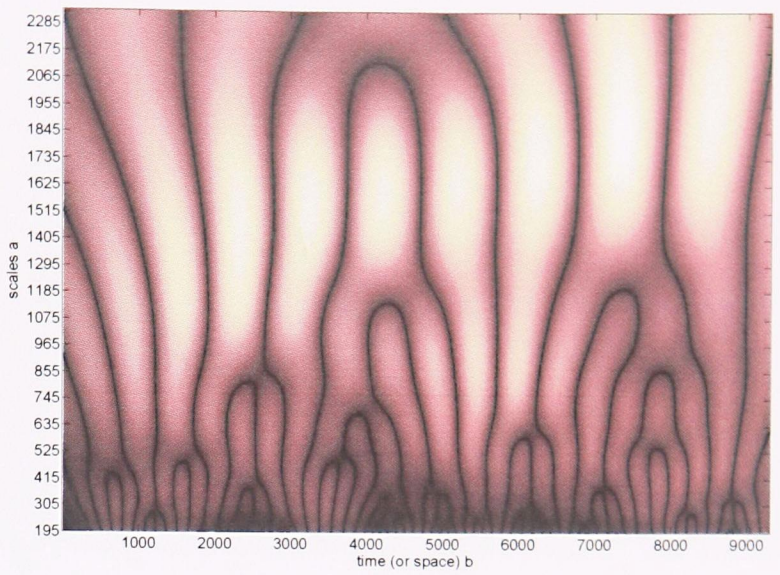


Caherglassaun 06/09

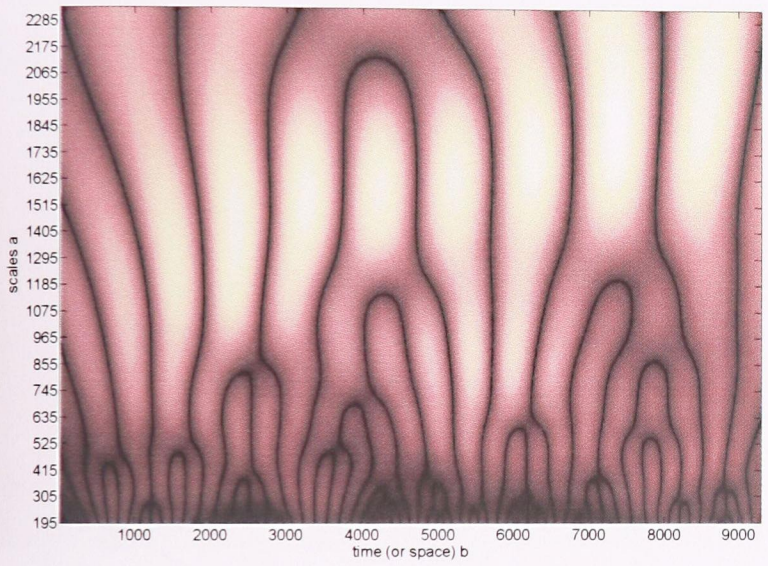
2008/09



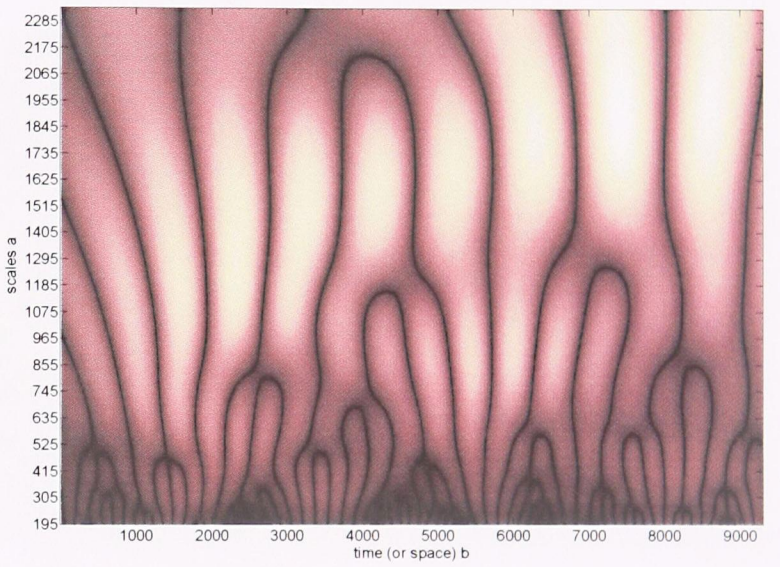
Blackrock 08/09



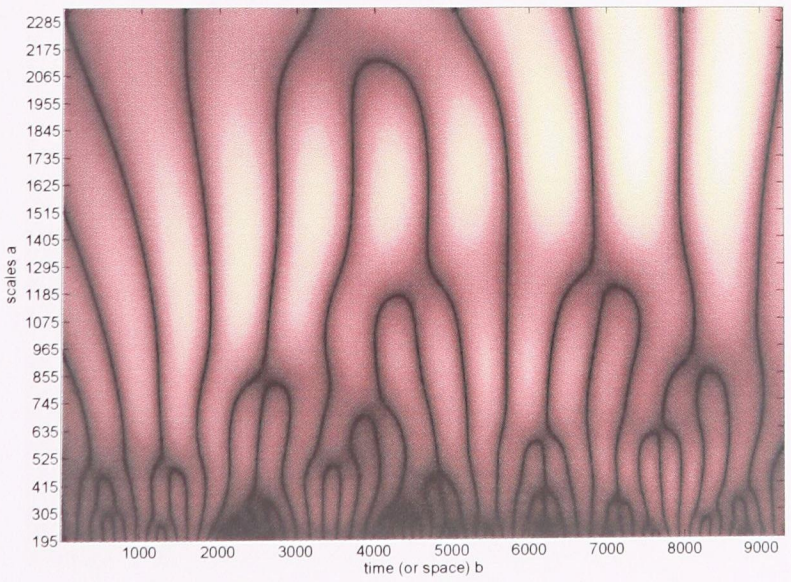
Coy 08/09



Coole 08/09

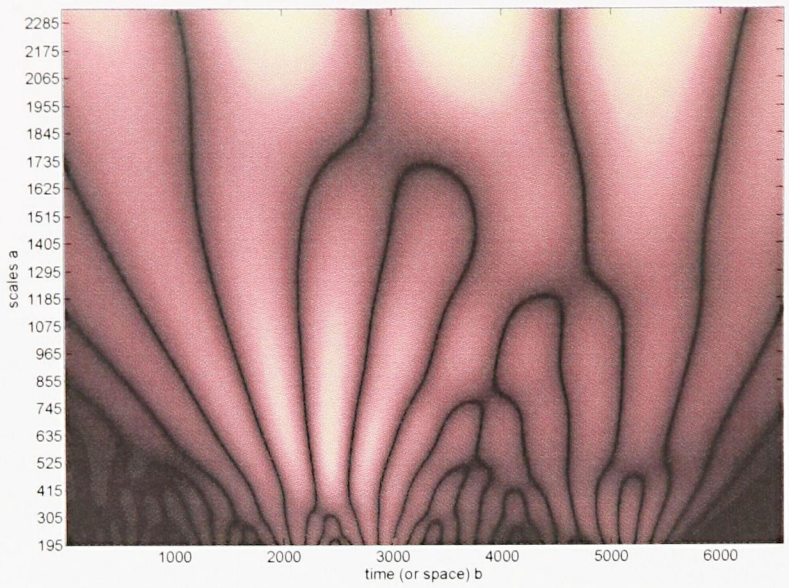


Garryland 08/09

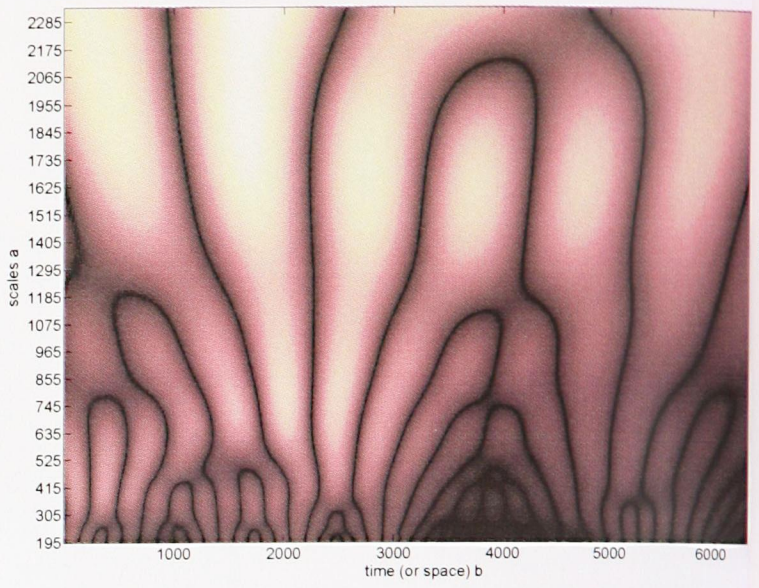


Caherglassaun 08/09

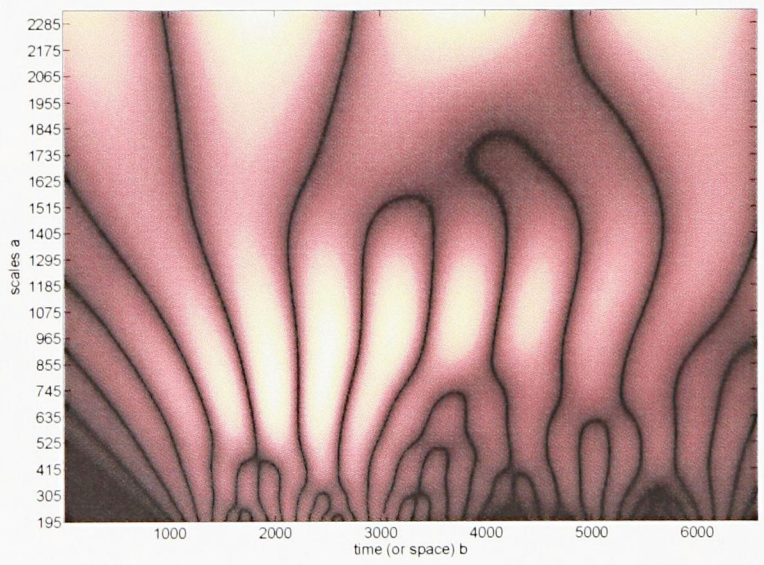
2007/08



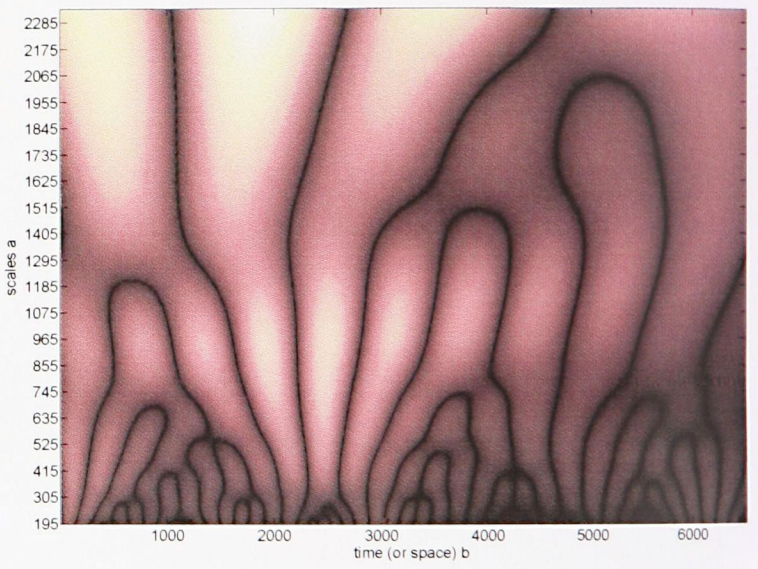
Blackrock 07/08



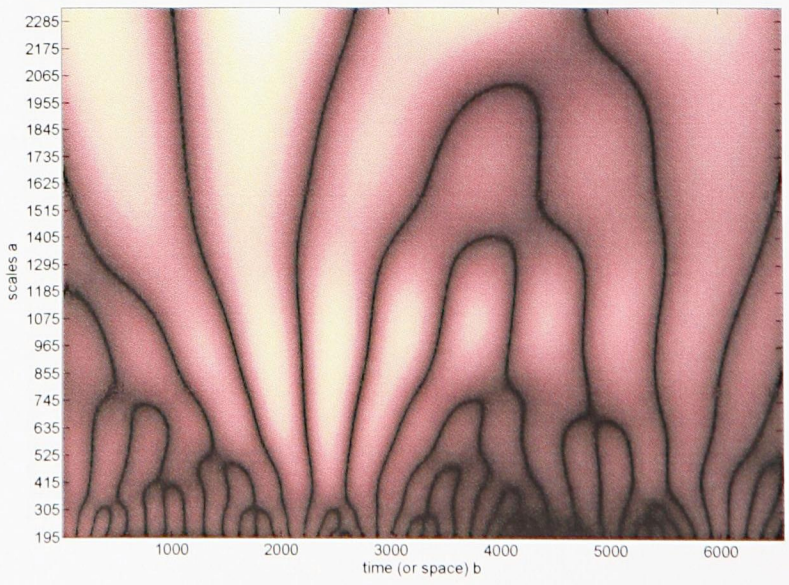
Coy 07/08



Coole 07/08

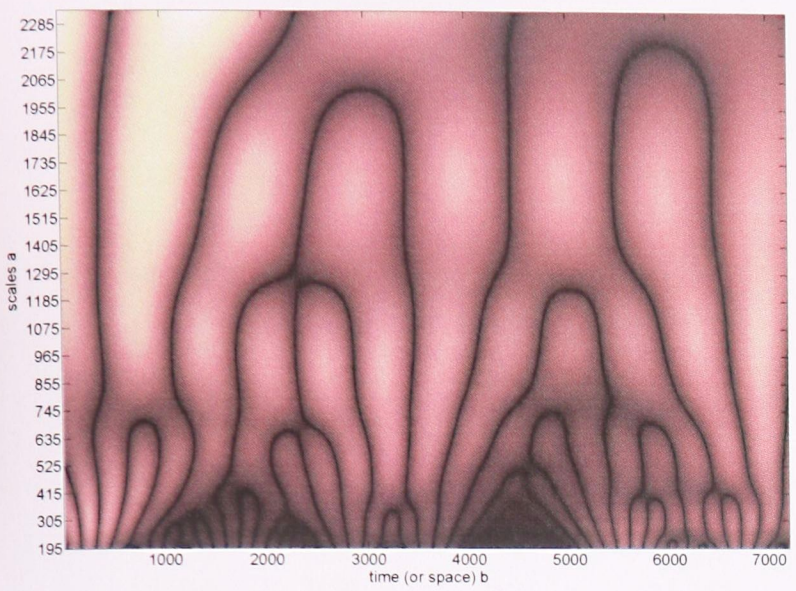


Garryland 07/08

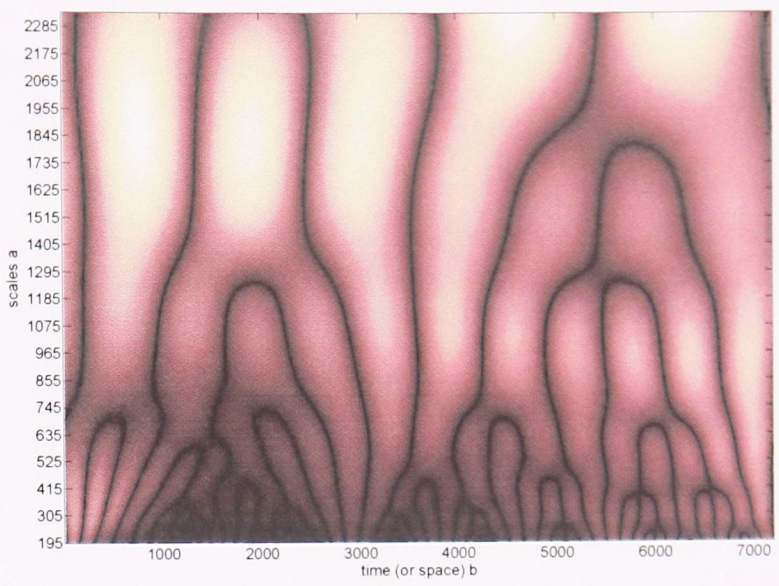


Caherglassaun 07/08

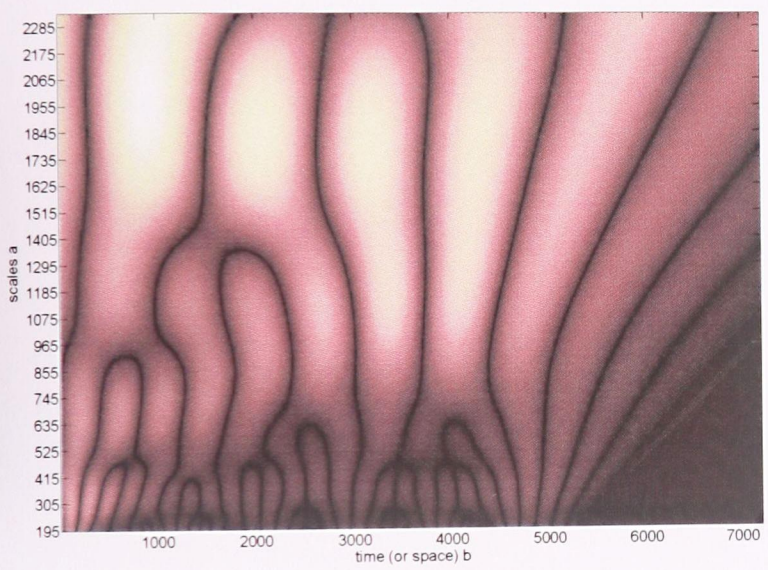
2006/07



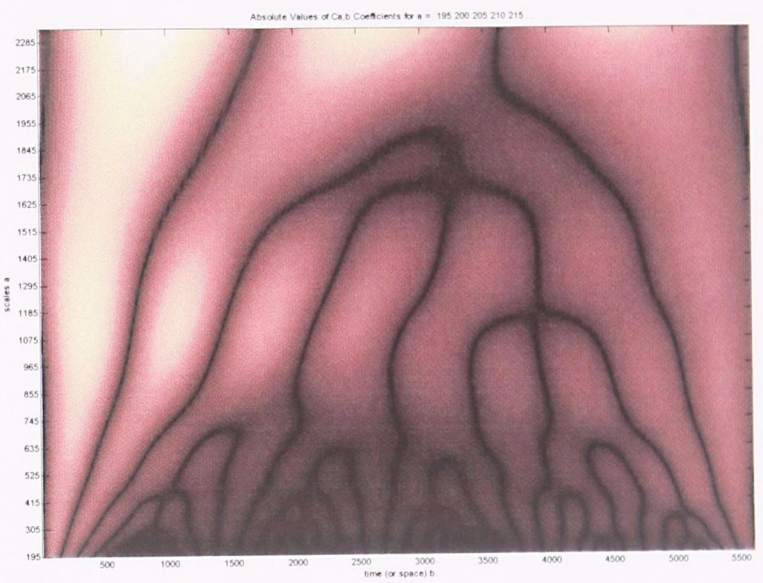
Blackrock 06/07



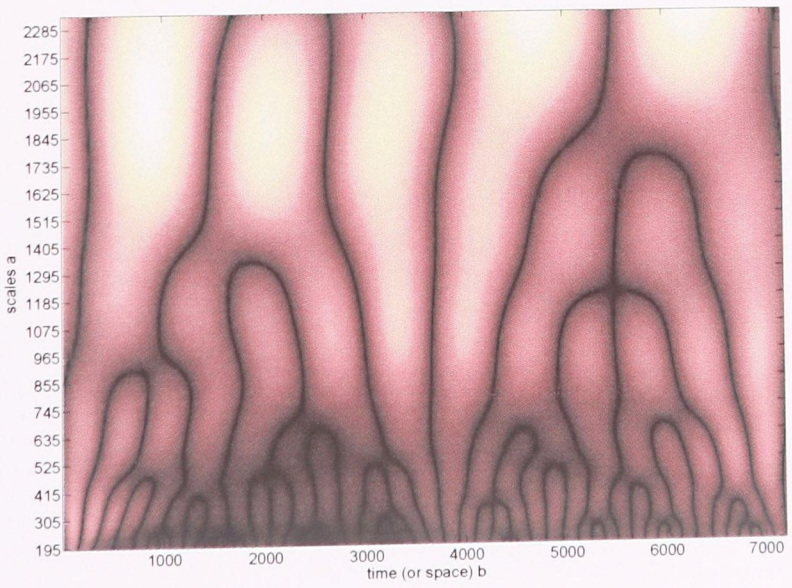
Coy 06/07



Coole 06/07



Garryland 06/07



Caherglassaun 06/07

TURLOUGH REPRESENTATION AS PONDS IN *INFOWORKS*

Blackrock pond dimensions

Elevation (mAOD)	Plan area (m^2)	Perimeter (m)
10.940	0.0	0.0
11.034	10.8	13.2
11.134	27.0	20.8
11.234	40.6	25.5
11.334	51.5	28.7
11.434	63.7	31.9
11.534	76.0	34.9
11.634	87.6	37.4
11.734	99.3	39.9
11.834	111.5	42.2
11.934	124.9	44.7
12.034	339.6	73.7
12.134	1366.0	147.8
12.234	3456.3	235.2
12.334	9749.0	394.9
12.434	14645.4	484.1
12.534	18041.3	537.3
12.634	21129.6	581.4
12.734	24918.6	631.4
12.834	31020.3	704.5
12.934	36774.5	767.1
13.034	43127.2	830.7
13.134	48416.7	880.2
13.234	53806.7	927.9
13.334	59299.3	974.1
13.434	65734.8	1025.6
13.534	72866.5	1079.8
13.634	79254.1	1126.1
13.734	84281.1	1161.2
13.834	87906.1	1186.0
13.934	91066.0	1207.1
14.034	93999.6	1226.4
14.134	96848.1	1244.8
14.234	100282.7	1266.7
14.334	104014.3	1290.1
14.434	107815.3	1313.4
14.534	112088.3	1339.2
14.634	116352.4	1364.4
14.734	119864.9	1384.9
14.834	122828.9	1401.9
14.934	125965.4	1419.7
15.034	129093.0	1437.2
15.134	132161.4	1454.2
15.234	135546.0	1472.7
15.334	138890.8	1490.7
15.434	141939.1	1507.0
15.534	145010.8	1523.2
15.634	147915.5	1538.4
15.734	150715.5	1552.9
15.834	153583.8	1567.6
15.934	156873.3	1584.3
16.034	159959.2	1599.8
16.134	162630.0	1613.1
16.234	165229.4	1625.9
16.334	167776.6	1638.4
16.434	170213.1	1650.3
16.534	172547.2	1661.6
16.634	174856.9	1672.6
16.734	177140.0	1683.5
16.834	179485.7	1694.6
16.934	182173.5	1707.3
17.034	184733.8	1719.2
17.134	187149.3	1730.4
17.234	189573.8	1741.6
17.334	191962.2	1752.5
17.434	194329.0	1763.3
17.534	196723.4	1774.1
17.634	199179.9	1785.2
17.734	201668.0	1796.3
17.834	204162.6	1807.4
17.934	206688.5	1818.5
18.034	209362.9	1830.2
18.134	212123.1	1842.3
18.234	215038.9	1854.9
18.334	218197.0	1868.5
18.434	221436.9	1882.3
18.534	224719.9	1896.2
18.634	227990.7	1909.9
18.734	231358.0	1924.0
18.834	234736.4	1938.0
18.934	237958.6	1951.2
19.034	241201.5	1964.5
19.134	244541.5	1978.0
19.234	248074.5	1992.3
19.334	251852.6	2007.4
19.434	255924.1	2023.6
19.534	260015.0	2039.7
19.634	263954.6	2055.1
19.734	268158.5	2071.4
19.834	272472.8	2088.0
19.934	277255.8	2106.2
20.034	281730.7	2123.1
20.134	286332.4	2140.4
20.234	290878.9	2157.3
20.334	295427.2	2174.1
20.434	300112.4	2191.3
20.534	304874.2	2208.6
20.634	309784.7	2226.3
20.734	314830.6	2244.4
20.834	320377.0	2264.1
20.934	325397.8	2281.7
21.034	330307.3	2298.9
21.134	335305.5	2316.2
21.234	340354.7	2333.6
21.334	345506.6	2351.2
21.434	350981.7	2369.7
21.534	356710.4	2389.0
21.634	363060.7	2410.2
21.734	368917.4	2429.5
21.834	374367.6	2447.4
21.934	379757.8	2465.0
22.034	385127.3	2482.3
22.134	390592.9	2499.9
22.234	396118.3	2517.5
22.334	401320.4	2534.0
22.434	406518.9	2550.4
22.534	412009.8	2567.5
22.634	417782.6	2585.4
22.734	423309.6	2602.5
22.834	428798.5	2619.3
22.934	434121.6	2635.5
23.034	439239.0	2651.0
23.134	444133.0	2665.7
23.234	448896.0	2680.0
23.334	453579.8	2693.9
23.434	458163.0	2707.5
23.534	462647.0	2720.7
23.634	467093.4	2733.8
23.734	471537.7	2746.7
23.834	475930.3	2759.5
23.934	480296.4	2772.1
24.034	484673.8	2784.7
24.134	489124.0	2797.5
24.234	493639.7	2810.4
24.334	498142.4	2823.2
24.434	502643.3	2835.9
24.534	507283.2	2849.0
24.634	512043.6	2862.3
24.734	516602.9	2875.0
24.834	520998.0	2887.2
24.934	525316.0	2899.1
25.034	529589.1	2910.9
25.134	533836.3	2922.6
25.234	538125.6	2934.3
25.334	542508.9	2946.2
25.434	547038.0	2958.5
25.534	551739.4	2971.2
25.634	556198.2	2983.1
25.734	560613.0	2995.0
25.834	565097.4	3006.9
25.934	569727.9	3019.2
26.034	574483.2	3031.8
26.134	579396.0	3044.7
26.234	584533.7	3058.2
26.334	589666.4	3071.6
26.434	594827.5	3085.0
26.454	595876.3	3087.7
26.474	596932.4	3090.5
26.494	597994.3	3093.2

Coy pond dimensions

Elevation (mAOD)	Plan area (m^2)	Perimeter (m)
8.600	41951.7	819.3
8.694	45333.3	851.7
8.794	49010.2	885.5
8.894	52408.1	915.7
8.994	55579.5	943.0
9.094	58684.7	969.0
9.194	61719.0	993.7
9.294	64848.2	1018.6
9.394	68214.9	1044.7
9.494	71855.0	1072.2
9.594	75470.5	1098.9
9.694	78834.1	1123.1
9.794	82035.6	1145.7
9.894	85477.0	1169.5
9.994	89236.4	1194.9
10.094	92617.5	1217.3
10.194	95811.1	1238.1
10.294	98938.2	1258.2
10.394	101911.9	1276.9
10.494	104854.5	1295.3
10.594	107268.2	1310.1
10.694	109425.5	1323.2
10.794	111513.0	1335.7
10.894	113394.1	1347.0
10.994	115154.1	1357.4
11.094	116844.5	1367.3
11.194	118487.8	1376.9
11.294	120105.0	1386.2
11.394	121753.7	1395.7
11.494	123509.8	1405.8
11.594	125139.9	1415.0
11.694	126770.7	1424.2
11.794	128449.7	1433.6
11.894	130086.9	1442.7
11.994	131639.9	1451.3
12.094	133051.6	1459.0
12.194	134369.1	1466.3
12.294	135663.3	1473.3
12.394	136924.4	1480.1
12.494	138156.5	1486.8
12.594	139367.4	1493.3
12.694	140570.1	1499.7
12.794	141768.9	1506.1
12.894	142974.6	1512.5
12.994	144205.7	1519.0
13.094	145428.5	1525.4
13.194	146611.8	1531.6
13.294	147776.9	1537.7
13.394	148936.6	1543.7
13.494	150092.8	1549.7
13.594	151246.0	1555.6
13.694	152405.5	1561.6
13.794	153581.6	1567.6
13.894	154751.2	1573.5
13.994	155900.9	1579.4
14.094	157043.4	1585.1
14.194	158163.6	1590.8
14.294	159285.4	1596.4
14.394	160415.9	1602.1
14.494	161600.1	1608.0
14.594	162970.7	1614.8
14.694	164535.5	1622.5
14.794	166194.0	1630.7
14.894	167802.5	1638.5
14.994	169448.9	1646.6
15.094	171292.8	1655.5
15.194	173160.6	1664.5
15.294	175054.6	1673.6
15.394	176965.4	1682.7
15.494	178936.6	1692.0
15.594	180945.4	1701.5
15.694	182937.5	1710.8
15.794	184944.0	1720.2
15.894	186997.1	1729.7
15.994	189091.5	1739.4
16.094	191196.7	1749.0
16.194	193340.1	1758.8
16.294	195524.2	1768.7
16.394	197770.5	1778.9
16.494	200135.9	1789.5
16.594	202506.4	1800.0
16.694	205126.9	1811.6
16.794	207594.2	1822.5
16.894	210035.7	1833.2
16.994	212556.6	1844.2
17.094	215084.3	1855.1
17.194	217583.1	1865.8
17.294	220126.8	1876.7
17.394	222710.4	1887.7
17.494	225370.0	1898.9
17.594	228029.7	1910.1
17.694	230649.5	1921.0
17.794	233356.7	1932.3
17.894	236311.6	1944.5
17.994	239547.3	1957.7
18.094	243331.8	1973.1
18.194	246909.8	1987.6
18.294	250589.3	2002.4
18.394	254450.0	2017.7

Coole pond dimensions

Elevation (mAOD)	Plan area (m^2)	Perimeter (m)
1.694	96901.3	1245.2
1.794	141687.9	1505.7
1.894	195437.4	1768.3
1.994	246649.6	1986.6
2.094	289249.2	2151.3
2.194	324067.8	2277.1
2.294	356200.3	2387.3
2.394	384856.6	2481.5
2.494	409912.0	2561.0
2.594	433728.6	2634.3
2.694	455724.8	2700.3
2.794	475970.2	2759.6
2.894	494231.0	2812.1
2.994	511029.0	2859.5
3.094	528055.6	2906.7
3.194	543984.2	2950.2
3.294	558900.3	2990.4
3.394	572592.4	3026.8
3.494	585723.7	3061.3
3.594	598575.8	3094.7
3.694	611807.1	3128.7
3.794	626831.4	3166.9
3.894	642828.5	3207.1
3.994	660584.1	3251.1
4.094	679873.5	3298.2
4.194	698615.7	3343.3
4.294	718492.7	3390.6
4.394	737999.4	3436.3
4.494	756183.3	3478.4
4.594	773303.7	3517.5
4.694	790061.2	3555.4
4.794	807649.1	3594.8
4.894	825022.2	3633.2
4.994	841383.1	3669.1
5.094	856651.6	3702.2
5.194	871351.3	3733.8
5.294	886119.2	3765.4
5.394	901578.5	3798.1
5.494	916537.2	3829.4
5.594	933665.5	3865.1
5.694	951108.5	3901.0
5.794	968925.8	3937.4
5.894	985158.5	3970.2
5.994	1000139.0	4000.3
6.094	1014261.1	4028.4
6.194	1028118.5	4055.8
6.294	1040838.0	4080.9
6.394	1052879.9	4104.4
6.494	1064283.5	4126.6
6.594	1075685.5	4148.6
6.694	1086597.5	4169.6
6.794	1097002.7	4189.5
6.894	1107158.8	4208.9
6.994	1117193.6	4227.9

Elevation (mAOD)	Plan area (m^2)	Perimeter (m)
7.094	1127122.2	4246.6
7.194	1137001.6	4265.2
7.294	1146920.2	4283.8
7.394	1156955.0	4302.5
7.494	1167677.7	4322.4
7.594	1178878.4	4343.0
7.694	1189820.7	4363.2
7.794	1200804.6	4383.2
7.894	1211845.8	4403.4
7.994	1222547.1	4422.8
8.094	1232915.4	4441.5
8.194	1243367.3	4460.3
8.294	1253739.3	4478.8
8.394	1264338.8	4497.7
8.494	1275586.9	4517.7
8.594	1286735.2	4537.4
8.694	1297506.1	4556.3
8.794	1307711.7	4574.2
8.894	1317779.4	4591.8
8.994	1327845.6	4609.3
9.094	1337940.6	4626.8
9.194	1348066.7	4644.3
9.294	1358277.6	4661.8
9.394	1368658.8	4679.6
9.494	1379163.6	4697.5
9.594	1389777.3	4715.6
9.694	1400490.8	4733.7
9.794	1411328.1	4752.0
9.894	1422303.9	4770.4
9.994	1433477.0	4789.1
10.094	1444817.9	4808.0
10.194	1456356.6	4827.2
10.294	1468152.7	4846.7
10.394	1480291.9	4866.7
10.494	1492802.6	4887.2
10.594	1505980.7	4908.7
10.694	1519189.3	4930.2
10.794	1532651.4	4952.0
10.894	1546493.6	4974.3
10.994	1560992.3	4997.6
11.094	1576223.5	5021.9
11.194	1591997.5	5047.0
11.294	1608532.7	5073.1
11.394	1625301.4	5099.5
11.494	1642557.3	5126.5
11.594	1660264.1	5154.0
11.694	1678376.2	5182.1
11.794	1696986.5	5210.7
11.894	1716377.0	5240.4
11.994	1736659.1	5271.3
12.094	1757814.3	5303.304
12.194	1779681.9	5336.189
12.294	1802001.7	5369.546
12.394	1824971.8	5403.661
12.494	1849331.1	5439.604
12.594	1873815.9	5475.496
12.694	1898310.6	5511.168
12.794	1923966.3	5548.284
12.894	1951532.6	5587.891
12.994	1980588	5629.335

Garryland pond dimensions

Elevation (mAOD)	Plan area (m^2)	Perimeter (m)
1.620	0.0	0.0
1.634	0.1	1.2
1.734	17.8	16.9
1.834	60.3	31.1
1.934	248.8	63.1
2.034	1985.5	178.2
2.134	3903.9	249.9
2.234	7123.8	337.6
2.334	14191.3	476.5
2.434	20175.9	568.2
2.534	26164.1	647.0
2.634	31696.3	712.1
2.734	36919.9	768.6
2.834	41983.1	819.6
2.934	47055.1	867.7
3.034	51738.7	909.8
3.134	56329.0	949.3
3.234	61168.9	989.3
3.334	65866.4	1026.6
3.434	70538.7	1062.4
3.534	75123.6	1096.3
3.634	79369.0	1126.9
3.734	83407.6	1155.2
3.834	87375.5	1182.4
3.934	91264.1	1208.4
4.034	95047.1	1233.2
4.134	98870.9	1257.7
4.234	102756.5	1282.2
4.334	106726.8	1306.8
4.434	111013.9	1332.7
4.534	115326.3	1358.4
4.634	119513.9	1382.8
4.734	123654.0	1406.6
4.834	127729.2	1429.6
4.934	131704.5	1451.6
5.034	135550.7	1472.7
5.134	139349.2	1493.2
5.234	143119.9	1513.2
5.334	146724.6	1532.2
5.434	150260.9	1550.5
5.534	153807.9	1568.7
5.634	157410.2	1587.0
5.734	161044.3	1605.2
5.834	164605.5	1622.9
5.934	168110.1	1640.0
6.034	171594.2	1657.0
6.134	175092.8	1673.8
6.234	178670.0	1690.8
6.334	182313.4	1707.9
6.434	185963.8	1724.9
6.534	189574.4	1741.6
6.634	193077.1	1757.6
6.734	196593.0	1773.6
6.834	199740.3	1787.7
6.934	202817.4	1801.4
7.034	205870.7	1814.9
7.134	208925.4	1828.3
7.234	211962.8	1841.6
7.334	214997.2	1854.7
7.434	218067.7	1867.9
7.534	221183.2	1881.2
7.634	224346.2	1894.6
7.734	227472.9	1907.8
7.834	230578.1	1920.7
7.934	233732.4	1933.8
8.034	236721.2	1946.2
8.134	239636.5	1958.1
8.234	242516.6	1969.8
8.334	245295.1	1981.1
8.434	248041.9	1992.2
8.534	250788.9	2003.2
8.634	253532.0	2014.1
8.734	256278.2	2025.0
8.834	259039.2	2035.8
8.934	261826.3	2046.8
9.034	264653.5	2057.8
9.134	267518.9	2068.9
9.234	270423.8	2080.1
9.334	273379.2	2091.4
9.434	276377.2	2102.9
9.534	279425.1	2114.4
9.634	282538.8	2126.2
9.734	285723.3	2138.1
9.834	288997.2	2150.3
9.934	292396.9	2162.9
10.034	295956.8	2176.1
10.134	299728.9	2189.9
10.234	303422.0	2203.4
10.334	307199.7	2217.0
10.434	310956.7	2230.5
10.534	314742.2	2244.1
10.634	318590.5	2257.8
10.734	322524.0	2271.6
10.834	326538.1	2285.7
10.934	330637.8	2300.0
11.034	334849.8	2314.6
11.134	339181.4	2329.6
11.234	343644.1	2344.8
11.334	348241.0	2360.5
11.434	352780.4	2375.8
11.534	357287.9	2390.9
11.634	361709.9	2405.7
11.734	366148.2	2420.4
11.834	370582.1	2435.0
11.934	375123.5	2449.9
12.034	379667.9	2464.7
12.134	384375.2	2479.9
12.234	389031.9	2494.9
12.334	393726.2	2509.9
12.434	398321.5	2524.5
12.534	403037.9	2539.4
12.634	407794.9	2554.4
12.734	412514.5	2569.1
12.754	413474.9	2572.1

Caherglassaun pond dimensions

Elevation (mAOD)	Plan area (m^2)	Perimeter (m)
0.500	29773.5	690.2
0.514	30207.6	695.2
0.614	34577.5	743.8
0.714	40154.4	801.5
0.814	46588.9	863.4
0.914	53151.5	922.2
1.014	59481.9	975.6
1.114	66124.2	1028.6
1.214	72154.6	1074.5
1.314	77835.0	1116.0
1.414	83191.1	1153.7
1.514	88222.9	1188.1
1.614	93212.3	1221.2
1.714	98908.4	1258.0
1.814	104149.3	1290.9
1.914	108836.8	1319.6
2.014	113136.3	1345.4
2.114	117160.5	1369.1
2.214	120800.3	1390.3
2.314	124119.1	1409.2
2.414	127163.6	1426.4
2.514	129990.1	1442.2
2.614	132706.8	1457.2
2.714	135279.0	1471.2
2.814	137765.4	1484.7
2.914	140191.1	1497.7
3.014	142566.1	1510.3
3.114	144950.0	1522.9
3.214	147402.7	1535.7
3.314	149873.3	1548.5
3.414	152410.7	1561.6
3.514	155224.7	1575.9
3.614	158286.3	1591.4
3.714	161697.3	1608.5
3.814	165366.4	1626.6
3.914	169214.3	1645.4
4.014	173446.1	1665.9
4.114	178183.0	1688.5
4.214	183441.9	1713.2
4.314	189563.0	1741.6
4.414	195889.5	1770.4
4.514	201977.5	1797.7
4.614	208362.2	1825.9
4.714	214690.3	1853.4
4.814	221367.0	1882.0
4.914	227449.1	1907.7
5.014	233432.3	1932.6
5.114	239598.0	1957.9
5.214	246294.1	1985.1
5.314	253146.4	2012.5
5.414	260200.8	2040.4
5.514	267703.3	2069.6
5.614	276329.9	2102.7
5.714	284691.3	2134.3
5.814	293568.2	2167.3
5.914	302812.3	2201.1

Elevation (mAOD)	Plan area (m^2)	Perimeter (m)
6.014	311819.0	2233.6
6.114	320932.9	2266.0
6.214	329637.4	2296.6
6.314	338697.1	2327.9
6.414	347930.9	2359.4
6.514	356372.7	2387.9
6.614	364648.6	2415.4
6.714	373356.8	2444.1
6.814	381847.3	2471.8
6.914	390069.9	2498.2
7.014	397956.6	2523.4
7.114	405762.8	2548.0
7.214	413858.0	2573.3
7.314	422142.3	2598.9
7.414	430198.9	2623.6
7.514	438133.7	2647.7
7.614	445914.2	2671.1
7.714	453735.7	2694.4
7.814	461080.7	2716.1
7.914	467910.3	2736.2
8.014	474593.8	2755.6
8.114	481237.0	2774.9
8.214	488002.6	2794.3
8.314	494791.3	2813.7
8.414	501460.4	2832.6
8.514	508177.0	2851.5
8.614	514646.8	2869.6
8.714	521241.0	2887.9
8.814	527841.2	2906.1
8.914	534527.0	2924.5
9.014	540972.0	2942.0
9.114	547337.5	2959.3
9.214	553709.6	2976.5
9.314	560137.6	2993.7
9.414	566433.4	3010.5
9.514	572658.5	3027.0
9.614	578847.3	3043.3
9.714	584908.4	3059.2
9.814	590959.2	3075.0
9.914	597011.5	3090.7
10.014	602889.6	3105.8
10.114	608756.6	3120.9
10.214	614559.3	3135.8
10.314	620301.2	3150.4
10.414	626038.2	3164.9
10.514	631857.9	3179.6
10.614	637687.9	3194.2
10.714	643499.0	3208.7
10.794	648162.9	3220.3

RUNOFF MODELS

Runoff volume model

The following runoff volume models are available in *Infoworks*.

- Fixed - runoff losses after initial losses can be defined as fixed independent of antecedent conditions. Only advisable for use with impervious areas, or pervious areas where runoff does not vary significantly with antecedent conditions.

- Wallingford - The Wallingford model is applicable to typical urban catchments in the UK. It uses a regression equation to predict the runoff coefficient depending on the density of development, the soil type and the antecedent wetness of each subcatchment. Runoff losses defined by:
  PR = 0.829 PIMP + 25.0 SOIL + 0.078 UCWI - 20.7 etc

- NewUK - a replacement to the UK PR equation defined above which addresses some problems:
  the old equation stated that PR remained constant throughout a rainfall event irrespective of catchment wetness. Clearly for long duration storms lower losses towards the end of the event may be significant in terms of urban drainage design. Also, problems had been encountered in applying the PR equation to partially separate catchments and to catchments with low PIMP and low SOIL values.

- SCS - a widely accepted model for predicting storm flow volumes from rural catchments. The method is used in the USA, France, Germany, Australia and parts of Africa. It was derived for rural catchments with uniform conditions. A simple runoff model that allows for variation in the runoff coefficient depending on the catchment wetness. The wetness is updated during the storm and the runoff coefficient increases as the catchment wetness increases. The catchment response is described by two parameters: *storage depth and catchment wetness index*

- Horton - Infiltration either on pervious surfaces or on semi-pervious surfaces can be directly modelled using a variant of the Horton equation (Horton, 1940). This is

an empirical formula derived from infiltrometer/small catchment studies and is usually expressed as a function of time.

- Green-Ampt - The SWMM runoff model uses the Mein and Larson (1973) implementation of the Green-Ampt infiltration equation. You define the following three parameters to use this infiltration model: average capillary suction, saturated hydraulic conductivity and initial moisture deficit.

- Constinf - The Constant Infiltration Model allows you to represent an infiltration drainage surface, such as a permeable pavement, that has a constant infiltration loss to groundwater. This infiltration loss is represented by the Infiltration Loss Coefficient field in the runoff surface definition. In other respects, the ConstInf surface acts in the same way as a fixed runoff surface. Thus not useful for this application.

- Horner - The Horner runoff volume model is used to determine net rainfall on urban subcatchments. The model was developed for use on impervious surfaces in medium sized subcatchments. The Horner model takes into account the decrease in rainfall losses on impervious surfaces throughout the rainfall event via a loss coefficient, Cp. Loss coefficient, Cp, is related to the ruggedness of roads, potholes etc. Cp decreases with time and is not constant. Not relevant here.

SCS model

The basis of the SCS model is the continuity equation:

$$P = I_a + F + Q \qquad \text{Eqn. G.1}$$

where I_a = initial losses (mm), F = cumulative actual storage (mm), Q = total runoff (mm) and P = total rainfall (mm).

Along with the following relationship between rainfall, runoff and storage

$$\frac{F}{S} = \frac{Q}{P - I_a} \qquad \text{Eqn. G.2}$$

where S = maximum potential storage.

The two equations combine to give the SCS model.

$$Q = \frac{(P - I_a)^2}{P - I_a + S} \quad \text{for } P \geq I_a \qquad \text{Eqn. G.3}$$

The form of model has been adapted within the Wallingford software for continuous simulation as follows:

$$\frac{dQ}{dt} = \frac{(P - I_a)(P - I_a + 2S)}{(P - I_a + S)^2} \frac{dP}{dt} \qquad \text{Eqn. G.4}$$

With numerical representation of the derivative per timestep as:

$$\frac{q}{p} = \frac{(P - I_a)(P - I_a + 2S)}{(P - I_a + S)^2} \qquad \text{Eqn. G.5}$$

Where q = runoff over time step (mm) and p = rainfall over time step.

The two parameters S and I_a are related by $I_a = kS$ where $0<k\leq0.2$

Many studies have suggested that SCS initial losses (k) value of between 0.05 and 0.1 – using 0.1. The storage parameter is related to an index known as the Runoff Curve Number (CN) which represents the combined influence of soil type, land management practices, vegetation cover, urban development and antecedent moisture conditions on hydrological response.

Routing models

The following routing models are available in Infoworks.

- Wallingford Procedure

  The flow is routed using two equal linear reservoirs in series, whose routing coefficient depends on rainfall intensity, contributing area and surface slope.

- Large catchment model

  The flow is routed using two equal linear reservoirs in series, whose routing coefficient depends on rainfall intensity, contributing area, and surface slope as in the Wallingford model. The software also applies a timestep lag and routing. factor

multiplier. The timestep lag and routing multiplier are functions of sub-catchment area, ground slope and catchment length.

- Sprint

  The flow is routed using a single linear reservoir, whose routing coefficient depends on sub-catchment area, ground slope and percentage impermeable.

- Desbordes

  The flow is routed using a single linear reservoir, whose routing coefficient depends on sub-catchment area, ground slope, percentage impermeable, catchment length, storm duration and storm depth.

- SWMM

  The flow is routed using a single non-linear reservoir, whose routing coefficient depends on surface roughness, surface area, ground slope and catchment width.

- Unit

  The flow is routed using a unit hydrograph. Time of peak flow and total runoff time are either user defined or calculated from one of six built in methods.

Large catchment model

This model contains two elements that attenuate the peak discharge from the single pipes: routing coefficient multiplier and runoff shift time.

The ***routing coefficient multiplier*** is derived from:

$$K = C_k.A.k_1 s.k_2.L.k_3$$

Where K = routing factor

A = area of sub-catchment (m^2)

s = slope (m/m)

L = length (m)

Default values of coefficients are:

$C_k = 0.03$, $k_1 = 0.030$, $k_2 = -0.228$, $k_3 = 0.460$

The ***runoff time shift*** is derived from:

$$T = C_t.A.t_1.s.t_2.L.t_3$$

Default values of coefficients are:

$C_t = 4.334$, $t_1 = 0.009$, $t_2 = -0.173$, $t_3 = 0.462$

Table G.1 Conduit parameters for Owenshree river calibration.

Conduit ID	Cross-section (mm)	Length (m)	u/s invert (mAOD)	d/s invert (mAOD)
	trapezoidal open channel (OTT 1:1)			
1.1	8000 x 2000	750	58.3	56.6
2.1	8000 x 2000	750	56.6	55.0
3.1	8000 x 2000	750	55.0	53.3
4.1	8000 x 2000	750	53.3	51.6
5.1	8000 x 2000	750	51.6	50.0
6.1	8000 x 2000	750	50.0	48.3
7.1	8000 x 2000	750	48.3	46.6
8.1	8000 x 2000	750	46.6	45.0
9.1	8000 x 2000	750	45.0	43.3
10.1	8000 x 2000	750	43.3	41.6
11.1	8000 x 2000	750	41.6	40.0
12.1	8000 x 2000	750	40.0	38.3
13.1	8000 x 2000	750	38.3	36.7
14.1	8000 x 2000	750	36.7	35.0
15.1	8000 x 2000	750	35.0	33.3
16.1	8000 x 2000	750	33.3	31.7
17.1	8000 x 2000	750	31.7	30.0
	diffuse network (rectangular cross-sections)			
21.1	2000 x 2000	1000	64.0	57.6
21.2	2000 x 1000	500	60.0	56.6
31.1	2000 x 2000	1000	58.0	56.0
31.2	2000 x 1000	500	60.0	56.0
41.1	2000 x 2000	1000	63.0	54.3
41.2	2000 x 1000	500	59.0	54.3

51.1	2000 x 2000	1000	63.0	52.6
51.2	2000 x 1000	500	58.0	52.6
61.1	2000 x 2000	1000	61.0	51.0
61.2	2000 x 1000	500	58.0	61.0
71.1	2000 x 2000	1000	60.0	49.3
71.2	2000 x 1000	500	57.0	50.0
81.1	2000 x 2000	1000	57.0	47.6
81.2	2000 x 1000	500	57.0	47.6
91.1	2000 x 2000	1000	58.0	46.0
91.2	2000 x 1000	500	56.0	46.0
101.1	2000 x 2000	1000	56.0	44.3
101.2	2000 x 1000	500	56.0	44.3
111.1	2000 x 2000	1000	57.0	42.6
111.2	2000 x 1000	500	56.0	42.6
121.1	2000 x 2000	1000	56.0	41.0
121.2	2000 x 1000	500	55.0	41.0
131.1	2000 x 2000	1000	56.0	39.3
131.2	2000 x 1000	500	55.0	39.3
141.1	2000 x 2000	1000	55.0	37.7
141.2	2000 x 1000	500	55.0	37.7
151.1	2000 x 2000	1000	54.0	36.0
151.2	2000 x 1000	500	55.0	36.0
161.1	2000 x 2000	1000	54.0	34.3
161.2	2000 x 1000	500	54.0	34.3
171.1	2000 x 2000	1000	54.0	32.7
171.2	2000 x 1000	500	54.0	32.7

Table G.2 Conduit parameters for final calibrated network model.

Conduit ID	Diameter (mm)	Length (m)	u/s invert (mAOD)	d/s invert (mAOD)
	trapezoidal open channel (OTT 1:1)			
1.1	8000 x 2000	750	58.3	56.6
2.1	8000 x 2000	750	56.6	55.0
3.1	8000 x 2000	750	55.0	53.3
4.1	8000 x 2000	750	53.3	51.6
5.1	8000 x 2000	750	51.6	50.0
6.1	8000 x 2000	750	50.0	48.3
7.1	8000 x 2000	750	48.3	46.6
8.1	8000 x 2000	750	46.6	45.0
9.1	8000 x 2000	750	45.0	43.3
10.1	8000 x 2000	750	43.3	41.6
11.1	8000 x 2000	750	41.6	40.0
12.1	8000 x 2000	750	40.0	38.3
13.1	8000 x 2000	750	38.3	36.7
14.1	8000 x 2000	750	36.7	35.0
15.1	8000 x 2000	750	35.0	33.3
16.1	8000 x 2000	750	33.3	31.7
17.1	8000 x 2000	750	31.7	30.0
18.1	8000 x 2000	750	30.0	28.3
19.1	8000 x 2000	750	28.3	26.7
20.1	8000 x 2000	750	26.7	25.0
		circular pipe		
21.1	2000	500	25.0	17.5
22.1	2000	500	17.5	12.0
23.1	2000	100	12.0	10.0
Black.2	2000	50	10.94	10.0
24.1	1200	80	10.0	9.8
25.1	2000	100	9.8	9.6
26.1	2000	500	9.6	9.0

27.1	2000	500	9.0	8.0
28.1	2000	100	8.0	7.8
Coy.1	2000	50	8.6	7.8
29.2	980	80	7.8	7.75
30.1	2000	100	7.75	7.7
31.1	2000	750	7.7	7.6
32.1	2000	750	7.6	7.5
33.1	2000	100	7.5	7.45
34.1	3000	100	7.45	7.4
35.1	3000	750	7.4	7.3
36.1	3000	750	7.3	7.2
37.1	3000	750	7.2	7.1
38.1	3000	750	7.1	7.0
39.1	3000	750	7.0	6.9
	trapezoidal open channel (OTT 1:1)			
40.1	12000 x 3000	1500	6.9	6.8
	circular pipe			
Coole.2	2200	300	1.694	1.694
G42.1	2200	300	1.694	1.694
Garryland.1	2200	100	1.62	1.61
G43.1	2200	300	1.61	1.6
Coole.1	1800	500	1.695	1.65
G42.1	1800	200	1.65	1.6
43.1	2500	750	1.6	1.3
44.1	2500	750	1.3	1.0
45.1	2500	750	1.0	0.65
46.1	2500	200	0.65	0.3
47.1	2500	100	0.3	0.0
48.1	2500	100	0.0	-0.05
49.1	2500	200	-0.05	-0.1
50.1	2500	750	-0.1	-0.2
51.1	2500	750	-0.2	-0.3
52.1	2500	750	-0.3	-0.4
53.1	2500	750	-0.4	-0.5

54.1	2500	750	-0.5	-0.6
55.1	2500	500	-0.6	-0.7
56.1	2500	200	-0.7	-0.8
→ River Ballycahalan		*trapezoidal open channel (OTT 1:1)*		
BO.1	8000 x 2000	750	36.0	33.0
B1.1	8000 x 2000	750	33.0	30.0
B2.1	8000 x 2000	750	30.0	27.0
B3.1	8000 x 2000	750	27.0	24.0
B4.1	8000 x 2000	750	24.0	21.0
B5.1	8000 x 2000	750	21.0	18.0
B6.1	8000 x 2000	100	18.0	17.0
		circular pipe		
B7.1	3000	100	17.0	8.0
→ River Beagh		*trapezoidal open channel (OTT 1:1)*		
X0.1	8000 x 2000	750	39.0	38.0
X1.1	8000 x 2000	750	38.0	37.0
X2.1	8000 x 2000	750	37.0	36.0
X3.1	8000 x 2000	750	36.0	35.0
X4.1	8000 x 2000	750	35.0	34.0
		circular pipe		
X5.1	2000	650	34.0	30.0
X6.1	2000	650	30.0	26.0
		trapezoidal open channel (OTT 1:1)		
X7.1	8000 x 2000	750	26.0	25.5
X8.1	8000 x 2000	750	24.5	23.0
X9.1	8000 x 2000	750	23.0	21.0
X10.1	8000 x 2000	750	21.0	18.5
X11.1	8000 x 2000	750	18.5	17.5
X12.1	8000 x 2000	750	17.5	15.0
X13.1	8000 x 2000	750	15.0	12.0
		circular pipe		
X14.1	2000	750	12.0	9.0